



TNT 2010

Trends in NanoTechnology

Braga (Portugal)
September 06-10, 2010

PHANTOMS
foundations



Universidad
de Oviedo

INL
INTERNATIONAL IBERIAN
NANOTECHNOLOGY
LABORATORY

UAM
UNIVERSIDAD AUTONOMA
DE MADRID

**UNIVERSITAS
FRIBURGENSIS**

UAB

Universitat Autònoma de Barcelona



ibec Institute for Bioengineering
of Catalonia



UNIVERSITAT DE BARCELONA

leti

CIC
nanogUNE
NANOSCIENCE COOPERATIVE RESEARCH CENTER

cea

**Georgia
Tech**

dipc
Dipartimento di Fisica

NIMS
Nanomaterials Laboratory



Fermi Gap Engineering by Au doping of the Ag/Cu(111) Dislocation Network

Z. M. Abd El-Fattah¹, M. Matena², F. Schiller¹, and J. E. Ortega^{1,2,3}

¹Centro de Física de Materiales CSIC/UPV-EHU, Materials Physics Center-MPC, San Sebastián, Spain, ²Donostia International Physics Center DIPC, San Sebastián, Spain, ³Departamento de Física Aplicada I, Universidad del País Vasco, San Sebastián, Spain.

zakaria.eldegwy@gmail.com

Self-assembled metallic superlattices have attracted much attention in the context of nanoscale fabrication, due to their suitability for nanostructured templates with 1-10 nm periodicities. Ag/Cu(111) represents one of the most simple and promising metallic superlattices. The fact that this system features a surface state with a gap at the Fermi energy^[1] makes it a suitable candidate for surface state nanoelectronics materials^[2]. In this context, we present an Angle Resolved Photoemission Spectroscopy study of Au-doped 1ML and 2ML Ag/Cu(111) systems. The \bar{M} -point Fermi gap of 1ML Ag/Cu(111) system has been found to move smoothly below the Fermi level as a function of Au doping. The 2ML Ag/Cu(111) system does not reveal a gap below the Fermi level, but such gap arises with Au doping. Such control over the Fermi gap in 1ML and 2ML Ag/Cu(111) might open a new way for further application in the very same analogue to the graphene-based technology.

References:

- [1] F. Schiller, J. Cordon, D. Vyalikh, A. Rubio and J. E. Ortega. Phys. Rev. Lett 94, 016103 (2005)
 [2] F. J. García de Abajo, J. Cordon, M. Corso, F. Schiller and J. E. Ortega. Nanoscale, 2, 717 (2010)

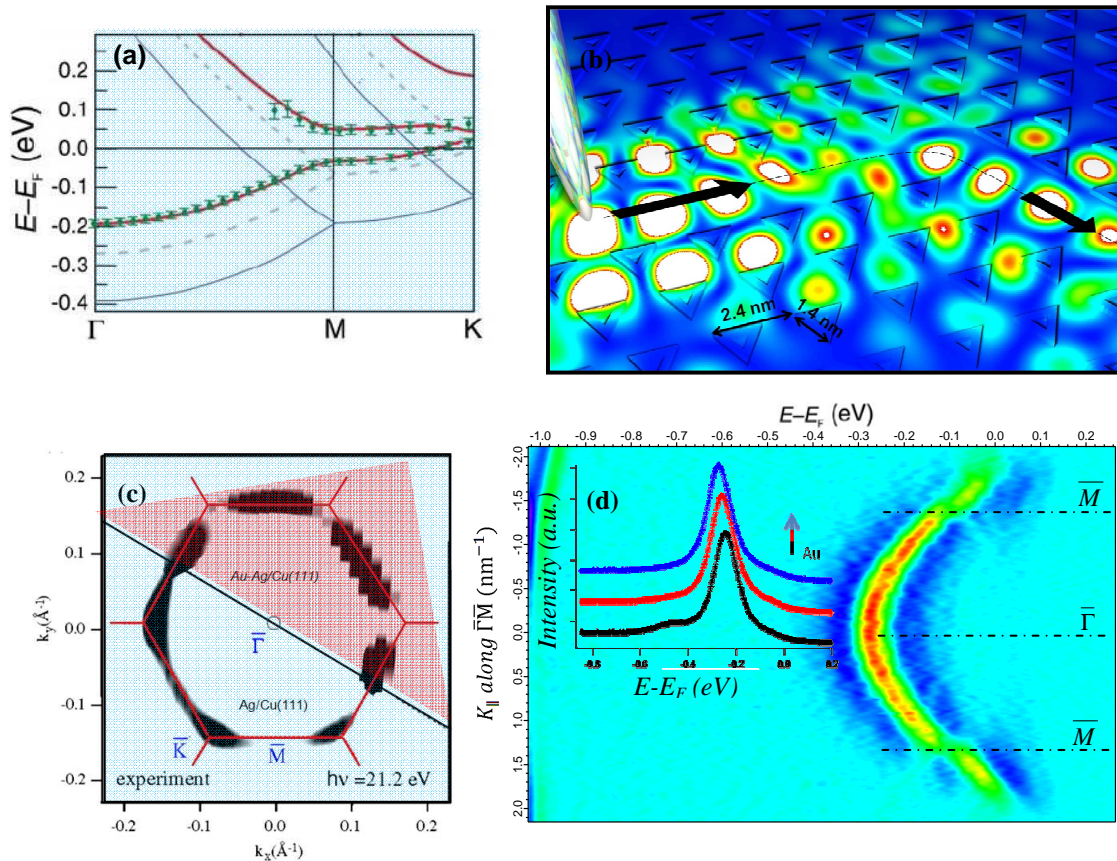


Figure: (a) Surface bands for Cu(111) (blue), a simple model band structure calculation of the 1ML Ag without triangular dislocations (dotted), with triangles (red), and experimental photoemission data (symbols) for the triangular network^[2]. (b) Principle of waveguiding and bending of electronic surface states (EESs)^[2]. (c) Fermi surface of 1ML Ag/Cu(111) and Au doped Ag/Cu(111). (d) Surface state of 1ML Ag/Cu(111) doped with certain amount of Au and the corresponding energy distribution curves as a function of Au doping.

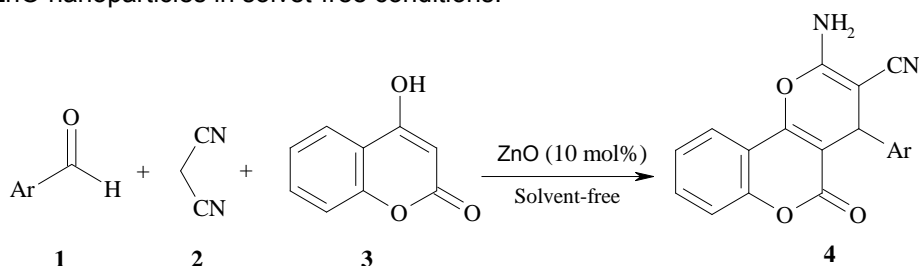
Solvent-Free Synthesis of 3,4-Dihydropyrano[*c*]chromene Derivatives Over ZnO Nanoparticles as an Economical and Efficient Catalyst

Shahrzad Abdolmohammadi

Department of Chemistry, East Tehran Branch (Qiam Dasht), Islamic Azad University, PO Box 33955-163, Tehran, Iran, and Fax: +98-21-3359 4332

E-mail: abdolmohamadi_sh@yahoo.com

Dihydropyrano[*c*]chromenes and their derivatives are of considerable interest because these compounds have a wide range of biological property, such as spasmolytic, diuretic, anti-coagulant, anti-cancer, anti-anaphylactic activity. In addition they can be used as cognitive enhancers, for the treatment of neurodegenerative diseases, including Alzheimer's disease, amyotrophic lateral sclerosis, Huntington's disease, Parkinson's disease, AIDS associated dementia and Down's syndrome as well as for the treatment of schizophrenia and myoclonus. Finally, a number of 2-amino-4*H*-pyrans are useful as photoactive materials. In recent years, the use of zinc oxide (ZnO) as an inexpensive, moisture stable, reusable, commercially available and environmentally benign catalyst in the synthesis of organic compounds has been interested. Thus continuing our research on new one-pot reactions,¹⁻³ we considered ZnO nanoparticles to be an ideal catalyst for effecting synthesis of dihydropyrano[*c*]chromenes via a three-component reaction of 4-hydroxycoumarin, aromatic aldehydes and malononitrile. Herein we describe our very simple, green and efficient route to the synthesis of 2-amino-4-aryl-5-oxo-4*H*, 5*H*-pyrano[3,2-*c*]chromene-3-carbonitriles using of a catalytic amount of ZnO nanoparticles in solvent-free conditions.



[1] S. Abdolmohammadi and S. Balalaie, *Tetrahedron Lett.*, 48, 3299 (2007).

[2] S. Balalaie, S. Abdolmohammadi, H. R. Bijanzadeh and A. M. Amani, *Mol. Divers.*, 12, 85 (2008).

[3] S. Balalaie, S. Abdolmohammadi and B. Soleimanifard, *Helvetica Chem. Acta*, 92, 932 (2009).

Nanoliposomes for encapsulation and delivery of the potential antitumoral methyl 6-methoxy-3-(4-methoxyphenyl)-1*H*-indole-2-carboxylate

Ana S. Abreu^{a,b}, Elisabete M. S. Castanheira^a, Maria-João R. P. Queiroz^b, Paula M. T. Ferreira^b

^aCentro de Física (CFUM) and ^bCentro de Química (CQ-UM), Universidade do Minho, Campus de Gualtar, 4710-057 Braga, Portugal
anabreu@quimica.uminho.pt

Nanoliposomes are new technological developments for the encapsulation and delivery of bioactive agents. Because of their biocompatibility and biodegradability, along with their size, nanoliposomes have potential applications in a vast range of fields, including nanotherapy. Nanoliposomes are able to enhance the performance of bioactive agents by improving their bioavailability, *in vitro* and *in vivo* stability, as well as preventing their unwanted interactions with other molecules [1].

Nanoliposomes may contain, in addition to phospholipids, other molecules such as cholesterol (Ch) which is an important component of most natural membranes. The incorporation of Ch can increase stability by modulating the fluidity of the lipid bilayer preventing crystallization of the phospholipid acyl chains and providing steric hindrance to their movement.

Further advances in liposome research found that polyethylene glycol (PEG), which is inert in the body, allows longer circulatory life of the drug delivery system [2].

In this work, a potential antitumoral fluorescent indole derivative **1**, methyl 6-methoxy-3-(4-methoxyphenyl)-1*H*-indole-2-carboxylate (Figure 1), previously synthesized by us [3], has been encapsulated in different nanoliposome formulations, composed of egg-yolk phosphatidylcholine (Egg-PC), dipalmitoyl phosphatidylcholine (DPPC), dipalmitoyl phosphatidylglycerol (DPPG), distearoyl phosphatidylcholine (DSPC), with or without Ch and distearoyl phosphatidylethanolamine-(polyethylene glycol)2000 (DSPE-PEG).

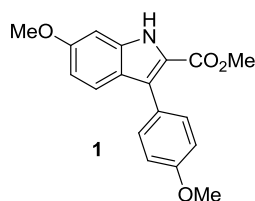


Figure 1. Structure of methyl 6-methoxy-3-(4-methoxyphenyl)-1*H*-indole-2-carboxylate.

Compound **1** was evaluated for the *in vitro* cell growth inhibition on three human tumor cell lines, breast adenocarcinoma (MCF-7), non-small cell lung cancer (NCI-H460) and a melanoma cell line (A375-C5), after a continuous exposure of 48 h, exhibiting low GI₅₀ values in the three tumor cell lines (Table 1).

Table 1. Values of compound **1** concentration needed for 50% of cell growth inhibition (GI₅₀).

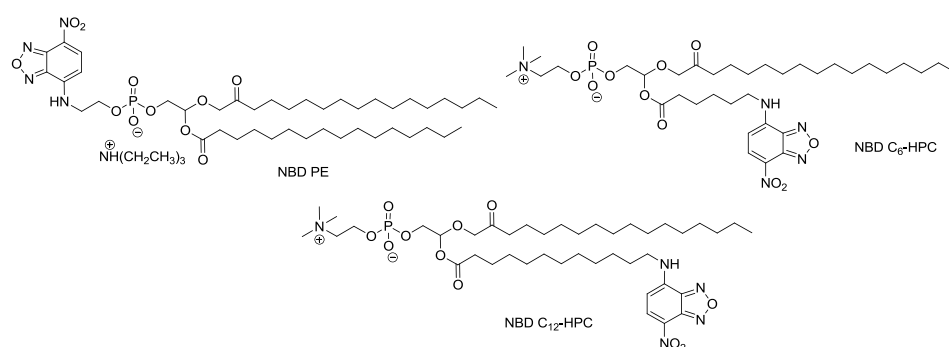
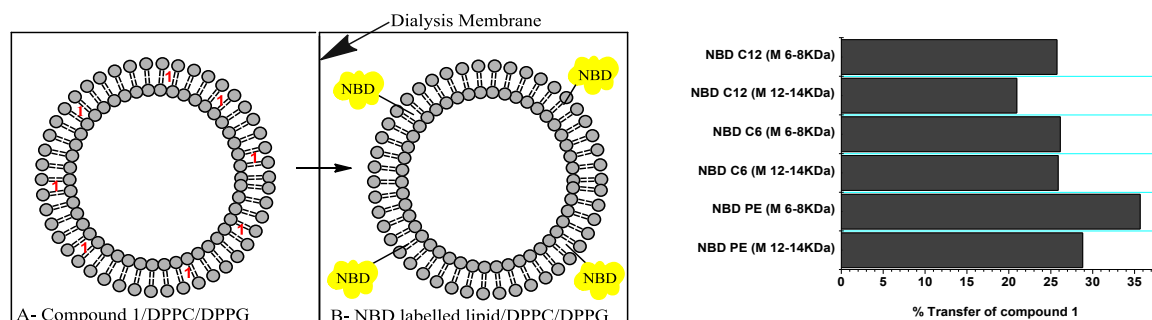
	GI ₅₀ (μM)		
	MCF-7	NCI-H460	A375-C5
1	0.37 ± 0.02	0.33 ± 0.03	0.25 ± 0.02

Different formulations of nanoliposomes were prepared by injection of an ethanolic solution of the lipid mixture and compound **1** in an aqueous media under vigorous stirring, above the melting transition temperature of the lipids. The nanoliposomes prepared were then extruded (3 cycles) through a 100 nm polycarbonate filter. Hydrodynamic diameter, size distribution and zeta potential were measured by dynamic light scattering (DLS). These parameters were monitored in different days in order to determine the more stable formulations (Table 2). The results showed that nanoliposomes have sizes ≤ 120 nm and are generally monodisperse and stable after two weeks. Evaluation of the zeta potential of a nanoliposome preparation can help to predict the stability and *in vivo* fate of liposomes.

Table 2. Hydrodynamic diameter, polydispersity and zeta potential of several nanoliposomes.

	Mean Diameter (nm)	Polidispersity	Zeta potential (mV)
Egg PC/Ch/DPPG	103.5 ± 0.9	0.124 ± 0.009	-51.9 ± 5.84
2 weeks after	95.4 ± 0.53	0.138 ± 0.010	
DPPC/Ch/DSPE-PEG	115.4 ± 0.51	0.146 ± 0.008	-29.5 ± 1.16
1 week after	116.3 ± 1.62	0.154 ± 0.008	
2 weeks after	116.0 ± 0.77	0.152 ± 0.011	
DSPC/Ch/DSPE-PEG	119.8 ± 2.00	0.190 ± 0.012	-26.9 ± 3.66

Permeability studies of compound **1** between DPPC/DPPG liposomes (donor liposomes) and nitrobenzoxadiazole(NBD)-labelled DPPC/DPPG liposomes (acceptor liposomes) were performed using two different sizes of dialysis membranes (6-8 KDa and 12-14 KDa). For these experiments, three different fluorescent labelled lipids, bearing a NBD moiety in different positions of the phospholipids, NBD-PE (labelled at headgroup), NBD-C₆-HPC and NBD-C₁₂-HPC (labelled at fatty acid) were used (Figure 2 and 3). The transfer of compound **1** from DPPC/DPPG liposomes was monitored by FRET (Förster Resonance Energy Transfer) from compound **1** (energy donor) to the NBD-labelled lipids (energy acceptor).

**Figure 2.** Chemical structure of the fluorescent-labelled lipids incorporated in nanoliposomes.**Figure 3.** Schematic dialysis experiment and percentage of drug transfer through a dialysis membrane.

Comparing the energy transfer to the several NBD-labelled lipids (Figure 3, right side), it can be concluded that compound **1** locates mainly near the polar head groups of phospholipids in the acceptor liposomes. It is also observed that compound **1** transfer is more efficient for the smaller dialysis membranes (6-8 KDa).

References

- [1] M.R. Mozafari, S.M. Mortazavi, Nanoliposomes: From Fundamentals to Recent Developments (2005) Trafford, printing in Victoria, BC Canada.
- [2] T.L. Andresen, S.S. Jensen, K. Jorgensen, Progress in Lipid Research **44** (2005) 68-97.
- [3] M.-J.R.P. Queiroz, A.S. Abreu, E.M.S. Castanheira, P.M.T. Ferreira, Tetrahedron **63** (2007) 2215-2222.

Acknowledgements

This work was funded by FCT-Portugal and FEDER through CFUM, CQ-UM, Project PTDC/QUI/81238/2006 (cofinanced by FCT and by program FEDER/COMPETE, ref. FCOMP-01-0124-FEDER-007467) and Post-doc. grant of A.S. Abreu (SFRH/BPD/24548/2005).

Novel Cellulosic titanium Dioxide Nanocomposites as a Protective Coating for Preserving Valuable Manuscripts

Maryam Afsharpour, Fereshteh Talaierad, Alireza Mahjoub

Nanoscience and Technology Research Center, University of Tehran, Tehran, Iran,
m_afsharpour@yahoo.com

Paper-art-works such as old manuscripts are susceptible objects that need to protect from damaging effect of ultraviolet radiation, visible light, pollutant gasses, mold and bacteria. Preventive conservation is an important element of collections care.

Since TiO_2 is broadly used in modern and contemporary pictorial art, acting both as a pure white pigment or a moderator of hue and saturation, the present paper is trying to investigate the TiO_2 role in the inherent protection of paper works of art. Titanium dioxide coatings have received much attention as photocatalysts in practical applications such as environmental purification, deodorization, sterilization and self-cleaning. A variety of physical and chemical approaches have been used to prepare titanium dioxide coating. However, the preparation of TiO_2 thin coatings is usually achieved at relatively high temperature or mechanical impact condition. Using this coating in the substrates with low thermal and mechanical resistance such as old manuscripts needs more attention. Non-impact spray based techniques are generally preferred to avoid breaks and streak defects. Also paper objects should be placed far enough away from display cases that oxide does not affect on the chemical and physical properties of fibers over time. So we use a cellulosic nano-composite of TiO_2 for coating oxides on the surface of fibers. This layered nano-composite can act as a consolidate materials too. Furthermore, to determine how well paper works screen objects from the damaging effects of ultraviolet radiation, a selection of colored fabrics were exposed to light and the fading of color are discussed.

In these studies on the aging of paper materials, the two accelerated aging mechanisms described are those due to light and heat. Degradation of mechanical properties of paper with thermal aging has been measured in tensile strength of papers. Results show good stability of papers with nano-composite coating. Also, a good light stability was shown in the colored paper that treated with this nano-composite. Furthermore, to demonstrate the degree of antifungal properties of coated papers, papers was treated with two common molds and the good preventive effect of coated paper against molds is discussed.

In addition, a paper of an old book was selected to test this coating method. The coated paper was analyzed by FT-IR spectroscopy and the effect of coating on the ink of the manuscript was examined too.

References

- [1] N. Kerr, L. Capjack, R. Fedosejeves, JAIC, **39** (2000) 3.
- [2] K. Ghule, A.V. Ghule, B. Chen ,Y. Ling, Green Chem., **8** (2006) 1034.
- [3] R. J. Feller, R. L. Feller, C. W. Bailie, M. Curran, JAIC **23**(1984) 114 .

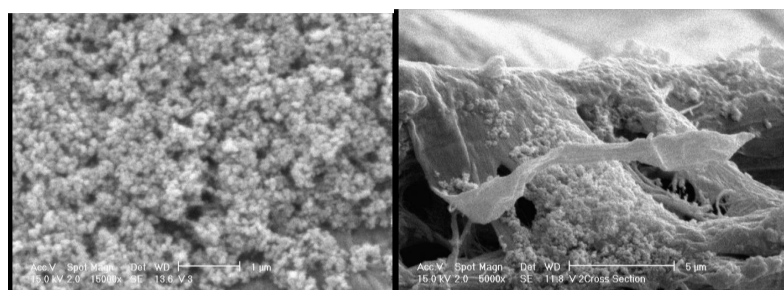


Figure 1 SEM images of paper coated by TiO_2 nanocomposites

Selective Oxidation Catalysts Based on Carbon Nanotubes with Covalently Attached to Molybdenum Oxides

Maryam Afsharpour, Alireza Mahjoub

Nanoscience and Technology Research Center, University of Tehran, Tehran, Iran,
m_afsharpour@yahoo.com

Selective oxidation of organic compounds is an extremely important and useful reaction in the chemical industry. Following discovery of carbon nanotubes, they have been studied extensively in versatile fields because of their novel structural characteristics. Carbon nanotube reactivity can be improved by functionalizing their sidewalls with chemical groups. Alternatively, metal oxides can be employed to decorate carbon nanotube sidewalls. Since metal oxides show a wide range of advanced physico-chemical properties such as high catalytic activity, adsorption capacity, efficient charge transfer, etc. Carbon nanotubes based on transition metal derivatives are being also widely studied, among them molybdenum oxide MoO_3 is an oxide which have been used for the development of materials potentially useful for catalysis, electrodes and sensors. Improvement in catalytic reactions such as selectivity, reactivity, stability and reusability are controlled by the electronic structure of the oxide system used, as well as by the chemical composition, crystal structure and morphology of the oxide surface. On the other hand, the high surface area of CNTs with a narrow pore size distribution is very important to applications used as substrates for external coating. The initial attempts for covalent functionalization took advantage of the higher reactivity of carbon atoms at the ends of the nanotubes to carry out the series of reaction steps leading to the covalent attachment.

Here we describe the rapid and facile chemically controlled deposition of MoO_3 in the cavity of CNTs. The structure and morphology of MoO_3/CNTs hybrid studied with IR spectra, Scanning electron microscopy (SEM), Transmission electron microscopy (TEM), Thermal gravimetric analysis (TGA) and X-ray diffraction (XRD).

In this paper, MoO_3/CNTs hybrids were prepared due to the strong chemical bonding of molybdenum oxide on carbon materials. In one step, the CNTs applied to functionalize and then the functionalized nanotubes were decorated with MoO_3 nanoparticles. MoO_3 were found to show a strong interaction with CNTs and resulting MoO_3/CNTs hybrids were proven to be a good catalyst for alcohol oxidation. The selectivity of the hybrid was found to increase dramatically when MoO_3 react with functional group of CNTs.

References

- [1] J.M. Planeix, N. Coustel and R. Dutartre, *J.Am.Chem.Soc.* , **116** (1994) 7935.
- [2] K. Jurkschat, S.J. Wilkins and R.G. Compton, *Small*, **2** (2006) 95.

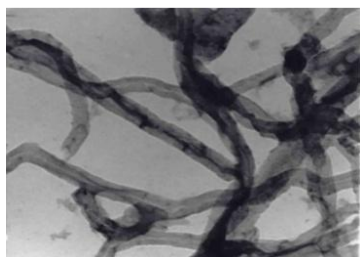


Figure 1: TEM image of MoO_3/CNTs hybrid

Synthesis and characterisation of conductive dna-templated polymer nanowires

Mahdi M. Almaky, B. R. Horrocks, and A. Houlton.

School of chemistry, Newcastle University. UK.

mahdimakki@hotmail.com

In this study, conducting polymer nanowires are prepared by the chemical oxidation of monomers to form polymer on DNA strands processed into polymer nanowires. During the project a series of Pyrrole - pyridine derivatives were prepared and characterised using a range of techniques (NMR, MS, and FTIR). The design of these monomers in modular with a polymerisable group, pyrrole with a flexible linker (alkyl group) will be combined with Pyridine derivatives with a metal ion binding site in order to provide the metal-binding functionality for metal deposition to improve the conductivity in addition to the morphology of the hybrid templated nanowire[1].

For the characterisation of the polymers as a bulk film, the prepared pyrrole-pyridine derivatives monomers were chemically polymerised in aqueous solution in the presence of oxidising agent such as FeCl₃. Then, the polymerisation of those monomers takes place in the presence of λ -DNA where cationic (positive charges) polymer interacts electrostatically with anionic (negative charges) DNA which direct the growth of polymer along DNA chains, hence, the conductive nanowire was obtained [2]. The nanowires will be analysed using suitable techniques especially Atomic Force Microscopy (AFM), FTIR, and electrical characterisation using I/V measurements at various temperatures. **References**

1. B. R. Horrocks, R. Hassanien., J. Hannant, M. A. Galindo, S. Pruneanu, A. R. Pike, A. Houlton and S. A. Al-Said, *Electrochem. Com.*, **11** (2009) 550 - 553.
2. L. Dong, S. Fishwick, B. A. Connolly, N. G. Wright, B. R. Horrocks, and A. Houlton, *Chem. Eur. J.*, **13** (2007), 822 - 828.

Scanning tunneling microscopic investigations into electron transport through graphene

Simon Altenburg, Jörg Kröger and Richard Berndt

Christian-Albrechts-Universität zu Kiel, IEAP, Olshausenstr. 40, D-24098 Kiel, Germany
altenburg@physik.uni-kiel.de

Graphene exhibits advantageous electronic properties that render it a promising candidate for carbon-based microelectronic applications and spintronic devices. To make use of these properties in devices, the graphene layer has to be contacted via macroscopic electrodes. It is therefore of utmost importance to (a) study the interaction of graphene with different electrode materials and to (b) determine the influence of graphene-electrode combinations on the electron transport through the graphene layer.

So far extended metal contacts to graphene have been studied [1-3]. Here, we use the tip of a cryogenic scanning tunneling microscope to contact graphene layers on Ru(0001) and Ir(111). Both surfaces exhibit a moiré lattice, which introduces a periodic variation of graphene-surface interactions. In these experiments the electrical conductance of graphene junctions is characterized with atomic precision. We find that the resulting contact conductances vary systematically with the strength of the graphene-substrate interaction due to the moiré lattice and substrate material. The results are analyzed by means of model calculations, utilizing density functional theory and nonequilibrium Green's functions techniques.

References

- [1] Y. M. Blanter and I. Martin, Phys. Rev. B, **76** (2007) 155433.
- [2] H. Schomerus, Phys. Rev. B, **76** (2007) 045433.
- [3] N. Nemeč, D. Tománek, and G. Cuniberti, Phys. Rev. B, **77** (2008) 125420.

Fabrication of nanofiber reinforced polymer microstructures through two photon polymerization

Mohammed-Amin Alubaidy

Ryerson University (Canada)

Femtosecond laser micromachining has become increasingly important in recent years for many fields, including micro-optics, micro-electronics, micro-biology, and micro-chemistry. Laser ablation, because of its non-contact nature, allows the micromachining and surface patterning of materials with minimal mechanical and thermal deformation. It is now well known that for many of these applications, the femtosecond regime offers advantages over the nanosecond regime. These advantages lie in its ability to deposit energy into a material in a very short time period, before thermal diffusion can occur. As a result, the heat-affected zone, where melting and solidification can occur, is significantly reduced. Smaller feature sizes, greater spatial resolution, and better aspect ratios can hence be achieved.

Another advantage of femtosecond laser micromachining is its versatility in terms of both the materials that can be processed and the type of processing. A variety of materials have been demonstrated to be suitable for femtosecond laser micromachining, such as metals, semiconductors, polymers, oxide ceramics, silica aerogels, optical glasses, and crystals. A variety of processing methods have been used, including the fabrication of photonic crystals, waveguides, gratings and single mode couplers, and the storage of data.

Two-photon polymerization (2PP) is a direct laser writing technique, which allows the fabrication of 2D and 3D structures with a resolution (structure size) down to 100nm [4, 5]. This microstructuring technique is based on the interaction of femtosecond laser radiation with a photosensitive material which induces a highly localized chemical reaction leading to polymerization of the photosensitive material. 2PP allows the fabrication of computer-generated 2D and 3D structures by direct laser "recording" into the volume of a photosensitive material. Due to the threshold behavior and nonlinear nature of the 2PP process, resolution beyond the diffraction limit can be realized by controlling the laser pulse energy and the number of applied pulses.

Polymer is an important material for constructing biomedical microelectromechanical systems (MEMS). Its flexure provides more comfort to patient than conventional silicon based MEMS [6]. More importantly, polymers are biocompatible. However, microdevices made of polymers have lower mechanical strength and modulus compared to metals. By filling the polymer matrix with another material, normally fillers such as particles, tubes and fibers, the mechanical strength of polymer can be improved. When the size of filler reduces to nanoscale, surface area of polymer/filler interface can be much larger than that created with conventional fillers [8, 9]. Therefore, significant improvement in mechanical strength is possible with nanofiller-enhanced composite. Moreover, nanofibers have very special properties compared to bulk materials or even micron-sized particles. These special properties encompass thermodynamic, chemical, mechanical and optical behavior.

In this work, we describe a new fabrication method via two photon polymerization of resin dispersed with nanofibers. This research proposal presents a new method for the formation of microfeatures with reinforced polymer using femtosecond laser material processing. The femtosecond laser was used for the generation of three-dimensional interweaved nanofiber and the construction of microfeatures, like microchannels and voxels, through two photon polymerization of nanofiber dispersed polymer resin. This new method has the potential of direct fabrication of reinforced micro/nano structures. The mechanical properties and of nanofiber reinforced polymer microstructures were investigated by means of nanoindentation.

The electrical conductivity of the nanocomposite formed by the incorporation of the generated nanofibers in a polymer matrix is investigated. The conductivity of the microstructure was measured by a two-probe system at room temperature and the conductivity-temperature relationship was measured between 20-140 oC. The effect of the repetition rate of the femtosecond laser on the electrical conductivity of the reinforced polymer was also studied. Results showed that the electrical conductivity of the reinforced polymer increases with the increase in the repetition rate of the femtosecond laser. Finally, the concept of electrical sensitivity was introduced to show how sensitive and to what extent the reinforced polymer resistance responds after being stimulated by the temperature change.

Even though extensive work has been done on the fabrication of polymeric two or three dimensional structures, to the best of our knowledge, no work has been done on the direct writing of nanofiber reinforced polymeric structures.

Probing electron dynamics in ozone-doped graphene by Raman spectroscopy

H. Tao^(a), J. Moser^(a), **F. Alzina**^{(a)*}, Y. Yamila^(a), A. Bachtold^(a), and C. M. Sotomayor-Torres^{(a),(b)}
^(a) CIN2 (Institut Català de Nanotecnologia-Consejo Superior de Investigaciones Científicas), Campus UAB, 08193 Bellaterra (Spain)
^(b)Institució Catalana de Recerca i Estudis Avançats (ICREA), 08010 Barcelona (Spain)
[* francesc.alsina.icn@uab.cat](mailto:francesc.alsina.icn@uab.cat)

Graphene linear carrier dispersion in the vicinity of two inequivalent points (\mathbf{K} , \mathbf{K}') of the Brillouin zone creates the conditions for the occurrence of unusual effects on the dynamics of both electrons (holes) and phonons, which are related to the electron-phonon interaction [1-4]. Sequential ozone short-exposure cycles increase the p doping of the graphene sheets, as concluded from both the position and the intensity of the Raman peaks. The dynamics of the photoexcited electron-hole pairs has been proven in graphene by the two-phonon Raman peaks intensity. We could determine the electron-phonon coupling for the phonon modes near the \mathbf{K} point, and to monitor the electron-electron scattering contribution with increasing charge concentration as well as with the number of graphene layers. Nevertheless the Raman spectra show the typical features related to different degrees of bond disruption and disorder at high ozone exposure.

[1] Tsuneya Ando, J. Phys. Soc. Jpn. 75, 124701 (2006).

[2] Michele Lazzeri and Francesco Mauri, Phys. Rev. Lett. 97, 266407 (2006).

[3] S. Pisana, M.Lazzeri, C. Casiraghi, K. S. Novoselov, A. K. Geim, A. C. Ferrari, and F. Mauri, Nat. Mat. 6, 198 (2007).

[4] J. Yan, Y. Zhang, and A. Pinczuk, Phy. Rev. Lett. 98, 166802 (2007).

Self catalyzed GaAs nanowires on GaAs (100): growth and characterization

S. Ambrosini^{1,2,3}, M. Fanetti^{1,2}, V. Grillo^{4,5} and S. Rubini¹

¹ Istituto Officina dei Materiali CNR, Laboratorio TASC, S.S. 14, Km. 163.5, I-34149 Trieste, Italy.

² Sincrotrone Trieste S. C. p. A., Elettra Laboratory, S.S. 14, Km. 163.5 I-34149 Trieste, Italy.

³ Università degli Studi di Trieste, via Monte Valerio 1, Trieste, Italy.

⁴ Centro S3, CNR-Istituto Nanoscienze, Via Campi 213A, 41125 Modena, Italy.

⁵ Also with IMEM-CNR, Parco Area delle Scienze 37/A, 43010 Parma, Italy.

ambrosini@tasc.infm.it

Nanowires (NWs) are quasi-one-dimensional crystals with diameter ranging between 30 and 100 nm and length up to several μm . NWs made of semiconductor materials are promising building blocks for the next generation optoelectronic devices and have received in the last years growing attention and interest [1]. They combine semiconductor properties with nanoscale dimensions and this can be exploited for device construction, such as solar cells [2], opto-electronics components [3–7], field emission devices [8] and sensor probes [9].

NWs are typically obtained either by top-down processes, involving patterning of a crystal, or by bottom-up methods, typically involving the presence of a metal nanoparticle, mainly Au, that induce and drive the 1D growth, or through the preparation of the substrate surface by nanofabrication methods. Avoiding Au as catalyst is particularly important when integration with the actual silicon technology is wanted, because Au creates in Si deep carrier traps that reduce Si semiconducting capacities [11].

We present here the growth of GaAs NWs on GaAs (100) without any catalyst deposition and without mechanical or chemical treatments of the substrate surface. Our 1D nucleation sites are obtained by depositing by MBE a sub-nm thick Si layer on GaAs (100) and then oxidizing it by atmospheric oxygen.

Most of the obtained NWs (fig.1A foreground) appear to grow following a VLS-like mechanism [12]: metallic nanoparticles present on the surface act as preferential adsorption sites for the reactants in gaseous phase. Once the nanoparticles are oversaturated, reactants precipitate and eventually nucleate at the interface among the nanoparticles and the substrate. In our case the metal is Ga. The high temperature employed during the growth ($T_g > 580\text{ }^\circ\text{C}$), suggests an incongruent evaporation of As atoms from the oxidized Si surface [13] at early stages of the growth. This allows Ga atoms to diffuse onto the surface and merge to create the nanoparticles. These wires have a growth rate of 20 μm per hour. A minority fraction of NWs don't display a Ga nanoparticle at the tip (fig.1A background), but are pyramid terminated and have a growth rate one order of magnitude smaller.

The structural properties of the two kind of wires are also different: the presence of Ga nanoparticle (fig 1C) is associated with pure zincblende crystal phase, the absence of the nanoparticle (fig 1B) is instead associated with wurtzite crystal phase (fig. 2 left, top part of the NW). Intermediate cases are also observed, where the Ga nanoparticles is consuming (fig. 1D). This situation is associated with a very high mix of zincblende and wurtzite phases through very dense stacking faults along the NW body (fig 2 left, middle part of the NW).

Optical properties of the as grown samples reflect the coexistence of the different structures. A representative low temperature photoluminescence spectrum is shown in Fig. 2 right. It presents a sharp photoluminescence peak around GaAs free exciton energy together with a structured band at lower energy. According to Ref 15, we interpret this band as due to the coexistence of zincblende and wurtzite sections with staggered band alignment.

The Ga-catalyzed wires are a very good example of VLS growth: it proceeds at high rate and leads to absence of stacking faults. When the Ga nanoparticle starts consuming, the catalysis driving force in NW growth competes with the very small energy difference between wurtzite and zincblende stacking [14] and this results in a mixing of the two phases to a lower growth rate. When the Ga nanoparticle has completely disappeared, NW growth is very slow with a direct vapour-to-solid reaction. This reaction happens faster on the pyramidal tip facets than the wall facets [17], resulting in a dominant axial to radial growth and no tapering.

Experiments show that the dominance between the two growth mechanisms can be tuned through to the As to Ga beam pressure ratio (BPR). If the As/Ga BPR is low, the Ga nanoparticle is clearly visible at the end of the growth for durations as high as 1 hour. When the As/Ga BPR is high, the total number of Ga adatoms arriving to the NW tip (direct impinging from the vapour phase plus diffusion) is too low to maintain the Ga nanoparticle on top and the Ga nanoparticle gets consumed.

References

- [1] Barth S. *et al.* Progress in Mater. Sci. 55, 563 (2010)
- [2] Tian B. *et al.*, Nature 449 (7164), pp. 885–889
- [3] Huang Y. *et al.*, Science 294 (2001) 1313.
- [4] Huang M.H. *et al.*, Science 292 (2001) 1897.
- [5] Panev N. *et al.*, Appl. Phys. Lett. 83 (2003) 2238.
- [6] Duan X. *et al.*, Nature 421 (2003) 241.
- [7] Wang J. *et al.*, Science 293 (2001) 1455
- [8] Xia, Y. *et al.*, Adv. Mater 15 (5), pp. 353–389 (2003)
- [9] Wan, Q.a *et al.*, APL Volume 84, Issue 18, 3 May 2004, Pages 3654–3656
- [10] Sorba L. *et al.*, J. Cryst. Growth 127 (1–4), 121–125 (1993).
- [11] Brotherton S. D., Lowther J. E., Phys. Rev. Lett. 44, 606–609 (1980)
- [12] Wagner R S and Ellis W C 1964 Appl. Phys. Lett. 4 89
- [13] Fontcuberta i Morral A., APP. PHYS LETT 92, 063112 2008
- [14] Glas F., Harmand J–C. and Patriarche G., PRL 99, 146101 (2007)
- [15] Spirkoska D. *et al.*, Phys. Rev. B 80, 245325 (2009)
- [16] Pavesi L., Guzzi M., J. Appl. Phys. 75 (10), (1994)
- [17] Ikejiri K. *et al.*, J. Cryst Growth 298 (2007) 16–619

Figures

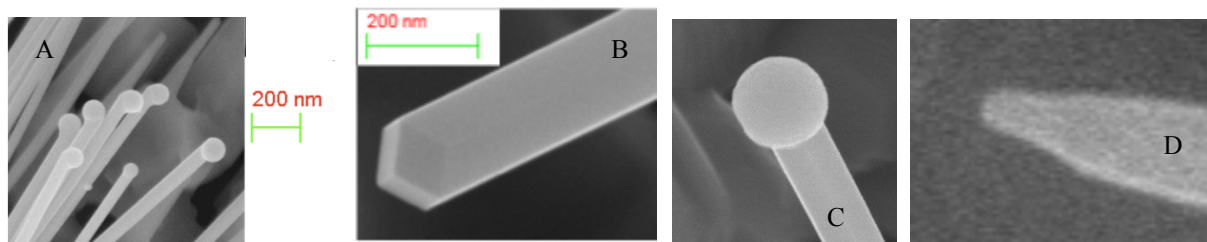


(Fig. 1) A: scanning electron microscopy images of the different GaAs NW types grown on GaAs (100). B: example of high As/Ga BPR growth, NWs are pyramid terminated; C: example of low As/Ga BPR growth, NWs are droplet terminated; D: example of growth with average As/Ga BPR, the nanoparticle is being consumed.

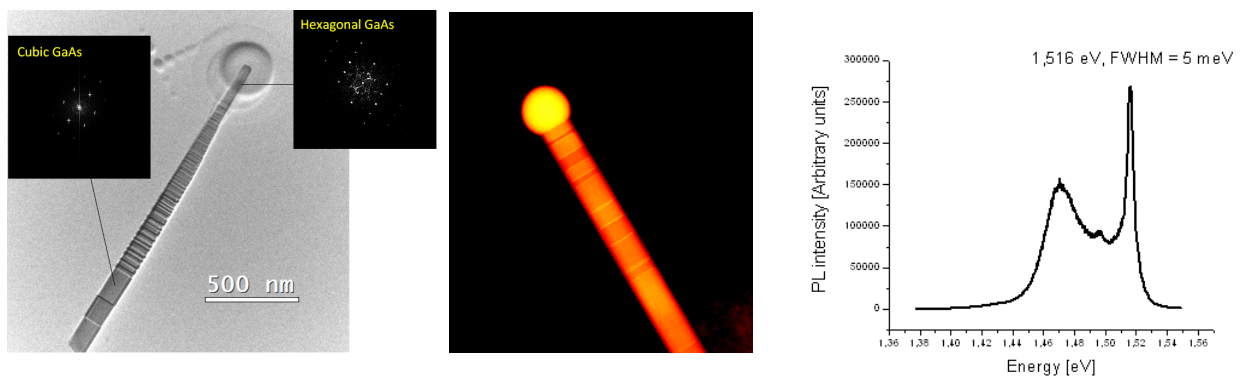


(Fig. 2) transmission electron microscopy images of the different GaAs NW types. Left: pyramid terminated NWs showing from the base, a pure zincblende phase, followed by a mix of zincblende and wurtzite and finally pure wurtzite phase in the top part; middle: droplet terminated NWs with pure zincblende structure; right: low temperature photoluminescence spectrum of the wires ensemble.

Fabrication of Functional Micro- and Nanoneedle electrodes using Template of Carbon Nanotube Nanoneedle and Electrodeposition

Taechang An¹, WooSeok Choi¹, Eunjoo Lee², In-tae Kim¹, Geunbae Lim^{1,3*}

¹Department of Mechanical Engineering,

²School of Interdisciplinary Bioscience and Bioengineering,

³Department of Integrative Bioscience and Biotechnology,

Pohang University of Science and Technology (POSTECH), Pohang, Korea

limmems@postech.ac.kr

With the development of nanotechnology, demands of information about microscale system have increased.[1][2] Micro- and Nanoneedle electrode provides opportunities for electrochemical and biological studies of micro-environments such as AFM-SECM[3][4][5] and single cell analysis[6][7][8]. Although a lot of fabrication methods of nanoneedles were reported, those methods have a limitation of material because most nanoneedles were fabricated using carbon nanotube[7][9][10] and silicon[6][11]. Yet the fabrication of nanoneedle using various materials is very difficult.

In this research, we report a fabrication method for functional micro- and nanoneedle using template of carbon nanotube (CNT) nanoneedle and electrodeposition. Because various materials such as metal, metal oxide and polymer can be coated to the desired location, electrodeposition are very useful for the fabrication of functional nanoneedle.

First, CNT nanoneedles were fabricated at tungsten tip and AFM tip using dielectrophoresis (DEP) and surface tension.[8][12] As shown in figure 1a, two tungsten tips are placed a few micrometers apart, and an AC electric field is applied between them. When the suspension droplet is placed between the electrodes, CNTs are attracted toward the region between the tips of the electrodes due to the DEP force. The suspension was the partially removed and the remaining suspension formed a water meniscus between tungsten tips. The collected CNTs were compressed by the surface tension and attached to the tungsten tip. As a result, CNT bundle nanowire was fabricated between tungsten tips. For the fabrication of CNT nanoneedle, center of the CNT bundle nanowire, weak point, was cut using high electric current. As shown in figure 2, diameter of the CNT nanoneedle was *ca.* 100nm, which could be controlled by changing the concentration of suspension, amplitude of AC voltage and collection time. Length of the CNT nanoneedle was determined by spacing between the tungsten tips.

For the fabrication of functional micro- and nanoneedle, desired material was coated on the CNT nanoneedle by electrodeposition (figure 1b). CNT nanoneedle was submerged electrodeposition solution up to desired position using micro stage and microscope. Au, Ni, ZnO and Ppy were successfully coated on the CNT nanoneedle (figure 3). Thickness and morphology of coating material could be controlled by electrodeposition conditions such as electric potential, solution concentration and deposition time.

In summary, functional micro- and nanoneedle were successfully fabricated using template of CNT nanoneedle and electrodeposition. Because this fabrication method is very simple and able to use various materials, it can be applied to fabrication of micro- and nanoneedle having the desired properties.

This work was supported by Mid-career Researcher Program through NRF grant funded by the MEST (No. 2009-0085377).

References

- [1] P. Sun, F.O. Laforge, T.P. Abeyweera, S.A. Rotenberg, J. Carpino, and M.V. Mirkin, *Proceedings of the National Academy of Sciences*, **105** (2008) 443-448.
- [2] A. Schulte and W. Schuhmann, *Angewandte Chemie International Edition*, **46** (2007) 8760-8777.
- [3] J.V. Macpherson and P.R. Unwin, *Analytical Chemistry*, **72** (2000) 276-285.
- [4] A. Kueng, C. Kranz, B. Mizaikoff, A. Lugstein, and E. Bertagnoli, *Applied Physics Letters*, **82** (2003) 1592.
- [5] D.P. Burt, N.R. Wilson, J.M.R. Weaver, P.S. Dobson, and J.V. Macpherson, *Nano Letters*, **5** (2005) 639-643.
- [6] D. Nawarathna, T. Turan, and H.K. Wickramasinghe, *Applied Physics Letters*, **95** (2009) 083117.
- [7] K. Yum, S. Na, Y. Xiang, N. Wang, and M. Yu, *Nano Letters*, **9** (2009) 2193-2198.

- [8] N.A. Kouklin, W.E. Kim, A.D. Lazareck, and J.M. Xu, *Applied Physics Letters*, **87** (2005) 173901.
 [9] J. Shen, W. Wang, Q. Chen, M. Wang, S. Xu, Y. Zhou, and X. Zhang, *Nanotechnology*, **20** (2009) 245307.
 [10] K. Yum, H.N. Cho, J. Hu, and M. Yu, *ACS Nano*, **1** (2007) 440-448.
 [11] H. Shin, P. Hesketh, B. Mizaikoff, and C. Kranz, *Sensors and Actuators B: Chemical*, **134** (2008) 488-495.
 [12] T. An, K.S. Kim, S.K. Hahn, and G. Lim, *Lab on a Chip*, in pressed.

Figures

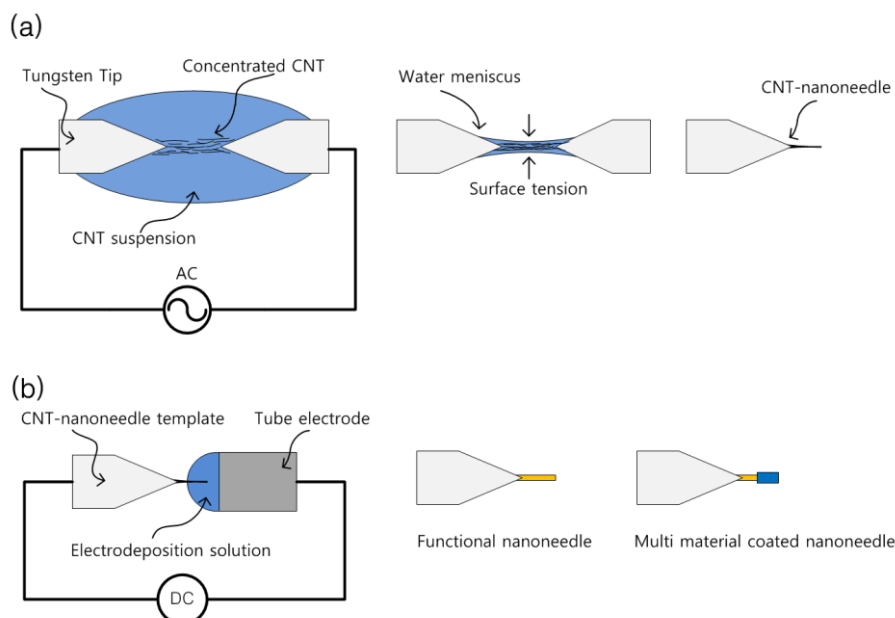


Figure 1. Fabrication process of functional nanoneedle. (a) fabrication process of CNT nanoneedle template, (b) electrodeposition process.

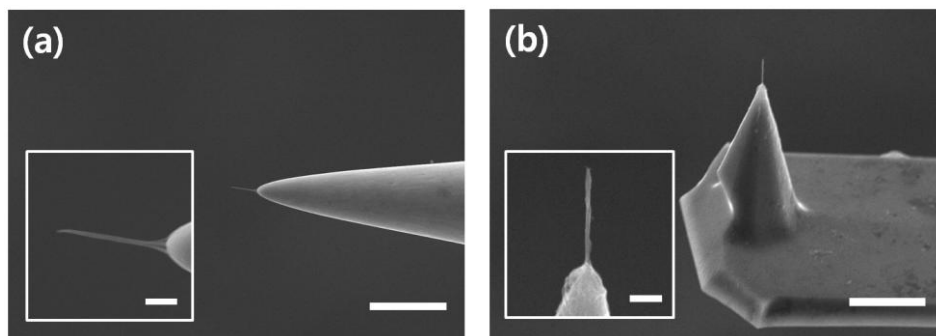


Figure 2. SEM image of (a) nanoneedle at tungsten tip and (b) AFM tip (Scale bar : 10 μm). Insert show magnification view (Scale bar : 1 μm)

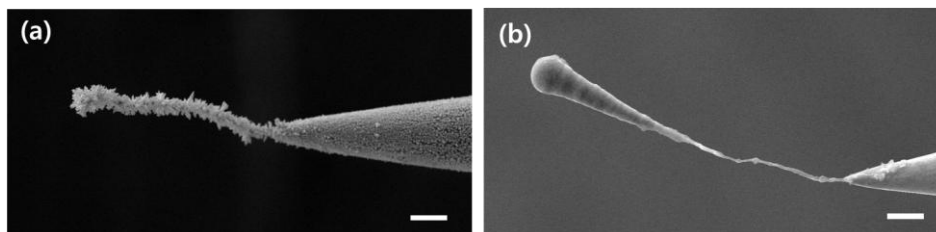


Figure 3. SEM image of functional nanoneedle coated by (a) Au and (b) Ni (Scale bar : 10 μm).

High photocatalytic activity of Zn_2SnO_4 among various structures of $Zn_{2x}Sn_{1-x}O_2$ prepared by a hydrothermal method

Azam Anaraki Firooz, Ali Reza Mahjoub, Abbas Ali Khodadadi, Maryam Movahedi
Department of Chemistry, Tarbiat Modares University, 14115-175, Tehran, Iran

azam_a_f@yahoo.com

In recent years, heterogeneous photocatalysis has received increasing attention for environmental applications such as air purification, water disinfection, hazardous remediation and water purification [1, 2]. The high photocatalytic degradation of semiconductors, such as TiO_2 and ZnO has attracted extensive attention of many researchers [3].

In this paper, different structures and morphologies of SnO_2 containing various amounts of ZnO , was synthesized via a hydrothermal method (without any template), characterized by scanning electron microscopy and powder X-ray diffraction, and used for photocatalytic degradation of Congo red. The results revealed that using different ratios of Zn^{+2}/Sn^{+2} affects the phase and morphology of the $Zn_{2x}Sn_{1-x}O_2$ compounds (see Fig. 1). This type of morphology tailoring of SnO_2 nanoparticles, ZnO doped SnO_2 porous structure, $ZnSnO_3$ flower-like, and Zn_2SnO_4 octahedrals was possible, by varying the Zn^{+2}/Sn^{+2} ratio of 0, 1/10, 1/5 and 1/1, respectively. These products could be formed by decomposition of $ZnSn(OH)_6$ phase. Zn_2SnO_4 with octahedral morphology exhibited a significant enhancement of photocatalytic activity toward degrading Congo red, as compared to other samples. This could be attributed to enhanced oxygen vacancies and crystallite defects formed by substitution of Zn^{+2} in the lattice of SnO_2 , revealed in photoluminescence measurements (see Fig. 2).

References

- [1] A. Fujishima, T. N. Rao, D. A. Tryk, J. Photochem. Photobiol., C photochem.1 (2000) 1-21.
- [2] B. Pal, T. Hata, K. Goto, G. Nogami, J. Mol. Catal.,A Chem. 169 (2001) 147-155.
- [3] H. Lachheb, E. Puzenat, A. Houas, M. ksibi, E. Elaloui, C. Guillard, et. al, Appl. Catal. B: Env. 39 (2002) 75-90.

Figures

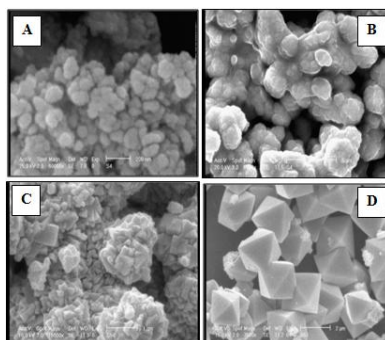


Fig. 1: SEM images of samples, a) SnO_2 nanoparticles, b) ZnO doped SnO_2 porous structure, c) $ZnSnO_3$ flower-like d) Zn_2SnO_4 octahedral.

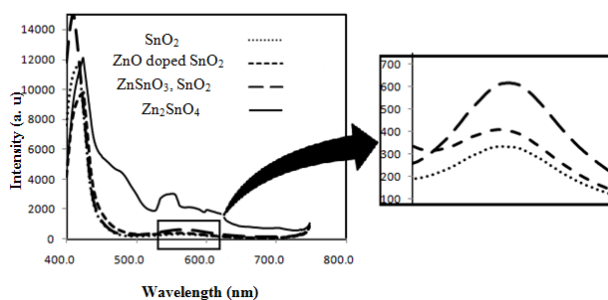


Fig. 2: The PL spectra of the samples.

Small Length-Scale Instabilities in Soft Elastic Films Bonded to Patterned Substrates

Hemalatha Annepu, Jayati Sarkar

Department of Chemical Engineering, Indian Institute of Technology Delhi, New Delhi, India-208016
hema.iitd@gmail.com

Soft elastic films (shear modulus $<1\text{MPa}$) exhibit instabilities at a length scale $\lambda \sim 3h$ (where h is the thickness of the elastic film) below a critical separation distance (d_{critical}) from a contactor. This is due to a competition between the destabilizing interaction forces (like VDW or electrostatic) and the stabilizing restoring elastic forces. In the present work we study the instabilities that develop when a patterned substrate is used instead of a flat substrate. It is found that it is possible to attain length scales as small as $0.296h$ (h being the mean thickness of the film) depending on the substrate pattern parameters. These instabilities are strongly dependant on and decrease with the substrate pattern amplitude as well as the roughness. Increasing the amplitude (β) of the substrate pattern and/or the surface roughness results in smaller and smaller length scales. This, however, also increases energy penalty required in the form of interaction stiffness to create the patterns, which indicates that, in case of VDW interactions, the contactor has to be now brought down to smaller distances to create the instabilities. This setback is overcome if electric field is used instead, making it possible to create instabilities even in very stiff films by externally applying very low voltage at a specified gap distance. More importantly, the critical voltage at which the instabilities are triggered decreases with increase in substrate patterning. The substrate pattern wavelength was found to be of minimal consequence in determining the surface morphology of the film. This opens up avenues to create surface patterns upto length scales as small as $0.32h$ ($\ll 3h$) just by patterning the substrate differently and ruling out the necessity to go for complex bilayer configurations where the smallest length scale reported was $0.5h$.

References

- [1] Mönch, W., Herminghaus, S.; *Europhys. Lett.* **2001**, *53*, 525–531.
- [2] Ghatak, A., Chaudhury, M. K., Shenoy, V., Sharma, A.; *Physical Review Letters* **2000**, *85*, 4329.
- [3] Sarkar, J., Shenoy, V., Sharma, A.; *Physical Review E* **2003**, *67*, 1–11.
- [4] Shenoy, V., Sharma, A.; *J. Applied Physics* **2003**, *94*, 6376.
- [5] Sarkar, J., Shenoy, V., Sharma, A.; *Physical Review Letters* **2004**, *93* (1). 018302-1 -018302-4.
- [6] Ghatak, A., Mahadevan, L., Chaudhury, M.K.; *Langmuir*, **2005**, *21*, pp. 1277-1281.
- [7] Sarkar, J., Sharma, A., Shenoy, V.; *Langmuir*, **2005**, *21* (4), 1457–1469
- [8] Shenoy, V., Sharma, A.; *Physical Review Letters* **2001**, *86*, 119.
- [9] Shenoy, V., Sharma, A.; *J. Mech. Phys. Of Solids* **2002**, *50*, 1155.
- [10] Seeman, S., Herminghaus, S., Jacobs, K.; *Physical Review Letters* **2001**, *86*, 5534.
- [11] Reiter, G., Khanna, R., Sharma, A. *Physical Review Letters* **2000**, *84*, 1432.
- [12] Sharma, A., Khanna, R.; *Physical Review Letters* **1998**, *81*, 3463.
- [13] Kargupta, K., Sharma, A.; *Journal of Colloids and Interface Science* **2002**, *245*, 99.
- [14] Tomar, G., Sharma, A., Shenoy, V., Biswas, G.; *Physical Review E* **2007**, *76*, 011607.
- [15] Bandyopadhyay, D., Sharma, A., Shankar, [J. Chem. Phys.](#) **2008**, *128*, 154909.
- [16] Sarkar, J., Sharma, A., and Shenoy, V.; *Journal of Adhesion* **2005**, *81*, 1-25.
- [17] Mukherjee, R., Pangule, R.C., Sharma, A., Banerjee, I.; *J. Chem. Phys.* **2007**, *127*, 064703.

Organoclay reinforced compatibilized nanocomposites of polypropylene with an amorphous polyamide

N. Aranburu, J. I. Eguiazabal, J. Nazabal

Departamento de Ciencia y Tecnología de Polímeros and Instituto de Materiales Poliméricos "POLYMAT", Facultad de Ciencias Químicas, Manuel de Lardizabal 3, 20018, Donostia, Spain
naramburu003@ikasle.ehu.es

Polymer blending offers a cost effective way to produce new commercially successful polymeric materials. However, compatibilization of the blends is often necessary to achieve the desired property combination due to the immiscibility of most polymers [1,2]. The compatibilization of polymer blends promotes a morphology improvement while facilitating the interfacial adhesion between the components, both leading to improved overall properties [3]. Blends of polypropylene (PP) and polyamides (PA) have been extensively studied because they offer the combination of low cost, good mechanical performance, high barrier properties to moisture and easy for processing of the PP with the excellent mechanical and thermal properties of the polyamides. The compatibilization of PP/PA blends has been obtained by the addition of a third component that consists of a polypropylene chain grafted with functional groups which can react with terminal amine groups in the PA.

For the last years, polymer/organoclay nanocomposites have been widely studied because of the ability of the clay platelets to enhance different properties such as mechanical properties, thermal stability, barrier properties or flame retardancy, at low clay contents. The properties improvement of the nanocomposites lies in the high aspect ratio and rigidity of the dispersed and well-exfoliated individual silicate layers into the polymer matrix [4]. The affinity between the polymer matrix and the organoclay is one of the most important factors in achieving good exfoliation; to a certain extent, affinity can be enhanced by optimizing the structure of the organoclay for a given polymer matrix. For polyamide nanocomposites, montmorillonite (MMT) modified with a quaternary ammonium salt containing one long alkyl tail has been seen to be the best achieving a good dispersion. The highest exfoliation levels have been observed in polyamide-6/organically modified montmorillonite nanocomposites, while nanocomposites with high degrees of dispersion have been obtained with other polyamides, such as PA66, PA12, PA11 or amorphous polyamides (aPA).

Recently, research attention has focused on polymer/polymer/clay ternary nanocomposites because they can combine the advantages offered by polymer blends and conventional nanocomposites [5,6].

In this work, we analyze the effects of the addition of an octadecylamine-modified MMT (OMMT) on the morphology, and the mechanical and thermal properties of efficiently compatibilized blends of PP with an amorphous polyamide (aPA) in 75/25 and 60/40 (PP/aPA) compositions. The compatibilizer was a maleic anhydride-grafted PP (PP-g-MA).

The PP/aPA/OMMT ternary nanocomposites (Figure 1) showed a biphasic structure, regardless of the PP/aPA composition and the OMMT content. The organoclay was found solely inside the aPA particles due to its higher affinity for this component and it showed an exfoliated nanostructure.

The addition of the organoclay to the blends promoted an increase in the average particle size of the aPA dispersed phase and an interfacial adhesion decrease between the components, which was more noticeable at increasing OMMT concentration. This behaviour was in part attributed to the competition between the OMMT surfactant and the aPA to interact with the MA groups of the PP-g-MA compatibilizer, which leads to a decrease of the compatibilization efficiency and to the observed morphological response.

The Young's modulus of the ternary nanocomposites (Figure 2) increased linearly with the OMMT concentration. The addition of 10% OMMT to aPA led to a modulus increase of 20% comparing to that of the unreinforced blend, both in the 75/25 and 60/40 compositions. The yield stress, the ductility and the impact strength were affected by the exclusive location of the OMMT inside the dispersed phase and, also, by the compatibilization efficiency decrease induced by its addition.

Acknowledgements

The financial support of the Basque Government (project n. GIC07/48-IT-234-07) is gratefully acknowledged. N. Aranburu also acknowledges the grant awarded by the Basque Government.

References

- [1] Paul, D. R.; Bucknall, C. B. *Polymer Blends*, Wiley, New York (2000).
- [2] Datta, S.; Lohse, D. J. *Polymeric Compatibilizers*, Hanser, Munich (1996).
- [3] Manning, S. C.; Moore, R. B. *Polymer Engineering and Science*, **39** (1999) 1921.
- [4] Utracki, L. A. *Clay-Containing Polymeric Nanocomposites*, Rapra Technology, Shropshire (2004).
- [5] Motamedi, P.; Bagheri, R. *Materials and Design*, **31** (2010) 1776.
- [6] Gahleitner, M.; Kretzschmar, B.; Pospiech, D.; Ingolic, E.; Reichelt, N.; Bernreitner, K. *Journal of Applied Polymer Science*, **100** (2006) 283.

Figures

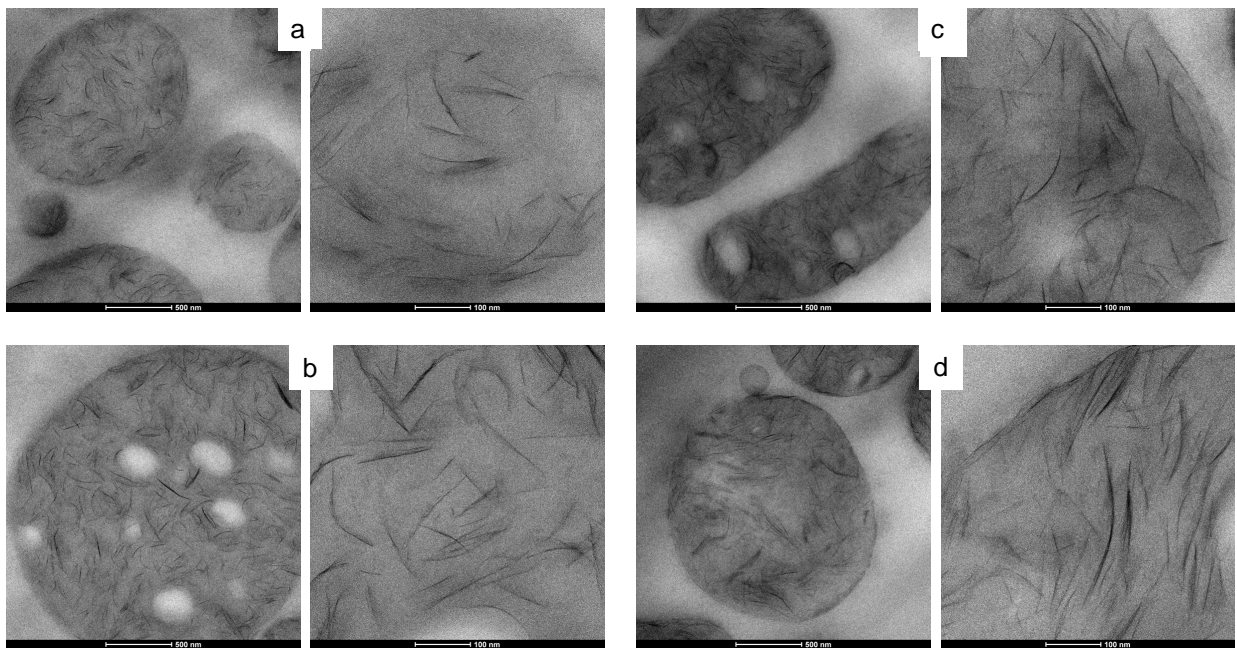


Figure 1. TEM micrographs of 75/25 PP/aPA blends with 5% OMMT (a) and 10% OMMT (b) and 60/40 PP/aPA blends with 5% OMMT (c) and 7% OMMT (d).

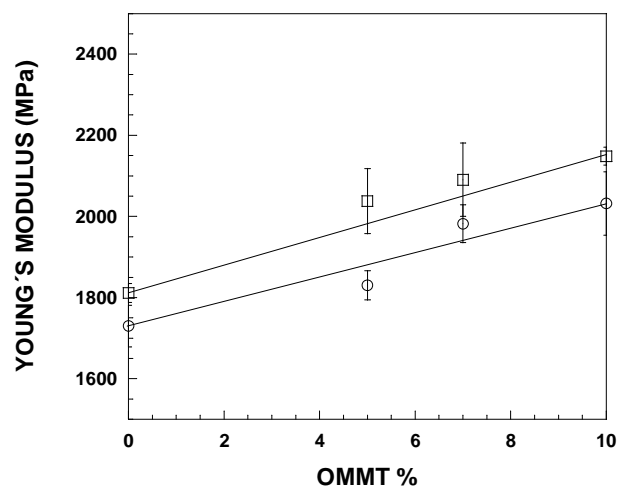


Figure 2. Young's modulus of 75/25 (○) and 60/40 (□) PP/aPA composition blends as a function of the OMMT content.

Preparation and Surface Functionalization of MWCNTs: study of the composite materials produced by interaction with a iron phthalocyanine complex

E. Asedegbe-Nieto¹, M. Pérez-Cadenas¹, J. Carter², J.A. Anderson², A. Guerrero-Ruiz¹

1. Dpto. Química Inorgánica y Técnica. Facultad de Ciencias UNED. Paseo Senda del Rey nº 9, 8040 Madrid, Spain.

2. Surface Chemistry and Catalysis Group, Dept Chemistry, University of Aberdeen, UK
easedegbe@ccia.uned.es

The production and application of nanocomposite materials can find various fields of interest, such as electronic components, selective sensors, heterogeneous catalysts, energy storage, etc. Many of these composites are formed due to (or are created by) specific interactions that occur at the **nanomaterials surfaces**. In the present case we have studied the interactions of multiwall carbon nanotubes (MWCNTs) with a commercially available iron organometallic compound, Iron(III) phthalocyanine-4,4',4'',4'''-tetrasulfonic acid (FePc), which is a hydrated monosodium salt, compound that contains oxygen (see scheme 1). Considering the above mentioned importance of the solid surface interactions with molecular compounds, as reported for instance for the graphene oxide with phthalocyanine hybrids [1] where the pi-pi bonds seem to be the key factors, we have previously treated the MWCNTs in order to modify their surface functionalities. So lab produced MWCNTs, prepared as described in [2], were treated with nitric acid solutions, in order to incorporate oxygen (carboxylic acids, phenols, etc) functions and, subsequently, aliquots of these oxidized samples were contacted with ethylenediamine, in order to turn the surface active sites to basic properties. In short in the way of preparing hybrids materials MCNTs-FePc, we present here the main features associated with the preparation and characterization of these composites solids.

A part from the preparation and surface functionalization of MWCNTs, the production of MWCNTs-FePc hybrids involves the contact of the solids with FePc (Aldrich) aqueous solutions. These suspensions were stirred using a magnetic stirrer for 17 hours at room temperature. Once the excess of solvent was removed using a rotary evaporator the resulting solids materials were dried in an oven at 373 K for 18 hours to ensure it was completely solvent-free. The resulting materials were studied by a battery of techniques. For the MWCNTs surface area and pore size distribution were determined from nitrogen adsorption isotherms at 77 K (NAI), and the incorporated functional groups were evaluated by thermogravimetric analysis under inert gas (ATG) and temperature programmed desorption under vacuum (TPD). In addition their surfaces were analyzed by X-ray Photoelectron Spectroscopy (XPS). The MWCNTs-FePc samples were also studied by XPS and by Infrared Spectroscopy (FTIR). This second method would aid in the determination of modifications in the molecular structure of the FePc molecule, if any. Finally the amounts of FePc incorporated on the hybrid solids were determined by ATG.

Figure 1 presents some images by Transmission Electron Microscopy (TEM) of the as prepared MWCNTs, methods described in reference [2]. The TEM analysis of the surface functionalized materials does not reveal any significant structural modification. From the NAI surface area values (BET method) were determined. So for the as-synthesized MCNTs a value of 90 m²/g was obtained, while the oxidation treatment results in an increase of surface area, up to 120 m²/g, the reaction with ethylenediamine gave a surface area value of 82 m²/g. By FTIR it is not possible to establish features about the surface groups, due to the absorbent-reflecting character of MWCNTs. However TGA and TPD determinations and the complementary XPS analysis, clearly provide valuable information that we have tried to summarize in the Scheme 1, which is relevant from the point of view of the surface species existing in the modified materials.

For the composite or hybrid solids, FTIR does not provide significant insides, with the exception that FePc compound suffers a loss of hydrated water molecules (see scheme 1), which can be the responsible of the weight loss observed in the ATG experiments. Also comparing the ATG of the three composite samples (MWCNTs-FePc, Oxidized-MWCNTs-FePc and Aminated-MWCNTs-FePc) we are able to detect that the amount of incorporated FePc complex is close to 14 wt %. It appears that the lowest amount of FePc is incorporated on de aminated surfaces. On the other hand Binding Energies determined from the XPS spectra, for the Fe2p_{3/2} species are not modified when interacting with the functionalized surfaces. This is indicating that covalent or ionic bonds are produced, thus we have to conclude that the **surface dominant interactions** in these composites are pi-pi types, as has been repeatedly reported for graphitic surfaces and aromatic compounds [3]. From the XPS analysis we have also determined chemical composition (surface atomic percentage) of the hybrid materials. These results are presented in Table 1. It can be noticed that percentage of Fe detected just in the original

FePc complex is significant lower than theoretical chemical content. Also in the composite solids the Fe percentage is high due to the additional presence of residual iron, which was incorporated in the MWCNTs during the preparation procedure (from the $\text{Fe}(\text{CO})_5$ used as catalyst). All these differences observed and summarized in Table 1 underline the relevance of the surface modification treatments in the final compositions of the prepared hybrid materials.

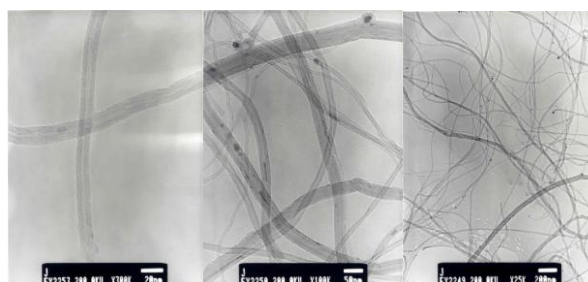
References

- [1] Zhang XQ, Feng YY, Tang SD, Feng W, Carbon, **48-1** (2010) 211-216.
 [2] Sampedro-Tejedor P, Maroto-Valiente, A, Nevskaja, DM, Muñoz V, Rodriguez-Ramos I, Guerrero-Ruiz A, Diamond & Related Mater., **16** (2007) 542-549.
 [3] Castillejos-Lopez E, Nevskaja DM, Muñoz V, Rodriguez-Ramos I, Guerrero-Ruiz A, Langmuir, **20-4**, (2004) 1013-1015.

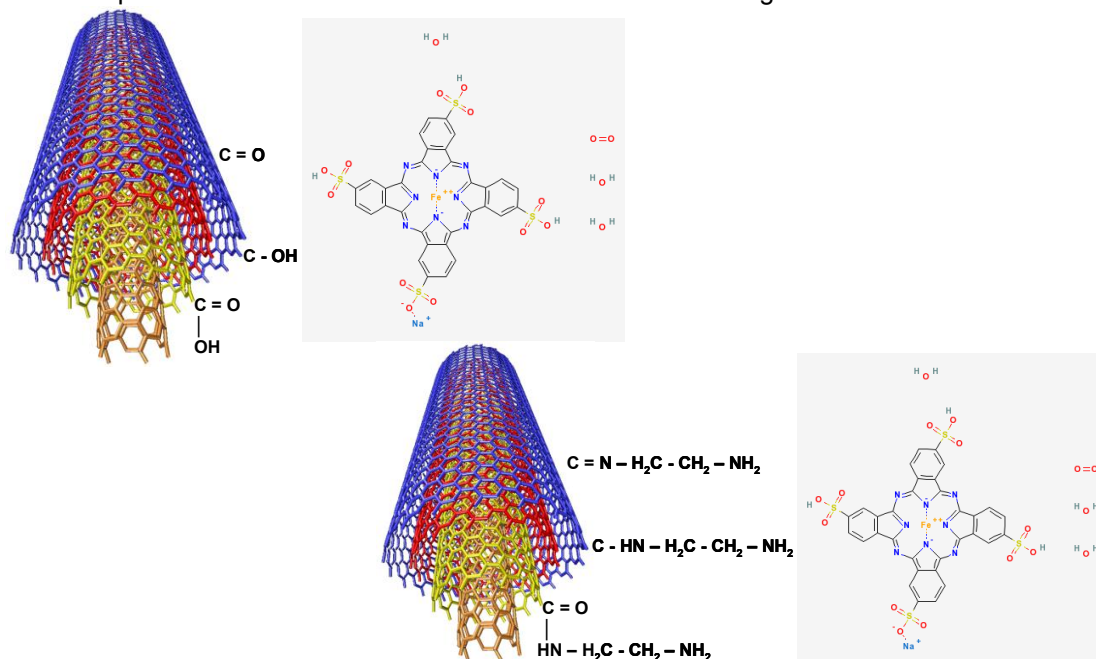
Table 1: Chemical composition of the composite materials as determined from XPS

Sample	Atomic percentage %				
	C1s	O1s	Fe2p 3/2	N1s	S2p
MWCNTs-FePc	86.64	10.28	0.27	1.63	1.20
Oxidized-MWCNTs-FePc	83.64	10.05	0.20	2.94	2.46
Amminated-MWCNTs-FePc	85.88	9.15	0.22	3.03	1.33
FePc	69.65	21.98	0.14	3.94	4.10
FePc (theoretical)	53.33	23.33	1.67	13.33	6.67

Figure 1: TEM images of the original MWCNTs sample.



Scheme 1: Representation of surface modified NWCNTs and the reagent FePc molecules.



Adsorption of Cationic Dye (Methylene Blue) from Water Using Polyaniline Nanotubes Base

Mohamad M. Ayad and Ahmed Abu El-Nasr

Department of Chemistry, Faculty of Science, University of Tanta, Tanta, Egypt

Email :Mohamed.ayad@science.tanta.edu.eg

Polyaniline nanotubes (PANI NTs) base has been utilized as an adsorbent for the removal of cationic dyes such as methylene blue (MB) from aqueous solution. This observation was evidenced from the measurements of quartz crystal microbalance (QCM) and the UV-visible spectroscopy. Experiments were conducted by varying parameters namely: initial concentration of MB and contact time. The percentage of colour removal decreased with increase of initial dye concentration. Adsorption equilibrium of the dye was reached after 120 minutes of contact time. Equilibrium data were fit to Langmuir, Freundlich and Tempkin isotherms and their constants were determined. The linear correlations coefficient showed that the Langmuir isotherm best fits the MB adsorption data on PANI NTs. The kinetic models: pseudo-first order, pseudo-second order and the intraparticle diffusion models were applied to the experimental data. It was observed that pseudo-second order kinetic model described the adsorption process better than any other kinetic models. Results obtained indicate that PANI NTs could be employed as an efficient adsorbent much more than the conventional PANI powder for dye removal from water.

Keywords: Polyaniline nanotubes; Methylene blue; Adsorption isotherm; Kinetics.

Pesticide detection using a surface stress micro cantilever system

Michael Bache, Rafael Jozef Taboryski, Silvan Schmid, Mogens Havsteen Jakobsen

Department of Micro- and Nanotechnology, Technical University of Denmark, DTU Nanotech, Building 345 East, DK-2800 Kongens Lyngby, Denmark;

Michael.bache@nanotech.dtu.dk

Keywords: Pesticide detection, cantilever, surface stress, characterization

Abstract

A 2,6 dichlorbenzamide (BAM) pesticide residue assay has been performed using a surface stress induced cantilever based detection system. The stress induced is measured using the CantiLab4[®] system from cantion with 4 gold coated cantilevers and piezo resistive readout. The detection mechanism is in principle label free, but fluorescent marked antibodies have been used to subsequently verify the binding on the cantilever surface. The profile and vibration mode of each cantilever has also been investigated using a light interferometer and resonance vibrometer device. The system has been analyzed during repeated measurements to verify the BAM assay and characterize the CantiLab4[®] system.

Introduction

During the last 10 years an increasing number of water wells in Denmark have been polluted by pesticides or its break down products. Pesticide analysis of drinking water is currently being done by manual sampling and laboratory analysis. This means weeks in between sampling and the analysis result. An in-line sensor based on a competitive immunological reaction for the detection of BAM will therefore vastly improve water quality monitoring. The BAM molecules in the water sample compete with BAM attached to a cantilever surface for the binding to anti-BAM monoclonal antibodies. [1][2]. The binding of anti-BAM antibodies to the surface of the cantilever will change the surface stress, causing bending of the cantilever. The bending is then detected by a change in resistance of the imbedded piezoelectric layer in the cantilever (fig 1).[2][3]

Experimental

On an inspected, tested and clean CantiChip4[®], a mixture of BAM-ovalbumine conjugate is spotted on cantilever B and C. Cantilever A and D is used as reference and spotted with ovalbumine alone. After overnight incubation the chip is placed in the CantiLab4[®] and a series of stabilization test are conducted. When the system is stable 100 μ l of 0.1 mg/ml unspecific Cy5 labeled mouse IgG mix is added to the chip, to test for any unspecific signal. This is followed by the adding of 100 μ l of 0.1 mg/ml Cy3 labeled BAM antibody in 1x PBS 0,05% Tween20 at a flow rate of 20 μ l/min. The signal is recorded and the data treated. The visible light and fluorescent pictures are taken of the chip, before and after spotting and hybridization (fig 2). The bending profile and vibration mode of each cantilever is recorded using a light interferometer, and a laser based vibrometer with a piezo actuator, before and after spotting and antibody hybridization (fig 3 and 4).

Results and Discussion

The BAM assay has given repeated positive measurements on the cantilever system; however a signal from the unspecific IgG antibody has also been obtained. The fluorescent labelling of the antibodies has verified the attachment of antibodies on the cantilever surface. A clear mass increase has been detected after BAM pesticide has been spotted on the cantilever surface; however, the addition of antibodies has not given a consistent decrease in resonance frequency using the vibrometer device (fig. 3). The bending profile and mass/stiffness values of each cantilever have been a useful tool for the interpretations of the results obtained with the pesticide assay.

References

[1]P.A. Rasmussen, J. Thaysen, O. Hansen, S.C. Eriksen, A. Boisen; Ultramicroscopy 97 (2003) p.371–376
 [1]L. Bruun, C. Koch, B.Pedersen, M.H. Jakobsen and J. Aamand; J. Immunological Methods 240(2000) p.133-142.
 [1]R.Marie, [Jensenius H](#), [Thaysen J](#), [Christensen CB](#), [Boisen A](#). Ultramicroscopy, [Volume 91, Issues 1-4](#), May 2002, p. 29-36

Figures

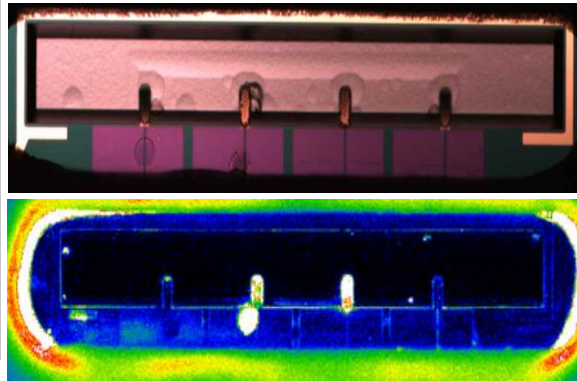
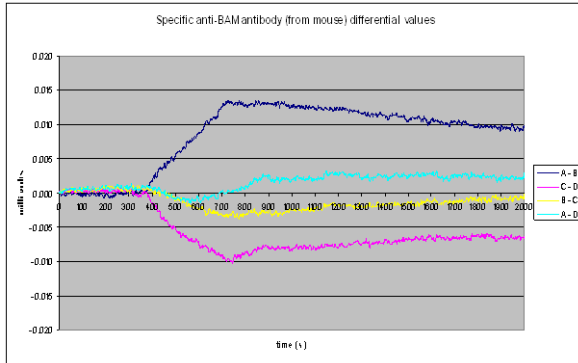


Figure 1. A typical differential signal obtained during the hybridization of anti-BAM to a BAM coated cantilevers..

Figure 2. A set of images of a Cation chip after an experiment, notice the bottom picture shows a clear fluorescent Cy3 signal on cantilever B and C, no signal was obtained from the unspecific IgG antibody

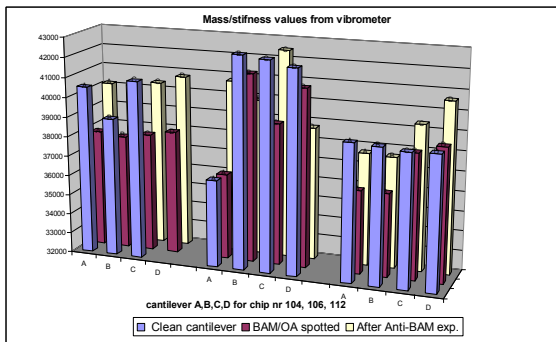


Figure 3. A graph showing 3 clusters of results of vibration frequency of each cantilever from 3 different chips (z axis series: clean, after spotting, after exp). Notice the large variation in between chips and after spotting.

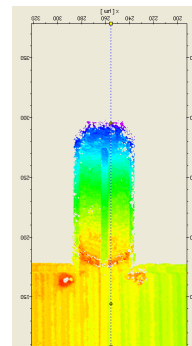


Figure 4. An example of a light interferometer profile image of one of the cantilevers after a pesticide has been spotted onto the surface

The influence of colloidal parameters on the specific power absorption of magnetite nanoparticles with core-shell structure.

M. Bañobre-López¹, Y. Piñeiro-Redondo¹, G. F. Goya² and J. Rivas¹

¹Applied Physics Department, University of Santiago de Compostela, E-15782 Santiago de Compostela, Spain.

²Instituto de Nanociencia de Aragón and Condensed Matter Physics Department, University of Zaragoza, 50018-Zaragoza, Spain.

manuel.banobre@usc.es

Magnetic nanoparticles with appropriate coatings are increasingly being used in many biomedical applications, such as magnetic resonance imaging, drug delivery, cell and tissue targeting or hyperthermia [1-3]. For hyperthermia therapy, nanotechnology offers a powerful tool to the design of nanometer heat-generating sources, which can be activated remotely by the application of an external alternating magnetic field.

Adequately coated iron oxide-based nanoparticles have been the most extensively studied material in hyperthermia experiments because they are thought to be biocompatible and nontoxic, making them suitable for in vivo applications [4-5]. The effective use of magnetic nanoparticles for these applications depends on several factors related to the size, shape, solvent and magnetic properties of the biocompatible nanoparticles. Although the size dependence of the heating power has been already investigated and indicates the existence of an optimal particle size in which the heating power is maximum [6], there is no systematic data on the influence of particle concentration, coating or solvent properties. In order to study the influence of these effects on the heating properties of the system, several dispersions containing single-domain magnetite nanoparticles with particle size between 4 and 12 nm coated with poly-acrylic acid (PAA) have been chemically synthesized through the coprecipitation method. The PAA-coated magnetite nanoparticles showed both crystallinity and magnetic properties similar to the bulk material. The specific power absorption (SPA) of the magnetic dispersions has been evaluated separately by changing both their magnetite nanoparticle concentration and their coating agent in water solution. In this sense, several functionalizing polymers/molecules have been used to coat the magnetic nanoparticle surface (i.e. PAA, oleic acid). Two different silica shell thicknesses coating the PAA-coated magnetite nanoparticles have been also studied. The effect of heat diffusion through the nonmagnetic silica shell coating on the heating power generated by the magnetic nanoparticles is discussed.

In order to evaluate separately the Brownian contribution to the general hyperthermia mechanism, the heating properties of magnetic dispersions at a fixed particle concentration have been evaluated as a function of the solvent viscosity, η . It is important to remark that the magnetite concentration was kept constant and the final dispersions showed a very good stability.

In conclusion, our approach in this work includes the synthesis of biocompatible core-shell magnetite based nanoparticle dispersions and has been focused on the SPA dependence of several factors related to the particle concentration, coating agents and solvent properties, mainly in those dispersions containing PAA-coated magnetite nanoparticles. The results obtained will be shown and discussed.

References

- [1] Q. A. Pankhurst, J. Connolly, S. K. Jones and J. Dobson, *J. Phys. D: Appl. Phys.*, **36** (2003) R167.
- [2] S. Laurent, D. Forge, M. Port, A. Roch, C. Robic, L. Vander Elst and R. N. Muller, *Chem. Rev.*, **108** (2008) 2064.
- [3] C. G. Hadjipanayis, M. J. Bonder, S. Balakrishnan, X. Wang, H. Mao and G. C. Hadjipanayis, *Small*, **4(11)** (2008) 1925.
- [4] R. B. Campbell, *Nanomedicine*, **2** (2007) 649.
- [5] A. K. Gupta, R. R. Naregalkar, V. Deep Vaidya and M. Gupta, *Nanomedicine* **2(1)** (2007) 23.
- [6] M. A. González-Fernández, T. E. Torres, M. Andrés-Vergés, R. Costo, P. de la Presa, C. J. Serna, M. P. Morales, C. Marquina, M. R. Ibarra and G. F. Goya, *J. Solid State Chem.*, **182** (2009) 2779.

Gold-Nanoprobes for specific targets enrichment

Letícia Giestas, Madalena Pinto, Milton Cordeiro, **Pedro V. Baptista**

CIGMH/DCV, Faculdade de Ciências e Tecnologia, Universidade Nova de Lisboa, Caparica, Portugal
pmbv@fct.unl.pt

Noble metal nanoparticles functionalized with ssDNA oligonucleotides have wide scope application for nucleic acid detection and characterization^[1,2]. Their extensive use has relied on the optical properties of Au-nanoparticles that convey increased sensitivity upon molecular recognition of a specific target. Here, we present a simple approach to allow the enrichment of a nucleic acid mixture for a specific sequence/target of interest. We take advantage of the ease of functionalization provided by the Au-nanoparticles' surface via a thiol bond – capture nanoprobe. Upon centrifugation, the capture-nanoprobes can be retrieved allowing isolation of the target; iteration of the process provides for a considerable enrichment that is of utmost relevance in gene expression assays. Recovery of the target sequence might be completed by heat or alkaline denaturation followed by centrifugation and removal of the AuNPs (Figure 1). Here, we demonstrate the potential of use of this approach, as well as quantification of target recovery from complex mixtures via a fluorescence based technique.

References

- [1] M.M. Cheng, G. Cuda, Y.L. Bunimovich, M. Gaspari, J.R. Heath, H.D. Hill, C.A. Mirkin, A.J. Nijdam, R. Terracciano, T. Thundat, M. Ferrari, *Current Opinion in Chemical Biology*, **10** (2006) 11-19.
[2] Baptista P., Pereira E., Eaton P., Doria G., Miranda A., Gomes I., Quaresma P. and Franco R., *Analytical Bioanalytical Chemistry*, **391** (2008) 943-950.

Figures

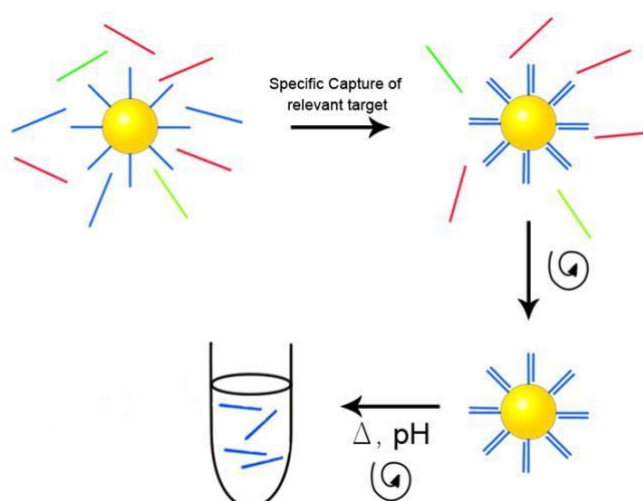


Figure 1: Illustration of target capture and recovery using specifically functionalized gold nanoparticles.

Synthesis and Characterisation of VO₂-based Thermo-chromic Thin films for Energy Efficient Windows

C. Batista*, R. M. Ribeiro, V. Teixeira

University of Minho, Department of Physics, Campus de Gualtar, 4710-057 Braga, Portugal

Abstract

Within the field of “smart” materials, thermo-chromic coatings are demonstrating a high potential to be applied as energy effective building and automotive window coatings due to their self-adaptative optical properties which actively modulate the solar radiation. Vanadium dioxide is the most promising candidate for this application since it reversibly changes its transmission/reflection in the infra-red wavelength range near room temperature, 68°C.

Solar control coatings are a technology with growing interest due to the necessity of improving the energy efficiency of buildings avoiding excessive energy consumption with cooling systems on summer. The latest approach is based on the use of thermo-chromic coatings on so-called “smart” windows. These coatings possess the ability of actively changing their optical properties as a consequence of a reversible structural transformation when going through a critical temperature.

Vanadium dioxide is an example of a thermo-chromic material which is a promising candidate for this kind of application. The change on its optical and also electrical properties takes place at approximately 68°C as a result of a first-order structural transition, going from a monoclinic to a tetragonal phase on heating. The low temperature semiconducting phase which is transparent to radiation in the visible and infrared spectral ranges maximizes the heating due to blackbody radiation, while the metallic high temperature phase filters the infrared radiation and maintains at the same time the transparency required, in the visible range, to keep an environment of natural

* Corresponding author: cbatista@fisica.uminho.pt

light. A transition temperature of 68°C is too high for this application and must therefore be reduced. At present, there are two approaches to reduce the transition temperature, the substitution of part of the vanadium cations by other metals such as tungsten, molybdenum or niobium, or the substitution of part of the oxygen anions by other elements, e.g. fluorine.

In this study, magnetron sputtered VO₂ thin films have been prepared with different doping elements such as W, Mo and Nb and different doping concentrations. We report on the influence of each element and respective concentrations on the crystal structure of the films, optical/thermochromic performance, electrical resistance, surface morphology, and effectiveness on the reduction of the semiconductor-metal transition from 68°C to room temperature, envisaging the application on energy efficient windows.

NUCLEATION OF SrTiO₃ (STO) NANOSTRUCTURES ON Si SUBSTRATES PREPARED BY METALORGANIC DECOMPOSITION (MOD)

M. Benedicto, L. Vázquez and P. Tejedor

Instituto de Ciencia de Materiales de Madrid, CSIC. Sor Juana Inés de la Cruz 3, 28049-Madrid, Spain

marcos.benedicto@icmm.csic.es

Presently, the semiconductor industry faces several technological challenges which must be addressed to preserve their competitiveness. To reduce the leakage current through the conventional gate oxide, SiO₂, this material has been replaced in recent years by high-k dielectrics which exhibit high thermal stability interfaces with Si, dielectric constants higher than that of SiO₂ and high bandgap energies. But the introduction of high-k oxides in complementary-metal-oxide-semiconductor (CMOS) devices causes a carrier mobility reduction in the transistor channel. The replacement of the Si channel by a III-V compound semiconductor, which possess much higher electron mobilities than Si, has been proposed as an alternative to improve the circuit characteristics. But direct growth of a III-V semiconductor (e.g., GaAs) on Si presents very difficult technical problems derived from the nucleation of a polar material (GaAs) on a non-polar one (Si), the high lattice mismatch (4.1%) and the high difference in thermal expansion coefficients (60%), which leads to the formation of a high defect density in the III-V channel. One of the most promising techniques to tackle this problem is selective epitaxy of GaAs on Si using the so-called epitaxial lateral overgrowth (ELO) ⁽¹⁻³⁾.

The aim of this work is to develop a new process to obtain self-organized nanostructures of strontium titanate (STO) on Si by metalorganic decomposition (MOD) which act as a buffer template for subsequent selective growth of GaAs by molecular beam epitaxy (MBE). There is an extensive bibliography describing the deposition of STO layers on various substrates, such as glass, STO or LaAlO₃ using MOD ⁽⁴⁻⁷⁾, MBE ⁽⁸⁻¹¹⁾, chemical vapor deposition (CVD) ⁽¹²⁾ and liquid phase deposition (LPD) ⁽¹³⁾. However, the deposition of STO layers on Si substrates by MOD has only been reported by Ng. ⁽¹⁴⁾

The precursor solutions were prepared in dry Ar atmosphere due to the hygroscopicity of the precursor, SrTi(OCHMe₂)₆. The solvent was isopropanol. The solutions, with concentrations between 1.0x10⁻³ and 1.0x10⁻²M, were deposited over Si (001) substrates in a clean room by spin coating and, subsequently, drying, pyrolysis and crystallization steps were applied. The crystallization was carried out by two alternative heating procedures: (i) rapid thermal annealing (RTA), which was performed in O₂ atmosphere at 650, 750 and 800°C, and (ii) conventional heating in air to 900°C. The surface morphology of the STO deposits and the chemical state of surface species were studied by atomic force microscopy (AFM) and infrared spectroscopy (IRS), respectively.

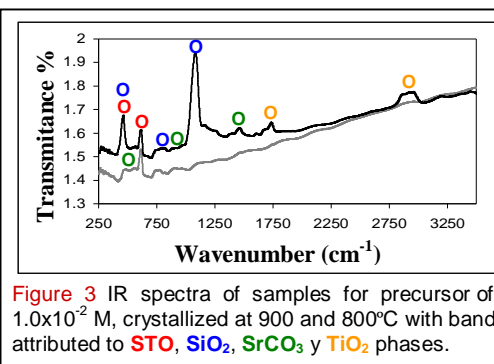
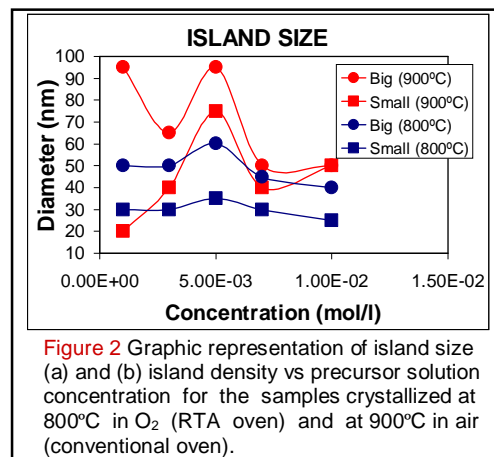
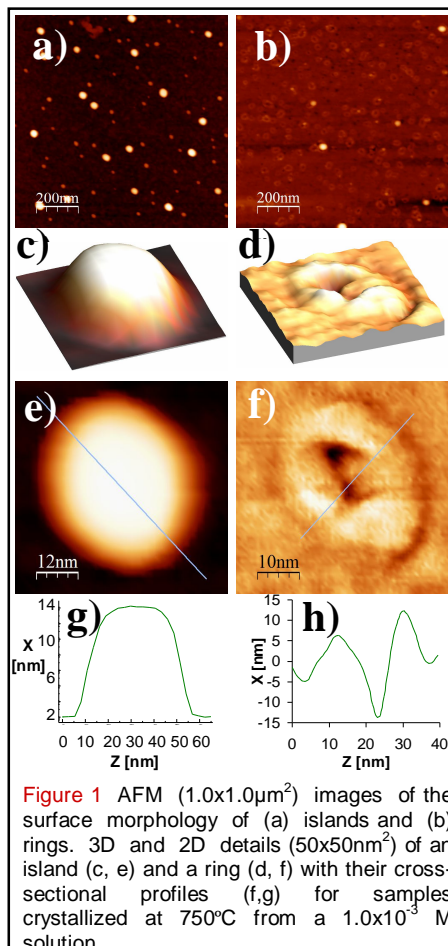
In the samples crystallized at 650°C, the STO phase coexists with organometallic macromolecules due to incomplete reaction. In the other series, the STO self-organizes by the formation of three kinds of nanostructures. Low precursor solution concentrations lead to the formation of islands grouped in two populations with diameters of ≈65 and ≈35nm and heights of ≈9 and ≈6nm, respectively. The estimated density have been found to be between 3.0x10⁸ and 2.0x10¹⁰ cm⁻². Medium concentrations favor the appearance of rings with external and internal diameters of ≈50nm and ≈20nm, respectively, and an average height of ≈4nm. Full uniform layers were obtained for the highest concentrations. The circular islands became rectangular when the annealing temperature increased due to an improved crystallization process (STO phases crystallize in cubic and rectangular systems). The island size was found to increase with precursor solution concentration up to a critical value (5.0x10⁻³M), where an island to ring transition takes place. This nucleation mechanism agrees with the growth models proposed by Doudevski ⁽¹⁵⁾ and Lorke ⁽¹⁶⁾ for other material systems. The island formation begins with the adsorption of organometallic molecules on the substrates constituting a matrix of crystallization nucleus. When the temperature is increased the solvent evaporates and molecules diffuse on the surface interacting among them. As concentration increases, the nuclei density increases and surface collisions become more frequent. At this stage the aggregation of new atoms to the nuclei is the limiting step. When the islands reach a critical dimension the upper atoms are in an energetically unfavourable state and they migrate out of the island re-incorporating to the surrounding substrate where the ring is formed.

The IR spectra prove the absence of water or solvent residues. The SrTrO₃ phase was present in both 800 (RTA) and 900°C (conventional oven) samples. By contrast the 900°C samples exhibit bands corresponding to secondary crystalline phases (SiO₂, TiO₂ and SrCO₃).

References

- [1] G. Vanamu, A.K. Datye, R. Dawson, S.H. Zaidi, Appl. Phys. Lett., 88 (2006) 251909.
- [2] S. Naritsuka, Y. Tejima, K. Fujie and T. Maruyama, J. Cryst. Growth, 310 (2008) 1642.
- [3] Y.S. Chang, S. Naritsuka and T. Nishinaga, J. Cryst. Growth, 312 (2010) 629.
- [4] M. J.-. Hua, M. X.-. Jian, S. J.-. Lan, L. Tie, S. F.-. Wen and C. J.-. Hao, Chinese Physics, 14 (2005) 3
- [5] T. Kawata, H. Iwasaki, S. Yufune, T. Ishibashi and K. Sato, Physica, C (2006)
- [6] T. Ishibashi, T. Kawata, S. Yufune and K. Sato, Journal of Physics: Conference Series 43 (2006) 255-258
- [7] A. Pomar, M. Coll, A. Cavallaro, J. Gázquez, N. Mestres, F. Sandiumenge, T. Puig, and X. Obradors, J. Mater. Res., 21 (2006) 5
- [8] K. Eisenbeiser, J.M. Finder, Z. Yu, J. Ramdani, J.A. Curless, J.A. Hallmark, R. Droopad, W.J. Ooms, L. Salem, S. Bradshaw and C.D. Overgaard, Applied Physics Letters, 76 (2000) 10
- [9] F. Niu and B.W. Wessels, Journal of Crystal Growth, 300 (2007) 509-518
- [10] K. Eisenbeiser, R. Emrick, R. Droopad, Z. Yu, J. Finder, S. Rockwell, J. Holmes, C. Overgaard and W. Ooms, IEEE Electron Device Letters, 23 (2002) 6
- [11] K. Eisenbeiser, J. Finder, R. Emrick, S. Rockwell, J. Holmes, R. Droopad, Z. Yu, J. Ramdani, L. Hilt, A. Talin, J. Edwards Jr, W. Ooms, J. Curless, C. Overgaard and M. O'Steen, Physical Sciences Research Labs/Motorola Labs, Motorola Inc.
- [12] J. Peña A. Martínez, F. Conde, J.M. González Calbet and M. Vallet-Regí, Solid State Ionics, 101-103 (1997) 183-190
- [13] Y. Gao, Y. Masuda, T. Yonezawa and K. Koumoto, Chem. Mater., 14 (2002) 5006-5014
- [14] T.B. Ng, J.B. Xu, G.D. Hu, W.Y. Cheung and I.H. Wilson, Electron Devices Meeting, Hong Kong (2002) 15-19
- [15] I. Doudevski and D.K. Schwartz, J. Am. Chem. Soc., 123 (2001) 6867-6872
- [16] A. Lorke, R.J. Luiken, J.M. García and P.M. Petroff, Jpn. J. Appl. Phys., 40 (2001) 1857-1859

Figures



NUCLEATION OF SrTiO₃ (STO) NANOSTRUCTURES ON Si SUBSTRATES PREPARED BY METALORGANIC DECOMPOSITION (MOD)

M. Benedicto and P. Tejedor

Instituto de Ciencia de Materiales de Madrid, CSIC. Sor Juana Inés de la Cruz 3, 28049-Madrid, Spain

marcos.benedicto@icmm.csic.es

Presently, the semiconductors industry faces several technological challenges which must be addressed to preserve their competitiveness. To reduce the leakage current through the conventional gate oxide, SiO₂, this material has been replaced in recent years by high-k dielectrics which exhibit high thermal stability interfaces with Si, dielectric constants higher than that of SiO₂ and high bandgap energies. But the introduction of high-k oxides in complementary-metal-oxide-semiconductor (CMOS) devices causes a carrier mobility reduction in the transistor channel. The replacement of the Si channel by a III-V compound semiconductor, which possess much higher electron mobilities than Si, has been proposed as an alternative to improve the circuit characteristics. But direct growth of a III-V semiconductor (e.g., GaAs) on Si presents very difficult technical problems derived from the nucleation of a polar material (GaAs) on a non-polar one (Si), the high lattice mismatch (4.1%) and the high difference in thermal expansion coefficients (60%), which leads to the formation of a high defect density in the III-V channel. One of the most promising techniques to tackle this problem is selective epitaxy of GaAs on Si using the so-called epitaxial lateral overgrowth (ELO) ⁽¹⁻³⁾.

The aim of this work is to develop a new process to obtain self-organized nanostructures of strontium titanate (STO) on Si by metalorganic decomposition (MOD) which act as a buffer template for subsequent selective growth of GaAs by molecular beam epitaxy (MBE). There is an extensive bibliography describing the deposition of STO layers on various substrates, such as glass, STO or LaAlO₃ using MOD ⁽⁴⁻⁷⁾, MBE ⁽⁸⁻¹¹⁾, chemical vapor deposition (CVD) ⁽¹²⁾ and liquid phase deposition (LPD) ⁽¹³⁾. However, the deposition of STO layers on Si substrates by MOD has only been reported by Ng. ⁽¹⁴⁾.

The precursor solutions were prepared in dry Ar atmosphere due to the hygroscopicity of the precursor, SrTi(OCHMe₂)₆. The solvent was isopropanol. The solutions, with concentrations between 1.0x10⁻³ and 1.0x10⁻²M, were deposited over Si (001) substrates in a clean room by spin coating and, subsequently, drying, pyrolysis and crystallization steps were applied. The crystallization was carried out by two alternative heating procedures: (i) rapid thermal annealing (RTA), which was performed in O₂ atmosphere at 650, 750 and 800°C, and (ii) conventional heating in air to 900°C. The surface morphology of the STO deposits and the chemical state of surface species were studied by atomic force microscopy (AFM) and infrared spectroscopy (IRS), respectively.

In the samples crystallized at 650°C, the STO phase coexists with organometallic macromolecules due to incomplete reaction. In the other series, the STO self-organizes by the formation of three kinds of nanostructures. Low precursor solution concentrations lead to the formation of islands grouped in two populations with diameters of ≈65 and ≈35nm and heights of ≈9 and ≈6nm, respectively. The estimated density have been found to be between 3.0x10⁸ and 2.0x10¹⁰ cm⁻². Medium concentrations favor the appearance of rings with external and internal diameters of ≈50nm and ≈20nm, respectively, and an average height of ≈4nm. Full uniform layers were obtained for the highest concentrations. The circular islands became rectangular when the annealing temperature increased due to an improved crystallization process (STO phases crystallize in cubic and rectangular systems). The island size was found to increase with precursor solution concentration up to a critical value (5.0x10⁻³M), where an island to ring transition takes place. This nucleation mechanism agrees with the growth models proposed by Doudevski ⁽¹⁵⁾ and Lorke ⁽¹⁶⁾ for other material systems. The island formation begins with the adsorption of organometallic molecules on the substrates constituting a matrix of crystallization nucleus. When the temperature is increased the solvent evaporates and molecules diffuse on the surface interacting among them. As concentration increases, the nuclei density increases and surface collisions become more frequent. At this stage the aggregation of new atoms to the nuclei is the limiting step. When the islands reach a critical dimension the upper atoms are in an energetically unfavourable state and they migrate out of the island re-incorporating to the surrounding substrate where the ring is formed.

The IR spectra prove the absence of water or solvent residues. The SrTrO₃ phase was present in both 800 (RTA) and 900°C (conventional oven) samples. By contrast the 900°C samples exhibit bands corresponding to secondary crystalline phases (SiO₂, TiO₂ and SrCO₃).

References

- [1] G. Vanamu, A.K. Datye, R. Dawson, S.H. Zaidi, Appl. Phys. Lett., 88 (2006) 251909.
 [2] S. Naritsuka, Y. Tejima, K. Fujie and T. Maruyama, J. Cryst. Growth, 310 (2008) 1642.
 [3] Y.S. Chang, S. Naritsuka and T. Nishinaga, J. Cryst. Growth, 312 (2010) 629.
 [4] M. J.- Hua, M. X.- Jian, S. J.- Lan, L. Tie, S. F.- Wen and C. J.- Hao, Chinese Physics, 14 (2005) 3
 [5] T. Kawata, H. Iwasaki, S. Yufune, T. Ishibashi and K. Sato, Physica, C (2006)
 [6] T. Ishibashi, T. Kawata, S. Yufune and K. Sato, Journal of Physics: Conference Series 43 (2006) 255-258
 [7] A. Pomar, M. Coll, A. Cavallaro, J. Gázquez, N. Mestres, F. Sandiumenge, T. Puig, and X. Obradors, J. Mater. Res., 21 (2006) 5
 [8] K. Eisenbeiser, J.M. Finder, Z. Yu, J. Ramdani, J.A. Curless, J.A. Hallmark, R. Droopad, W.J. Ooms, L. Salem, S. Bradshaw and C.D. Overgaard, Applied Physics Letters, 76 (2000) 10
 [9] F. Niu and B.W. Wessels, Journal of Crystal Growth, 300 (2007) 509-518
 [10] K. Eisenbeiser, R. Emrick, R. Droopad, Z. Yu, J. Finder, S. Rockwell, J. Holmes, C. Overgaard and W. Ooms, IEEE Electron Device Letters, 23 (2002) 6
 [11] K. Eisenbeiser, J. Finder, R. Emrick, S. Rockwell, J. Holmes, R. Droopad, Z. Yu, J. Ramdani, L. Hilt, A. Talin, J. Edwards Jr, W. Ooms, J. Curless, C. Overgaard and M. O'Steen, Physical Sciences Research Labs/Motorola Labs, Motorola Inc.
 [12] J. Peña A. Martínez, F. Conde, J.M. González Calbet and M. Vallet-Regí, Solid State Ionics, 101-103 (1997) 183-190
 [13] Y. Gao, Y. Masuda, T. Yonezawa and K. Koumoto, Chem. Mater., 14 (2002) 5006-5014
 [14] T.B. Ng, J.B. Xu, G.D. Hu, W.Y. Cheung and I.H. Wilson, Electron Devices Meeting, Hong Kong (2002) 15-19
 [15] I. Doudevski and D.K. Schwartz, J. Am. Chem. Soc., 123 (2001) 6867-6872
 [16] A. Lorke, R.J. Luiken, J.M. García and P.M. Petroff, Jpn. J. Appl. Phys., 40 (2001) 1857-1859

Figures

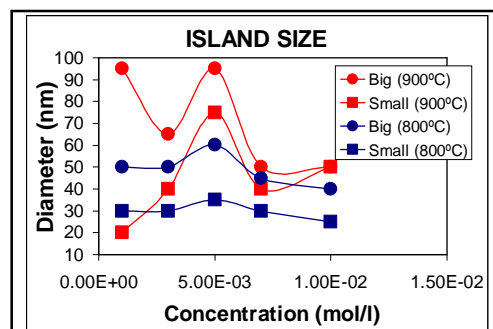
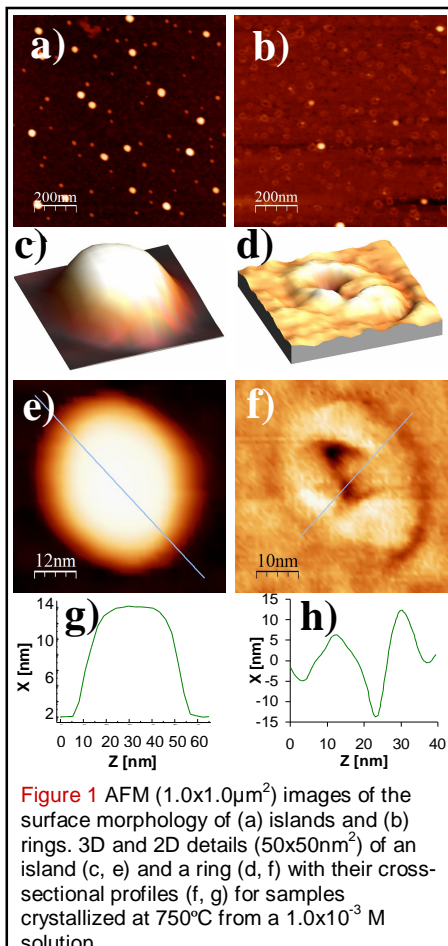


Figure 2 Graphic representation of island size (a) and (b) island density vs precursor solution concentration for the samples crystallized at 800°C in O_2 (RTA) and at 900°C in air (conventional oven).

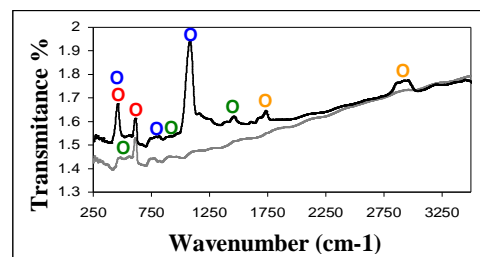


Figure 3 IR spectra of samples for precursor of $1.0 \times 10^{-2} \text{M}$, crystallized at 900 and 800°C with band attributed to **STO**, **SiO₂**, **SrCO₃** y **TiO₂** phases.

Developing nanotechnology based cancer therapeutics: RNA interference as a powerful tool in gene silencing for p53

Ioana Berindan Neagoe^{1,2}, Cornelia Braicu¹, O.Balacescu¹, Oana Tudoran¹, Loredana Balacescu¹,

Claudia Burz², T.Kaucsar², Roxana Redis², V.Cristea², Al.Irimie^{1,2}

1 – Institute of Oncology Ion Chiricuta Cluj Napoca Romania

2 – University of Medicine and Pharmacy Iuliu Hatieganu Cluj Napoca Romania

Discovered only in the last ten years, RNA interference is a powerful tool that can be used to silence any gene of interest in many biological systems. To date, this technology has been used largely for research applications, involving cells grown in the laboratory or model organisms, as well as new therapeutics for cancer. Multi-disciplinary teams are involved to develop this technology forward so that it can be used as soon as possible to inhibit the function of cancer genes for cancer therapy. Our goal is to develop improved delivery methods such that RNAi molecules that can be given with less toxicity and more efficient in cancer patients. Again, targeting the RNAi molecules selectively only to cancer cells will likely be required to achieve the desired therapeutic results. Similar approaches are being developed for delivering therapeutic DNA molecules to cancer cells *in vivo*, including to replace the function of mutated tumor suppressor genes like p53.

p53 gene, discovered almost 35 years ago, keeps the main role in cell cycle control, apoptosis pathways and transcription. *p53* gene is found mutated in more than 50% of all human cancers in different locations. Many structures from viral to non viral were designed to incorporate and deliver in appropriate conditions, forms of *p53* gene or its transcripts, systemically, to target tumor cells and to eliminate them through apoptosis or to restore the normal tumor suppressor gene role. Each delivery system presents advantages and low performance in relation to immune system recognition and acceptance. One of the major discoveries in the last years, silencing of RNA, represents a powerful tool for inhibiting post transcriptional control of gene expression. According to several studies, the RNA silencing technology for p53 transcripts together with other carriers or transporters at nano level for *p53* gene can be used for creating new therapeutic models. RNA interference for p53 uses different ds (double strand) molecules like short interfering RNA and despite the difficulty of introducing them into mammalian cells due to immune system response it can be exploited into therapy.

Our study was focused in different types of human cancers, looking for inhibition by RNA interference of mutant p53 gene expression and implicitly the restoration of the wild type p53 model as apoptotic feature of a dying cell.

Key words: nanotechnologies, apoptosis, cancer, p53, restoration, RNA interference, transcription

Influence of the pH on the Hydrothermal-Assisted Synthesis of Graphene

Concha Bosch-Navarro¹, Eugenio Coronado¹, Carlos Martí-Gastaldo¹, Ana Cros², Maribel Gómez-Gómez², Juan F. Sánchez-Royo³

¹Molecular Materials Research Team (UIMM), Instituto de Ciencia Molecular (ICMol), Universidad de Valencia

² Instituto de Ciencia de los Materiales (ICMUV), Universidad de Valencia

³ Instituto de Ciencia de los Materiales, Dpto. Física Aplicada y Electromagnetismo, Universidad de Valencia

email: concepcion.bosch@uv.es

Graphene (G) is an allotropic form of carbon which can be described as single sheets of aromatic sp² carbon atoms. From 2004, when Novoselov *et al.* reported its isolation through the so-called scotch-tape method,¹ it has attracted increasing interest, becoming one of the hottest scientific topics to date. Its importance is undoubtedly associated to the sophisticated electronic properties predicted for G sheets. Among them, ballistic transport, high conductivity, extraordinary optical or thermal properties, high surface area or its mechanical resistance, which turns it into one of the strongest materials on earth, justify the current importance devoted to this material, confirming it as a one of the most promising candidates for the future development of technologically advanced applications.²⁻⁵

Concerning the synthesis of G, several physical routes such as the Chemical Vapor Deposition (CVD) or the micromechanical exfoliation of graphite (more commonly known as the scotch-tape method) has emerged as the most exploited synthetic recipes.⁶ Though these routes lead to high-quality G sheets, the scalable production of G in good yields remains one of the main challenges for its potential employment into further technological applications. With this regard, the chemical synthesis of graphene has become as a promising alternative, since it would permit synthesizing large-scale quantities of G. Depending on the chemical nature of the G precursor, these chemical methods can be divided in two general categories: a) Those starting directly from graphite – a layered material built up from the stacking of G sheets through weak van der Waals interactions – and b) Those relying on the sequential exfoliation and reduction of graphite oxide (GO), which is generally prepared in a preliminary stage through acidic oxidation of graphite.⁷ This oxidation promotes an increment of the interlayer space separating the G sheets in the solid state, thus permitting the exfoliation of the layers under continuous cycles of sonication and mechanical stirring. Afterwards, the exfoliated material is subjected to a reduction reaction, necessary to recover the electronic properties of pristine unmodified G. So far, this reduction has been accomplished through several strategies, which typically relied on the use of hazardous reduction agents (i.e. hydrazine, dimethylhydrazine or L-ascorbic acid).^{8,9} Recently, it has been demonstrated that supercritical water may act as a reducing agent for GO in hydrothermal conditions, offering a new and “green” route for the production of graphene.¹⁰

Herein we provide further insights on this biocompatible method for the production of graphene from the exfoliation/reduction of GO (**Figure 1**). GO is obtained by the Hummers method,¹¹ and afterwards reduced *via* a hydrothermal (HT) treatment in water (G_{red}). The effect of the pH on this latter step, which was found to produce different nanocarbon forms with variable reduction degrees, was studied in the 3-11 interval. We will describe the chemical nature of the resulting species on basis of the collective employment of High Resolution Transmission Electron Microscopy (HRTEM), Raman and X-ray Photoelectron Spectroscopy (XPS), amongst other experimental techniques.

1. Novoselov, K. S.; Geim, A. K.; Morozov, S. V.; Jiang, D.; Zhang, Y.; Dubonos, S. V.; Grigorieva, I. V.; Firsov, A. A., *Science* **2004**, *306* (5696), 666-669.
2. Rao, C. N. R.; Biswas, K.; Subrahmanyam, K. S.; Govindaraj, A., *Journal of Materials Chemistry* **2009**, *19* (17), 2457-2469.
3. Charles, E.; Sykes, H., *Nature Chemistry* **2009**, *1*, 175-176.
4. Eda, G.; Chhowalla, M., *Advanced Materials* **9999** (9999), NA.
5. Liu, J.; Tao, L.; Yang, W.; Li, D.; Boyer, C.; Wuhler, R.; Braet, F.; Davis, T. P., *Langmuir*.
6. Park, S.; Ruoff, R. S., *Nat Nano* **2009**, *4* (4), 217-224.
7. Rao, C. N. R.; Sood, A. K.; Subrahmanyam, K. S.; Govindaraj, A., *Angewandte Chemie International Edition* **2009**, *48* (42), 7752-7777.
8. Stankovich, S.; Dikin, D. A.; Piner, R. D.; Kohlhaas, K. A.; Kleinhammes, A.; Jia, Y.; Wu, Y.; Nguyen, S. T.; Ruoff, R. S., *Carbon* **2007**, *45* (7), 1558-1565.
9. Zhang, J.; Yang, H.; Shen, G.; Cheng, P.; Zhang, J.; Guo, S., *Chemical Communications* **46** (7), 1112-1114.
10. Zhou, Y.; Bao, Q.; Tang, L. A. L.; Zhong, Y.; Loh, K. P., *Chemistry of Materials* **2009**, *21* (13), 2950-2956.
11. Hummers, W. S.; Offeman, R. E., *Journal of the American Chemical Society* **1958**, *80* (6), 1339-1339.

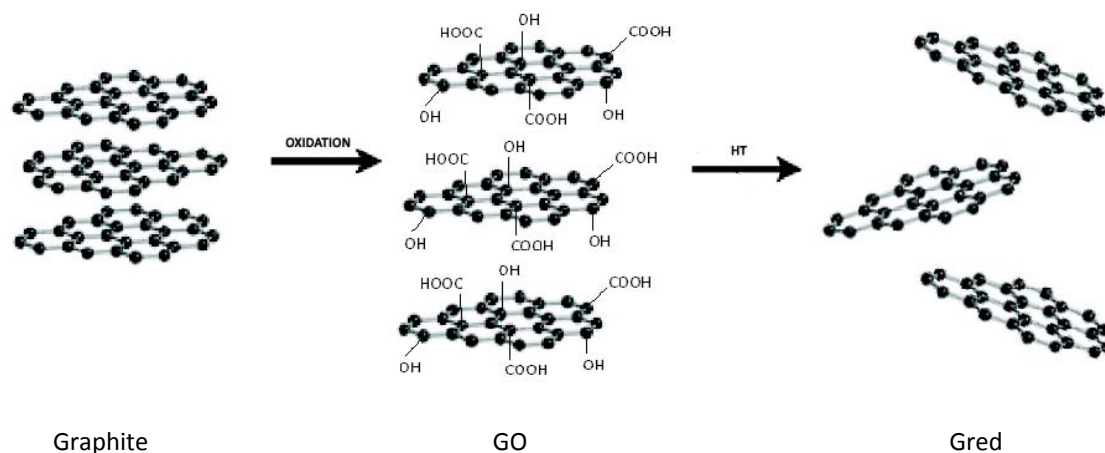


Figure 1. Scheme describing the chemical production of graphene (G_{red}) through the reduction of GO.

Production of nanoparticles from natural and synthetic hydroxylapatite by laser ablation

M. Boutinguiza, R. Comesaña, F. Lusquiños, A. Riveiro, J. Pou

Dpto. Física Aplicada, Universidad de Vigo, Lagoas-Marcosende, 9,
36310 Vigo, SPAIN
mohamed@uvigo.es

Nanoparticles represent an important object of investigation in the field of biomaterials due to the new properties and functionalities obtainable when operating at nanoscale [1-3]. Calcium phosphate compounds in particular, such as hydroxylapatite, $\text{Ca}_{10}(\text{PO}_4)_6(\text{OH})_2$ are getting special attention as biomaterials due their characteristics to induce bone-integration and to anchor rigidly prostheses or implants to the bone [4]. Hydroxylapatite (HA) has a special importance because of its similarities with the mineral constituents of bones and teeth, where this material is present as nanometric particles with a platelet shape [5]. On the other hand it seems that the use of β -tricalcium phosphate (β -TCP), $\text{Ca}_3(\text{PO}_4)_2$ in nanosize scale and low crystallinity improves the bioactivity [6]. HA from both synthetic and natural origins is widely used in the biomaterials field.

There are different and diverse techniques for producing calcium phosphate nanoparticles, among them aqueous solutions [7], the templating technique to achieve nano-porous hydroxylapatite structure [8], or the microwave irradiation to synthesize hydroxylapatite nanostructure [9], etc. In this work we report the results of calcium phosphate nanoparticles obtained from calcined fish bones and synthetic HA using laser ablation in de-ionized water. This technique offers some advantages, such as: direct formation of nanoparticles in solutions, the absence of contamination, all particles are collected, easiness of preparation, low costs of processing, etc.

In previous work we obtained calcium phosphate micro and nanoparticles from fish bones by laser ablation in ambient conditions [10] and laser-induced fracture [11]. In the present study we report the production of β -TCP and HA nanoparticles from a natural source such as calcined fish bones and commercial synthetic HA. Pellets of calcined fish bones and commercial HA (Sigma Aldrich) were prepared as precursor material to be ablated in de-ionized water by two different lasers operating at 1064 and 1075 nm wavelength respectively. The first system used was a pulsed Nd:YAG laser delivering a maximum average power of 500 W. The laser beam was coupled to an optical fiber of 400 μm diameter and focused onto the upper surface of the target by means of 80 mm of focal length lens, where the spot diameter at normal incidence for a pulsed laser was about 0.2 mm. Other parameters were varied as follows: laser pulse width 1–3 ms, frequency 5–10 Hz, and pulse energy 2–8 J. The second laser system used was a monomode Ytterbium doped fiber laser (YDFL). This laser works in continuous wave mode delivering a maximum average power of 200 W. Its high beam quality allowed setting the irradiance range between 2×10^5 and 10^6 W/cm^2 . The laser beam was coupled to an optical fiber of 50 μm diameter using the same focusing system and processing set up than in the case of the Nd:YAG laser. Precursor material was characterized by means of X-ray diffraction (XRD) using a Siemens D-500 equipment and by X-Ray Fluorescence (XRF) taken by a Siemens SRS 3000 unit. Transmission electron microscopy (TEM), selected area electron diffraction (SAED) and high-resolution transmission electron microscopy (HRTEM) images were taken on a JOEL-JEM 210 FEG transmission electron microscope equipped with a slow digital camera scan, using an accelerating voltage of 200 kV, to reveal their crystalline. The morphology as well as the composition is described by the Scanning Electron Microscopy (SEM) using a JOEL-JSM-6700F.

The results from X-ray diffraction patterns of the material obtained from calcined fish bones reveal that the powder is well crystallized calcium phosphate phases composed mainly by HA. Figure 1 exhibits the XRD patterns of the used fish bones and the commercial HA compared with those of stoichiometric HA (JCPDS 1993).

When the laser beam impinges on the target, its surface is exposed to thousands of high energy pulses, which cause a rapid increase of temperature, leading to material fracturing, melting and/or evaporation [12]. According to the size and morphology of the collected material, there are different kinds of particles. Some of them exhibit a rounded shape and nanometric size, as can be seen from figure 2 showing their lattice fringes. The measurement of the inter-planar spacing shows good agreement with the HA and TCP. The shape and size of these particles suggest they are obtained by melting and rapid solidification of the starting material, while the presence of TCP might be due to the crystalline transformation phase from precursor HA to β -TCP promoted by long pulse and high temperature. Other kind of particles consisted of rounded and amorphous ones with tendency to agglomeration. This kind of particles is obtained by the use of pulsed laser, which can promote the condition of thermal confinement

due to low thermal diffusivity of the starting particles together with the high pulse energy and millisecond pulses. The particles obtained from fish bones preserve the presence of some trace elements such as, Mg, K, etc. which are usual in biological apatites.

In this work nanoparticles of HA and β -TCP have been obtained by the ablation of fish bones and synthetic HA suspended in de-ionized water using pulsed as well as continuous wave laser. The use of the first one promotes the nanoparticles formation by the mechanism of evaporation and rapid condensation, while the latter one favours the melting particles formation mechanism. The presence of the β -TCP is due to the transformation of HA into β -TCP caused by the high temperature.

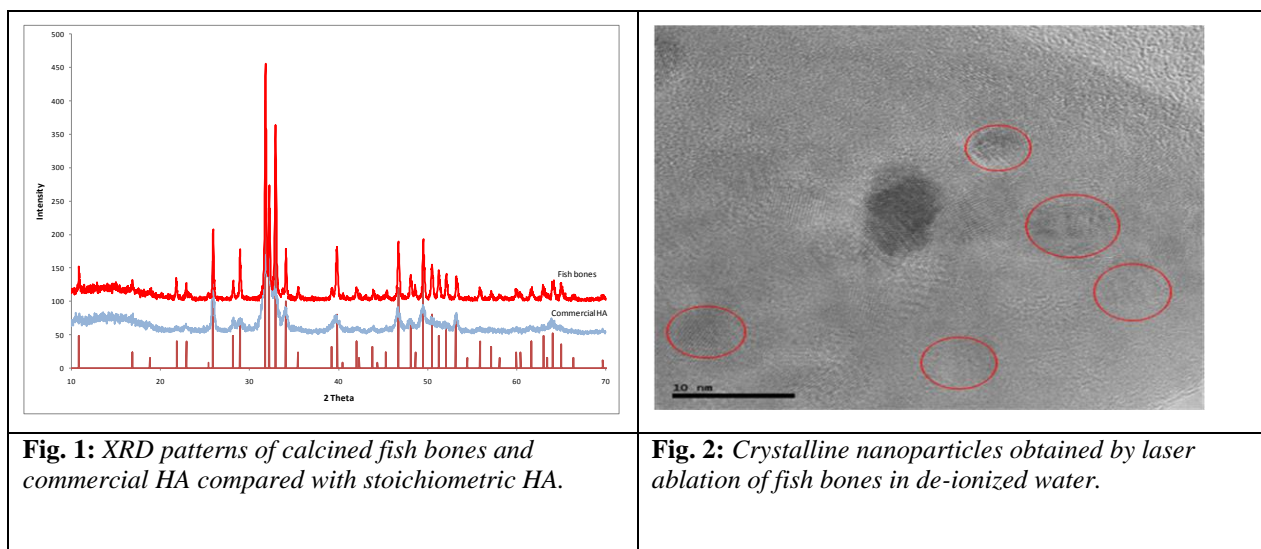
Acknowledgements

This work was partially supported by the European Union program POCTEP project (0330_IBEROMARE_1_P), the Spanish government (CICYT/FEDER MAT2006-10481) and by Xunta de Galicia (INCITE08PXIB303225PR, INCITE09E2R303103ES).

References

- [1] W. Wang, D. Shi, J. Lian, G. Liu, L. Wang and R. C. Ewing: Appl. Phys. Lett. **89** (2006),183106. Authors, Journal, **Issue** (Year) page.
- [2]. D. Aronov and G. Rosenman: Appl. Phys. Lett. **88** (2006)163906.
- [3]. H.H.K. Xu, M.D. Weir, L. Sun, S. Takagi, and L.C. Chow: J. Dent. Res. **86** (4) (2007) 378.
- [4] S.M Barinov, Y.V. Baschenko. Krajewski A (editor). Bioceramics and the human body. UK: Elsevier Science Publishers (199) 206.
- [5] T. Koshino, T. Murase, T. Takagi and T. Saito. Biomat.**22** (2001) 1579.
- [6] O. D. Schneider, S. Loher, T. J. Brunner, L. Uebersax, M. Simonet, R. N. Grass, H. P. Merkle, and W. J. Stark. J. Biomed. Mat. Res. B: Appl. Biomat. **84B** 2 (2007) 350.
- [7] L. Yubao, K. De Groot, J. De Wijn, C.P.A.T. Klein and S.V.D. Meer. J. Mater. Sci. Mater. Med. **5** (1994) 326.
- [8] J. Yao, W. Tjandra, Y.Z. Chen, K.C. Tam, J. Ma and B. Soh. J. Mater. Chem. **13** (2003) 3053.
- [9] J. Liu, K. Li, H. Wang, M. Zhu, H. Xu and H. Yan. Nanotechnology **16** (2005) 82.
- [10] M. Boutinguiza, F. Lusquiños, R. Comesaña, A. Riveiro, F. Quintero and J. Pou. App. Surf. Sci. **254** (4) (2007) 1264.
- [11] M. Boutinguiza, F. Lusquiños, A. Riveiro, R. Comesaña and J. Pou. App. Surf. Sci. **255** (10) (2009) 5382.
- [12] Y. Chen, V. Bulatov, L. Singer, J. Stricker and I. Schechter. Anal. Bioanal. Chem. **383** (2005) 1090.

Figures



Room Temperature Sputtered Ta₂O₅ for Solid State Biosensors

R. Branquinho^{*1,2}, J. V. Pinto¹, P. Barquinha¹, L. Pereira¹, P. Estrela³, P. Baptista⁴, R. Martins¹, E. Fortunato¹

¹ CENIMAT, I3N and CEMOP/UNINOVA, Faculdade de Ciência e Tecnologia da Universidade Nova de Lisboa (FCT-UNL), Campus de Caparica, 2829-516 Caparica, Portugal

² INL, International Iberian Nanotechnology Laboratory, Braga, Portugal

³ Department of Electronic and Electrical Engineering University of Bath, BA2 7AY, UK

⁴ CIGMH/Departamento de Ciências da Vida, FCT-UNL, 2829-516 Caparica, Portugal

*ritasba@fct.unl.pt

Since the enzyme modified electrode was invented by Clark in 1962 this area of research has been ever growing. Biosensors have application in many areas of interest from agriculture to industrial control, pharmaceutical to health care. Consequently much effort is put into new and improved materials for device optimization and sensitivity enhancement.

Ion sensitive field effect transistors (ISFETs) based biosensors have a fast response and are suitable for miniaturization, since the signal-to-noise ratio is independent of the device area. It is also possible to integrate several ISFET sensors to allow the simultaneous measurement of various parameters by coating each gate dielectric with a specific biological agent.

High-k dielectrics that are used as the gate oxide, such as Ta₂O₅, show sensitivity to pH so the optimization of this sensitive layer is crucial.

An advantageous technique for oxide thin films deposition is radiofrequency (rf) magnetron sputtering because it permits good quality films to be obtained at room temperature and the use of low cost disposable substrates such as plastic and even paper.

We present a study of Ta₂O₅ thin films deposition conditions and their influence on pH sensitivity. The films were produced by varying some deposition parameters, such as argon and oxygen partial pressure ratio and deposition pressure. The influence of post-production treatments such as annealing temperature and plasma surface treatments with argon and oxygen, performed under several conditions, were also studied in order to assess their contribution to pH sensitivity. The films were deposited on p-doped Si/SiO₂ substrates in an electrolyte-insulator-semiconductor (EIS) capacitive structure that was used to evaluate the sensors' response to pH (Fig.1). EIS devices mimic the gate structure of the ISFET and have the advantage of being easier to fabricate. Capacitance measurements were performed in a standard three electrode configuration (Fig.2).

An enzyme modified sensor was successfully constructed by adsorptively immobilizing penicillinase onto the surface of the Ta₂O₅ film that yielded the optimal pH sensitivity. The underlying pH sensor detects the variation in H⁺ concentration resulting from the catalyzed hydrolysis of penicillin G by penicillinase, which is dependent on the penicillin concentration in the solution.

The application of the studied sensitive Ta₂O₅ films to ISFET biosensor structures was also studied and will be discussed.

References

- [1] Turek, M., M. Keusgen, et al., Journal of Contemporary Physics-Armenian Academy of Sciences, **43**(2) (2008) 82-85.
- [2] Pan, T. M. and J. C. Lin., Sensors and Actuators B-Chemical, **138**(2) (2009) 474-479.
- [3] Yan, F., P. Estrela, et al., Sensors, **5**(4-5) (2005) 293-301.

Figures

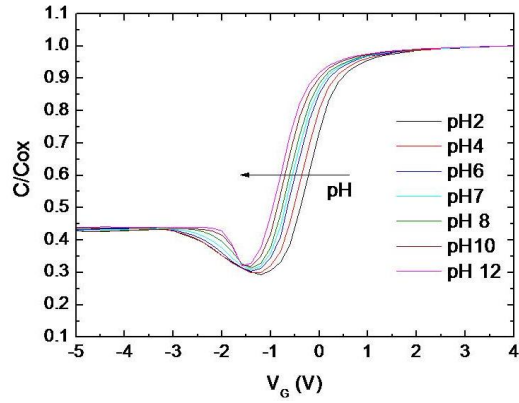


Fig. 1 – EIS device's capacitance vs voltage characteristics variation due to pH.

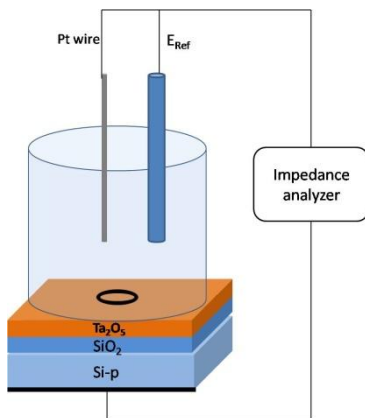


Fig. 2 – Experimental set-up used for EIS structure capacitance measurements

***In vitro* transdermal delivery of caffeine-loaded alginate particles**

Maguie Cangueiro¹, Catarina P. Reis¹, Catarina Rosado¹, Patrícia Carvalho¹ and Luís Monteiro¹ Rodrigues

Laboratory of Nanoscience and Biomedical Nanotechnology, Universidade Lusófona de Humanidades e Tecnologias, 376 Campo Grande, Lisbon, Portugal
maguie.cangueiro@hotmail.com

Introduction

Encapsulation technique has emerged a few years ago as a promising technology for new drug delivery systems. The production of alginate microspheres via internal gelation offers a method of encapsulation a variety of biologically active agents including drugs [1], proteins [2] and enzymes [3], among others compounds.

In this study, alginate microspheres were prepared by emulsification/internal gelation technique. The purpose of this study was the improvement of absorption of caffeine through an *in vitro* permeation model. This carrier will be applied as carriers for anticellulitic treatment.

In our study, the polymer chosen was alginate. Alginate is a natural polysaccharide found in brown algae and used in the food and pharmaceutical Industries. Alginates have been successfully employed as a matrix for the encapsulation of drugs, macromolecules and biological cells [4].

Material and methods

Preparation of alginate particles: A 2% (w/v) sodium alginate solution was prepared with caffeine at 1% (w/v). A suspension of CaCO₃ at 5% (w/v) was added to the alginate solution and dispersed at 400 rpm into 50 mL of paraffin oil containing 1.5 mL of Span 80. 15 min later, 20 mL of paraffin oil containing 300 µL of acetic acid were added to the w/o emulsion in order to solubilize calcium salt and stirring continued for 30 minutes. Microparticles were recovered using acetate buffer at pH 4.5 and centrifugation cycles [4]. A gel and cream containing caffeine at 1% were also prepared.

Viscosity of the caffeine gel and the gel without caffeine were measured by a viscometer.

Morphological and particles size analysis: Morphology was determined by optical microscopy. Size distribution of microparticles was determined by laser diffractometry with a size range from 0.02 to 2000 µm. Particle size was expressed as volume mean diameter (µm). Polydispersity was determined by the SPAN factor [4].

Encapsulation efficiency: The encapsulation efficiency was calculated by indirect method measuring the absorbance at 273 nm of the non-encapsulated caffeine. The encapsulation efficiency of the caffeine was then calculated from the difference between the total free caffeine and the initial amount of the drug. The other method that we calculated the encapsulation efficiency was by dissolving the microparticles with a solution of sodium citrate in pH 7.4 phosphate buffer. Then, the solution was centrifuged and caffeine in supernatant was quantified at 273 nm.

In vitro release study: The *in vitro* skin permeation studies were performed on Franz diffusion cell using silicone as permeation membrane. The profile of *in vitro* skin permeation was compared between caffeine gel, caffeine cream, and microparticles of caffeine prepared by emulsification/internal gelation technique.

Results: An encapsulation efficiency of 51% was obtained. The morphology of microparticles was determined. Particles were round as seen in Figure 1 with a mean diameter of 45 µm (Figure 2). SPAN factor was 2,014. The result of the viscosity of the caffeine gel was 212 cP and the gel without caffeine 126 cP.

The results of the *in vitro* skin permeation performed by Franz diffusion cell revealed that microencapsulation of caffeine by emulsification/internal gelation method can be an alternative for the transdermal delivery of this drug.

Discussion: Optimization of drug delivery through human skin is important in current therapies. Polymeric microparticles can be considered as promising drug delivery systems since they demonstrated biocompatibility with tissue and cells, singular properties and subcellular size. Herein, the emulsification/internal gelation technique offers several advantages over other conventional methods, and shows a great promise in the development of encapsulation of drugs. This study confirmed that this technique successfully produced smaller particles with medical and pharmaceutical applications and may be applied to other drugs.

References

- [1] Ribeiro, A.J., Neufeld, R.J., Arnaud, P., Chaumeil, J.C. Microencapsulation of lipophilic drugs in chitosan-coated alginate microspheres. *Int. J. Pharm.*, 1999, 187, 115-123.
- [2] Coppi, G., Iannuccelli, V., Leo, E., Bernabei, M.T., Camerini, R., 2002. Protein immobilization in crosslinked alginate microparticles. *J. Microencapsul.*, 2002, 19, 37-44.
- [3] Boadi, D.K., Neufeld, R.J. Encapsulation of tannase for the hydrolysis of tea tannins. *Enz. Microbial Technol.* 2001, 28, 590-595
- [4] Silva, C.M., Ribeiro, A.J., Figueiredo, I.V., Gonçalves, A.R., Veiga, F., Alginate microspheres prepared by internal gelation: Development and effect on insulin stability, *International Journal of Pharmaceutics*, 2006

Figures

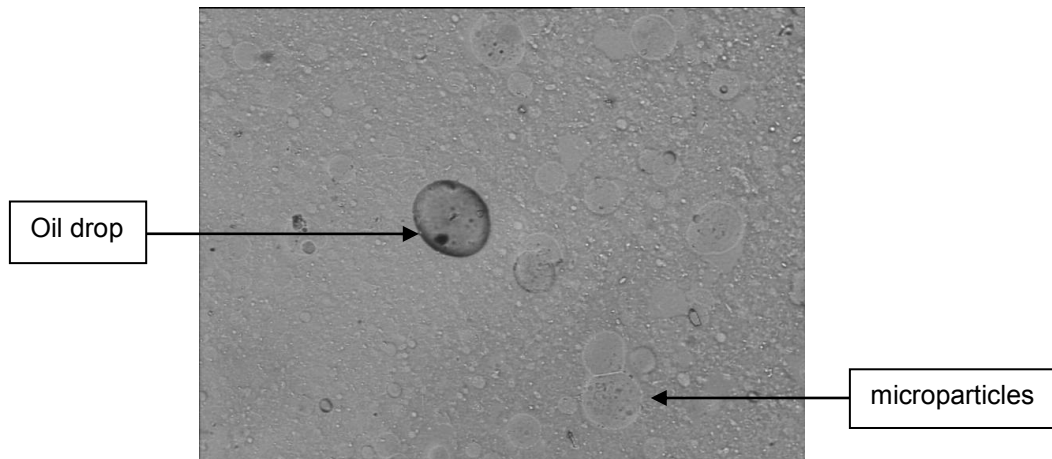


Figure 1 - Photograph of alginate particles.

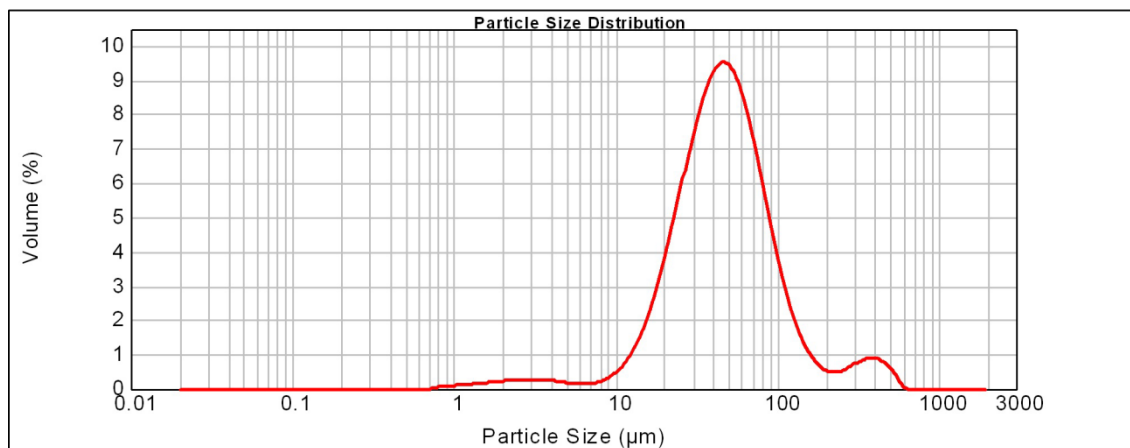


Figure 2 – Particle size distribution using Fraunhofer model.

Effect of the carbon nanotube surface characteristics on the percolation threshold and conductivity of carbon nanotube/poly(vinylidene fluoride) composites

S.A.C. Carabineiro,¹ J. Pereira,² C. Caparros,² V. Sencadas,² M.F.R. Pereira,¹
S. Lanceros-Mendez²

¹ Universidade do Porto, Faculdade de Engenharia, LSRE/LCM – Laboratório Associado,
Rua Dr. Roberto Frias, s/n, 4200-465 Porto, Portugal

² Centro/Departamento de Física da Universidade do Minho, Campus de Gualtar,
4710-057 Braga, Portugal
sonia.carabineiro@fe.up.pt

In order to increase the application range of polymers, highly conductive nanoscale fillers can be incorporated into the polymeric matrix. As carbon nanotubes (CNT) present high electrical conductivity (10^3 - 10^4 S/cm), they have been widely used [1]. Therefore, CNT/polymer composites are expected to have several important applications, namely in the field of sensors and actuators [2]. However, in order to properly tailor the composite material properties for specific applications, the relevant conduction mechanisms must be better understood.

The experimental percolation thresholds for CNT composites results on a wide range of values for the same type of CNT/polymer composites [3], being a deviation from the bounds predicted by the excluded volume theory and a dispersion for the values of the critical exponent (t) [4-5]. It was demonstrated that the conductivity of CNT/polymer composites can be described by a single junction expression [6] and that the electrical properties also strongly depend on the characteristics of the polymer matrix [7].

In the present work, commercial multi-walled carbon nanotubes (Nanocyl - 3100) have been used as received (sample CNTs) and functionalised through oxidation under reflux with HNO₃ (7 M) for 3 h at 130°C, followed by washing with distilled water until neutral pH, and drying overnight at 120 °C (sample CNTox). The CNTox material was heat treated under inert atmosphere (N₂) at 400 °C for 1 h (sample CNTox400) and at 900°C for 1h (sample CNTox900). The obtained samples were characterised by adsorption of N₂ at -196°C and by temperature programmed desorption (TPD). The results obtained are shown in Table 1. The different surface oxygenated groups created upon oxidising treatments decompose through heating, releasing CO and/or CO₂ (Figure 1). As this release occurs at specific temperatures, identification of the surface groups is thus possible [8]. In nanotubes, the oxygenated groups (Figure 2) are formed at the edges/ends and defects of graphitic sheets [10]. The total amounts of CO and CO₂ evolved from the samples were obtained by integration of the TPD spectra and are also presented in Table 1. The peaks were deconvoluted using the nonlinear least-squares procedure, assuming a multi Gaussian peak shape [8-9]. It is clear that the treatment with HNO₃ produces a large amount of acidic oxygen groups, like carboxylic acids, anhydrides and lactones, which decompose to release CO₂. Part of these groups (carboxylic acids) are removed through heating at 400°C. A treatment at 900°C removes all the groups, so that the obtained sample is similar to the original, but with an increase of the surface area (Table 1).

CNT/poly(vinylidene fluoride) composites were prepared using the above CNT samples, with different filler fractions up to 0.5 %wt. It was found that oxidation reduces composite conductivity for a given concentration and shifts the percolation threshold to higher concentrations. The theoretical analyses of these facts help to get interesting insights on the conduction mechanism of these composites.

Acknowledgements: Authors thank Fundação para a Ciência e a Tecnologia (FCT), Portugal, for financial support through the projects PTDC/CTM/69316/2006 and NANO/NMed-SD/0156/2007), and CIENCIA 2007 program for SAC. VS and JP also thank FCT for the SFRH/BPD/63148/2009 and SFRH/BD/66930/2009 grants.

References

- [1] M.H. Al-Saleha, U. Sundarara, Carbon 47 (2009) 2.
- [2] E.T. Thostenson, C. Li, T.-W.Chou, Compos. Sci. Technol. 65 (2005) 491.
- [3] W. Bauhofer, J.Z. Kovacs, Compos. Sci. Technol. 69 (2009) 1486.

- [4] D. Stauffer, A. Aharony, Introduction to Percolation Theory, Taylor and Francis, London (1992).
- [5] A. Celzard, E. McRae, C. Deleuze, M. Dufort, G. Furdin, J.F. Mareche, Phys. Rev. B 53 (1996) 6209.
- [6] P. Cardoso, J. Silva, A. J. Paleo, F.W.J. van Hattum, R. Simões, S. Lanceros-Mendez, Phys. Status Solidi A 207 (2009) 407.
- [7] V. Sencadas, J. Gomes, P. Costa, F.W.J. van Hattum, J.G. Rocha, S. Lanceros-Mendez, Carbon, 7 (2009) 2590.
- [8] J.L. Figueiredo, M.F.R. Pereira, M.M.A. Freitas, J.J.M. Órfão, Carbon 37 (1999) 1379.
- [9] J.L. Figueiredo, M.F.R. Pereira, M.M.A. Freitas, J.J.M. Órfão, Ind. Eng. Chem. Res. 46 (2007) 4110.
- [10] S. Barnerjee, T. Hemraj-Benny, S.S. Wong, Adv. Mater. 17 (2005) 17.

Table 1 - BET surface areas (m^2/g) obtained by adsorption of N_2 at $-196^\circ C$ and amounts of CO_2 and CO ($\mu mol/g$) obtained by integration of areas under TPD spectra.

Sample	CNTs	CNTox	CNTox400	CNTox900
BET surface area (m^2/g)	254	400	432	449
CO_2 ($\mu mol/g$)	70	778	230	24
CO ($\mu mol/g$)	193	1638	1512	204
CO / CO_2	2.76	2.11	6.57	8.50

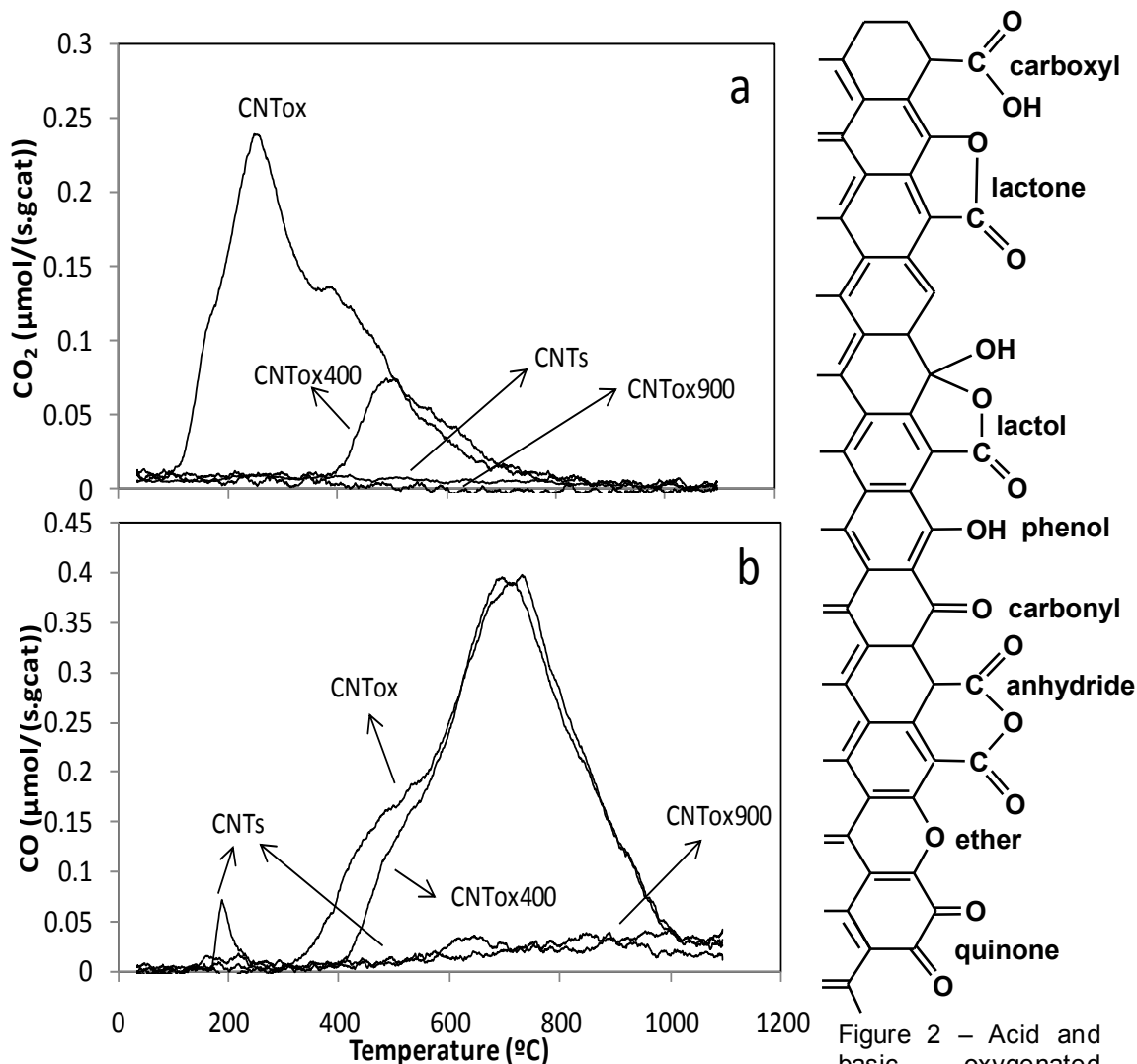


Figure 1 - TPD spectra of the CNT samples before and after the oxidizing treatments: CO_2 (a) and CO (b) evolution.

Figure 2 - Acid and basic oxygenated groups on CNT surface.

Gold nanoparticles supported on magnesium oxide for CO oxidation

S.A.C. Carabineiro,¹ N. Bogdanchikova,² A. Pestryakov,³ P.B. Tavares,⁴ L.S.G. Fernandes,⁴ J.L. Figueiredo¹

¹ Universidade do Porto, Faculdade de Engenharia, LSRE/LCM – Laboratório Associado, Rua Dr. Roberto Frias, s/n, 4200-465 Porto, Portugal

² Universidad Nacional Autónoma de México, Centro de Nanociencias y Nanotecnología, Carretera Tijuana-Ensenada, 22800, Ensenada, Baja California, Mexico

³ Tomsk Polytechnic University, 30, Lenin Avenue, Tomsk, 634050, Russia

⁴ Universidade de Trás-os-Montes e Alto Douro, CQVR Centro de Química –Vila Real, Departamento de Química, 5001-911 Vila Real, Portugal
sonia.carabineiro@fe.up.pt

It is well known from the literature that for gold to be active as a catalyst, a careful preparation is needed in order to obtain nanoparticles well dispersed on the support [1-4]. Many supports have been used so far, including MgO [2-4]. However, when compared with other supports, MgO is considered “inactive” [5-8] since it is basically an irreducible oxide, such as Al₂O₃. These materials have a low ability to adsorb or store oxygen at low temperatures [5].

However, several authors like Margitfalvi et al. [9] and Gates and co-workers [10-11] managed to prepare Au/MgO catalysts that had high activity for low temperature CO oxidation. Also Grisel et al. found that gold on magnesium oxide catalysts supported on alumina were also extremely active for this reaction [12].

As Co-Precipitation (CP) [1-5] and Deposition-Precipitation (DP) [1-4, 12] are the most common ways to prepare oxide supported gold catalysts, in the present work, we wanted to use less usual Au loading methods (1% wt.), such as double impregnation (DIM) [13], liquid phase reductive deposition (LPRD) [14] and sonication (US) [15], in order to prepare Au nanoparticles. To the best of our knowledge, the only reports on the use of DIM is the work of Bowker et al. dealing with TiO₂ samples [13] and our previous works with CeO₂ [16-17] and ZnO [15] catalysts. This method represents an environmentally and economically more favorable route to the production of high activity gold catalyst, when compared with the traditional DP method [13]. As far as we know, LPRD has only been used by Sunagawa et al. to prepare Pt and Au catalysts on Fe₂O₃, FeOOH, ZrO₂ and TiO₂ supports [14], and also by us for CeO₂ [18] and TiO₂ [19] catalysts. US method was only used by our group to prepare Au/ZnO materials [15]. These methods include a washing procedure, in order to eliminate residual chloride that causes sintering of Au nanoparticles, thus turning them inactive [1-4].

Figure 1 shows the XRD micrographs obtained for the MgO support alone (commercial sample obtained from Merck, with a BET surface area of 32 m²/g), and loaded with Au by DIM. The identified phase for the unloaded material is the respective oxide (cubic, Fm-3m, 01-078-0430); however, when gold is loaded, a new Mg(OH)₂ phase (hexagonal, P-3m1, 01-076-0667) was formed (Figure 1). 99% of this hydroxide phase was detected along with 1% MgO. Gold was not detected, most likely due to the low loading and small particle size. The hydroxide is most likely formed by reaction with water, in which the gold precursor is dissolved (MgO + H₂O → Mg(OH)₂). Similar results were obtained for the other loading methods. Figure 2 shows a HRTEM image of the MgO support which is quite different from what is observed in Figure 3 (MgO with Au loaded by DIM), as the support structure changes from large crystals (Figure 2) into a fiber appearance (Figure 3). Gold particles are also observed with sizes ranging from 2-12 nm. Other methods showed larger gold nanoparticle sizes between 3 to 15 nm. Also the average size of gold particles is 5.4 nm for DIM, while it is above 6.7 nm for LPRD and US.

All samples prepared were tested for the oxidation of CO (Figure 4), which is a simple established model reaction to evaluate gold catalysts that has many potential applications, namely in CO removal from H₂ streams for fuel cells and gas sensing [1-4, 15-18]. Loading MgO with Au leads to the total conversion of CO at much lower temperatures than with MgO alone, as expected. The best results were obtained with DIM. This can be explained in terms of the nanoparticle size, well known to be related with catalytic activity of gold catalysts [1-4].

Acknowledgements: Authors thank Fundação para a Ciência e a Tecnologia (FCT), Portugal, for financial support (CIENCIA 2007 program for SAC), and project PTDC/EQU-ERQ/101456/2008, financed by FCT and FEDER in the context of Programme COMPETE.

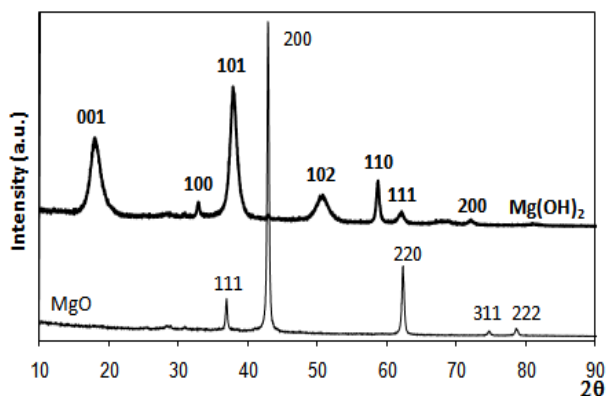


Figure 1 - X-ray diffraction spectra of MgO (thin line) and loaded with Au (thicker line), with phases and crystal planes (Miller indexes) identified. Gold was not detected by XRD.

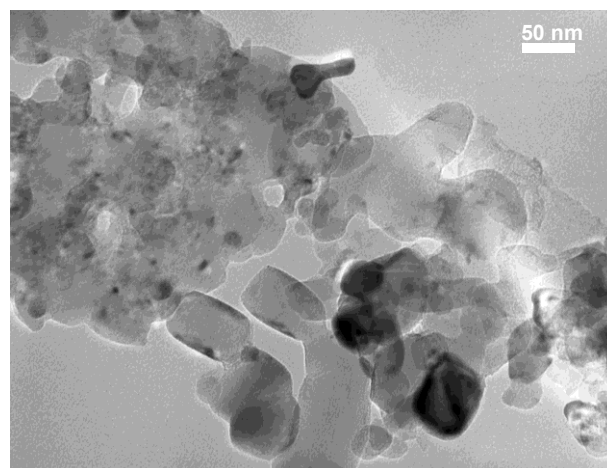


Figure 2 – HRTEM image of the MgO support.

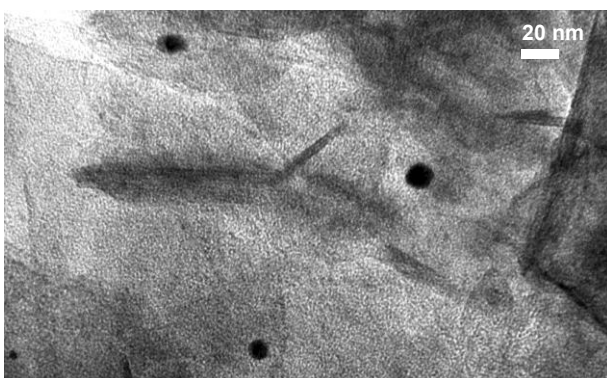


Figure 3 – HRTEM image of the MgO with Au loaded by DIM.

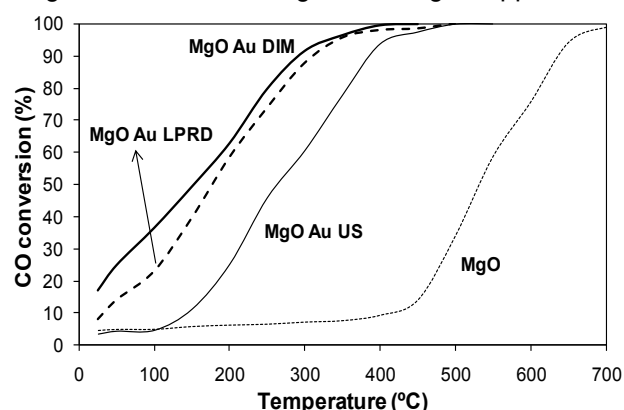


Figure 4 – CO conversion (%) versus temperature for the MgO support alone and with Au loaded by different methods.

References

- [1] G.C. Bond, D.T. Thompson, *Gold Bull.* 33 (2000) 41.
- [2] G.C. Bond, C. Louis, D.T. Thompson, *Catalysis by Gold. Catalytic Science Series*, ed. G.J. Hutchings. Vol. 6. 2006, London, United Kingdom: Imperial College Press.
- [3] S.A.C. Carabineiro, D.T. Thompson, *Catalytic Applications for Gold Nanotechnology*, in *Nanocatalysis*, E.U. Heiz and U. Landman, Editors. 2007, Springer-Verlag: Berlin, Heidelberg, New York. p. 377-489.
- [4] S.A.C. Carabineiro, D.T. Thompson, *Gold Catalysis*, in *Gold: Science and applications*, C. Corti and R. Holliday, Editors. 2010, CRC Press, Taylor and Francis Group: Boca Raton, London, New York. p. 89-122.
- [5] M.M. Schubert, S. Hackenberg, A.C. Veen, M. Muhler, V. Plzak, R.J. Behm, *J. Catal.* 197 (2001) 113.
- [6] M. Gasior, B. Grzybowska, K. Samson, A. Ruszel, J. Haber, *Catal. Today* 91-2 (2004) 131.
- [7] S. Ivanova, V. Pitchon, C. Petit, *J. Mol. Catal. A: Chem.* 256 (2006) 278.
- [8] G. Glaspell, H.M.A. Hassan, A. Elzatahry, V. Abdalsayed, M.S. El-Shall, *Top. Catal.* 47 (2008) 22.
- [9] J. Margitfalvi, A.Fasi, M. Hegedus, F. Lonyi, S. Gobolos, N. Bogdanchikova, *Catal. Today* 72 (2002) 157.
- [10] Y. Hao, M. Mihaylov, E. Ivanova, K. Hadjiivanov, H. Knozinger, B.C. Gates, *J. Catal.* 261 (2009) 137.
- [11] Y.L. Hao, B.C. Gates, *J. Catal.* 263 (2009) 83.
- [12] R.J.H. Grisel, B.E. Nieuwenhuys, *J. Catal.* 199 (2001) 48.
- [13] M. Bowker, A. Nuhu, J. Soares, *Catal. Today* 122 (2007) 245.
- [14] Y. Sunagawa, K. Yamamoto, H. Takahashi, A. Muramatsu, *Catal. Today* 132 (2008) 81.
- [15] S.A.C. Carabineiro, B.F. Machado, R.R. Bacsá, P. Serp, G. Dražić, J.L. Faria, J.L. Figueiredo, *J. Catal.* (2010), in press, DOI: 10.1016/j.jcat.2010.05.011.
- [16] S.A.C. Carabineiro, A.M.T. Silva, G. Dražić, P.B. Tavares, J.L. Figueiredo, *Gold nanoparticles on ceria supports for the oxidation of carbon monoxide. Catal. Today* (2010), in press, DOI: 10.1016/j.cattod.2010.01.036.
- [17] S.A.C. Carabineiro, S.S.T. Bastos, J.J.M. Órfão, M.F.R. Pereira, J.J. Delgado, J.L. Figueiredo, *Appl. Catal. A: Gen.* 381 (2010) 150.
- [18] S.A.C. Carabineiro, A.M.T. Silva, G. Dražić, P.B. Tavares, J.L. Figueiredo, *Catal. Today* (2010) in press, DOI: 10.1016/j.cattod.2009.12.017.
- [19] V.P. Santos, S.A.C. Carabineiro, P.B. Tavares, M.F.R. Pereira, J.J.M. Órfão, J.L. Figueiredo, *Appl. Catal. B: Env.*, in press, DOI: 10.1016/j.apcatb.2010.06.020.

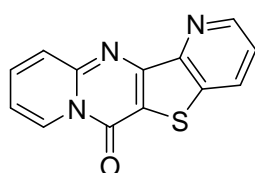
New potential antitumoral fluorescent tetracyclic thieno[3,2-*b*]pyridine derivatives: Interaction with DNA and encapsulation in nanoliposomes

Elisabete M. S. Castanheira,^a M. Solange D. Carvalho,^{a,b} A. Rita O. Rodrigues,^a R. C. Calhelha^b and Maria-João R. P. Queiroz^b

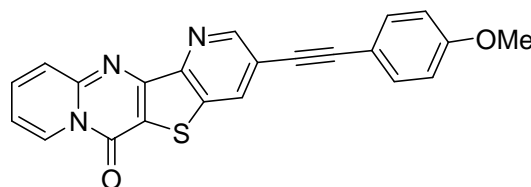
^aCentre of Physics (CFUM) and ^bCentre of Chemistry (CQ-UM), University of Minho, Campus de Gualtar, 4710-057 Braga, Portugal
ecoutinho@fisica.uminho.pt

Nanosized liposomes are among technological delivery methods for chemotherapeutic drugs in the treatment of cancer. This technique can potentially overcome many common pharmacologic problems, such as those involving solubility, pharmacokinetics, in vivo stability and toxicity [1,2]. Liposomes are closed spherical vesicles consisting of a lipid bilayer that encapsulates an aqueous phase in which hydrophilic drugs can be stored, while water insoluble compounds can be incorporated in the hydrophobic region of the lipid bilayer [3].

In this work, two new potential antitumoral fluorescent tetracyclic thieno[3,2-*b*]pyridine derivatives **1** and **2** (structures shown below), previously synthesized by some of us [4], were encapsulated in nanosized liposomes of DPPC (dipalmitoyl phosphatidylcholine), egg lecithin (phosphatidylcholine from egg yolk) and DODAB (dioctadecyldimethylammonium bromide). The phospholipids DPPC and egg lecithin (Egg-PC) are neutral components of biological membranes, while cationic liposomes based on the synthetic lipid DODAB have been used as vehicles for DNA transfection and drug delivery [5].



Compound 1



Compound 2

The investigation based on DNA interactions has a key importance in order to understand the mechanisms of action of antitumor and antiviral drugs and to design new DNA-targeted drugs [6]. Both compounds **1** and **2** were tested for their interaction with salmon sperm DNA using spectroscopic methods. These studies allowed to determine the binding constants and binding site sizes (in base pairs), through the McGhee and von Hippel modification of Scatchard plot [7] (Equation 1 and Table 1),

$$\frac{r}{c_f} = K_i (1 - nr) \left[\frac{(1 - nr)}{(1 - (n - 1)r)} \right]^{n-1} \quad (1)$$

where K_i is the intrinsic binding constant, n is the binding site size, r is the ratio $c_b/[DNA]$, c_b and c_f are the concentrations of bound and free compound, respectively. Fluorescence quenching experiments using external quenchers are also very useful to establish the DNA-binding modes, since intercalated chromophores are less accessible to anionic quenchers due to electrostatic repulsion with negatively charged DNA [8]. Quenching measurements using iodide ion showed that both compounds exhibit some intercalation in DNA, compound **2** being the more intercalative one, with a lower fraction of molecules accessible to quencher (Table 1).

Table 1. Binding constants to DNA (K_i), binding site sizes (n) and fraction of compound molecules accessible to external quenchers (f_a)

	K_i (M^{-1})	n (base pairs)	f_a
Compound 1	$(8.7 \pm 0.9) \times 10^3$	11 ± 3	0.89
Compound 2	$(5.9 \pm 0.6) \times 10^3$	7 ± 2	0.65

Considering the antitumoral potential of these compounds, the encapsulation in nanoliposomes is important for future drug delivery assays. Monodisperse and nanosized liposomes were prepared by injection of an ethanolic solution of the lipid in an aqueous media under vigorous stirring, above the lipid melting transition temperature ($T_m \sim 41$ °C for DPPC and 45 °C for DODAB). The hydrodynamic diameters of 87 ± 11 nm for DPPC, 51 ± 2 nm for Egg-PC and 268 ± 37 nm for DODAB were obtained by dynamic light scattering.

Fluorescence experiments of both compounds encapsulated in nanosized liposomes were carried out (Figure 1), in both gel (below T_m) and liquid-crystalline (above T_m) phases. Fluorescence anisotropy measurements allowed to conclude that compound 1 prefers a hydrated environment in the nanoliposomes, while compound 2 can be transported in the hydrophobic region of the lipid bilayer, especially in Egg-PC nanoliposomes.

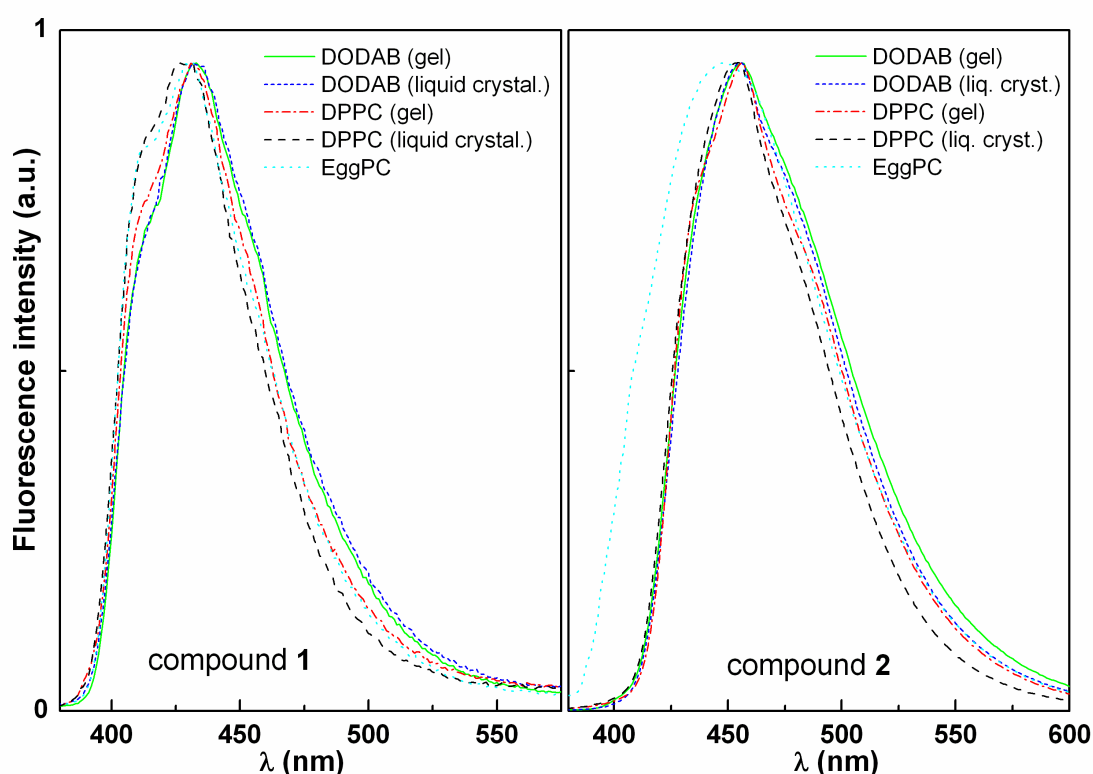


Figure 1. Normalized fluorescence emission spectra of compounds 1 and 2 incorporated in nanoliposomes of DPPC, Egg-PC and DODAB.

Acknowledgements

This work was funded by FCT-Portugal and FEDER through CFUM, CQ-UM, Project PTDC/QUI/81238/2006 cofinanced by FCT and program FEDER/COMPETE (FCOMP-01-0124-FEDER-007467) and PhD grants of M.S.D. Carvalho (SFRH/BD/47052/2008) and R.C. Calhela (SFRH/BD/29274/2006).

References

- [1] T. L. Andresen, S. S. Jensen, K. Jorgensen, *Prog. Lipid Res.* **44** (2005) 68-97.
- [2] N.A. Ochekepe, P.O. Olorunfemi, N.C. Ngwuluka, *Tropical J. Pharm. Res.* **8** (2009) 265-274; 275-287.
- [3] Y. Malam, M. Loizidou, A. M. Seifalian, *Trends Pharmacol. Sci.* **30** (2009) 592-599.
- [4] R. C. Calhela, M.-J. R. P. Queiroz, *Tetrahedron Lett.* **51** (2010) 281-283.
- [5] M. C. Pedroso de Lima, S. Simões, P. Pires, H. Faneca, N. Düzgünes, *Adv. Drug Deliv. Rev.* **47** (2001) 277-294.
- [6] S. Mahadevan, M. Palaniandavar, *Inorg. Chim. Acta* **254** (1997) 291-302.
- [7] J. D. McGhee, P. H. von Hippel, *J. Mol. Biol.* **86** (1974) 469-489.
- [8] C. V. Kumar, E. H. Asuncion, J. K. Barton, N. J. Turro, *J. Am. Chem. Soc.* **115** (1993) 8547-8553.

Nano -engineering of bio-arrays at 157 nm

A. C. Cefalas^a, E. Sarantopoulou^a, Z. Kollia^a, P. Petrou^b, S. Kakabakos^b

^a National Hellenic Research Foundation. Theoretical and Physical Chemistry Institute. 48 Vassileos Constantinou Avenue, Athens 11635 Greece

^b Institute of Radioisotopes and Radiodiagnostic Products,
NCSR "Demokritos", Aghia Paraskevi, Athens, 15310, Greece

ccefalas@eie.gr

Laser surface functionalization and micro/nano patterning of polymeric substrates at 157 nm, is a novel and simple methodology for bio-array fabrication, which allows surface etching with atomic resolution, strengthens localized protein binding on surfaces and increases writing density of arrays [1].

Surface morphology and functionalization in VUV depend on material and irradiation parameters. In this work selective protein binding on polystyrene substrates coated with a 2nm protective BSA inert protein was obtained following BSA removal with laser light at 157nm.

Different proteins were bind separately on the polystyrene surface following first laser treatment and then protein binding by dipping in solutions in repetitive steps. This finding simplifies the DNA chip fabrication with laser ablation at 157nm as it eliminates the need of developing new polymeric materials for the intermediate steps.

References

1. A.M Douvas, P.S Petrou, S.E. Kakabakos K. Misiakos, P. Argitis, E Sarantopoulou,.., Z. Kollia, A.C Cefalas,. Anal. Bioanal. Chem. 381, 1027, 2005.

Palladium nanoparticles on InP for hydrogen detection

Ondřej Černohorský, Karel Žďánský, Jiří Zavadil, Pavel Kacerovský, Kateřina Piksová

Czech Technical University in Prague - Faculty of Nuclear Sciences and Physical Engineering -
Department of Physical Electronics, V Holešovičkách 2, Prague, Czech Republic
cernohorsky@ufe.cz

Metal layer on semiconductor form energetic barrier called Schottky barrier. On this interface, we are able to detect hydrogen molecules in air. The presence of hydrogen is detected by the change of I-V characteristics of these structures. In this work, we prepared and studied interfaces with various metals in nanoparticle form on n type InP substrates. Metals which were studied were Pd, Pt, Au, and Ag.

Nanoparticles of metals were prepared by reverse micelle technique in isooctane. In this nonpolar solvent, the metal nanoparticles are embedded in reverse micelles of surfactant AOT (bis-(2-ethylhexyl) sulfosuccinate) [1]. The size of nanoparticles was about 20 nm. From these solutions, nanoparticles were deposited onto single crystal wafer of n type InP by electrophoresis. The schematic drawing of the structure is shown on Fig.1. Two types of layers were prepared by applying both polarities of deposition. Further, the layers were annealed in high vacuum at 400°C to remove surfactant from the structure.

These structures were studied by current-voltage measurements, where the diodes prepared by positive potential on InP wafer showed better rectifying properties than diodes prepared by the other way. The typical current-voltage characteristics are shown on Fig.2. From current-voltage characteristics, the Schottky barrier height was calculated. For Pd/InP interfaces with positive potential on the wafer the Schottky barrier height was over 1 eV. Other methods of characterization were secondary-ion mass spectroscopy, AFM, SEM (Fig.3.), capacitance-voltage measurements, and measurements of response of the structure on the presence of hydrogen [2]. The last measurements showed that the current was about two orders of magnitude higher in the presence of hydrogen.

References:

[1] CHEN D.H.; WANG Ch.Ch.; HUANG T.Ch. *Preparation of Palladium Ultrafine Particles in Reverse Micelles*. **Journal of Colloid and Interface Science**, 1999, č. 210, s. 123-129. ISSN 0021-9797/99

[2] Žďánský K., Zavadil J., Kacerovský P., Lorinčík J., Vaniš J., Kostka F., Černohorský O., Fojtík A., Reboun J., Čermák J.: *Electrophoresis deposition of metal nanoparticles with reverse micelles onto InP*, **International Journal of Materials Research**, 2009, vol. 9., p. 1234-1238, ISSN 1862-5282

Figures:

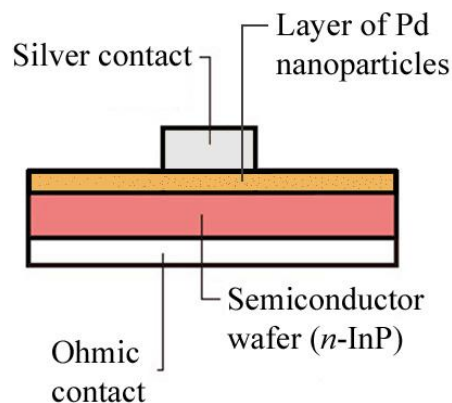


Fig.1. The schematic drawing of structure

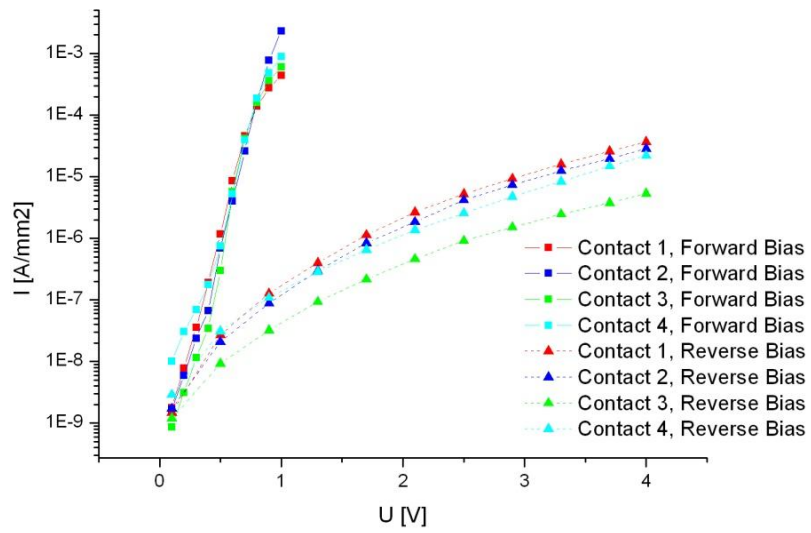


Fig.2. Current-voltage characteristics of Pd/InP interface

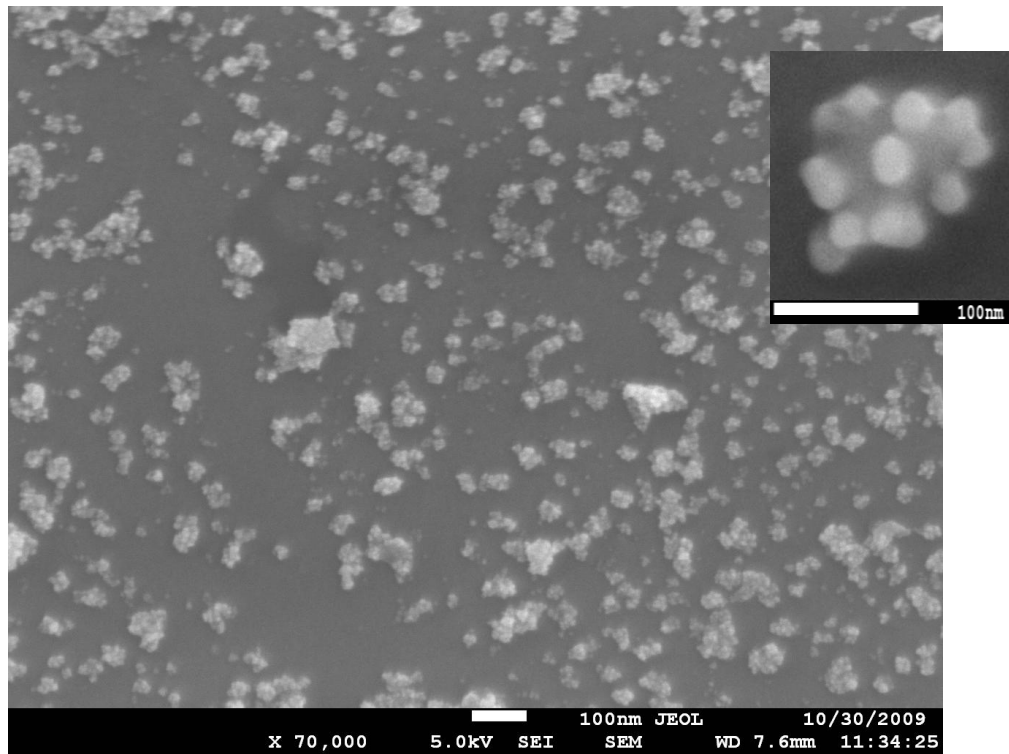


Fig.3. Current-voltage characteristics of Pd/InP interface

Field Enhancement Dependence on the Shape and Size of Au Nanoparticles in Surface-Enhanced Raman Spectroscopy-Active Substrates

Hui-Wen Cheng¹, Chia-Hui Yu¹, and, Yiming Li^{1,2,*}

¹Department of Electrical Engineering and Institute of Communications Engineering,
National Chiao Tung University, 1001 Ta-Hsueh Road, Hsinchu City, Hsinchu 300, Taiwan

²National Nano Device Laboratories, Hsinchu 300, Taiwan

*Tel: 886-3-571-2121 ext. 52974; Email: ymli@faculty.nctu.edu.tw

Introduction

Surface-Enhanced Raman spectroscopy (SERS) has recently got a lot of attention due to its rapid identification of chemical, bacterial samples and single molecule detection. Various studies on nanostructures have been reviewed [1]. The fabricated nanostructures for both bottom-up and top-down approaches have been reported. And, the degree of Raman enhancement is strongly dependent on the morphology of formulated nanostructures. Recently, a top-down approach for the fabrication of SERS-active substrate was proposed [2]. However, the expensive substrate, equipments and complicated process are needed. Therefore, a low cost, environment friendly and simple fabrication for SERS-active substrates will be of great interest for basic and clinical researchers as well as for biotechnologies. In this study, we experimentally and computationally study the local field enhancements of nanoparticles on hydrothermally roughened SERS-active substrates [3], where application of the fabricated samples in identification of Rhodamine 6G (R6G) is discussed.

Computational Model

The Fig. 1(a) shows the three-dimensional (3D) view of the gold-coated nanoparticulate structure, where the 3D finite-difference time-domain (FDTD) numerical simulation is adopted to investigate the field enhancement of substrates. The 3D FDTD method solves a set of Maxwell's equations by first discretizing the equations via central differences in time and space. Then, we base on Yee's mesh and the electric and magnetic field components at points on a grid with grid points to solve these equations. The Maxwell's equations are iteratively solved in a leapfrog manner, alternating between computing the E and H fields at subsequent $\Delta t / 2$ intervals [4], as shown in Fig. 2.

Results and Discussion

For chemical sensing, the hydrothermally roughened substrates are treated with aqueous solutions of 10^{-4} M R6G, where AFM images of titanium thin films treated under hydrothermal conditions for 12 h treatment duration as shown in Fig. 1(b). Fig. 3 shows the characteristic Raman vibrational modes of R6G immobilized on the substrate with or without hydrothermal treatment. The substrate with hydrothermal treatment shows larger intensity than that without hydrothermal treatment due to the roughness on the surface. Through using the FDTD simulation, the evaluation of electric field on the substrates is carried out by directing light with a wave length of 633 nm. Notably, the nanosensor also can be fabricated by other synthesis methods to achieve different shape of nanoparticles. Therefore, we further consider cubic and pyramid shapes of nanoparticles. The 3D simulation results show that the electric field (E_x) enhancement of cube is larger than that of spherical and pyramid shapes, as shown in Fig. 4. Then, we consider different samples which are gold nanoparticle, gold nanocage and gold/silver alloy (from left to right) for spherical, cubic and pyramidal shapes, as shown in Fig. 1(c). From the results of Fig. 4, the Au/Ag alloy is adopted for spherical shape. For pyramid, the nanocage or metal alloy is the same. The corresponding distributions of electric field are shown in Figs. 5, 6 and 7, respectively.

Conclusions

In conclusion, we have successfully prepared SERS-active substrates with low background for the detection of both Rhodamine 6G and Staphylococcus aureus. The enhancement can be controlled by tuning the surface roughness of the substrates through varying treatment duration. Through the FDTD simulation, the field enhancement of spherical and cubic shape nanoparticles can be enhanced by using Au/Ag alloy and nanocage samples, where the different shape of nanoparticles also can be fabricated by other synthesis method for local field enhancement in diverse nanosensor applications.

Acknowledgment

This work was supported in part by Taiwan National Science Council (NSC) under Contract NSC-97-2221-E-009-154-MY2.

References

- [1] S. Lal et al., Chem. Soc. Rev., vol. 37, 2008, pp. 898-911.
- [2] A. Dhawan et al., in: IEDM, 2008, pp. 487-490.
- [3] J.-Y. Yang et al., in Proc. IEEE Int. Conf. Nano/Molecular Medicine and Engineering, 2009, pp. 96-99.
- [4] Y. Li et al., Comp. Phys. Commun., vol. 179, 2008, pp. 107-111.

Figures

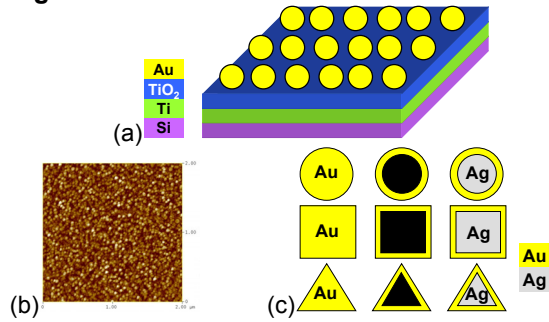


Figure 1. (a) A schematic plot of the 3D view of simulated structure. (b) The AFM images of titanium thin films treated under hydrothermal conditions for 12 h treatment durations. (c) Gold nanoparticle, gold nanocage and gold/silver alloy (from left to right) for spherical, cubic and pyramidal shapes, respectively.

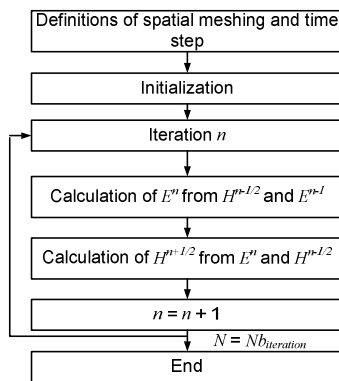


Figure 2. The simulation procedure of solving the Maxwell's equations.

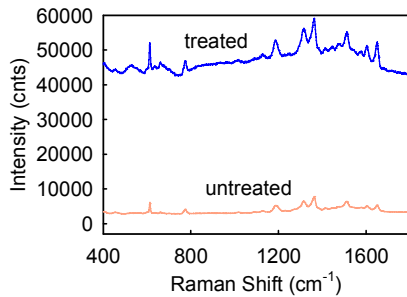


Figure 3. The Raman spectra for Rhodamine 6G (10^{-4} M) immobilized on hydrothermally untreated (blue) and treated (orange) substrates.

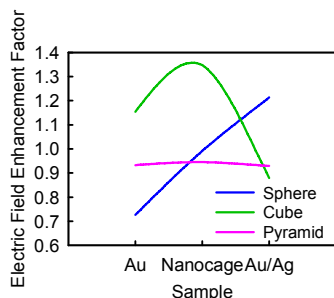


Figure 4. The plot of electric field enhancement factor versus different samples.

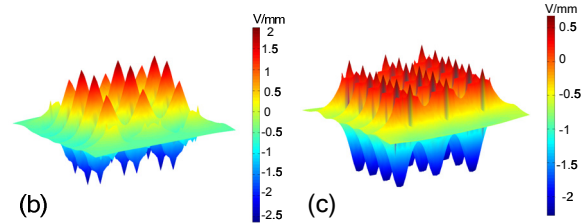
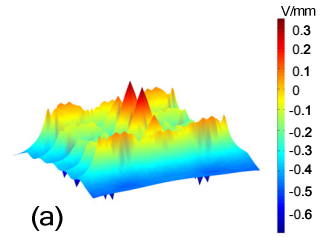


Figure 5. The top view of electric field distribution with spherical shape of (a) Au nanoparticle, (b) Au nanocage and (c) Au/Ag alloy, respectively.

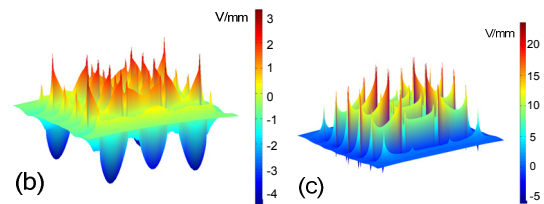
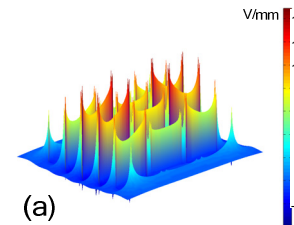


Figure 6. The top view of electric field distribution with cubic shape of (a) Au nanoparticle, (b) Au nanocage and (c) Au/Ag alloy, respectively.

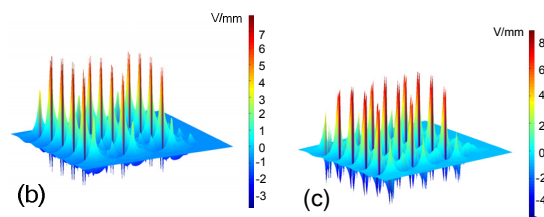
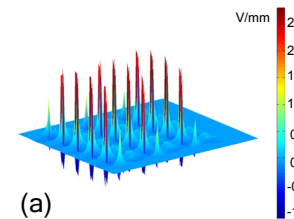


Figure 7. The top view of electric field distribution with pyramidal shape of (a) Au nanoparticle, (b) Au nanocage and (c) Au/Ag alloy, respectively.

Organic Electrochemical Transistors Based on Dielectrophoretically Aligned Nanowire Array

WooSeok Choi¹, Taechang An¹, Geunbae Lim^{1,2*}

¹Department of Mechanical Engineering, Postech, Pohang, Korea

²Department of Integrative Bioscience and Biotechnology, Postech, Pohang, Korea

limmems@postech.ac.kr

In the past 20 years, a large amount of research has been progressed in the area of organic thin film transistors (OTFTs) due to the many profits of organic semiconductors such as structural flexibility, low temperature processing, and especially low cost [1]. In recent years, organic electrochemical transistors (OECTs), the subset of OTFTs, have been attracted the area of sensing because of their ability of operating in aqueous environments with relatively low voltage and the integration with microfluidics [2]. Moreover, nanowires are owing to their unique properties and their potential for fabrication into high density nanoscale devices [3]. It needs to be integrated into an existing device for transistors and sensing elements, however, various methods fabricating nanowires between the electrodes have some limitation [3],[4].

In this research, we introduce the fabrication of individually addressable organic nanowires array on a single chip using dielectrophoresis and pH sensing based on OECT. Figure 1 shows the traditional MEMS process for preparation of the electrode array having cantilever shape for synthesis of nanowire [5]. Carbon nanotube based nanowire is synthesized by the dielectrophoresis and surface tension between the patterned cantilever electrodes. The solution which consists of CNT-COOH suspension and organic materials such as monomer of conducting polymer and nafion was place on between electrodes. Applying AC electric field, positive dielectrophoretic force gathered the CNTs with high electric conductivity between the electrodes where the electric field gradient is larger. After removing the solution, remaining CNT solution forms a concave meniscus because of their capillary force and contains CNTs gathered by dielectrophoretic force (Figure 2). Figure 3 shows a SEM image of a polypyrrole-CNT nanowire and polyaniline-CNT nanowire with a few hundreds nanowire thickness. Because the nanowire is synthesized only the electrodes applied electric field, it is possible to synthesize different kind of nanowire individually on a single chip.

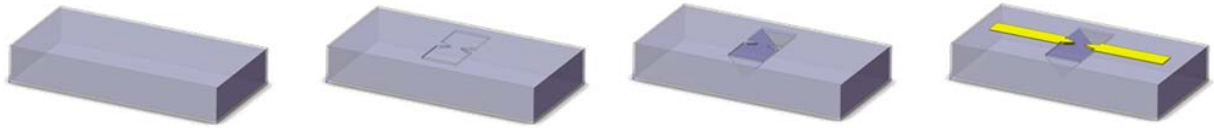
As an example of OECT sensor, it is applied to pH sensor using CNT-nafion nanowire. Figure 4 shows the schematic diagram of OECT measurement. A drain-source voltage V_{DS} is applied 0.5V and electrolyte gate voltage V_G is swept from 0 to 0.5V. Figure 5 is the graph of drain source current ratio I_{DS} to current at zero gate voltage I_0 according to some pH buffer solutions. Owing to increase of the gate voltage, the cations are attached CNT-nafion nanowire by the repulsive force and obstruct the current through the nanowire between drain-source electrodes. The incline of the I_{DS} according to the change of V_G is steeper at lower pH because of larger quantity of hydrogen ions. The slope of current ratio is linearly dependent of pH value.

This work was supported by Mid-career Researcher program through NRF grant funded by the MEST (No. 2009-0085377).

References

- [1] C.D. Dimitrakopoulos, R.L. Malenfant, *Adv. Mater.* **14** (2002) 99-117
- [2] D.A. Bernardis, G.G. Malliaras, *Adv. Func. Mater* **17** (2007) 3538-3544.
- [3] A.K. Wanekaya, W. Chen, N.V. Myung, A. Mulchandani, *Electroanal.* **18** (2006) 533-550.
- [4] D. Lee, T. Cui, *Biosens. Bioelectron.* **25** (2010) 2259-2264.
- [5] W. Choi, T. An, G. Lim, *IEEE Sensor 2009 Conference* (2009) 1151-1153.

Figures



(a) Silicon nitride deposition (b) RIE etching (c) TMAH bulk etching (d) Electrode deposition
Figure 1. Schematic process of cantilever electrodes fabrication

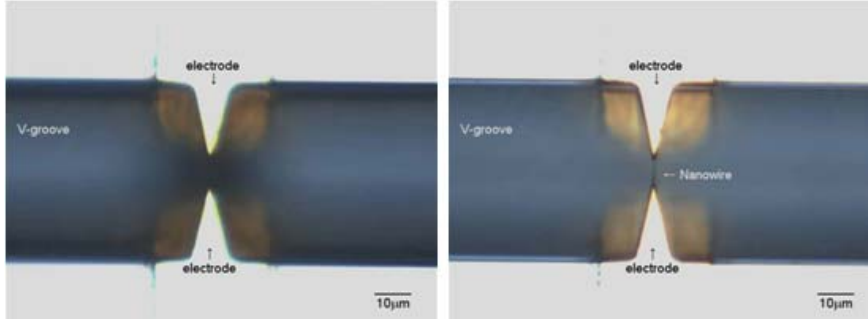


Figure 2. Microscope images of nanowire fabrication process, (a) attraction of CNT between electrodes with AC voltage; (b) nanowire synthesized between electrodes after removal of solutions.

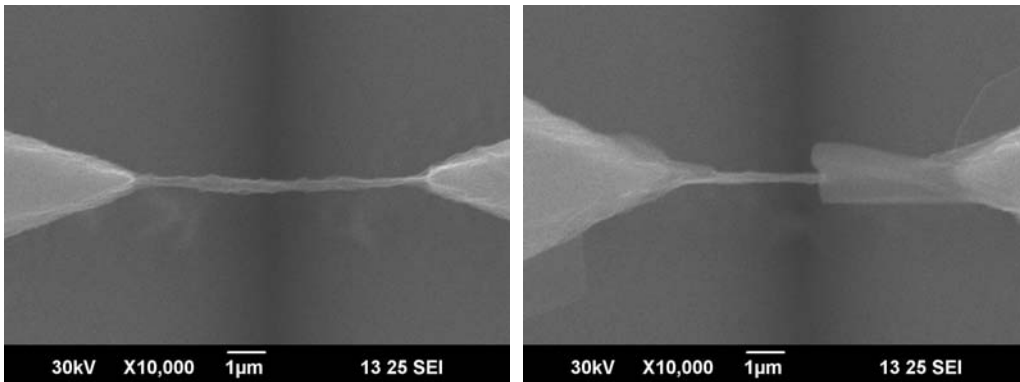


Figure 3. SEM image of (a) CNT-polypyrrole nanowire and (b) CNT-polyaniline nanowire.

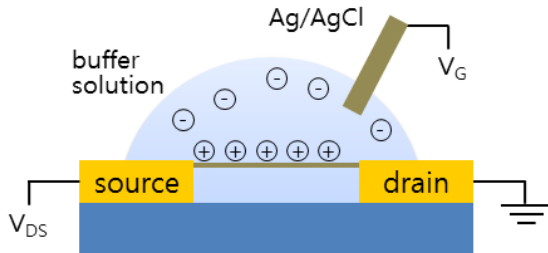


Figure 4. Schematic diagram of OECT measurement

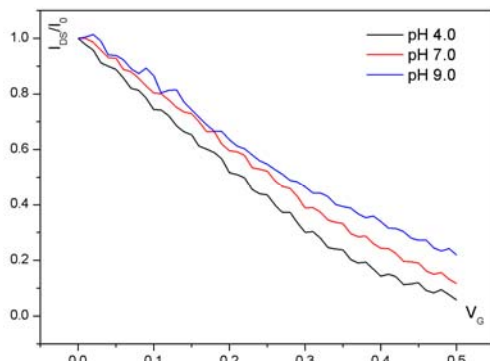


Figure 5. The graph of current ratio vs. gate voltage

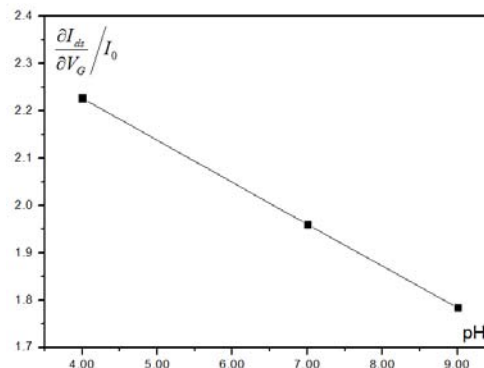


Figure 6. The graph of slope of current ratio according to gate voltage vs. pH

Modulation mechanisms of the genotoxicity of organic pollutants by carbon nanotubes

Gisela de A. Umbuzeiro¹, **Vitor R. Coluci**¹, Jaqueline Honório¹, Diego Stefani², Ronaldo Giro¹, Daniel A. Morales¹, Antonio G. S. Filho³, Oswaldo L. Alves²

¹ Faculdade de Tecnologia, UNICAMP, Limeira, SP Brazil

² LQES, Instituto de Química, UNICAMP, Campinas, SP Brazil

³ Departamento de Física, Universidade Federal do Ceará, Fortaleza, CE, Brazil

vitor@ft.unicamp.br

Carbon nanotubes (CNTs) represent a very important class of nanomaterials due to their many potential and current applications [1]. With the rapid growth of the number of CNT-based products, it is reasonable to expect an increase of the exposure of population and biota. Once in the environment, CNTs can interact with other compounds. Among those compounds is the important class of polycyclic aromatic hydrocarbons (PAHs) and nitro-PAHs which has been largely investigated due to its mutagenic and carcinogenic effects. These compounds are generated from fossil fuels combustion or burning of organic material [2]. Among nitro-PAHs, 1-nitropyrene (1-NP) is the most abundant in the environment [3].

This work aimed to study the modulation of the genotoxicity of 1-NP in the presence of CNTs in water. Multi-walled carbon nanotubes were produced by chemical vapour deposition process and characterized by LQES-UNICAMP. The mutagenicity of the 1-NP was evaluated after incubation with well characterized acid-treated multiwalled carbon nanotube samples. The Salmonella/microsome assay was performed with TA98 strain in dose-response experiments of 1-NP (10 - 1000 ng) exposed to different concentrations of carbon nanotubes (10, 50, and 100 µg) after different pre-incubation times. Reduction of the 1-NP mutagenicity was observed as the carbon nanotube concentration increased. The mutagenicity reduction is mainly attributed to non-covalent functionalization of carbon nanotubes by the 1-NP, expected to occur at free-defect regions. Atomistic calculations and transmission electron microscopy analysis suggested that this mechanism can lead to the capture of 1-NP molecules by the carbon nanotubes surfaces, reducing 1-NP availability for the bacteria cells and inhibiting its mutagenicity. The understanding of the pollutant-carbon nanotubes interactions can help in the development of new environmental applications as well as in the determination of the possible impacts of carbon nanotubes when released into the environment.

References

[1] R. H. Baughman, A. A. Zakhidov and W. A. de Heer, *Science* **297**, (2002) 787.

[2] G. A. Umbuzeiro, *et al.*, *Environmental and Molecular Mutagenesis* **49**, (2008) 249.

[3] K. El-Bayoumy *et al.*, *Cancer Research* **48**, (1988) 4256.

Pegylated nanoparticles for encapsulation of bisnaphthalimidopropyl derivatives against *Leishmania infantum*

Sofia Costa Lima¹, Vasco Rodrigues¹, Jorge Garrido², Fernanda Borges², Paul Kong Thoo Lin³ and Anabela Cordeiro da Silva^{1,4}

¹IBMC-INEB, Biology of Infection and Immunology Division - Parasite Disease Group. Rua do Campo Alegre, 823, 4150-180 Porto, Portugal

²CIQUP Departamento de Química, Faculdade de Ciências, 4169 – 007 Porto, Portugal

³School of Life Sciences, The Robert Gordon University, Aberdeen AB29 9SB, Scotland, UK

⁴Faculdade de Farmácia da Universidade do Porto, Laboratório de Bioquímica. Rua Aníbal Cunha, 164, 4050-047 Porto, Portugal

slima@ibmc.up.pt

Alternative antileishmanial agents are an urgent need since currently available drugs for the treatment of leishmaniasis are associated with emerging resistance and elevated toxicities. Recently, bisnaphthalimidopropyl (BNIP) compounds showed promising anti-*Leishmania* activity [1,2], despite presenting some associated toxicity and low aqueous solubility, therefore claiming the use of a delivery system able to target infected tissues and increase efficiency.

The present work aimed to develop a nanoparticulate system for BNIP compounds based on PLA and PLGA polymers and evaluate the activity of the nanoformulations against the *Leishmania infantum* parasite. The effect of PEGylation on the anti-*Leishmania* activity of the nanoformulations was also assessed. BNIP-loaded nanoparticles were prepared by nanoprecipitation and PEGylation was achieved through introduction of a PLA-PEG copolymer in the preparation procedure. Physicochemical characterization of the nanoformulations included size, polydispersity index, ζ -potential, encapsulation efficiency and *in vitro* drug release determinations. The anti-*Leishmania* activity was evaluated in intracellular *L. infantum* amastigotes.

All nanoformulations presented a mean diameter in the range of 180-235 nm, low polydispersity (≤ 0.102), anionic surface charge (-1 to -7 mV) and encapsulation efficiency of BNIP compounds in the range of 80-90 %. The optimal drug loading was 5 % (w/w), since it didn't led to major disturbance of the particles characteristics and kept the encapsulation efficiency around 80 %. *In vitro* drug release studies revealed a biphasic pattern of drug release. PEGylation of nanoparticles resulted in increased release of the drugs *in vitro*; however, after 7 days of incubation, the majority of the compound stays retained in the particle matrix, in both uncoated and PEG-coated nanoparticles. Empty nanoparticles were able to inhibit the growth of intracellular amastigotes. This effect was more pronounced for uncoated nanoparticles. Based on these findings, optimization of polymer amount in the nanoformulation was carried out. For PLGA and PLA nanoparticles the maximum concentration that didn't exhibit considerable anti-*Leishmania* activity was 0.20 mg/ml, while for PLA- and PLGA-PEG nanoparticles it was of 1.00 mg/ml. Incorporation of BNIP compounds in the nanoparticles reduced the toxicity of the compounds to human and mouse macrophages by at least 10-fold. Growth inhibition assays revealed that BNIP compounds encapsulated in PEG coated nanoparticles were more effective than the free compounds in inhibiting the growth of intracellular amastigotes in human THP1 macrophages.

In resume, BNIP compounds were efficiently encapsulated in uncoated and PEG-coated nanoparticles, leading to a reduction in the toxicity of the compounds on macrophage cells. Therefore, these BNIP nanoformulations tolerate the administration of higher doses because the slow and sustained release of the drug from the nanoparticles, which reduces the toxic effect associated with the administration of the free drug. PEG-coated nanoparticles containing the BNIP compounds were more effective in the growth inhibition of intracellular *L. infantum* amastigotes than free compound.

References

[1] Oliveira, J., L. Ralton, J. Tavares, A. Codeiro-da-Silva, C.S. Bestwick, A. McPherson and P.K. Thoo Lin, The synthesis and the *in vitro* cytotoxicity studies of bisnaphthalimidopropyl polyamine derivatives against colon cancer cells and parasite *Leishmania infantum*. *Bioorg Med Chem*, 2007. 15(1): p. 541-5.

[2] Tavares, J., A. Ouaissi, P. Kong Thoo Lin, I. Loureiro, S. Kaur, N. Roy and A. Cordeiro-da-Silva, Bisnaphthalimidopropyl Derivatives as Inhibitors of *Leishmania* SIR2 Related Protein 1. *ChemMedChem*, 2010, 5, 140-7.

Acknowledgments

S Costa Lima thanks Fundação para a Ciência e Tecnologia (FCT) for the grant SFRH/BPD/37880/2007 and Fundação Calouste Gulbenkian for the funded project P-105348.

CdSe/TiO₂ core-shell nanoparticles produced in AOT reverse micelles: applications in pollutant photodegradation using visible light

Paulo J. G. Coutinho, Arlindo M. F. Garcia, Marisa S. F. Fernandes

Centre of Physics (CFUM), University of Minho, 4710-057 Braga, Portugal
pcoutinho@fisica.uminho.pt

Over the last decade, nanostructured semiconductor materials have been the focus of intense research efforts [1]. The striking feature of a nanometric solid is that conventionally detectable properties are no longer constant, but are tunable by simply controlling its shape and size and this has originated a revolution in materials science and device technology. Their photophysics shows high luminescence with tunable emission maxima and narrow bandwidth. Semiconductor nanocrystals (CdSe, ZnS, ...), metallic nanocrystals (Ag, Au, ...) and magnetic nanocrystals (Ni, Fe₃O₄, ...) can be prepared by templating with the aqueous cavities existent in self-organized structures of water-in-oil microemulsions [2]. The main aspects that control structure of these nanoparticulate systems are the nucleation and growth processes, which are determined by the microemulsions dynamics, the interaction between nanoparticle surface and surfactant molecules and, if needed, by the presence of metal complexing agents. Core-shell nanoparticles (CdSe/ZnS) have also been made by templating techniques [2], opening the range of possibilities for tailoring the material to specific needs of application and improving its biocompatibility.

In this work we succeeded in the production of CdSe nanocrystals with ~2.7nm size emitting with high quantum yield at 545nm with a halfwidth of 30 nm (Figure 1).

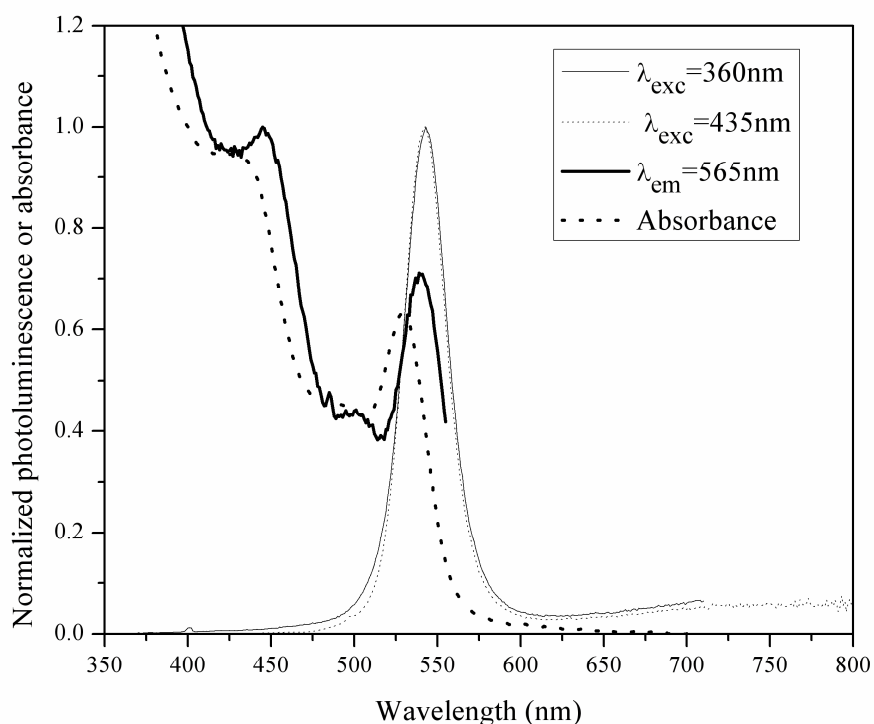
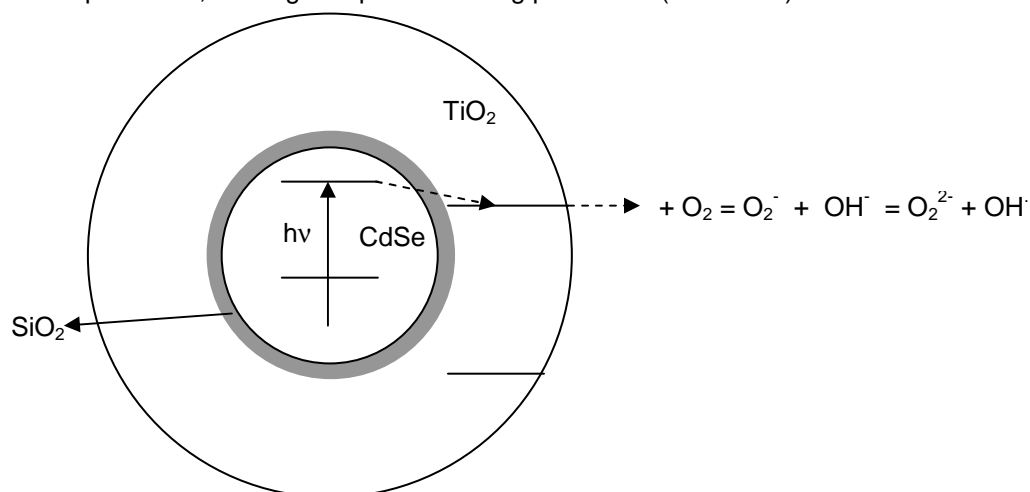


Figure 1. Absorption and photoluminescence spectra of CdSe nanoparticles.

We have used AOT reverse micelles templating procedure and cadmium nitrate and polyselenide as precursors. The nucleation and growth processes proceed in the water pools and the resulting particles are probably stabilized by non-covalent surface covering with AOT surfactant molecules. The particles surface can thus be easily changed, either by adding other molecules that covalently bind to the particles surface displacing the surfactant (capping/functionalization agents), or by growing other materials on it (core-shell nanoparticles). We have grown a titanium dioxide shell above the cadmium selenide core using a mercapto derivative of a silicon alkoxide as coupling agent followed by the addition of TBOT (titanium tetrabutoxide). The observed huge decrease of the photoluminescence quantum yield of the resulting particles indicates the formation of core-shell CdSe/TiO₂ nanoparticles as it was reported a photoinduced electron transfer from CdSe to TiO₂ in a linked arrangement [3]. This process can thus capacitate the TiO₂ outer layer for electron transfer reactions with adsorbed or

surrounding molecules. These can be oxygen generating superoxide or hydroxyl radicals, which can act as strong oxidants of pollutants, leading to a photocleaning procedure (scheme 1).



Scheme 1. Photodegradation mechanism using CdSe/TiO₂ core-shell nanoparticles (dashed line represents electron path).

TiO₂ can originate this photocatalytic process by itself but, due to a high band gap, UV radiation is needed with $\lambda < 387$ nm. The advantage of the prepared nanoparticles is the possibility of efficiently using visible light for the same purpose. In Figure 2, our results show a significant photodegradation of the dye methylene blue (generally used as a standard) under 405nm irradiation with a 150W Xe arc source and a 405 ± 5 nm interference filter. The light intensity in the irradiation cell was 3.2×10^{-8} Einstein $\text{cm}^{-2} \text{s}^{-1}$ and the resulting initial first order kinetics constant for the photodegradation process was $2.7 \times 10^{-3} \text{ min}^{-1}$. As the initial methylene blue concentration was 1.4×10^{-5} M, we estimate a photodegradation quantum yield of 0.034%.

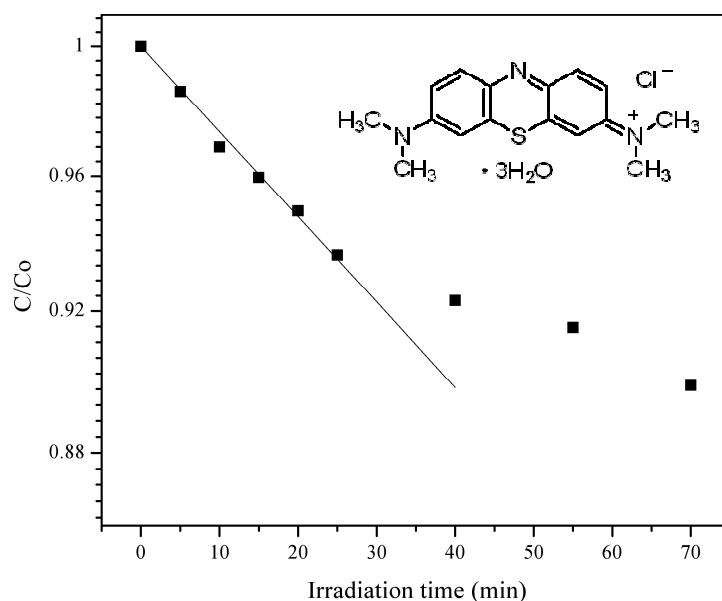


Figure 2. Photodegradation of methylene blue using CdSe/TiO₂ core-shell nanoparticles.

References

- [1] Wenwan Zhong, *Anal. Bioanal. Chem.* **394** (2009) 47-59.
- [2] A. R. Kortan, R. Hull, R. L. Opila, M. G. Bawendi, M. L. Steigerwald, P. J. Carroll, Louis E. Brus, *J. Am. Chem. Soc.* **112** (1990) 1327-1332.
- [3] István Robel, Masaru Kuno, Prashant V. Kamat, *J. Am. Chem. Soc.* **129** (2007) 4136-4137.

Acknowledgements

Financial support to CFUM by FCT-Portugal and FEDER is acknowledged.

Studies on carbon nanotubes/silver clusters composites
Jelena Cveticanin, Zlatko Rakocevic, Djordje Trpkov, Olivera Neskovic
Vinca Institute of Nuclear Sciences, PO Box 522, 11001 Belgrade, Serbia
e-mail: cvetic@vinca.rs

Keywords: carbon nanotubes, silver, functionalization

Since their discovery in 1991 by Iijima [1], carbon nanotubes (CNTs) have attracted great interest in most fields of science and engineering due to their unique physical and chemical properties. These properties allow them to be applied for a wide range of applications [2, 3]. The major areas of CNTs research are the polymer composites [4] and biomedical materials and devices including biosensors, drug and vaccine delivery vehicles [5].

Carbon nanotubes/silver clusters composites were produced by functionalization of both single walled and multi walled CNTs (SWCNTs and MWCNTs) by Ag nanoparticles, achieved via anchoring of the polymer to the surface of CNTs and simultaneous reduction of Ag^+ ions under the γ -irradiation. Two different synthesis procedures were employed. The presence of Ag on the nanotubes was confirmed using energy dispersive X-ray spectroscopy. CNTs/silver clusters composites were visualized using microscopic techniques STM and TEM. The particle size distribution measurements were taken. Ag nanoparticles were formed and successfully decorated CNTs. Making a CNT type of composites is of interest for their further application in different fields of biology and technology.

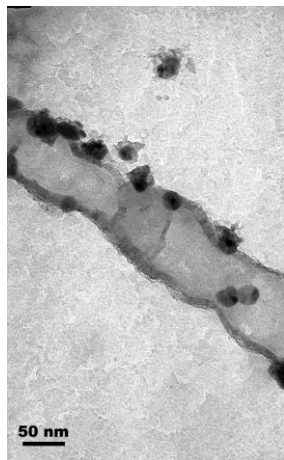


Figure 1. TEM image of as-prepared Ag/PVA/SWCNTs.

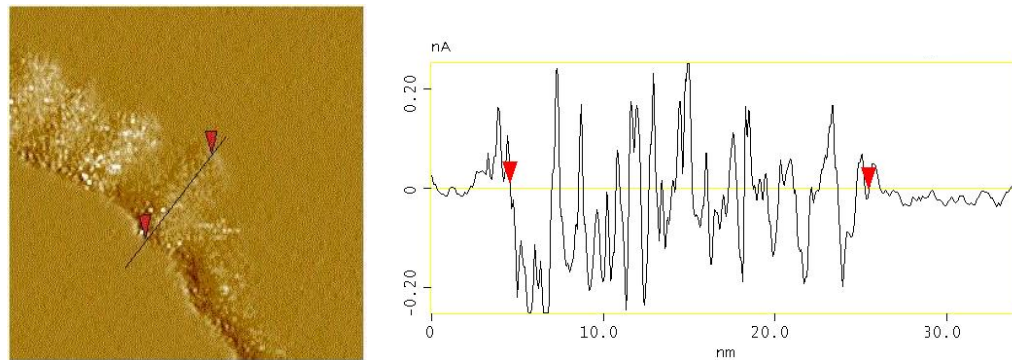


Figure 2. STM image (69nm x 69nm) of Ag/PVA/SWCNTs

References

- [1] S. Iijima, *Nature* **354** (1991) 56–8.
- [2] R. H. Baughman, A. A. Zakhidov, W. A. de Heer, *Science* **297** (2002) 787–92.
- [3] J. Gooding, *J. Electrochim. Acta* **50** (2005) 3049–60.
- [4] J. N. Coleman, U. Khan, W. J. Blau, Y. K. Gun'ko, *Carbon* **44** (2006) 1624–52.
- [5] Y. Lin, S. Taylor, H. Li, K. A. S. Fernando, L. Qu, W. Wang, L. Gu, B. Zhou, Y. P. Sun, *J. Mater. Chem.* **14** (2004) 527–41.

NIR Photoresponce in New Up-Converting CdSe/NaYF₄:Yb,Er Nano-Heterostructures

Afshin Dadvand^{a,b}, Chenglin Yan^{a,b}, Dmitrii F. Perepichka^b, and Federico Rosei^a

^aINRS-EMT, Université du Québec 1650 Boul. Lionel Boulet, J3X 1S2 Varennes (QC) Canada,

^bDepartment of Chemistry and Center for Self-Assembled Chemical Structures, McGill University, 801 Sherbrooke Street West, Montréal, Quebec, Canada H3A 2K6.

E-mail: dadvand@emt.inrs.ca

Multi-component hetero-nanostructures containing two or more nanosized components arranged in a controlled manner are of fundamental and practical significance for many rapidly developing fields.[1] An interaction between the components of such systems may significantly improve the application performance and even induce new chemical [2] and electronic properties.[3] In this research work, we demonstrate energy up-conversion of near-infrared (NIR) photons, subsequent energy transfer (ET) from lanthanide nanocrystals to quantum dots (QDs), and the dissociation of thus formed excitons leading to pronounced photoconductivity.[4]

Efficient up-conversion of sub-band-gap energy photons to create a hole-electron pair in a semiconductor would allow breaking a fundamental limitation of single junction photovoltaic devices. We note that energy transfer from NaYF₄:Yb,Er onto CdSe has been recently shown for a core-shell structure.[5] However, using silica shell to attach CdSe to the lanthanide nanocrystals precludes electronic interaction between the CdSe and renders its semiconducting properties irrelevant.

Therefore, the aim of this research is to develop a simple method for the synthesis of nano-heterostructures consisting of lanthanide-doped NaYF₄ nanocrystals dendritically decorated with CdSe QDs.

To demonstrate feasibility of using CdSe/NaYF₄:Yb,Er (CSNY) up-converted energy transfer system in electronic devices, we have studied its photoconductivity upon NIR excitation. The two-contact devices were prepared by spin-coating of solution of studied nanoparticles in toluene on Si/SiO₂ substrates pre-patterned with Au electrodes. These devices showed a reversible and stable NIR photoconductivity switch. To our knowledge, this is the first example of using up-converting nanocrystals in optoelectronic devices and it could have a potential application in photovoltaics to harvest sub-band-gap energy photons.[6]

References

- [1] Mokari, T.; Sztrum, C.; Salant, A.; Rabani, E.; Banin, U. *Nat. Mater.* **4** (2005) 855; (b) Catala, L.; Brinzer, D.; Prado, Y.; Gloter, A.; Stephan, O.; Rogez, G.; Mallah, T. *Angew. Chem. internat. Edit*, **1** (2009) 183.
- [2] Lim, B.; Jiang, M.; Camargo, P.; Cho, E. C.; Tao, J.; Lu, X.; Zhu, Y.; Xia, Y. *Science*, **324** (2009) 1302.
- [3] Gudiksen, M. S.; Lauhon, L. J.; Wang, J. F.; Smith, D. C.; Lieber, C. M. *Nature*, **415** (2002) 617.
- [4] Grieve, K.; Mulvaney, P.; Grieser, F. *Curr. Opin. Colloid Interface Sci.* **5** (2000) 168.
- [5] Li, Z. Q.; Zhang, Y.; Jiang, S. *Adv. Mater.* **20** (2008) 4765.
- [6] Shalav, A.; Richards, B. S.; Trupke, T.; Kramer, K. W.; Gudel, H. U. *Appl. Phys. Lett.* **86** (2005) 013505.

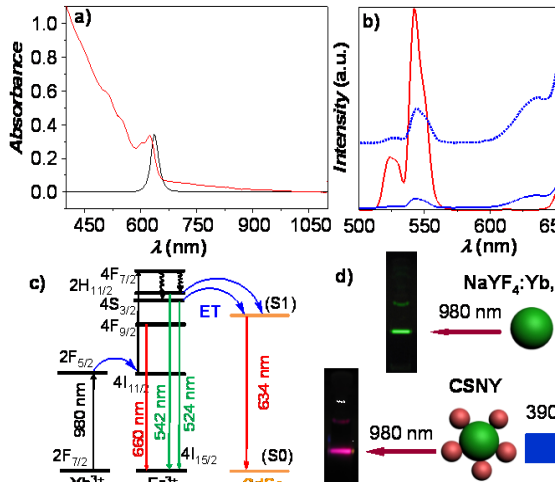


Figure 1. (a) Absorption and emission spectrum of CSNY excited at 390 nm; (b) emission spectra of the seed NaYF₄:Yb,Er nanocrystals (red line) and of resulting CSNY (solid blue line); a dotted line shows an expansion of the same in toluene (both ~1 wt%) excited by NIR laser ($\lambda_{exc} = 980$ nm); (c) a simplified schematic of the excitation and ET in CSNY; (d) photographs of the emission from NaYF₄:Yb,Er nanocrystals (top) and CSNY heterostructures (bottom) under excitation at 390 nm and 980 nm.

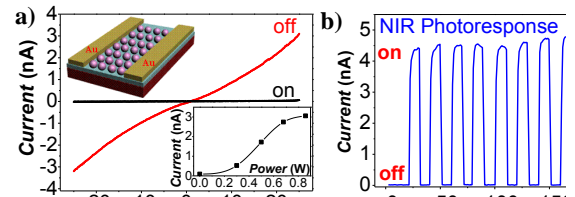


Figure 3. (a) I - V characteristics of the CSNY-based device (shown in top inset) in dark (black line) and under 980 nm radiation; bottom inset shows photocurrent-laser power dependence. (b) On-off switching at laser power 0.86 W and bias voltage of 35 V.

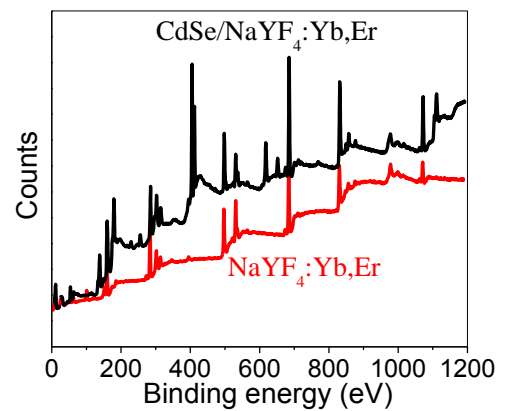


Figure 4. XPS spectra of NaYF₄:Yb,Er nanocrystals and CSNY hetero-nanostructures,

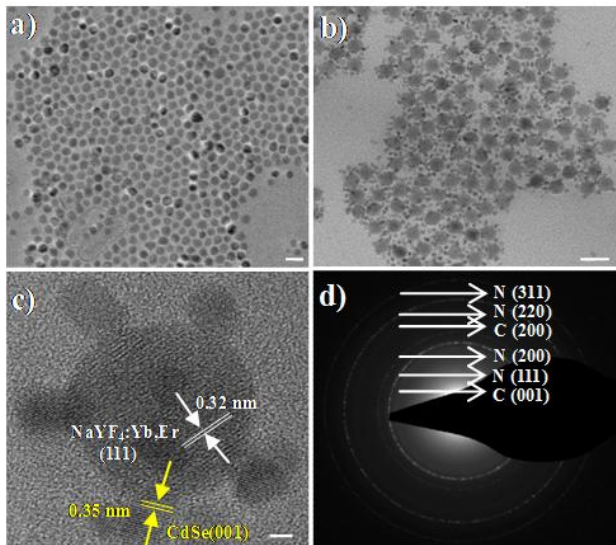


Figure 2. (a) TEM images of original NaYF₄:Yb,Er nanocrystals and (b) and (c) CSNY hetero-nanostructures (d) SAED pattern of a CSNY hetero-nanostructure. Scale bar is: 50 nm (a, b) and 3 nm (c). N represents NaYF₄:Yb,Er; and C represents CdSe.

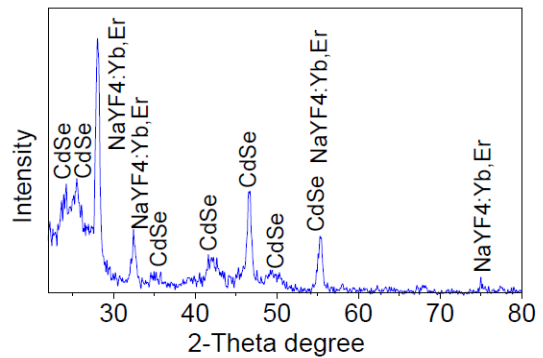


Figure 5. XRD pattern of CSNY hetero-nanostructures, where indexed peaks were assigned to the planes of hexagonal phase CdSe and cubic phase NaYF₄:Yb,Er.

Biotemplated polyaniline nanowires as building blocks for spin-valves

T.V.A.G. de Oliveira⁽¹⁾, N. Amsharov⁽²⁾, C. Wege⁽³⁾, L.E. Hueso^(1,4), A.M. Bittner^(1,4)

⁽¹⁾ CIC nanoGUNE Consolider, Tolosa Hiribidea 76, E-20018 San Sebastián, Spain.

⁽²⁾ Max-Planck-Institute for Solid State Research, Heisenbergstraße 1, D-70569 Stuttgart, Germany.

⁽³⁾ Institute of Biology, University of Stuttgart, Pfaffenwaldring 57, D-70569 Stuttgart, Germany.

⁽⁴⁾ IKERBASQUE, Basque Foundation for Science, E-48011 Bilbao, Spain.

t.oliveira@nanogune.eu

The Tobacco Mosaic Virus (TMV) has been extensively used as scaffold for the controlled one-dimensional assembly of particles and molecule. While the research in this area was largely focused on understanding the assembly and the fundamental properties of such composites, it now shifts to the fabrication of actual devices with functionalized TMVs as its main building blocks.

Here, we investigated the feasibility of fabricating organic spin valves by using TMV coated with polyaniline (PANI)^[1] as the non-magnetic interlayer of the device. In this device, spin-polarized electrons are injected from a first ferromagnetic (FM1) electrode, transported through the conductive polymer-coated TMV, and injected back in a second FM2 electrode, see the inset in Fig.1(a). Depending on the relative orientation of the magnetization of the electrodes, two different resistance levels appear in our device.

This magnetoresistance variation is well known for metals and semiconductor as the non-magnetic channel, but just recently it has been demonstrated that organic semiconductors could also be used as spin transporting materials^[2]. Indeed, the small spin-orbit interaction and the reduced coupling to nuclear spins make organic semiconductors perfect candidates for spintronic applications.

In this study, a biomolecule is used for the first time as the building block of a spintronic device. Moreover, we have selected polyaniline as the non-magnetic, charge-transporting layer – this conjugated polymer is one of the unique examples of organic semiconductors that can be synthesized in a true metallic state through doping^[3]. Therefore, the PANi-TMV device is expected to have superior spin diffusion length, together with its intrinsic long spin relaxation time.

References

- [1] Z. Niu, J. Liu, L.A. Lee, M.A. Bruckman, D. Zhao, G. Koley, Q. Wang. *Nano Letters*, **7** (2007) 3729–3733.
- [2] V. A. Dediu, L.E. Hueso, I Bergenti, C. Taliani. *Nature Materials*, **8** (2009) 707–716.
- [3] K. Lee, S. Cho, S. Heum Park, A. J. Heeger, C.-W. Lee, S.-H. Lee. *Nature*, **441** (2006) 65–68.

Figures

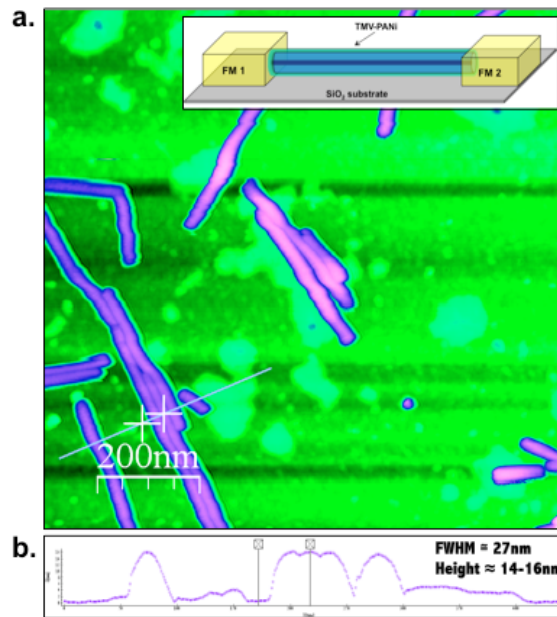


Fig. 1: In (a), an AFM image of the PANi-coated TMV deposited on Si/SiO₂ wafer. The inset shows a schematic view of the TMV-PANi spin-valve. A profile of the coated nanowires is shown in (b), its reduced height is due to the strong interaction of the wires with SiO₂.

Virus-Based Assemblies as Nanocontainers and Nanoreactors

Andrés de la Escosura,^{a,b} Marta Comellas-Aragónés,^b Friso Sikkema,^b Martijn Verwegen,^b
Anne van der Ham,^b Jeroen J. L. M. Cornelissen^b and Roeland J. M. Nolte^b

¹ Universidad Autónoma de Madrid, Organic Chemistry Department (Módulo 01), Cantoblanco 28049, Madrid, Spain. E-mail: andres.delaescosura@uam.es

² Institute for Molecules and Materials, Radboud University Nijmegen, Toernooiveld 1, Nijmegen 6525 DE, The Netherlands.

The Cowpea Chlorotic Mottle Virus (CCMV) is a plant virus (28 nm in diameter) whose protein shell defines an inner cavity of approximately 18 nm. One of the interesting features of this virus is its sensitivity to pH and ionic strength. Depending on these factors, CCMV capsids can rapidly be disassembled *in vitro* into protein dimmers and then re-assembled again. In this lecture, new concepts related to the use of CCMV capsids as nanoreactors will be presented (Figure 1).¹ The following topics will be discussed: (i) the encapsulation of DNA-templated chromophore assemblies within virus protein nanotubes;² (ii) the controlled integration of synthetic polymers within the CCMV cavity;³ (iii) the use of the CCMV capsid as a nanoreaction vessel for the controlled free radical polymerization of water soluble monomers; and (iv) the templated synthesis of well-defined inorganic nanoparticles inside CCMV.⁴

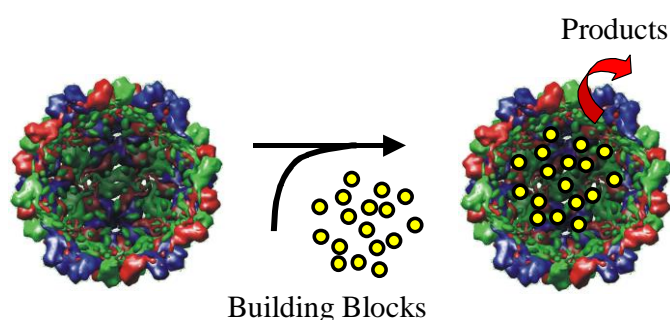


Figure 1. Schematic illustration of the use of viral capsids as nanoreactors

- (1) de la Escosura, A.; Nolte, R. J. M.; Cornelissen, J. J. L. M. *J. Mater. Chem.* **2009**, *19*, 2274-2278.
- (2) de la Escosura, A.; Janssen, P. G. A.; Schenning, A. P. H. J.; Nolte, R. J.; Cornelissen, J. J. L. M. *Angew. Chem. Int. Ed.* **2010**, *49*, 1-5.
- (3) Comellas-Aragones, M.; de la Escosura, A.; Dirks, A. J.; van der Ham, A.; Fuste-Cune, A.; Cornelissen, J. J. L. M.; Nolte, R. J. M. *Biomacromolecules* **2009**, *10*, 3141-3147.
- (4) de la Escosura, A.; Verwegen, M.; Sikkema, F. D.; Comellas-Aragones, M.; Kirilyuk, A.; Rasing, T.; Nolte, R. J. M.; Cornelissen, J. *Chem. Commun.* **2008**, 1542-1544.

The active layer thickness effect of Dye sensitized solar cell (DSSCs) containing multi-walled carbon nanotubes (MWCNTs).

Kadiatou Thérèse Dembélé^{1,2}; Federico Rosei¹; Enrico Traversa^{2,3}; Silvia Licoccia²; Clara Santato⁴.

1. Université de Québec INRS-EMT canada;
2. Departement of Chemical Science and Technology (NAST), Université of Rome Tor Vergata; Italy
3. International Research Center for Materials Nanoarchitectonics (MANA), National Institute for Materials Sciences (NIMS) at Japan
4. École Polytechnique de Montréal, Canada.

The active layer thickness is very important to DSSCs performance. The optimal thickness changes according to the semiconductors materials used in the cells. Here we report its effects in DSSCs performance in general and in DSSCs containing carbon nanotubes performance. When the thickness is least than 10 μm , the risks to create a short circuit in the device increase and the current becomes very low. Up to this value, (from 15 μm to 20 μm) the resistance increase while the current still low, so the device performance decreases.

Carbon nanotubes are used in DSSCs to increase their performances, but its addiction can change all the parameters. In DSSCs containing CNTs, the optimal value of the thickness is 15 μm . Under this value, first there is an experimental difficulty because during the annealing process, the CNTs try to remove TiO_2 of the surface to create a hole, second we have a very low current. Because after annealing, while TiO_2 nanoparticles are well synthesized on the substrate, CNTs don't change a lot because the anneal temperature (500°C) is not enough to synthesize them. So the surface won't be uniform, there will be a pick of CNTs, which can create a short circuit in the device after cell assembling or just decrease the current, because CNTs are have a very good electrical conductivity. By increasing the active layer thickness of DSSCs containing CNTs the voltage and the resistance increase while the current decrease. For best performance of the device we need to increase only voltage not the resistance, so the compromise should be done between the voltage and resistance increasing and the current decreasing because at some value (20 μm) the voltage increase is not enough to compensate current decrease, which will decrease the device performance.

It is difficult to electron to move through a thick layer till the electrode in a case of very thick active layer in DSSCs, and just a short circuit will be created if this layer is too thin. The compromise should be done for best performance.

Characterization of morphology, crystallization and melting behaviour of films of ethylene-vinyl acetate (EVA) by means of AFM and DSC

J. Diaz¹, E. Xuriguera², S. González-Martín²

¹ Nanometric Techniques Unit. Scientific-Technical Services. University of Barcelona. C/ Lluís Solfe i Sabarís 1-3. 08028 Barcelona

²Diopma, IN2UB, Departament de Ciència dels Materials i Enginyeria Metal·lúrgica, Universitat de Barcelona, Martí i Franquès 1, E-08028 Barcelona, Spain
jdiaz@sct.ub.es

The crystallization, the morphology and the thermal behaviour of films of ethylene-vinyl acetate copolymer (EVA) were investigated by means of Atomic Force Microscopy (AFM) and differential scanning calorimetry (DSC). Real-time AFM phase imaging enables us to observe the crystallization process of EVA24.

The EVA used was polydispersed random copolymer with 24 wt% nominal of vinyl acetate (EVA24).

The strategy to characterize the behaviour of EVA24 was an isothermal crystallization, a time-to-event experiment. A typical method consists of raising the sample above its melt temperature and holding isothermally for a couple of minutes to ensure that it was completely melted. The sample was then rapidly cooled and stabilized at the desired test temperature [1-2].

The dynamic crystallization process of EVA24 was directly observed using tapping-mode AFM (TM-AFM). For this purpose, a heater was coupled to the AFM to realize the isothermal crystallization of EVA24.

The isothermal crystallization temperature (T_c) used for in-situ observations with AFM was previously optimized with DSC. The study with DSC reproduces the same conditions, i.e., EVA24 film was melted and next cooled at the desired temperature. The melting and crystallization temperatures were verified through a standard DSC with a typical temperature-scanning rate of 10°C/min. These are 64°C for T_m and 51°C T_c . Isothermal DSC at different temperatures in the vicinity of T_c were performed in order to choose the appropriate T_c , which brings enough time to observe the crystallization process in AFM. The selected temperature was 61°C.

During crystallization ethylene-vinyl acetate (EVA) is ejected on the surface of the film forming droplet-like domains. A different morphology is observed. AFM images recorded at different temperatures demonstrated height changes of different domains caused by crystallization of ethylene-vinyl acetate [3].

References

- [1] R. Pearce and G. J. Vancso. *Macromolecules*, **30** (1997) 5843–5848
- [2] Chi-Ming Chan and Lin Li, *Adv. Polym. Sci.*, **188** (2005) 1-41.
- [3] Ruth L. McEvoy, Sonja Krause and Peter Wut. *Polymer* **39** (1998) 5223-5239.

The authors would like to thank David González and Lluís Mañosa, Departament Estructura i Constituents de Matèria de la Universitat de Barcelona, for use of their DSC. The authors are also grateful to Dr Gerard Oncins from the Nanometric Techniques Unit of the Scientific-Technical Services of the University of Barcelona for useful discussions on the results.

Analysis of the process variables in Laser Spinning controlling the geometry of nanofibers

O. Dieste, F. Quintero, J. Pou, R. Comesaña, F. Lusquiños, A. Riveiro

Dpto. Física Aplicada, Universidade de Vigo, ETSEI, R/ Maxwell, 36310 Vigo, Spain
fquintero@uvigo.es

The great interest that quasi-1D structures involve in nanotechnology applications have triggered many researches about methods to produce nanofibers[1]. Special importance has the control of composition, structure and geometry to obtain useful nanofibers[2].

Laser spinning is a new technique enabling the production of large quantity of ultra-long amorphous ceramic nanofibers, showing extremely high length to diameter ratio and with tailored composition. This technique has been demonstrated successfully with several compositions, probing its capability to produce fibers of inorganic oxides that can not be fiberized by any other technique[3]. The process involves a high power laser focused over the surface of the precursor plate, so a very small volume of material is melted, at the same time as a high speed gas jet stretches the molten material to produce a viscous filament. A relative movement between the plate of precursor material and the laser keeps the process ongoing to sustain a uniform mass flow of the liquid volume[4] In order to make possible the rapid cooling and elongation of the viscous filament by the high speed gas jet before it breaks, the process must be carefully controlled[5]. In this way large quantity of intertwined micro- and nanofibers can be obtained in a very short time (figure 1 shows typical appearance of the fibers). The ceramic nanofibers obtained by this technique are always amorphous due to the rapid cooling of the molten material. Furthermore, the composition of the fibers can also be easily controlled just by adjusting precursor composition are obtained from a small melted volume and cooled at ultra-short time.

In the present work we study how working conditions influence on nanofibers geometry and the quantity of nanofibers produced. We carried out several series of experiments varying different working conditions to study their influence on the process and on the fibers produced. The area irradiated by the laser beam on the surface of the precursor material is expected to have an important influence as it changes the energy density supplied to the molten volume and affects to its temperature. In fact, the area of the surface of precursor material irradiated by the laser changes the quantity of fibers obtained: there is an optimum distance which maximizes the quantity of fibers produced. The speed of the cut is likely to have an influence since it may change the shape of the melting front and, again, its temperature. Figures 2.a and 2.b illustrate some of the results we observed depending on this parameter. Cutting speed is the most relevant variable to control geometry of the fibers as expected from the outcomes of the previous theoretical work[5]. Thus, an interesting conclusion from this result is that the distribution of diameters can be controlled by simply changing the speed of the process. Gas pressure was found to be not an influential variable, as it does not produces any change on geometry or quantity of fibers, provided that supersonic regime is reached in the gas jet. Three types of assist gas were used: argon, dry air and wet air. Switching assist gas between argon and dry air do not produce changes on the fibers. However, using wet air enlarges the diameters, which means that thicker fibers are obtained by using wet air as drag gas. This result may be explained by the fact that heat losses are greater on wet air than on dry air due to the change in convective factor. Therefore cooling of the fibers is faster and, consequently, elongation process finishes sooner.

Acknowledgments

This work was partially supported by the European Union program POCTEP project (0330_IBEROMARE_1_P), the Spanish government (CICYT/FEDER MAT2006-10481) and by Xunta de Galicia (INCITE08PXIB303225PR, INCITE09E2R303103ES).

References

1. C.N.R. Rao, F.L. Deepak, G. Gundiah, A. Govindaraj: Progress in Solid State Chemistry 31, 5-147 (2003)
2. S.V. Kuchibhatla, A. Karakoti, D. Bera, S. Seal: Progress in Materials Science 52, 699-913 (2007)
3. F. Quintero, J. Pou, F. Lusquiños, A. Riveiro, Experimental analysis of the production of micro- and nanofibres by laser spinning, 2007
4. F. Quintero, A.B. Mann, J. Pou, F. Lusquinos, A. Riveiro, Rapid production of ultralong amorphous ceramic nanofibers by laser spinning, 2007
5. F. Quintero, O. Dieste, J. Pou, F. Lusquinos, A. Riveiro: J Phys D Appl Phys 42, (2009)

Figures

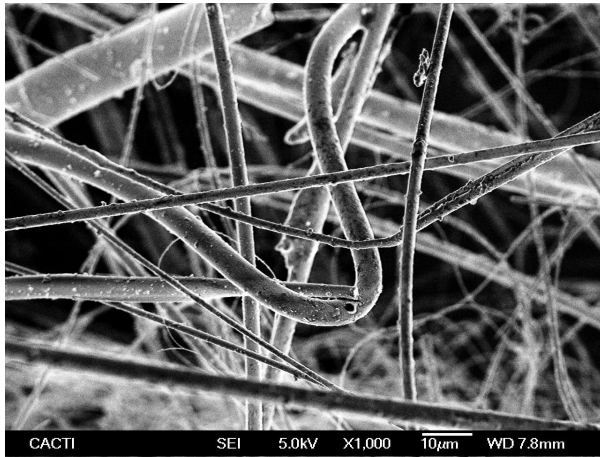


Figure 1. SEM micrograph showing the typical appearance of the micro- and nanofibers produced by Laser Spinning.

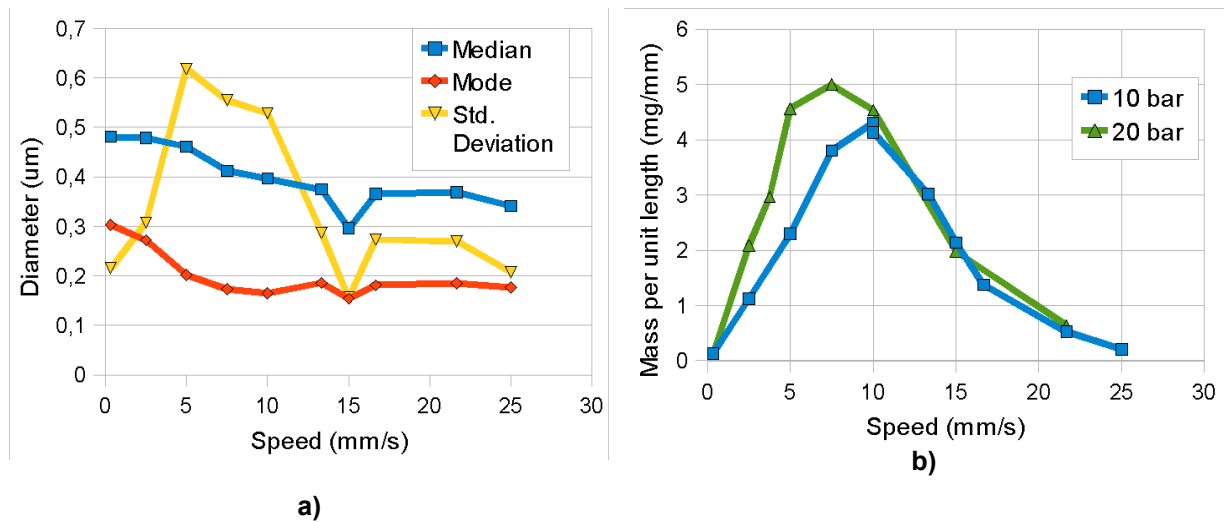


Figure 2. a) Diameters Distribution of the fibers produced as a function of the speed of the cut. b) Mass of the fibers obtained per unit length of precursor material processed as a function of speed of cut.

Polymer-stabilized Palladium Nanoparticles for catalytic membranes: *ad hoc* polymer fabrication.

B. Domènech¹, M. Muñoz¹ and J. Macanás²

Unitat de Química Analítica, Departament de Química, Universitat Autònoma de Barcelona, Campus UAB, 08193 Bellaterra, Barcelona, Spain.

Berta.Domenech@uab.cat

Novel Energy-Oriented Materials Group, Centre d'Investigació en Nanociència i Nanotecnologia CIN2 (ICN-CSIC), Campus UAB, 08193 Bellaterra, Barcelona, Spain.

Jorge.Macanas@cin2.es

Metal nanoparticles (MNPs) are especially effective catalysts because of their relatively large percentage of surface atoms [1,2]. Additionally, these materials often possess unusual electronic properties due to their unique size, which is between the bulk and molecular regimes [3]. For most practical catalytic applications, however, the nanoparticles must be immobilized on solid supports to prevent aggregation and facilitate catalyst recovery [4,5].

Encapsulation by polymers [6] seems advantageous because in addition to stabilizing and protecting the particles, polymers offer unique possibilities for modifying both the environment around catalytic sites and the access to these sites [7-9]. Including nanoparticles inside polymeric membrane would yield to a useful material for process intensification [10,11] since the combination of catalysis and membrane processes may, for instance, change and separate pollutants through a single step. Anyway, it is imperative to adequate the polymeric matrix to the MNPs synthesis and to their final application since the protective polymer not only influences particle size and morphology but can also have a tremendous influence on catalytic activity and/or selectivity.

In this presentation we report the development Pd-MNPs by Intermatrix Synthesis (IMS) [12,13] in asymmetric SPES-C (sulfonated polyethersulphone with Cardo group) membranes as synthetic media. The aim to use SPES-C is to improve of the final nanocomposite properties for catalytic applications such as microfiltration. Up to now, we have optimized the sulfonation degree of the polymer taking into account the following issues: (i) the needed of a high enough ion-exchange capacity (because sulfonic groups act as metal ion binders and nanoreactors) and (ii) the solubility properties of the polymer required for membrane formation by phase inversion procedure (a large degree of sulfonation would cause polymer dissolution).

In Figure 1 a Transmission Electron Microscopy image is shown, where the obtained Pd-MNPs in SPES-C membranes can be seen. Almost spherical small nanoparticles are found with a low degree of aggregation.

The characterization of the catalytic effect of the membrane samples was performed using a reaction model [14] widely used in the evaluation of new catalysts for reactions in aqueous phase: the reduction of p-nitrophenol in presence of sodium borohydride and metallic catalyst (Figure 2.) Quick p-nitrophenol degradation has been observed in batch experiments.

References

- [1] A. Alonso, D. N. Muraviev, J. Macanás, A. Shafir, M. Muñoz, A. Vallribera, D. Prodius, S. Melnic, C. Turta, Dalton Trans., 39 (2010) 2579.
- [2] R. Pool, Science 248 (1990), 1186.
- [3] L.D. Pachón and G. Rothenberg, Appl. Organomet. Chem. 22 (2008), 288
- [4] D.E. Meyer and D. Bhattacharyya, J. Phys. Chem. B 111 (2007), 7142.
- [5] L. Brandao, D. Fritsch, A.M. Mendes and L.M. Madeira, Ind. Eng. Chem. Res. 46 (2007), 5278.
- [6] A.D. Pomogailo, G.I. Dzhardimalieva, A.S. Rozenberg, D.N. Muraviev, J. Nanoparticle Res., 5 (2003) 497.

- [7] C.A. Mirkin, *Small*, **1** (2005), 14.
[8] J.M. Campelo, D. Luna, R. Luque, J.M. Marinas, A.A. Romero, *ChemSusChem*, **2** (2009), 18.
[9] S. Kidambi, J. Dai, J. Li and M.L. Bruening, *J. Am. Chem. Soc.* **126** (2004), 2658.
[10] I.F.J. Vankelecom, *Chem. Rev.*, **102** (2002), 3779.
[11] M. Králik and A. Biffis, *J. Mol. Catal. A: Chem.* **177** (2001), 113.
[12] D.N. Muraviev, P. Ruiz, M. Muñoz, J. Macanás, *Pure Appl. Chem.*, **80**(11) (2008), 2425.
[13] P. Ruiz, M. Muñoz, J. Macanás, C. Turta, D. Prodius, D.N. Muraviev, *Dalton Transactions.*, **39**(7) (2010), 1751.
[14] D.M. Dotzauer, J. Dai, L. Sun and M.L. Bruening, *Nano Lett.* **6** (2006), 2268.

Figures

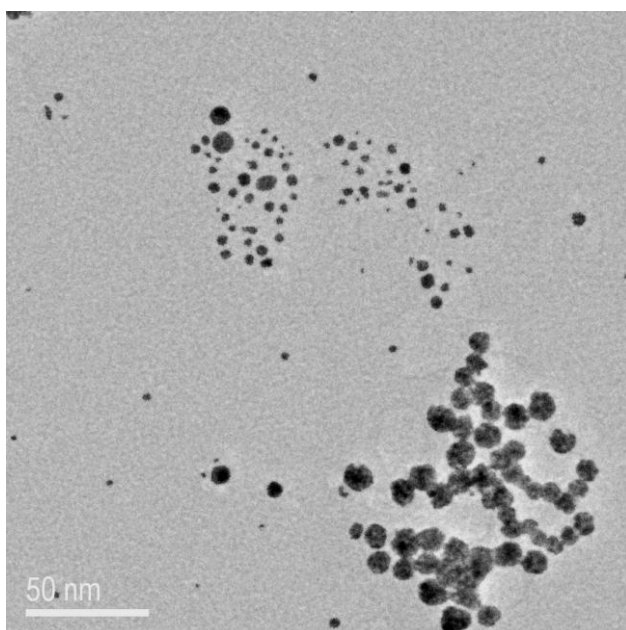


Figure 1: TEM image of Pd-MNPs obtained by IMS inside a SPES-C membrane.

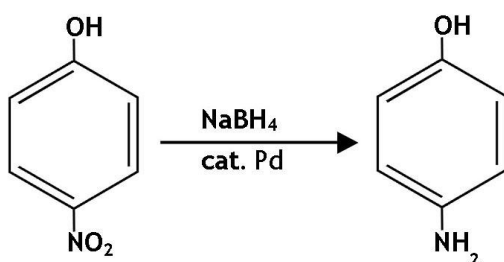


Figure 2: catalytic reduction of p-Nitrophenol in basic media with NaBH₄

Multiplex genetic characterization via noble metal nanoprobos

Gonçalo Doria^{1,*}, João Conde^{1,2}, Miguel Larginho^{1,3} and Pedro Baptista¹

¹CIGMH/DCV, Faculdade de Ciências e Tecnologia, Universidade Nova de Lisboa, Caparica, Portugal;

² Instituto de Nanociencia de Aragón, Universidad de Zaragoza, Zaragoza, Spain;

³ BIOSCOPE/Physical-Chemistry Department, Faculty of Science, University of Vigo, Ourense, Spain;

*Tel/Fax: (+351) 212 948 530; E-mail: doria_go@fct.unl.pt

Cancer is a multigenic complex disease where is usually required that multiple gene loci are characterized simultaneously and/or in association (e.g. tumor suppressor gene TP53, *c-myc* oncogene, BCR-ABL fusion oncogene, among others)^[1,2]. Here, we present the use of noble metal nanoparticles with different compositions in a one-pot multi-color DNA detection strategy for multiplex cancer diagnostic. Synthesis and functionalization with thiol-ssDNA of pure gold and gold-silver alloy nanoparticles was successfully achieved, yielding different nanoprobos with tunable colors and distinct absorption peaks, characteristic of each nanoparticles' surface plasmon resonance. These nanoprobos were combined in a one-pot reaction to allow for the simultaneous differential detection of different nucleic acids sequences related to cancer, following a non-cross-linking method that has been previously developed by our group using gold nanoprobos alone^[3,4,5]. The method is based on the colorimetric comparison of solutions before and after salt-induced nanoprobe aggregation. Only the presence of a complementary target stabilizes the corresponding nanoprobe, preventing aggregation and colorimetric change after salt addition, while the absence of a complementary target leads to the aggregation of nanoprobos with a concomitant color change of solution (Figure 1)^[6].

References

- [1] Afar DE *et al.*, Science, **264** (1994) 424-6;
- [2] Ho JS *et al.*, Mol Cell Biol, **25** (2005) 7423–31;
- [3] Baptista P *et al.*, J Biotechnol, **119** (2005) 111-7;
- [4] Baptista P *et al.*, Clin Chem, **52** (2006) 1433-4;
- [5] Doria G *et al.*, IET Nanobiotechnol, **1** (2007) 53-7.
- [6] Doria G *et al.*, Nanotechnology, **21** (2010) 255101;

Acknowledgements

We thank FCT/MCTES for financial support: PTDC/SAU-BEB/66511/2006; PTDC/EEA-ELC/74236/2006; Nanotruck-Action NanoSciEra+ and CIGMH.

Figures

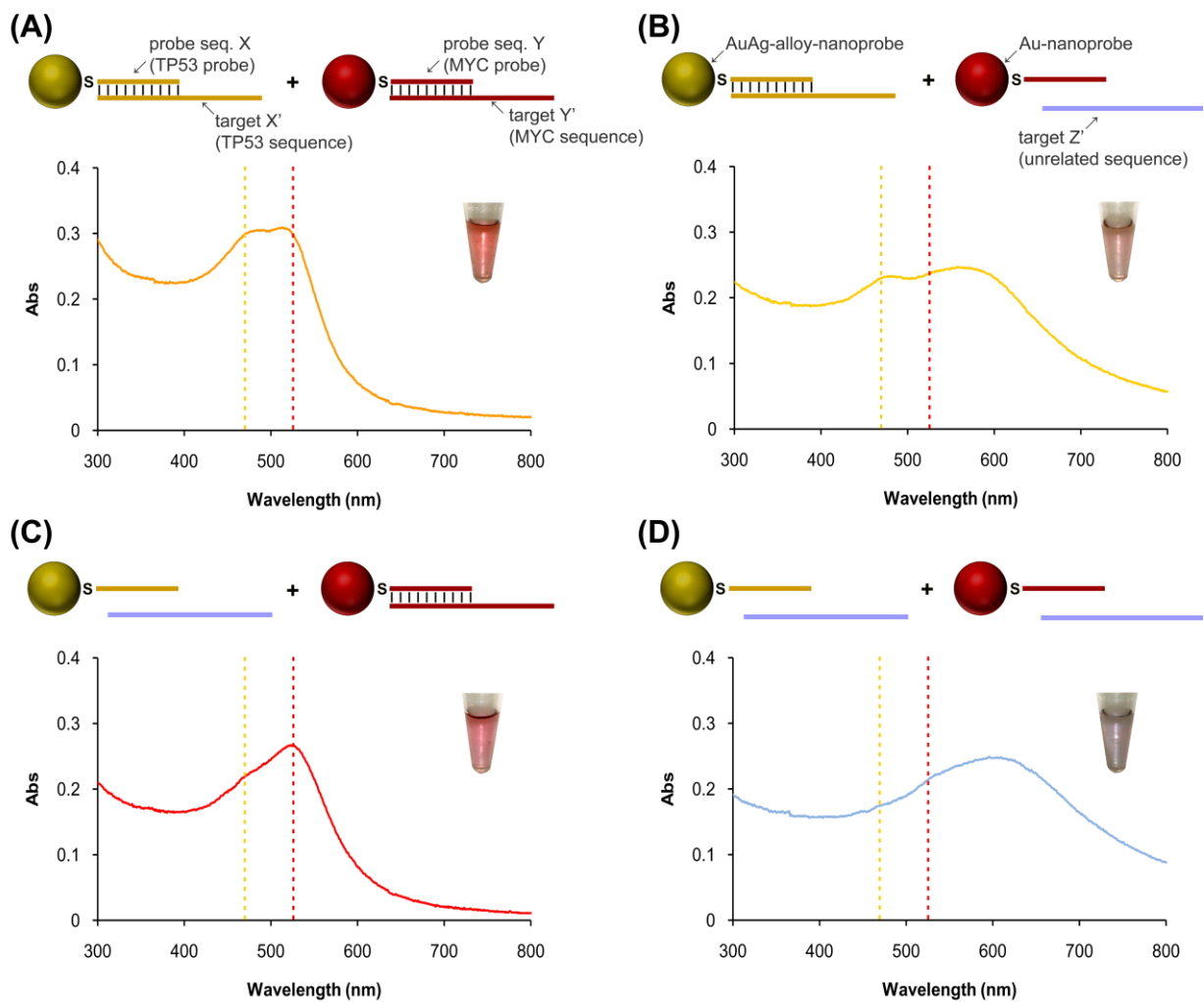


Figure 1 - One-pot colorimetric multi-target detection ^[1]. UV-visible spectrum and digital photograph of AuAg-alloy- and Au-nanoprobe mix in the presence of: (A) complementary targets to both the AuAg-alloy- and Au-nanoprobe; (B) a complementary target to the AuAg-alloy-nanoprobe; (C) a complementary target to the Au-nanoprobe; (D) a non-complementary target to both AuAg-alloy- and Au-nanoprobes. Vertical dashed lines represent the absorption peaks of AuAg-alloy-nanoprobes (orange broken line; 470 nm) and Au-nanoprobes (red broken line; 526 nm) when dispersed in solution.

TiO₂ highly ordered quantum dots prepared by anodization techniques on Si wafer

Jana Drbohlavová^a, Marina Vorozhtsova^a, Radim Hrdý^a, René Kizek^b, Petr Babula^c and Jaromír Hubálek^a

^aBrno University of Technology, Faculty of Electrical Engineering and Communication, Department of Microelectronics, Údolní 53, 602 00 Brno, Czech Republic

^bMendel University in Brno, Faculty of Agronomy, Department of Chemistry and Biochemistry, Zemědělská 1, Brno, Czech Republic

^cUniversity of Veterinary and Pharmaceutical Sciences, Department of Natural Drugs, Palackého 1/3, 612 42 Brno, Czech Republic

drbohla@feec.vutbr.cz, hubalek@feec.vutbr.cz

Quantum dots (QDs) from semiconductor material are very promising candidates for medicinal purposes, mainly as biosensors and labels in biological imaging. QDs exhibit unique physical and optical properties and moreover, there is a possibility of various biomolecules attaching to their surface [1], which allows the detection of DNA and proteins [2, 3].

QDs designed for usage in biological systems are mostly applied in solution (colloidal form) [4, 5]. Nevertheless a demand of deposited QDs on various solid surfaces for biomedical application was also emphasized in some papers [6, 7]. It was found that traditional top-down patterning methods as photolithography and e-beam lithography are time-consuming and expensive processes; therefore there is a demand for new more sophisticated techniques for QDs fabrication [8].

The template-based nanoengineering techniques are probably the most favorable techniques from the price availability point of view. Concerning the templates, many different materials such as porous alumina, polymer gel, surfactant, activated carbon and carbon fiber have been used to synthesize different kinds of nanostructured porous materials. It could be very promising and interesting to use the template-based techniques for fabrication of QDs as a sensor array for in situ biosensing applications mainly due to the simplicity of biomolecules detection [9]. Thanks to this sensors arrangement, where each sensor can be created from QDs emitting the light at the different wavelength, it could be possible to easily detect many different biomolecules at the same time.

This work focuses on developing TiO₂ planar nanostructures (quantum dots, eventually nanowires) for detection of various biomolecules (DNA, proteins) in vitro, which may replace currently used slow and low-sensible methods of detection in medicine. The new way of QDs synthesis is employing of electrochemical deposition through high-ordered nanoporous ceramic template, which belongs to low-cost and rapid preparation technique compared to traditionally used ones, photolithographic or epitaxial depositions. Ordered arrays of titania nanodots can be achieved by successive anodization and utilization of different anodizing conditions of evaporated aluminium (2 μm) and sputtered titanium (200 nm) layers in the same electrolyte. We observed the sulphuric acid solution used as electrolyte provides smaller dimensions of pores and hence of QDs compared to oxalic acid (30 nm vs 50 nm). Finally, the titania QDs were heat treated in order to obtain thermodynamically stable phase, anatase and the anodic alumina mask was removed by etching in mixture of H₃PO₄ and CrO₃ at 60 °C. The following figures (Fig. 1, Fig. 2) represent the nanostructures deposition process using anodically prepared template. Raman spectroscopy measurement will be used to characterize the titania nanodots crystallographic composition. Fluorescence spectra and AFM characterization of prepared samples will be discussed.

The financial support from the grants GACR P102/10/P618 and KAN 208130801 is highly acknowledged.

References

- [1] Sapsford KE, Pons T, Medintz IL and Mattoussi H, *Sensors*, **6** (2006) 925.
- [2] Huang FH and Chen GN: *Spectrochimica Acta Part a-Molecular and Biomolecular Spectroscopy*, **70** (2008) 318.
- [3] Tansil NC and Gao ZQ: *Nano Today*, **1** (2006) 28.
- [4] Walling MA, Novak JA and Shepard JRE: *Int. J. Mol. Sci.*, **10** (2009) 441.
- [5] Yong KT: *Nanotechnology*, **20** (2009) 10.
- [6] Bodas D and Khan-Malek C: *Sens. Actuator B-Chem.*, **128** (2007) 168,
- [7] Ma Q, Song TY, Yuan P, Wang C and Su XG: *Colloids and Surfaces B-Biointerfaces*, **64** (2008) 248.
- [8] Dai CA, Wu YL, Lee YH, Chang CJ and Su WF: *J. Cryst. Growth*, **288** (2006) 128.
- [9] Drbohlavova J, Adam V, Kizek R and Hubalek J: *Int. J. Mol. Sci.*, **10** (2009) 656.

Figures

Fig. 1: SEM image of hexagonal pores in alumina template prepared by anodization

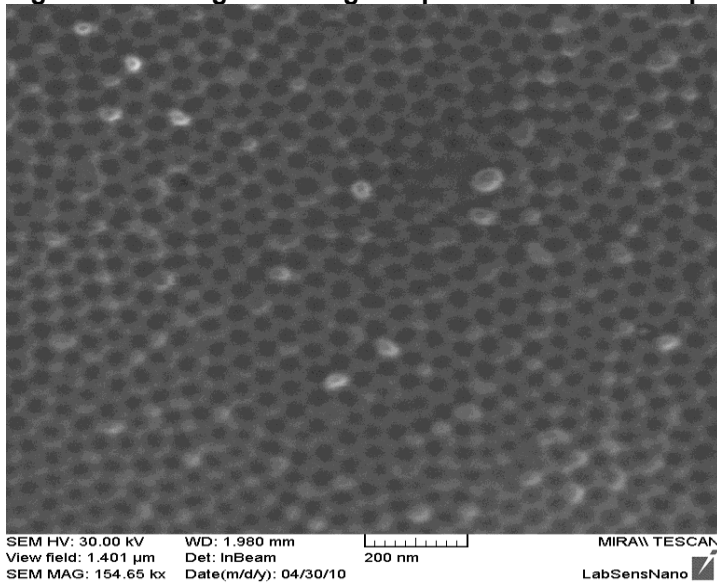
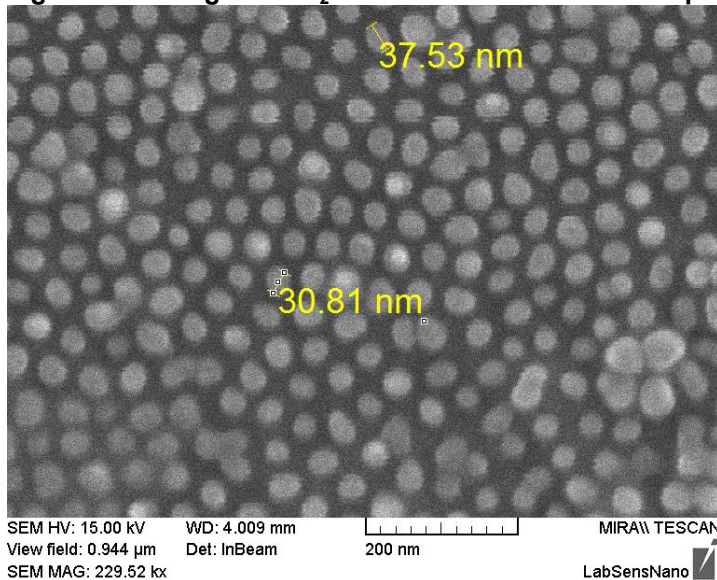


Fig. 2: SEM image of TiO₂ nanodots after alumina template dissolving



CdTe quantum dots based chemical nanosensors

Abel J. Duarte¹, Maria do Carmo V.F. Vaz¹ e Joaquim C.G. Esteves da Silva²

¹REQUIMTE, Instituto Superior de Engenharia do Porto, R. António Bernardino Almeida 431, 4200-072 Porto, Portugal. E-mail: ajd@isep.ipp.pt

²Centro de Investigação em Química, Departamento de Química e Bioquímica, Faculdade de Ciências da Universidade do Porto, Rua Campo Alegre 687, 4169-007 Porto, Portugal. E-mail: jcsilva@fc.up.pt

Quantum dots (QDs) are semiconductor alloy crystal with dimensions on the order of nanometers that show remarkable fluorescent properties with a relatively narrow emission spectrum and high photostability [1-3]. CdTe QDs are composed of atoms of cadmium and tellurium and have interesting physical and chemical properties that can be successfully used as chemical sensors if they are stabilized and functionalized with selected chemical substances [1-4]. The synthesis of QDs in aqueous media has improved its solubility in water and decreasing the toxicity. Soluble fluorescent nanomaterials are highly promising nanosensors that can be used for chemical and/or biochemical analysis and in vivo bioimaging [1-6].

The stabilization of QDs is usually done with a bifunctional organic molecule, S-R, in which one group is a thiol or mercapto, which binds to the semiconductor, and other functional group confers water solubility. These QDs can be made even more stable by passivation for depositing another semiconductor with a bigger band-gap energy, such as ZnS.

This communication presents CdTe QDs synthesized in water using mercaptoacetic acid as stabilizing agent with and without passivation with ZnS. Besides the morphological characteristics of the nanomaterials and their photophysical properties their utilization as pH nanosensors will be discussed.

Acknowledgements: Financial support from Fundação para a Ciência e Tecnologia (Lisboa, Portugal) (FSE-FEDER) (Project PTDC/QUI/71001/2006) and (Project PTDC/QUI/71336/2006) is acknowledged.

References

- [1] Leitão, J.M.M.; Gonçalves, H.M.R.; Mendonça, C.; Esteves da Silva, J.C.G., *Analytica Chimica Acta*, 628 (2008) 143-154.
- [2] Gonçalves, H.M.R.; Mendonça, C.; Esteves da Silva, J.C.G., *Journal of Fluorescence*, 19 (2009) 141-149.
- [3] Maule, C.D.; Gonçalves H.M.R.; Mendonça, C.; Sampaio, P.; Jorge, P.A.S.; Esteves da Silva, J.C.G., *Talanta*, 80 (2010) 1932–1938.
- [4] Campos, B.B.; Algarra, M.; Alonso, B.; Casado, C.M.; Esteves Da Silva, J.C.G., *Analyst*, 134 (2009) 2447-2452.
- [5] Gonçalves, H.M.R.; Esteves da Silva, J.C.G., *Journal of Fluorescence*, (2010) DOI: 10.1007/s10895-010-0652-y.
- [6] Gonçalves, H.M.R.; Duarte, A.J.; Esteves da Silva, J.C.G., *Biosensors and Bioelectronics*, (2010) DOI: doi:10.1016/j.bios.2010.07.018.

Controllable Synthesis of ZnO Nanoparticles and Flower-like by Microwave Irradiation as Highly Sensitive Ethanol Sensors

N. F. Hamedani¹, A.R. Mahjoub*¹, A. A. khodadadi², Y. Mortazavi²

¹Department of Chemistry, Tarbiat Modares University, Tehran, Iran.

²School of Chemical Engineering, University of Tehran, Tehran, Iran.

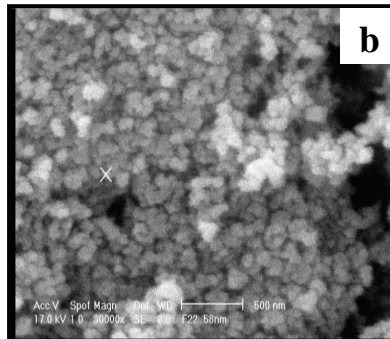
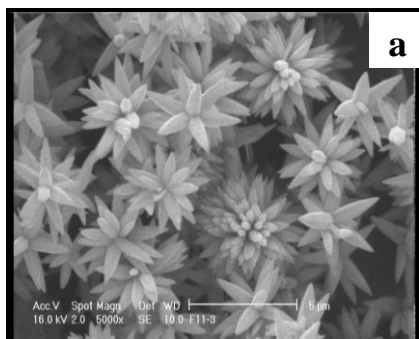
Email:mahjouba@modares.ac.ir

Metal oxide semi conductors play very important roles in many areas of chemistry, physics and material science. Among oxide semiconductors, ZnO has attracted much attention because of its basis of several properties such as n-Type semi conducting compound, UV absorber and gas sensor [1, 2]. Recently, the studies reveal that the performances of ZnO are closely depending on its morphology. Thus several different methods have been reported for the preparation ZnO nano structures including nano rods, nano belts, nano sheets and flowerlike structures. Compared with the conventional heating, microwave irradiation has unique features such as rapid heating, short reaction time, highly reaction rate and energy storage [3].

In gas sensor application ZnO has some advantages because of its high Sensivity, selectivity and chemical stability [4]. In this study ZnO nano particles and flowerlike have been successfully prepared by a fast, simple and controllable microwave-assisted method using zinc acetate as the starting materials and water as solvent under microwave irradiation for 2 minutes. The morphology, shape and size of the synthesized ZnO samples were determined by using X-ray powder diffraction (XRD) and scanning electron microscopy (SEM). The morphology was controlled by adapting experimental conditions such as pH and power of microwave. In consider to sensing properties ZnO nano particles sensors exhibit higher response to 500 ppm ethanol in 350 C.

References

- [1] N.S. Ramgir, I.S. Mulla, K.P. Vijayamohanam, J. Sens. Actuators B., 708, (2005) 107.
- [2] H.Gong, J.Q.Hu, J.H.W ang, C.H.Ong, F.R.Zhu, J. Sens. Actuators B., 115, (2006) 247.
- [3] T.Krishnakumar, R.Jayaprakash, N.Pinna, N.Donata, A.Bonavita, G.Micali, G.Neri, J. Sens. Actuators B., 143, (2009).
- [4] A.B.Bodade, A.M. Bende, G.N. Chaudhari, J. Vaccum, 82, (2008)588.



SEM images of ZnO (a) Flower-like (b) Nanoparticles

Biosynthesis of silver nanoparticles by *Aspergillus oryzae* and *Penicillium chrysogenum*

Sara Fernandes, Manuel Mota and Nelson Lima

IBB-Institute for Biotechnology and Bioengineering, Centre of Biological Engineering, Universidade do Minho, Campus de Gualtar, 4710-057, Braga, Portugal

sara.fernandes@deb.uminho.pt

Development of reliable and eco-friendly processes for synthesis of metallic nanoparticles is an important step in the field of application of nanotechnology. Also the importance of bactericidal nanomaterials study due to the increase in new resistant strains of bacteria and fungi against most potent antibiotics has promoted research in the well known activity of silver ions and silver-based compounds, including silver nanoparticles. For this reason, there is an essential need to develop environmentally benign procedures for synthesis of silver nanoparticles for commercialization purposes. In relation to other microorganisms fungi present key characteristics such as tolerance and metal bioaccumulation abilities that are advantageous for production of nanoparticles.

In this study, silver nanoparticles were synthesised extracellularly from silver nitrate using the fungi *Aspergillus oryzae* MUM 97.19 and *Penicillium chrysogenum* MUM 03.22, supplied by Micoteca da Universidade do Minho (MUM) fungal culture collection, and the morphology of the nanoparticles was characterised by Scanning Electron Microscopy (SEM). In addition, the potential to manipulate key parameters, which control growth and other cellular activities, to achieve an optimised production of nanoparticles were investigated. A complete screening of different pH, temperature and salinity conditions was conducted. The main results obtained will be presented and discussed.

Microinjection moulding of nanocomposites with modified carbon nanotubes: correlation between dispersion and electrical conductivity

Tânia Ferreira¹, Andrea Cunha¹, Maria C. Paiva¹, António J. Pontes¹

¹ Institute for Polymers and Composites/I3N, University of Minho, Campus of Azurém, 4800-058
Guimarães, Portugal
ex1931@dep.uminho.pt

Introduction

Carbon nanotubes (CNT) exhibit unique thermal, electrical and mechanical properties, and their nanocomposites have attracted the attention of many scientists due to the strong application potential in electronics, chemical and biological sensing and reinforced composite materials[1]. The processes of micro molding (MIM) and microinjection molding (μ IM) are the most efficient and cost-effective processes for the large-scale production of thermoplastic nanocomposite microparts with low reinforcement content and exceptional electrical properties.

The present work reports the dispersion of CNT in polyamide 6 (PA 6) for the production of nanocomposites with different CNT content using μ IM. The CNT were used as received and chemically functionalized. The nanocomposites were micro injection moulded and the electrical and mechanical properties of the specimens obtained were measured. The dispersion, distribution and interface of the CNT in the PA 6 were analysed.

Experimental

The CNT (Nanocyl NC 7000) were functionalized using the 1,3-dipolar cycloaddition reaction of an azomethine ylide to the CNT, generating pyrrolidine groups at the surface [2], under solvent-free conditions.

The nanocomposites with polyamide 6 (Badamid®B70) and pure or functionalized CNT were prepared in a prototype mini-twin screw extruder under different processing conditions; small specimens were obtained by microinjection moulding in a Boy 12 equipment (Fig. 1).

The nanotube agglomerate size, distribution and dispersion were measured using optical microscopy (OM) and the CNT/polymer interface was observed by scanning SEM. The electrical resistivity of the composites was measured. The specimens were tensile tested using a microtester equipped with a load cell of 1 kN.

Results

The images of the composites obtained by OM allowed the statistical study of CNT agglomerate size and distribution, and CNT dispersion (Fig. 2). The SEM images evidence the effect of the chemical modification of the CNT, illustrating the improvement of the CNT interface in PA 6 in the case of functionalized CNT (Fig. 3). The improvement in CNT dispersion affected the electrical and mechanical properties of the composites, as illustrated in Table 1 for the composites with 1,5% wt of as received and functionalized CNT. As expected, the composites of PA 6 with 1,5-4,5% CNT are semiconductors, and the conductivity increased with the CNT content. The addition of pure CNT to PA 6 increased the elastic modulus and the increase was proportional to the amount of CNT incorporation. Samples with functionalized CNT presented the higher values for elastic modulus.



Fig. 1 - Microinjection moulded composite specimens: a) tensile and b) impact.

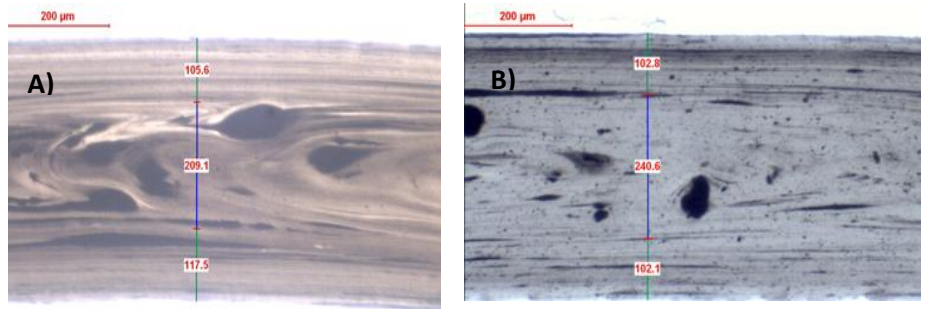


Fig. 2 – Examples of optical microscope images and statistical study for pure A) and functionalized B) 1,5% CNT nanocomposites for tensile specimens.

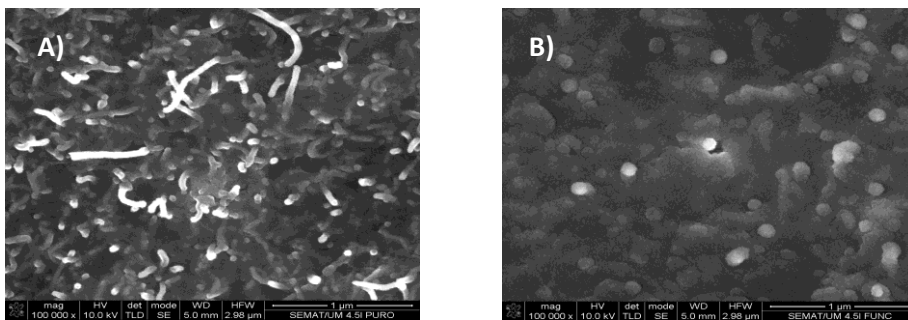


Fig. 3 – SEM images for pure A) and functionalized B) 4,5% CNT nanocomposites.

Table 1 – CNT dispersion results and electrical and mechanical properties for the nanocomposites with 1,5% of pure CNT and functionalized CNT (FCNT).

Composite	Number of agglomerates	Average area (μm^2)	Electrical conductivity ($\text{S}\cdot\text{m}^{-1}$)	Elastic Modulus (MPa)
CNT	94	3017 ± 682	$7,3 \times 10^{-04}$	$2,66 \pm 0,42$
FCNT*	242	839 ± 151	$1,7 \times 10^{-04}$	$3,99 \pm 0,64$

*The CNT content in FCNT nanocomposites is 1,26%, the remaining weight is due to the functional groups at the CNT surface.

Acknowledgements

The authors acknowledge the financial support from FCT through project POCI/QUI/59835/2004 and the PhD grant to T. Ferreira (SFRH/BD/39119/2007).

References

- 1 – Baughman RH, Zakhidov AA, de Heer WA. Carbon nanotubes—the route toward applications. *Science* 2002;297:787-92.
- 2 - Araújo, R. F., Paiva, M. C., Proença, M. F., Silva, C. J. R. *Comp. Sci. Technol.* 2007, 67, 806–810.

Serial MTJ sensors based on MgO in bridge configuration for in-chip current field detection

Raquel Flores^{1,2,a}, F. Cardoso^{1,2}, R. Ferreira^{1,3}, S. Cardoso^{1,2}, P. P. Freitas^{1,2}, C. Reig⁴

¹INESC-Microsistemas e Nanotecnologias (INESC-MN) and IN-Institute for Nanosciences and Nanotechnologies, Rua Alves Redol, 9 - 1, 1000-029 Lisboa Portugal

²Physics Department, Instituto Superior Técnico-Universidade Técnica de Lisboa, 1049-001 Lisbon, Portugal

³Iberian International Nanotechnology Laboratory (INL), Braga, Portugal

⁴Department of Electronic Engineering, Universitat de Valencia, Av. Dr. Moliner, 50 - Burjassot, 46100 Valencia (Spain)

^aflores.rakel@gmail.com

Nowadays and more than ever, control and precision regarding electronic circuits became very important, especially concerning microelectronic devices where electrical current, power and energy measurements have been a matter of concern. New precise, integrable, low power consumption and low cost devices are demanded and they are mainly needed in integrated circuits (IC), systems-on-chip (SOC), micro-electromechanical systems (MEMS), among others.

Magnetic tunnel junctions (MTJ) have been currently used as sensors for electrical currents measurements in IC. In addition, these sensors have also been used in Wheatstone bridge configuration for low current measurements [1]. Current lines are integrated on top of the sensor.

In this work a new configuration is being used: instead of a Wheatstone bridge of 4 singular sensors, we are using a bridge of 4 series of MTJ's. Each bridge's branch has 380 sensors connected in series. The design was projected using CAD and besides bridges, isolated sensors and isolated series were also designed as reference (Fig.1). MTJ's structure was deposited by magnetron sputtering in Nordiko 2000 sputtering system [2] and microfabricated using photolithography by direct write laser. Each active sensing element has an area of $2 \times 30 \mu\text{m}^2$.

Devices were characterized using an external magnetic field in the range $[-140, 140] \text{Oe}$. An isolated individual MTJ sensor presented a TMR of 101.7% for a 5.0mV of bias voltage, with a linear range between 0 Oe and 50 Oe and $R \times A = 90.9 \text{ k}\Omega\mu\text{m}^2$. A sensibility of $13.05 \Omega/\text{Oe}$ was achieved for this sensor (Fig. 2).

Concerning a bridge (4 MTJ series of 380 sensors) it was obtained a TMR of 56.54% using a bias current of $5.0 \mu\text{A}$. Output had a linear response between 0 Oe to 55 Oe, presenting a sensibility in this range of $2.29 \text{ k}\Omega/\text{Oe}$ (Fig. 3).

Using MTJ elements connected in series increases the total magnetic volume of the sense layer ($\sim N \times V_{\text{free}}$) and thus allows using bias currents as large as needed, up to several amperes, which means a higher output of the sensor for the same input when comparing to single sensors. It also has the advantage of getting a lower noise level in measurements.

References

[1] "Magnetic Field Sensors Based on Giant Magnetoresistance (GMR) Technology: Applications in Electrical Current Sensing", Càndid Reig, María-Dolores Cubells-Beltrán, Diego Ramírez, *Sensors* 2009, vol9, pp. 7919-7942, October 2009.

[2] "Effect of CoFeB thickness and shape anisotropy on the transfer curves of MgO Magnetic Tunnel Junctions", P.Wisniowski, S.Cardoso, P.P.Freitas, *J.Appl.Phys.*, vol.103, pp.07A910-07A912, April 2008.

Figures

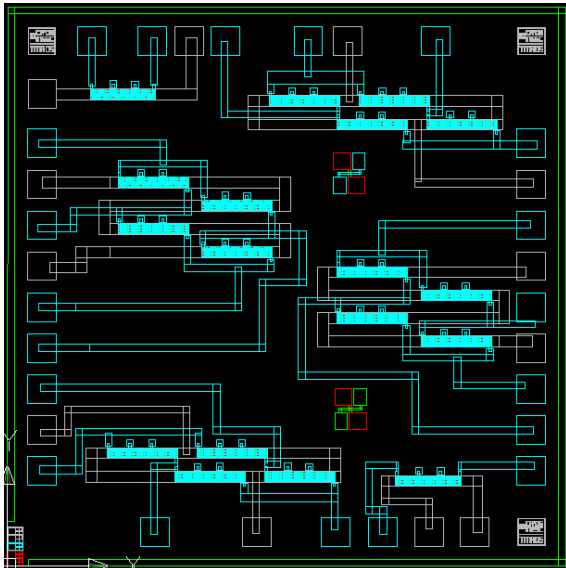


Figure 1: Mask design

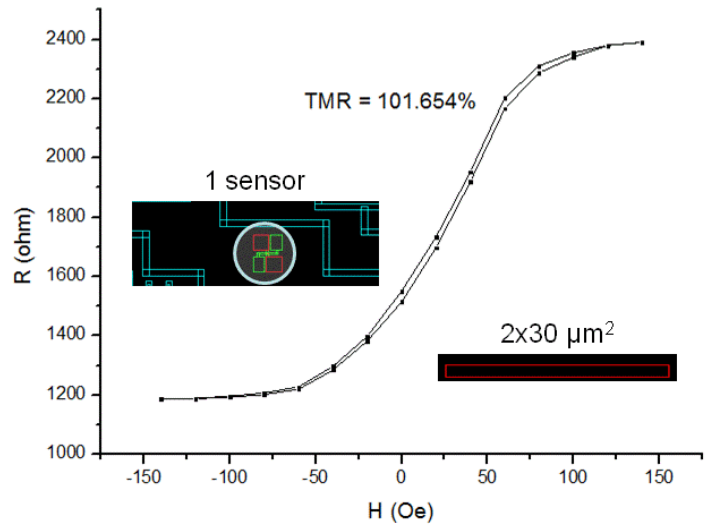


Figure 2: Isolated sensor output

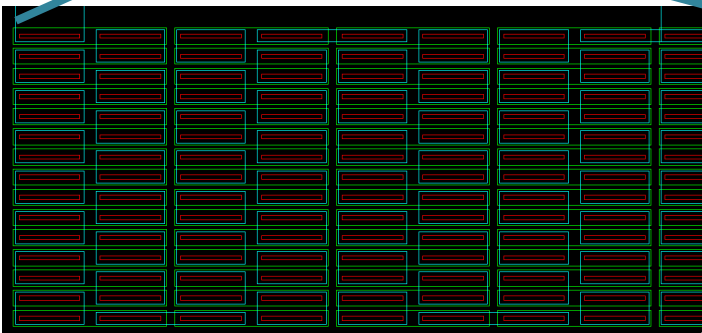
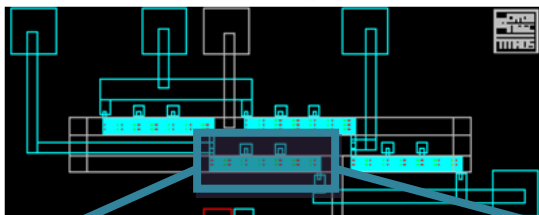
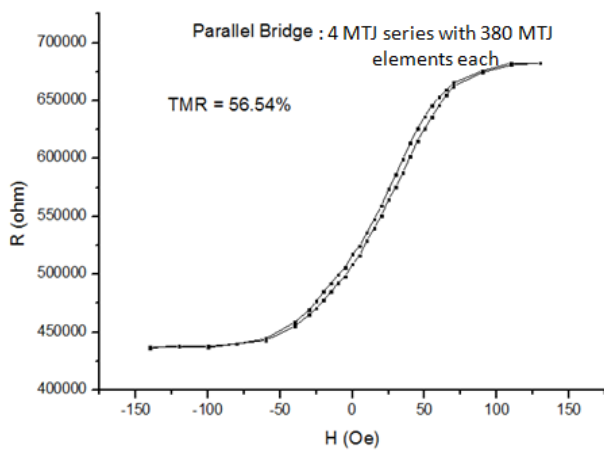


Figure 3: Bridge (4 MTJ series) output

TiWN2 150Å
Ta 50Å
Ru 50Å
CoFeB 100Å
MgO 17Å
CoFeB 30Å
Ru 9Å
CoFe 20Å
MnPt 200Å
Ta 30Å
Ru 180Å
Ta 50Å
Al2O3 600Å
Si

Figure 4: Sample structure

Core@Shell Fluorescent-Magnetic Glyco-ferrites as Specific Targeted Contrast Agents for Magnetic Resonance Imaging

Juan Gallo, Isabel García, Nuria Genicio, Daniel Padro, Soledad Penadés

Magnetic resonance imaging (MRI) has been used for several years for non-invasive medical diagnostic. Until now its use in clinics has been based on non-specific contrast agents, but nowadays a fast shift towards specific targeted agents is taking place. In order to prepare these specific probes a careful design of the new contrast agents is needed. Our group has experience in preparing gold and magnetic nanoparticles for their application as T₁ and T₂ MRI contrast agents.^{1,2}

We present here superparamagnetic glyconanoparticles designed to specifically label cells, tissues or organs. For the preparation of the magnetic nanoparticle platform we have selected the thermal decomposition methodology³ followed by deposition of a gold shell⁴ in non-polar solvents. To render these nanoparticles water soluble a ligand exchange reaction with amphiphilic sugar conjugates and carboxylic linkers was performed. The carbohydrates confer the nanoparticles interesting properties as biocompatibility, lack of immunogenicity and reduction of non-specific adsorption. To the carboxylic group protein G and a fluorescent dye were coupled. Protein G guarantees the well-oriented capture of antibodies. High specificity was achieved by choosing antibodies (Ab) as targeting molecules.

Finally the ability of these glyconanoparticles to label specifically cell populations was tested both by MRI and by fluorescence techniques with two different cell lines and with a complex real biological media as blood.

1. Marradi, M.; Alcantara, D.; de la Fuente, J. M.; Garcia-Martin, M. L.; Cerdan, S.; Penades, S., Paramagnetic Gd-based gold glyconanoparticles as probes for MRI: tuning relaxivities with sugars. *Chem Commun (Camb)* **2009**, (26), 3922-4.
2. de la Fuente, J. M.; Alcantara, D.; Eaton, P.; Crespo, P.; Rojas, T. C.; Fernandez, A.; Hernando, A.; Penades, S., Gold and gold-iron oxide magnetic glyconanoparticles: synthesis, characterization and magnetic properties. *J Phys Chem B* **2006**, 110, (26), 13021-8.
3. Sun, S.; Zeng, H.; Robinson, D. B.; Raoux, S.; Rice, P. M.; Wang, S. X.; Li, G., Monodisperse MFe₂O₄ (M = Fe, Co, Mn) nanoparticles. *J Am Chem Soc* **2004**, 126, (1), 273-9.
4. Wang, L.; Luo, J.; Fan, Q.; Suzuki, M.; Suzuki, I. S.; Engelhard, M. H.; Lin, Y.; Kim, N.; Wang, J. Q.; Zhong, C. J., Monodispersed core-shell Fe₃O₄@Au nanoparticles. *J Phys Chem B* **2005**, 109, (46), 21593-601.

Crystallographic Characterization of ZnO Thin Films by Electron Backscattered Diffraction

C.B. Garcia, C.J Tavares, L. Rebouta, E. Ariza
Universidade do Minho, Campus de Azurém 4800-058, Guimarães, Portugal
ctavares@fisica.uminho.pt

Zinc Oxide, ZnO, has been used in numerous applications [1] as solar cells [2], window material for displays, transparent high power electronics, transducers, piezoelectric, UV light emitters, varistors [3] and acoustic wave devices [4]. The performance of these applications depends on the degree of crystallinity; the crystals have to render a high quality. Preferred orientation or crystallographic texture or has long been known to powerfully influence material properties [5].

The purpose of this work is to show the crystallographic characterization of the ZnO thin films produced by magnetron sputtering. Electron backscattered diffraction (EBSD) has been used to characterize the crystallography of these coatings, deposited on glass. Combined with a Field Emission Gun Scanning Electron Microscope (FEG-SEM), EBSD is a technique that allows the crystallographic study correlated with the surface and chemical properties. Moreover, it enables the analysis of microstructure and texture [6], grain size [7], grain orientation, grain boundary and misorientation [8], phase identification [9] and strain [10].

References:

- [1] Hamid, M., et al., *Deposition and characterization of ZnO thin films from a novel hexanuclear zinc precursor*. Inorganica Chimica Acta, 2008. **361**(1): p. 188-194.
- [2] Keis, K., et al., *Nanostructured ZnO electrodes for dye-sensitized solar cell applications*. Journal of Photochemistry and Photobiology A: Chemistry, 2002. **148**(1-3): p. 57-64.
- [3] Viswanath, R.N., et al., *Preparation and characterization of nanocrystalline ZnO based materials for varistor applications*. Nanostructured Materials, 1995. **6**(5-8): p. 993-996.
- [4] Wu, M.S., et al., *Low-loss ZnO optical waveguides for SAW-AO applications*. Ultrasonics, Ferroelectrics and Frequency Control, IEEE Transactions on, 1989. **36**(4): p. 442-445.
- [5] Adam J. Schwartz, M.K.a.B.L.A., *Electron Backscatter Diffraction in Materials Science*. 1^a ed. 2000: Kluwer Academic/Plenum Publishers.
- [6] Petrov, R., et al., *Microstructure and texture of a lightly deformed TRIP-assisted steel characterized by means of the EBSD technique*. Materials Science and Engineering: A, 2007. **447**(1-2): p. 285-297.
- [7] Humphreys, F.J., *Characterisation of fine-scale microstructures by electron backscatter diffraction (EBSD)*. Scripta Materialia, 2004. **51**(8): p. 771-776.
- [8] Randle, V., H. Davies, and I. Cross, *Grain boundary misorientation distributions*. Current Opinion in Solid State and Materials Science, 2001. **5**(1): p. 3-8.
- [9] Small, J.A. and J.R. Michael, *Phase identification of individual crystalline particles by electron backscatter diffraction*. Journal of Microscopy, 2001. **201**(1): p. 59.
- [10] Hurley, P.J. and F.J. Humphreys, *The application of EBSD to the study of substructural development in a cold rolled single-phase aluminium alloy*. Acta Materialia, 2003. **51**(4): p. 1087-1102.

Figures:

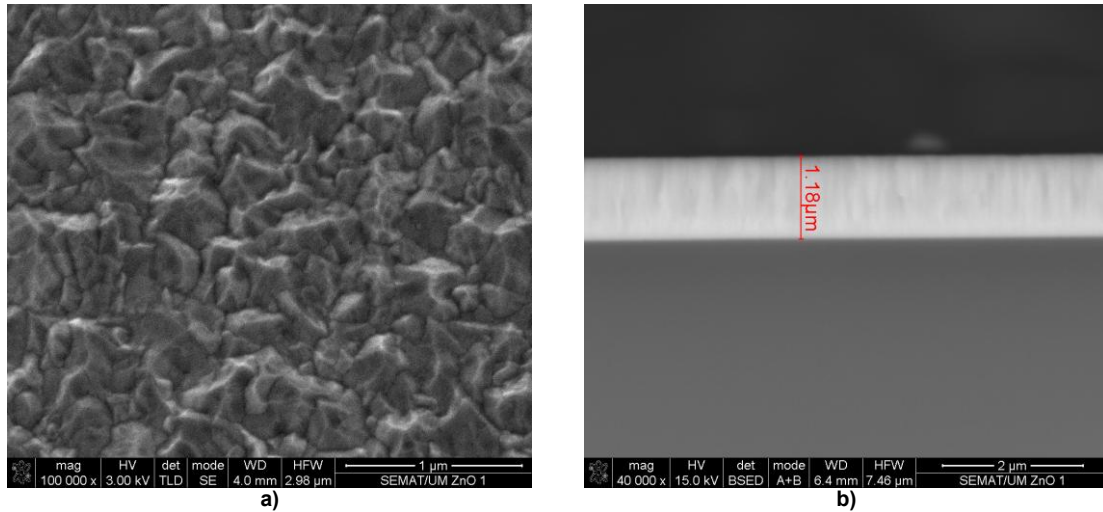


Figure 1 – SEM micrographs of the a) surface morphology and its b) cross-section for a ZnO thin film.

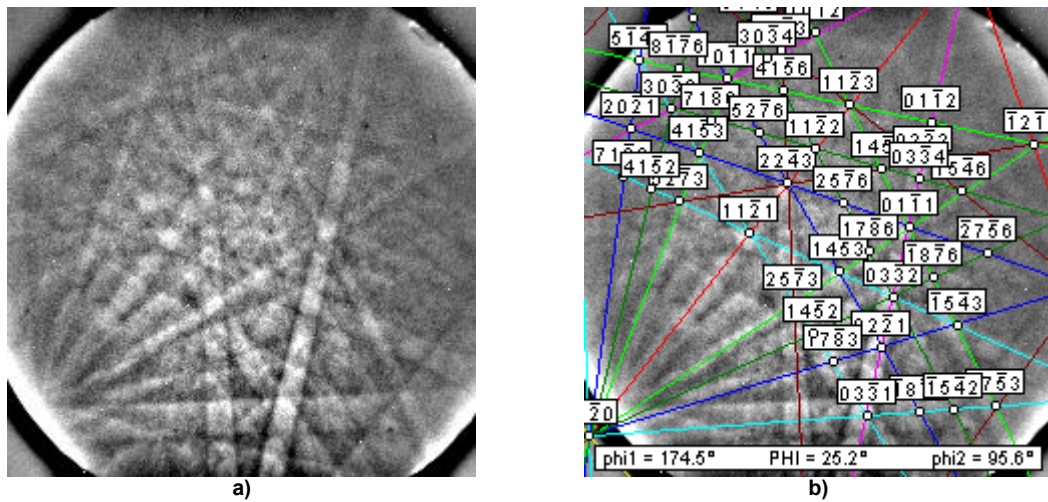


Figure 2 - a) Diffraction Pattern with characteristic Kikuchi Bands and b) respective indexing for a ZnO thin film. The Images were acquired by means of a EBSD detector coupled to a FEG-SEM microscope. Indexing was carried out using the TSL OIM software.

Acknowledgement:

The authors kindly acknowledge the financial support from the Portuguese FCT scientific program for the National Network of Electron Microscopy (RNME) REDE/1511/RME/2005.

Enhanced emission and tunability in self-assembled photonic crystals by hybrid photonic-plasmonic modes

M. López-García⁽¹⁾, J.F. Galisteo-López⁽¹⁾, A. Blanco⁽¹⁾, C. López⁽¹⁾, **A. García-Martín**⁽²⁾

(1) Instituto de Ciencias de Materiales de Madrid (CSIC), c/ Sor Juana Inés de la Cruz 3, 28049, Cantoblanco, (Madrid) Spain

(2) Instituto de Microelectrónica de Madrid (CSIC), c/ Isaac Newton 8, 28760, Tres Cantos, (Madrid) Spain

antonio@imm.cnm.csic.es

Tunability is challenging in photonics. The possibility to either passively or actively modify the optical properties of photonic devices opens new applications especially in sensing and light emitting devices. Among all the structures suitable to be implemented as tuning devices, photonic and plasmonic crystals have become two of the most powerful techniques. Recently, coupling between both kinds of structures has shown to provide exceptional properties especially concerning light emission control at visible and near infrared range [1]. From this point of view, more affordable implementations compared to usual lithographic techniques has been proposed making use of the high quality self-assembled photonic crystals fabrication methods. By growing a monolayer of polystyrene spheres (diameter size similar to working wavelength) on a gold substrate it is possible to obtain hybrid photonic-plasmonic resonances coupling [2]. Modal distribution of those hybrid modes is largely dependent on the lattice parameter as well as on the filling fraction of the monolayer of spheres. In addition, if an emitter is placed in the field confinement region for one given mode, emission can be enhanced as well as tuned to the required frequency by choosing the appropriate sphere diameter.

In this work we present an easy implementation method to tune the modal distribution of that system by homogeneously reduce sphere diameter while lattice parameter is kept constant. Applying oxygen plasma etching for a very accurate controlled time we have obtained control over filling fraction (ff) of the photonic crystal. Reductions were performed from the as-grown close packed ($ff = 0.52$) to largely reduced sphere size ($ff < 10$) while quality of the photonic lattice was shown to keep very high. Both experimental and theoretical study of the optical response was performed in normal incidence reflectance. Modes of the system (shown as large dips in reflectance) largely blueshift with sphere reduction, especially those with waveguided character. Sensibility of mode spectral position to filling fraction variations was investigated for 1 μm diameter polystyrene spheres by reflectance measurements in diameter reduction steps as low as 10 nm. Almost linear blueshift was observed for every mode. Numerical simulations for reflectance have shown good agreement with experimental results. Field profile into the structure was studied in order to evaluate how changes on sphere diameter affect mode shape. Larger changes were found for waveguided-like modes compared to plasmonic ones as would be expected from studies reported in bibliography for these structures.

As a step forward, changes on emission distribution with filling fraction was studied. To do that, red dye doped PS 520 nm diameter spheres (emission maxima at aprox. 590 nm) were grown on gold substrate. Several steps on sphere reduction were performed and changes for emission maxima were measured typically happening at the same spectral position were a dip in reflectance is shown. It was found that, as expected, emission spectrum was blueshift in the same amount that was is monitorize for reflectance. This provides a proof of principle of tuning of the emission peaks to the required spectral position while the structural modification is very accurately monitorize by normal reflectance measurements.

This results demonstrate that this fine tuning process could be used for passive or active devices leading to high performance but low cost structures as for example biosensors or OLED.

References

[1] R.F Oulton, V.J. Sorger, T. Zentgraf, R. Ma, C. Gladden, L. Dai, G. Bartal, X. Zhang, *Nature* **461** (2009) 629.

[2] R. M. Cole, Y. Sugawara, J. J. Baumberg, S. Mahajan, M. E. Abdelsalam, P. Barlett. *Phys. Rev. Lett.* **97** (2006) 137401.

Figures

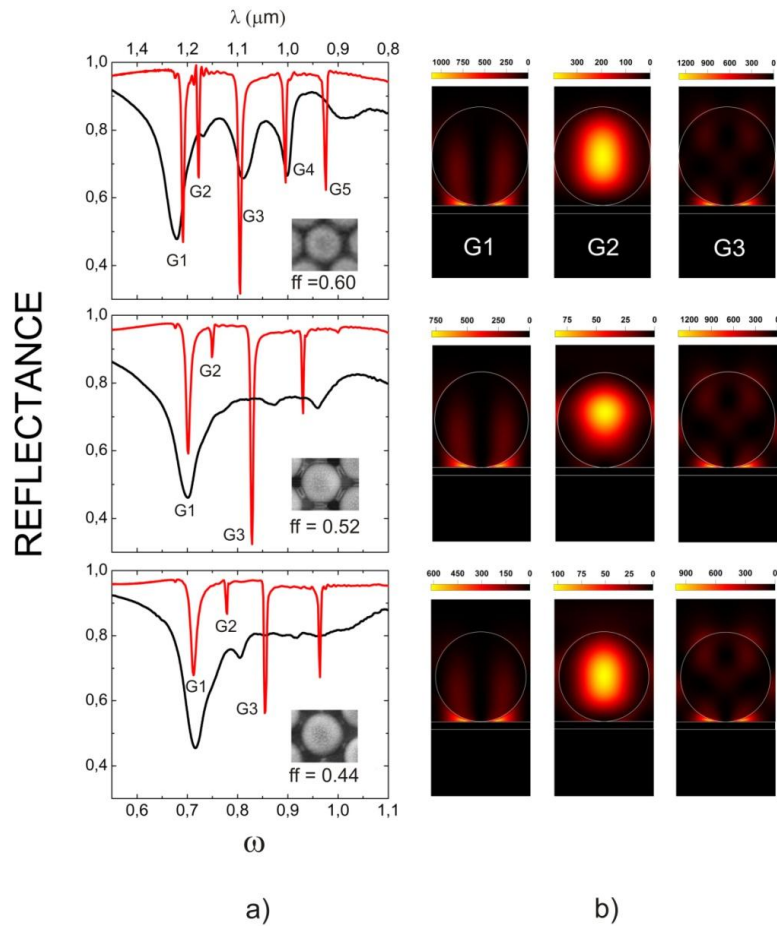


Figure 2. a) Normal incidence reflectance for three different filling fractions. Top to bottom: $ff=0.6$, $ff=0.52$, $ff=0.44$ corresponding to $\gamma=1$, $\gamma=0.95$ and $\gamma=0.9$ respectively. Experimental (black) and theoretical spectra (red) are presented. b) Total field intensity distribution and its evolution with sphere resizing for the first three modes in the left panel.

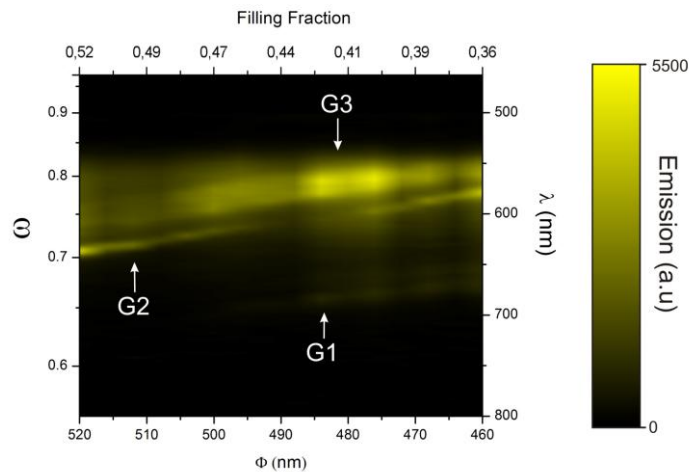


Figure 2. Emission (in arbitrary units) contour plot for a monolayer of 520 nm dye doped PS spheres in a continuous filling fraction reduction process. Oxygen plasma etching was carried out from the close packed scenario ($ff = 0.52$) to a final filling fraction of $ff = 0.36$.

Modelling chemical nanosensor devices based on graphene ribbons

C. G. Rocha, P. Rathi, D. Nozaki, and G. Cuniberti

Dresden University of Technology, Institute for Materials Science, 01069, Dresden, Germany
cgomes@nano.tu-dresden.de

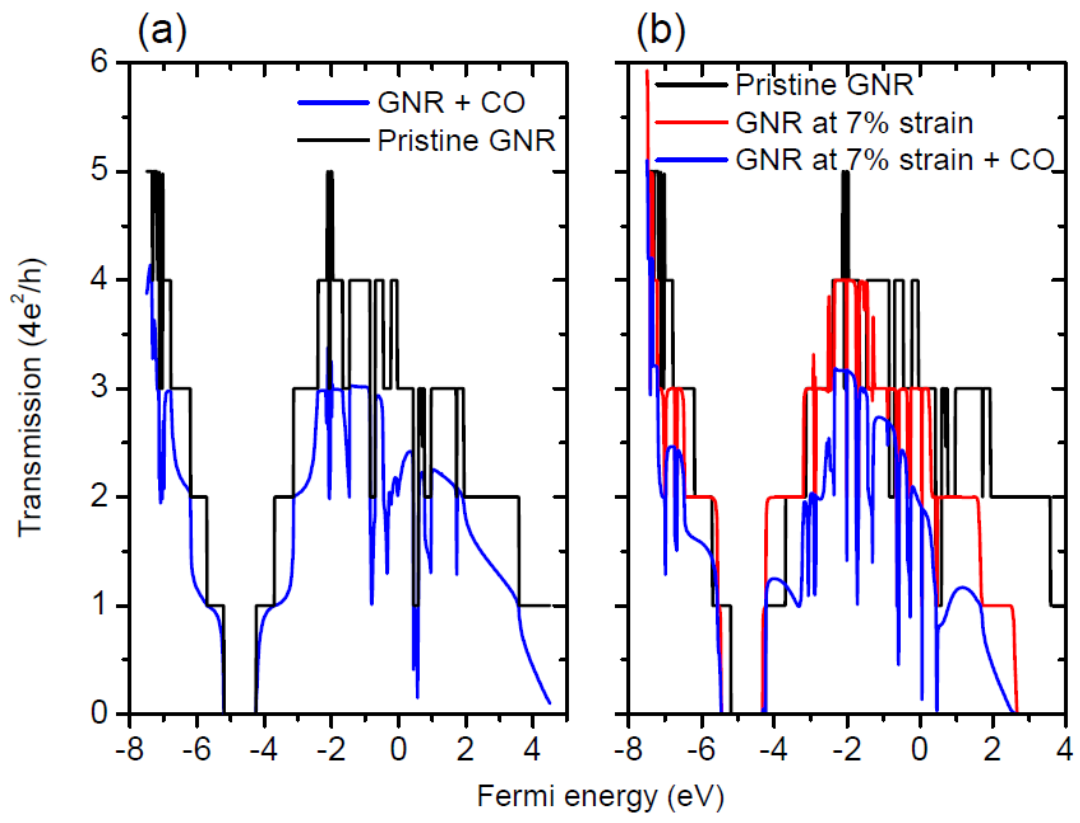
The search for novel nanoscale materials combined with the fabrication of ultra small circuit architectures are immediate priority for industry and research branches. Nanoelectronic devices based on carbon nanostructures, such as carbon nanotubes[1] and graphene[2], rise as a promising alternative to Si-based apparatus due to their extraordinary physical properties, for instance, outstanding mechanical strength[3] and electronic character strictly dependent on geometrical aspects[4]. The applicability of these materials also ranges the field of chemical and biological sensors at nanoscale offering promising applications in the realms of Medicine diagnosis and environmental pollution control. One has confirmed that graphene and nanotubes can discriminate low concentrations of contaminants and they can pose as suitable host materials for sensing a considerable number of different molecules and gases[5,6].

The experimental achievements in this field have progressed at fast pace, however its theoretical counterpart has not shared the same success, mainly due to the large computational complexity required to model highly doped structures. The theoretical description of more realistic systems turns into a big challenge since larger number of impurities and disordered features should be taken into account. For this reason, the main goal of this work is to improve the theoretical understanding of the physical properties of carbon-based hosts interacting with foreign structures. Different foreign entities such as nanoparticles, individual atoms, small molecules, polymers and metallic contaminants are attached to graphene hosts and the systems are theoretically addressed within robust semi-empirical approaches that are able to treat highly imperfect systems[7]. The electronic transmission of the sensors are also modulated by mechanical strain. The performance of the devices and their response to the application of external mechanical forces are probed in order to determine optimal physical conditions that can maximize the chemical sensibility of graphene hosts[8].

Preliminary results are shown in the figure below which displays the electronic transmission as a function of Fermi energy for pristine and doped graphene nanoribbon. Carbon monoxide is adsorbed on graphene's surface and one can notice that the presence of the impurity is detected by the transmission curve although the energy gap itself is not modified. In the following, the ribbon is uniaxially stretched by the aid of mechanical forces which elongate the ribbon with a mechanical strain of 7%. The system demonstrate remarkable sensibility to mechanical strain since its energy gap size is altered with the strain application. Still, carbon monoxide adsorption can be perceived by the ribbon.

References

- [1] J.-C. Charlier, X. Blase, and S. Roche, *Rev. Mod. Phys.* **79**, (2007) 677 (2007);
- [2] K. S. Novoselov, *et al.*, *Science* **306**, (2004) 666;
- [3] C. Lee, X. Wei, J. W. Kysar, and J. Hone, *Science* **321**, (2008) 5887;
- [4] A. H. Castro Neto, *et al.*, *Rev. Mod. Phys.* **81**, (2009) 109;
- [5] F. Schedin, *et al.*, *Nat. Mat.* **6**, (2007) 652;
- [6] Y. Dan, *et al.*, *Nano Lett.* **9**, (2009) 1472;
- [7] C. G. Rocha, *et al.*, *J. Phys.: Cond. Matt.* **19**, (2007) 346201; C. G. Rocha, and M. S. Ferreira, *Europhys. Lett.* **82**, (2008) 27004;
- [8] M. Poetschke, C. G. Rocha, L. E. F. Foa Torres, and G. Cuniberti, *Phys. Rev. B* **81** (2010) 193404.



Tyrosinase-Gold Nanoparticles Bionanoconjugates on Nanostructured Gold Surfaces: Development of an Enzymatic Biosensor of Phenolic Compounds

I. Gomes¹, A. P. Serro², A. P. Carapeto², P. Paradiso³, J. Cortez¹, S. Cardoso⁴, P. P. Freitas⁴, B. Saramago² and R. Franco¹

¹REQUIMTE, Departamento de Química, Faculdade de Ciências e Tecnologia, Universidade Nova de Lisboa, 2829-516 Caparica, Portugal

²Centro de Química Estrutural, Instituto Superior Técnico, Av. Rovisco Pais, 1049-001 Lisboa, Portugal

³Departamento de Engenharia de Materiais, Instituto Superior Técnico, Av. Rovisco Pais, 1049-001 Lisboa, Portugal

⁴Instituto de Engenharia de Sistemas e Computadores - Microsistemas e Nanotecnologias (INESC-MN) and Institute for Nanosciences and Nanotechnologies (IN, Associated Lab.), Rua Alves Redol 9, 1000-029 Lisboa, Portugal
inesgomes@dq.fct.unl.pt

Tyrosinase (1.14.18.1) is a copper monooxygenase that catalyzes the *o*-hydroxylation of monophenols and the oxidation of *o*-diphenols to *o*-quinones [1]. The development of enzymatic biosensors based on the tyrosinase enzyme has attracted great interest for the detection of phenolic compounds (pesticides, pollutants) in ground or wastewaters [2,3]. Our objective is to develop a biosensor based on bionanoconjugates of tyrosinase on gold nanoparticles (AuNPs), taking advantage of the high surface areas of AuNPs, its unique electrochemical properties and ideal protein conjugation chemistry afforded by suitable functionalization.

Self-Assembled Monolayers (SAM) of thiolates form nanostructured surfaces with a diversity of functionalities and chemical characteristics that can favor the immobilization of enzymes in gold surfaces [4]. The immobilization of enzymes and bioactive conjugates in this type of nanostructured gold surfaces is a highly suited strategy for the development of biosensors with high activity and specificity.

In the present work, the immobilization of bionanoconjugates of tyrosinase and gold nanoparticles on nanostructured gold surfaces containing SAMs of alkanethiols, was studied by Quartz Crystal Microbalance (QCM) and Atomic Force Microscopy (AFM). AuNPs were functionalized with mercaptoundecanoic acid (MUA) and second conjugated with tyrosinase, producing bionanoconjugates. The tyrosinase-MUA-AuNP bionanoconjugates were then adsorbed on the surface of the cationic SAM (11-amino-1-undecanethiol hydrochloride) on the piezoelectric quartz crystal coated with gold, and the change in mass was estimated from the shift in the measured oscillation frequency [5]. The catalytic activity of the enzyme adsorbed on to the gold crystal was measured using a spectrophotometric assay to detect the formation of reaction products.

QCM results confirm the high adsorbed amount of tyrosinase-MUA-AuNP bionanoconjugates on the surface of the gold crystal, comparatively with the lower values that were obtained for the deposition of the MUA-AuNP alone on the same type of cationic SAM (Figure 1).

AFM was used as a tool for the visualization of bionanoconjugates on gold surfaces deposited on silicon substrates. The bare surfaces topography enabled the observation of individual bionanoconjugates and provided information on the bionanoconjugates-surface interaction.

AFM images show high immobilization of the conjugates on the cationic SAM (Figure 2), when compared with the gold surface alone or the cationic SAM on gold surface.

References:

- [1] Gormally, M. V. *et al.*, *Langmuir*, **25**, (2009), 10014-10019.
- [2] Kim, G. *et al.*, *J. Environ. Monit.*, **10**, (2008), 632-637.
- [3] Abdullah, J. *et al.*, *Sensors and Actuators B*, **114**, (2006), 604-609.
- [4] Love, J.C. *et al.*, *Chem Rev.*, **105**, (2005), 1103-70.
- [5] Gispert, M.P. *et al.*, *Surf. Interface Anal.*, **40**, (2008), 1529-1537.

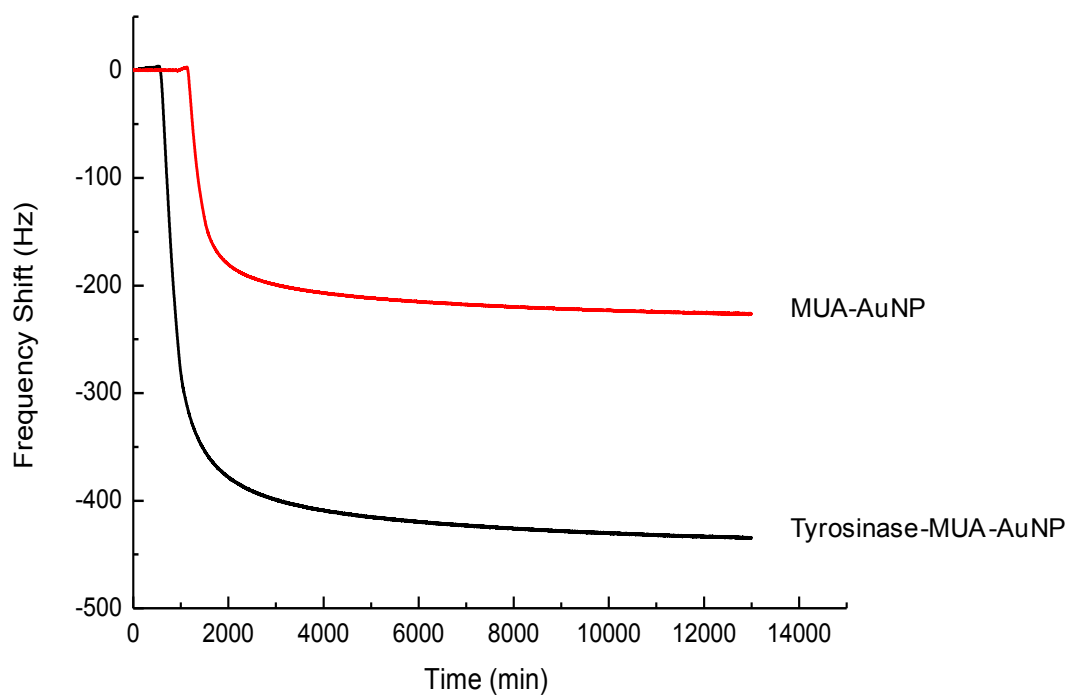


Figure 1. Change of frequency in the 3rd harmonic, obtained by QCM for the deposition of Tyrosinase-MUA-AuNP bionanoconjugates and MUA-AuNP alone on the cationic SAM on a gold coated crystal.

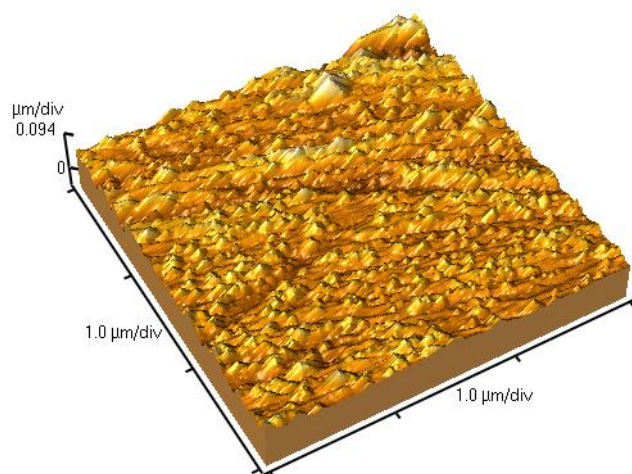


Figure 2. 3D AFM image of the immobilization of Tyrosinase-MUA-AuNP bionanoconjugates adsorbed on cationic SAM over the gold surface.

NMR Studies on the Phosphonic Acid Oxide Capping of Colloidal Semiconductor Nanocrystals

Raquel Gomes[‡], Agnieszka Sczygiel[†], José C. Martins[†], Zeger Hens[‡]

[‡] Physics and Chemistry of Nanostructures, Ghent University, Krijgslaan 281-S3, 9000 Ghent, Belgium

[†] NMR and Structure Analysis Unit, Ghent University, Krijgslaan 281-S4, 9000 Ghent, Belgium
raquelfilipa.gomespintofernandes@ugent.be

Shape control of colloidal nanomaterials with a wurtzite crystal structure like CdSe and CdS can be attained by translating the intrinsic crystal anisotropy into an anisotropic growth kinetics. Especially in the presence of phosphonic acids like octadecylphosphonic acid (ODPA), it was found that when the reaction is under kinetic control, the crystals generally grow faster along the *c*-axis, leading to the formation of quantum rods.[1] This experimental result has been substantiated by theoretical calculations on the relative binding strength of different ligands, which confirmed that phosphonic acids bind more strongly than fatty acids, amines, phosphines or phosphine oxides to the CdSe surface, with a specific affinity for the 11 $\bar{2}$ 0 surfaces parallel to the *c*-axis.[2] In spite of their key role in the formation of anisotropic nanoparticles like quantum rods, [1,3,4] the interaction of phosphonic acids with CdSe nanoparticles, and especially their binding strength relative to other ligands has not been experimentally investigated so far.

Here, we use solution nuclear magnetic resonance (NMR) spectroscopy to analyze the binding of phosphonic acid to CdSe quantum dots (QDs). Especially in the case that free/bound exchange is slow with respect to the NMR time scale, solution NMR is a suitable technique for this purpose.[5,6] Resonances of bound ligands appear broadened and shifted with respect to free ligand resonances, which enables to identify and quantify the ligands. Moreover, additional information can be obtained using diffusion ordered spectroscopy (DOSY), where the resonances of the free and surface-bound ligands are separated along the diffusion dimension, or using Nuclear Overhauser Effect Spectroscopy (NOESY), where efficient cross relaxation is indicative of ligand/nanoparticle interaction.[5]

In this work, we apply both ¹H and ³¹P-NMR to study ODPA capped CdSe nanocrystals. As a starting point, we present the results regarding CdSe QDs that are used as seeds in the growth of highly luminescent CdSe/CdS QRs.[4] Although the reaction mixture to synthesize these CdSe QDs is complex and includes other possible ligands such as TOP (trioctylphosphine) and TOPO (trioctylphosphine oxide),[4] ODPA could be identified as the only ligand adsorbed at the QDs, using ³¹P-NMR. As shown in Fig. 1A the spectra of ³¹P-NMR CdSe QDs in THF is broad. Indeed, after the addition of ODPA a sharp signal develops at 30 ppm, thus assigned to the free ligand. Moreover, upon extraction of the organic part of the sample, the remaining free molecules give rise to a single peak at ca 30 ppm coincident with the one found for ODPA. Taking into account that TOP has a resonance at -33 ppm and TOPO at 40 ppm in ³¹P-NMR spectrum, we conclude that ODPA is the only ligand of these CdSe QDs. In Fig. 1B, the ¹H-NMR shows also broad resonances corresponding to bound ODPA. From the integral of the peak at 1.31 ppm and using a reference of known concentration, a concentration of ODPA of 59.5 mM was determined. This corresponds to 4.45 ligands/nm².

In order to get a further insight into the system, we added excess oleic acid (OA) to the ODPA capped CdSe QD suspension. OA can be easily monitored in NMR by means of the resonance of the alkene protons at around 5.5 ppm. Even with an excess of 8:1, only free OA is observed, as shown in Fig. 2A. This result was corroborated by NOESY and DOSY measurements. Alternatively, two ligand exchange procedures (ODPA→OA) were performed successively, by adding a 100-fold excess of OA and heating the sample up to 60 °C. After this treatment, we find that the alkene resonance is composed of a broad and a sharp component, indicative of bound and free OA. Based on the integration of the resonance, we find an OA:ODPA ratio of only 1:12. When excess ODPA is added to this sample, ¹H-NMR reveals that the intensity of the sharp feature in the alkene resonance increases, while the broad resonance goes down (Fig. 2B). This indicates that OA desorbs and is most likely replaced by the added ODPA. From the trend of the titration (see inset Fig. 2B), it is expected that when the added ODPA reaches 4 mM, the OA is completely replaced, that is, one molecule of ODPA replaces on average 1.1 molecules of OA.

In conclusion, we find that OA is readily and quantitatively replaced by ODPA on CdSe QD surfaces, while the reverse process is extremely difficult, that is, the binding strength of ODPA to CdSe QDs is indeed several orders of magnitude higher than that of OA. This study constitutes the first step towards the understanding of ligand exchange in the different facets of QRs and consequently the mechanisms for rod growth.

References

- [1] X. Peng, L. Manna, W. Yang, J. Wickham, E. Scher, A. Kadavanich, A. P. Alivisatos, *Nature*, **404** (2000) 59.
 [2] J. Y. Rempel, B. L. Trout, M. G. Bawendi, K. F. Jensen, *J. Phys. Chem. B*, **110** (2006) 18007.
 [3] L. Manna, E. C. Scher, A. P. Alivisatos, *J. Am. Chem. Soc.*, **122** (2000) 12700.
 [4] L. Carbone, C. Nobile, M. De Giorgi, F. D. Sala, G. Morello, P. Pompa, M. Hytch, E. Snoeck, A. Fiore, I. R. Franchini, M. Nadasan, A. F. Silvestre, L. Chiodo, S. Kudera, R. Cingolani, R. Krahn, L. Manna, *Nano Lett.*, **7** (2007) 2942.
 [5] a) Z. Hens, I. Moreels, J. C. Martins, *ChemPhysChem*, **6** (2005) 2578. b) I. Moreels, J. C. Martins, Z. Hens, *ChemPhysChem*, **7** (2006) 1028. c) I. Moreels, B. Fritzing, J. C. Martins, Z. Hens, *J. Am. Chem. Soc.*, **130** (2008) 15081. d) L. Van Lokeren, G. Maheut, F. Ribot, V. Escax, I. Verbruggen, C. Sanchez, J. C. Martins, M. Biesemans, R. Willem, *Chem.-Eur. J.* **13** (2007) 6957. e) B. Fritzing, I. Moreels, P. Lommens, R. Koole, Z. Hens, J. C. Martins, *J. Am. Chem. Soc.*, **131** (2009) 3024.
 [6] a) J. Aldana, Y. A. Wang, X. G. Peng, *J. Am. Chem. Soc.*, **123** (2001) 8844. b) S. A. Majetich, A. C. Carter, J. Belot, R. D. Mccullough, *J. Phys. Chem.*, **98** (1994) 13705. c) J. R. Sachleben, V. Colvin, L. Emsley, E. W. Wooten, A. P. Alivisatos, *J. Phys. Chem. B*, **102** (1998) 10117. d) F. Ribot, V. Escax, C. Roiland, C. Sanchez, J. C. Martins, M. Biesemans, I. Verbruggen, R. Willem, *Chem. Commun.* (2005) 1019. e) H. T. Liu, J. S. Owen, A. P. Alivisatos, *J. Am. Chem. Soc.*, **129** (2007) 305. f) J. S. Steckel, B. K. H. Yen, D. C. Oertel, M. G. Bawendi, *J. Am. Chem. Soc.* **128** (2006) 13032. g) O. Kohlmann, W. E. Steinmetz, X. A. Mao, W. P. Wuelfing, A. C. Templeton, R. W. Murray, C. S. Johnson, *J. Phys. Chem. B*, **105** (2001) 8801. h) L. Shen, R. Soong, M. F. Wang, A. Lee, C. Wu, G. D. Scholes, P. M. Macdonald, M. A. Winnik, *J. Phys. Chem. B*, **112** (2008) 1626.

Figure 1 – A) ^{31}P -NMR of ODPA capped CdSe QDs, the same after addition of ODPA and also after extraction of the organic part of the sample (free ligands only). **B)** ^1H -NMR of ODPA capped CdSe QDs. For all spectra CdSe QDs (2.9 nm, $[\text{QD}]=506\ \mu\text{M}$, d_8 -THF).

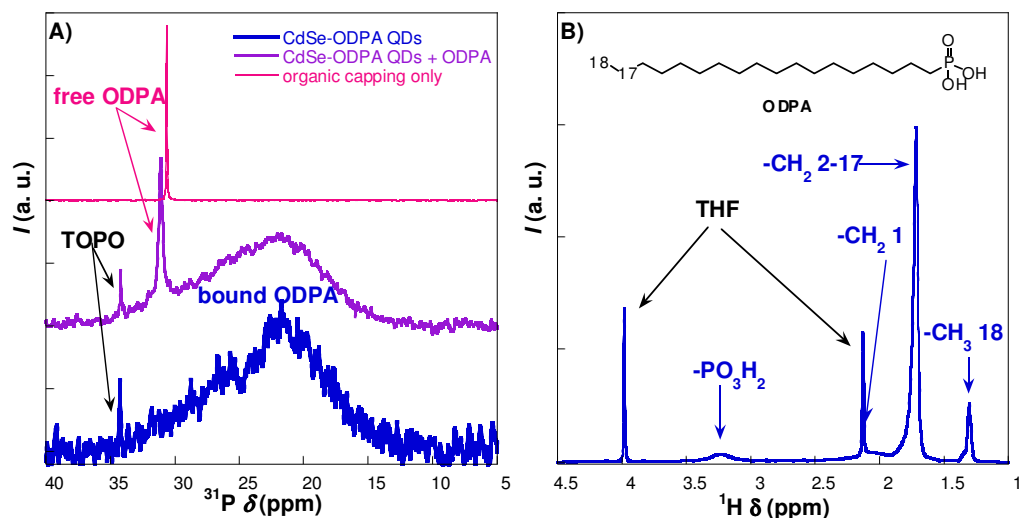
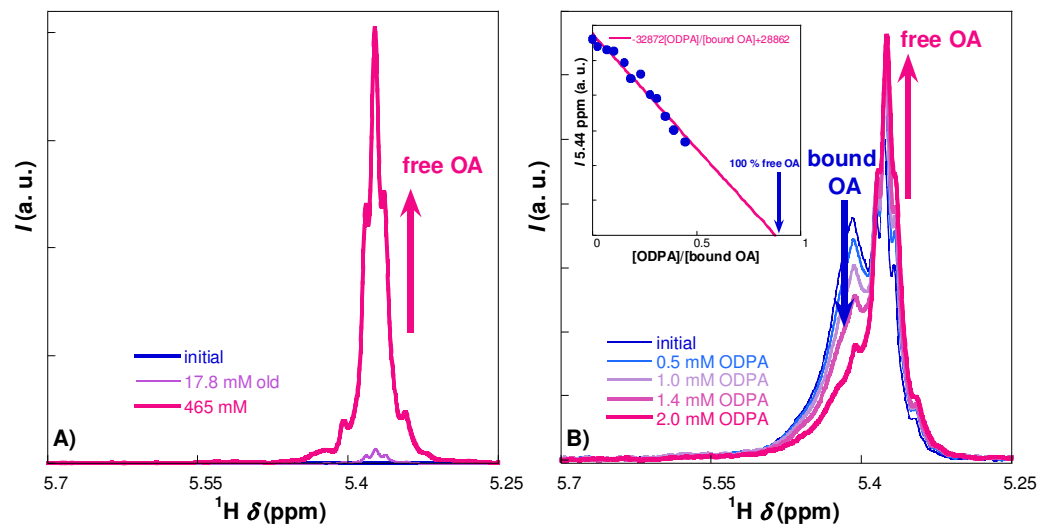


Figure 2 – ^1H -NMR spectra zoomed in the double bond region of OA. A) Addition of OA to ODPA capped CdSe QDs. **B)** Addition of ODPA to OA/ODPA capped CdSe QDs, *inset* intensity of the peak at 5.44 ppm in function of the concentration ratio added ODPA-bound OA.



One-step microwave synthesis and characterization of gadolinium-doped titania nanoparticles

Virginia Gómez, Silvia Irusta, Francisco Balas and Jesús Santamaría

Instituto de Nanociencia de Aragón (INA), Edificio I+D, c/ Mariano Esquillor s/n, 50018 Zaragoza (Spain)
virgomez@unizar.es

TiO₂ nanoparticles are widely used for applications such as photocatalysts, pigments, and cosmetic additives. In the last years, the relevance of different methods to synthesize titanium dioxide nanoparticles has been emphasized. An effective way to improve the TiO₂ photocatalytic efficiency is doping nanoparticles with different metals. There is not much literature about titanium oxide doped with gadolinium, usually; sol-gel synthesis or hydrothermal methods were used [1-4].

The homogeneity of the particle-size distribution is a critical factor for designing nanomaterials. The modification of the surface chemistry of TiO₂ particles is used to control the aggregation, but reduces the final properties of the nanomaterials. It has been found that the incorporation of trace-amount lanthanides into TiO₂ structure results in a reduction of the final aggregation in both solution and solid phases. Therefore, the main objective of the present work is obtaining Gd-doped TiO₂ nanoparticles with a narrow particle-size distribution and homogeneous shapes that prevent aggregation.

Microwave radiation has been applied to prepare different nanomaterials. Using microwave energy has many advantages as a rapid transfer of heat to medium and selective heating [5]. Synthetic methods that combine microwave and hydrothermal treatments have been developed to form different oxides [6, 7]. The synthesis procedure of Gd-TiO₂ nanoparticles combines a sol-gel processing followed by microwave treatment. This procedure leads to anatase nanoparticles avoiding the aggregation due to high temperature treatments.

Monodispersed Gd-doped anatase nanoparticles were prepared from titanium tetraisopropoxide. Several Gd(III) amounts were added using Gd(NO₃)₃ as precursor up to 0,5, 1, 3, 6 and 9% Gd/Ti atomic ratio. The precursors were heated to 120 °C in a microwave oven during 15 min. The synthesized Gd-TiO₂ nanoparticles were analyzed by XRD, TEM, SEM, EDX, SQUID magnetometry, nitrogen adsorption, UV-VIS and DLS.

XRD patterns show the characteristic anatase diffraction peaks, regardless the amount of Gd doping amount no signals of Gd (III) or Gd (III) oxide were detected. Crystallite sizes calculated using the Scherrer equation were found between 6 to 7 nm. The morphology of Gd-TiO₂ samples can be seen in the TEM images of Figure 1, which show the homogenous particle shapes together with an average particle size about 15 nm.

Gadolinium doping was analyzed by using XPS and EDX. Gd3d XPS spectra of nanoparticles with 0.5, 1 and 3 % Gd/Ti atomic ratio are shown in Figure 2. The Gd/Ti atomic ratio calculated from XPS spectra was higher than the bulk concentration suggesting that Gd is mostly in the surface of the titanium dioxide nanoparticles. An SEM-EDX mapping was performed for 3% Gd sample indicating a homogeneous distribution of Gd in the particles. The 9 % Gd doped nanoparticles were found to have paramagnetic behavior when characterized using SQUID magnetometry.

The surface area of Gd-TiO₂ was determined by N₂-Adsorption, giving a S_{BET} of 272 m²/g. This surface area value is slightly larger than that for pure TiO₂ nanoparticles (239 m²/g). Finally, the aggregation of Gd-TiO₂ nanoparticles aggregation was studied in aqueous dispersions by ζ-potential measurements at different pH. DLS measurements show good nanoparticles dispersion in aqueous acid solutions.

References

- [1] J. Xu, Y. Ao, D. Fu, C. Yuan, Colloids and Surfaces A: Physicochemical and Engineering Aspects 334 (2009) 107-111.
- [2] M. Zawadzki, L. Kepinski, Journal of Alloys and Compounds 380 (2004) 255-259.
- [3] D. Zhao, T. Peng, M. Liu, L. Lu, P. Cai, Microporous and Mesoporous Materials 114 (2008) 166-174.
- [4] W. Zhou, Y. Zhou, S. Tang, Materials Letters 59 (2005) 3115-3118.
- [5] X. Chen, S.S. Mao, Chemical Reviews 107 (2007) 2891-2959.
- [6] A.V. Murugan, V. Samuel, V. Ravi, Materials Letters 60 (2006) 479-480.
- [7] Z. Chen, W. Li, W. Zeng, M. Li, J. Xiang, Z. Zhou, J. Huang, Materials Letters 62 (2008) 4343-4344.

Figures

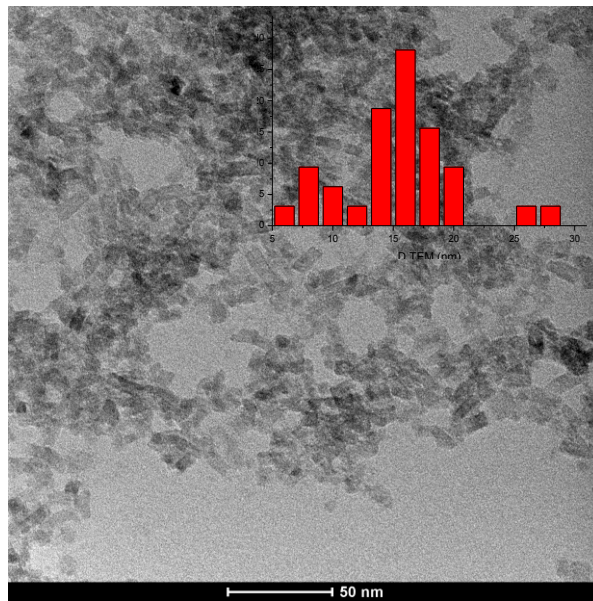


Fig 1. TEM image 3 % at gadolinium doped titania nanoparticles and histogram sizes calculated with imaQ Vision Builder.

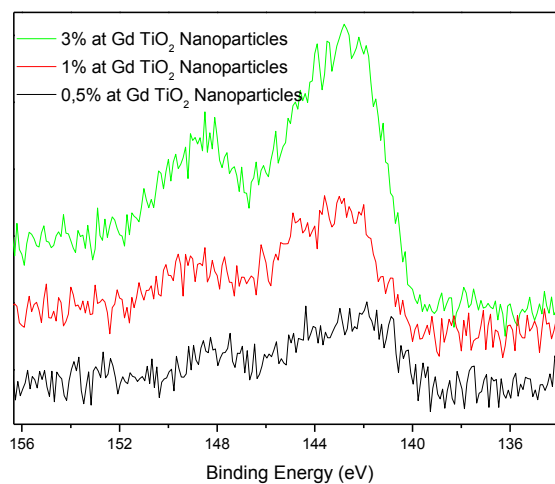


Fig. 2 Gadolinium 4d core level for nanoparticles with different amounts of gadolinium.

Deposition and Modification of Nanowires by FluidFM technology

Raphael Grüter,¹ Pascal Behr,^{1,2} Michael Gabi,² Jérôme Polesel Maris,³ János Vörös,¹ Tomaso Zambelli¹

¹Laboratory of Biosensors and Bioelectronics, D-ITET, ETH Zurich, Switzerland

²Cytosurge GmbH, Zurich, Switzerland

³Commissariat à l'énergie atomique, SACLAY, France

<mailto:grueter@biomed.ee.ethz.ch>

The FluidFM [1] combines AFM technology with nanofluidics. A channel incorporated directly in the cantilever and an aperture at the apex of the tip allows local liquid dispensing of soluble molecules in air and in liquid. Therefore, the FluidFM is the adapted tool for local chemistry with high resolution. Especially for synthesis and modification of nanowires, it provides new opportunities.

Nanowires have attracted great interest in biological sensing research. The high contact area between analyst and nanowire leads to a high sensitivity. A novel protocol for local synthesis and functionalization by FluidFM technology is presented thanks to the opportunity of filling the microchannel with specific soluble molecules. Both, metal and conductive polymer nanowires can be deposited in liquid and at desired position of the substrate. Because of the dimension of the aperture at the apex of the tip, the FluidFM can later be used for individual functionalization of closely packed nanowires with specific receptor molecules.

Additionally, the FluidFM can be used as an electrochemical lithographic tool. A non-conducting organic coating can be locally electrografted on a conducting substrate by incorporation of a counter electrode into the connected fluidic circuit and applying a potential between counter electrode and conducting substrate.

Acknowledgements

The authors acknowledge the financial support from the Swiss federal program Nano-Tera.ch.

References

[1] A. Meister, M. Gabi, P. Behr, P. Studer, J. Vörös, P. Niedermann, J. Bitterli, J. Polesel-Maris, M. Liley, H. Heinzelmann, T. Zambelli, *Nano Letters* **9** (2009) 2501.

Figures

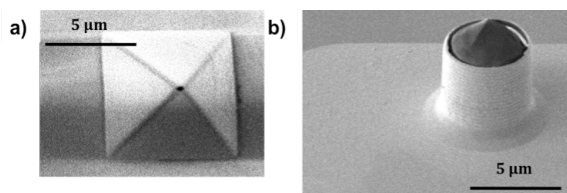


Figure 1: Different geometries of microchanneled cantilever tips. **a)** Pyramidal tip with an aperture of 200 nm at the apex. **b)** Cylindrical tip with embedded pyramid for high-resolution scanning.

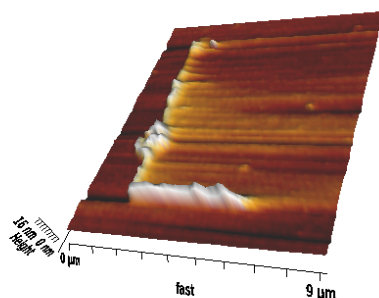


Figure 2: Deposition (in air) of Au-colloids (5nm) onto a PEI-coated Si-wafer.

Epitaxial growth of highly mismatched GaInAs layers on nanoporous GaAs substrates

Jan Grym¹, Dušan Nohavica^{1,2}, Petar Gladkov^{1,2}, Eduard Hulicius², Jiří Pangrác²

¹Institute of Photonics and Electronics, ASCR, Prague, Czech Republic

²Institute of Physics ASCR, Prague, Czech Republic
grym@ufe.cz

Pore formation in A^{III}B^V materials was reported in a number of recent papers [1-4]. On the contrary, their technological applications in epitaxial growth have not been thoroughly investigated yet.

Epitaxial growth has always been a marriage of convenience between deposited layer and substrate. In the simplest case, both layer and substrate are of the same material, providing a homoepitaxial match. Frequently, it is impractical to use the same material for both the layer and the substrate since certain large single crystals are not available, are expensive, or their properties are inappropriate for the intended application. Different strategies were suggested to achieve high quality single-crystal thin films grown on a lattice mismatched substrate. Significant development in defect density reduction in semiconductor materials has been accomplished using epitaxial lateral overgrowth techniques [5]. Recently, semiconductor epitaxial growth has progressed to pseudomorphic, lattice mismatched systems where a small amount of strain is accommodated in very thin layers [6].

A new approach extending the critical layer thickness in highly mismatched heterostructures is nanoheteroepitaxy [7]. Nanoheteroepitaxy exploits the three-dimensional stress relief mechanisms that are available in nanoscale objects and applies this property to reduce the strain energy in lattice mismatched heterojunctions. While in conventional planar structures the epilayer can only deform vertically, in a nanopatterned substrate a selectively growing epilayer can deform vertically and laterally, and the strain energy decreases exponentially with the distance from the growth interface [8].

We take advantage of a novel concept of the epitaxial growth of largely lattice mismatched layers on nanoporous substrates [9]. It is essential that the substrate takes over most of the strain of the layer at the initial growth stage. We report on the preparation of nanoporous GaAs substrates and on the growth of GaInAs epitaxial layers by the liquid phase epitaxy and metal organic vapour phase epitaxy (MOVPE) on these nanoporous substrates.

The pore etching was carried out in an electrochemical cell containing a fluoride-iodide aqueous electrolyte (H₂O-HF-KI) using a configuration equivalent to four electrodes. A home-made potentiostat/galvanostat was computer-controlled and allowed to register all process variables. (100)-oriented GaAs:Si substrates with a carrier concentration of $2 \times 10^{18} \text{ cm}^{-3}$ were used for the pore preparation. The layers of Ga_{0.8}In_{0.2}As were grown in AIXTRON 200 MOVPE apparatus. The porous structures before and after the epitaxial overgrowth were observed by scanning electron microscopy (SEM) and atomic force microscopy (AFM). The composition of the grown layer was determined by the electron microprobe with wavelength-dispersive spectrometer and correlated with the results of low temperature photoluminescence (PL) spectroscopy. The surface morphology of the layers was observed by Nomarski differential interference contrast microscopy (NDICM).

Figure 1 shows a cross-section of a GaAs substrate with a porous layer of 5 μm in thickness, which was overgrown by 0.7 μm thick layer of Ga_{0.8}In_{0.2}As. A comparison of the surface morphology of the epitaxial layer grown on porous and nonporous substrates observed by NDICM is shown in figure 2. While a typical cross-hatching pattern corresponding to a large misfit between the substrate and the layer is observed on the nonporous substrate, a random pattern is observed on the porous substrate. This observation, together with the results of low temperature PL measurements indicate that the porous substrate gives rise to the decrease in the density of extended defects at the heterointerface.

The work was supported by the project P108/10/0253 of the Czech Science Foundation.

References

- [1] Föll, H., et al., *Advanced Materials*, **3** (2003) 183-198.
- [2] Santinacci, L. and Djenizian, T., *Comptes Rendus Chimie*, **9** (2008) 964-983.
- [3] Ulin, V. and Konnikov, S., *Semiconductors*, **7** (2007) 832-844.
- [4] Ulin, V. and Konnikov, S., *Semiconductors*, **7** (2007) 845-854.
- [5] Nishinaga, T., *Journal of Crystal Growth*, **237-239** (2002) 1410-1417.
- [6] Atkinson, A., Jain, S.C., and Harker, A.H., *Journal of Applied Physics*, **5** (1995) 1907-1913.
- [7] Zubia, D., et al., *Journal of Vacuum Science & Technology B*, **6** (2000) 3514-3520.
- [8] Luryi, S. and Suhir, E., *Applied Physics Letters*, **3** (1986) 140-142.
- [9] Sitnikova, A.A., et al., *Semiconductors*, **39** (2005) 523-527.

Figures

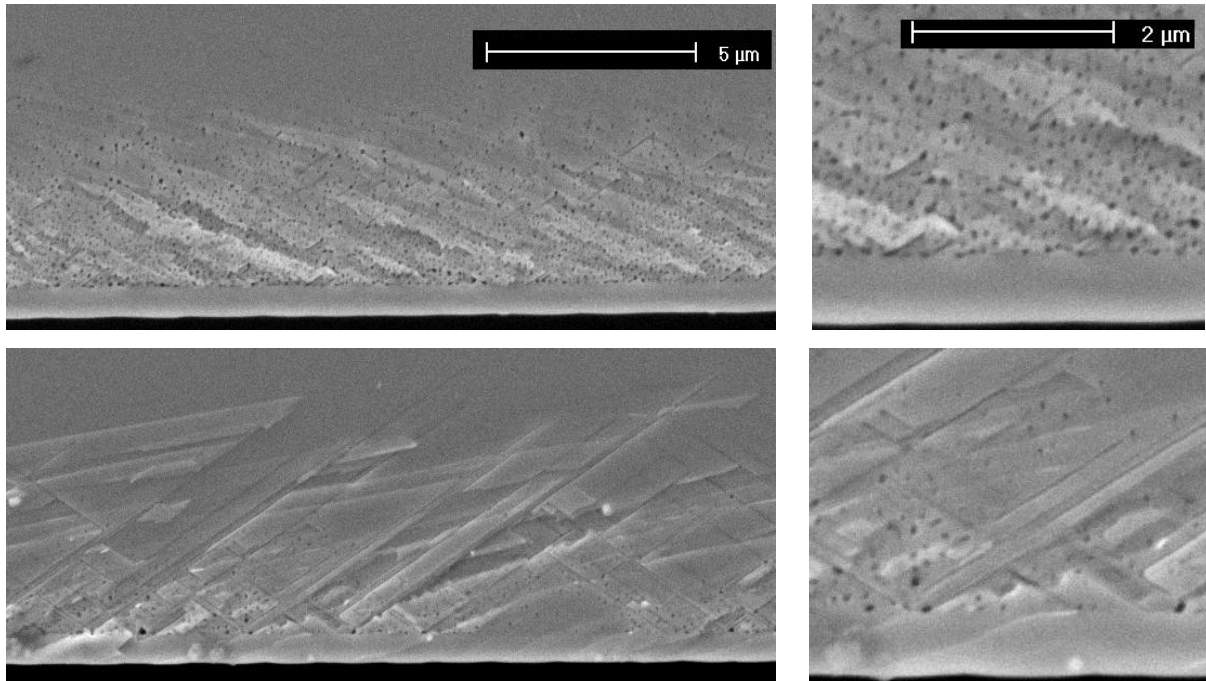


Figure 1: SEM micrographs of the cross section of porous GaAs substrate overgrown by 700 nm thick layer of GaInAs. The sample was cleaved along two perpendicular directions shown on the upper and lower panel respectively. The right panel shows the same with a higher magnification.

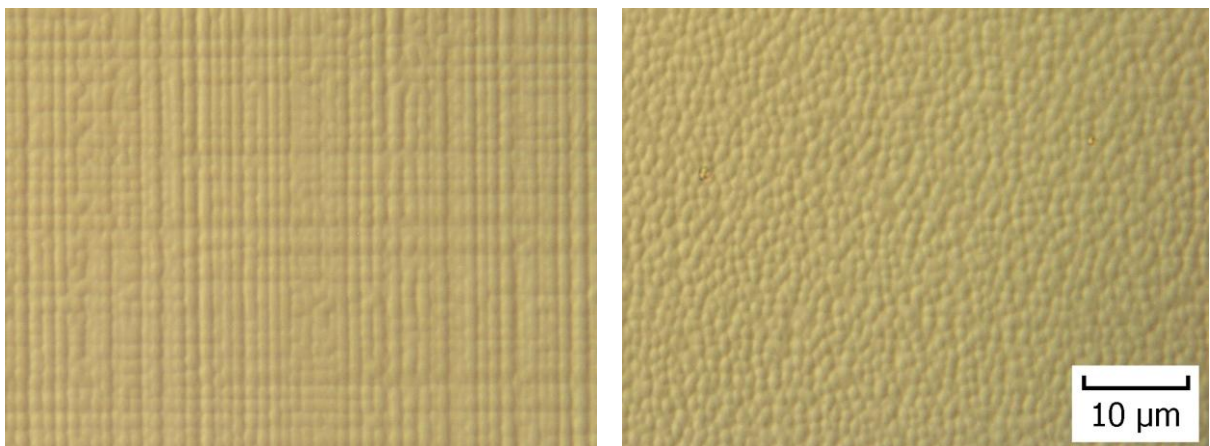


Figure 2: Nomarski contrast optical micrograph of the InGaAs layer grown on standard GaAs substrate (left panel) and porous GaAs substrate (right panel).

Hydrogen Sensors Based on Electrophoretically Deposited Pd Nanoparticles onto InP

Jan Grym¹, Olga Procházková¹, Roman Yatskiv¹, Kateřina Piksová²

¹Institute of Photonics and Electronics, ASCR, Prague, Czech Republic

²Faculty of Nuclear Science and Physical Engineering, CTU in Prague, Czech Republic
grym@ufe.cz

Metal nanoparticles (MNPs) form a bridge between bulk materials and atomic or molecular structures. Bulk metals show constant size independent physical properties while the properties of MNPs are driven by their size, shape, and inter-particle distance. Surface properties are crucial because the number of surface atoms becomes significant as the MNP reaches the nanoscale limit [1]. III-V semiconductors have established their position in electronic devices thanks to their unique properties. As compared to silicon, they offer higher operating speeds, lower power consumption, or higher light emission efficiency. However, to fully exploit their properties, there is one key point remaining to be solved. III-V semiconductor structures suffer from a high density of surface/interface states causing so called Fermi level pinning [2]. The Fermi level pinning leads to low Schottky barrier heights (SBH) on n-type III-Vs, which are metal independent when prepared by standard evaporation techniques [3]. In this paper we report on the preparation of Schottky barriers on InP substrates with increased SBHs by the electrophoretic deposition of palladium NPs. We also demonstrate their application in hydrogen sensors.

Pd nanoparticles with the diameters of 7 and 10 nm were prepared in isooctane colloid solution by the reverse micelle technique [4]. The electrophoretic deposition from the colloid solution took place in a cell with two parallel electrodes. The upper electrode was made from a high-purity graphite, the lower electrode was formed by an InP substrate of n-type conductivity with the background concentration of about $6 \times 10^{15} \text{ cm}^{-3}$. Pulsed DC voltage with a duty cycle of 50 % was applied for a selected period of time to deposit a Pd nanolayer.

We discuss the influence of (i) the final substrate surface treatment, (ii) the properties of the deposited colloid solution, (iii) the electrophoretic deposition conditions (time, electrode polarity, applied voltage), and (iv) the post-deposition treatment of the layers (chemical treatment in peroxide and annealing at elevated temperatures) on the morphology of the deposited layers, their electrical properties, and their sensitivity towards hydrogen.

Layers of nanoparticles were observed in JEOL JSM 7500F scanning electron microscope and by AFM. Selected layers were contacted by the spots of a conductive silver or graphite colloid paint. These structures were further characterized by the measurement of current-voltage characteristics and their detection towards hydrogen was tested in a cell with a through-flow gas system.

The coverage of the surface strongly depends on the applied voltage. The higher the voltage, the better the coverage and the smaller the size of deposited clusters. Figure 1 shows the morphology of the layers deposited at 100 V for 1 hour and 18 hours respectively. The high values of SBH reaching 0.9 eV – in comparison with thermally evaporated Pd reaching 0.45 eV only – indicate a very low degree of Fermi level pinning. This is further proved by the hydrogen detection measurement. The best results reached for a mixture of hydrogen (20 %) and nitrogen gases show an increase of current by six orders of magnitude (see Figure 2). The hydrogen molecules are absorbed and dissociated at Pd surface, atomic hydrogen rapidly diffuses to the Pd/InP interface, where the dipole layer develops. Subsequently, the Schottky barrier height decreases and the electric current increases.

The work was supported by the projects 102/09/1037 of the Czech Science Foundation and grant KJB200670901 of the ASCR.

References

- [1] Hossam, H., Journal of Physics D: Applied Physics, **23** (2007) 7173-7186.
- [2] Hasegawa, H. and Akazawa, M., Applied Surface Science, **24** (2008) 8005-8015.
- [3] Hasegawa, H., Solid-State Electronics, **10** (1997) 1441-1450.
- [4] Chen, D.-H., Wang, C.-C., and Huang, T.-C., Journal of Colloid and Interface Science, **1** (1999) 123-129.

Figures

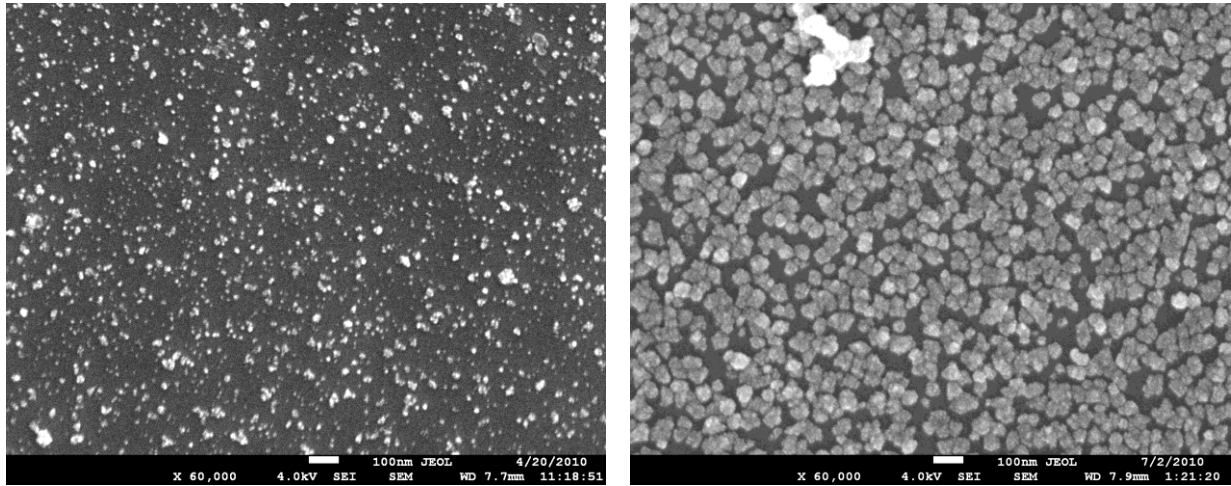


Figure 1: SEM images of Pd NPs deposited onto the InP substrate with the applied voltage of 100 V with different deposition times: 1 hour (left panel) and 18 hours (right panel).

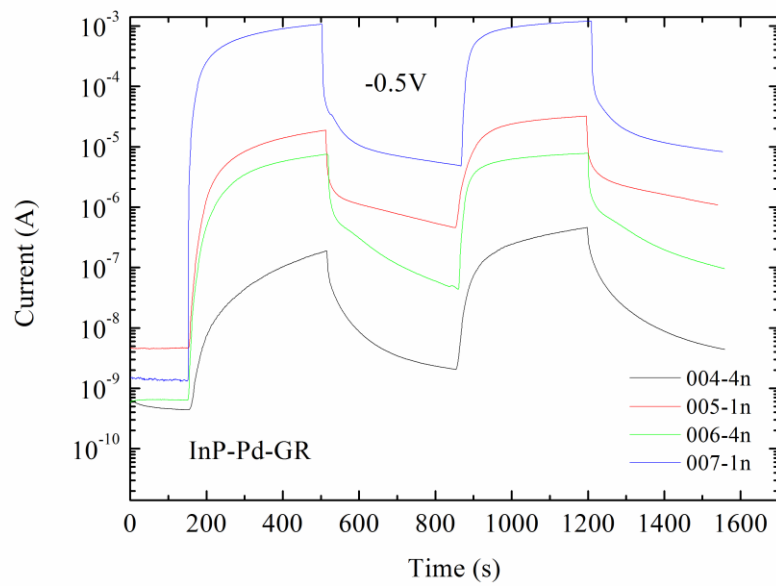


Figure 2: Current-transient characteristics of Pd-InP Schottky diodes exposed to hydrogen/nitrogen gas mixture. Samples 004 to 007 were deposited at a different applied voltage ranging from 30 V to 100 V.

Reducing zinc oxide in rubber industry use through the development of mixed metal oxide nanoparticles

Manuel Guzmán, Núria Agulló, Salvador Borrós

Grup d'Enginyeria de Materials (GEMAT), Institut Químic de Sarrià-Universitat Ramon Llull, Via Augusta 390, Barcelona, Spain
manuelguzmanm@iqs.es

Zinc oxide is a widely used compound in rubber industry due to the excellent properties that shows as activator for sulphur vulcanisation. The tire industry remains the largest single market for ZnO, consuming more than half of the total worldwide demand of 1,200,000 metric tons¹. Traditionally, ZnO is used in rubber formulations in concentrations of 3–8 parts per hundred rubber (phr).

Despite its superior characteristics, there is an increased concern about the environmental effects that zinc oxide causes and over the years lower levels of zinc have been tried in order to decrease its impact and to minimise the production costs. Different approaches have been considered for reducing zinc levels. Between all the alternatives proposed, the use of nano-sized ZnO particles with high surface area seems to be promising. However, it was found that the use of more active forms of zinc oxide did not substantially reduce further the minimum zinc content that can be achieved with conventional zinc oxide although the dispersion of high surface area ZnO during mixing was found to be significantly better, which could enable low levels of this zinc oxide to be used in industry with more confidence².

There have been a number of studies comparing different metal oxides as vulcanisation activators in order to find substitutes for zinc oxide. Several metal oxides have been used, CaO, MgO, CdO, CuO, PbO and NiO. Among them, MgO is the most promising candidate since it is a non heavy metal oxide that provokes the breakdown of the accelerator to be faster than when ZnO is used and it is able to form active sulphurating agents. However the crosslink level achieved is lower than that obtained with zinc oxide, which has limited its industrial application.

In this article, a new approach to overcome the problems between ZnO and MgO is presented. It consists in the development of a new activator based in the mixture of both mixed oxides at nanoscale to take advantage of the behaviour of both zinc and magnesium oxides as nanoparticles. The new activator is nanometer-sized mixed metal oxide particles of zinc and magnesium ($Zn_{1-x}Mg_xO$) with very precise stoichiometry prepared employing a polymer-based method. In this accelerator, magnesium is incorporated into the ZnO structure and this inclusion and its size are expected to show a better performance taking advantage of the behaviour of both ZnO and MgO in sulphur vulcanisation.

Basically, the method consists on the preparation of a polymer/metal salt complex that is water-soluble, its purification by precipitation/redissolution cycles and finally the calcination of the dried purified complex to give nanosized crystals³. The polymer used to form the polymer/metal salt complex is poly [acrylic acid]. Magnesium nitrate hexahydrate, and zinc nitrate hexahydrate are the starting materials.

Dynamic Light Scattering was employed to measure the particle size of the $Zn_{1-x}Mg_xO$ particles, which was found to be in the range of 100 to 175 nm with a narrow distribution as seen in Figure 1. No apparent dependence of the particle size with the magnesium content was found.

X-Ray diffraction was employed to characterise the crystal structure of the mixed metal oxide particles. Figure 2 shows the X-ray diffraction patterns of the oxide products obtained in the different syntheses. The patterns of the pure ZnO are indexed according to the known hexagonal phase (zincite)⁴, and that of MgO is indexed according to its cubic phase (periclase)⁵. In **¡Error! No se encuentra el origen de la referencia.**, the vertical line corresponds to the standard reflections of the ZnO phase and the dashed vertical lines are the standard reflections of the MgO phase which planes are indicated with a star. The scans showed a weak (200) peak of the MgO phase, which demonstrates that the material is mostly present in the hexagonal phase (zincite) and that magnesium has been incorporated into the ZnO structure. In addition, the lattice constant *c* of the synthesized nanoparticles has decreased in comparison to the corresponding ZnO phase. As magnesium replaces zinc in the hexagonal phase, due to the smaller radius of Mg^{2+} than that of Zn^{2+} , there is a shrinking of the lattice constant along the *c*-axis and a displacement of the diffraction peaks to higher angles. These findings indicate Mg^{2+} ions replace the Zn^{2+} ions into the zincite.

The model compound vulcanisation (MCV) approach with squalene as a model molecule for natural rubber and N-Cyclohexylbenzothiazole-2-sulphenamide (CBS) as accelerator has been used to study the role of the mixed metal oxide along the reaction. The results obtained with $Zn_{1-x}Mg_xO$ nanoparticles

as activator for sulphenamide accelerated sulphur vulcanisation have shown when $Zn_{1-x}Mg_xO$ nanoparticles are used it is possible to take advantage of the behaviour of both ZnO and MgO in sulphur vulcanisation. It has been seen that the reactions that take place during the scorch time, the breakdown of the accelerator and the formation of MBT occur faster, which could be due to the presence of magnesium into the zinc oxide structure.

Nevertheless, the crosslink degree achieved is higher than those obtained with zinc oxide nanoparticles. It is worth noting that mixed metal oxide nanoparticles of zinc and magnesium lead to around a 30 % higher crosslink degree than the one obtained with standard zinc oxide. This effect can be partly attributed to the small particle size of the $Zn_{1-x}Mg_xO$ since Bhowmick et al.⁶⁻⁷ found that ZnO nanoparticles (30-70 nm) increased the crosslink degree by 15 % compared with standard ZnO. On the other hand, the fact that, even with bigger sizes, higher amounts of crosslinked products are formed suggests that $Zn_{1-x}Mg_xO$ nanoparticles are more active and more effective transporting sulphur into the hydrocarbon chain than ZnO nanoparticles. Therefore, $Zn_{1-x}Mg_xO$ nanoparticles not only overcome the disadvantages of the use of a mixture of ZnO and MgO reported previously in the literature⁸, which shows a crosslink degree similar to the one obtained with magnesium oxide, but a better performance is achieved.

References

- [1] Walter, J., Tire Technology International, **March** (2009) 18.
- [2] Chapman, A. V., Johnson, T., *Kautschuk Gummi Kunststoffe* **58** (2005) 358.
- [3] Lu, G., Lieberwirth, I., Wegner, G., *Journal of the American Chemical Society* **128** (2006) 15445.
- [4] JCPDS Card No 36-1451.
- [5] JCPDS Card No 45-0946.
- [6] Sahoo, S., Kar, S., Ganguly, A., Maiti, M., Bhowmick, A. K., *Polymers & Polymer Composites* **16** (2008) 193.
- [7] Sahoo, S., Kar, S., Ganguly, A., George, J.J., Bhowmick, A. K., *Journal of Applied Polymer Science* **105** (2007) 2407.
- [8] Vega, B., Doctoral Thesis, Universitat Ramon Llul, Barcelona (2008).

Figures

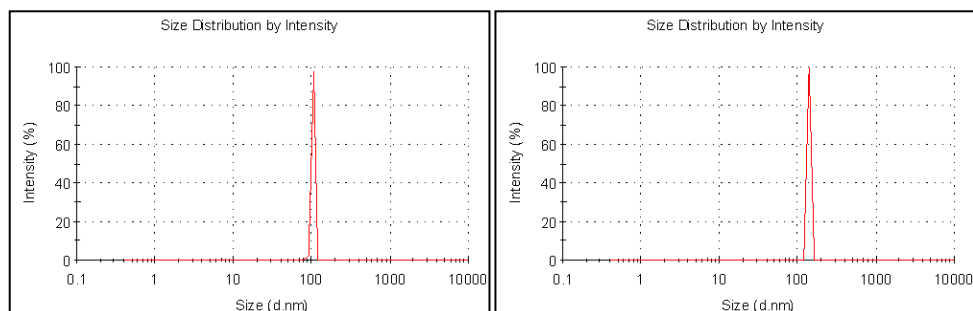


Figure 1. Particle size measurement of a) MG1.2 and b) MG1.5.

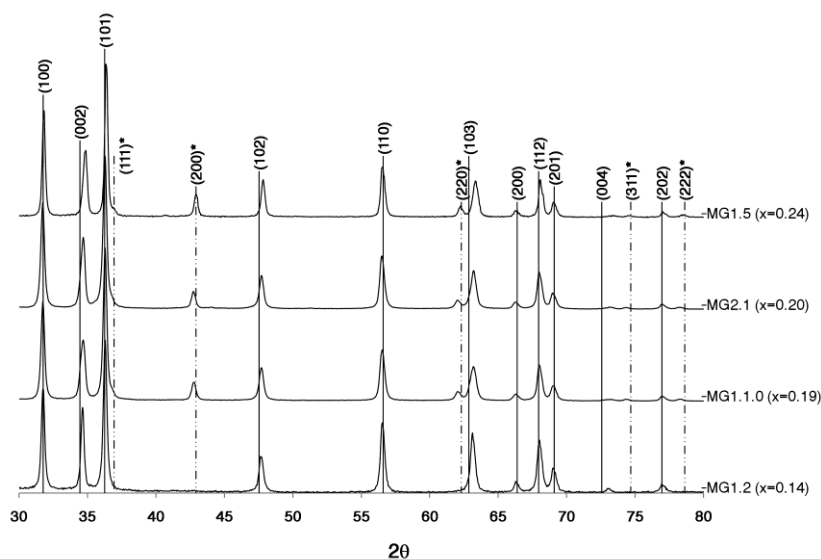


Figure 2. XRD patterns of $Zn_{1-x}Mg_xO$.

Towards alternative 2D polymers based on coordination polymers

Cristina Hermosa,^a Almudena Gallego,^a Oscar Castillo,^b Salomé Delgado,^a Julio Gómez-Herrero,^c Félix Zamora^a

^a Departamento de Química Inorgánica, Universidad Autónoma de Madrid, 28049, Madrid, Spain

^b Departamento de Química Inorgánica, Facultad de Ciencia y Tecnología, Universidad del País Vasco, Apartado 644, E-48080 Bilbao, Spain

^c Dpto. de Física de la Materia Condensada, Universidad Autónoma de Madrid, 28049 Madrid, Spain
cristina.hermosa@uam.es

Coordination polymers are a class of compounds formed by two building-blocks, the metal units (metal ions or complexes) and the ligands (molecules or ions), connected by means of coordination bonds. A wide variety of architectures with a broad panel of properties can be achieved by suitable selection of the building-blocks. Large amount of work has been done towards potential applications of materials based on coordination polymers. Probably, the most studied being gas storage and gas separation [1]. However, little is known about their potential use as alternative materials of nanometric dimensions. We have recently pointed out that a particular type of 1D coordination polymers seems particularly suitable as molecular wires [2]. In addition, the development of the unique properties of graphene has originated a scientific “revolution” around this material. This scenario has motivated us to consider new alternatives for the isolation of 2D polymers, in other words, new 2D materials with one atom or molecule of thickness [3]. As for the preparation of graphene, one feasible route to achieve this end consists of delamination of a layered compound [4].

Herein, we present the synthesis and structure of a laminar Cu(I) coordination polymer $[\text{Cu}(\mu\text{-pymS}_2)(\mu\text{-Cl})]_n \cdot n\text{MeOH}$ (Fig. 1). It was synthesized by diffusing a dipyrimidindisulfide (PymS_2) MeOH:MeCN solution into a $\text{CuCl}_2 \cdot 2\text{H}_2\text{O}$ methanolic solution. Isolated red crystals of $[\text{Cu}(\mu\text{-pymS}_2)(\mu\text{-Cl})]_n \cdot n\text{MeOH}$ exhibit semiconducting and luminescent properties. X-ray diffraction analyses evidenced that the sheets are weakly face-to-face stacked through pyrimidine ligand moieties (Fig 1a). The packing of these sheets allocate channels along the *c* axis which are occupied with disordered guest methanol molecules (Fig1b). The solvent molecules can be selectively exchanged by *ie.* water or ethanol molecules, resulting in a slight shift in the relative position of the layers. As evidenced by crystallographic data and interchange host-guest properties let us to envision a feasible compound exfoliation.

In fact, crystalline $[\text{Cu}(\mu\text{-pymS}_2)(\mu\text{-Cl})]_n$ can be exfoliated into colloidal sheets by micromechanical cleaving. Both hydrophilic and hydrophobic sites can be found in the layer structure, hence mica (hydrophilic) and HOPG (hydrophobic) surfaces were explored in order to adsorb the compound by casting deposition of previously sonicated and diluted sample suspensions. Atomic force microscopy techniques were employed to characterise deposited sheets of $[\text{Cu}(\mu\text{-pymS}_2)(\mu\text{-Cl})]_n$ on HOPG (Fig.2) and mica (Fig.3). Its is noticeable the morphological features of the sheets adsorbed on HOPG which angles resemble to those observed in the monocrystals of this material.

References

- [1] C.Janiak, Dalton Transactions, **14** (2003) 2781.
- [2] L. Welte, A. Calzolari, R. di Felice, F. Zamora, J. Gómez-Herrero, Nature Nanotechnology, **5** (2010) 110.
- [3] P. Amo-Ochoa, L. Welte, R. González-Prieto, P. J. Sanz Miguel, C. J. Gómez-García, S. Delgado, J. Gómez-Herrero, F. Zamora, Chemical Communications, **19** (2010) 3262.
- [4] A.J.Jacobson, In Comprehensive Supramolecular Chemistry, Vol 7, G.Alberti and T. Bein (Ed) (1996) 315.

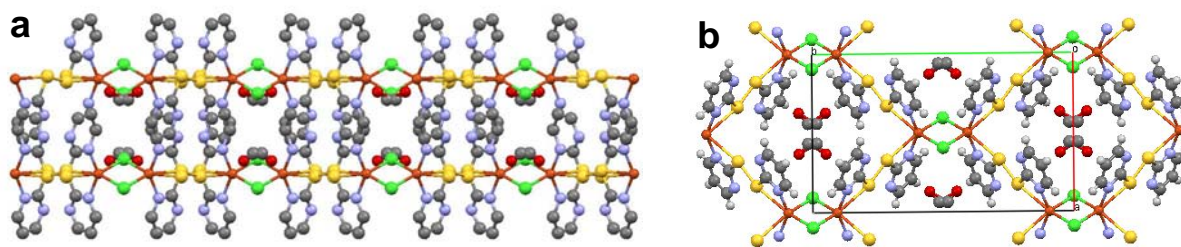


Figure 1. (a) *bc* plane view showing the interlayer interactions and (b) *ab* plane view of $[\text{Cu}(\mu\text{-pymS}_2)(\mu\text{-Cl})]_n \cdot n\text{MeOH}$ showing the structure of a layer with the cavity filled by molecules of methanol.

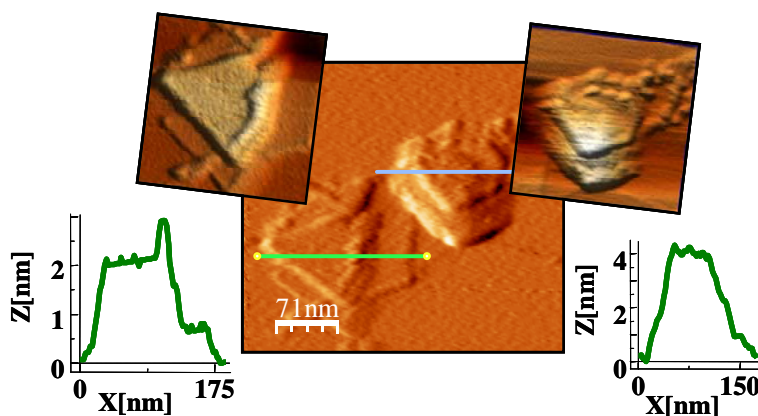


Figure 2. AFM image and two zoomed areas with their height profiles showing two sheets of $[\text{Cu}(\mu\text{-pymS}_2)(\mu\text{-Cl})]_n$ deposited on HOPG.

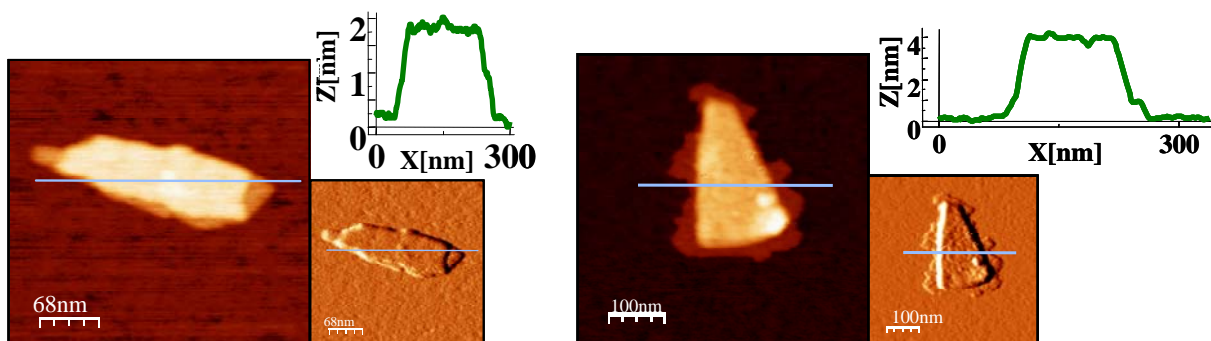


Figure 3. Two AFM images and their height profiles sheets of $[\text{Cu}(\mu\text{-pymS}_2)(\mu\text{-Cl})]_n$ deposited on mica.

Measurement of tip-sample interaction forces under infrared irradiation toward high-spatial-resolution infrared spectroscopy using FM-AFM

Yoshihiro Hosokawa, Kei Kobayashi, Hirofumi Yamada and Kazumi Matsushige

Kyoto University, A1-326 Katsura Campus Nishikyo Kyoto, Japan
hosokawa@piezo.kuee.kyoto-u.ac.jp

Infrared (IR) spectroscopy is a superior, analytical technique which is capable of identifying functional groups having characteristic vibration frequencies. However, the spatial resolution in the conventional IR spectroscopy is on the order of micrometers because of the diffraction limit. Recently, several researchers demonstrated high-spatial-resolution IR spectroscopy by detecting thermal expansions on the surface using atomic force microscopy (AFM) during IR irradiation[1,2]. They succeeded in detecting a cantilever deflection induced by the thermal expansion by the contact-mode AFM. However the spatial resolution was still limited around 100 nm because of the contact radius of the cantilever tip. Frequency-modulation AFM (FM-AFM) is capable of detecting tip-sample interaction forces with a very high sensitivity. While the cantilever is oscillated it at its resonance frequency using a self-oscillation loop, the tip-sample interaction forces induce either a shift in the resonance frequency (conservative interaction) or an change in the oscillation amplitude (dissipative interaction). The conservative and the dissipative force can be independently measured. In this presentation, we show the measurement results of a preliminary experiment on the measurement of the tip-sample interaction forces on polymer thin films under IR irradiation using FM-AFM.

Figure 1 shows a schematic of an experimental setup. We used a commercially available AFM apparatus (JEOL: JSPM-5200) and home-built FM electronics. We used an automatic gain controller (AGC) which kept the oscillation amplitude of the cantilever constant. The energy dissipated by the tip-sample interaction was measured from the output of the AGC quantitatively. We used a Si cantilever (Nanosensors: NCH), whose nominal spring constant and resonance frequency were 40 N/m and 300 kHz, respectively. The quality factor of the cantilever was 10,000 in a vacuum environment (10^{-1} Pa). The typical oscillation amplitude was set at 10 nm_{p-p}.

We prepared a polyethylene glycol (PEG) film by spin-coating its toluene solution on a silicon surface. We irradiated the sample under the cantilever tip with a collimated quantum cascade laser (QCL) (Hamamatsu Photonics) through a zinc selenide window from outside of the vacuum chamber. The power density on the sample was approximately 1.3 mW/cm². The center wavenumber of the QCL was 1050 cm⁻¹. The temperature of the QCL was controlled by a thermoelectric cooler, which was also used for tuning the wavenumber with a range of +/- 6 cm⁻¹.

Figure 2 shows a topographic image of the sample. The thickness of the PEG film measured from a step in the image was approximately 200 nm. To measure a relationship between the tip-sample interaction forces and IR irradiation, we modulated the power of the QCL at 750 Hz and detected the modulation component in the frequency shift signal and the energy dissipation of the cantilever using a lock-in amplifier. We measured the relationship between the magnitude of these components and the wavenumber of the QCL. Figure 3 shows plots of the magnitude of the modulated components in the frequency shift (black, thin) and the energy dissipation (red, bold) measured on Si (dotted) and the PEG film (solid) as indicated in Fig. 2. The wavenumber of the QCL was calibrated using a Fourier transform IR spectroscopy of the QCL beam. We found that the magnitude of the modulation component in the energy dissipation induced by IR irradiation was different between those on the PEG film and on the Si surface. In Figure 4, we also show an infrared absorption spectrum of the PEG film using the QCL. We found that two absorption peaks in the absorption spectrum indicated by the arrows, which might be corresponding to the peaks at the same wavenumbers in the dissipative force spectrum in Fig. 2, which are also indicated by the arrows.

Reference

- [1]F. J. Boerio and M. J. Starr, *Journal of Adhesion* (2008) **84** 874
- [2]A. Dazzi, R. Prazeres, F. Glotin and J. M. Ortega, *Optics Letters* (2005) **30** 18

Figures

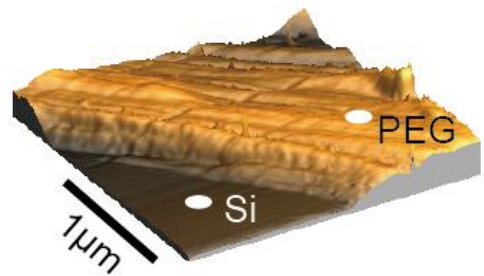
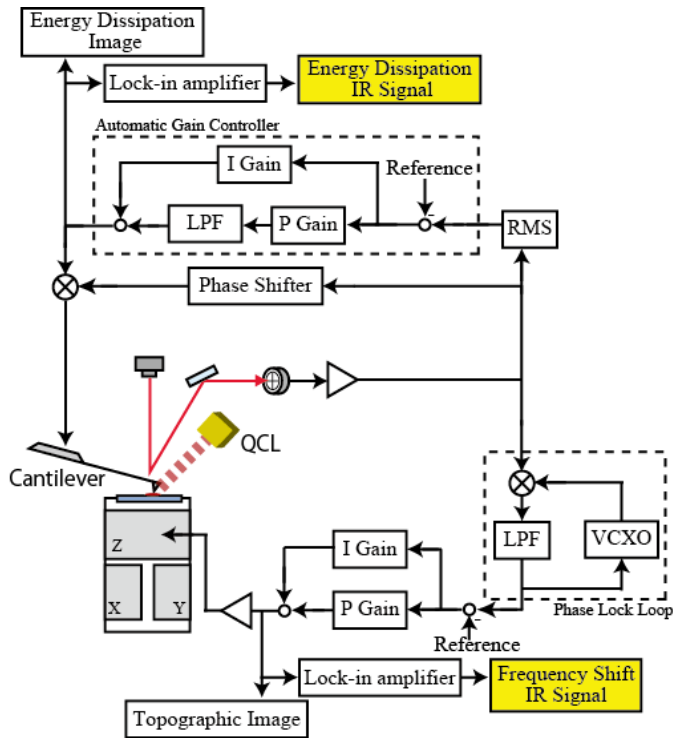


Figure 2: Topographic image of polyethylene glycol (PEG) thin film on the Si surface using FM-AFM.

Figure 1: Experiment setup of FM-AFM combined with irradiate infrared.

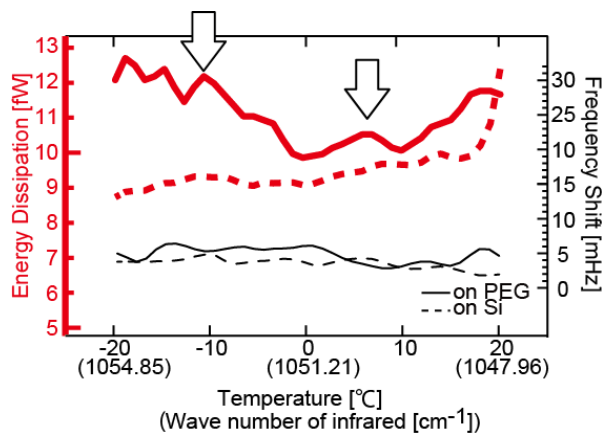


Figure 3: Frequency shift (black, thin) and energy dissipation (red, bold) induced by infrared irradiation measured on Si (dotted) and PEG (solid) as indicated in Fig.2.

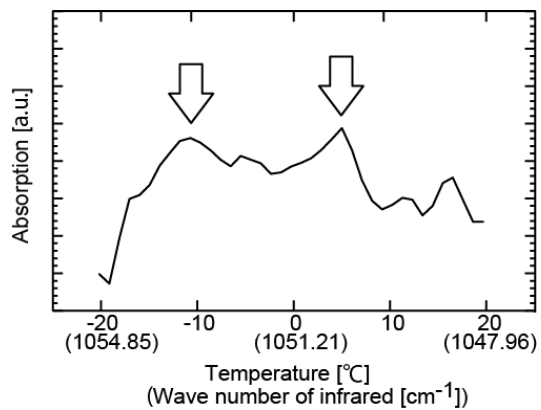


Figure 4: Infrared absorption spectrum of PEG detected by sweeping a temperature of QCL.

The effects of Fe/Al₂O₃ preparation technique as a catalyst on synthesized CNTs in CVD method.

A.A.Hosseini*, F.sh.Abhari, F.Taleshi

Department of Physics, University of Mazandran, Babolsar, 47416-95447, IRAN
hos-a-p1@umz.ac.ir

In this research, the growth of CNTs is carried out on Fe/Al₂O₃ substrate by CVD method. Preparation of Fe catalyst nanoparticle supported on Al₂O₃ substrate as catalyst system for growth of CNTs, were carried out by two different methods, in order to, investigate its effects on the quality of synthesized CNTs. In the first method, Fe nanoparticles (with the size of less than 60nm) were mixed with alumina powder, and in the second one impregnation method were employed to synthesis catalyst particle on alumina substrate from Fe(NO₃)₃.6H₂O salt. The qualities of CNTs growth on the substrates produced by above methods were compared using SEM images and XRD pattern of the produced samples.

Key words; catalyst, Fe/ Al₂O₃, CVD, CNT, impregnation, SEM, XRD

References

- [1] J. W. Ward and et al, Substrate effects on the growth of CNT by ..., *Chem. Phys. Let.* **376**(2003) 717-725.
- [2] Régis Philippe and et al, An original growth mode of MWCNTs on alumina supported iron catalysts, *Journal of Catalysis* *Journal of Catalysis*, Volume 263, Issue 2, 25 April 2009, Pages 345-358
- [3] William A. and et al, CNT reinforced ceramic and metals, materials today, ISSN:1369 7021 ©Elsevier Ltd 2004
- [4] Anne-Claire Dupuis, The catalyst in the CCVD of carbon nanotubes—a review, *Materials Science*, **Volume 50**, *Issue 8*, November 2005, Pages 929-961
- [5] L. Kumari and et al, Synthesis, microstructure and electrical conductivity of carbon nanotube–alumina nanocomposites, *Ceramics International*, **Volume 35**, *Issue 5*, July 2009, Pages 1775-1781
- [6] Jinwei Ning and et al, Fabrication and mechanical properties of SiO₂ matrix composites reinforced by carbon nanotube, *Materials Science and Engineering A* **357** (2003) 392_396
- [7] E.Teredo, aligned carbon nanotube grown on alumina and quartz substrate by simple thermal CVD processe, *Diamond Related Materials* **15**, July 2009, Pages 1775-1781
- [8] K. Balani and et al, (2008) , In situ carbon nanotube reinforcements in a plasma-sprayed aluminium oxide nanocomposite coating aluminium oxide nanocomposite coating, *Acta Material* **56**, 571–579

Direct Thermal Decomposition of $[\text{Cd}(\text{DADMBTZ})_3](\text{ClO}_3)_2$ Complex for the Synthesis of CdO-CdS nanocomposite

A. Hosseinian*¹, M. Movahedi²

¹Department of Engineering Science, University College of Engineering, University of Tehran,
Tehran, Islamic Republic of Iran.

²Department of Chemistry, Payame Noor University, Isfahan, Iran.

Hoseinian@ut.ac.ir

Recently, much effort has been devoted to the design and controlled fabrication of nanostructured materials with functional properties. Among these investigations, the nanocomposite materials can not only demonstrate small size effect, surface effect, and quantum–dimension effect, but also combine the advantages of all ingredients. Therefore, the nanocomposite materials have attracted more and more attention due to their tailored properties and potential application in photonic crystal, drug delivery, biological markers, bio-separation, and as catalyst. Various kinds of nanocomposite materials have been successfully fabricated such as metal/metal, metal/semiconductor, semiconductor/semiconductor, inorganic particle/polymer and inorganic particle/inorganic particle, showing tailored magnetic optical electrical properties [1, 2]. CdS, an important semiconductor with a wide band gap of 2.4 eV at room temperature. It has high potential application in light-emitting diodes, solar cells, optoelectronics and catalysts [3]. There are a variety of methods used to prepare this material. Changes in the photoactivity of CdS can also be achieved by combining the CdS semiconductor with other semiconductors at different energy levels (ZnS, ZnO, TiO₂...). Modification of CdS by impurity can efficiently adjust its electrical, optical, and magnetic properties. In spite of the absence of studies in literature on the effect of CdO presence on the activity of CdS under visible light, there are interesting results showing the increase in CdS activity for samples mixed with CdO [4,5].

The potential use of supramolecular coordination complexes as materials for nanotechnological applications would seem to be very extensive as nanometer- scaled materials often exhibit the new interesting size-dependent physical and chemical properties that cannot be observed in their bulk analogous. The use of bithiazole complexes as precursors for preparing inorganic nano-materials has not yet been investigated thoroughly [6].

The tris-chelate Cd(II) complex, $[\text{Cd}(\text{DADMBTZ})_3](\text{ClO}_3)_2$, DADMBTZ=2,2'-diamino-5,5'-dimethyl-4,4'-bithiazole, has been synthesized by reaction of $\text{Cd}(\text{CH}_3\text{COO})_2$ with DADMBTZ in 1:2 ratio in the presence of an excess amount of potassium chlorate. The complex was characterized by elemental analyses and IR, ¹H, ¹³C NMR, ¹¹³Cd NMR spectroscopy. The thermal behavior of compound $[\text{Cd}(\text{DADMBTZ})_3](\text{ClO}_3)_2$ was studied by thermal gravimetric and differential thermal analyses. The nanocomposite CdO-CdS has been prepared by direct thermal decomposition of $[\text{Cd}(\text{DADMBTZ})_3](\text{ClO}_3)_2$. The nanocomposite was characterized by scanning electron microscopy, X-ray powder diffraction (XRD), and IR Spectroscopy. Estimated from the Scherrer formula, the average size of the particles is about 43 nm for CdO-CdS nanocomposite after calcination of compound $[\text{Cd}(\text{DADMBTZ})_3](\text{ClO}_3)_2$ in agreement with that observed from SEM images.

References

- [1] Sebastian P J, Calixto M E. Thin solid films Research 360 (2000) 128.
- [2] R M. Navarro, F. D. Valle, J.L.G. Fierro. International Journal of hydrogen energy. 33 (2008) 4265.
- [3] A .Phuruangrat, T .Thongtem, S. Thongtem, Mater Lett., 63, (2009)1562.

Electrochemical Perforation of the Aluminum Oxide Barrier Layer in Thin Film Micro Sensors

Radim Hrdy, Marina Vorozthsova, Jana Chomoucka, Jana Drbohlavova, Jan Prasek, Jaromir Hubalek

Department of Microelectronics, Brno University of Technology, Udolni 53, Brno, Czech Republic
hrdy@feec.vutbr.cz

Nanoporous anodic aluminum oxide (AAO) has been used as a template for growth of various functional nanomaterials and as a scaffold for nanodevices and systems [1]. Porous AAO membranes have attracted significant interest during recent years due to the fact that they are readily synthesized through a simple procedure and extremely useful in nanoscience studies [2].

This work is focused on the fabrication of AAO in thin films applications. A new electrochemical approach was developed for selective oxide barrier perforation using of re-anodization technique for micro sensors application. The skip phasing of oxide barriers wet etching is the significant advantage of re-anodization. The dissolution of oxide barrier is carried out in the same acid such as the anodization process and the perforation is controlled only by current density and applied voltage.

The microsystem, which represents small comb-like electrochemical sensors system, was prepared by deposition of gold microstructures on silicon, silicon oxide and titanium multilayer. The thin aluminum film (2 μm) was deposited on surface of electrodes by evaporation method. The thin porous anodic alumina template was prepared by one-step oxidation process under potentiostatic voltage (40 V) in 0.3 M oxalic acid at 17 °C [3]. The anodization process ran to the point where the current density started to increase. At this time, all aluminium was consumed and the oxide barrier started to be dissolved. The continuous application of voltage caused complete dissolution of oxide barrier, approximately after 15 seconds. For the next application the opened alumina template could be used for the electrodeposition of nanowires or nanotubes with the same length and diameter as the template. The surface morphology and homogeneity of the fabricated samples were investigated with MIRA II Tescan scanning electronic microscope operated at 1–30 keV in high vacuum mode. The impedance spectroscopy was provided (Agilent 4284A) to characterize opening of nanoporous alumina. The original porous structure can be seen on Fig. 1. The pore diameter was in range of 30–80 nm and thickness was 2 μm .

This research was supported by the Czech Ministry of Education the frame of Research Plan MSM 0021630503 and Grand Agency of Czech Republic GA 102/09/1601.

References

- [1] J. Oh and C. V. Thompson, **Advanced Materials**, vol. 20, pp. 1368-1372, 2008.
- [2] C. Y. Han, G. A. Willing, Z. Xiao, and H. H. Wang, **Langmuir**, vol. 23, pp. 1564-1568, 2006.
- [3] K. Nielsch, F. Müller, A.-P. Li, and U. Gösele, **Advanced Materials**, vol. 12, pp. 582-586, 2000.

Figures

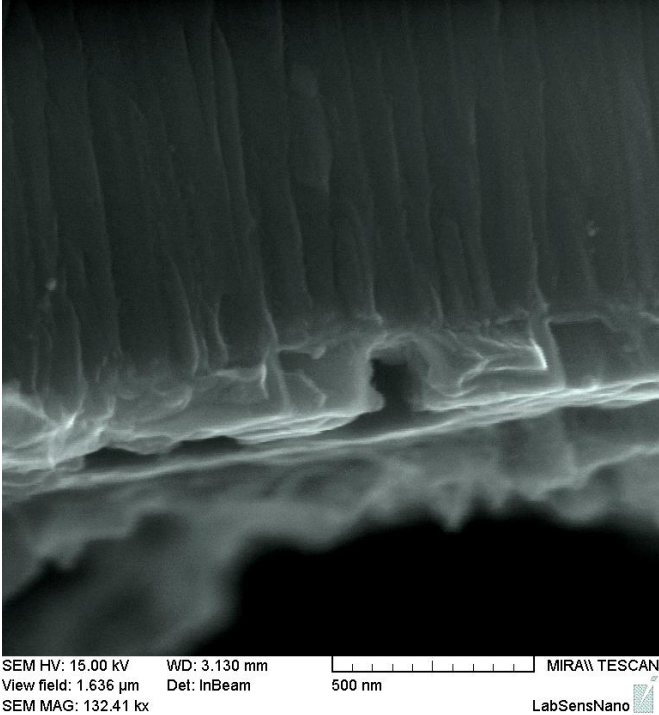


Fig.1. SEM cross-section image of nanoporous oxide alumina with perforation barrier

Preparation and Gas Sensing Characteristics of Mesoporous In₂O₃ Nanofibers

Sang Kyoo Lim, Soonhyun Kim, Daeic Chang and **Sung-Ho Hwang**

Division of Nano & Bio Technology, Daegu Gyeongbuk Institute of Science and Technology (DGIST),
Daegu 704-230, Republic of Korea

hsungho@dgist.ac.kr

Recently, one-dimensional nanostructured materials such as nanowires, nanofibers, nanorods, and nanotubes have received a great attention for their potential applications in numerous areas due to their special properties, which are distinct from conventional bulk materials. Since the first reported nanobelt structure of In₂O₃ [1], there have been a large number of studies on one-dimensional In₂O₃ nanostructures[2,3]. In₂O₃ nanowires have also been demonstrated to work as ultra-sensitive chemical sensors for NO₂ and NH₃, exhibiting significantly improved chemical sensing performance compared to existing thin film-based sensors due to their enhanced surface to volume ratio [4]. Thus, gas sensors based on one-dimensional In₂O₃ are very sensitive to low concentrations of oxidizing gases like O₃, NO_x and Cl₂.

In this work, a simple process is described for forming In₂O₃ nanofibers by thermal oxidation of polymer/indium precursor nanofibers that were prepared by electrospinning. Electrospinning has been found to be a unique and cost-effective route for fabricating large surface area nanofibers for a variety of applications. Here, mesoporous In₂O₃ nanofibers with high surface area were synthesized by calcinations of electrospun polyvinyl alcohol (PVA)/indium acetate composite fiber. A PVA solution and indium acetate were mixed and electrospun. After calcinations of these precursor PVA/indium acetate composite nanofibers, the mesoporous In₂O₃ nanofibers were successfully obtained. The mesoporous In₂O₃ nanofibers were characterized by thermogravimetric analysis, X-ray diffraction, Fourier transform infrared spectroscopy, scanning electron microscopy, transmission electron microscopy, and physical adsorption/desorption isotherms. The mesoporous In₂O₃ nanofibers with diameters in the range of 150 ~ 200 nm consisted of nanoparticles with a primary particle size of 10 nm ~ 20 nm and showed the cubic indium oxide crystals. The BET surface area of mesoporous In₂O₃ nanofibers was strongly affected by calcinations temperature. The sensitivity of these mesoporous In₂O₃ nanofibers to CO in air was high rather than commercial In₂O₃ nanopowder. The highly elevated sensitivity of In₂O₃ nanofibers calcined at 400 °C to CO in air could be attributed to the high surface area. The results demonstrate that the electrospinning approach is an easy and useful method to synthesize the metal oxides with mesopores and high surface area, which could be responsible for enhancing the gas sensing properties.

References

- [1] Z.W. Pan, Z.R. Dai, Z.L. Wang, *Science*, **291** (2001) 1947-1949.
- [2] M.J. Zheng, L.D. Zhang, G.H. Li, X.Y. Zhang, X.F. Wang, *Appl. Phys. Lett.*, **79** (2001) 839-841.
- [3] X.P. Shen, H.J. Liu, X. Fan, Y. Jiang, J.M. Hong, Z. Xu, *J. Cryst. Growth*, **276** (2005) 471-477.
- [4] C. Li, D.H. Zhang, X.L. Liu, S. Han, T. Tang, J. Han, C.W. Zhou, *Appl. Phys. Lett.*, **82** (2003) 1613-1615.

Figures

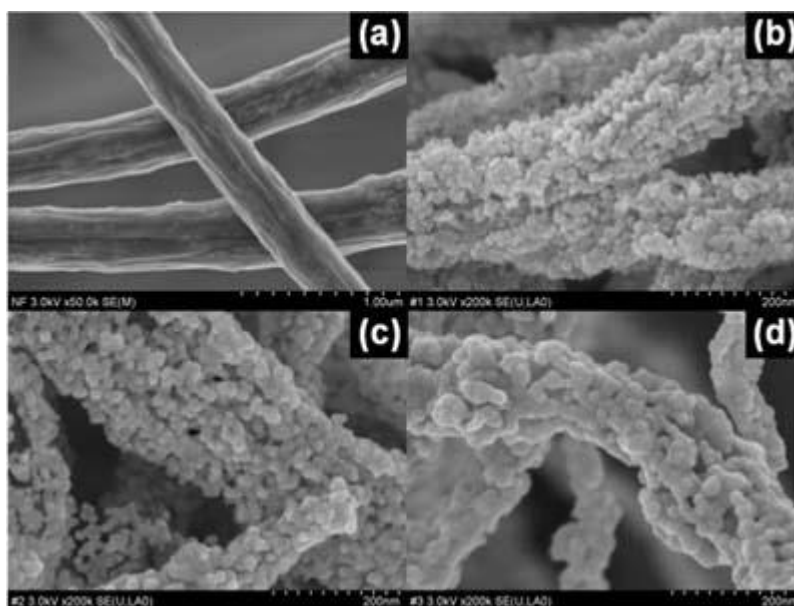


Figure 1. SEM images of (a) PVA/indium acetate composite nanofibers as-prepared, (b) INF-400, (c) INF-500, and (d) INF-600.

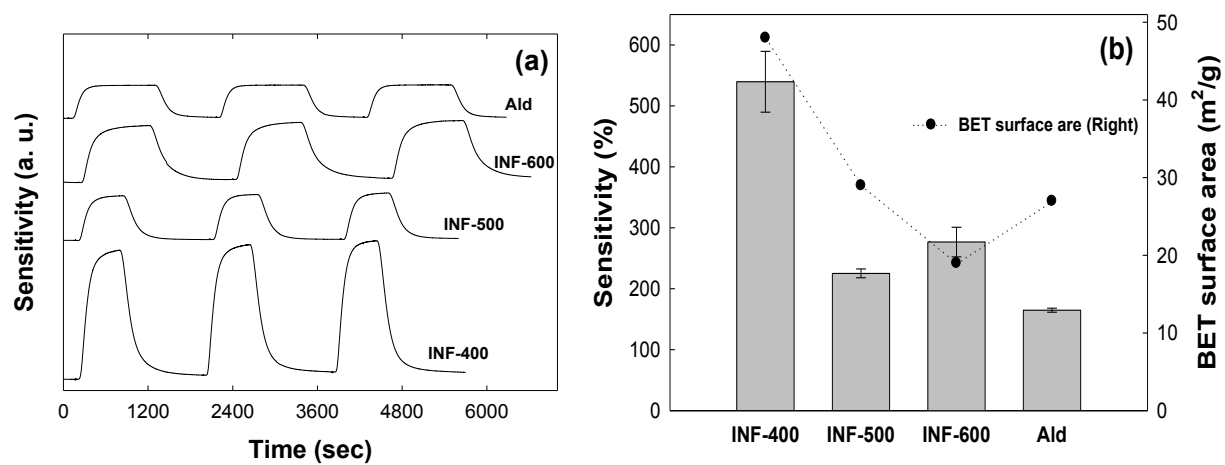


Figure 2. (a) Sensor response and (b) Sensitivity and BET surface area of INF-400, INF-500, INF-600, and commercial In_2O_3 (Ald) to 100 ppm of CO in air at 300 °C.

Local magnetic and electric state in pure and doped graphene

Michał Ingot¹ Vitalii Dugaev^{1,2}

¹*Department of Physics, Rzeszów University of Technology,
Al. Powstańców Warszawy 6, 35-959 Rzeszów, Poland and*

²*Department of Physics and CFIF, Instituto Superior Técnico,
Technical University of Lisbon, Av. Rovisco Pais, 1049-001 Lisbon, Portugal*

Graphene is very interesting and potentially important material for solid state physics and electronics. The problem of ferromagnetic state in monoatomic layer of carbon atoms is still not quite clear. We consider a possibility of creation of the local magnetic moment $M(\mathbf{r})$ and electric polarization $P(\mathbf{r})$ as a problem of induced magnetic and electric polarization of the electron gas in graphene. We use a model of perturbation with an impurity in state A or B with strongly localized potential $V(\mathbf{r})$. We find the energy level of electron localized at the impurity and the wave function using different methods (solving the Schrödinger equation and using the Green's function formalism). Then we use Green's function formalism to calculate the induced magnetization and induced electric polarisation of the electron system using the linear approach of Dirac's Hamiltonian. We consider two cases with chemical potential $\mu = 0$ (no free carriers) and $\mu \neq 0$. If the chemical potential is equal to zero, we have only pure polarization and distribution of local induced magnetization and electrical moment as $\sim 1/r^3$. If the chemical potential is not zero, the RKKY oscillations appear on top of pure polarization. At small carrier density it enhances the induced local moments but a larger impurity density destroys the local magnetization and electric polarization.

MgO MTJ biosensors for immunomagnetic lateral flow detection

R. Janeiro^{1,2}, F. Cardoso^{1,2}, R. Ferreira^{1,3}, S. Cardoso^{1,2}, P.P. Freitas^{1,2}, J.M. De Teresa⁴, D. Saurel⁵, D. Serrate^{4,5}

¹INESC-Microsistemas e Nanotecnologias (INESC-MN) and IN-Institute for Nanosciences and Nanotechnologies, Rua Alves Redol, 9 - 1, 1000-029 Lisboa Portugal.

²Physics Department, Instituto Superior Técnico-Universidade Técnica de Lisboa, 1049-001 Lisbon, Portugal

³Iberian International Nanotechnology Laboratory (INL), Braga, Portugal

⁴Instituto de Ciencia de los Materiales de Aragón, CSIC-Universidad de Zaragoza, Facultad de Ciencias, Zaragoza, 50009, Spain

⁵Instituto de Nanociencia de Aragón, Universidad de Zaragoza, Zaragoza, 50009, Spain

ricardo.janeiro@hotmail.com

In recent years, particularly in the last two decades we have seen an enormous expansion of so-called biosciences, which are currently showing themselves as an area of scientific knowledge with advances and achievements of major scientific and social impact, even more in the present context of the constant threat to public health by various diseases and pathogens of human transmission all over the world (on one side the big cities characterized by the proliferation of places with high human concentration that favor the spread, on the other side there are underdeveloped countries in which their general population doesn't have the means to prevent and contain epidemics becoming a fertile land to the spread of diseases).

In this context it is clear the potential of nanotechnology, capable of providing the necessary means for the detection and screening of pathogens in the form of sensors capable of detecting them, it is precisely this field that integrates the current project.

The aim is the fabrication of magnetoresistive (MR) sensors, with linear response capable of performing tests of recognition by the detection of biological nanoparticles functionalized magnetically polarized and previously linked to biomolecules. It is a requirement to provide a practical use: to build a portable platform with integrated MR sensors. In addition this work uses MTJ elements connected in series.

A deposition sputtering system Nordiko 2000 is responsible for the growth of the magnetic film with the following structure: Ta 50Å / Ru 180Å / Ta 30Å / MnPt 200Å / CoFe 20Å / Ru 9Å / CoFeB 30Å / MgO XÅ / CoFeB YÅ / Ru 50Å / Ta 50Å . The devices are patterned according to the mask that is presented under [Figure1]. The sensors are made of series of N=360 MgO tunnel junctions elements corresponding to a much layer magnetic volume of the free layer. This architecture allows devices robust enough to withstand the voltage drops on the order of few hundreds of volts without suffering disruption, and obtaining output values of the order of 200kOhm, beyond the obvious gain in the noise level (S_V) of the sensor and positive implications for the detectivity (D) that is the minimum field detectable [1].

$$S_V^2(f) = N \left(2eIR \coth \left(\frac{eV}{2K_B N T} \right) + \frac{\alpha V^2}{N^2 A f} \right)$$

$$D = \frac{S_V}{\Delta V / \Delta H}$$

where I is the bias current, R is sensor resistance, V is the bias voltage, α is a Hooge like parameter, A is the sensor area, T is the temperature, H is the applied magnetic field.

Values of TMRs of 70% [Fig.2], with a sensibility of the order of 440 are obtained, and the work focus in optimizing the stacks and MTJs dimensions in order to for improved the Signal Noise Ratio [SNR].

References

[1] R. Guerreroa, M. Pannetier-Lecoecura, C. Fermona, S.Cardoso,b R.Ferreirab and P.P.Freitas, "Low frequency noise in arrays of magnetic tunnel junctions connected in series and parallel."

[2] P.Wisniowski, S.Cardoso, P.P.Freitas, J.Appl.Phys., vol.103, pp.07A910-07A912. "Effect of CoFeB thickness and shape anisotropy on the transfer curves of MgO Magnetic Tunnel Junctions", April 2008.

Figures

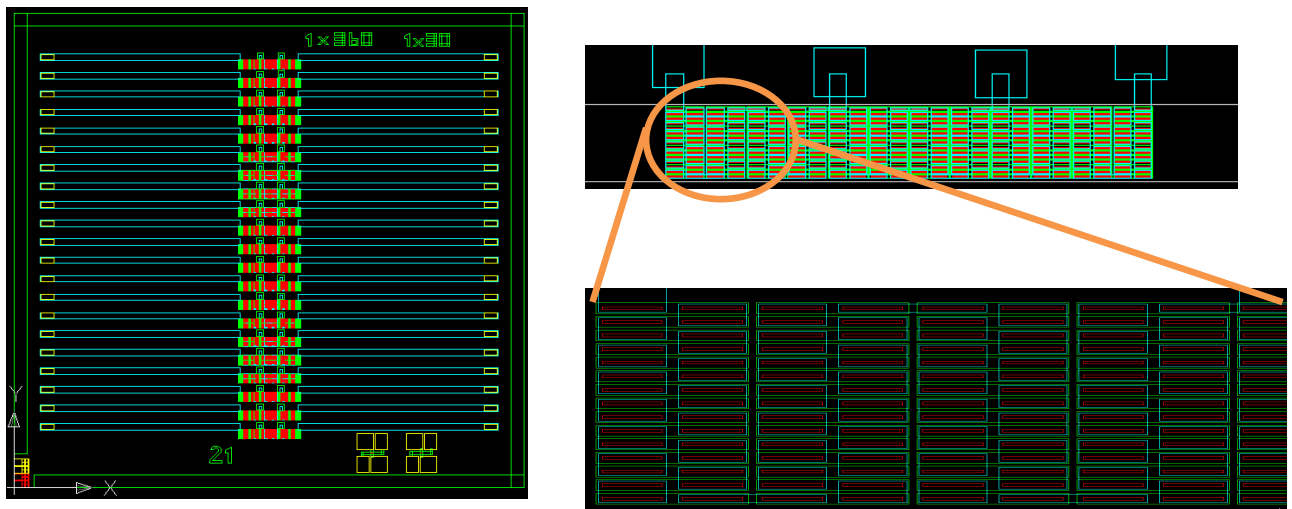


Fig.1 – Actual mask design and sensor detail.

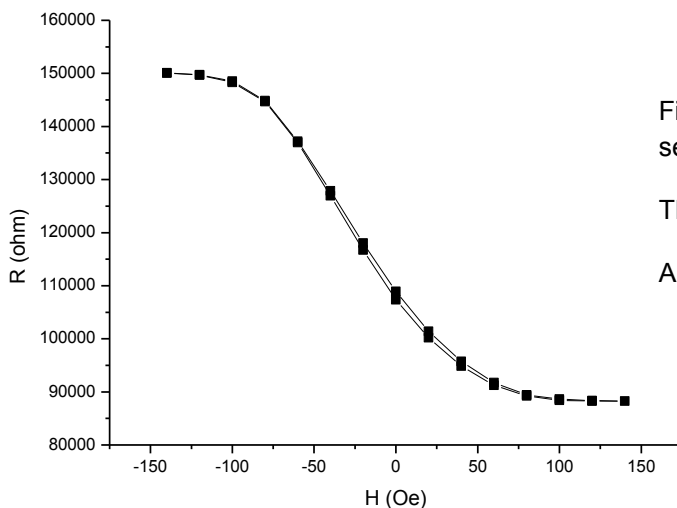


Fig.2 – Typical output result of 360MTJ in series (MgO 17Å, CoFeB 100Å);

TMR=70.5%;

Area 1 MTJ = 60μm²

Langmuir-Blodgett films of lead chalcogenide quantum dots

Yolanda Justo¹, Iwan Moreels¹, Karel Lambert¹, and Zeger Hens¹

¹Physics and Chemistry of Nanostructures, Ghent University, B-9000 Ghent, Belgium

Yolanda.Justo@UGent.be

The Langmuir-Blodgett (LB) technique provides a straightforward method for the fabrication of thin films of a diverse range of nanocrystals, including lead chalcogenide quantum dots (Qdots).[1] The development of densely packed and homogeneous monolayers of infrared emitting Qdots is important, not only for the study of the optical properties of the Qdots under thin film conditions, but also for the development of photonic devices like LEDs, lasers and solar cells.

In this poster, we compare the optical properties of LB films consisting of PbS, PbSe and PbSe/CdSe core-shell Qdots. As can be seen in Figure 1, we find that PbSe Qdots show an oriented attachment, most probably due to the rapid oxidation of these Qdots in air or in contact with water. However, we can resolve this issue by growing a CdSe shell around the PbSe core Qdots. The improved stability of the Qdots leads to a highly ordered hexagonal close-packed structure. Air-stable PbS Qdots show the same high-quality morphology. [2]

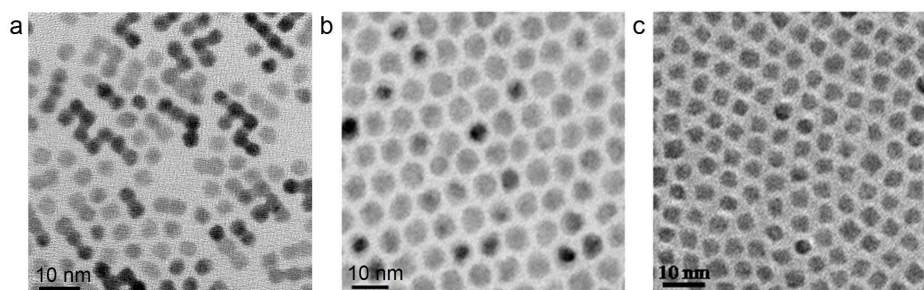


Figure 1: TEM images of LB depositions of (a) PbSe QDs, (b) PbSe/CdSe QDs, (c) PbS QDs.

However, despite the improved film quality for PbSe/CdSe and PbS Qdots, only the PbS Qdot LB films retain a high photoluminescence as it is shown in Figure 2. The PbS LB luminescence yield is similar to the yield of the PbS Qdots in suspension. For both PbSe and PbSe/CdSe, the LB film luminescence is almost completely quenched.[2]

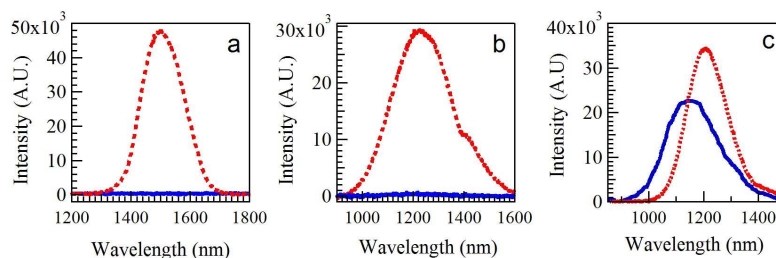


Figure 2: Photoluminescence of the colloidal solution (dotted line) and monolayer (full line), relative to the absorbance at 400 nm: (a) PbSe QDs, (b) PbSe/CdSe QDs, (c) PbS QDs.

Although PbS QD films are luminescent, they undergo oxidation under ambient conditions, causing a blue shift of the photoluminescence peak. Although this oxidation leads to a final decrease in effective size of about 1 nm after 1 month, the films maintain their photoluminescence (Figure 3). These results indicate that PbS QDs are the preferred material for near-infrared light-emitting applications based on lead chalcogenide LB films.

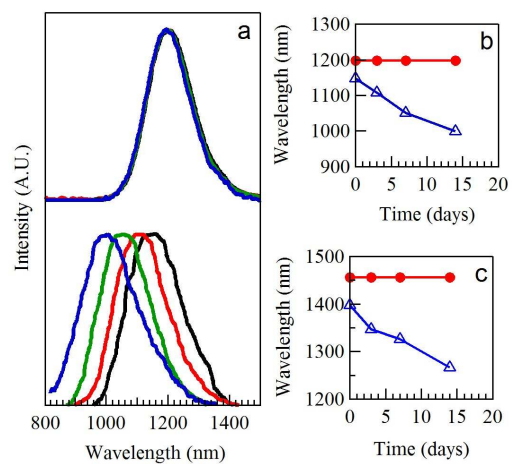


Figure 3: Effect of oxygen in PbS QDs. (a) Luminescence of a 3.7 nm colloidal solution (top) and monolayer (bottom) at different times. Evolution of the peak position versus time in colloidal QDs (dots) and monolayer (open triangles) in 3.7 nm QDs (b) and 5.2 nm QDs (c).

References

- [1] Lambert K, Moreels I, Van Thourhout D, Hens Z, *Langmuir* **24** (2008) 5961.
- [2] Justo Y, Moreels I, Lambert K, *Nanotechnology* **21** (2010) DOI: 10.1088/0957-4484/21/29/295606

Luminescence of Silicon Nanocrystals

Belkacem Kadari, Liliya Nikolova, Francois Martin, Guy Ross and Federico Rosei

Institut National de la Recherche Scientifique, Center Energy Materials Telecommunications,
1650, boul. Lionel-Boulet, Varennes, QC, J3X 1S2, Canada

rosei@emt.inrs.ca

Miniaturization of features in microelectronic devices has proceeded exponentially for several decades [1], yet is expected soon to be limited by technological challenges as well as intrinsic physical limitations. A possible solution to such problems is to replace electrical signals with photons transported through optical interconnections.

Silicon is group IV semiconductor known to be with indirect bandgap. Despite the large variety of devices based on Silicon, it is not a suitable material for a light emission source. In fact, if excitons are created, their recombination occurs on non-radiative sites. Since the discovery of photoluminescence of nanostructured silicon in 1990 [2], a lot of effort has been employed to develop an efficient source of light and to understand the mechanisms of electro- and photo-luminescence.

Nanostructured Silicon could be obtained by few different techniques Plasma Enhanced Chemical Vapor Deposition [3], Pulsed Laser Deposition [4], ion implantation [5], etc. For industrial applications a rigid and chemically stable system has to be made. Therefore, the best configuration is Silicon nanocrystals (Si-nc) embedded in silicon dioxide (SiO_2).

In this work we present our results on photo- (PL) and electro-luminescence (EL) of Si-nc embedded in SiO_2 . Ion implantation has been used to create an excess of Silicon in SiO_2 layer thermally grown on silicon wafer. The technique permits to control the depth of distribution of the emitting centers, the excess of Silicon thus giving control to the size of the formed crystals. The later is directly related to the emitted wave length. Double implantation at two different energies with similar fluences has been employed to obtain relatively uniform distribution and density of the silicon ions through the thickness of the SiO_2 layer. The fluences have been chosen to form a layer of Si-nc with high density to increase the number of the emitting center. The mean size has been evaluated to be of $\sim 3\text{nm}$ [7]. Thermal annealing in 95% Nitrogen + 5% Hydrogen has been made to give sufficient thermal energy to the ions to diffuse in the matrix and form the nanocrystals. The best results for electroluminescence have been obtained for electrical devices with top golden semitransparent contact and bottom silver contact.

EL measurements, shown in Figure 1, have been taken at a single luminescent spot (see Figure 2). Three peaks are present. The first peak, at 647 nm, is attributed mainly to non-bringing oxygen hole center (NBOHC) defects in the oxide [8]; the second and third peaks, at 804 nm and 879 nm, are attributed to the presence of the Si-nc, as the peaks positions coincide with the PL peak situated in the range $\sim 750\text{--}950\text{ nm}$, and for these peaks the intensity increases with the applied voltage. In samples without Si-nc, no peaks with these positions have been observed [9].

References

- [1] G.E. Moore, *Electronics*, **38** (1965) 114.
- [2] L.T. Canham, *Appl. Phys. Lett.*, **57** (1990) 1046.
- [3] G.V. Prakash, N. Daldossa, E. Degoli, F. Iacona, M. Cazzanelli, Z. Gaburro, G. Pucker, P. Dalba, F. Rocca, E.C. Moreira, G. Franzo, D. Pacifici, F. Priolo, C. Arcangeli, A.B. Filonov, S. Ossicini, and L. Pavesi, *J. Nanosci. Nanotechnol.*, **1** (2001) 159.
- [4] D. Riabinina, M. Chaker, and F. Rosei, *Appl. Phys. Lett.*, **89** (2006) 131501.
- [5] G.G. Ross, D. Barba, C. Dahmoune, Y.Q. Wang, and F. Martin, *Nucl. Instrum. Methods Phys. Res., Sect. B*, **256** (2007) 211.
- [6] B. Kadari, MSc degree thesis, Institut National de la Recherche Scientifique, 2007.
- [7] L. Nikolova, D. Riabinina, B. Kadari, J.M. MacLeod, M. Chaker, F. Rosei, *ECS Transactions Proceedings*, Submitted article, February 2010.
- [8] L. Ding, T.P. Chen, Y. Liu, M. Yang, J.I. Wong, K.Y. Liu, F.R. Zhu, and S. Fung, *Nanotechnology*, **18** (2007) 6.
- [9] A. Lacombe, B. Kadari, F. Beaudoin, D. Barba, F. Martin, and G.G. Ross, *Nanotechnology*, **19** (2008) 6.

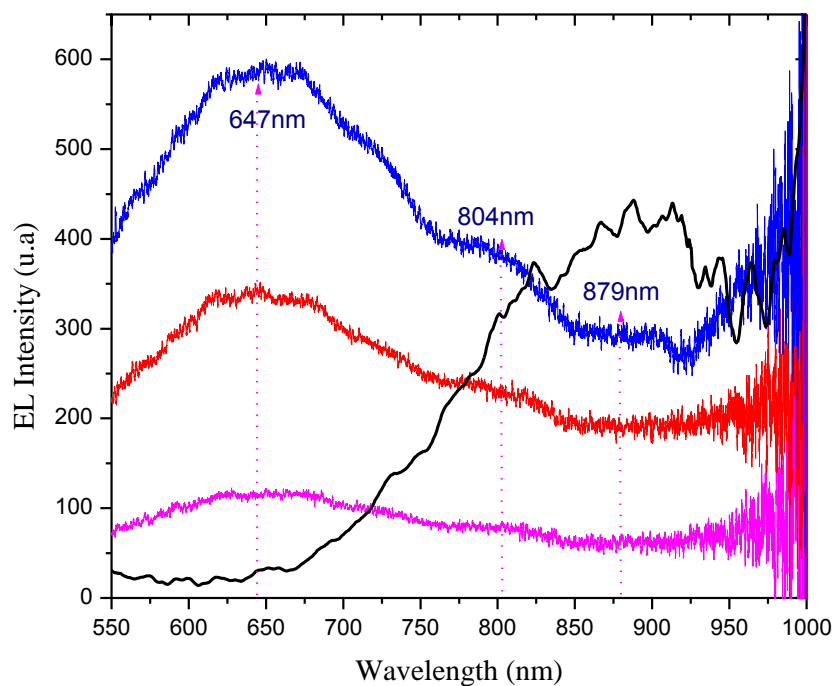


Figure 1. Micro-EL and PL spectra for Si-nc. Blue line: EL at 17V; Red line: EL at 14V; Pink line: EL at 10V; Black line: normalised PL [6].

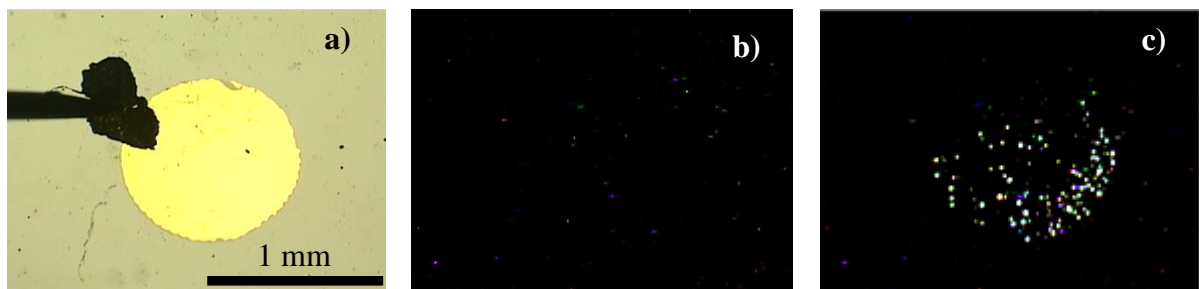


Figure 2. EL points under reverse voltage : (a) image of the electrode; (b) reference at 0V; (c) EL at -18V, -2.7 A/cm^2

Size dependent optical properties of zinc blende CdTe nanocrystals

Kamal John Sundar¹, Richard Karel Čapek¹, David De Muynck², Frank Vanhaecke², Q. Zhao³, A. Van Tomme³, Zeger Hens¹

1 Physics and Chemistry of Nanostructures, Ghent University, B-9000 Ghent, Belgium

2 Laboratory of Analytical Chemistry, Ghent University, B-9000 Ghent, Belgium

3 Instituut voor Kern- en Stralingsfysica and INPAC, K.U.Leuven, B-3001 Leuven, Belgium

Kamal.JohnSundar@UGent.be

Colloidal semiconductor nanocrystals are relatively a new class of fluorescent dyes with a tunable electronic band gap depending on their size due to the quantum confinement effect¹. The optical and electronic properties of these materials make them interesting for applications like LEDs, solar cells and bio-labeling.

We have quantitatively examined the size dependent optical properties of zinc blende CdTe nanocrystals at the bandgap and at high energies. The optical properties are pertinent to the precision of the molar extinction coefficients. These coefficients are interesting physical quantities to determine the concentration. The local field factor has been explicitly taken into account to obtain these coefficients. The interplay of the experimental data obtained by inductively coupled plasma spectroscopy (ICPMS), UV-Vis absorption spectroscopy, transmission electron microscopy (TEM) and Rutherford back scattering (RBS) enables us to determine the extinction coefficients. The intrinsic absorption coefficients deduced at the bandgap increases as power of 3.05 to diameter. Maxwell-Garnette effective medium theory²⁻⁶ enables us to calculate the oscillator strength and the exciton life times of the nanocrystals. The exciton life time is deduced to be between 8-14 ns.

References:

1. L. E. Brus, *Journal of Chemical Physics*, 1984, **80**, 4403-4409.
2. C. A. Leatherdale, W. K. Woo, F. V. Mikulec and M. G. Bawendi, *Journal of Physical Chemistry B*, 2002, **106**, 7619-7622.
3. R. K. Čapek, I. Moreels, K. Lambert, D. De Muynck, Q. Zhao, A. Van Tomme, F. Vanhaecke and Z. Hens, *The Journal of Physical Chemistry C*, 2010, **114**, 6371-6376.
4. I. Moreels, K. Lambert, D. Smeets, D. De Muynck, T. Nollet, J. C. Martins, F. Vanhaecke, A. Vantomme, C. Delerue, G. Allan and Z. Hens, *Acs Nano*, 2009, **3**, 3023-3030.
5. I. Moreels, K. Lambert, D. De Muynck, F. Vanhaecke, D. Poelman, J. C. Martins, G. Allan and Z. Hens, *Chemistry of Materials*, 2007, **19**, 6101-6106.
6. J. Jasieniak, L. Smith, J. van Embden and P. Mulvaney, *Journal of Physical Chemistry C*, 2009, **113**, 19468-19474.

Cause of Ferromagnetism in Copper doped ZnO thin films

Shumaila Karamat, R. S. Rawat, T. L. Tan, and P. Lee

Natural Science and Science Education, National Institute of Education, Nanyang

Technological University, Singapore 637616

shumailakaramat@gmail.com

The possibility of incorporating magnetic degrees of freedom into semiconductor devices has spawned a new field of electronics known as spintronics, and identifying suitable materials is being pursued world-wide. Diluted magnetic semiconductors (DMS) have attracted a lot of attention recently as potential candidates for use in spintronics applications [1]. The thrust on DMS has been aroused after theoretical predictions of Dietl [2] that Mn doped p-type ZnO might display Curie temperatures above room temperature. ZnO doped with Mn, Co, Cr, Ni, V or Fe systems were studied but the drawback to this approach is the segregation of the dopant material [3,4]. The effect of such ferromagnetic clusters must be examined more carefully before the usefulness of such materials for spintronics applications can be determined.

Interestingly, copper-doped zinc oxide (ZnO:Cu) has been predicted to be ferromagnetic and some initial experiments have shown signs of magnetic behavior. Copper is non-magnetic in nature, and neither Cu₂O nor CuO is ferromagnetic. Thus, Cu doped ZnO has potential of showing magnetic behavior only due to substitution of Cu on Zn sites and not due to clustering of Cu into nano-magnetic particles or other impurity phases. Initial studies of ZnO doped with Cu showed contradiction with each other showing non-magnetic and magnetic nature of ZnO:Cu system [5,6]. Some initial theoretical studies of 25% Cu doped ZnO system [4] showed nonmagnetic behavior. Later theoretical studies at lower doping levels indicated ZnO doped with 6.25% [5] and 3.125% Cu [6] should be ferromagnetic. This variation was reconciled by noting the proximity of the copper dopant atoms with respect to each other in the different studies. In this work, we studied copper doped ZnO system with small co-doping of aluminium to improve the conductivity.

In this study, ZnO thin films doped with Cu (1- 5%) and co-doped with Al (0.2%) were grown on *c*-plane (001) sapphire single crystal substrates by pulsed laser deposition. Target pellets, of various compositions, were prepared by the conventional solid-state reaction technique. A pulsed Nd:YAG laser with a wavelength of 532 nm was used for thin film deposition having repetition rate of 10 Hz. X-ray diffraction (XRD) of these films was carried out using a Siemens D5005 X-ray diffractometer with Cu-K α radiation. Chemical analysis of the films grown was carried out by X-ray photo spectrometry (XPS) performed using a Al-K α radiation. Magnetic measurements were performed using a vibrating sample magnetometer (VSM) at 300K. Optical properties were measured by Raman and PL spectroscopy.

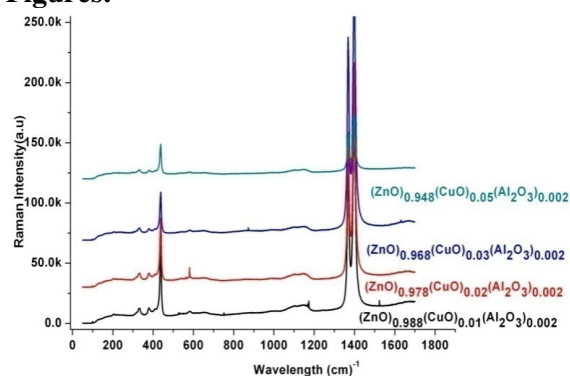
Thin films deposited by PLD are epitaxial in nature having (002) orientation for different compositions. Ferromagnetic signature was also observed for thin films. The cause of ferromagnetic behaviour is the substitution of Zn⁺² ions by Cu⁺² ions in ZnO lattice, which was confirmed from XPS analysis. Thin films are conductive in nature. Ferromagnetic signal and the obtained carrier concentration clearly showed that Cu doped ZnO system has a potential of applications in spintronics but more efforts are required to explore further the different aspects of Cu doped ZnO system.

Rest of the details will be presented in the detailed manuscript.

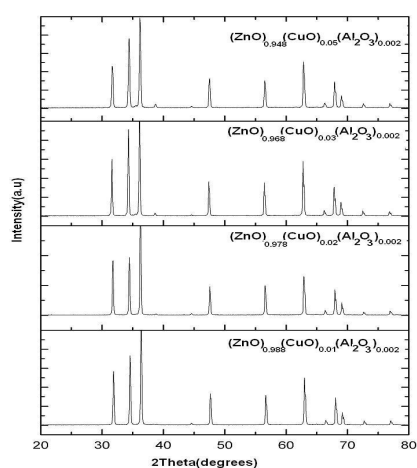
References:

- [1] D. Chakraborti, J. Narayan, J. T. Prater, Appl. Phys. Lett., **90** (2007) 062504.
- [2] T. Dietl, Nat. Mater., **2** (2003) 646.
- [3] S. J. Pearton, D. P. Norton, K. Ip, Y. W. Heo, and T. Steiner, J. Vac. Sci. Technol. B, **22** (2004) 932.
- [4] K. Sato and H. Katayama-Yoshida, Jpn. J. Appl. Phys., **Part 2 39** (2000) L555.
- [5] M. S. Park and B. I. Min, Phys. Rev. B, **68** (2003) 224436.
- [6] C. H. Chien, S. H. Chiou, G. Y. Gao, and Y. D. Yao, J. Magn. Magn. Mater., **282** (2004) 275.

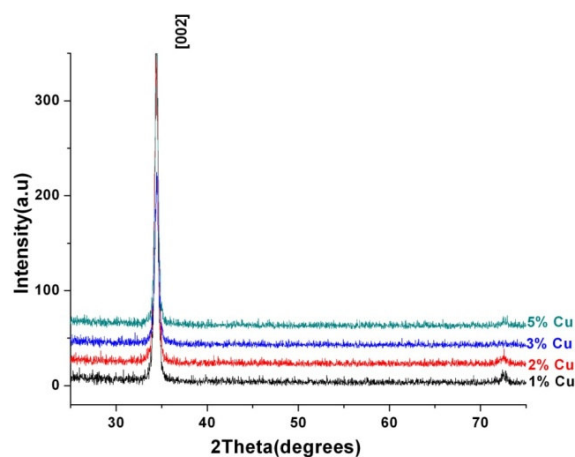
Figures:



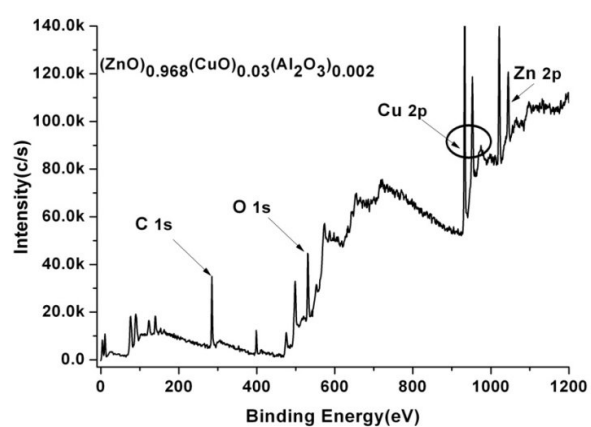
Raman spectra for $(\text{ZnO})_{1-x}(\text{CuO})_x(\text{Al}_2\text{O}_3)_{0.002}$ bulk samples



XRD graphs of $(\text{ZnO})_{1-x}(\text{CuO})_x(\text{Al}_2\text{O}_3)_{0.002}$ bulk samples



XRD graphs for thin film samples grown on sapphire (001) substrates



XPS survey scan for $(\text{ZnO})_{0.968}(\text{CuO})_{0.03}(\text{Al}_2\text{O}_3)_{0.002}$ thin film sample

Dependence of ZnO nanowires at different gas flow rates and flowing gas composition grown by Vapor deposition

Shumaila Karamat, R.S .Rawat, T.L. Tan and P. Lee

Natural Science and Science Education, National Institute of Education, Nanyang Technological

University, Singapore 637616

shumailakaramat@gmail.com

From last few years, motivation for the synthesis of nanostructure materials among researchers has been arisen because of their unique and fascinating properties which make them potential candidates in nano scale industrial applications. ZnO structures especially quasi-one dimensional nanostructures have stimulated intensive interest due to their distinguished performance in electronics, optics and photonics. ZnO is a key technological material. ZnO nano-clusters and thin films have also been shown to exhibit room temperature UV lasing properties. Due to the promising application of ZnO in nano scale optoelectronic devices, it is important to be able to synthesize these nanowires in single crystalline form and study their optical properties.

Nanowires have been grown using various methods including vapor liquid solid (VLS), one of the vapor phase transport form [1-4], chemical vapor deposition [5], arc discharge [6], laser ablation [7], template assisted synthesis [8]. Here we report the growth of ZnO nanowires by vapor liquid solid (VLS) method which is one of the forms of vapor phase transport deposition. In the present experiment, ZnO and graphite powders with a weight ratio of 1:1 were used to grow structures. The growth of ZnO nanostructures is conducted inside a double tube furnace system as shown in figure 1. The growth system comprises a standard quartz tube furnace, vacuum adaptors, a gas flow controller, and a vacuum system. A small quartz tube inside the furnace of 9mm diameter is placed in the middle position for uniform temperature in which ZnO powder and substrates were placed. A carefully calibrated mass flow controller, gas valve and gas regulator with gas cylinder was connected to the left end of the furnace tube. Different structures were obtained for different flow rates and different argon oxygen gas mixtures composition.

In the present approach, Au layer is used as a catalyst, Au droplet and wire formed under the reaction conditions. Au droplets serves as a preferential site for the absorption of gas phase ZnO and, when super saturated, the nucleation site for crystallization. During the growth, the catalyst droplet directs the nanowires growth direction and defines the diameter of the nanowire. In our experiments, we grow structures for different argon- oxygen gases percentage of gases in Argon gases for 90 mins. X- ray diffraction patterns were recorded by using SIEMENS D5000 X-ray diffractometer equipped with a Cu-K α ($\lambda=1.544 \text{ \AA}$) source. SEM images were obtained on a JEOL JSM-6700F field emission scanning electron microscope. The electronic states of elements were estimated by X-ray Photoelectron Spectroscopy (XPS) with Kratos Axis-Ultra spectrometer equipped with a focused monochromatic Al-K α X-ray beam. Optical measurements were done by using an Acton 2759 monochromator to estimate different emissions of ZnO.

XRD spectrum showed ZnO diffraction peaks. SEM micrographs showed the wires in the vertical and the horizontal direction for different flowing gas composition. Room temperature photoluminescence spectrum of as prepared nanowires shows two emissions in UV and visible regions that can be ascribed to the near band edge (NBE) transitions and to deep-level trap-state transitions, respectively. Compositional analysis was also done to investigate the change in the valance states of elements.

References:

- [1] Y. Cui, L.J. Lauhon, M.S. Gudiksen, J. Wang, and C.M. Lieber, Appl. Phys. Lett., 78, (2001) 2214
- [2] G. Gu, M. Burghard, G. T. Kim, G. S. Dusberg, P. W. Chiu, V. Krstic, S. Roth, and W.Q. Han, 90, (2001) 5747.
- [3] M. H. Huang, Y.Wu, H. Feick, N. Tran, Weber, E. and P.Yang, Adv. Mater., 13, (2001)113.
- [4] M.H. Huang, S. Mao, H. Feick, H.Yan, Y.Wu, H. Kind, E. Weber, R. Russo and P. Yang, Science, 292, (2001) 1897.
- [5] Y. Wu, R. Fan and P.Yang, Nano Lett., 2(2), (2002) 83.
- [6] Y.C. Choi, W.S. Kim, Y.S. Park, S.M. Lee, D.J. Bee, Y.H. Lee, G.S. Park, W.B. Choi, N.S. Lee and J.M. Kim, Adv. Mater., 12, (2000) 746.
- [7] A.M. Morales and C.M. Lieber, Science, 279, (1998) 208.

Figures:

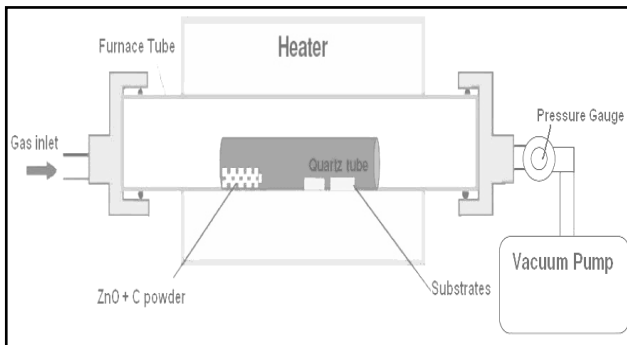


Fig 1. Schematic of the experimental setup

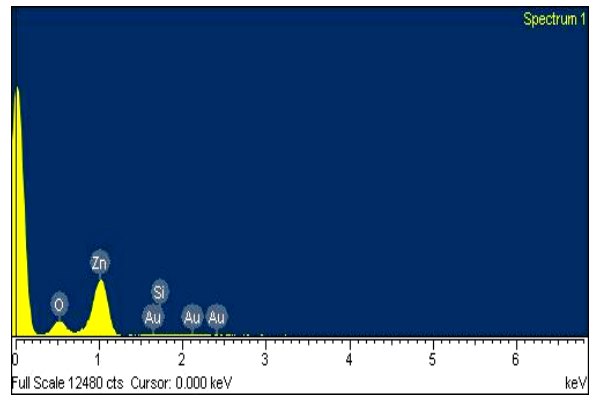


Fig 2. EDX spectrum of ZnO nanowires

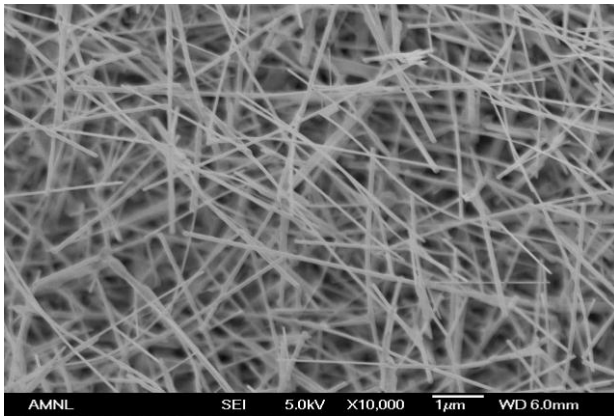


Fig 3. SEM micrograph of thin films grown in Ar-O₂ gas flow

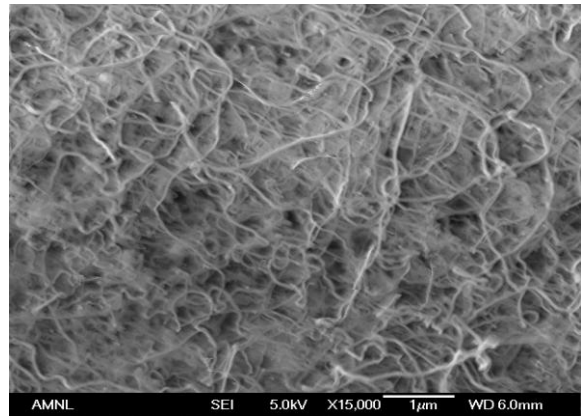


Fig 4. SEM micrograph of thin films grown in Ar gas flow

Plant Virus Drug Delivery

Abid Ali Khan¹, S. Emil Ruff², Christina Wege² and Alexander M. Bittner^{1,3}

¹ CIC nanoGUNE Consolider, Tolosa Hiribidea 76, 20018 Donostia – San Sebastian, Spain

² Institute of Biology, University of Stuttgart, Pfaffenwaldring 57, 70569 Stuttgart, Germany

³ IKERBASQUE, Basque Foundation for Science, 48011 Bilbao, Spain

a.khan@nanogune.eu

Tobacco Mosaic Virus is a tubular plant virus containing RNA and 2100 identical coat proteins. Our aim is filling up the 4nm wide and 300nm long channel of TMV with a cytostatic drug (e.g. otherwise highly toxic Pt compounds such as Cisplatin) and sealing the TMV ends by magnetic nanoparticles. The administration involves application of an alternating external magnetic field to break the seal to release the drug, as well as to generate heat, for simultaneous drug and hyperthermia treatment [1].

The Tobacco mosaic virus (TMV) can be metallized in aqueous suspension, resulting in unique dumbbell-, rod- and tube-shaped deposits with diameters down to 3 nm and lengths up to micrometers [2, 3]. The coating process is based on the adsorption of noble metal cations followed by autocatalytic electroless deposition (figure 1). Magnetometry measurements performed on these TMV samples (metallized with Ni) find a saturation magnetization of approximately 0.004 emu per gram of deposited solid (which contains Ni but also salts from the bath). This very low value can be accounted for by a cluster microstructure consisting of rather small Ni cores surrounded by NiO shells, which would be indicative of extensive oxidation. However, the measured coercivity of 90 Oe is similar to that of bulk Ni (100 Oe), suggesting that the cores are large enough to exhibit bulk ferromagnetism (figure 2). Previous work with TMV electroless deposition [3] showed that using the anionic surfactant Re-610/E makes Ni dots deposition only at ends of the TMV (figure 3). This was the basis for sealing the 4nm channel.

References

[1] MAGNIFYCO Project. (FP7-NMP-2007-SMALL-1). T. Pellegrino, NNL Lecce, Italy.

[2] S. Balci, K. Noda, AM Bittner, A. Kadri, C. Wege, H. Jeske and K. Kern. *Angew. Chemie Int. Ed.* **46** (2007) 3149-3151.

[3] Z. Wu, R. Zierold, A. Müller, E. Ruff, C. Ma, Abid A. Khan, F. Geiger, M. Knez, K. Nielsch, Alexander M. Bittner, C. Wege and Carl E. Krill III. *Submitted*.

Figures



Figure 1: Ni deposited on TMV via electroless deposition

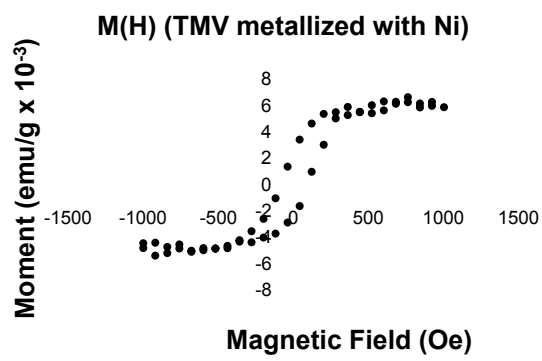


Figure 2: Magnetization of Ni deposited on TMV

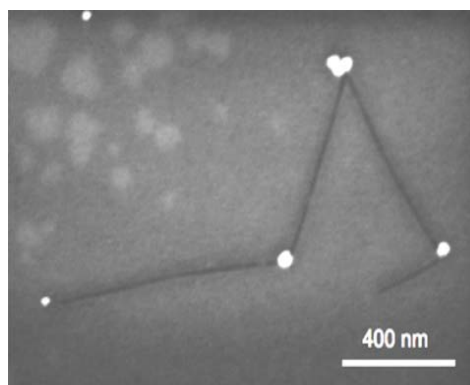


Figure 3: Ni-TMV-Ni dumbbells synthesized using Re-610/E in electroless deposition bath

Physical Change of Transparent Film Heaters Based on Single-Walled Carbon Nanotubes in High Temperature Environment

Duckjong Kim, Hyun-Chang Lee, Ju Yeon Woo, Chang-Soo Han

Korea Institute of Machinery and Materials, 171 Jang-dong, Yuseong-gu, Daejeon 305-343, Korea
cshan@kimm.re.kr

Carbon nanotube (CNT) is a cylindrical carbon nanostructure with good transport properties along tube's axis. As one approach of practical use, CNT networks are made and their application to many areas is investigated. In particular, since single-walled carbon nanotubes (SWCNTs) are very slender, network of SWCNTs can be transparent keeping the inherent transport characteristics. The transparent conducting film (TCF) has been studied for use as electrodes in photovoltaics, organic light-emitting diodes, touch screens, sensors, transistors, and speakers. Recently, we reported the possibility of creating a transparent heater using CNT-TCF [1]. In such a heater, we must consider various physical aspects, which affect each other during the heating of the CNT-TCF. Detailed research into the thermal characteristics of CNT-TCFs is essential if they are to be commercially used as transparent heaters.

In this research, we investigated the thermal behavior of transparent film heaters (TFHs) made of single-walled carbon nanotubes (SWCNTs). The temperature dependence of the electrical resistance of the TFHs heated by Joule heating was examined. The change in physical properties of the TFHs due to heating was investigated with an analysis of Raman and transmittance spectra.

We fabricated the TCF by using the spray coating method. We dispersed SWCNTs in deionized water with 1 wt% sodium dodecyl sulfate (SDS) and sonicated for several hours. The concentration of the SWCNT solution was 1 $\mu\text{g/ml}$. We sprayed the SWCNT solution on a glass substrate to form the TCF. The size of the glass substrate is 50 mm \times 50 mm \times 0.5 mm. As a result, we made TCFs with transparency of about 70 % at 550 nm. The sheet resistance of the TCFs was in the range of 130~160 Ω/sq . Finally, on the TCF, we formed electrodes by using silver paste to make a low-resistance electrical contact. We applied the voltage difference of 60 V across the electrodes by using a DC power supply (Agilent E3649A). We measured the voltage difference and the surface temperature of the TCF by using a data acquisition unit (Agilent 34970A) and monitored the electrical current through the TCF by using a current meter (Fluke 189). For temperature measurement, we used T-type thermocouples. We calculated the electrical resistance by dividing the applied voltage difference by the measured current. To analyze the Raman spectra of the TFHs before and after heating, Raman spectroscopy with wavelength of 633 nm (inVia, Renishaw) was used to detect changes in the RBM, D, and G modes. We measured the optical transmittance by using the absorption spectroscopy (Optizen 2120UV Plus).

After heating and leaving the samples at room temperature for several days, we measured the resistances of the films. The results are shown in Table 1. There was no significant change when the film was heated to 150°C; the resistance changes were too small. However, heating to 200°C did change the resistance. After recovery, the TFH resistance had increased by about 10%. Moreover, when the temperature was increased to 300°C, the resistance, even after a few days of recovery, increased significantly by over 300%.

To determine the reason why the resistances changed permanently above 200°C, we captured Raman spectra with excitation energy of 633 nm; the result is shown in Fig. 1. Figure 1 compares the results for unheated (pristine) samples, samples heated to 65°C, and samples heated to 200°C. For the pristine and samples heated to 65°C, the peaks in the RBM, D, and G bands did not change, demonstrating that there was no physical change caused by low-temperature heating. On the contrary, Joule heating of the TFH to 200°C caused a definite change in the physical aspects. The semiconducting peak in the RBM mode disappeared, and the peak in the G band increased. This means that some of the semiconducting nanotubes were removed. In the D band, several peaks, except for 1340 cm^{-1} , which denotes defects on the carbon lattice structure, were significantly reduced. A previous report indicated that a CNT is burned out when a large current is applied [2]. If the connection between electrodes includes metallic and semiconducting nanotubes, the metallic nanotubes are broken down first. According to the stepwise increase of the current, they could create a semiconducting device. However, we obtained unexpected results by heating the TFH above 200°C. This behavior requires further detailed research.

We heated the TFH to temperatures greater than 300°C and found that the optical morphology of the TCF definitely changed as shown in Fig. 2. In the region 2, the temperature was maximum and greater than 360°C. The higher temperature made the region 2 of the TCF more transparent. When we measured the transmittance of the TFH sample before and after the experiment, the transparency of region 2 improved significantly from 69.7% to 85.7% at 550 nm. On the other hand, the transmittance of the regions 1 and 3 of the TCF sample changed very little.

We are developing an explanation on the mechanism underlying the observed phenomena. This study would improve understanding of the heating effect on the physical properties of the transparent conducting film using SWCNTs which could be a good candidate for the heater in many applications requiring both heating function and transparency.

References

- [1] Yoon, Y. H., Song, J. W., Kim, D., Kim, J., Park, J., Oh, S. and Han, C.-S., *Advanced Materials*, **19** (2007) 4284-4287.
 [2] Collins, P. G., Arnold, M. S. and Avouris, P., *Science*, **292** (2001) 706-709.

Figures

Table 1 Permanent resistance change according to maximum heating temperature.

Maximum heating temperature (°C)	Electrical resistance (Ω)	
	Before heating	After heating
65	135.5	137.2
100	138.0	133.6
150	139.0	133.5
200	135.2	147.8
300	136.8	497.6

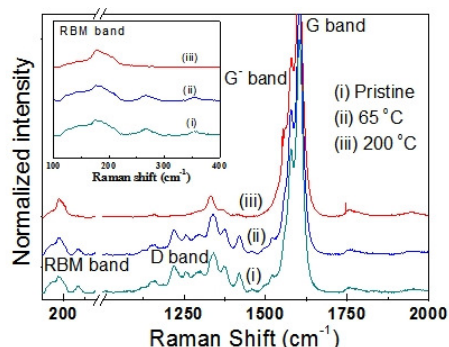


Fig. 1 Raman spectra of SWNT thin films at an excitation energy of 633 nm.

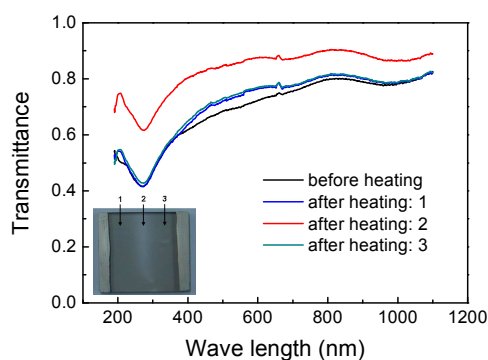


Fig. 2 Transmittances of the TFH heated above 300°C.

Cell adhesion study to new endosteal implant by atomic force microscopy

Petr Kolar¹, Katerina Tomankova¹, Hana Kolarova¹, Klara Safarova², Jana Frankova³, veronika Pivodova³ and Jitka Ulrichova³

¹Department of Medical Biophysics, Faculty of Medicine, Palacky University in Olomouc, Hnevotinska 3, 775 15 Olomouc, Czech Republic

²Centre for Nanomaterial Research, Faculty of Science, Palacky University in Olomouc, Slechtitelu 11, 783 71 Olomouc, Czech Republic

³Department of Medical Chemistry, Faculty of Medicine, Palacky University in Olomouc, Hnevotinska 3, 775 15 Olomouc, Czech Republic
peta.kolar@seznam.cz

Till now, commercially pure titanium has been the most successful and widespread material used for these implants [1]. We tested morphological and mechanical properties of cell lines of alveolar fibroblasts placed on newly developed materials. We used the following modified titanium targets as a substrate for cells: 1. polished titanium; 2. rough machined titanium; 3. rough machined and alkalic corroded titanium; 4. rough machined, sandblasted and acid corroded titanium; 5. rough machined, sandblasted, acid and alkalic corroded titanium; 6. rough machined titanium covered by zirconium nitride. We used cell lines placed on Thermanox plastic discs as a control group. We imaged these cell lines on individual new material targets and we tested mechanical and adhesive properties of these cells by atomic force microscopy (AFM) and scanning electron microscopy (SEM). Measuring was performed with 0.1% glutaraldehyde fixation in air or in liquid and without chemical fixation in liquid. This study demonstrated that AFM can be used to obtain high resolution topographical images of cells, and to quantify the tip–cell interaction force and the surface elasticity or cell adhesivity to the substrate [2]. With SEM we show control images of adhesive and topographic arrangement of cells and current results show that cells grow along topographic changes on substrate. AFM measuring determined the best properties of tested materials according to value of adhesive forces between cells and substrates.

Acknowledgement

This work has been supported by the Projects of the Ministry of Education of the Czech Republic MSM6198959216, MSM6198959218, 1M6198959201, Ministry of Industry and Trade MPO FI-IM5/218, Czech Science Foundation GACR 303/09 H048 and Institute of Molecular and Translational Medicine CZ.1.05/2.1.00/01.0030.

Reference

- [1] G. Lauer, M. Wiedmann-Al-Ahmad, J.E. Otten, U. Hubner, R. Schmelzeisen, W. Schilli., *Biomaterials* **22** (2001), 2799-2809.
- [2] C.B. Vollea, M.A. Ferguson, K.E. Aidala, E.M. Spainc, M.E. Núneza., *Colloids and Surfaces B: Biointerfaces* **67**, (2008) 32–40.

Lithographic processing for Large Area CVD Graphene

Shishir Kumar, N. Peltekis, K-H. Lee, H-Y. Kim, Georg S. Duesberg

CRANN and School of Chemistry, Trinity College, Dublin, Ireland
duesberg@tcd.ie

We present a study on making devices from large area chemical vapour deposition graphene. Starting from controlled CVD growth of graphene on Cu films, the large area graphene was transferred on to insulating substrates. Optical lithography followed by lift off and etching is used to structure graphene devices. We discuss the problems faced in etching large area graphene using conventional processes used in microlithography. This work will be useful for high volume processing of graphene using these scaleable processes steps, yielding FET and sensor devices on large areas. We also present a study of the effects of processing on graphene by AFM, SEM, TEM and XPS. Electrical measurements performed indicate p-doping of graphene. Further measurements oriented towards sensor applications are also presented.

Speeding up DNA purification for gold nanoprobe-based detection assays

Miguel Larginho^{a,b}, Gonçalo Doria^a, José Luis Capelo^b and Pedro Viana Baptista^{a*}

^a CIGMH/DCV, Faculdade de Ciências e Tecnologia, Universidade Nova de Lisboa, Campus da Caparica, 2829-516 Caparica, Portugal, Tel/Fax: +351 212 948 530;

^b BIOSCOPE Group, Faculty of Science, Physical-Chemistry Department, Campus Ourense, University of Vigo, 32004, Ourense, Spain;
E-mail: pmvb@fct.unl.pt

We have previously reported on a gold nanoprobe assay based on colorimetric differentiation between samples, after salt addition: DNA samples harbouring a complementary sequence to the nanoprobe prevent aggregation and the solution retains its original red colour; the absence of a complementary sequence does not stabilise the nanoprobe and aggregation occurs, with subsequent colour change from red to blue^{1,2}.

Sample pre-treatment is a crucial step in most biomolecular recognition assays. Current isolation and purification procedures often require enzyme digestion steps and organic solvent extractions in order to refine the sample for biosensing assays. Ultrasonic energy has already proven to be a viable and fast option in generating fragments from purified DNA samples³. We report an inexpensive, fast and simple methodology for nucleic acids extraction for improvement of the subsequent detection using a gold nanoprobe-based colorimetric assay. This work uses an ultrasonic platform as a means for simultaneous cell disruption and biomolecules fragmentation. Afterwards, a quick enzyme-free procedure for further DNA purification is used, in order to remove some contaminants which may hamper the detection step. By using the sonoreactor for simultaneous cell bursting and DNA fragmentation, this protocol saves time and enhances the target availability for hybridisation with the nanoprobes.

References

- [1] P. Baptista, G. Doria, D. Henriques, E. Pereira and R. Franco, *J. Biotechnol.* **119** (2005) 111.
- [2] J. Conde, J.M. de la Fuente, P.V. Baptista, *J. Nanobiotechnol.* **8** (2010) 5.
- [3] M. Larginho, H.M. Santos, G. Doria, H. Scholz, P.V. Baptista, J.L. Capelo, *Talanta* **81** (2010) 881.

Acknowledgements

We thank FCT/MCTES for financial support: CIGMH, PTDC/SAU-BEB/66511/2006 and PTDC/EEA-ELC/74236/2006. SFRH/BD/64026/2009 for Miguel Larginho. Dr. J. L. Capelo acknowledges Xunta de Galicia (Spain) for their Parga-Pondal Research contract and Universidade de Vigo (Spain) for Project ref. 2009-INOUE-15.

Damaging Graphene with Ozone Treatment : a Chemically Tunable Metal-Insulator Transition

N. Leconte¹, J. Moser², P. Ordejon², H. Tao², A. Lherbier¹, A. Bachtold², F. Alsina², C.M. Sotomayor Torres^{2,3}, J.-C. Charlier¹, S. Roche^{2,4}

¹ IMCN, Université catholique de Louvain, Place Croix du Sud 1 (NAPS-ETSF), B-1348, Louvain-la-Neuve, Belgium

nicolas.leconte@uclouvain.be

² CIN2 (ICN-CSIC) Barcelona, Campus UAB, E08193 Bellaterra, Spain

³ ICREA, 08010 Barcelona, Spain

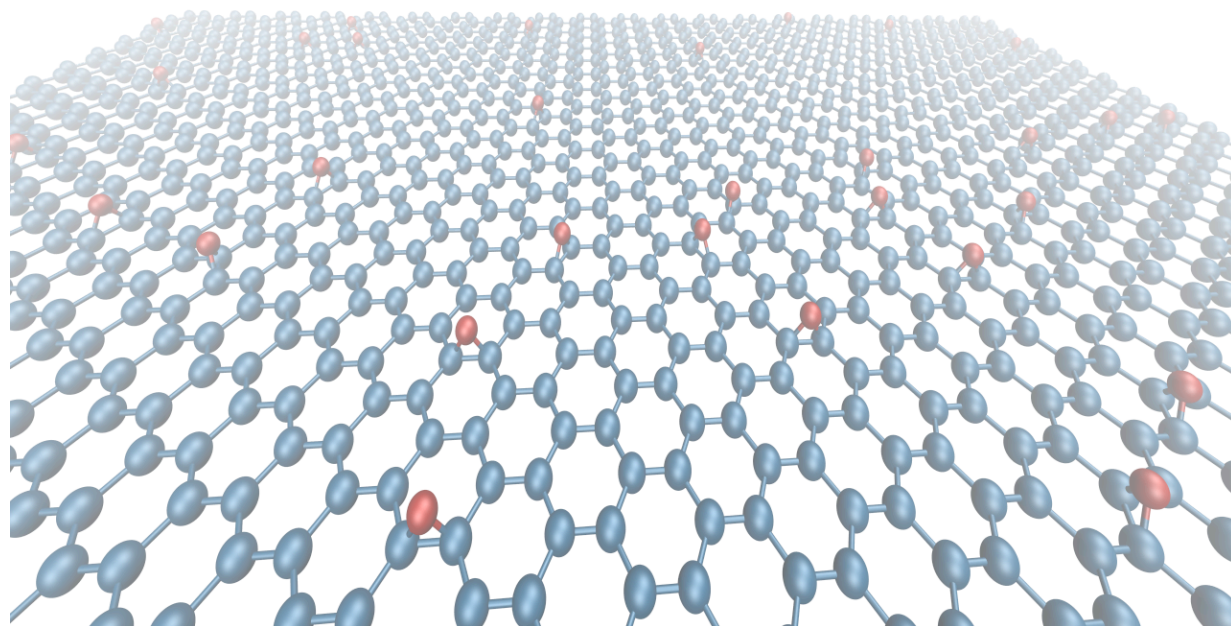
⁴ CEA, INAC, SP2M, L_Sim, 17 Avenue des Martyrs, 38054, France

We present an *ab initio* multiscale study of electronic and transport properties of two-dimensional graphene after epoxide functionalization via ozone treatment[1,2]. The orbital rehybridization induced by the epoxide groups triggers a strong intervalley scattering and changes dramatically the conduction properties of graphene. A DFT-parametrized tight-binding model within the Kubo formalism[3] allows us to simulate mesoscopic-sized systems up to 2 million atoms. By varying the random coverage density of epoxide defects from 0.1 to 4%, charge conduction can be tuned from a diffusive to a strongly localized regime, with localization lengths down to a few nanometers long. Experimental results[4] supporting the interpretation as a metal-insulator transition are also provided.

References

- [1] N. Leconte, J. Moser, P. Ordejon, H. Tao, A. Lherbier, A. Bachtold, F. Alsina, C.M. Sotomayor Torres, J.-C. Charlier, and S. Roche, submitted to ACS Nano (2010)
- [2] N. Leconte, P. Ordejon, A. Lherbier, J.-C. Charlier, and S. Roche (in preparation)
- [3] H. Ishii, F. Triozon, N. Kobayashi, K. Hirose, and S. Roche, C. R. Physique **10**, 283 (2009)
- [4] J. Moser, H. Tao, S. Roche, F. Alsina, C.M. Sotomayor Torres, and A. Bachtold, arXiv:1003.1299

Figures



Preparation and characterization of coordination polymer particles with various aspect ratio

Soo-Keun Lee, Sunhye Kim, Sang Kyoo Lim

Division of Nano-Bio Technology, Daegu Gyeongbuk Institute of Science and Technology (DGIST),
Samsung Financial Plaza, Duksan-dong 110, Jung-gu, Daegu 700-010, Korea
laser@dgist.ac.kr

Coordinated polymer particles (CPPs) have attracted a great attention because of their high surface area and fundamentally interesting unique structure, which allow for applications in non-linear-optics,[1] catalysis,[2] gas storage,[3, 4] and molecular recognition.[5] A sophisticated understanding of coordination polymer particle formation, as well as the concomitant size and shape control, is crucial for the practical application of these materials. However, the fine control of CPP shape has not been well studied. Herein we report the formation of rod shaped bimetal (In and Sn) coordinated polymer particles and control of their aspect ratio (4 to 20).

The rod shaped bimetal coordinated materials were synthesized by the following process: 1,4-benzenedicarboxylic acid (TPA) was dissolved in N,N-dimethylformamide (DMF) and methanol, and DMF containing InCl_3 and SnCl_4 was added to the prepared solution. The resulting mixture was heated at $100\text{ }^\circ\text{C}$ for 4 hours. The product generated in this time was isolated by cooling the reaction mixture to room temperature, collecting the precipitate by centrifugation, and washing several times with DMF and methanol. Field-emission scanning electron microscopy (SEM) images of In/Sn-CPP (Figure 1a) reveal rod formation with various length ($\sim 100\text{ nm}$ to $\sim 10\text{ }\mu\text{m}$). The chemical composition of In/Sn-CPP was determined by energy dispersive X-ray (EDX, Figure 1b) spectroscopy. The IR spectrum of In/Sn-CPP confirms the coordination of the carboxylate groups of TPA to metal ions, as evidenced by a shift in the CO stretching frequency to lower frequency compared to the CO stretching frequency for the uncoordinated TPA. The resulting In/Sn-CPP was found to be thermally stable to $460\text{ }^\circ\text{C}$, by thermogravimetric analysis. Furthermore, TGA data reveal that no significant guest molecules are involved in In/Sn-CPP after conventional vacuum treatment, as evidenced by no substantial weight loss until $460\text{ }^\circ\text{C}$. The aspect ratios of the rod shaped In/Sn-CPP were varied by changing the added amount of methanol. The more added methanol produced the lower aspect ratio materials. The reason for this phenomenon may relate with the amount of nuclei formation with different solvent conditions. The effect of such parameters upon the particle size was rationalized on the basis of crystal growth mechanism.

This work was supported by DGIST basic research program of the MEST.

References

- [1] Evans, O. R. & Lin, W., *Acc. Chem. Res.*, 2002, **35** (2002) 511.
- [2] Seo, J. S. et al., *Nature*, **404** (2000) 982.
- [3] Rosi, N. L. et al., *Science*, **300** (2003) 1127.
- [4] Yaghi, O. M. et al., *Nature*, **423** (2003) 705.
- [5] Kosal, M. E., Chou, J.-H., Wilson, S. R. & Suslick, K. S., *Nature Mater.*, **1** (2002) 118.

Figures

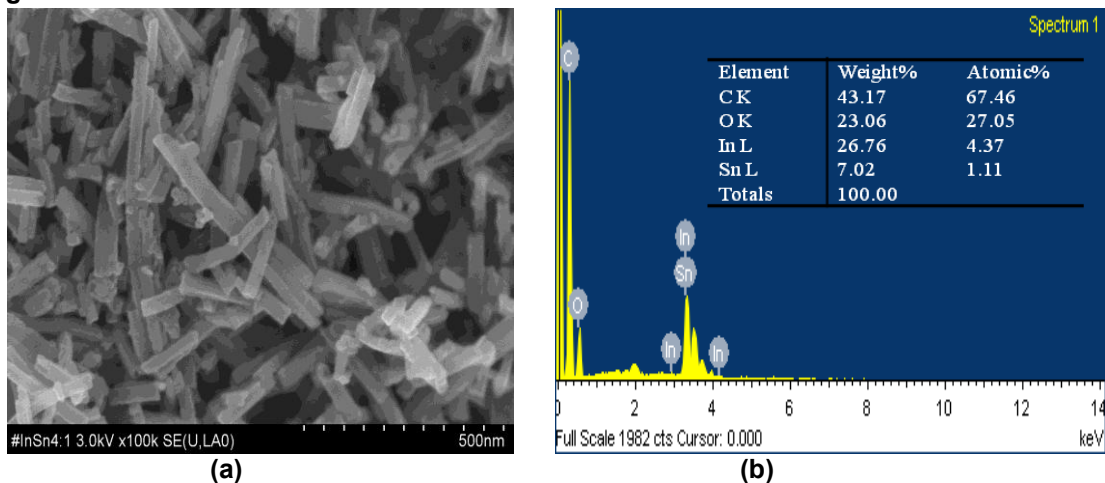


Figure 1. SEM image and EDX spectrum of In/Sn-CPP.

Size-controllable synthesis of hollow Calcium carbonate nanotube and its application for detoxifying reagent

Xuan Qi Li, Hua Chun Zeng*

Department of Chemical and Biomolecular Engineering, Faculty of Engineering
NUS Graduate School for Integrative Sciences and Engineering
National University of Singapore
10 Kent Ridge Crescent, 119260, Singapore
chezhc@nus.edu.sg

Calcium carbonate (CaCO_3) is one of the most important mineral materials with vast applications. In recent years, its crystallization and nucleation processes with or without template have been under extensive investigation [1]. On the other hand, fabrication of functional materials, including CaCO_3 , with hollow interiors has also received great attention, since it has potential applications in many fields, such as photonic crystals, host materials for intercalants, drug-delivery carriers, sensors and chemical reactors, etc [2].

In this work, we presented two synthetic methods to prepare CaCO_3 nanotubes with hollow structures at room temperature. In our experiments, sodium citrate and calcium citrate, which are commonly used as food additives, were used as precursor compounds. The diameter size of the nanotubes could be controlled in the range of 50 to 500 nm by changing the relative mass or concentration of reactants. In addition, the mechanism of the reaction, which combined both oriented attachment and Ostwald ripening, have been further investigated and discussed. Furthermore, detoxifying capability of the CaCO_3 material has also been tested, which showed that our CaCO_3 products were effective for removing heavy metal ions such as Pb^{2+} and Cd^{2+} from aqueous solution. One of interesting phenomena was that, the reaction between CaCO_3 and the heavy metallic ions would happen at first in the hollow areas inside the nanotube, implying that the inner surface was more activate than the outer surface, and the as-prepared CaCO_3 nanotubes could be used in removal of heavy metallic ions, as demonstrated in this work.

References

- [1] Hanying Li, Lara A. Estroff*, Journal of the American Chemical Society, 129 (2007) 5348.
- [2] Wei Wei, Guang-Hui Ma*, Gang Hu, Di Yu, Tom Mcleish, Zhi-Guo Su, Zhe-Yu Shen, Journal of the American Chemical Society, 130 (2008) 15808.

Nanotube Synthesis: Gold(I)–Alkanethiolate Nanotubes

Yu Xin Zhang, **Zheng Li**, Hua Chun Zeng*

Department of Chemical and Biomolecular Engineering, Faculty of Engineering
NUS Graduate School for Integrative Sciences and Engineering
National University of Singapore
10 Kent Ridge Crescent, 119260, Singapore
chezhc@nus.edu.sg

The prospect of new electronics, materials and biomedical applications has boosted research on the synthesis of carbon and metal-based nanotubes. However, no metal–organic supramolecular solids have yet been shaped into nanotube backbones. Our group has for the first time synthesized nanotubes that incorporate hybrid metal–organic complexes into their wall structure. Gold(I)-alkanethiolate nanotubes were successfully synthesized through the self-assembly approach to produce bilayer structure of platelets of gold ion bound to alkanethiolate ligands and then curl process of the sheets structure into nanotubes [1].

Nanotubes were produced by adding gold ion precursor-ligand mixture to an alkaline solution with the presence of a non-ionic surfactant. With specific hydrocarbon chain lengths, the bilayer structures were synthesized firstly and then curled into nanotube with good quality and uniformity, under the assistance of non-ionic surfactant. The different layers were held in the nanotube structures due to van der Waals interaction between the alkanethiolates. The synthesized nanotubes are very stable and remain intact when subjected to various strong acids, bases and reducing reagents, as well as common solvents. This exceptional chemical stability and robustness is thought to originate from the protection provided by the hydrophobic alkanethiolate chains. Besides, we also demonstrated that under the irradiation of electron beam, the gold ions in the bilayer can be reduced into metallic gold nanoparticles [1].

Further applications for the nanotubes include that they can be used as precursors for hybrid supernanotubes combining the properties of gold nanoparticles and nanotubes, with many new and promising applications. We are currently optimizing gold reduction and ordering of the resulting gold nanoparticles.

Reference

[1] Yu Xin Zhang, Hua Chun Zeng*, *Advanced Materials*, 21 (2009) 4962.

Preparation and characterization of ZnO Nanofibers by Electrospinning

Sang Kyo Lim, Sung-Ho Hwang, So Hee Bang, Daeic Chang, Soon Hyun Kim

Daegu Gyeongbuk Institute of Science & Technology, 5th Floor, Daegu Technopark Venture 2 Plant, 75 Gongdanbuk2gil, Dalseo-gu, 704-230, Daegu, Republic of Korea
limsk@dgist.ac.kr

Recently, one-dimensional nanostructured materials such as nanowires, nanofibers, nanorods, and nanotubes have received a great attention for their potential applications in numerous areas due to their special properties, which are distinct from conventional bulk materials. Among various semiconductor nanostructures, variety of nanostructures of ZnO has been investigated.

Pure ZnO is an n-type semiconductor with a wide bandgap (3.37 eV) and it is one of the most promising materials due to its use in a wide range applications in various fields, including short wavelength light-emitting diode and room temperature ultraviolet (UV) lasing diode, solar cell, UV-absorber, transparent conductor, gas sensor, etc.

The ZnO has been early and widely studied due to its high mobility of conduction electron, good chemical and physical stability, low cost, and so on. Compared to other structural types of ZnO gas sensors, nanostructured ZnO gas sensors are reported to exhibit higher sensitivity.

From this perspective, of ZnO nanofiber based gas sensors are expected to exhibit sensing performance at very low gas concentrations. We have prepared PAN nanofibers from PAN solutions by an electrospinning method. Subsequent calcination of PAN nanofibers under an N₂ atmosphere produced carbon nanofibers(CNF). The carbon nanofibers was coated with zinc oxide sol. Finally, thermal treatment of the zinc oxide sol coated CNF under oxidative conditions resulted in ZnO nanofibers. In this work, we prepared ZnO nanofibers using an electrospinning method.

The morphologies and microstructures of ZnO nanofibers as a function of annealing temperature were analyzed using X-ray diffraction (XRD) and scanning electron microscopy (SEM). Furthermore, the electrical and CO gas sensing properties of ZnO nanofibers were investigated.

References

- [1] S. Lee, T.R. Kim, A.A. Ogale, M.S. Kim, Synthetic Met. 157 (2007) 644.
- [2] Y. Wang, S. Serrano, J.J. Santiago-Aviles, Synthetic Met. 138 (2003) 423.
- [3] B.Y. Deng, X. Yan, Q.F. Wei, W.D. Gao, Mater. Character. 58 (2007) 854.
- [4] N. Kumar, R. Kaur, R.M. Mehra, J. Lumin. 126 (2007) 784.
- [5] Y.Y. Villanueva, D.R. Liu, P.T. Cheng, Thin Solid Films 501 (2006) 366.
- [6] S. Kim, S.K. Lim, Appl. Catal. B: Env. 84 (2008) 16.
- [7] S. K. Lim, S. H. Hwang, S. Kim, Cryst. Res. Technol. 45, (2010) 771.
- [8] Y.J. Kim, C.R. Park, Carbon 43 (2005) 2397.

Figure. 1 FE-SEM images of ZnO nanofibers

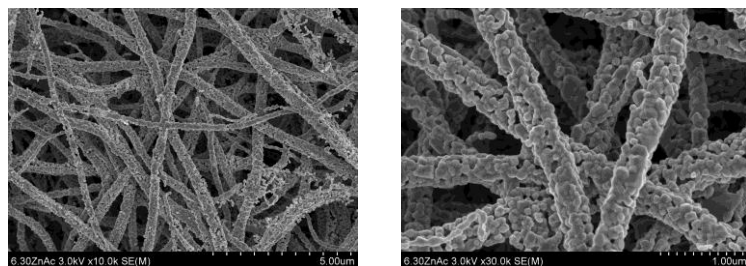
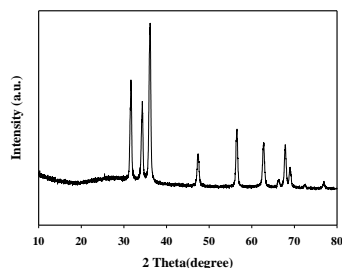


Figure. 2 XRD pattern of ZnO nanofibers



Phonon Transport in Large Scale Carbon-Based Disordered Materials: Implementation of an Efficient Order N and Real Space Kubo Methodology

Wu Li, Haldun Sevinçli, Stephan Roche and Gianaurelio Cuniberti

Institute for Materials Science and Max Bergmann Center of Biomaterials,
Dresden University of Technology, 01062 Dresden, Germany.
wu.li@nano.tu-dresden.de

In recent years, the understanding of phonon transport in carbon-based materials such as carbon nanotubes (CNTs) and graphene-based materials has become particularly important for both fundamental studies of coherent transport but also in view of novel applications. Conventional Green function approach cannot be used to study large system since it requires matrix inversions. An efficient computational approach is demanded in order to tackle large scale (and realistic) simulations of material of interest. In this poster, using the Kubo formalism[1] we demonstrate that a time-dependent phonon wavepacket formalism can be connected to the calculation of the thermal conductance, which has exactly the same form as the real space Kubo approach studying electronic transport[2]. After validating this numerical approach by comparing the obtained phonon mean free paths (MFP) in disordered CNTs (with isotope impurities) with previously computed ones by means of Green functions-based method [3], we apply the new algorithm to large width GNRs, and focus on the impact of edge disorder profiles. Scaling properties of phonon MFP and temperature-dependent thermal conductance are calculated as a function of edge disorder strength and for ribbon lateral sizes accessible to today's state-of-the-art lithography. A strong impact of smooth edge disorder on the thermal conductance was found, pinpointing towards good thermoelectrical properties of large width nanoribbons[4]. The broad generality of our method could offer a novel frame to explore other types of complex materials, including Boron-nitride-based materials or silicon-based materials (nanowires, superlattices, etc.).[5]

References

- [1]P. B. Allen and J. L. Feldman, Phys. Rev. B **48**, 12581 (1993).
- [2]F. Triozon et al., Phys. Rev. B **69**, 121410(R) (2004);
A. Lherbier et al., Phys. Rev. Lett. **100**, 036803 (2008).
- [3]I. Savić, N. Mingo, D. A. Stewart, Phys. Rev. Lett **101**, 165502 (2008).
- [4]H. Sevinçli and G. Cuniberti, Phys. Rev. B **81**, 113401 (2010).
- [5]W. Li, H. Sevinçli, G. Cuniberti and S. Roche, *submitted*

Figures

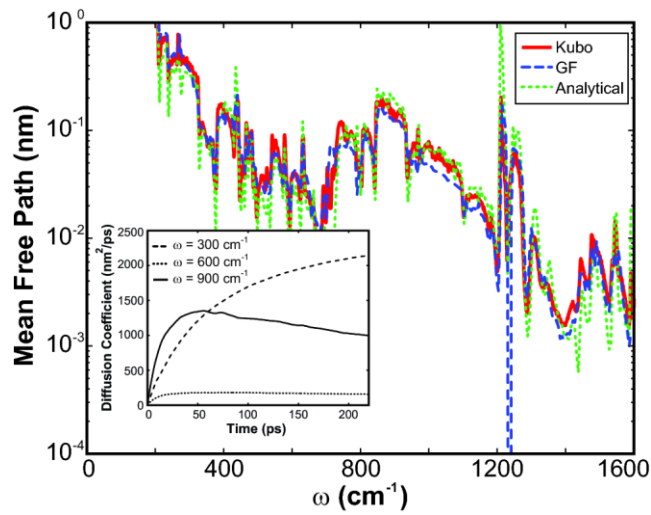


FIG.1. Main frame: frequency dependent MFP in CNT (7,0) with isotopic disorder with the GF method[3], Kubo method and the analytical formula. Inset: time dependent diffusion coefficients for three chosen frequencies.

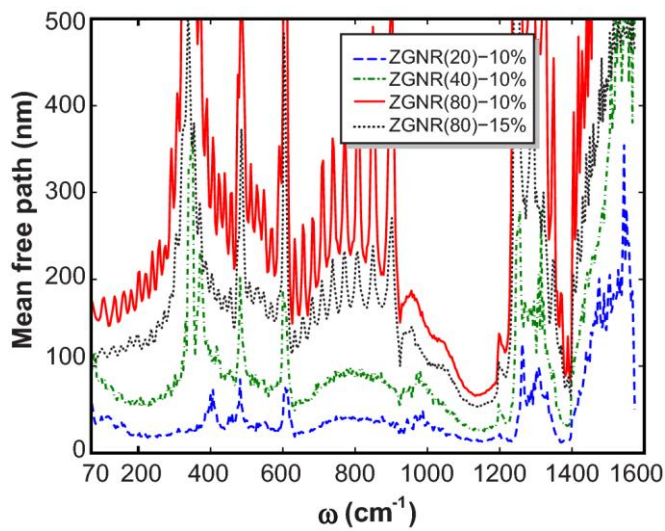


FIG.2. Elastic MFP for ZGNR of widths $N_z = 20, 40$ and 80 with disorder density of 10% , and also for 80 and 15% disorder for comparison.

Squaramide Magnetic Iron Nanoparticles for the Selective Removal of Hg²⁺ Ions in Water

Kenia López, M. Nieves Piña and Jeroni Morey

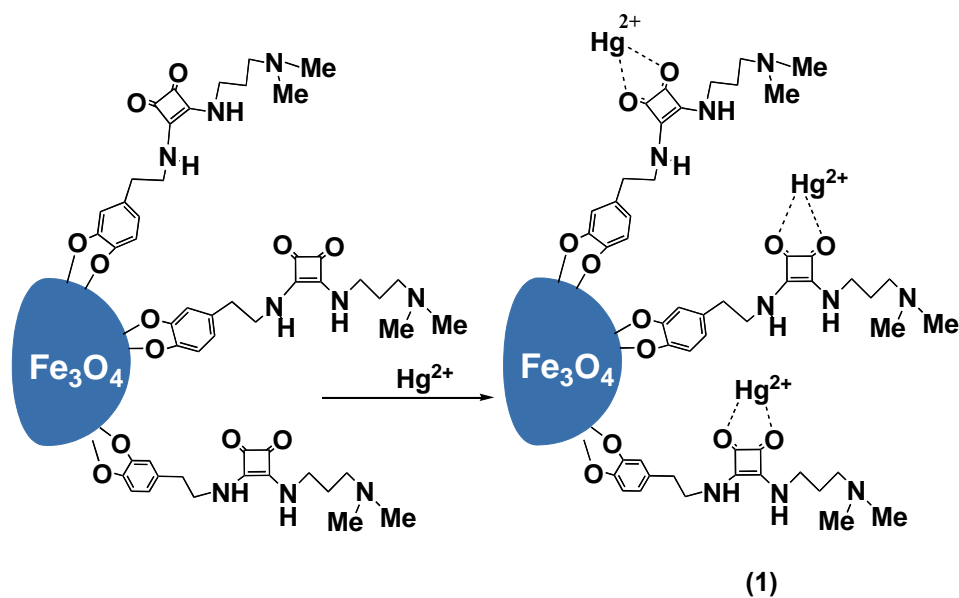
Department of Chemistry, University of the Illes Balears, Palma de Mallorca, Spain
jeroni.morey@uib.es

Elimination of mercury and its compounds in the environment is of great interest because of their high toxicity, wide usage in a number of industrial processes, and biomagnification in the food chain. Because the squaramide unit showed unusual selectivity^[1] for Hg²⁺, we have investigated the interactions of squaramide based on nanomagnetic iron particles (1) with Hg²⁺ at pH 4 in water.

The iron nanoparticles were synthesized as described by Sun^[2]. Here we report a simple approach to conjugate monodisperse Fe₃O₄ nanoparticles with various squaramide-dopamine units.

Our results^[3] show that 20 mg of hybrid nanomagnetic iron particles (1) remove 56% of a Hg²⁺ solution of 377 mg/L. However, the Fe₃O₄ nanoparticles without functionalization only remove 17%.

The regeneration of nanomagnetic iron particles (1) was carried out using 2 x 5 mL of 0.1 M EDTA as eluent. The removal of Hg²⁺ obtained with that recovery nanomaterial was lower, 34%, in the first two cycles and only 24% in the third cycle.



References

- [1] R. R. Avirah, K. Jyothish and D. Ramaiah, *Org. Lett.*, **2007**, 9, 121-124.
- [2] J. Xie, C. Xu, Z. Xu, Y. Hou, K. L. Young, S. X. Wang, N. Pourmond and S. Sun, *Chem. Mater.*, **2006**, 18, 5401-5403.
- [3] C. H. R. Nambiar, B. Narayana, B. M. Rao, B. Mathew, and B. Ramachandra, *Microchem. J.*, **1996**, 53, 175-179.

Generating and measuring anisotropic elastic behavior of Co thin films with oriented surface nano-strings on micro-cantilevers

V. Madurga, J. Vergara, C. Favieres

Public University of Navarre, Laboratory of Magnetism, Dept. of Physics, E31006 Pamplona, Spain
vmadurga@unavarra.es

Si micro-cantilevers, MCL, $\approx 450 \times 50 \times \approx 2 \mu\text{m}^3$ were coated with Co by the pulsed laser deposition, PLD, technique, using an off-normal incidence plasma procedure. A Nd:YAG laser beam $-\lambda = 1054 \text{ nm}$, 20 Hz repetition rate, 240 mJ per pulse of 4.5 ns ($\approx 12 \text{ Gw}$)– was driven to a pure Co target located inside a chamber with a base pressure of 10^{-6} mbar . The laser beam made an angle of 45° with the normal to the target, which rotated at 32 rpm. The generated Co plasma reached two MCL at an off-normal angle $\theta = 55^\circ$ when they were situated at the lateral surface of a cone with angle 2θ , which also rotated around its axis at 120 rpm. We used the advantage of micro-cantilevers [1, 2] measuring their mechanical and magneto-mechanical properties determining the elastic and magnetic properties of the Co thin films deposited on them.

The same two MCL were coated in consecutive processes. After determination of the resonant frequency of each MLC, ν_0 , they were positioned parallel and perpendicular to the generatrix of the cone respectively. So, the incidence plane of the plasma was parallel or perpendicular to the longitudinal direction of each MCL respectively. Then the generated nano-strings in the deposited film were perpendicular, (transverse) or parallel, (longitudinal) to the longitudinal direction of each MCL [2]. By scanning tunneling microscopy, STM, Fig. 1a, they were imaged these two different kind of nano-strings, Fig. 1b and 1c. After each deposition time, t , the resonant frequency of each coated micro-cantilever, $\nu_{(c \text{ MCL})}$, was measured again and so successively for the consecutive coating processes. So the change of this resonant frequency was measured, as shown in Fig. 2a. For a MCL the initial resonant frequency satisfies the expression $\nu_0^2 \sim k_0/m_0$, being k_0 the spring constant of the MCL and m_0 its mass. For the coated MCL the ratio $\nu_{(c \text{ MCL})}^2/\nu_0^2 = (k_{(c \text{ MCL})}/m_{(c \text{ MCL})})/(k_0/m_0)$, R2-FRQ, will vary when k or m change: an increase in the mass will produce a decrease in this ratio R2-FRQ and an increase of the spring constant will produce an increase in this ratio. Fig. 2b and 2c show the changes of R2-FRQ when coating processes with deposition time $t = 15 \text{ s}$ and 1 min. were performed respectively. The percolation phenomenon in the deposited Co over the MCL, was deduced for a total deposition time $\approx 1.6 \text{ min.}$, Fig. 2b, when the decrease of R2-FRQ changed its slope. The initial decrease of R2-FRQ produced by the increase of m was balanced by the increase in k produced then by the percolated film. Fig. 2c shows the evolution of R2-FRQ for deposition time $t = 1 \text{ min.}$ Because the mass deposited over the two MCL was equal, the split of the value of R2-FRQ (starting approximately at 2.2 min.) must be due to the generation of the nano-strings, which produced different values of k . In fact, the coated MCL with longitudinal nano-strings exhibited a value of k higher than the corresponding to the coated MCL with the transverse ones. Taking into account that the resonant frequencies ν_0 of the two MCL was in the interval $(8665 \pm 5) \text{ Hz}$, and the values of the density of the Si: $2.33 \cdot 10^3 \text{ kg/m}^3$, its Young modulus: $1.69 \cdot 10^{11} \text{ Pa}$, the MCL length: $450 \mu\text{m}$, and its width: $50 \mu\text{m}$, it was deduced the mass of the MCL, $m_0 = 6.66 \cdot 10^{-11} \text{ kg}$ and $k_0 = 0.200 \text{ N/m}$. The increment in m_0 for each min. of deposition time was $4.16 \cdot 10^{-13} \text{ kg}$. The relative change in the spring constant after 4 min. of deposition for the MCL coated with longitudinal nano-strings was at least 40% higher than the produced for the MCL coated with transverse nano-strings. This 40% was a measurement of the anisotropic elastic property consequence of the surface nano-strings morphology of these thin films.

References

- [1] P. S. Waggoner and H. G. Craighead, *Lab Chip*, **7** (2007) 1238
- [2] V. Madurga, C. Favieres, J. Vergara, *Nanotechnology*, **21** (2010) 095702

Figures

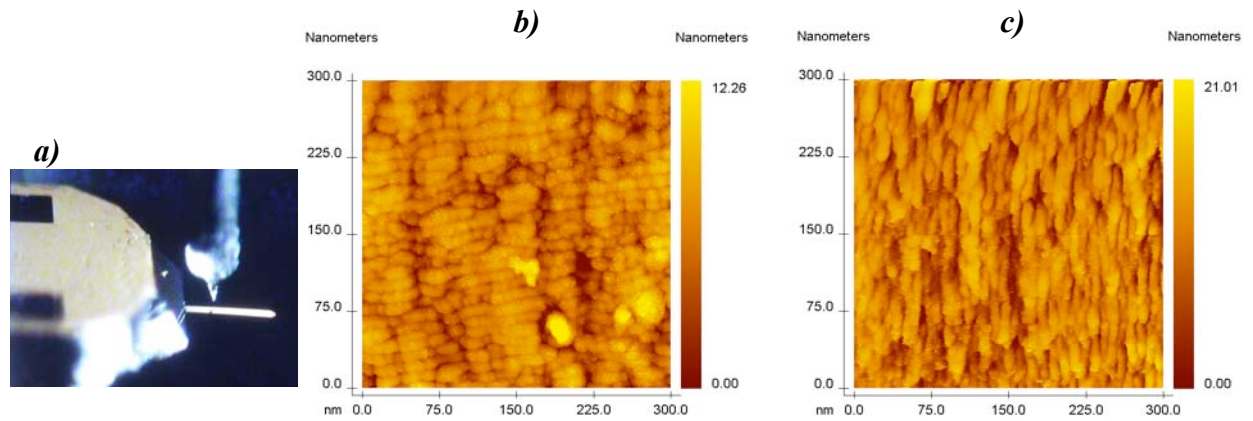


Fig. 1

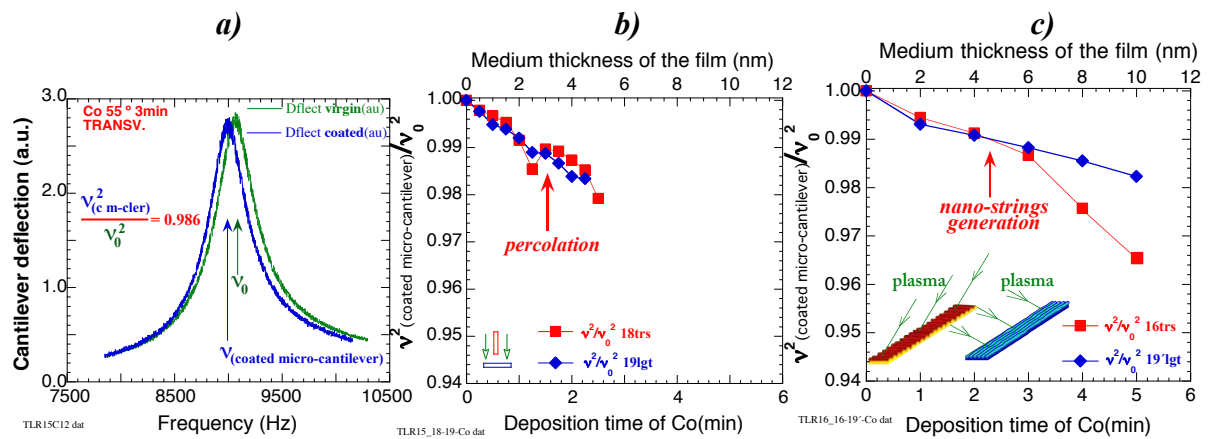


Fig. 2

Development of nanostructured 3D matrices to direct mesenchymal stem cells behaviour

F.R. Maia^{1,2,3}, K. Fonseca^{1,3}, P.L. Granja^{1,3}, C.C. Barrias¹

¹ INEB – Instituto de Engenharia Biomédica, Divisão de Biomateriais, R. Campo Alegre 823, 4150-180 Porto, Portugal.

² INL – International Iberian Nanotechnology Laboratory, Avda Central 100, 4710-229 Braga, Portugal.

³ Universidade do Porto, Faculdade de Engenharia, Departamento de Engenharia Metalúrgica e de Materiais. Rua Dr. Roberto Frias, 4200-465 Porto, Portugal.

raqmaia@ineb.up.pt

Introduction

New strategies for bone regeneration therapies evoke the development of improved biomaterials that reproduce key functions of the natural extracellular matrix (ECM), which serves both as a structural support for cells and as a dynamic biochemical network that directs cellular activities.

In this study, chemical functionalization of alginate hydrogels with an osteogenic signaling peptide was investigated. The selected peptide is based in the C-terminal sequence of OGP (Osteogenic Growth Peptide), known to increase bone mass and fracture healing in vivo, and to regulate cell proliferation and osteogenic differentiation in vitro [1]. Generally designated by OGP₁₀₋₁₄ (Tyr-Gly-Phe-Gly-Gly), this five amino-acid sequence retains full bioactivity, being responsible for binding to the OGP receptor [1]. OGP-alginate was further combined with alginate modified with a cell-adhesion peptide (RGD-alginate), previously shown to enhance the viability and osteogenic differentiation of cells in the entrapped state [2] and with alginate modified with a protease-sensitive peptide (PVGLIG-alginate) to allow cells to partially remodel the hydrogel and spread within the matrix. Alginate hydrogels containing the three peptides were used as a 3D matrix for culturing human mesenchymal stem cells (hMSC), and the effect of these multifunctional microenvironments in cell behaviour, namely on osteogenic differentiation was investigated.

Materials and Methods

Alginate (Protanal LF 20/40, FMC Biopolymers) was bulk-functionalized with the peptide sequence GGGYGFGG (OGP₁₀₋₁₄ with a poly-glycine spacer, GenScript) using standard aqueous carbodiimide chemistry [2]. Different amounts of peptide (10, 50 and 100 mg) per gram of alginate were used. The amount of coupled peptides was analyzed by UV spectroscopy and by using the bicinchoninic acid (BCA) assay. 3D cultures of hMSC within multifunctional alginate hydrogels were established by combining cells with gel precursor solutions prior to polymerization.

Cells inside the discs were cultured under basal and osteogenic induction conditions for up to 16 days. Osteogenic differentiation was analyzed by assaying alkaline phosphatase activity (ALP) using a cytochemical staining in situ.

Results and Discussion

UV spectroscopy and the BCA acid assay showed that the osteogenic peptide sequence was effectively grafted to alginate, and that the coupled amount increased with the amount of peptide initially available for reaction. The reaction yields varied from 84±3% (10 mg/g alginate) to 46±4% (100 mg/g alginate) (Figure 1). hMSC were cultured within RGD-alginate, PVGLIG/RGD-alginate and OGP/PVGLIG/RGD-alginate discs. Cells entrapped within alginate discs were only able to remodel the hydrogel matrix and spread when PVGLIG-alginate was used in combination with RGD-alginate.

The osteogenic differentiation of 3D cultured hMSC was analysed through ALP activity along the time of culture in cells entrapped in RGD-alginate, PVGLIG/RGD-alginate and OGP/PVGLIG/RGD-alginate discs, under basal and osteogenic induction conditions. In figure 2 is possible to observe that ALP activity increase along the time, especially under osteogenic induction conditions and in the presence of OGP₁₀₋₁₄. Moreover, under the same conditions, the degradation of the hydrogels was accelerated;

References

- [1] Chen Y-C et al. J Peptide Res 2000;56:147-156;
 [2] Evangelista MB et al. Biomaterials 2007;28:3644-3655;

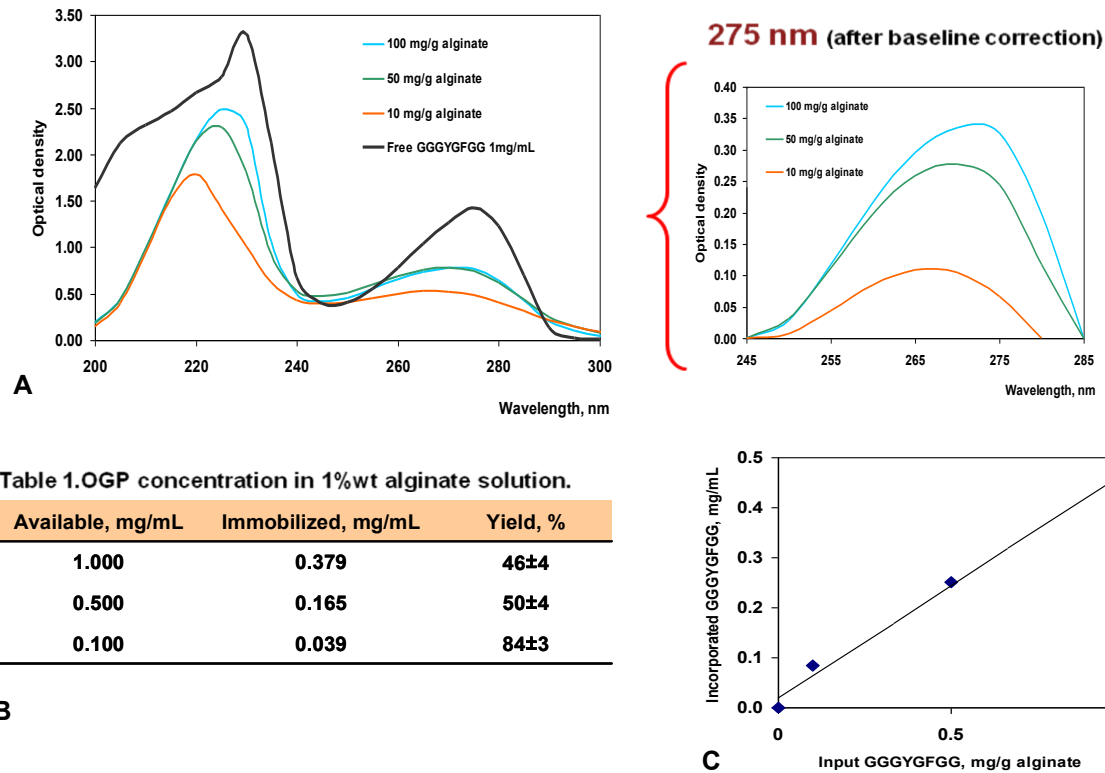


Figure 1. (A) The presence of peaks around 230/275 nm was observed, which indicates that the peptide was effectively grafted to the polymer backbone. (B) Table 1. lists the amount of immobilized OGP10-14 obtained using different initial amounts of peptide and the respective reaction yields. (C) A linear relationship between the amount of immobilized peptide and that initially available for reaction was obtained.

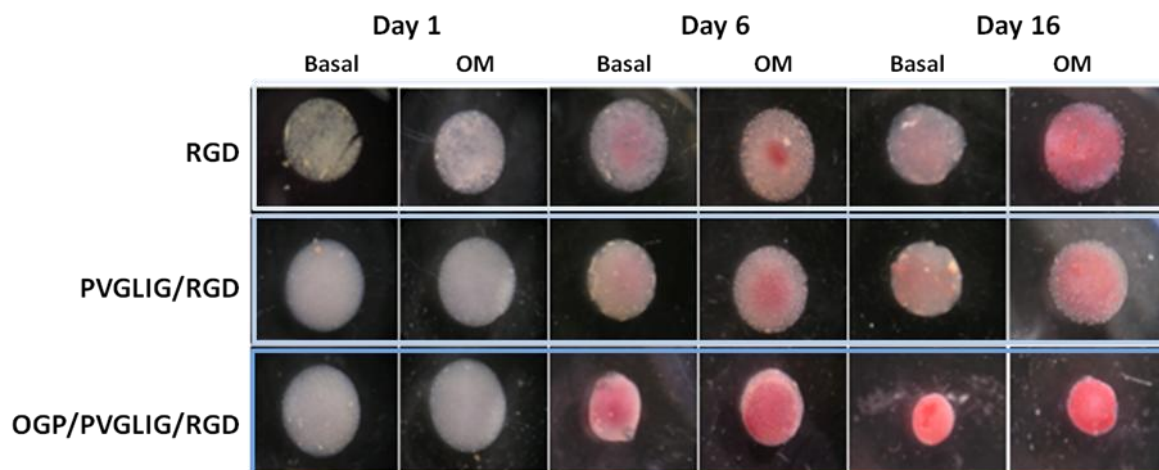


Figure 2. Expression of ALP activity along the time in cells entrapped in RGD-alginate, PVGLIG/RGD-alginate and OGP/PVGLIG/RGD-alginate discs, under basal and osteogenic induction conditions. ALP activity increase along the time, especially under osteogenic induction conditions, and in the presence of OGP₁₀₋₁₄. Moreover, in the presence of OGP₁₀₋₁₄ the degradation of the hydrogels was faster (original magnification 25x).

Identifying stable atomic configurations by the correlation analysis of conductance traces

Péter Makk¹, András Halbritter¹, Szymon Mackowiak², Szabolcs Csonka¹, Maciej Wawrzyniak³, Jan Martinek²

¹*Department of Physics, Budapest University of Technology and Economics and Condensed Matter Research Group of the Hungarian Academy of Sciences, 1111 Budapest, Budafoki út 8., Hungary*

²*Institute of Molecular Physics, Polish Academy of Sciences, 60-179 Poznan, Poland*

³*Faculty of Electronics and Telecommunications, Poznan University of Technology, Poznan, Poland and Organization, Address, City, Country*
peter.makk@gmail.com

Break junction techniques have been proved to be a suitable method for the creation of high stability single-atom or single-molecule junctions. However, as the detailed configuration of the nano-scale junction cannot be traced by direct microscopic imaging, all the information must be collected from current and voltage measurements. Several techniques applying the toolbox of mesoscopic physics were developed for the study of atomic and molecular junctions [1], including the identification of stable atomic configurations by conductance histogram technique, the study of the transmission eigenchannels by conductance fluctuation [2], shot noise [3], or superconducting subgap structure measurements [4,5], as well as the detection of the vibrational modes by point-contact spectroscopy [2].

Conductance histogram technique had a pioneering role in understanding electron transport on the single-atom scale [1], and presently it is widely applied in the field of molecular electronics to identify well-defined single molecule structures [6,7]. However, it is obvious that conventional conductance histograms – measuring statistical averages – can only provide limited information about the studied nanostructures. In several fields of physics it is well known that going beyond averages can supply fundamentally new information, as demonstrated by the success of quantum noise studies in mesoscopic systems, or correlation spectroscopy in NMR studies [8]. Implementing these ideas we have developed [9] a novel statistical method based on the 2D cross-correlation analysis of conductance versus electrode separation traces. This method is capable of resolving several features of nanocontact formation dynamics, which are completely hidden in traditional conductance histograms.

This analysis can show, whether two configurations are always occurring together, one configuration is excluding the other, or their occurrences are independent events. Furthermore, the correlation analysis can resolve fine structures related to different atomic configurations, which are smeared out in the conductance histogram.

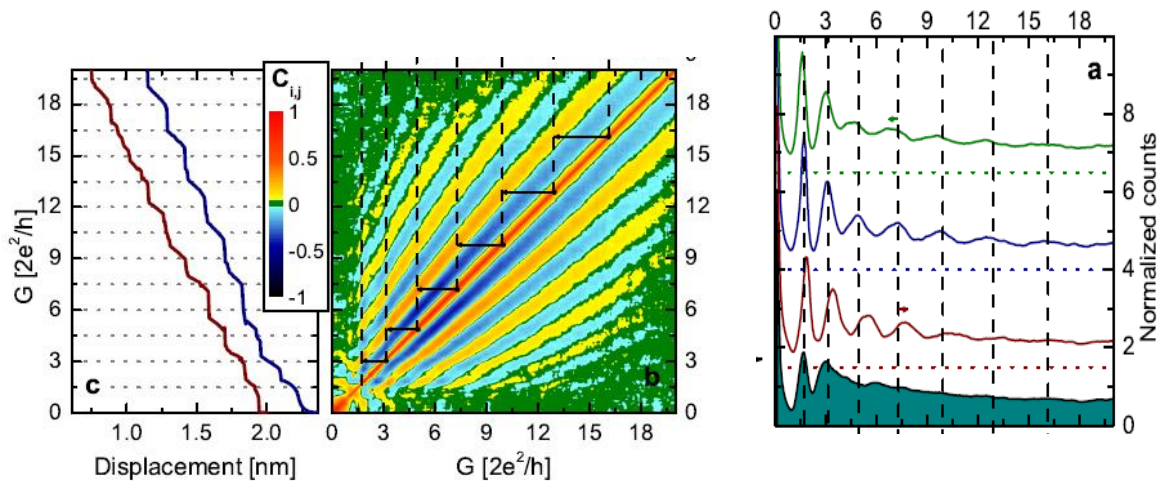
Applying this method we have studied the formation of atomic-scale nanocontacts in transition metal junctions, Ni, Fe, V [9]. In these metals low-symmetric *d* orbitals give an important contribution to the conduction, introducing an extreme sensitivity of conductance to precise junction geometry. Accordingly, traditional conductance histograms cannot show much more information than the conductance of a single-atom contact. Our analysis overcomes this difficulty, and opens a new window for resolving the typical evolutions of the conductance staircase starting from rather large contact diameters, and finding several, yet undetected stable atomic configurations. According to our novel analysis, Ni, Fe & V nanowires exhibit a very regular, atom by atom narrowing of the minimal cross section (figure 1), in contrast to the rather unordered rupture of Au junctions.

References

- [1] N. Agrait, A. Levy Yeyati, J. M. van Ruitenbeek, Quantum properties of atomic-sized conductors, *Physics Reports* 377, 81 (2003).
- [2] R. H. M. Smit, Y. Noat, C. Untiedt, N. D. Lang, M. C. van Hemert, J. M. van Ruitenbeek, Measurement of the conductance of a hydrogen molecule, *Nature* 419, 906 (2002).
- [3] D. Djukic and J.M. van Ruitenbeek, Shot noise measurement on a single molecule, *Nano Letters*, 6 (2006)
- [4] E. Scheer, N. Agrait, J. C. Cuevas, A. Levy Yeyati et al., The signature of chemical valence in the electrical conduction through a single atom contact, *Nature* 394, 154 (1998).
- [5] P. Makk, Sz. Csonka, A. Halbritter, Effect of hydrogen molecules on the electronic transport through atomic-sized metallic junctions in the superconducting state, *PRB* 78, 045414 (2008).
- [6] S. Wu, *et al.*, Molecular junctions based on aromatic coupling. *Nature Nanotechnology*. 3, 569-574 (2008).

- [7] L. Venkataraman, Jennifer E. Klare, Colin Nuckolls, Mark S. Hybertsen, and Michael L. Steigerwald, Dependence of singlemolecule junction conductance on molecular conformation. *Nature*. 442, 904-907 (2006).
- [8] R. R. Ernst, G. Bodenhausen and A. Wokaun, *Principles of Nuclear Magnetic Resonance in One and Two Dimensions*, (Oxford Univ. Press, Oxford 1987)
- [9] A. Halbritter, P. Makk, Sz. Mackowiak, Sz. Csonka, M. Wawrzyniak, J. Martinek, Atom by atom narrowing of transition metal nanowires resolved by 2D correlation analysis. arXiv:1006.1811v1, submitted to *Phys. Rev. Lett.* (2010).

Figures



Measurements on Ni junctions. Left: Representative conductance traces and 2D correlation histogram for the data set. Right: Refocused histogram for Ni contacts (arXiv:1006.1811v1)

Improving Magnetic Field Detection Limits of Spin Valve Sensors Using 3D Magnetic Flux Guide Concentrators

Z. Marinho, A. Gualdino, S. Freitas, R. Chaves, R. Ferreira, J. P. Conde, and P.P. Freitas

Instituto Nacional de Engenharia de Sistemas e Computadores
Microsistemas e Nanotecnologias (INESC-MN), 1000-029 Lisbon, Portugal
Instituto Superior Técnico (IST), 1000-029 Lisbon, Portugal

zitamarinho@gmail.com

Index Terms—*1/f noise, flux concentrator, low field detection, magnetoresistive sensors, spin valve sensitivity.*

This work will conduct a study regarding the improvement in low amplitude static magnetic field detection, following the research line of A. Guedes [1] [2]. To achieve measurements below the nano Tesla range an integration of magnetoresistive sensors, magnetic flux concentrators and microelectromechanical systems (MEMS) has been carried out. The operation range frequency is shifted from DC to high frequencies in order to decrease the $1/f$ noise. This process is achieved by mechanical modulation of a static magnetic field by the MEMS resonator [3].

The improvement made here is given by the optimization of the magnetic flux concentrators based on CoZrNb or CoFeB/Ru/CoFeB multi layers, increasing the detection limit of the magnetoresistive sensor [5]. 3D Magnetic Flux Concentrators were created [see Fig.1] in order to study its effect on the magnetic field gain at the sensor level. A 10 to 100 fold increase is expected to be obtained when integrating these concentrators with spin valve sensors or MgO based magnetic tunnel junctions. In addition an improvement in the design was made [4] in order to achieve a better performance of the overall system.

Different processing approaches for the fabrication of the concentrators have been studied and compared, both by ion milling under controlled angles and lift off processes. This work challenges the detection limits of low static magnetic field signals, aiming at the pico Tesla range.

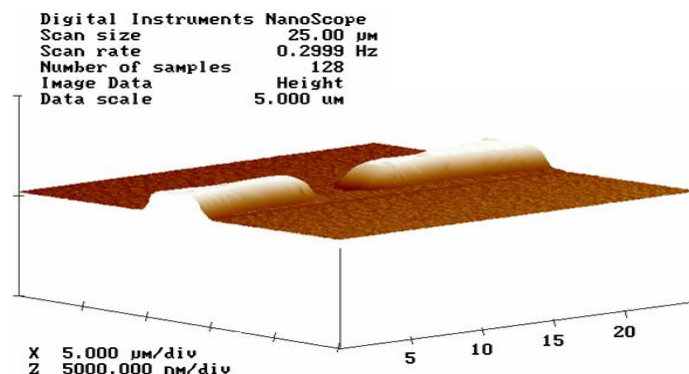


Fig.1 - Flux concentrator gap image obtained from AFM measurement. A 25.6 degree angle profile is obtained by ion milling processes in a CoZrNb 7000A layer.

References:

TNT2010 September 06-10, 2010 Braga, Portugal

[1] For the starting point of the research line see, _Improving Magnetic Field Detection Limits of Spin Valve Sensors Using Magnetic Flux Guide Concentrators ; A. Guedes , J. M. Almeida , S. Cardoso , R. Ferreira , and P. P. Freitas, (INESC-MN), IEEE Transactions on magnetics, Vol. 43, no. 6, June 2007.

[2] Hybrid Magnetic Tunnel Junction – MEMS High Frequency Field Modulator for 1/f Noise Suppression; A. Guedes , Samadhan B. Patil , Piotr Wisniowski , Virginia Chu , João P. Conde, and P. P. Freitas; IEE Transactions on magnetic, Vol. 44, no. 11, November 2008.

[3] Hybrid magnetoresistive microelectromechanical devices for static field modulation and sensor 1/f noise cancellation; A. Guedes, S.B. Patil, S. Cardoso, V. Chu, J.P. Conde, and P.P.Freitas; Journal of Applied Physics 103,07E924 (2008).

[4] P. Drljacca, F. Vincent, P. Besse, and R. Popovic, "Design of planar magnetic concentrator for high sensitivity Hall devices" *Sens. Actuators A*, vol. 97–98, pp. 10–14, 2002.

[5] C. Fermon, M. Pannetier-Lecoeur, N. Biziere, and B. Cousin, "Optimizing GMR sensor for low and high frequencies applications" *Sens. Actuators A*, vol. 129, pp. 203–206, 2006.

Carbon clathrates from fullerite under high pressure

L.Marques¹, M.Mezouar², J-L. Hodeau³

¹Universidade de Aveiro, Campus de Santiago, 3810 Aveiro, Portugal

²European Synchrotron Radiation Facility, BP220, 38043 Grenoble, France

³Institut Néel CNRS-UJF, BP166, 38042 Grenoble, France

lmarques@ua.pt

C60 fullerite displays a very rich phase diagram with a plethora of interesting new phases with new structural architectures. At pressures below 8 GPa different C60 polymers, based on 2+2 cycloaddition polymeric bond, have been found: a 1D polymeric phase and two 2D polymeric phases, involving square or triangular polymerized planes [1]. It must be noted that these high-pressure polymeric phases can be quenched to room conditions. Also in this pressure range but for temperatures above 850°C, C60 cages collapse irreversibly transforming into an amorphous sp²-carbon phase. Despite its graphitic nature this amorphous phase displays remarkable super-hard properties [2]. At pressures above 8GPa, and in contrast to low-pressure range, the phase diagram of C60 fullerite is not elucidated. We have used the Paris-Edinburgh large-volume press, employing sintered diamond anvils, to extend the analysis of the fullerite phase diagram to higher pressures [2]. The synchrotron diffraction patterns displayed by C60 samples compressed above 10GPa are complex indicating heterogeneous samples composed of several different phases and/or partial transformed grains. Despite this complexity the x-ray diffraction analysis clearly shows that C60 fullerite forms 3D polymers. The molecular near-neighbor (NN) distances in these 3D polymers are much smaller than the one corresponding to the 2+2 cycloaddition bond characteristic of the low-pressure polymers. This indicates that new intermolecular bonding schemes come into play at these pressures. Unfortunately the poor-crystallized samples, in addition to its heterogeneity, did not permit to obtain the detailed atomic structure of these new 3D polymeric phases, preventing the elucidation of the intermolecular bonding active at these pressures. It must be noted, and in contrast to low-pressure polymers, that the transformations above 10GPa are not reversible and thus these 3D polymers can be better viewed as carbon clathrates.

References

[1] M. Núñez-Regueiro, L. Marques, J.L. Hodeau, J.L., O. Béthoux, M. Perroux Physical Review Letters, 74 (1995) 278-281; B. Sundqvist, Advances in Physics, 48 (1999) 1-134.

[2] A. Lyapin, V. Brazhkin, E. Gromnitskaya, S. Popova, O. Stal'gorova, R. Voloshin, S. Bayliss, A. Sapelkin, Applied Physics Letters, 76 (2000) 712-714.

[3] G. Morard, M. Mezouar, N. Rey, R. Poloni, A. Merlen, S. Le Floch, P. Toulemonde, S. Pascarelli, A. San-Miguel, C. Sanloup, G. Fiquet, High Pressure Research, 27 (2007) 223-233.

Wavelength dependence of the SPP wavevector magnetic modulation in Au/Co/Au films

D. Martín-Becerra^{‡,1}, J. B. González-Díaz¹, V. V. Temnov², A. Cebollada¹, G. Armelles¹, T. Thomay³,
A. Leitenstorfer³, R. Bratschitsch³, A. García-Martín¹, M. U. González¹

¹IMM-Instituto de Microelectrónica de Madrid (CNM-CSIC), Isaac Newton 8, PTM,
E-28760 Tres Cantos, Madrid, Spain.

²Department of Chemistry, Massachusetts Institute of Technology, Cambridge (MA), USA

³Department of Physics and Center for Applied Photonics, University of Konstanz, Germany

[‡]diana.martin@imm.cnm.csic.es

Surface plasmons polaritons (SPP) are evanescent waves that propagate along a dielectric-metal interface. They can be confined in subwavelength metal structures, i.e. below the diffraction limit, which leads to many possible applications, including miniaturized optical devices. Within that context, the development of active plasmonics is important to achieve nanophotonic devices with advanced functionalities. This requires a system where the plasmon properties can be manipulated using an external agent. Among the different control agents considered so far, the magnetic field seems a promising candidate, since it is able to modify the dispersion relation of SPP [1] at reasonable magnetic field strengths, and with a high switching speed. This modulation comes from the non-diagonal elements of the dielectric tensor, ϵ_{ij} , appearing when the magnetic field is turned on. For noble metals, the ones typically used in plasmonics, these elements are proportional to the applied magnetic field but, unfortunately, very small at field values reasonable for developing applications. On the other hand, ferromagnetic metals have sizeable ϵ_{ij} values at small magnetic fields (proportional to their magnetization), but are optically too absorbent. A smart system to develop magnetic field tunable plasmonic devices is the use of multilayers of noble and ferromagnetic metals [2, 3]. That is the framework of the present work, where we analyze the magnetic field induced SPP wavevector modulation (Δk) in Au/Co/Au films as a function of the wavelength and the position of the Co layer inside the trilayer.

The experimental analysis of the SPP wavevector modulation has been performed via surface plasmon interferometry with tilted slit-groove microinterferometers [4]. A sketch of a magneto-plasmonic interferometer is shown in Fig. 1. Illumination with a p-polarized laser beam at normal incidence results in the excitation of SPPs at the groove that propagate towards the slit, where they are reconverted back into free-space radiation (I_{SP}) and interfere with light directly transmitted through the slit (I_r). The total intensity collected from the slit is:

$$I_{DC} = I_r + I_{SP} e^{-2k_{SP}^i d} + 2\sqrt{I_{SP}} e^{-k_{SP}^i d} \sqrt{I_r} \cdot \cos(k_{SP}^r \cdot d + \varphi_0),$$

where k_{SP}^r and k_{SP}^i are the real and imaginary part of the SPP wavevector respectively, φ_0 is an arbitrary phase and d is the groove-slit distance.

When the light intensity transmitted through the slit is recorded by scanning a photodiode along the slit axis (see optical interferogram in Fig. 2), a series of maxima and minima appears as a consequence of the different slit-groove distance for each slit position. To detect the magnetic modulation, we apply an external periodic magnetic field high enough to saturate the sample (about 20 mT) in the direction parallel to the slit axis. This generates a variation in the SPP wavevector, therefore shifting the interference pattern. Then, at each point of the slit, we measure the variation of intensity associated with this pattern shift, I_{MP} , with a lock-in amplifier. This constitutes the magnetoplasmonic interferogram, also shown in Fig. 2. Actually, when applying the magnetic field, both the real and the imaginary part of the SPP wavevector k_{SP} are modified and the I_{MP} signal can be expressed, up to a first order approximation, as:

$$I_{MP} = I(M) - I(-M) \approx (-2 \cdot \Delta k_{SP}^r \cdot d) \sqrt{I_{SP}} e^{-k_{SP}^i d} \sqrt{I_r} \cdot \sin(k_{SP}^r \cdot d + \varphi_0 + \Phi), \text{ with } \tan \Phi = \frac{\Delta k_{SP}^i}{\Delta k_{SP}^r}$$

Here Δk_{SP} represents the k_{SP} modulation with the sample magnetization and it is defined as $\Delta k_{SP} = k_{SP}(M) - k_{SP}(-M)$. As we can see in the equation, the modulation of k_{SP}^r (Δk_{SP}^r) is related to the amplitude of the magnetoplasmonic signal, while the modulation of k_{SP}^i (Δk_{SP}^i) induces a phase shift (Φ) between the optical and the magnetoplasmonic signal. We would like to notice here that for $\Delta k_{SP}^i = 0$; the optical and magnetoplasmonic interferograms are shifted by exactly 90° due to the cosine and sine dependence of each magnitude, and according to our definition Φ is zero in that case.

Thus, through the analysis of both interferograms we are able to determine the modulation of both the real and imaginary part of k_{SP} . We have performed this analysis as a function of the wavelength and Co position. Figure 3 shows the behaviour of Δk_{SP} as a function of Co depth for three different wavelengths.

We have observed that Δk_{SP} decays exponentially as the position of the cobalt layer goes deeper in the trilayer, a behaviour that can be correlated with the exponential decay of the SPP field inside the metal [4]. Regarding the wavelength dependence, Δk_{SP} decreases as the wavelength increases. We associate this behaviour with the dispersion relation of the plasmon, since the higher the wavelength, the closer the plasmon is to the light line, and the more its electromagnetic field is spread on the dielectric. For lower wavelengths, on the other contrary, the SPP electromagnetic field appears more squeezed at the interface, probing more inside the metal layer, where the magnetic activity lies.

The behaviour of the imaginary part is not so directly related with the extension of the SPP electromagnetic field in the interface, and the value of the α_{ij} and its dependence with the wavelength seem to be the relevant parameters in this case.

References:

- [1] R. F. Wallis, J. J. Brion, E. Burstein, and A. Hartstein, Phys. Rev. B **9** (1974) 3424.
- [2] J. B. González-Díaz, A. García-Martín, G. Armelles, J. M. García-Martín, C. Clavero, A. Cebollada, R. A. Lukaszew, J. R. Skuza, D. P. Kumah and R. Clarke, Phys. Rev. B **76** (2007) 153402.
- [3] E. Ferreiro-Vila, J. B. González-Díaz, R. Fermento, M. U. González, A. García-Martín, J. M. García-Martín, A. Cebollada, G. Armelles, D. Meneses-Rodríguez and E. Muñoz-Sandoval, Phys. Rev. B **80** (2009) 125132.
- [4] V. V. Temnov, G. Armelles, U. Woggon, D. Guzatov, A. Cebollada, A. Garcia-Martin, J. M. Garcia-Martin, T. Thomay, A. Leitenstorfer, and R. Bratschitsch, Nat. Photonics **4** (2010) 107.

Figures:

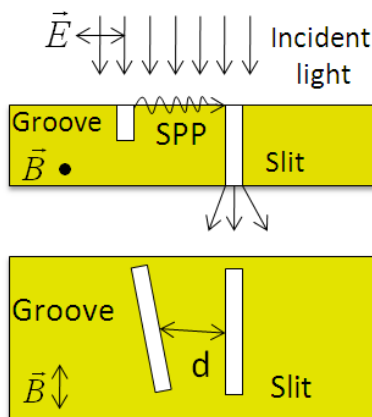


Figure 1: Interference pattern and sketch of the magnetoplasmonic micro-interferometer.

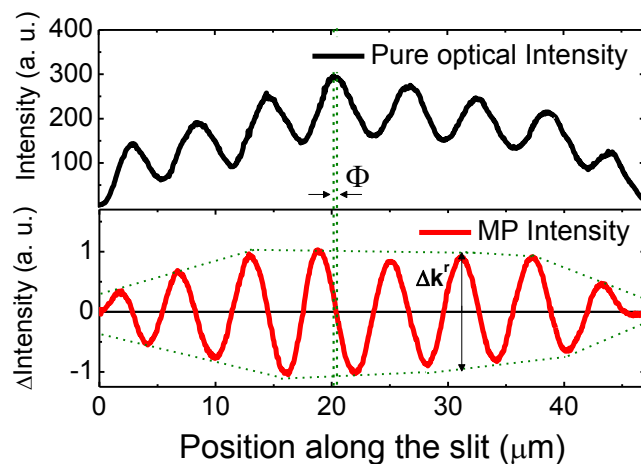


Figure 2: Optical and magnetoplasmonic interferogram

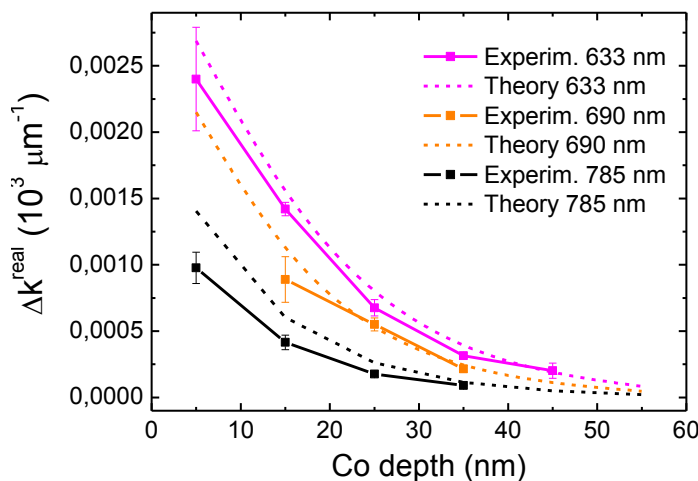


Figure 3: Dependence of the modulation of the real part of k_{SP} with the position of the cobalt layer and the incident wavelength.

Modification of Carbon Nanotubes and Graphene with 1-octadecylalcohol for Polymer Nanocomposites

Horacio J. Salavagione, **Gerardo Martínez**

Instituto de Ciencia y Tecnología de Polímeros, CSIC, Juan de la Cierva 3, 28006 Madrid, España

gmart@ictp.csic.es

Carbon nanostructures such as carbon nanotubes and graphene are promising materials to be employed as filler in polymeric nanocomposites. At present, nanocomposites employing carbon-based reinforcement materials are dominated by carbon nanotubes (CNTs). Graphene, one-atom-thick planar sheet of sp^2 bonded carbon atoms, is a quasi-2-dimensional (2D) material. The fascinating properties of graphene and few layer graphene (FLG) have made it one of the most promising materials.¹ Its greatest aspect ratio and lower cost of preparation, since it is obtained from the naturally occurring graphite, make the graphene will gradually replacing carbon nanotubes.

However, the development of nanocomposites reinforced with this kind of carbon materials has been impeded by their difficult dispersion in matrix. Therefore, sometimes it is crucial their functionalization to make it compatible with a wide range of polymers.

The esterification reactions is one of the most employed reaction to covalently bound functional groups to CNT. This reaction have been also employed in graphene by using graphite oxide and subsequent reduction.²

Here we report the functionalization of graphene and CNT with long alkyl groups through a simple esterification reaction. The success of the modification was confirmed by FTIR, Raman, HNMR and TGA-mass techniques. The final products are soluble in dimethylformamide (DMF) giving stable solution by months.

The functionalization makes these materials compatible with vinyl polymers. We prepared nanocomposites of poly (vinyl chloride) (PVC) with both modified carbon nanostructures. The FTIR spectrum of the nanocomposite shows some interesting differences compared to separate materials. In the case of nanocomposites of PVC with CNT the carbonyl band of the modified-CNT (1633 cm^{-1}) shift to higher wavenumber. Furthermore, the intensity ratio of the C-Cl bands of PVC (I_{615}/I_{635}) is remarkably higher in the nanocomposite. Both effects evidence the effective polymer/filler interaction mainly by halogen bonding. However, other interactions such as van de Waals or dipole-dipole should not be discarded. These interactions are responsible by changes in the final properties.

Acknowledgments. Financial support from the Spanish Ministry of Science and Innovation (MICINN) (MAT2009-09335) is grateful acknowledged.

References

[1] A. K. Geim, K. S. Novoselov, Nature Mater. 6 (2007) 183

[2] Horacio J. Salavagione, Gerardo Martínez, Marián A. Gómez. Macromolecules, 2009, 42, 6331

Figures

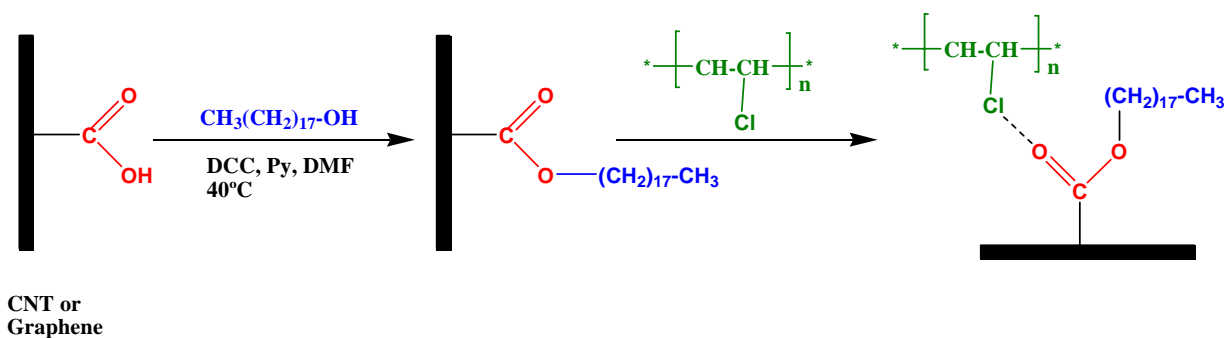


Figure 1. Schematic representation of the modification process and nanocomposite preparation.

Magnetic force microscopy characterization of the magnetization reversal processes in high density arrays of Co bars with strong dipolar interactions

J. I. Martín, F. Valdés-Bango, A. Hierro-Rodríguez, G. Rodríguez-Rodríguez, M. Vélez and J. M. Alameda

Departamento de Física, Universidad de Oviedo-CINN, 33007 Oviedo, SPAIN

J. M. Teixeira, G. N. Kakazei, Y. G. Pogorelov and J. B. Sousa

FIMUP and IN-Institute of Nanoscience and Nanotechnology, Departamento de Física da Faculdade de Ciências, Universidade do Porto, 4169-007 Porto, Portugal

ji.martin@cinn.es

Magnetic nanostructures have received increasing attention in recent years [1] both because of their potential as high density recording media and for their interesting fundamental properties. Magnetization reversal processes of ordered arrays of magnetic nanoelements depend strongly not only on the individual element characteristics (material, size, shape) but also on interparticle interactions mediated by dipolar magnetic coupling. Many interesting effects have been reported in interacting arrays of particles, such as changes in coercivity and switching width [2], in the dynamic response [3] and collective behavior including a superparamagnetic-ferromagnetic transition as a function of interdot distance [4].

Often, conflicting results are obtained regarding the role of dipolar interactions in dense arrays of nanoelements since dipolar interaction is a long range effect and presents a complex character that changes sign depending on the geometrical configuration of the nanoelements. Thus interactions may induce either a broadening or a sharpening of the reversal process depending on array geometrical characteristics and on the single element reversal process. For this reason, studies in arrays of magnetic nanoelements with a well defined magnetic anisotropy and highly symmetric geometrical arrangements can be optimum for the disentanglement of the different factors that govern interaction phenomena.

In this work, rectangular and rhomboidal arrays of Co bars have been fabricated by e-beam lithography combined with a lift-off process. Typical bar dimensions are 1.5 μm length, 0.3 μm width and 40 nm thickness with interelement distances in the range 0.2-0.5 μm (i.e. comparable to element width). Figure 1 shows a series of magnetic force microscopy images taken in a rectangular array of Co bars under a reversed in-plane magnetic field. The reversed domains that propagate in the array have a very anisotropic character (consisting of only one or two rows of bars) that can be attributed to the dominant ferromagnetic interaction between bars along their dipole axis. Hysteresis loops have been derived from these MFM images assigning a positive/negative dipole moment at each bar depending on the direction of its magnetic contrast (see Fig. 2). The small plateau that appears during the magnetization reversal process is an indication of the "antiferromagnetic" interaction between adjacent rows that helps to stabilize a magnetic configuration with a reduced global magnetic moment.

In order to analyze these results, Co bars could be treated as "magnetic dipoles" in order to compute dipolar interactions across the array. However, for dense arrays of magnetic nanoelements these simple models lead to overestimates of the strength of the interaction field and it is better to consider the interactions between individual magnetic charges to describe the array magnetic behavior [5]. Micromagnetic simulations performed with the OOMMF code [6] for different array geometries will also be presented to compare with the observed experimental results.

Work supported by Spanish MICINN (FIS2008-06249, HP2008-0032), Asturias FICYT (IB08-106) and CRUP of Portugal (grant no. E41/09) in the framework of the Spanish-Portuguese Integrated Action. G.N.K acknowledges support from FCT of Portugal through the "Ciencia 2007" program.

References

- [1] View review article J.I.Martin, J. Nogués, Kai Liu, J.L.Vicent, and Ivan K. Schuller, *J. Magn. Magn. Mat.* **256** (2003) 449 and references therein.
 [2] G. A. Gibson and S. Schultz, *J. Appl. Phys.* **73** (1993) 4516.
 [3] G. N. Kakazei, P. E. Wigen, K. Yu. Guslienko, V. Novosad, A. N. Slavin, V. O. Golub, N. A. Lesnik, and Y. Otani, *Appl. Phys. Lett.* **85** (2004) 443
 [4] R. P. Cowburn, A. O. Adeyeye, and M. E. Welland, *New J. Phys.* **1** (1999) 16.1
 [5] J. M. Teixeira et al (to be published)
 [6] OOMMF User's Guide Versión 1.2 a3 (October 2002); M.J. Donahue, D.G. Porter, R.D. McMichael and J. Eicke, *Physica status solidi*, **137** (1993) 207.

Figures

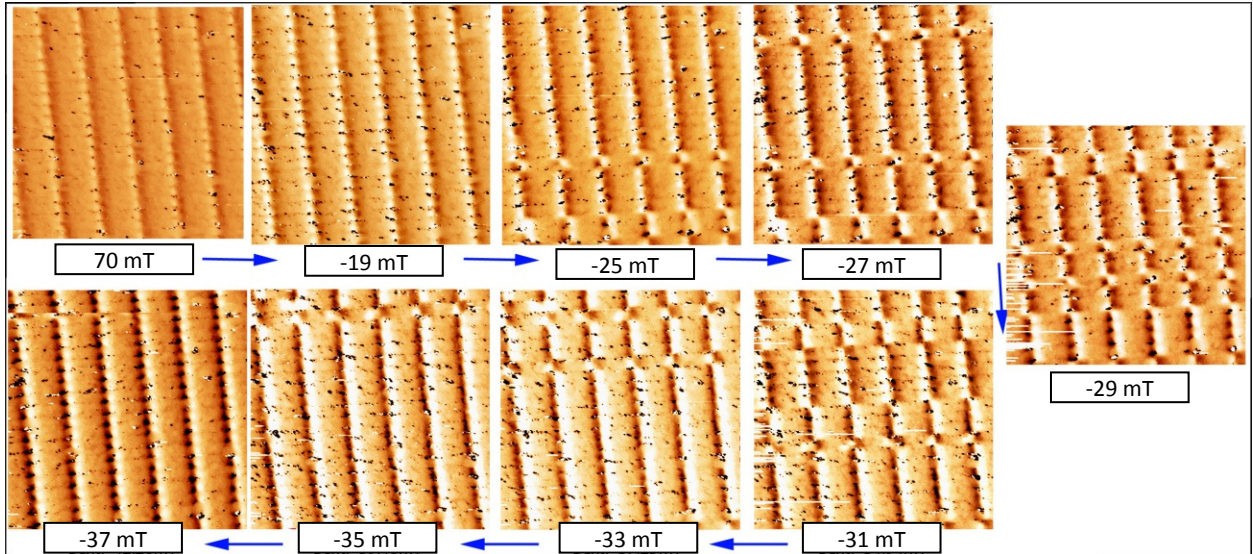


Figure 1: Magnetic Force Microscopy characterization of the reversal process of a dense array of Co bars. Each $10 \times 10 \mu\text{m}^2$ image was taken under a different constant magnetic fields as indicated by the labels. The field was applied in the sample plane, along the bars (i.e. in the magnetic easy axis of the patterned nanostructure). Blue arrows indicate the temporal sequence of applied fields from positive to negative saturation.

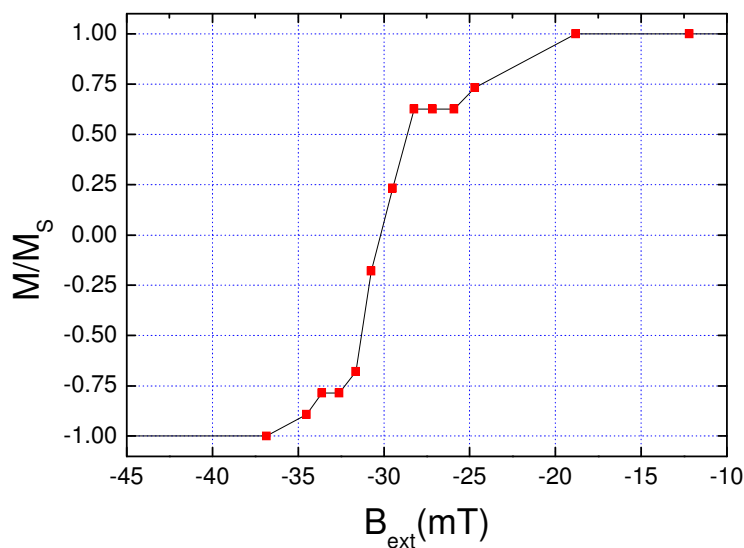


Figure 2: Decreasing field branch of the hysteresis loop deduced from the MFM measurements in Fig.1 by assigning a positive/negative dipole moment to each Co bar, depending on the sign of its magnetic contrast.

"High precision" macromolecular construction as a way to control self-assembly and micellar structure: the example of elastin-like co-recombinamers

Laura Martín¹, Emilio Castro², Artur Ribeiro¹, Matilde Alonso¹, J. Carlos Rodríguez-Cabello¹

¹ GIR Bioforge, Universidad de Valladolid, CIBER-BBN, Paseo de Belén 11, 47010 Valladolid, Spain.

² Grupo de Física de Coloides y Polímeros, Universidad de Santiago de Compostela, 15782 Santiago de Compostela, Spain.

lmartin@bioforge.uva.es

The increasing need for drug-delivery systems that improve specificity and activity whilst at the same time being biocompatible has led to the development of a wide variety of new materials, many of which polymeric systems because of their ability to form a range of different nanoparticulate structures, including micelles, nanospheres, nanocapsules, and polymersomes [1].

Elastin-like recombinamers (ELRs) provide tunable physicochemical properties and excellent biocompatibility. This has led to extensive biological and nanotechnological applications of ELRs [2]. The absolute control over the design of ELRs allows facile manipulation of their stimuli-responsive properties and other physical and functional characteristics. Biosynthesis allows the production of strictly monodisperse polymers with no possibility of randomness in the comonomer distribution.

Amphiphilic elastin-like di- and triblock corecombinamers are a new class of macromolecules that exhibit thermally triggered nanoscale self-assembly [3]. The control over the molecular weight and the hydrophilic-to-hydrophobic ratio afford different nanostructures as micelles or vesicles with several sizes as well as control of the temperature at which self-assemble occurs.

To study the effect of the amino-acid composition and distribution, we are biosynthesized different elastin-like block corecombinamers. They are a combination of two different blocks. The first block is [(VPGVG)₂-(VPGEV)₂-(VPGVG)₂]_n (E-block), a well known pH-responsive smart polymer, and the other is [(VPAVG)]_m (A-block), a thermoresponsive polymer with no pH responsiveness[3]. In this manner the set of corecombinamers studied includes three diblock with variable sizes of both blocks; E₅₀A₄₀, E₅₀A₆₀ and E₁₀₀A₄₀ and two triblock corecombinamers with a variable size of the A-block; E₅₀A₄₀E₅₀ and E₅₀A₆₀E₅₀. The structure of the nanoparticles was investigated as a function of the temperature and concentration using turbidimetry, DLS and SLS, DSC and Cryo-TEM amongst others in aqueous solution (Figure 1) showing different nanostructures with several diameters. The potential of ELRs to self-assemble in response to environmental changes as pH or temperature makes them very attractive for the construction of nano-devices for use as controlled delivery and stimuli-responsive systems or advanced nanobiotechnological applications.

Acknowledgements

We acknowledge financial support from the MICINN (projects MAT 2007-66275-C02-01, MAT 2007-61604, MAT 2009-14195-C03-03 and PSE-300100-2006-1), the JCyL (projects VA034A09 and VA030A08), the CIBER-BBN (project CB06-01-0003), the JCyL and the Instituto de Salud Carlos III under the "Network Center of Regenerative Medicine and Cellular Therapy of Castilla and León". E.C. acknowledges the Angeles Alvaríño (Xunta de Galicia, Spain) program.

References

- [1] Letchford, K., Burt, H., *European Journal of Pharmaceutics and Biopharmaceutics*, **65**, 2007, 259-269.
- [2] Rodríguez-Cabello, J. C., Martín L., Alonso, M., Arias, F. J., Testera, A. M., *Polymer*, **50**, 2009, 5159-5169.
- [3] MacKay, J. A., Chen, M., McDaniel, J. R., Liu, W., Simnick, A. J., Chilkoti, A. *Nature Materials*, **8**, 2009, 993-999.
- [4] Ribeiro, A., Arias, F. J., Reguera, J., Alonso, M., Rodríguez-Cabello, J. C., *Biophysical Journal*, **97**, 2009, 312-320.

Figures

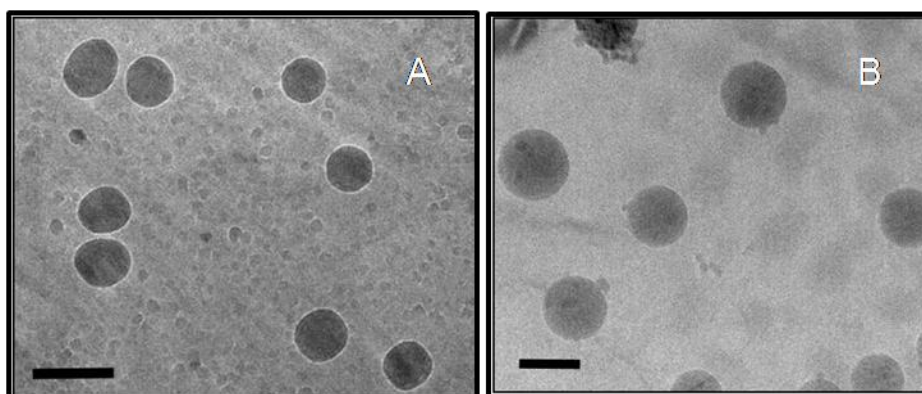


Fig 1. Cryo-TEM images in aqueous solution. (A) $E_{50}A_{60}E_{50}$, (B) $E_{50}A_{60}$. Scale bars: 200nm.

Defects distribution and geometrical disturbances in Carbon Nanotube Heterojunctions

Francisco J. Martín-Martínez, Santiago Melchor, Jose A. Dobado

Grupo de Modelización y Diseño Molecular, Departamento de Química Orgánica, Facultad de Ciencias,
Universidad de Granada, 18071, Spain

fjmm@ugr.es

The relative stability of a family of carbon nanotubes (CNT) with defects has been investigated theoretically with first-principles density functional theory (DFT) calculations, B3LYP/6-31G*. A set of (12,0)-(8,0) CNT heterojunctions with an increasing number ($n=1-4$) of pentagon/heptagon defects were studied systematically in different arrangements, and the results compared with a set of small graphene defective fragments. The structures were constructed with CoNTub Software.^{[1][2]} In addition, tubular structures with two pairs of defects distributed variedly (along and around the CNT) with increasing distances were considered. Within the defective structures, that containing the well-known Stone-Wales defect resulted the most stable one. However, if more than two pairs of defects coexist, situations where the defects appear together seem to be preferred, in sharp contrast to the isolated pentagon rule (IPR) for fullerenes, although this is in accordance with some previous works on this topic. The junctions studied here constitute different arrangements that allow us to discuss which effects (geometric and energetic) arise from the particular positions and orientations of the defects in nanotubes. Moreover, a hefty correlation between the energetic stability and the geometric deformation was found, measured with the average pyramidalization angle (POAV) and the average trigonal deformation (D_{120}), as well as Main Bond Length (MBL) and Ring Bond Dispersion (RBD), which has been already demonstrated useful parameters in analyzing geometrical features in graphite-like structures^[3]. For such purpose, the different contributions to molecular strain were analyzed with the TubeAnalyzer software.

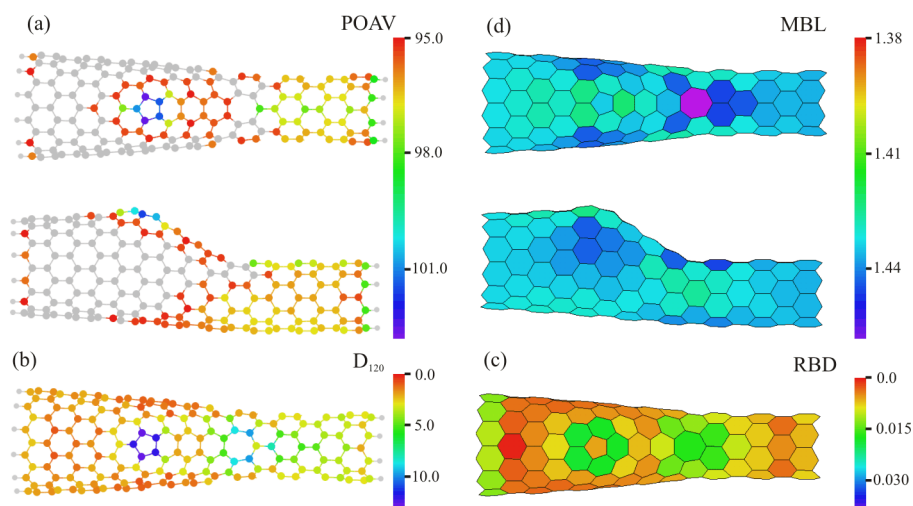
References

[1] Melchor, S.; Dobado, J.A., *J. Chem. Inf. Comput. Sci.* **44** (2004) 1639

[2] <http://www.ugr.es/local/gmdm/contub.htm>

[3] Martín-Martínez, F.J.; Melchor, S.; Dobado, J.A., *Org. Lett.* **10**, (2008) 1991

Figures



Morphological and structural characterization of Ge nanoparticles produced by Pulsed Laser Deposition

A. J. Martins, **J. Martín-Sánchez**, L. Marques, E. M F. Vieira, A. G. Rolo, M. M. D. Ramos, M. J. M. Gomes

University of Minho, Centre of Physics and Physics Department, Braga, 4710-057, Portugal

e-mail: Javierms@fisica.uminho.pt; Javier.martin.nano@gmail.com

Pulsed laser deposition (PLD) is a versatile technique to grow high quality multicomponent thin films and nanometer-sized particles (nanoparticles) when a gas atmosphere is introduced in the deposition chamber at low substrate temperatures [1]. In the last years, much effort has been devoted to the production and characterization of Si nanoparticles [1-3], while less works can be found concerning Ge nanoparticles [4-6]. In this regard, Ge material has been proposed as a good alternative to Si for memory device applications due to the smaller band-gap energy that Ge presents [7]. For the development of flash memory devices based on nanoparticles as storage nodes with an optimal performance, it would be highly desirable to control the nanoparticles size and density distribution while avoiding the micron-sized particles deposition on the substrate surface, usually obtained in the ablation process.

In this work, we have systematically studied the morphological and structural properties for Ge nanoparticles (NPs) obtained by Pulsed Laser Deposition (PLD) on Si (100) substrates in an Ar environment at room temperature (RT). In our experimental setup, we have used a KrF excimer laser ($\lambda = 248$ nm, $t_p = 10$ ns). We demonstrate that it is possible to control the nanoparticles distribution by controlling the experimental deposition conditions. We also demonstrate that both the occurrence of micron-sized particulates on the surface and uniformity in the nanoparticles size distribution can be controlled by introducing a mechanical filter (solid disk) between the target and the substrate. We have also evaluated the crystallinity of the produced nanoparticles at RT.

The size distribution and dispersion of the obtained Ge nanoparticles were evaluated using Atomic Force Microscopy (AFM), Scanning Electron Microscopy (SEM) and Transmission Electron Microscopy (TEM). The structural properties of the nanoparticles were characterized by X-ray diffraction and Raman Spectroscopy.

Acknowledgements

This work has been partially supported by FCT-Fundação para a Ciência e a Tecnologia-Portugal and by the "Programa Operacional Ciência e Inovação 2010-POCI 2010" co-financed by FEDER through the Project PTDC/FIS/70194/2006. JMS and EMFV thanks to FCT for the financial support through the grants SFRH/BD/64850/2009 and SFRH/BD/45410/2008.

References

- [1] W. Marine, L. Patrone, B. Luk'yanchuk, M. Sentis, *Applied Surface Science* **345** (2000) 154.
- [2] L. Patrone, D. Nelson, V.I. Safarov, M. Sentis, W. Marine, S. Giorgio, *Journal of Applied Physics* **87** (2000) 3829.
- [3] Y.L. Wang, W. Xu, Y. Zhou, L.Z. Chu, and G.S. Fu, *Laser Part. Beams* **25** (2007) 9.
- [4] P.F. Lee, X.B. Lu, J.Y. Dai, H.L. WChan, E. Jelenkovic, and K.Y. Tong, *Nanotechnology* **17** (2006) 1202.

[5] X. Ma, J. Phys. Conf. Series **152** (2009) 012020.

[6] M. Yang, T.P. Chen, J.I. Wong, Y. Liu, A.A. Tseng, and S. Fung, J. Nanosci. Nanotechnol. **10** (2010) 4517.

[7] S. Tiwari, F. Rana, H. Hanafi, A. Hartstein, E.F. Crabbe, K. Chan, Applied Physics Letters **68** (1996) 1377.

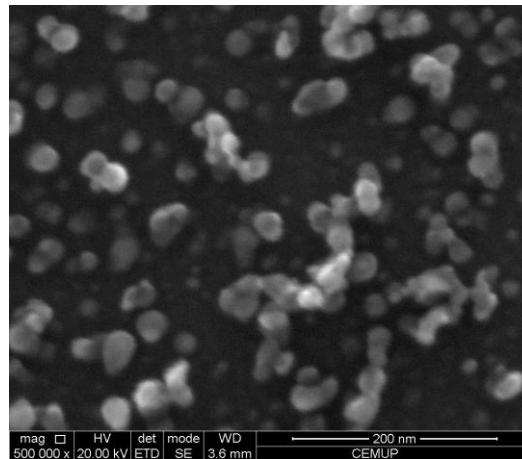


Figure 1: SEM image of Ge nanoparticles produced by Pulsed Laser Deposition at room temperature.

Chalcogenide As-S Glass Infilled Colloidal Photonic Crystals

Joe McGrath¹, Maria Bardosova¹, Hiroshi Fudouzi², Tomas Kohoutek³, and Martyn E. Pemble¹

¹ Tyndall National Institute, Lee Maltings, Prospect Row, Cork, Ireland

² Optronics Materials Center, National Institute for Material Science (NIMS), 1-2-1 Sengen, Tsukuba, Ibaraki 305-0047, Japan

³ Centre for Material Science, University of Pardubice, Studentska 95, 53210 Pardubice, Czech Republic.

Contact e-mail: joe.mcgrath@tyndall.ie

In this work, we have studied porous colloidal particle assemblies deposited onto glass substrates. The assemblies consist of silica nanoparticles ($d \sim 250\text{nm}$), organised into regular 3D patterns. Initially, the voids between the particles are filled with air. These structures have been prepared by three different methods: controlled evaporation [1], under-oil crystallisation [2] and the Langmuir-Blodgett method [3].

An SEM examination of the cross-sections of the resulting structures reveals differences in assembling of the SiO_2 nanoparticles that can only be attributed to their respective preparation methods. These differences lead to quantitative changes in reflectance/transmittance spectra that are manifested by Bragg peak maxima shifts.

The assemblies on their own have a refractive index contrast between the constituent materials (SiO_2 and air) which is insufficient for an achievement of a full (3D) photonic band gap. This fact makes them unsuitable for most photonic applications.

To try to obtain a complete PBG, the colloidal crystals made here were used as templates and their voids infilled with a high refractive index chalcogenide $\text{As}_{30}\text{S}_{70}$ glass [4]. The infiltration, which was carried out by spin-coating method leads to a red shift of the Bragg peak of about 150 nm at an incidence angle of 90 degrees for samples made from spheres of diameter 280 nm using the under oil fabrication method. Red shifts of 160 nm and 192 nm were then observed for samples made from spheres of diameters 210 nm and 250 nm assembled using the LB technique. It is calculated that infilling with chalcogenide glass opals increases the effective refractive index of the composite material from $n = 1.334$ to $n = 1.687$ for the samples prepared using the under oil method. Comparable increases in effective refractive index occur for the LB grown samples.

Although the refractive index contrast achieved is still insufficient for the achievement of full (3D) PBG, we suggest that the inclusion of the chalcogenide glass opens up the possibility of using the infilled structures for non-linear optical applications, while doping of the glass with rare earth ions can also be exploited to make a range of new or improved photonic devices.

References

[1] P. Jiang, J.F. Bertone, K.S. Hwang, V.L. Colvin, Chem. Mater, 1999, 11, 2132.

[2] H. Fudouzi, Journal of Colloidal Interface and Science, 2004, 275, 277.

[3] M. Bardosova. P. Hodge, L. Pach. M.E. Pemble, R.H. Tredgold and D.E. Whitehead Thin Solid Films 2003, 437, 276.

[4] T. Kohoutek, T. Wagner, M. Frumar, A. Chrissanthopoulos, O. Kostadinova, S.N. Yannopoulos, Journal of Applied Physics, 2008, 103, Art N 063511.

Multispectral Imaging of Natural Photonic Nanostructures

José M. Medina¹, Sérgio M. C. Nascimento¹ and Pete Vukusic²

¹ Center for Physics, University of Minho, Campus de Gualtar, Braga, 4710-057, Portugal

² School of Physics, University of Exeter, Stocker Road, Exeter, EX4 4QL, UK

Corresponding author: jmanuel@fisica.uminho.pt

Introduction

Many insects and birds contain photonic structures assembled at the nanometer-scale, some of which produce structural colors. Structural colors are the result of the manipulation of the flow of light due to scattering, multilayer interference or diffraction to produce special goniochromatic effects. That is, their reflectance spectra depend markedly on both the illumination and the viewing angle and can create metal-pearl-like and iridescent effects [1]. Structural colors represent a key growth research area because they provide the basis to develop novel applications such as synthetic nanopigments for industrial coatings or new nanomaterials for displays and for life sciences [1]. Surface characterization is often carried out using electron microscopy whereas reflectance spectra are collected using conventional spectrophotometers [2]. Multispectral imaging is a common spectroscopy technique in non-invasive sensing analysis. In comparison with conventional multi-angle spectrophotometers and RGB cameras, multispectral imaging has the advantage of combining reflectance data with detail spatial information of the scene, thereby providing information beyond that discernible by the human eye. From images taken at a series of narrow-bandwidth wavelengths, multispectral imaging methods differentiate from small-scale structures to entire samples. These images are then combined producing a three dimensional block or *cube* for further processing and analysis. The development of new optical imaging applications for structural colors requires innovative methods to optimize the signal-to-noise ratio, the dynamic range as well as new data processing analysis.

The aim of this study was to apply a new multispectral imaging system in the analysis of the reflectance spectra underlying the structural colors of a series of different structurally colored butterfly wings. In particular, it was intended to take advantage of the unique spatial-spectral information obtained with the multispectral system to investigate the possibility of extracting structural information through an analysis of principal components (PCA).

Experimental device

The experimental device consisted of an illumination source or xenon lamp filtered with an ultraviolet and an infrared filter (FGL400S, FM01, Thorlabs). The light was collimated using a standard convergent lens and a circular diaphragm. A tunable liquid crystal filter (Varispec VS-VIS2-10HC-35-SQ, Cambridge Research and Instrumentation, Inc., Boston, Mass.) was mounted in front of the light source. The filter has a transmission wavelength range between 400-720nm with a bandwidth at half-maximum of 10nm at 550nm. The bandwidth decreases to 6nm at 400nm and increases to 16nm at 720nm, in the same way as standard Lyot filters. The filter has a 35 mm aperture and a field-of-view of 7.5 degrees. The filter was mounted inside a cooler system to maintain the operating temperature fixed and below 30°C. Two mirrors project the light over the sample at a fixed illumination angle close to 45 degrees. To acquire multispectral images, a monochrome CCD camera (Hamamatsu C4742-80-12AG) was mounted normal to the sample so the specular component was excluded. The CCD camera has a spatial resolution of 1344x1024 pixels with a frame rate of 8.9Hz. The camera also has an electronic shutter with a timer controlled by an external signal. A conventional objective (Cosmicar TV zoom lens 12.5–75 mm, 1:1.8 n° 57827) was placed in the CCD camera. The lens had an aperture of *f*/2.8 and a focal distance around 50mm. The images were acquired with a frame grabber (Matrox Corona/8/E, Matrox Electronic Systems, Ltd., Quebec, Canada). The frame grabber also provides the external signal to control the time shutter of the CCD camera. Setup, synchronization and control of the frame grabber, the filter and the CCD camera were done using specific software in a PC. The illumination-measuring geometry was therefore fixed and simulates the standard CIE geometry (45/0). The entire multispectral system except the illumination source was covered with a piece of black cloth in a dark room.

Methods and materials

Eight different biological structurally-colored samples were examined. They were butterfly wings from the following species: *Morpho deidamia*, *Papilio palinurus*, *Morpho didius*, *Morpho aega*, *Morpho rhetenor*, *Callophrys rubi*, *Papilio lorquinianus* and *Diachrysis chrysitis*. The brightly colored side of each butterfly wing was mounted vertically in a panel containing a black hole of 3cm or 1cm diameter. The

hole ensured a proper black background within the field of view of the scene. Multispectral data were calibrated using a white and a black (noise) reference image. The white reference image was obtained from a white diffuser (Edmund Optics opal diffuser 50mm), to correct spatial roughness. The spectral reflectance function of the white diffuser was measured using a spectrophotometer Shimadzu UV-310-PC with an integrating sphere. The black reference image was obtained by switching off the light source and preventing any light into the CCD camera. The wavelength range between 400-718nm was sampled at 6nm intervals. Each multispectral set consisted of 54 images. For each sample including both the white and the black reference samples, the exposition time at each wavelength was calculated using an optimization algorithm so that maximum pixel output was within 86- 90% of the CCD saturation value [3]. Therefore, the spectral reflectance function at each pixel was calculated after correcting for the intensity of the dark noise current and normalizing as a function of the white diffuser image corrected to the illuminant.

Results

Figure 1A,B (left) represents two examples corresponding to the *Papilio palinurus* and the *Morpho aega*, respectively. The visual area indicates a portion of the butterfly wing with size 400 x 400 pixels in gray scale. Figure 1A,B (right) also indicates an example of the spectral reflectance function calculated at different pixel positions (black and red solid lines). For each butterfly wing, spectral correlation analysis of reflectance spectra over the entire selected area was done using PCA. Although the number and spectral signature of the basis functions depend on the specific sample, our results indicate that between 9-32 bases can take into account more than 99% of the variability of reflectance spectra. This finding confirms the presence of characteristic nanostructures within butterfly wings. These results also show that multispectral imaging is a useful tool for structural colors and complement optical and electron microscopy observations.

The Fundação para a Ciência e Tecnologia and the Center for Physics, University of Minho, Portugal and the School of Physics at the University of Exeter, United Kingdom supported this work.

References

- [1] Kinoshita, S., Yoshioka, S., & Miyazaki, J. Reports on Progress in Physics, **71** (2008) 076410.
- [2] Vukusic, P., & Stavenga, D. G. (2009). Journal of the Royal Society Interface, **6** (2009) S133-S148.
- [3] Foster, D. H. Amano, K., Nascimento, S.M.C. & Foster, M.J. Journal of the Optical Society of America A, **23** (2006) 2359-2372.

Figures

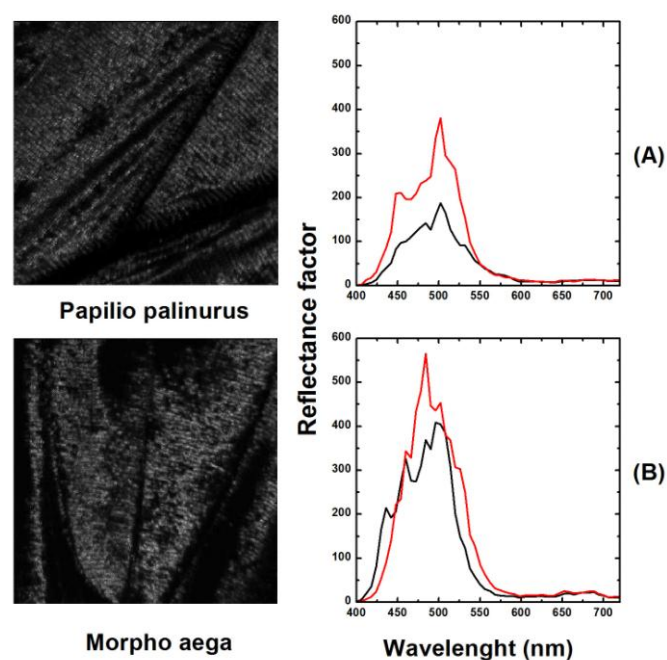


Figure 1. (A) Visual area of the *Papilio palinurus* (left, gray scale) and the estimated spectral reflectance function (right). Reflectance examples are given at different pixels positions. (B) Example of the *Morpho aega*.

Structural modification of TiO₂ nanorod films with an influence on the photovoltaic efficiency of a dye-sensitized solar cell (DSSC).

Lijian Meng^{a,b)*} and Can Li^{c)}

- a). Departamento de Física, Instituto Superior de Engenharia do Porto, Rua Dr. António Bernardino de Almeida, 431, 4200-072 Porto, Portugal.
 - b). Centro de Física, Universidade do Minho, 4800-058 Guimarães, Portugal.
 - c). State Key Laboratory of Catalysis, Dalian Institute of Chemical Physics, Chinese Academy of Sciences, 457 Zhongshan Road, Dalian 116023, China.
- *Corresponding author (ljm@isep.ipp.pt)

TiO₂ nanorod films have been deposited on ITO substrates by dc reactive magnetron sputtering technique. The structures of these nanorod films were modified by variation of the oxygen pressure during the sputtering process. Although all these TiO₂ nanorod films deposited at different oxygen pressures show an anatase structure, the orientation of the nanorod films varies with the oxygen pressure. Only a very weak (101) diffraction peak can be observed for the TiO₂ nanorod film prepared at low oxygen pressure. However, as the oxygen pressure is increased, the (220) diffraction peak appears and the intensity of this diffraction peak is increased with the oxygen pressure. The results of the SEM show that these TiO₂ nanorods are perpendicular to the ITO substrate. At low oxygen pressure, these sputtered TiO₂ nanorods stick together and have a dense structure. As the oxygen pressure is increased, these sputtered TiO₂ nanorods get separated gradually and have a porous structure. The optical transmittance of these TiO₂ nanorod films have been measured and fitted by OJL model. The porosities of the TiO₂ nanorod films have been calculated. The TiO₂ nanorod film prepared at high oxygen pressure shows a high porosity. The dye-sensitized solar cells (DSSCs) have been assembled using these TiO₂ nanorod films prepared at different oxygen pressures as photoelectrode. The optimum performance was achieved for the DSSC using the TiO₂ nanorod films with highest (220) diffraction peak and highest porosity.

Nanoparticle heterostructures: Selective growth of metal dots onto dihexagonal pyramidal CdSe nanocrystals

M. Meyns,¹ N. G. Bastús,¹ Y. Cai,¹ A. Kornowski,¹ B. H. Juárez² and C. Klinké.¹

¹Institute of Physical Chemistry, University of Hamburg, Grindelallee 117, 20146 Hamburg, Germany.

²IMDEA Nanociencia, Avda. Fco. Tomás y Valiente 7, 28049 Cantoblanco, Madrid, Spain.
meyns@chemie-uni-hamburg.de

During the past decades, a high degree of tunability of sizes, shapes and related physico-chemical properties of single component nanoparticles has been achieved.¹ Within the aim of improving materials for advanced applications, it is the rational next step to combine materials with different characteristic properties and thus obtain more complex structures. Following this strategy, it is possible to integrate favourable features of different materials in a single nanostructure or even obtain new properties resulting from interaction of the components. Especially interesting is the case of hybrid semiconductor-metal nanoparticles regarding the respective optical and electronic properties.

A successful approach for the chemical synthesis of hybrid-nanoparticles is the seeded growth method.² Semiconductor nanoparticles are used as seeds for the nucleation of one or more crystalline metal domains on their surface. The deposition behaviour is closely related to the geometry and surface reactivity of the seed particles. In our studies, we employed dihexagonal pyramidal CdSe nanocrystal seeds with a high number of vertices and thus reactive sites.^{3,4} This enabled us to investigate different parameters affecting the deposition, such as the oxidation state of the precursor, but also to tune the number, size and surface distribution of metallic domains in the final hybrid structures. Apart from an overview of the synthesis and physical properties, an interesting phenomenon observed in cases where the reduction of gold precursor was incomplete will be addressed: the migration of gold atoms on CdSe surfaces induced by a TEM beam.

The possibility to selectively stabilize Au deposits of down to cluster size (< 2 nm) on the surface of CdSe nanocrystals, for instance, seems promising in terms of both optoelectronic and photocatalytic applications.

References

- [1] C. Burda, X. Chen, R. Narayanan, M. El-Sayed, *Chem. Rev.*, **105** (2005) 1025.
- [2] P. D. Cozzoli, T. Pellegrino, L. Manna, *Chem. Soc. Rev.*, **35** (2006) 1195.
- [3] B. H. Juárez, M. Meyns, A. Chanaewa, Y. Cai, C. Klinké, H. Weller, *J. Am. Chem. Soc.*, **130** (2008) 15282.
- [4] A. B. Hungria, B. H. Juárez, C. Klinké, H. Weller, P. Midgley, *Nano Res.*, **1** (2008) 89.

Tunneling-current-induced light emission from chiral binaphthylene–perylenebiscarboxydiimide dimer

Y. Miyake¹, A. Fujiki¹, M. Kasaya-Akai¹, A. Saito^{1,2}, and Y. Kuwahara¹

¹ Department of Precision Science and Technology, Graduate School of Engineering, Osaka University, 2-1 Yamada-oka, Suita, Osaka 565-0871, Japan

² PRESTO, Japan Science and Technology Agency (JST), 4-1-8 Honcho, Kawaguchi, Saitama 332-0012, Japan

E-mail: miyake@ss.prec.eng.osaka-u.ac.jp

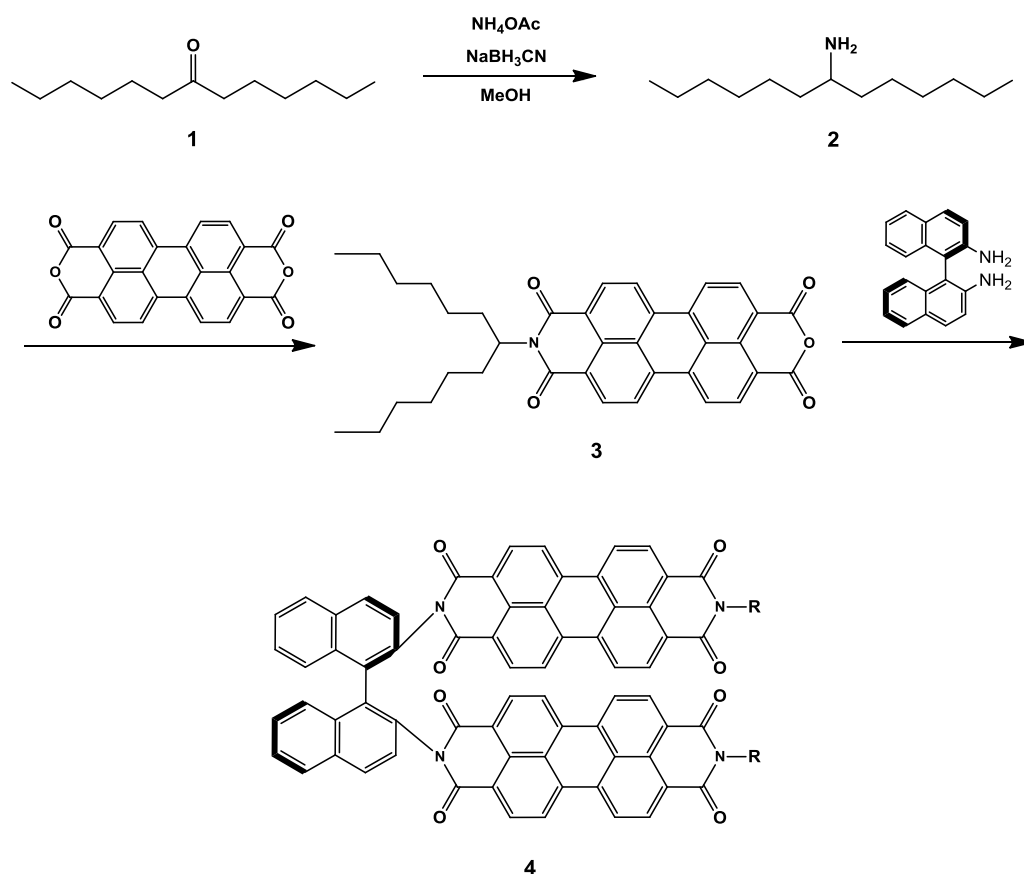
Chiral π -conjugated molecules and their self-organized structures have been attracted much attention for characteristic chiroptical behaviors such as dichroism (CD) and circularly polarized luminescence (CPL). Chiral molecular thin films and self-organized structures are expected to be potential candidates for chiroptical sensors and sources for circularly polarized light. [1] In this work, we have investigated the emission properties of chiral binaphthylene–perylenebiscarboxydiimide dimer (Scheme 1) thin films on the highly oriented pyrolytic graphite (HOPG) and the Au(111) surfaces using tunneling electrons from a scanning tunneling microscope (STM). The STM-induced light emission (STM-LE) analysis is a useful tool for characterizing the optical and electric properties of inorganic materials and organic molecules (Figure 1). So far, STM-LE has been utilized for analyzing achiral molecules. [2-4] The light emission from chiral molecules provides specific information about optical chirality of the molecules in the excited states. So, STM-LE analysis of chiral molecules can be a powerful tool for analyzing the excited state of chiral molecules on the surface. We adopt chiral binaphthylene–perylenebiscarboxydiimide dimer (**4**) for model compound chiral chromophore of light emission. Perylene diimides and the analogues show strong fluorescence. The central binaphthylene unit promotes chiral structure for the two perylene chromophore.

Compound (**4**) was synthesized via a slightly modified method reported previously. [5] 1-hexylheptylamine (**2**) was obtained by the reaction between dihexyl ketone (**1**) and $\text{NH}_4\text{OAc}/\text{NaBH}_3\text{CN}$. [6,7] N-(1-hexylheptyl)perylene-3,4,9,10-tetracarboxyl-3,4-anhydride-9,10-imide (**3**) was prepared by the reaction between 1-hexylheptylamine (**2**) and excess perylene-3,4,9,10-tetracarboxylic dianhydride (PTCDA) in DMF. The crude product of the reaction between 1-hexylheptylamine and PTCDA included symmetric dialkylated compound and asymmetric monoalkylated compound. Monoalkylated compound (**3**) was purified by column chromatography on a silica gel (eluent: chloroform). Chiral perylene diimide dimer (**4**) was synthesized via condensation reaction between binaphthyl diamine and (**3**). All compounds were identified using ^1H NMR, IR and elemental analysis. Cast films and spin coated films of compound (**4**) were prepared for STM-LE experiments.

In the present work, we will report surface morphology and STM-LE properties of chiral binaphthylene–perylenebiscarboxydiimide dimer (**4**) on the HOPG and the Au(111) surfaces.

References

- [1] H. Tsumatori, T. Nakashima, T. Kawai, *Org. Lett.*, **10** (2010) 2362.
- [2] H. W. Liu, U. Le, T. Yoshinobu, Y. Aso, H. Iwasaki, R. Nishitani, *Appl. Phys. Lett.*, **6** (2006) 061901.
- [3] H. W. Liu, R. Nishitani, Y. Le, K. Sudoh, M. Nowicki, T. Yoshinobu, Y. Aso, H. Wasaki, *Ultramicroscopy*, **8-9** (2006) 785.
- [4] T. Uemura, M. Furumoto, T. Nakano, M. Akai-Kasaya, A. Saito, M. Aono, Y. Kuwahara, *Chem. Phys. Lett.*, **4-6** (2007) 232.
- [5] H. Langhals, J. Gold, *Liebigs. Ann-Recl.*, **6** (1997) 1151.
- [6] Y. K. Che, A. Datar, K. Balakrishnan, L. Zang, *J. Am. Chem. Soc.*, **23** (2007) 7234.
- [7] M. W. Holman, R. C. Liu, D. M. Adams, *J. Am. Chem. Soc.*, **41** (2003) 12649.



Scheme 1. Synthetic scheme of compound (*R*)-4 [R=CH (C₆H₁₃)₂].

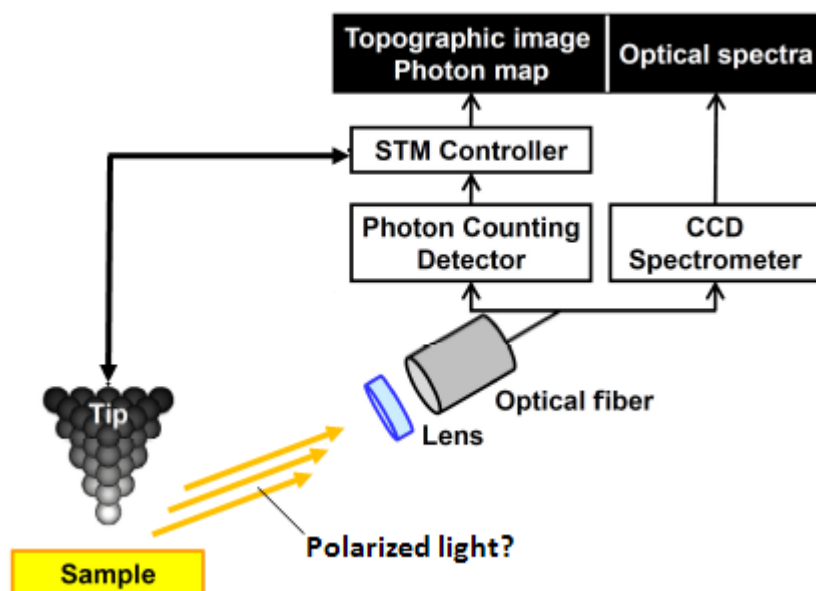


Figure 1. Schematic diagram of the photon detection system equipped with an STM under ambient condition.

Electrical resistance of CNT-peek composites under temperature and compression

Mohammad Mohiuddin, S. V. Hoa

Concordia Centre for Composites, Department of Mechanical and Industrial Engineering, Concordia University, 1455 de Maisonneuve Blvd. W Montréal, Québec, Canada H3G 1M8
E-mail: moh_mohi@encs.concordia.ca, hoasuo@alcor.concordia.ca

ABSTRACT

Electrically conductive carbon nano tube composites have attracted a great deal of scientific and industrial interest in the last few years. The electrical conductivity of the nanotube filled polymer composites is due to continuous conductive network formed in a specific arrangement by the nanotubes [1]. Enhancement of electrical conductivity of polymer by mixing them with multiwalled carbon nanotubes has found significant applications in newer areas such as electrostatic charge dissipation, electronic equipment, pressure sensors, sensor of vehicle weight to collect tolls in the highways, selective gas sensors, important strategic materials such as EMI/RFI shielding in computer and cellular phone housing etc. [2-4]. Smart materials can identify a change in the environment and respond to it by performing both sensing and actuation.

The level of electrical conductivity in the heterogeneous polymer nanocomposites primarily depends on several factors such as nature of the polymer matrix, morphology of conducting filler materials, processing parameters such as mixing time, mixing temperature and speed of mixing device and the test conditions such as pressure and temperature [5]. The electrical resistance of conductive polymeric composites changes with externally applied heat and pressure [6]. Scanning of literature shows that most of the researchers so far explored the applicability of pressure sensors made of carbon black (CB), carbon fiber, carbon nanotube (CNT), metallic powders, graphite etc. as conducting element and elastomeric rubber materials like NBR, SBR, EPDM etc. as matrix [7-10]. Results of those researches in engineering practice still need to be improved or adjusted according to the specific requirements of the sensor applications. No extensive research has yet been done to find out the possibility of using advanced thermoplastic materials e.g. PEEK, PEKK, PMMA as matrix in manufacturing pressure sensing element.

In the present article, the temperature and pressure dependent electrical resistance of advanced thermoplastic composites made of MWCNT and Poly Ether Ether Ketone (PEEK) for different CNT loadings are investigated. Different weight percentages of carbon nano tubes were dispersed with PEEK through intense shear mixing by calendaring technique in Brabender at 100 rpm and 380°C for 20 minutes. The resulting nanocomposites were processed into round shaped pieces of 25.4 mm diameter and 1.5 mm thickness. The samples are then simultaneously compressed by applying a pressure from zero to 40 MPa with an interval of 2 MPa and heated from 40°C to 140°C at an interval of 10°C. It has been found that electrical resistance decreases significantly with the application of heat and pressure. The results are graphically represented and supported by SEM images of the sample before and after applying pressure and temperature.

Keywords: Compression Pressure, Carbon nanotubes, electrical conductivity, micro structure.

References

- [1] Zheng WG, Wong SC and Sue HJ, *Polymer*, **43** (2002), 6767.
- [2] Volf J, Holy S and Vlcek J, *Sensors and Actuators A*, **62** (1997), 556.
- [3] Ghosp, P. and Chakrabart A. *European Polymer Journal*, **36** (2000)1043.
- [4] Chen, X. Jiang, Y., Wu, Z. Li and D Yang J, *Sensors and Actuators B*, **66** (2000), 37.
- [5] N.C. das, T. K. Chaki and D. Khastgir. *Carbon* **40** (2002) 807
- [6] X.W. Zhang, Y.Pan, Q. Zheng and X.S.Yi, *J.Polym.Sci B, Polym. Phys.***38** (2000), 2739.
- [7] K.P. Sau, T. K. Chaki and D. Khastgir, *Polymer*, **39** (1998), 6461.
- [8] Guohua Chen, Jinrong Lu, Wei Lu, Dajun Wu and Cuiling Wu, *Polym Int.***54** (2005)1689.
- [9] Wei Lu, Hongfei Lin, Dajun Wu and Guohua Chen, *Polymer* **47** (2006) 4440
- [10] K. Yoshimura, K. Nakano, T. Miyake, Y. Hishikawa, C. Kuzuya. *carbon* **45** (2007)1997

Acknowledgement

Financial support from the natural Sciences and Engineering Research Council of Canada (NSERC) is appreciated.

Figures

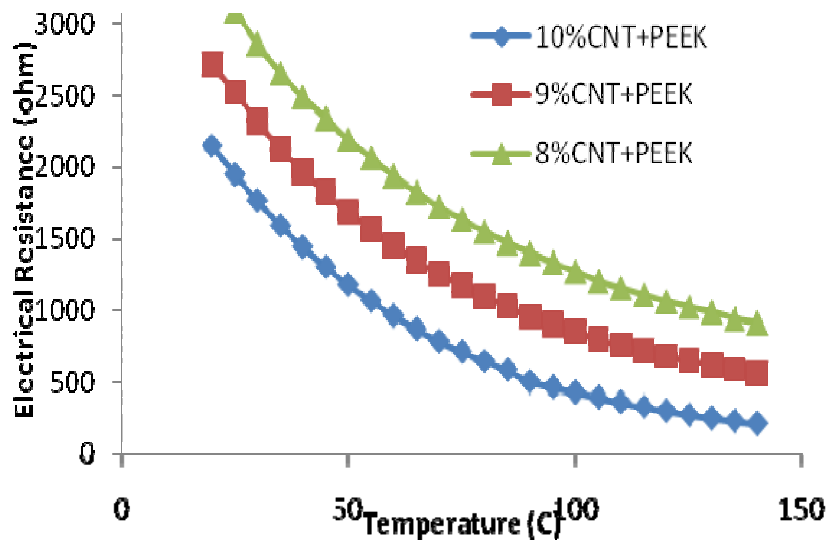


Figure 1: Electrical Resistance as a function of Temperature for 8%, 9% & 10% CNT-PEEK composites

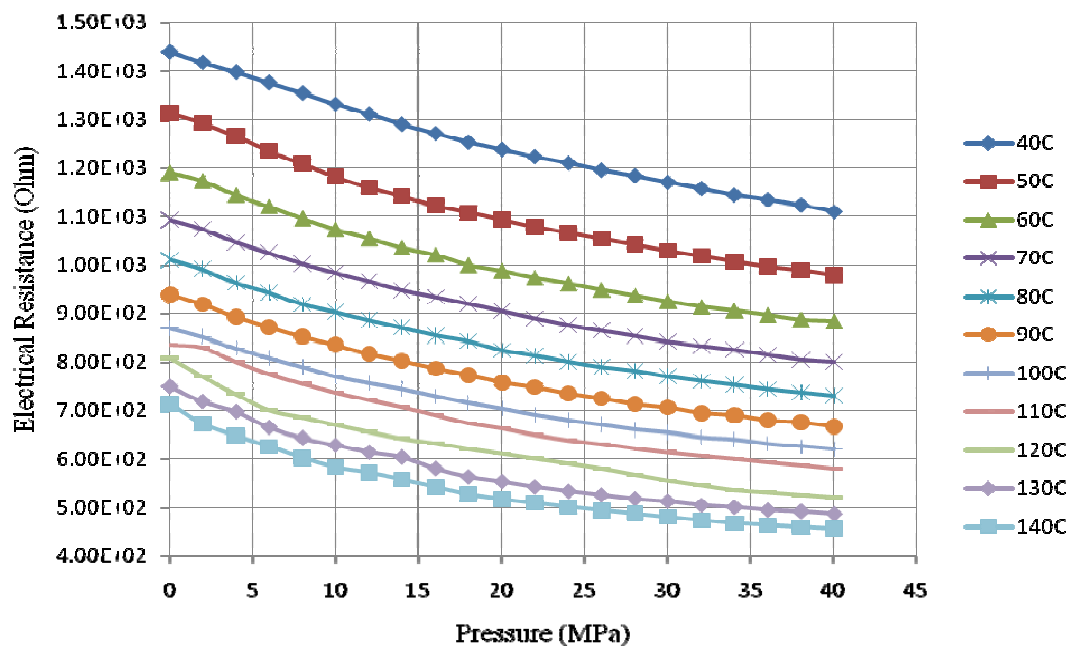


Figure 2: Electrical resistance of 9% CNT-PEEK at different temperatures and pressures

Theoretical Analysis of the Electronic Properties of the Endohedral Clusters $M@Al_{12}$ (M= B, Al, Si, N, P) and their ions

B. Molina^a, J. J. Castro^b, and J.R. Soto^a

^aDepartamento de Física, Facultad de Ciencias, UNAM, Apdo. Post. 70-646, 04510 México, D.F.

^bDepartamento de Física, CINVESTAV del IPN, Apdo. Post. 14-740, 07000 México, D.F.
mlnbrt@yahoo.com

It is well established that endohedral anion clusters $M@Al_{12}$ (M= B, Al, Si, N, P) have high stable icosahedral structures with a HOMO-LUMO gap comparable to C₆₀ and Au₂₀. However, when ionized, they present a vibronic instability tending to break their symmetry. In this work we present an analysis, based on an all-electron full relativistic DFT calculation, showing that through the ionization process ending with 39 and 41 electrons, these anion clusters suffer a Jahn-Teller symmetry breaking. The original Ih structure symmetry of the anion clusters (with 40 electrons), is lowered to D_{2h} for B and D_{3d} for Al, Si, N, and P in the 39 electrons case; and D_{5d} for the 41 electrons structure, except for N. We present the results for the corresponding density of states, vertical detachment energies and vertical ionization potentials. We discuss our results within the framework of the superatom model.

Novel Hybrid Nanoparticles Based on Squaramides

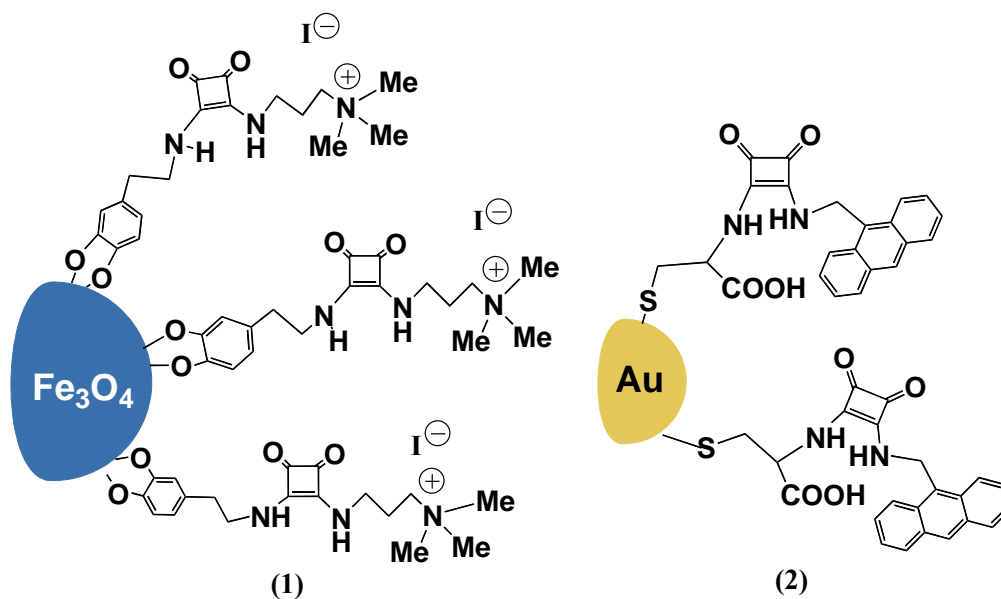
Jeroni Morey, M. Nieves Piña, Juan Robles and Kenia López

Department of Chemistry, University of the Illes Balears, Palma de Mallorca, Spain
jeroni.morey@uib.es

Squaramides have been used in combination with various receptors for molecular recognition of carboxylic acids, carboxylates and several inorganic anions: sulfate, hydrogen phosphate. Nanoparticles provide an adaptable platform for the incorporation of an enormous array of functionalities. In this contribution we describe the preparation of a new hybrid nanomaterials based on the conjunction of iron nanoparticles (1) and gold nanoparticles (2) with squaramide groups. (Figure).

Here we report a simple approach to conjugate monodisperse Fe_3O_4 nanoparticles with various squaramide-ammonium iodide salts, via a readily available linker, dopamine hydrochloride. The iron nanoparticles were synthesized as described by Sun[1]. Dynamic light scattering (DLS) measurements on the dispersed Fe_3O_4 show that the nanoparticles have an average hydrodynamic diameter of 9 nm. Preliminary results seem to indicate the availability of the new hybrid iron nanoparticles for the determination of the following anions: benzoate, tartrate and citrate in water at pH = 8.

The gold nanoparticles (2) were synthesized as described by Hegmann^[2] with few changes. This design reflects the need of cystein as an anchor group in fluorescent squaramide groups to stabilize gold nanoparticles. Transmission electron microscopy (TEM) analysis indicated an average core diameter for (2) of 15 nm. The fluorescence spectrum of the gold nanoparticles (2) showed that the emission of anthracene was dependent on the pH.



References

- [1] J. Xie, C. Xu, Z. Xu, Y. Hou, K. L. Young, S. X. Wang, N. Pourmond and S. Sun, *Chem. Mater.* **2006**, *18*, 5401-5403.
[2] H. Qi and T. Hegmann, *J. Am. Chem. Soc.* **2008**, *130*, 14201-14203.

Enzymatic Synthesis of Amorphous Calcium Phosphate-Ciprofloxacin-Chitosan Nanocomposites as Potential Bone Substitutes

Stefania Nardecchia, María C. Gutiérrez, María L. Ferrer, Francisco del Monte

Instituto de Ciencia de Materiales de Madrid, Consejo Superior de Investigaciones Científicas,
C/Sor Juana Inés de la Cruz, 3. 28049 Cantoblanco, Madrid, Spain.
nardecchia@icmm.csic.es

Bone is made from calcium phosphates in the form of apatitic mineral phases with a large number of proteins. Recent studies reveal that, despite the complicated hierarchical structures of bone and teeth, their basic building blocks are nanoparticles of calcium phosphate which chemical and biological properties are strictly linked to their nanoscale dimensions (the mineral phase of bone is constituted of carbonated hydroxyapatite crystals with a length of about 100 nm, width of 0-30 nm, and thickness of 3-6 nm). Then, biomimetic calcium phosphates need to be synthesized with similar nanoscale dimensions, as well as with properties such as low crystallinity, nonstoichiometric composition and crystalline disorder, which require a nanoscience approach. [1]

In natural bone synthesis, the biomineralization process starts with the formation of poorly crystalline calcium apatites (preceded by possible transient amorphous calcium phosphates, ACP), which are then modified through crystalline phase transitions to form the more stable mature bone apatites with increased crystallinity (HAP). Previous studies also confirm that ACP has improved bioactivity compared to HAP since more adhesion and proliferation of osteogenic cells are observed on the ACP substrates. [2]

The development of a new generation of bonelike composite materials calls for a biomimetic synthetic approach using natural bone as a guide. In bone regeneration, scaffolds serve as template for cell interactions and formation of bone-extracellular matrix to provide structural support to the newly formed tissue. Therefore, it is necessary that the scaffolds should, in some respect, mimic host bone morphology in order to optimize integration into surrounding tissue. [3] Enzymatically assisted routes offer the possibility to synthesize a number of materials with excellent control of the structural organization. In particular, HAP precursors could be obtained in solution by enzyme-catalyzed decomposition of urea by urease, and, in the same way, monolithic and homogeneous chitosan (CHI) hydrogels with a homogeneous 3D network structure have recently been prepared. [4] On the other hand, the controlled release of antibiotics from scaffold structures has been widely demonstrated to be of great utility to reduce the risks of infection after surgery. For this purpose, in a previous study, we have incorporated the antibiotic ciprofloxacin (CFX) into the macroporous structure of CHI scaffolds. [5]

Furthermore, the surface functionalization of calcium phosphate with bioactive molecules makes them able to transfer information to and act selectively on the biological environment, and this represents a main challenge for innovative bone substitute materials. In this context, the synthesis of ACP nanoparticles loaded with antibiotic drug that can be released by a controlled kinetic process represents an attractive goal. [6]

Herein, we applied the urease assisted hydrolysis of urea for the preparation of nanocomposites of calcium phosphate, CFX and CHI for bone regeneration. The base generated by urea hydrolysis promoted both CHI gelation and ACP-CFX simultaneous precipitation at biological temperatures (37 °C). Macroporous hierarchical structures were obtained by a cryogenic process (so-called ISISA, ice segregation induces self-assembly) that is simply based on the unidirectional freezing (at -196 °C) of the hydrogel nanocomposite. After freeze-drying, the resulting hierarchical structures consist of well aligned micrometer-sized pores in the freezing direction corresponding to the empty areas where ice crystals originally resided, being the macrostructure supported by the matter (e.g., calcium phosphate nanoparticles and CFX nanocrystals dispersed within CHI matrix) accumulated between adjacent ice crystals (Fig.2). We have analyzed the delivery kinetics of CFX crystals entrapped in CHI scaffolds by UV-vis spectrometry.

References

- [1] S. V. Dorozhkin, *J. Mater. Sci.* **42** (2007) 1061.
- [2] J. Song, V. Malathong, C. R. Bertozzi, *J. Am. Chem. Soc.* **127** (2005) 3366.
- [3] C. Sanchez, H. Arribart, M. M. Giraud Guille, *Nature Materials*, **4** (2005) 277.
- [4] M. C. Gutiérrez, M. Jobbágy, M. L. Ferrer, F. del Monte, *Chem. Mater.* **20** (2008) 11.
- [5] I. Aranaz, M. C. Gutiérrez, L. Yuste, F. Rojo, M. L. Ferrer, F. del Monte, *J. Mater. Chem.* **19** (2009) 1576.
- [6] B. Palazzo, M. Iafisco, M. Laforgia, N. Margiotta, G. Natile, C. L. Bianchi, D. Walsh, S. Mann, N. Roveri, *Adv. Funct. Mater.* **17** (2007) 2180.

Figures

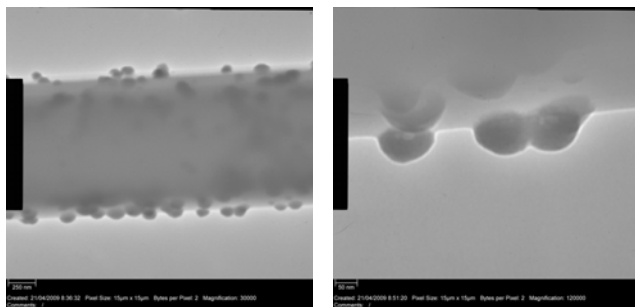


Fig.1_TEM micrographs of ACP and CFX obtained by enzymatic synthesis at 37 °C.

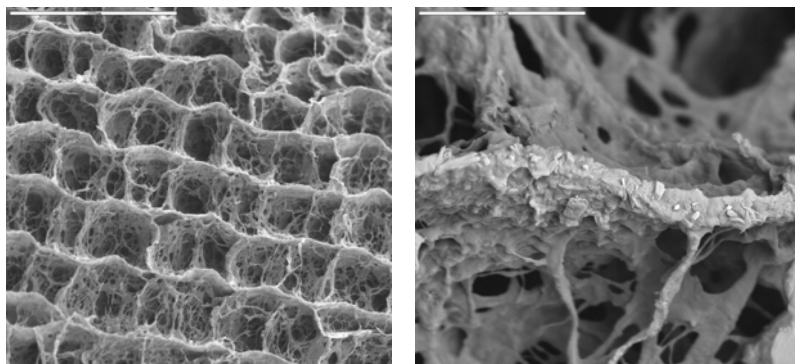


Fig.2_SEM micrographs of hierarchical structure resulting from freezing hydrogel nanocomposites.

Poly(acrylonitrile-butadiene styrene)/Poly(methylmethacrylate)/nanoclay nanocomposite and its properties

Tayebe Nazari, Hamid Garmabi, Ahmad Arefazar

Polymer Engineering Department, Amirkabir University of Technology, Tehran, Iran
E-Mail: garmabi@aut.ac.ir, t_nazari@aut.ac.ir

Acrylonitrile–butadiene–styrene (ABS) is one of the most important rubber-toughened thermoplastics, but its application is limited because of its low thermal stability and lack of flame retardancy. These problems can be overcome by some of the strategies such as physical blending of high heat resistant polymer and some fillers with ABS, although fluidity and impact properties of ABS may be decreased [1]. Poly(methyl methacrylate) (PMMA) which is compatible with poly(styrene-co-acrylonitrile) (SAN), is characterized by higher heat-distortion temperature (HDT) and is cheaper than other high-performance polymers for blending with ABS. PMMA can improve thermal properties of ABS, so can nanoclays. We want to investigate both of their effects on ABS.

In this work, for the first time blend nanocomposite of ABS/PMMA/nano-organoclay has been prepared in four various processing conditions with melt blending in the co-rotating twin screw extruder. It's necessary that the melt viscosity ratios of polymer grades must be near one to reach a fine and uniform distribution of the minor component in the major component [2]. So, the rheology curves of PMMA and ABS at melt temperature were obtained, figure 1. Then polymers with 2% wt nanoclay (cloisite 30B) have been blended. The amount of PMMA in the hybrid is 25 %wt. We varied the processing condition (screw speed and feeding rate to extruder) to find out optimum compounding condition. Mechanical properties and morphology of prepared samples were characterized using tensile test, Izod impact test and X-ray diffraction (XRD).

The result shows that samples were extruded in the higher screw speed and lower feeding rate, have good elongation at break, higher modulus, figure 2, and higher tensile strength, because of the better dispersion of nanoclays [3], as a result these samples show lower Izod impact strength, figure 3, due to the reduction of polymer molecular chains mobility close to nanoclay surface [4]. In comparison with virgin ABS, addition of both PMMA and organoclay to ABS matrix improves heat deflection temperature of hybrid nanocomposite. Also XRD pattern in figure 4 illustrates some intercalation of polymer chains between C30B galleries but on the other hand the characteristic peak of the C30B was shifted to higher degree somewhat. This event indicates that some nanoclay gallery height decreased upon compounding [5]. A possible explanation for this unexpected result in two different processing conditions is that perhaps clay type had not been suitable.

References:

- [1] Q. Li, M. Tian, D. Kim, L. Zhang and R. Jin, *Journal of Applied Polymer Science*, **85**, 2002, 2652-2660.
- [2] K. Yang, S.H. Lee and J.M. Oh, *Polymer Engineering and Science*, **39**, 1999, 1667-1677.
- [3] G. Ozkoc, G. Bayram, J. Tiesnitsch, *Polymer Composites*, **29**, 2008, 345–356.
- [4] S. Qin, M. Zhang and et al, *Journal of Macromolecular Science PartB: Physics*, **48**, 2009, 910–918.
- [5] R. J. Opalko, MSC Thesis, University of Akron, 2008.

Table 1- Prepared samples name and processing condition

Nanocomposite name	Screw speed of extruder (rpm)	Feeding rate to extruder (kg/h)	Temperature profile (°c)
250-H	250	10	200-220
250-L	250	5	"
500-H	500	10	"
500-L	500	5	"

Figure 1:

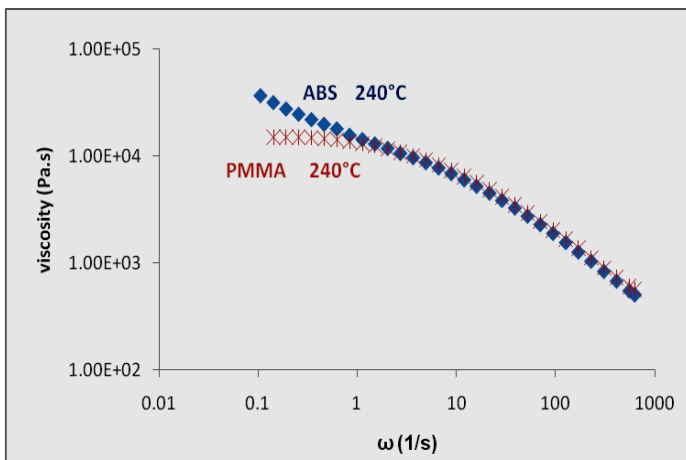


Figure 2:

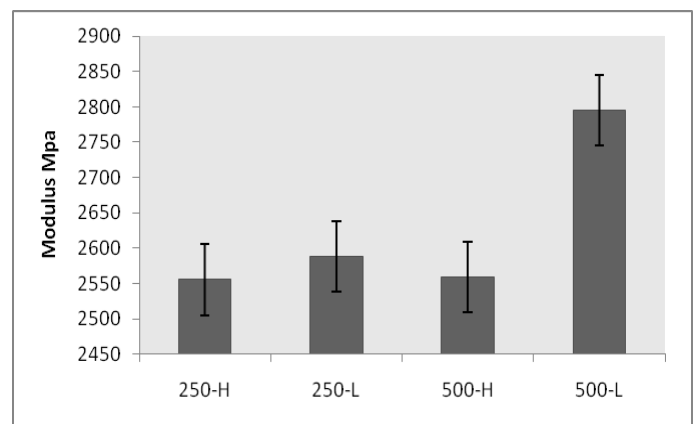


Figure 3:

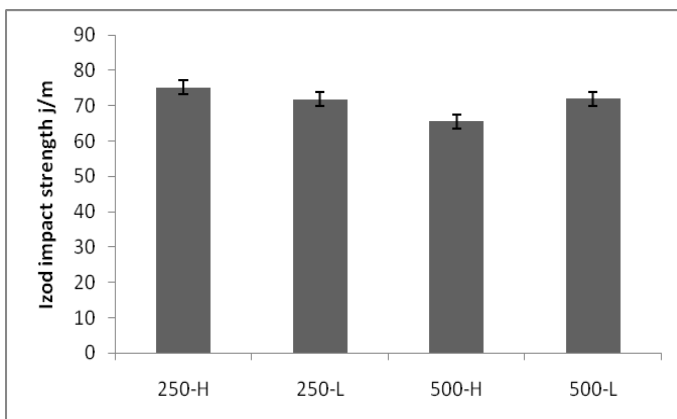
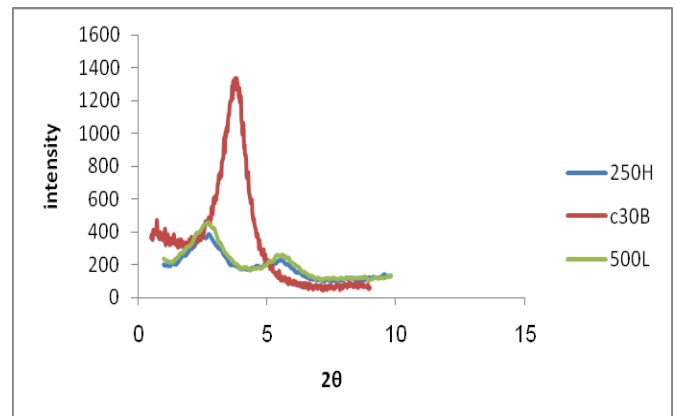


Figure 4:



Electrical Measurements on Graphene Inside Scanning Electron Microscope Using Four Point Probes

M. B. Olesen, B. Malm, D. H. Petersen, P. Bøggild

DTU Nanotech, Technical University of Denmark, Build. 345E, DK-2800 Kgs. Lyngby, Denmark
mikkel.olesen@nanotech.dtu.dk

Since the discovery of the experimental technique for fabricating graphene by cleaving Highly Oriented Pyrolytic Graphite (HOPG)^[1], the interest of graphene as a electronic component has increased dramatically^[2]. Graphene is a two dimensional, single-layer carbon material arranged in a hexagonal grid. It is a semi-metal, meaning it has discrete K points where conduction band and valence band intersect^[3]. The interest in graphene as a electronic device comes from fact that the electrons acts as massless Dirac fermions^[4], which gives rise to the high electron mobility and long mean free path^[2] even at room temperature.

Graphene fabricated from HOPG can be placed on 90nm or 300nm silicon dioxide (SiO₂) for highest optical contrast between the substrate and the graphene^[5]. In this manner, pieces of graphene, multilayered graphene and graphite attach to the surface, and the contrast increases with the number of layers^[5]. Another, albeit more time consuming method, is to use Raman spectroscopy, which gives rise to a peak at 2600 cm⁻¹^[6]. We here present a characterization method for graphene, using scanning electron microscopy (SEM). The contrast between a graphene sample and the substrate depends on the tilting angle of sample, ie. the angle between the electron beam and the normal of the sample surface.

Since graphene is a two dimensional material, the surface to volume ratio is very high, and the electrical properties are highly influenced by environmental variations. Theoretical calculations show electron mobilities of 100.000 cm²/Vs^[2], and experimental measurements on graphene on top of SiO₂, shows mobilities of 44.000 cm²/Vs^[7]. Characterization of graphene on an atomic level has been performed inside TEM^[8], and it has been shown that the electron induces damage on the graphene^[9], but not to what extend it effects the electrical properties. To better understand the electrical properties of graphene under the influence of an electron beam, four point probe (4pp) measurements are performed inside a SEM.

SEM Contrast on Graphene

Graphene cleaved from HOPG is placed on a wafer with 90nm of SiO₂. The sample are examined inside SEM. Using acceleration voltages ranging from 1keV to 10keV, and tilting the sample in angles of 0 (zero) to 55 degrees, a contrast difference between the substrate and the graphene is observed. Higher angles gives results in higher contrast. The contrast is calculated from,

$$contrast = \frac{I_{substrate} - I_{graphene}}{I_{substrate}}$$

where I_i is the brightness intensity of material i . Fig. 2 shows the visible contrast difference on a sample at zero degrees and 55 degrees.

The tilting measurements are done on graphene samples with 1,2,3,>5 layers, and the result shows that the fewer layers, the less contrast difference when tilting. By measuring the contrast difference on graphene samples, the number of layers can be calculated. The output from the SE2 detector increases as the sample is tilted towards the detector. The intensities are related to the SEM brightness and contrast settings, in order to evaluate the data.

Electrical Measurements Using Four Point Probes

Cleaved graphene placed on SiO₂, are placed inside a SEM on a SmarAct manipulator arm. On another arm, a 4pp is placed and electrical connections are made, so that the manipulator and the 4pp can be controlled from outside the chamber. Using this structure of setup, electrical measurements can be performed while the sample is exposed to the electron beam. By performing the measurements in vacuum, the effects from the air is eliminated. When the 4pp has electrical contact to the graphene, the electron beam can be turned on and off to measure the conductance with and without the beam affecting the sample. Thereby, the contamination induced by the beam on the graphene sample is estimated.

Measurements are done on different number of layers of graphene, on graphene on top of SiO₂ and on suspended graphene. Fig. 2 shows a four point probe contacted to a graphene sheet suspended inside SEM. Our findings suggests a difference in conductance over time, when the graphene sample is exposed to an electron beam.

References

- [1] K. S. Novoselov, A. K. Geim, S. V. Morozov, D. Jiang, Y. Zhang, S. V. Dubonos, I. V. Grigorieva, A. A. Firsov, *Science* 306, (2004) 666
- [2] A. K. Geim, K. S. Novoselov, *Nature Mat.* 6, (2007) 183-191
- [3] C. H. Park, L. Yang, Y. W. Son, M. L. Cohen, S. G. Louie, *Nature phys.*, vol 4 (2007) 213-217
- [4] K. S. Novoselov, A. K. Geim, S. V. Morozov, D. Jiang, M. I. Katsnelson, I. V. Grigorieva, S. V. Dubonos, A. A. Firsov, *Nature Lett.* Vol 438, 10, (2005) 04233
- [5] P. Blake, E. W. Hill, A. H. Castro Neto, K. S. Novoselov, D. Jiang, R. Yang, T. J. Booth, A. K. Geim, *App. Phys. Lett.* 91 (2007) 063124
- [6] A. Gupta, G. Chen, P. Joshi, S. Tadigadapa, P. C. Eklund, *Nano Lett.* Vol. 6, No. 12 (2006) 2667-2673
- [7] R. S. Shishir, D. K. Ferry, *J. Phys.: Condens. Matter* 21 (2009) 232204
- [8] H. Zhang, P. X. Feng, *Elsevier*, 48 (2010) 359-364
- [9] D. Teweldebrhan, A. A. Balandin, *App. Phys. Lett.* 94 (2009) 013101

Figures

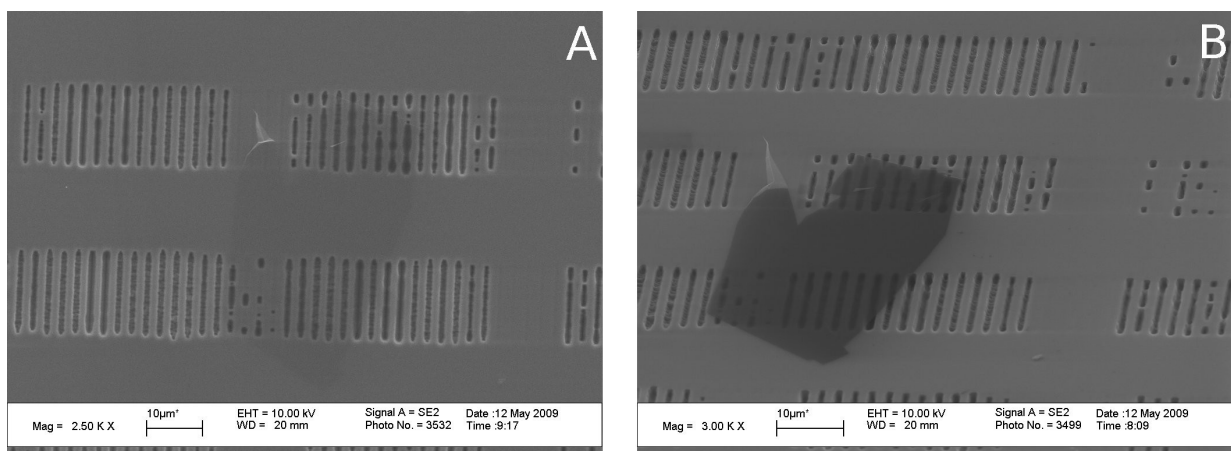


Fig. 1: Multilayered graphene at different tilting angles. (A) zero degrees, (B) 55 degrees. The contrast difference between substrate and graphene is increasing with increasing tilting angle.

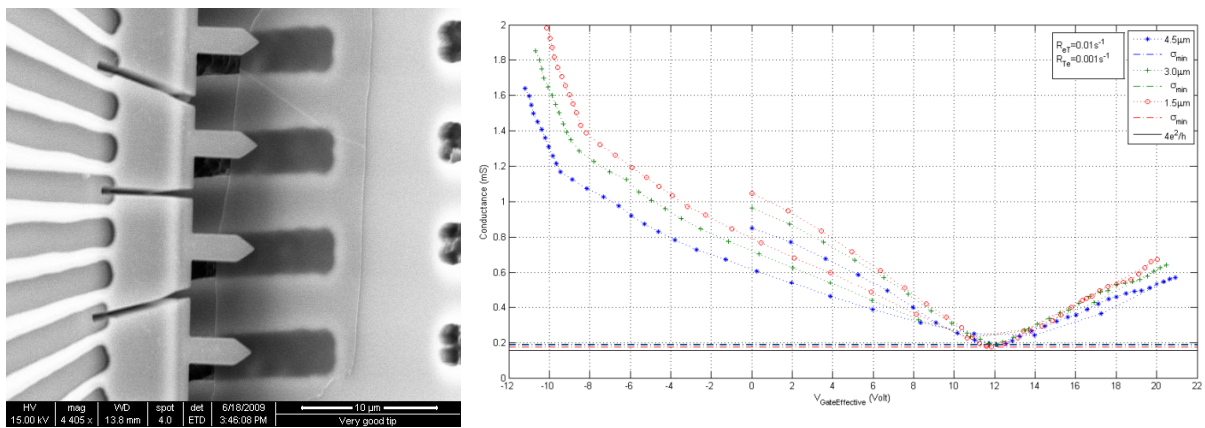


Fig. 2: (Left) Micro four point probes in contact with graphene suspended over ridges. (Right) Four point probe measurements performed on graphene in air. The curves are for different probe pitches.

Fluorinated Cholesterol based system with DOTAP for DNA Transfection

Diana Paiva¹, Gerald Brezesinski², Sandra Rocha¹, Maria do Carmo Pereira¹

¹LEPAE, Faculty of Engineering, University of Porto, Rua Dr. Roberto Frias, 4200-465 Porto, Portugal

²Max-Planck Institute of Colloids and Interfaces, Am Mühlenberg 1, 14476 Potsdam, Germany
deq08007@fe.up.pt

Cationic liposomes are extremely advantageous for DNA transfection due to stability and health safety when compared with viral vectors. Liposomal delivery systems are formed by a cationic lipid bilayer usually combined with helper lipids, such as cholesterol, in order to improve their stability, reduce the toxicity of cationic lipids and increase their plasma half-life time. One of the best properties of cationic liposomes is that they interact efficiently with negatively charged molecules, such as DNA, mainly by electrostatic interactions. This becomes a fast and easy method to prepare delivery systems which do not require an encapsulation step.

A new system has been developed and characterized using the cationic lipid DOTAP and fluorinated cholesterol (F7-cholesterol), as the helper lipid. Liposomes were prepared by the lipid film hydration method and extruded through polycarbonate membranes of pore size from 800 to 100 nm. The system was characterized by dynamic light scattering and zeta-potential measurements. The study confirms the formation of a liposome-monodisperse sized population and a positive zeta-potential (55 ± 5 mV) of the system. Their positively charged surfaces efficiently compact DNA by means of a strong entropically driven surface interaction that yields the formation of lipoplexes as confirmed by zeta-potential values.

Langmuir monolayers of the lipid system were obtained and have shown that the fluorinated cholesterol does not induce a first order phase transition, although its addition has an ordering effect in DOTAP layers. The results obtained by Brewster angle microscopy evidence a complete miscibility between the compounds, which confirms the previous results. It was noticed that for the same pressure, the area per molecule is smaller than the expected at all ratios tested (DOTAP:F7-cholesterol 9:1, 4:1, 7:3, 3:2, 1:1, 2:3, 3:7, 1:4 and 1:9), which indicates a strong interaction between DOTAP and fluorinated cholesterol reducing the area per molecule occupied by the compounds.

The infrared reflection absorption spectroscopy (IRRAS) studies show the adsorption of DNA to lipid monolayers of pure DOTAP and mixtures DOTAP:F7-cholesterol 2:1, 1:1 and 1:2. Pure F7-cholesterol monolayer does not show any DNA at the interface. The DNA migrates to the interface due electrostatic interactions. For the tested mixtures, the amount of DNA at the interface decreases with the decreasing amount of DOTAP. However, the amount of absorbed DNA is higher than the values expected by the linear relation, meaning that even when DOTAP was combined with F7-cholesterol, it has enough free charges to establish electrostatic interactions with DNA.

Nanoparticle induced phase transformation and dielectric response of core/shell Fe/MgO–poly(vinylidene fluoride) nanocomposites

A. J. Paleo¹, C. Martínez-Boubeta², Ll. Balcells³ and S. Lanceros-Mendez⁴

1- IPC - Institute for Polymers and Composites, University of Minho, Campus de Azurém, 4800-058 Guimarães, Portugal

2- IN2UB and Departament d'Electrònica, Universitat de Barcelona, 08028, Spain

3- ICMAB-CSIC, Campus UAB, Bellaterra 08193, Spain

4- Center/Department of Physics, University of Minho, Campus de Gualtar, 4710-057 Braga, Portugal

Magnetic materials with high permeability and low magnetic loss at high frequency can play an important role in high frequency communication devices [1, 2]. In this case the magnetic material should have high saturation magnetization, high magnetic anisotropy and high electrical resistivity. In order to get suitable materials for applications accomplishing both high saturation magnetization and high electrical resistivity, the preparation of nanocomposite materials composed of nanoparticles with high saturation magnetization and insulating matrix such as polymer seem to be one of the preferred ways [3].

Here we report on Fe(Co) particles covered by a uniform 3 nm thick MgO epitaxial shell. Among commonly used schemes, we followed simple physics-derived solutions based on gas-aggregation methods that assure industrial scalability and ecology. Nearly spherical crystals self-assembled nanomagnets were obtained by means of vapor-phase condensation [4]. Nanocomposites of the core-shell particles (0.02, 0.2 and 2%wt) with poly(vinylidene fluoride) were prepared by solution casting under conditions leading to the non-electroactive β -phase in the pure polymer [5]. The dielectric and thermal and mechanical properties of the composites were evaluated.

Far infrared spectroscopy and differential scanning calorimetry indicate that the nanoparticles seem to act as nucleating agents in the polymer crystallization process, affecting both the melting temperature (increases with increasing nanoparticle concentration) and the degree of crystallinity and the polymer phase. In this way, the material is obtained in the electroactive polar β -phase, with the possibility of interplay of the magnetic and electrical response of the material. The dielectric response of the composite, on the other hand slightly affected by the presence of the magnetic nanoparticles.

References

- [1] M. Saidani and M. A. Gijs, Appl. Phys. Lett. 84, 4496 (2004).
- [2] B. Lu, H. Huang, X. L. Dong, X. F. Zhang, J. P. Lei, J. P. Sun, and C. Dong, J. Appl. Phys. 104, 114313 (2008).
- [3] S. X. Wang, N. X. Sun, M. Yamaguchi, and S. Yabukami, Nature London, 407, 150 (2000).
- [4] C. Martínez-Boubeta et al. 94, 262507 (2009); Nanomed.: Nano. Bio. Med. 6, 362 (2010).
- [5] M. C. Branciforti, V. Sencadas, S. Lanceros-Mendez, R. Gregorio, Jr. Journal of Polymer Science Part B-Polymer Physics, 45, 19, 2793 (2007).

Acknowledgments

The authors acknowledge the Foundation for Science and Technology, Lisbon, through the 3^o Quadro Comunitario de Apoio, the POCTI and FEDER programs, the PTDC/CTM/69316/2006 grant, the NANO/NMed-SD/0156/2007 project, EU-DG RTD's SFERA (BIONANOS) and the Spanish MICINN (MAT2009-08024, CONSOLIDER (CSD2007-00041)) for financial support. C. M. Boubeta gratefully acknowledges financial support from the Spanish "Ramón y Cajal" program.

The radio frequency systems to potentate the therapeutic properties of nanostructures and nanosystems as carriers into the cell.

D.Pantis^{1,2}, S.Spinean², Al.Efimov³, R.Ion⁴, M.Borda¹

1- Technical University Cluj Napoca, Romania

2- ROMATSA Cluj Napoca, Romania

3 - Science Biocreative, Bucharest, Romania

4 – The National Institute for Research & Development in Chemistry and Petrochemistry, Bucharest, Romania

Key words:

SWNT, radio frequency, cancer, hyperthermia

Introduction

The purpose of the study was to use viabilised nanostructures, as carriers for delivery of different drugs or structures into the cells using different methods (injected intratumoral or send via blood flow) in cancer treatment.

To use SWNT as „carrier” several properties and features have to be demonstrated. Among them the demonstration that thermal effects on the indicated viabilised nanostructure has effects only on the structure sent and the combination between SWNT and viabilisation will be not affected by SWNT

Material and methods

Our study was designed for some specific structures knowkn to be used as carriers for several nucleic acids sequences or different drugs, like SWNT originally produced in ITIM Laboratories in Cluj Napoca.

Knowing that in hyperthermia, the targeted temperature range is between 40 and 46°C, we demonstrated that at that temperature, the SWNT structure is not affected.

The experiments were carried out in ICECHIM Bucharest Laboratories, Romania on nanotubes produced by TIM Cluj and also from Bucharest.

The experiment was made on TGA / SDTA 851E Mettler-Toledo., which is evaluating the weight loss with the temperature of the tested materials. The same thermal effect is produced by a Radiofrequency Generator (the device was built in Cluj, generating 400-500 W in a range of 2-30 MHz (range including the frequency allocated to medical purposes).

The results are demostrating that SWNT are ideals transporters, due to a remarcable thermal conductivity and thermal resistance.

Conclusion

The experiments on SWNT structures were carried out to evaluate several properties and parameters :

- Radiation power
- Radiation frequency
- Radiation time
- Thermal effects of the radiation in different tissues, under different angles

Our results demonstrates that under certain conditions these type of transporters can be used under the precise control of a radio frequency generator with better results in targeting the cell membrane, being potential candidates for cancer treatment.

The effects of hyaluronan –coated gold nanoparticles on cell migration, proliferation and viability

Hanna Parkkola¹, Laura Vivero¹, Marc Ramis¹, Mark Slevin², Joaquin Querol¹, Judith Sendra¹

1-Endor Nanotechnologies, Helix Building, Parc Científic de Barcelona, Baldiri i Reixac 15, 08028 Barcelona, Spain

2- British Institute of Technology & Ecommerce Avicenna House/Kalam House 258-262 Romford Road, London

e-mail: hanna.parkkola@endornanotech.com, judith.sendra@endornanotech.com

Hyaluronan (HA) is a non-sulfated glycosaminoglycan of a molecular mass as high as 10⁶ kDa that consists of repeating units of (β,1– 4)-D-glucuronic acid-(β,1–3)-N-acetyl-D-glucosamine. HA is abundant in extracellular matrix and an important component of e.g. skin and synovial joint. HA is a potent regulator of vascular endothelial cell function and because of its role in tissue remodeling it has been shown to be involved in pathologies such as cerebrovascular disease and cancer. Native high molecular HA is antiangiogenic but degradation products of specific size, oligosaccharide-HAs (o-HA), have been reported to stimulate angiogenesis, cell proliferation and migration. (1, 2)

Our laboratory prepared 5 kDa o-HA conjugated to gold nanoparticles (HA-GNPs) and the effects of these HA-GNPs *in vitro* were studied in fibroblasts, endothelial and breast cancer cells. The proliferation and migration rates and also cell viability in the presence HA-GNPs were evaluated to investigate the angiogenic effects of this nanoconjugate. We detected neither promotion nor inhibition of cell proliferation and our wound healing experiments with cancer cells showed mild inhibition of cell migration. The HA-GNPs didn't reduce cell viability so these effects were not due to toxicity.

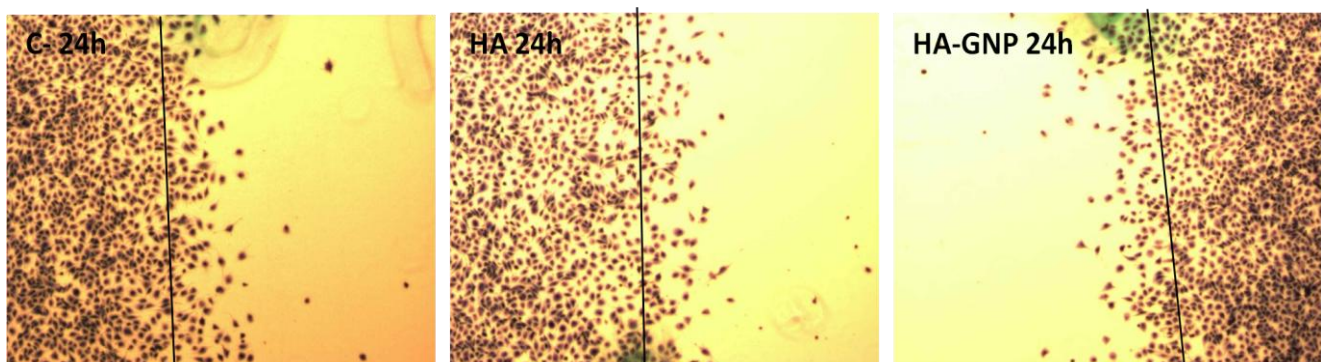
The stimulatory effects of o-HA seem to be highly size-dependent. It has been reported earlier that low molecular weight o-HA promotes events related to angiogenesis and tissue remodeling but our results show that 5 kDa o-HA conjugated to gold nanoparticles doesn't possess these properties. In fact, a specific size o-HA has also been shown to display anticancer effects by causing apoptosis and reducing drug resistance (3). In conclusion, when designing nanoscale therapeutics, it's essential to carefully consider the possible effects of conjugate size modification on desired effects. Different sizes may lead to completely different responses on cellular level.

References:

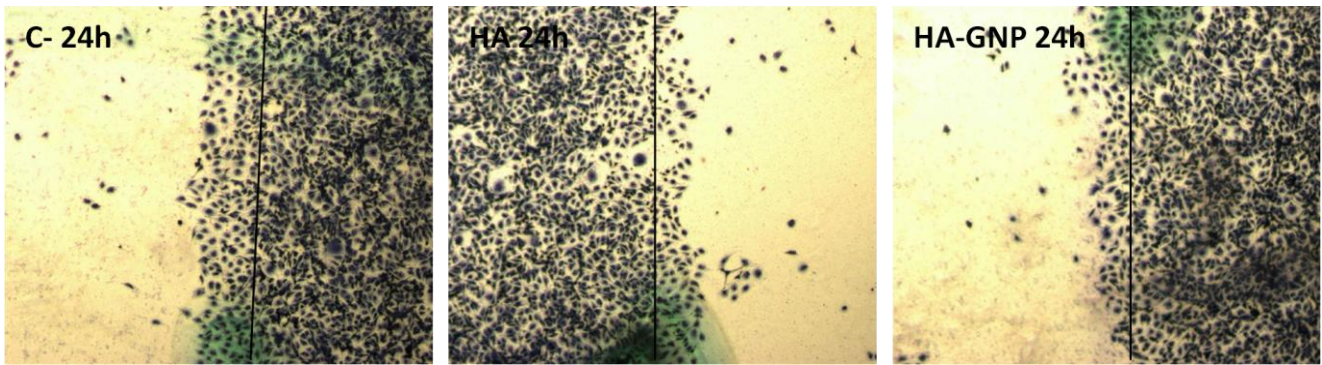
1. West DC, Kumar S, Ciba Found Symp, **143:187-201**, (1989) discussion 201-7, 281-5.
2. Slevin M, Kumar S, Gaffney J, J Biol Chem, **277(43)**, (2002) 41046-59.
3. Toole BP, Clin Cancer Res, **15(24)**, (2009) 7462–8

Figures:

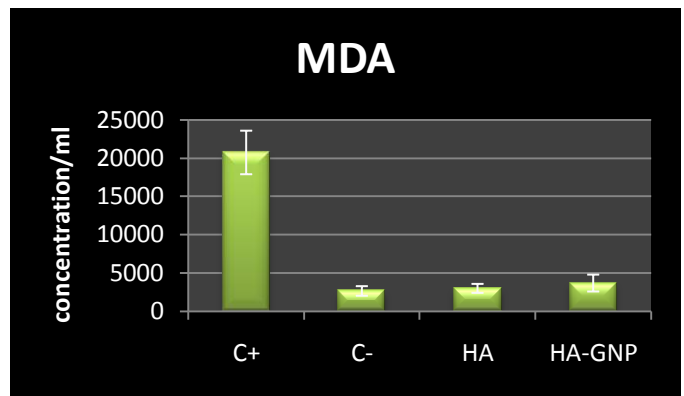
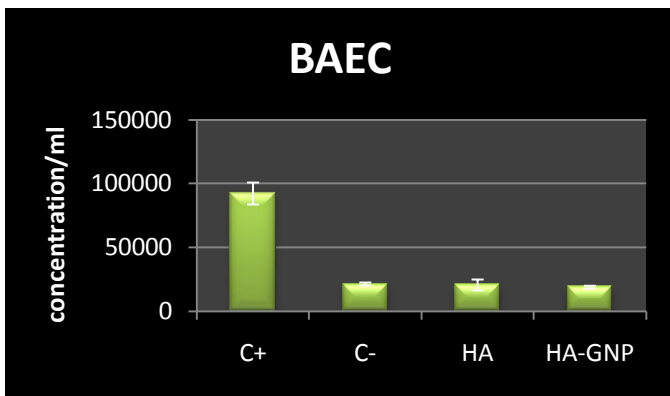
1. Migration (Wound healing assay): a) Bovine aortic endothelial cells (BAEC):



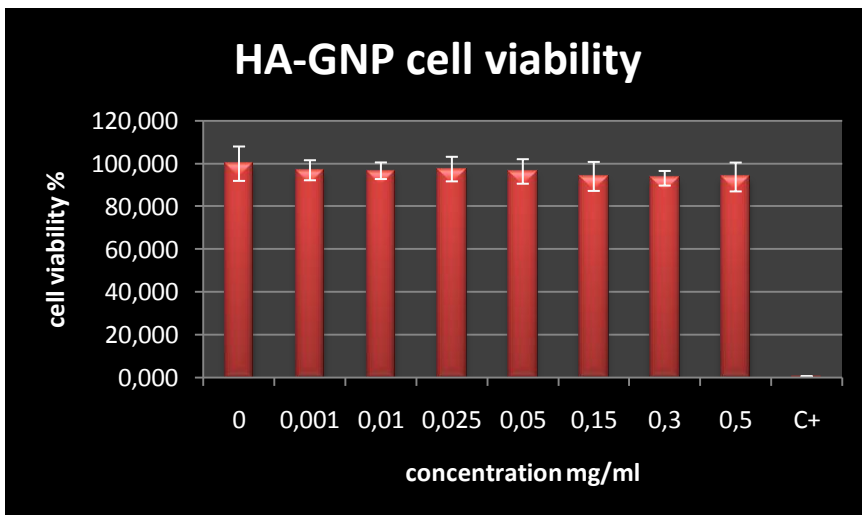
b) MDA-231 human breast cancer cells:



2. Proliferation with bovine aortic endothelial cells (BAEC) & MDA-231 human breast cancer cells



3. Cell viability with human dermal fibroblasts:



Sol-gel derived nano-glass-ceramics comprising RE-doped KYF₄ nanocrystals

A. Santana-Alonso, A.C. Yanes, J. Méndez-Ramos, J. del-Castillo, V.D. Rodríguez and **J. Peraza**

Departamento de Física Básica y Departamento de Física Fundamental y Experimental, Electrónica y Sistemas, Universidad de La Laguna, 38206, La Laguna, Tenerife, Spain

ayanesh@ull.es; jperaza@ull.es

Glass-ceramics containing rare-earth (RE) doped nanocrystals are considered to play an important role in the development of new luminescent materials in areas such as photo-electronic devices, white light up-conversion phosphors, solid state lasers, solar cells and biological labels [1]. These materials can be synthesized by the room temperature sol-gel method with the advantages of its low cost, easiness, controlled concentration and size, excellent purity and dispersion [2]. KYF₄ is very attractive host for RE ions for providing high intensity VUV and visible up-conversion emissions, under IR excitation, due to its very low phonon energy environment which enhances luminescence. Among RE ions, Eu³⁺ is highly sensitive to the local structure and it is used as a probe of final environment for the ions, key factor for resultant quantum efficiency of the luminescent materials. Tm³⁺ is well known for its IR to UV and blue up-conversion emissions. By co-doping with Yb³⁺, these emissions can be intensified remarkably due to larger absorption cross-section of Yb³⁺ and the high efficient energy transfer to Tm³⁺ ions. We have successfully developed, for the first time to our knowledge, sol-gel derived nano-glass-ceramics containing RE-doped KYF₄ nanocrystals, after adequate heat treatment of precursor glasses. Here, we report a complete site selective resolved spectroscopic study by means of Eu³⁺-doped samples as a function of heat-treatment temperature. By other side, we also report high efficient UV up-conversion emissions in Yb³⁺-Tm³⁺ co-doped samples as a function of Yb³⁺ concentration and thermal treatment temperature. These unusually high energetic UV emissions, protected from non-radiate decays provided by the low phonon energy host of KYF₄ nanocrystals, represent a significant progress in the search of new stable species for applications in optical materials for solid state UV sources.

References

- [1] Y. Ying and A.P. Alivisatos, *Nature* **437** (2005) 664
- [2] J. Méndez-Ramos et al. *J. Nanosci. Nanotechnol.* **10** (2010) 1273

Up-conversion and down-shifting in sol-gel derived glass-ceramics containing rare-earth doped SnO₂ and LaF₃ nanocrystals

A.C. Yanes, J. del-Castillo, J. Méndez-Ramos, V.D. Rodríguez and J. Peraza

Departamento de Física Básica y Departamento de Física Fundamental y Experimental, Electrónica y Sistemas, Universidad de La Laguna, 38206, La Laguna, Tenerife, Spain

ayanesh@ull.es; jperaza@ull.es

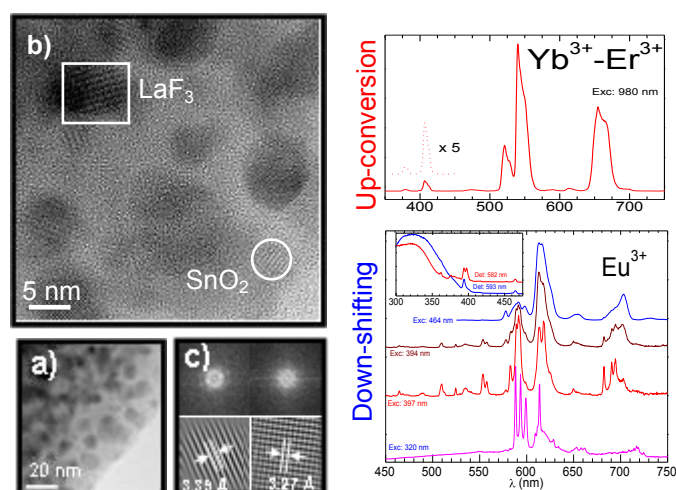
The increase in the efficiency of solar cells is a challenge issue at present in the race for sustainable renewal energy sources against climate change. It is known that the limited spectral response of commercial semiconductor solar cells to the wide solar spectrum constitutes the main cause of losses in photovoltaic technology [1, 2]. That is why the efficiency of current solar cells could be appreciably increased by means of up-conversion and down-shifting processes which convert photons from the NIR and UV-blue, respectively, into the green-red, where the solar cell response be maximum. These effects could be obtained by means of luminescence layers without interfering with the active material [3].

Here we report a novel class of nanostructured glass-ceramics comprising two co-existing rare-earth doped nanocrystalline phases, SnO₂ semiconductor nanocrystal (quantum dot) and LaF₃, embedded into a silica glass matrix for an efficient simultaneous UV and IR to visible photon conversion. On one hand, the wide and strong UV absorption by SnO₂ quantum dot and subsequent efficient energy transfer to Eu³⁺ [4] and, on the other hand, the also very efficient IR to visible up-conversion with the pair Yb³⁺-Er³⁺ partitioned into low phonon LaF₃ nanocrystalline environment, yield to visible emissions with application in improving the spectral response of photovoltaic solar cells.

References

- [1] Richards, B.S.; Solar Energy Materials and Solar Cells, **90**, (2006), 1189.
- [2] Strümpel, C.; McCann, M.; Beaucarne, G.; Arkhipov, V.; Slaoui, A.; Svrcek, V.; del Cañizo, C.; Tobias, I.; Solar Energy Materials and Solar Cells, **91**, (2007), 238.
- [3] Shalav, A.; Richards, B.S.; Green, M.A.; Solar Energy Materials and Solar Cells **91**, (2007), 829.
- [4] Yanes, A.C.; del-Castillo, J.; Torres, M.E.; Peraza, J.; Rodríguez, V.D; and Méndez-Ramos, J.; Appl. Phys. Lett., **85**, (2004), 2343.

Figures



Melting temperature of icosahedral metallic nanowires

J. A. Pérez Finol (1), S. Peláez (1), P. García-Mochales (2) and P. A. Serena (1).

(1) Consejo Superior de Investigaciones Científicas (CSIC), Instituto de Ciencia de Materiales de Madrid (ICMM), C/Sor Juana Inés de la Cruz 3, 28049-Madrid, Spain

(2) Departamento de Física de la Materia Condensada, C-III, Universidad Autónoma de Madrid, 28049, Madrid, Spain

japerezfinol@icmm.csic.es

During the last two decades, the study of the properties of nanowires has been one of the keystones in the development of nanotechnology, since these nano-objects exhibit electrical and mechanical properties of interest in fundamental knowledge as well as technological applications. In particular, the formation of ultra-thin metallic nanowires from the breaking of nanocontacts has been subject of many experimental and theoretical studies. For instance, the formation of linear atomic chains (LAC) has been observed in both scanning tunneling microscopy (STM) or mechanically controllable break junction (MCBJ) experiments on different metallic species [1]. By means electron beam irradiation of thin Au films long nanowires of helical structures can be obtained [2]. Moreover, theoretical works have shown the formation of a great variety of weird nanowires which present a higher stability than the a priori expected fcc/bcc crystalline nanowires [3].

A few years ago, it has been suggested that icosahedral (a.k.a. pentagonal) nanowires are formed spontaneously in MCBJ ruptures of Cu nanocontacts[4]. In a recent work we have reported Molecular Dynamics (MD) simulations of the breaking process of Al, Ni and Cu nanowires in which these icosahedral nanowires are observed [5]. We have shown that these structures are long, very stable and are formed at relatively high temperatures compared to the corresponding bulk melting temperature. Indeed there is an optimal temperature at which the probability of formation of pentagonal nanowires is highest. The existence of this optimal temperature is the result of a balance between two phenomena. On one hand a high temperature favors the formation of a disordered region in the narrowest section of the nanowire. It is from this disordered region that atoms diffuse to form pentagonal rings. On the other hand, a too high temperature induces the melting of the narrowest section of the nanowire, and the breaking of the contact.

In the present work we are interested in the temperature dependence of the stability of the icosahedral nanowires. We use MD simulations to study the dynamical evolution of the nanowires as the temperature increases. Infinite pentagonal nanowires are simulated by using periodic boundary conditions along the nanowire axis. Different sizes of the unit cell along the nanowire axis direction are tested, in order to identify size effects in our simulations. Interatomic interactions are modeled using a parameterization of the Embedded Atom Method (EAM). Temperature is controlled by a Nosè-Hover chain algorithm. We have taken account the linear thermal expansion coefficients of the pentagonal nanowires.

Here we report the melting temperature T_m of the icosahedral nanowire structures for three metallic species: Al, Ni and Cu. This T_m is determined from a statistical analysis of many MD simulations at slowly increasing temperature. For every simulation the diffusion coefficient and the total cohesive energy are monitored. An abrupt jump in these observables indicates that the nanowire has abandoned its pentagonal structure. It has been observed that once the pentagonal structure is altered, the nanowire is rapidly distorted and becomes a nearly-spherical cluster (see figure 1). A statistical analysis of the temperatures at which this structural change takes place gives a good estimation of the melting temperature T_m (see figure 2).

References

- [1] N. Agrait, A. Levy-Yeyati, and J.M. van Ruitenbeek, Phys. Rep. **377**, 81 (2003).
- [2] K. Kondo and K. Takayanagi, Science **289**, 606 (2000).
- [3] O. Gülseren, F. Ercolessi and E. Tosatti, Phys. Rev. Lett. **80**, 3775 (1998).
- [4] J.C. González, V. Rodrigues, J. Bettini, L. G. C. Rego, A. R. Rocha, P. Z. Coura, S. O. Dantas, F. Sato, D. S. Galvão, D. Ugarte. Phys. Rev. Lett. **93** 126103-1 (2004)
- [5] S. Pelaez, C. Guerrero, R. Paredes, P. García-Mochales and P. A. Serena, in preparation.

Figures

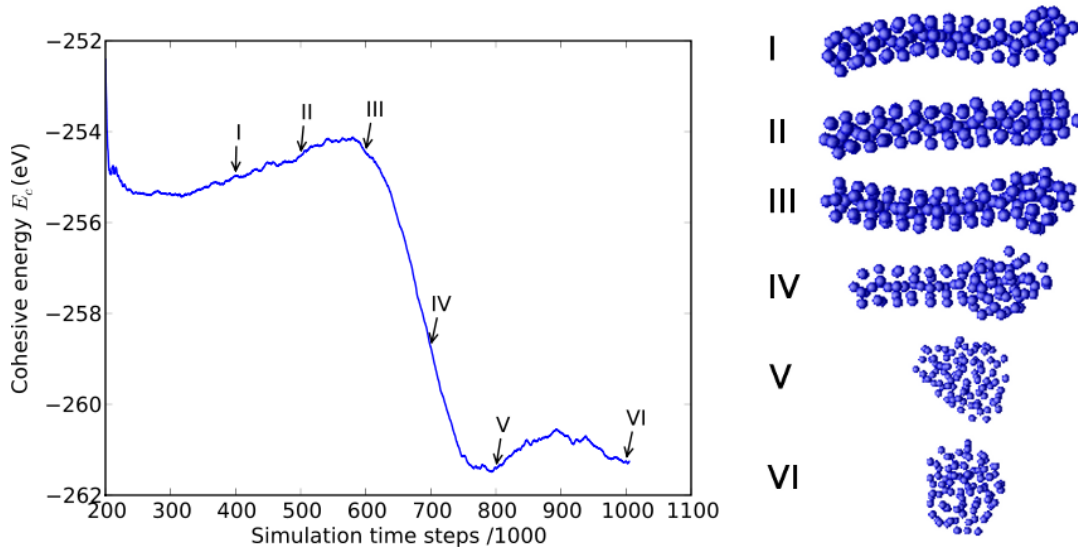


Figure 1. (Right) Time evolution of the cohesive energy E_c during the melting process of a pentagonal Cu nanowire. The cohesive energy E_c exhibits a jump, which clearly indicates that this transformation has taken place. (Left) Several snapshots correspond to the Cu nanowires whose cohesive energy is shown. Note that once the pentagonal structure is distorted due to a high temperature anywhere along the nanowire, it rapidly transforms into a cluster.

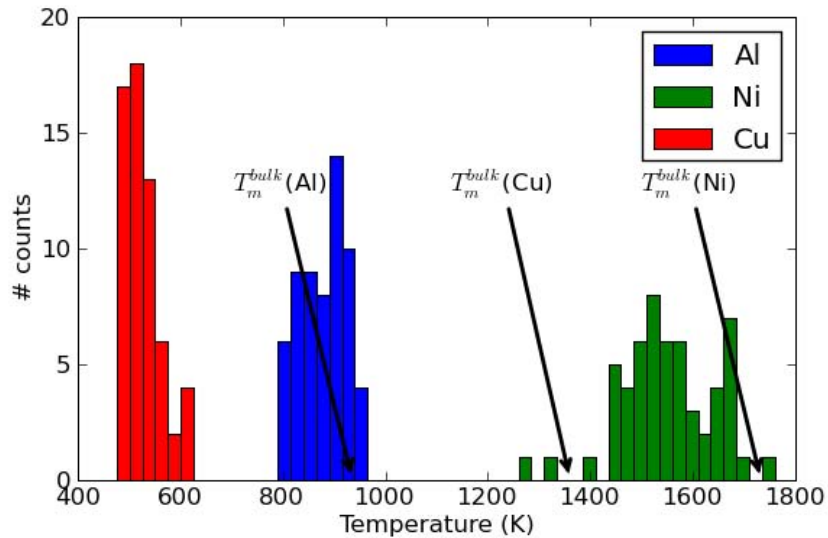


Figure 2. Histograms of the melting temperature of pentagonal nanowires. These histograms have been obtained from 60 independent melting simulations for each material. The arrows point to the melting temperatures of the corresponding bulk system. Notice the large difference between T_m and T_m^{bulk} for the Cu case.

Synthesis and Characterization of Mercuric Iodide Nanoparticles

M. E. Pérez, H. Bentos Pereira, L. Fornaro

Grupo de Semiconductores Compuestos

Facultad de Química, Universidad de la República, General Flores 2124

Montevideo, Uruguay

toty@fq.edu.uy

Mercuric iodide (HgI_2) is a compound semiconductor that belongs to the layered compounds family MX_n (M: heavy metal, X: no metal, $n > 1$); their crystalline planes are perpendicular to the c axis, thus they have a strong crystallographic, morphologic and other anisotropies. It is this anisotropy which leads the mercuric iodide crystals to growth with “platelet” habit [1]. The HgI_2 also has the best properties to act as an ionizing radiation sensor. On the other hand, the trend in HgI_2 films has been the polycrystalline growth and then the oriented growth; results showed that the detector performance is better when the crystalline film is oriented [2].

In the last years there has been a great development of nanotubes and nanoparticles similar to fullerenes (inorganic fullerenes (IF)) which are compounds of the NY_2 family such as MoS_2 , WS_2 , NiCl_2 and CdCl_2 [3,4]. Because of the structure similarity between IF structures and HgI_2 , we started to synthesize mercuric iodide nanoparticles in order to use them to obtain the first monolayer of a film; in this way the further film growth should be guided by the monolayer orientation.

We have synthesized mercuric iodide nanodiscs by a suspension method, which will be used as a first layer in the film growth. The nanodiscs were obtained from $\text{Hg}(\text{NO}_3)_2 \cdot \text{H}_2\text{O}$ and I_2 with Octadecene as solvent. The reaction lasted 2 hours at 70°C and another 10 minutes at 100°C . HgI_2 nanoparticles were then washed with ether [5].

Mercuric iodide identity was first checked by X-ray diffraction, a XRD diffractogram is showed in Figure 1. The nanoparticles synthesized were observed by Transmission Electron Microscopy, Figure 2 shows the image of the nanodiscs obtained. The nanodiscs diameter ranges between 80-140 nm. Electron Diffraction Spectroscopy was performed to the nanodiscs in order to bear out the compound identity, Figure 3 shows the EDS diagram of one of the nanodiscs showed in Figure 2. It still remains to check the crystallinity of the nanoparticles and their growth axis. We also must standardize nanodiscs diameters—by changing the synthesis conditions.

It is the first time that mercuric iodide nanoparticles are obtained by a suspension method; this also a promising method to obtain nanoparticles of adequate morphology to be employed in compound semiconductors monocrystalline film growth.

Authors thank the Laboratorio de Microscopia Electrónica (LME), Laboratorio Nacional de Luz Sincrotrón (LNLS), and Prof. Dr. Jesiel Freitas Carvalho from the Física de Materiais group, Universidad Federal de Goiás for the use of the TEM and for the XRD measurements respectively.

References:

- [1] Fornaro L., Luchini L., Knöcke M., Mussio L., Quagliata E., Chattopadhyay K., Burger A., *Journal of Crystal Growth*, vol. 217 N°3, (2000), pp. 263-270.
- [2] L. Fornaro, A. Cuña, A. Noguera, I. Aguiar, M. Pérez, L. Mussio, A. Gancharov, *IEEE Trans. Nucl. Sci* 52 (6) part 2, (2006) pp 3107-3110.
- [3] Reshef Tenne, www.weizmann.ac.il/ICS/booklet/20/pdf/reshef_tenne.pdf
- [4] C. Schuffenhauer, R. Popovitz-Biro and R. Tenne, *J. Matter Chem.* 12, (2002), p. 1587.
- [5] Dingsheng Wang, Chenui Hao, Wen Zheng, Xiaoling Ma, Deren Chu, Qing Peng, and Yadon Li, *Nano Res.* 2 (2009), 130-134.

Figures:

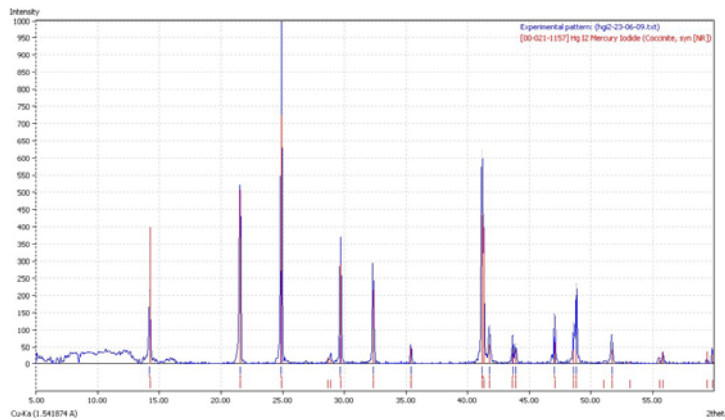


Figure 1. X-ray Diffractogram of HgI_2 nanoparticles

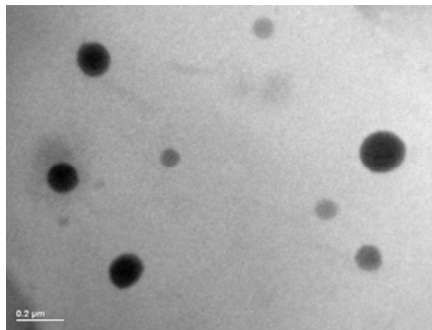


Figure 2. Transmission electron micrograph of HgI_2 nanodiscs kV= 200 eV

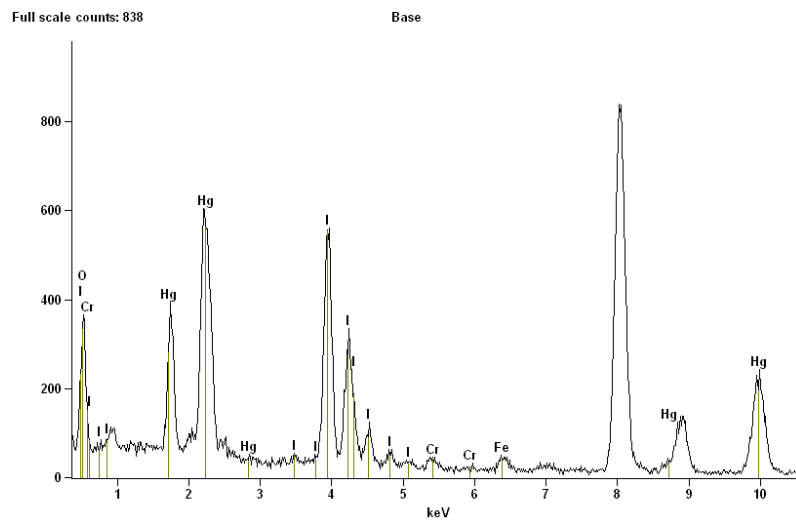


Figure 3. EDS Spectrum of a nanodisc showed in figure 2.

SEM Imaging of Films of Metal Nanoparticles Deposited on Semiconductors

Piksová K.^a, Grym J.^b, Procházková O.^b, Žďánský K.^b, Zavadil J.^b, Yatskiv R.^b, Fiala P.^a

^a*Department of Physical Electronics, Faculty of Nuclear Sciences and Physical Engineering, Czech Technical University in Prague, Břehová 7, 115 19 Prague 1, Czech Republic*

^b*Institute of Photonics and Electronics AS CR, Chaberska 57, 18251 Prague 8, Czech Republic*

katerina.piksova@jfifi.cvut.cz

Layers of metal nanoparticles on semiconductor surfaces show interesting effects which may be desirable for practical applications. Association of metal nanoparticles with semiconductor materials opens up novel means to gain structures with remarkable properties.

Schottky barriers with layers of nanosized metal particles on semiconductor wafers can be used as hydrogen sensors which are more sensitive than those prepared by conventional deposition techniques.

Colloids of metal nanoparticles stabilized by AOT reverse micelles in isooctane were prepared. The colloids contain nanoparticles with the size distribution of 5-10 nm in diameter. Nanolayers were deposited by electrophoresis onto semiconductor wafers.

The morphology of the deposited layers was observed by JEOL JSM 7500F scanning microscope.

We discuss the influence of:

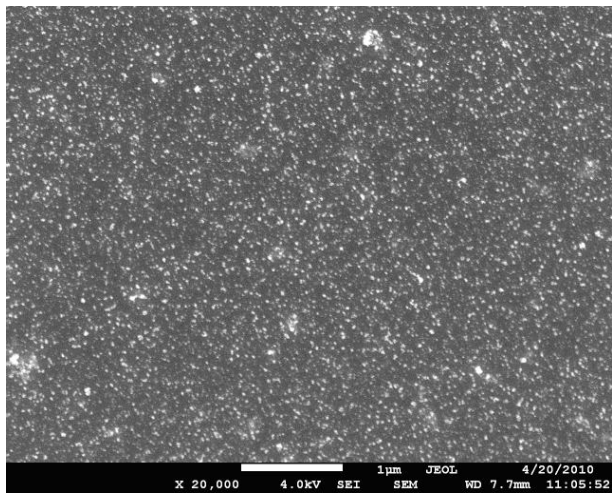
- conditions of the electrophoretic deposition, i.e. electrode polarity, time of the deposition and applied voltage,
- the post-deposition treatment, i.e. thermal annealing,
- the properties of deposited colloids

This work has been supported by the Czech Ministry of Education, Youth and Sports in the framework of the Research Plan 60840770022 and by the Grant Agency of the Academy of Science of the Czech Republic, project KAN401220801 and the Czech Science Foundation grant 102/09/1037.

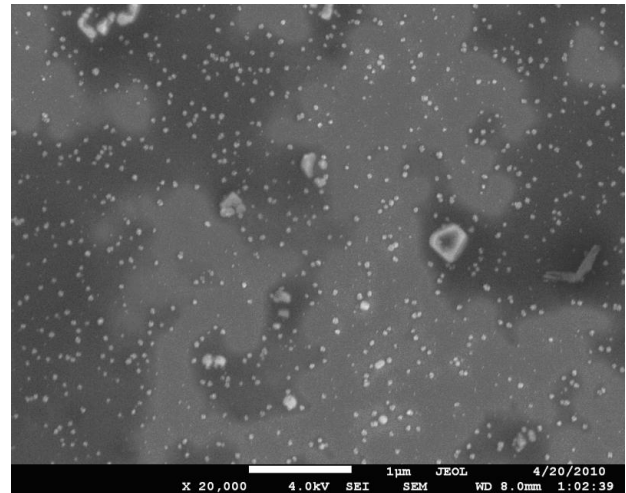
References

- [1] CHEN D.H.; WANG Ch.Ch.; HUANG T.Ch. *Preparation of Palladium Ultrafine Particles in Reverse Micelles*. **Journal of Colloid and Interface Science**, 1999, č. 210, s. 123-129. ISSN 0021-9797/99
- [2] Žďánský K., Zavadil J., Kacerovský P., Lorinčík J., Vaniš J., Kostka F., Černohorský O., Fojtík A., Reboun J., Čermák J.: *Electrophoresis deposition of metal nanoparticles with reverse micelles onto InP*, **International Journal of Materials Research**, 2009, vol. 9., p. 1234-1238, ISSN 1862-5282.

Figures:

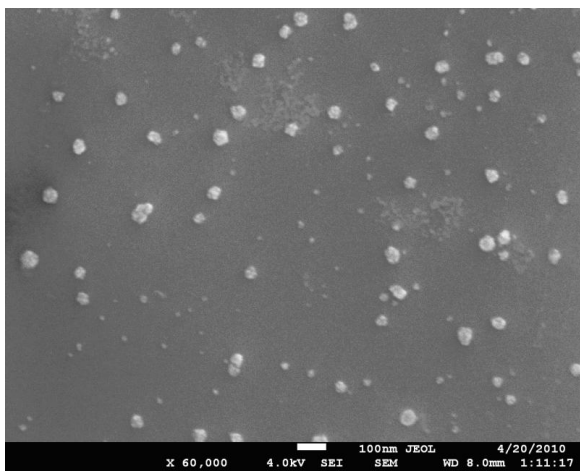


a) applied voltage - 100V

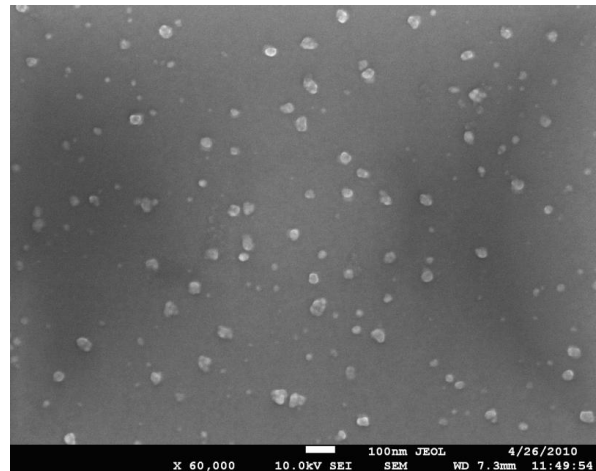


b) applied voltage - 30V

Fig. 1: Comparison morphology – dependence on applied voltage



a) non-annealed sample



b) annealed sample

Fig. 2: Comparison morphology – dependence on annealing

Remote magnetic heating of smart thermoresponsive PNIPAM-Fe₃O₄ nanocomposites

Y. Piñeiro Redondo¹, Manuel Bañobre López¹, Chiara Dionigi², Valentin Dediu², Sangram Keshari Samal², José Rivas¹

¹ Applied Physics Dept., University of Santiago de Compostela, E-15782 Santiago de Compostela, Spain

² Consiglio Nazionale delle Ricerche – Istituto per lo Studio dei Materiali Nanostrutturati, Via P. Gobetti 101, I-40129 Bologna, Italy

y.pineiro.redondo@usc.es

The interest on biocompatible smart materials for medical applications has been growing progressively in the last decade.

In particular hydrogels based on PNIPAM (poly N-isopropyl acrylamide) are considered an advance for drug delivery due to their peculiar thermal response. PNIPAM undergoes a reversible phase transition from a swollen hydrated state to a shrunken dehydrated state when heated in water above a critical temperature that is about 32°C (Lower Critical Solution Temperature, LCST)

Magnetic functionality has been recently added to PNIPAM hydrogels and magnetic cores coated with PNIPAM shells have been synthesized in order to induce the PNIPAM shrinkage by controllable high-frequency magnetic field [1].

In particular, our approach in this field refers to reverse composite- hydrogels consisting in PNIPAM-co-acrylic acid hydrogels used as templates for the deposition of magnetic nanoparticles [2]. Non coated and superparamagnetic (SPM) magnetite (Fe₃O₄) nanoparticles, with a narrow size distribution around 8 nm, have been used in order to assure effective magnetic functionality and biocompatibility for remote magnetic manipulation of in-vivo applications.

Similarly to the core- shell hydrogels, the reverse composite-hydrogels easily undergo to LCST under high-frequency magnetic field.

From the TGA profile of the various reverse composite-hydrogels we found that there is a limit for the loading of magnetite nanoparticle (MNP). This limit is achieved using a starting MNP/NIPAM ratio bigger than 2% (w/w).

The LCST of the fully loaded composite-hydrogels has moved to temperatures around 40°C with an average diameter decrease of ≈ 20%.

Remote magnetic heating has been successfully achieved by application of an alternating RF magnetic field (B=27 mT and f=260KHz) to the thermoresponsive PNIPAM-magnetite nanocomposites. The observed temperature increase overcomes the LCST where the MNP/NIPAM nanocomposites shows thermal shrinking, making this system suitable for externally controlled drug delivery .

References

- [1] J. Rubio-Retama, N. E. Zafeiropoulos, C. Serafinelli, R. Rojas-Reyna, B. Voit, E. Lopez Cabarcos, M.d Stamm, *Langmuir* 23 (2007) 10280-10285
- [2] S. Purushotham, R.V. Ramanujan, *Acta Biomaterialia* 6 (2010) 502–510

Structural study of multilayers of Si_{1-x}Ge_x Nanocrystals embedded in SiO₂ matrix

S. R. C. Pinto¹, A. G. Rolo¹, M. Buljan², A. Chahboun^{1,3}, S. Bernstorff⁴, and M. J. M. Gomes¹

sarapinto@fisica.uminho.pt

¹ Physics Department, University of Minho, 4710 – 057 Braga, Portugal

² Rudjer Boskovic Institute, Bijenicka cesta 54, 10000 Zagreb, Croatia

³ Physics Department, Dhar Mehraz Sciences Faculty, BP 1796, Fès, Morocco

⁴ Sincrotrone Trieste, 34012 Basovizza, Italy

Si_{1-x}Ge_x ($0 \leq x \leq 1$) nanocrystals (NCs) systems have attracted considerable attention because of their potential applications in nonvolatile memory and integrated optoelectronics applications.

In this work, SiO₂/Si_{1-x}Ge_x + SiO₂/SiO₂ multilayer structures were grown on p-Si (100) substrate using the RF co-sputtering technique and annealed at different temperature. Different thicknesses of oxide layer and Si_{1-x}Ge_x have been produced to perform the structural characterization and to achieve the optimization of the growth parameters. The annealing temperature ranged from 700 to 1100 °C with the aim to optimize the annealing temperature that promotes well separated layered NCs structures.

The total films thicknesses were obtained by Scanning Microscopy Spectroscopy (SEM) (figure 1), and the thickness of each layer was estimated by Rutherford Backscattering Spectroscopy (RBS). SiO₂/Si_{1-x}Ge_x + SiO₂/SiO₂ homogeneous multilayer films were produced in the range 2 to 6 nm and 6 to 16 nm for, respectively, the Si_{1-x}Ge_x and silica layers.

The samples were structurally characterized by X-ray diffraction, Raman spectroscopy, Grazing Incidence X-ray Diffraction (GIXRD), Grazing Incidence Small angle X-ray Scattering (GISAXS) (figure 2) and High Resolution Transmission Electron Microscopy (HRTEM). The NCs shape, size distribution and the spatial arrangement were determined by GISAXS and TEM measurements, while Raman, HRTEM and diffraction measurements provided detailed data about the NCs composition and their inner structure. The results of the analysis show that the average size of NCs, the composition of Si_{1-x}Ge_x heterostructure and the strain in the formed NCs are very sensitive to the parameters of the deposition and annealing procedures.

Figures

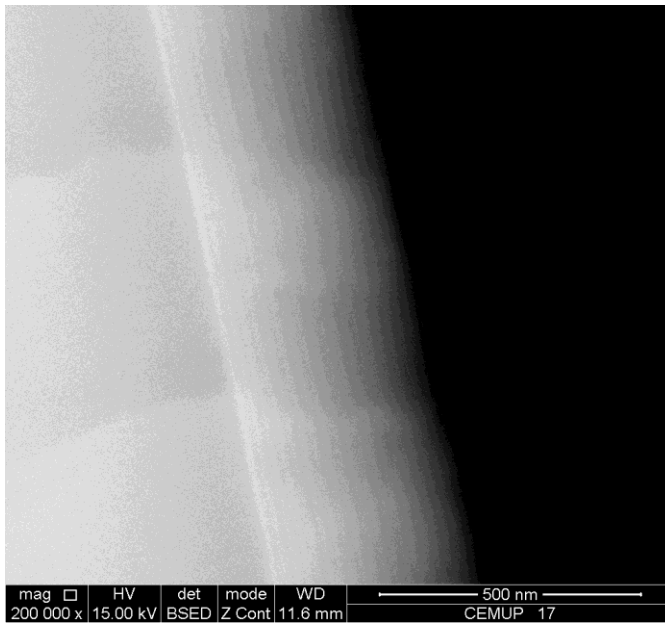


Figure 1: SEM image of $(\text{Si}_{1-x}\text{Ge}_x/\text{SiO}_2) \times 20$ layers. It is possible to see the different layers well separated. The total thickness is about 300 nm.

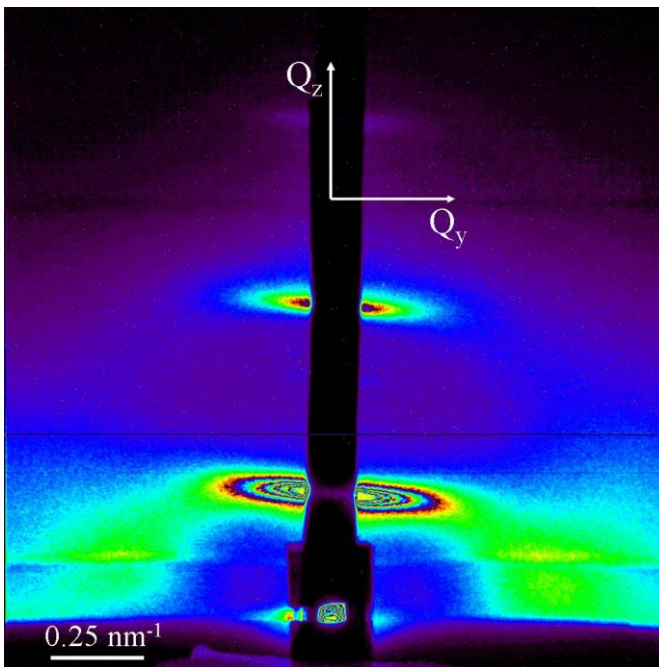


Figure 2: GISAXS map measured on the as-deposited multilayer

A novel DNA chip for single molecule analysis

T.Plénat^{1,2}, C.Tardin^{1,2}, C.Vieu^{3,2}, C.Thibault^{3,2}, E.Trévisiol^{3,4}, and L.Salomé^{1,2}

¹CNRS; IPBS (Institute of Pharmacology and Structural Biology); 205 route de Narbonne, F-31077 Toulouse, France and ²University of Toulouse; UPS; IPBS; F-31077 Toulouse, France

³LAAS, Nanobiosystems, 7, Avenue du Colonel Roche, F-31077 Toulouse, France

⁴UMR 5504, UMR 792, Ingénierie des Systèmes Biologiques et des Procédés & Plate-forme Biopuces, CNRS, INRA, INSA, 135, avenue de Rangueil, 31077 Toulouse, France

plenat@ipbs.fr

The last two decades have seen the emergence of single-molecule experiments [1]. By avoiding the ensemble averaging inherent to traditional bulk-phase biochemistry, the study of molecular machineries at the single-molecule level permits a better understanding of the behavior of living systems. Indeed the dynamics of the machineries processes can be characterized and rare subpopulations can be identified [2].

One of the main shortcoming of single molecule experiments is that the acquisition of statistically solid data is very time consuming, which explains the fact that they are still not widely used in laboratories.

We will present the development of a new single DNA chip, allowing the simultaneous analysis of hundreds of single DNA molecules by the Tethered Particle Motion (TPM) technique, therefore giving high-throughput capabilities to this approach.

The principle of a TPM experiment consists in tracking a bead tethered at the free end of a DNA molecule which is immobilized by the other end to a coverslip thanks to optical videomicroscopy. The amplitude of the Brownian motion of the bead is related to the effective length of the DNA molecule [3]. Any conformational change of the DNA molecule due to external factors (proteins, ions, temperature), that induces a variation of the effective length of the DNA tether, can be thus monitored by TPM [4].

References

- [1] Cornish, P. V.; Ha, T., *Acs Chemical Biology* **1** (2007) 53.
- [2] van Oijen, A. M., *Nature Chemical Biology*, **8** (2008) 440.
- [3] Yin, H.; Landick, R.; Gelles, J., *Biophys J*, **6** (1994) 2468.
- [4] Pouget, N. et al.; *Nucleic Acid Res.*, **9** (2004) e73

Controlling Light Inside Disordered Materials: Matrix Model and Applications

S. M. Popoff, G. Lerosey, R. Carminati, M. Fink, A.C. Boccara, S. Gigan

Institut Langevin, ESPCI ParisTech, CNRS UMR 7587, ESPCI, 10 rue Vauquelin, 75005 Paris, France

sebastien.popoff@espci.fr

Abstract : We introduce a method to experimentally measure the monochromatic transmission matrix of a complex medium in optics. This method is based on a spatial phase modulator together with a full-field interferometric measurement on a camera. We determine the transmission matrix of a thick random scattering sample. We show that this matrix exhibits statistical properties in good agreement with random matrix theory and allows light focusing and imaging through the random medium.

Recently, a method has been proposed by I. Vellekoop et al. [1] to focus light through a multiple scattering material, using a spatial light modulator as a tool to shape the incoming beam to obtain a maximal interference on a speckle spot of the output speckle pattern. The result is a bright, diffraction limited, spot which can be several hundred time brighter than the rest of the speckle. By the same method, the same group also demonstrated the enhancement of the optical activity of a fluorescent object embedded in the material [2], and even shown strong evidence of the existence of open channels in a random medium [3].

However, there is a much more general approach to the problem of imaging and controlling light in a random medium. It consists of measuring the transmission matrix, i.e. the matrix linking the amplitude of the input to the output modes of the multiple scattering material. This approach not only gives several new possibilities for imaging, but also allows direct insight on the material itself, as has been demonstrated in acoustics [4] or electromagnetism [5] for instance.

We present here an original method [6] based on an interferometric measurement of the speckle on a camera, which has allowed us to measure the transmission matrix of an opaque slab of ZnO powder.

The experimental setup is presented in fig1. A laser is expanded and reflected off a phase-only spatial light modulator (SLM) and sent on the sample. The light on the other side of the sample is collected by a microscope objective and imaged on a CCD camera.

We choose as our input modes a 16x16 macropixels matrix of the SLM. The light that is shone on the sample but was reflected outside of this matrix is our reference and has been used as a reference to measure the amplitude of the output speckle on a 16x16 macropixels matrix on the CCD.

By choosing the Hadamart basis to encode our input vectors, and by extracting the amplitude and phase of the speckle produced by the input modes by a 4-phase full-field interferometric method, we have been able to extract the matrix K_{obs} , which is directly related to the transmission matrix K of the medium, but has a contribution due to the reference speckle that we can account for. This matrix is acquired in approximately 3 minutes, a time comparable to iterative methods.

As soon as we have measured the transmission matrix, it is in principle possible to perform a virtual phase conjugation to focus on any output E_{target} , by sending $E_{\text{in}}=K^{\dagger} E_{\text{target}}$ (where † denotes the transpose conjugate). The result is a bright focus with the same SNR ratio as the one obtained by iterative methods. It is also possible to infer simply, by measuring the output speckle, the input image (this is the reciprocal problem of the focusing). Results are summarized on figure 2. All these results are obtained in one step.

To reconstruct a more complex image, one have to increase the number of degrees of information, either by averaging results obtained with different illuminations of the same amplitude object, or by increasing the number of segments recorded on the CCD camera. A typical result of the reconstruction of a complex pattern is shown in figure 3.

We also have been able to measure the singular value distribution of the transmission matrix, after filtering the effect of the reference on K_{obs} , as well as the effect of residual correlations between neighboring pixels. We verified a well-known prediction of random matrix theory, i.e. that the normalized singular values follow the so-called quarter-circle law [8]. The result is shown on figure 4.

We believe that this method is very promising, both for imaging application, and for the study of wave propagation in complex materials.

References

- [1] I. Vellekoop et al., Opt. Lett. **32** (2007) 2309.
- [2] I. Vellekoop et al., Opt. Lett **1** (2007) 53.
- [3] I. Vellekoop et al., Phys. Rev. Lett., **101** (2008) 120601.
- [4] A. Derode et al., Phys. Rev. Lett., **90** (2003) 014301.
- [5] G. Lerosey et al., Science, **315** (2007) 1120.

- [6] S.M. Popoff et al., Phys. Rev. Lett., **104** (2010) 100601.
 [7] A. Dubois et al., Appl. Opt, **41** (2002) 805.
 [8] V. Marcenko and L. Pastur, Sbornik: Mathematics, **1** (1967) 457.

Figures

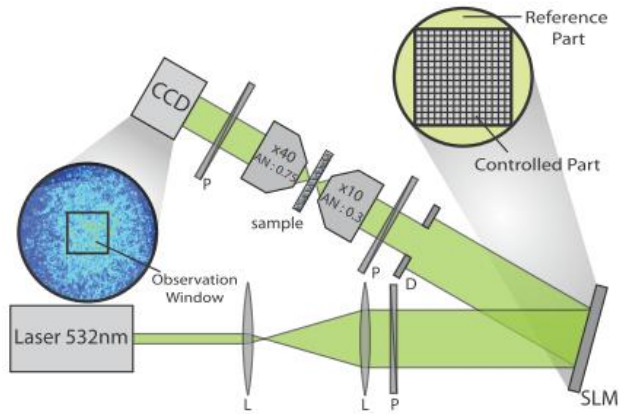


Figure 1 : Experimental setup

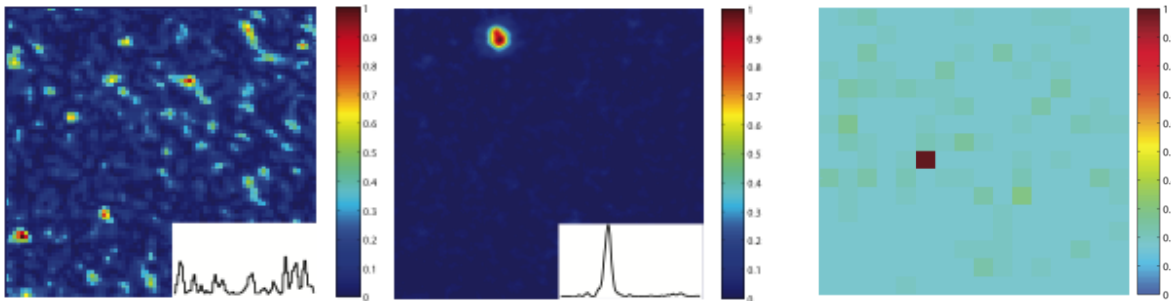


Figure 2 : Imaging by using the transmission matrix. (left) initial speckle at the output of the sample. (center) focusing on a single point. SNR of the focus over the background is 54, equal to approximately 40% of the ideal phase conjugation. (right) detection of a single ON pixel at the input by analysing the output speckle. Insets show profile along one direction.

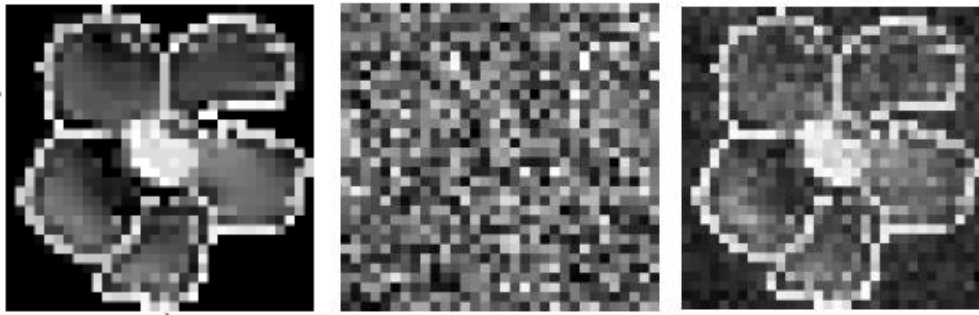


Figure 3 : A complex image reconstruction using the transmission matrix. (left) amplitude image displayed on the SLM. (center) the resulting output speckle. (right) the reconstruction using the transmission matrix.

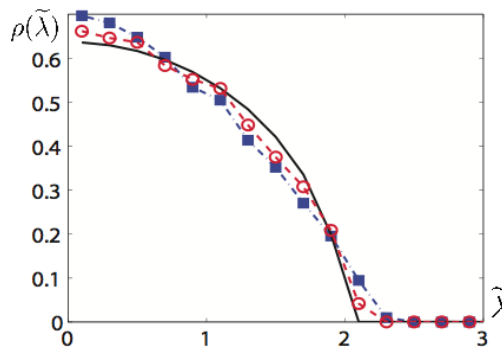


Figure 4 : Distribution of the normalized singular values. Solid line : quarter-circle law as predicted by random matrix theory. Squares : distribution for the transmission matrix. Circles : distribution for the measured transmission matrix when removing nearest neighbors to eliminate residual correlations.

Utilizing Vertically Aligned Carbon Nanotubes Based Working Electrodes for Detection of Heavy Metal Ions and Thiols

Jan Prasek¹, Jaromir Hubalek¹, Ondrej Jasek², Lenka Zajickova², Dalibor Huska³,
Vojtech Adam³, Petr Majzlik³, Rene Kizek³

¹Department of Microelectronics, Brno University of Technology, Udolni 53, Brno, Czech Republic

²Department of Physical Electronics, Masaryk University, Brno, Czech Republic

³Department of Chemistry and Biochemistry, Mendel University, Brno, Czech Republic

prasek@feec.vutbr.cz

It is a common knowledge that toxic heavy metal ions (lead, cadmium and mercury) are able to enter to organisms and interfere several important metabolic processes. However, essential heavy metals have high affinity to biologically active molecules, and, under specific conditions, can alter key biochemical pathways. The presence of the metal ions induces and/or damages cell homeostasis, transcription, translation, cell dividing etc. Proteins and nucleic acids belong to the main and most important target of both essential and toxic metal ions. Among very sensitive analytical methods for detection of heavy metal ions belong the electrochemical ones. The classic electrochemical instruments are consisted of potentiostat/galvanostat with electrochemical cell including three electrodes (working, reference and auxiliary). However, the trend of analytical techniques is to miniaturize the whole instrument due to many advantages of small devices including portability, low costs and demands on service and operations, sufficient sensitivity and selectivity. Today, the solid electrodes are commonly used as a substitution of formerly used mercury drop electrode due to its toxicity. Moreover, the solid electrodes could be miniaturized easily. The problem is that in comparison to standard electrodes used in laboratories the miniaturized electrodes have much lower response due to their small electrode active area. Therefore it is necessary to preserve the active electrode area though the geometrical size of the electrode is miniaturized. One of the possibilities of preserving the active electrode area is to create nanostructures on the electrode surface.

In the last two decades, nanomaterials in the form of nanotubes and nanowires have begun to be reported as promising materials for wide field of applications. Such materials could be also used for fabrication of miniaturized electrodes. The nanostructured electrodes could be fabricated using several techniques. The easiest fabrication technique is to use a mixture of nanomaterial as a filler with a suitable vehicle, which could be deposited on the electrode substrate using screen-printing, drop-coating, dip-coating, spraying, etc [1-3]. The disadvantage of these nanocomposition-based electrodes is the irreproducible electrode surface with undefined active electrode area. The reproducible nanostructured electrode surface could be fabricated using lithography as a common tool for microelectronics devices implementation, anodization process for nanorods or nanotubes creation [4], etc. One of these techniques is creation of vertically aligned multiwalled carbon nanotubes (MWNTs) grown directly on the electrode surface using CVD.

The aim of this work was to fabricate several types of nanostructured working electrodes of three-electrode electrochemical sensor which is fabricated using standard thick film technology with working electrode made of direct grown MWNTs. These electrodes were compared on various stationary and flow electrochemical instruments for an easy and sensitive determination of heavy metal ions and biologically important thiol called phytochelatin2 (Fig. 1), which belongs to plant peptides playing key role in protection of cell compartments against heavy metals and can be easily detected by electrochemical instruments [5, 6]. The basic shape of the three-electrode electrochemical sensor and its real fabricated sample with gold (ESL 8844-G, Electroscience, UK) working electrode before MWNTs deposition is shown in the figure 1. The MWNTs have been deposited using plasma enhanced CVD direct grown on different electrode underlay on the atmospheric pressure. The deposition was done on the pure Au, Ag and Pt layer without any catalyst and on the 10 nm thick Fe catalyst using the same underlay. The SEM comparison of the electrodes fabricated on the Ag (ESL 9912-K) thick film paste with (up) and without (down) use of catalyst is shown in the figure 2. From the comparison it is clear that both electrodes are covered with vertically aligned MWNTs. Moreover, the electrode with catalyst consists of more clumps. We tested the following working electrodes: i) fabricated direct grown MWNTs based electrodes, ii) hanging mercury drop electrode, iii) carbon tip and connected them to three types of potentiostats: a standard potentiostat (Autolab), a commercially available miniaturized potentiostat (PalmSens) and a home-made potentiostat.

Primarily we aimed our attention at the detection of three metal ions, zinc(II), cadmium(II) and copper(II). Electrochemical detection of these ions at a mercury working electrode is routinely used. Redox signals for zinc(II) were observed at -0.9 V, for cadmium(II) at -0.6 V and for copper at -0.2 V versus Ag/AgCl 3M KCl. The calibration curves were strictly linear with detection limits on the order of hundreds of pM. Relative standard deviation did not exceed 2%. Differential pulse anodic stripping voltammetry using HMDE as a working electrode is among the most sensitive analytical techniques

used for heavy metal ion detection. However, from a technological point of view, the non-solid electrodes have much lower miniaturization potential than solid electrodes, like silver, gold, carbon or platinum. The MWNTs electrodes nanostructuring is a promising technology for further miniaturization. Fabricated electrodes and carbon tips electrodes were sensitive enough to detect ions down to tens and hundreds nM, respectively. The measured voltammogram is shown in Fig. 4. Various potentiostats were also tested, but the effect of their usage on detection limits was in one order of magnitude. Further, we tested all used potentiostats and working electrodes on analysis of environmental samples. Besides, we analyzed phytochelatin2 by using the instruments and found that the thiol gave well developed response at all electrodes with detection limit app. units or subunits of μM .

Acknowledgement

The work was supported by the Czech grant projects GACR 102/09/P640, GACR 102/08/1546 and GACR P205/10/1374.

References

- [1] Johnosn, L., et al., Journal of Materials Chemistry, Vol. 20, No. 9 (2010), pp. 1737-1743.
- [2] Prasek J., et al., 5th IEEE Sensors Conference, Vol. 1, No 1 (2006), pp. 1257-1260.
- [3] Thielemans, W., et al., Green Chemistry, Vol. 11, No. 4 (2009), pp. 531-537.
- [4] Klosova, K., et al., Phys. stat. sol. A, Vol. 205, No. 6 (2007), pp. 1435-1438.
- [5] Adam, V., et al.: Int. J. Electrochem. Sci., Vol. 5 (2010), pp. 429-447.
- [6] Strouhal, M., et al.: Bioelectrochemistry, Vol. 60, No. 1-2, (2003), pp. 29-36.

Figures

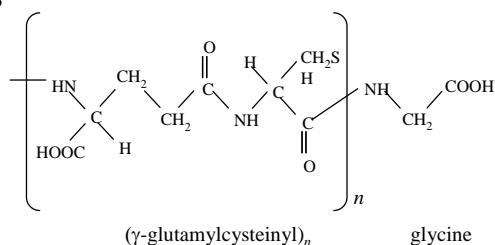


Fig. 1: Structure of phytochelatin.

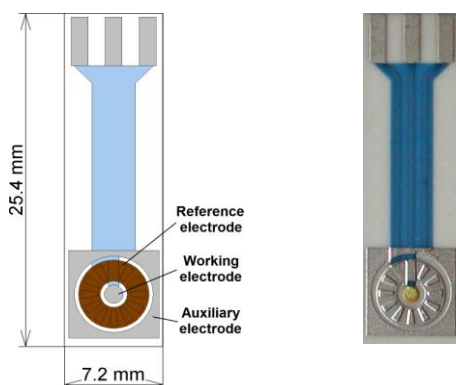


Fig. 3: Three electrode electrochemical sensor design (up) and its fabricated sample before MWNTs deposition (down).

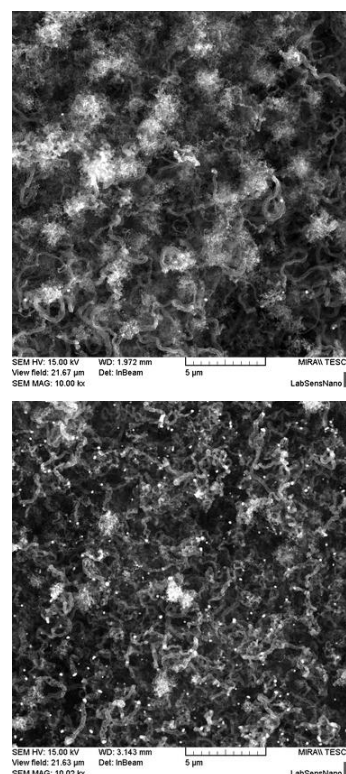


Fig. 2: SEM micrographs of the electrodes fabricated on the Ag based thick film paste with (left) and without (right) use of 10 nm Fe catalyst.

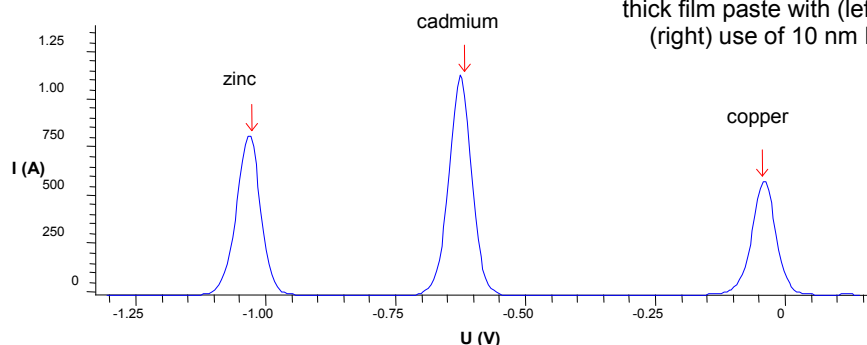


Fig. 4: Typical voltammogram of zinc, cadmium and copper, respectively.

Magneto-optical characterization of $\text{Cr}^{\text{II}}_{3/2}[\text{Cr}^{\text{III}}(\text{CN})_6]$ Prussian Blue Analogue films performed by Kerr magnetometry

Juan Pablo Prieto¹, Eugenio Coronado¹, Magdalena Makarewicz¹, Helena Prima¹, Francisco Romero¹.

1- Molecular Science Institute, University of Valencia, C/Catedrático José Beltrán 2, 46980 Paterna (Valencia), Spain.

juan.prieto@uv.es

Magneto-Optical Kerr Effect (MOKE) technique is a surface technique, which allows to acquire magnetic information from the surface region of a film. This represents an important difference respect to other magnetometry techniques, such as SQUID or PPMS, where the characterization is performed on the overall sample. Moreover, for the magnetic characterization the Kerr magnetometer uses a laser as polarized light source, with a laser spot that can be focalized on the surface of the film with a size of less than 1 μm , allowing to measure magnetic properties with high lateral resolution. Using a variable temperature Magneto-Optical Kerr Effect set-up we have characterized Prussian Blue Analogue (PBA) films obtained by electrochemical deposition.

PBA's are molecule-based magnetic materials that are good candidates for the obtaining of molecular analogues of the inorganic spintronic structures [1]. These materials present great advantages respect to conventional inorganic metals and semiconductors such as their flexibility, transparency, processability, chemical versatility and novel added functionalities. Furthermore certain families of Prussian Blue Analogues are molecule-based ferromagnets ordering near room temperature. In this way, the study of PBA's films with Kerr magnetometer is motivated by the development of molecular spintronics systems such as spin-injecting electrodes and components of spin valves structures.

In this poster, measurements on films of the $\text{Cr}^{\text{II}}_{3/2}[\text{Cr}^{\text{III}}(\text{CN})_6]$ PBA [2-3], carried out with a MOKE magnetometer, are going to be shown. Moreover, a study of the morphology of these films has been performed using an AFM microscope with the aim of relating the magnetic properties of these systems with their nanostructure determined by the growth of the sample during the electrodeposition.

[1] J.Camarero,E. Coronado; Journal of Materials Chemistry, **19** (2009),1678-1684.

[2] T. Mallah, S. Thiébaud, M. Verdaguer, P. Veillet; Science, **262**, (1993), 15541557.

[3] O. Sato, T. Iyoda, A. Fujishima, K. Hashimoto; Science, **271**, (1996), 49-51.

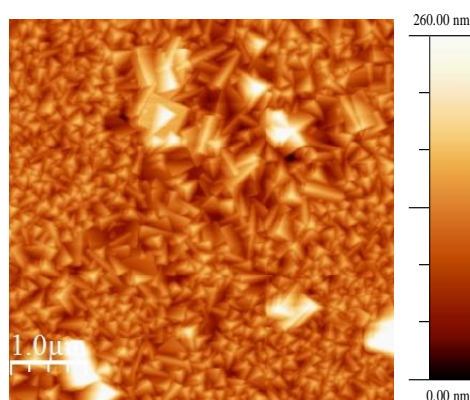


Figure 1: Topography AFM image ($5\mu\text{m} \times 5\mu\text{m}$) of a 50 seconds deposition time film of PBA $\text{Cr}^{\text{II}}_{3/2}[\text{Cr}^{\text{III}}(\text{CN})_6]$ obtained by electrodeposition showing a granular structure

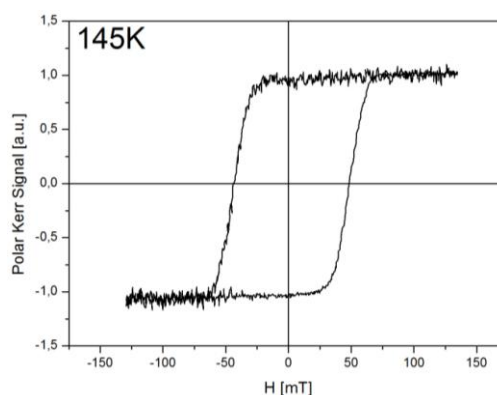


Figure 2: Hysteresis loop of a 50 seconds electrodeposition time film of PBA $\text{Cr}^{\text{II}}_{3/2}[\text{Cr}^{\text{III}}(\text{CN})_6]$ measured at 145 K with the MOKE magnetometer.

Fast deposition of elongated Nickel nanowires inside nanoporous alumina templates

Mariana P. Proenca, C.T. Sousa, D.C. Leitao, J Ventura, M. Vazquez, J.P. Araujo

IFIMUP and IN – Institute of Nanoscience and Nanotechnology, Rua do Campo Alegre 687, 4169-007
Porto, Portugal

Instituto de Ciencia de Materiales ICMM – CSIC, Campus Universitario 28049 Cantoblanco Madrid,
Spain

mproenca@fc.up.pt

One-dimensional metallic nanostructured materials have attracted extensive attention in recent years because of their technological importance in nanometer-scale devices and information storage systems. By combining deposition techniques with highly ordered nanoporous templates we can easily tune the growth of these nanostructures and form nanowires (NWs) with controlled diameters and lengths.

In this work we used electrochemical techniques to fabricate Ni NWs [1] inside nanoporous alumina templates. The depositions were performed in a Watts bath, applying a constant potential using 3 electrodes: gold sputtered on one side of the porous membrane as working electrode (WE), platinum mesh as counter electrode (CE) and Ag/AgCl (in KCl) as reference electrode. Linear voltammetry was performed prior to the deposition process in an attempt to find the optimum potential for Ni deposition. We present a comparative study of the deposition process at different constant potentials. The deposition rate was found to be different for each potential. Furthermore, the maximum length of the nanowires grown was found to depend on the applied potential, so that, for lower potentials, the nanowires do not reach the top of the 50 μm membrane. The uniformity of the Ni deposition was found to be dependent on the quality of the membranes and gold contact underneath. The length of the NWs (5 to 50 μm) was controlled by the time of deposition, for a specific applied potential, and their outer diameters correspond to the alumina pores' diameter (30 to 200 nm).

A study of the structural, morphological and magnetic properties of the Ni NWs was performed using Scanning Electron Microscopy (SEM), X-Ray Diffraction (XRD) and Vibrating Sample Magnetometer (VSM).

References

[1] K. Nielsch *et. al.*, Applied Physics Letters, **79** (2001) 1360-1362.

Figures

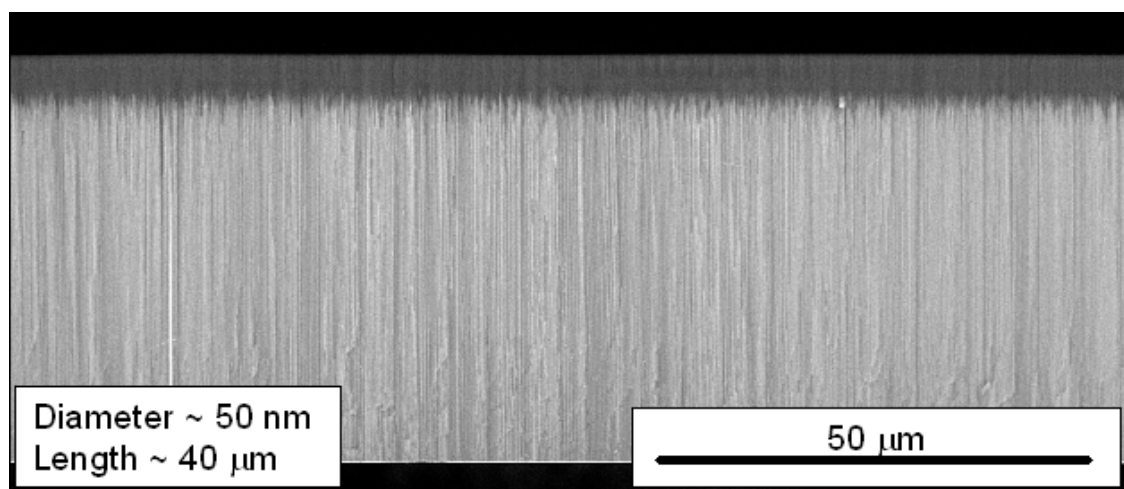


Fig. 1. SEM image of nickel nanowires electrodeposited inside a nanoporous alumina membrane

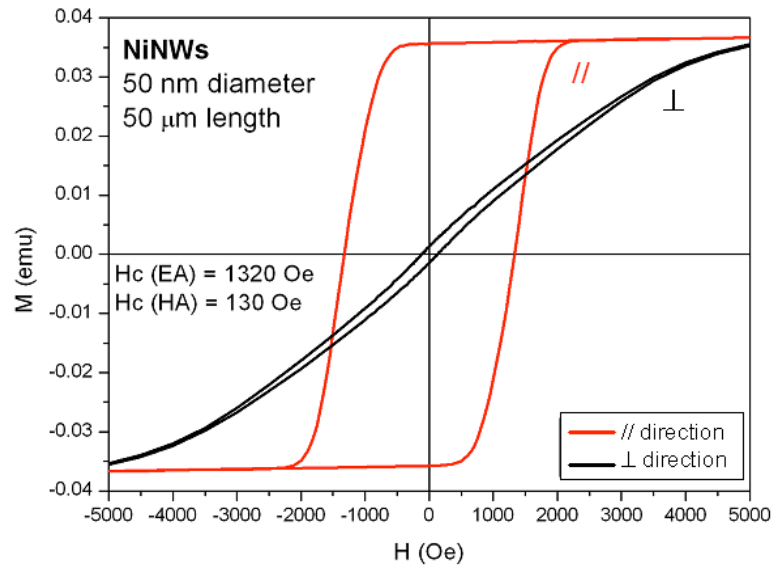


Fig. 2. Magnetization curve of nickel nanowires electrodeposited inside a nanoporous alumina membrane

Structure and magnetism of the V/Ta(001) surface: A DFT calculation

A.A. Ramanathan, J.M. Khalifeh, and B.A. Hamad

University of Jordan (Jordan)

Thin slab calculations using the density functional theory (DFT) and norm-conserving pseudopotentials, show a $p(1\times 1)$ in-plane ferromagnetic (FM) ordering with appreciable magnetic moment of $2.2\mu\text{B}$ for the V monolayer (ML). The surface V atoms are anti-ferromagnetically (AF) coupled with the Ta layers below (LAF). The results have been obtained by performing complete geometrical optimization at absolute zero. Structural relaxation of the clean V(001) and Ta(001) surfaces, show large inward relaxations of 9.8% and 11.2% respectively in good agreement with experiment and other calculations. The inward relaxation is reduced to 6.0% for the vanadium surface overlayer in V/Ta(001) and could be the result of its spin polarization.

Keywords: *Vanadium, DFT, magnetic moment, LAF, pseudopotential, relaxation*

Preparation Two different Morphology of Ag/Ag₂O Nanoparticles from the Same Initial Nanorods of Silver (I) Coordination Polymer

Z. Rashidi Ranjbar, A. Morsali

Department of Chemistry, Faculty of Sciences, Tarbiat Modares University, Tehran, Islamic Republic of Iran

Silver as a useful metal has been utilized in several applications: catalysis, electronics, photonics, biology and so on. Ag₂O is used as catalysts and has different application, too. It is notable that both size and shape of solid materials influence on the Chemical and physical properties. By decreasing the size of structures; the ratio of surface area to volume would be increased. Therefore some chemical and physical (color, phase transition temperatures, and the values of band-gaps) properties of them would be altered. Therefore, by the size and shape control of solid materials, their chemical and physical properties can be altered as desired.

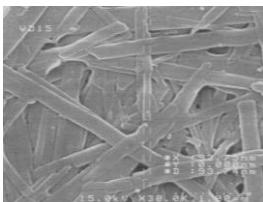
Two different (morphology and size) interesting nanorod as nano coordination polymer (NCP) of silver (I), [Ag(bpfb)(NO₃)]_n, have been synthesized by using two distinct sonochemical baths with different power -305 w and 0.135 KW- (Figure 1a, b). This compound were obtained from initial reagents addition (AgNO₃: bpfb) in 1:1 molar ratio at sonochemical process.

It is notable that this polymer was synthesized in single crystal form and characterized by X-ray crystallography.

This NCP (Nano Coordination Polymer) as nanorod was used to prepare silver/silver Oxide by thermolysis. Decomposition of nano coordination polymer occurs at high temperature without surfactant and at lower temperature in presence of surfactant. We use from a laboratorial electric furnace for heat treating. When initial NCP heated directly at 873K, grey powder of Ag/Ag₂O nanoparticles obtained. Also, we heated this polymer at 473K after immersing in oleic acid as surfactant. Some grey powder was isolated after washing the product with excess ethanol. XRD pattern (Figure 2) of these products shows that a mixture of silver metal and silver (I) Oxide has been fabricated.

The SEM images show that when oleic acid used for decomposing, nanoparticles with perfect dispersion obtained (Figure 3a, b). So, the synthesis methods have important roles and could control the products.

a) Power 305 W



b) Power 0.135 KW

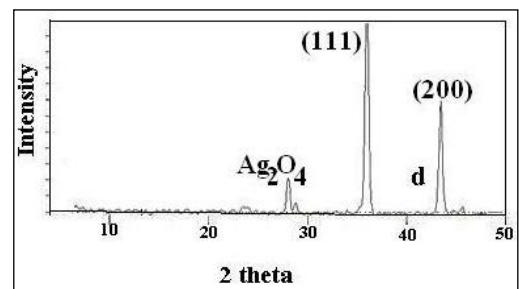
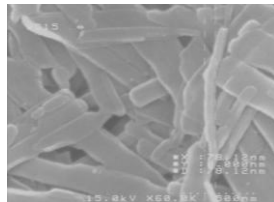
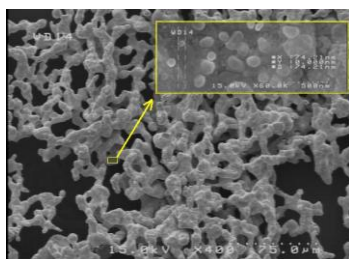


Figure 2. SEM images of silver (I) nanorods coordination polymer

Figure 2. XRD pattern of Ag/Ag₂O

a) Direct decomposition



b) Decomposition by surfactant

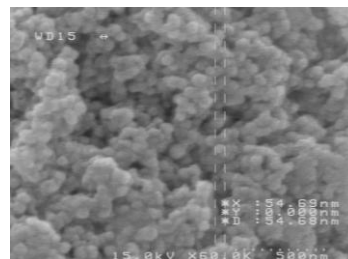


Figure 3. SEM images of Ag/Ag₂O nanoparticles

Design and transdermal delivery of indomethacin nanosystem

Felipe de Freitas Nunes¹, **Catarina Pinto Reis**², Catarina Rosado², Luis Monteiro Rodrigues²

¹ Laboratório de Farmacotécnica, Universidade Federal do Paraná, Av. Pref. Lothário Meissner 632, 80210-170 Curitiba, PR - Brasil

² Experimental Dermatology Unit and Laboratory of Nanoscience and Biomedical Nanotechnology, Universidade Lusófona de Humanidades e Tecnologias, Campo Grande 376, 1749-024 Lisboa – Portugal

catarinapintoreis@gmail.com

Presently, transdermal drug delivery is one of the most promising methods for drug application. Increasing numbers of drugs are being added to the list of therapeutic agents that can be delivered to the systemic circulation *via* skin. The transdermal route offers several advantages over conventional dosage forms including extended duration of activity, avoidance of first-pass metabolism by the liver, minimization of pain, reduction of side effects, reduction in the fluctuations of drug concentrations in the blood and possible sustained drug release.

Indomethacin was selected as a model since it has been widely used as a non-steroidal anti-inflammatory drug (NSAID) for external pharmaceutical preparations. It works by inhibiting the production of prostaglandins, molecules known to cause symptoms such as pain, stiffness and swelling. In fact, oral therapy with indomethacin is very effective but its clinical use is often limited because of its potential to cause adverse effects. The administration of indomethacin *via* the transdermal route has been adopted to overcome the disadvantages of the oral route and maintain relatively consistent plasma levels for long-term therapy. The present study was carried out to design a viable and practically effective transdermal system of indomethacin. As well-known, the stratum corneum, the outermost layer of the skin, acts as a barrier. It is therefore necessary to disrupt this function to improve the transdermal delivery of this drug.

Thus, nanoencapsulation technologies were applied in order to enhance bioavailability and reduce toxicity of indomethacin after transdermal administration. Nanoparticles are solid sub-micronic drug carriers of natural, semisynthetic, or synthetic polymeric nature in the nanometer size range. Nanoparticles may or may not be biodegradable and they have many advantages over traditional formulations and this is why the interest about them has increased in the past years. Nanoparticles appear as a very good alternative system to deliver and to protect drugs. As well, a promising strategy in nanotechnology field is the use of multifunctional biodegradable polymers exhibiting permeation enhancing and mucoadhesive properties. The polymer selected was gelatine because it is a non-toxic polymer with broad spectrum of use and easy access.

Methods:

Nanoparticles were produced by two-step desolvation process [1]. Parameters such as mean particle size and zeta potential were studied. The skin permeability of this nanosystem was also studied by using Franz cells. Free-indomethacin in cellulose-based system and indomethacin-loaded nanoparticles were considered. The cumulative amount of indomethacin passing across silicone membrane was calculated using the measured indomethacin concentrations in the receiver solutions. Drug release was determined by ultraviolet–visible spectrophotometer.

Results and Discussion:

Nanoparticles appear as a very good alternative system to deliver and to protect drugs [2, 3]. Gelatine nanoparticles were easily included in cellulose-based system as seen in figure.

Gelatine nanoparticles showed a small mean particle size. Particle size ranges from 290 to 350 nm. The polydispersity index was lower than 0,199. At the skin surface, molecules contact with other molecules which negligibly affect permeation. The penetrant has three potential pathways to the viable tissue: through hair follicles with associated sebaceous glands, via sweat ducts, or across continuous stratum corneum between these appendages. Sizes up to 200–300 nm can penetrate intact skin [4]. They may penetrate follicles and stratum corneum. In general, colloidal particles >10 μm remain on the skin surface; those 3–10 μm concentrate in the follicle and when < 3 μm they penetrate follicles and stratum corneum alike [5].

Zeta potential was negative (mean -9 mV). Values were between -10 and -6.4 mV. Since the human skin has zeta potential around +23 mV [6], opposite charge may increase time contact between drug and skin.

Concerning permeation studies of indomethacin, this study showed that gelatin nanoparticles led to a better controlled release of indomethacin especially on burst release effect but additional experiments are needed.

Conclusions:

The present data confirm the feasibility of developing indomethacin transdermal nanosystem on an industrial scale. Further studies, now in progress, will deal with the application of the presently reported findings to human skin permeation, involving *in vivo* testing.

References

- [1] Z. Lu, T.-K. Yeh, M. Tsai, J.L.-S. Au, M.G. Wientjes, *Clinical Cancer Research*, 10 (2004) 7677.
- [2] C.P. Reis, R.J. Neufeld, A.J. Ribeiro, F. Veiga, *Nanomedicine: Nanotechnology, Biology and Medicine*, 2 (2006) 8.
- [3] C.P. Reis, R.J. Neufeld, A.J. Ribeiro, F. Veiga, *Nanomedicine: Nanotechnology, Biology and Medicine*, 2 (2006) 53.
- [4] B.W. Barry, *Eur. J. Pharm. Sci.*, 14 (2001) 101.
- [5] H. Schaefer, T.E. Redelmeier, in: Karger (Ed.), *Skin Barrier* Basel, 1996, p. 235.
- [6] M.J. Morykwas, J.W. Thornton, R.H. Bartlett, *Plastic and Reconstructive Surgery*, 79 (1987) 732.

Figure

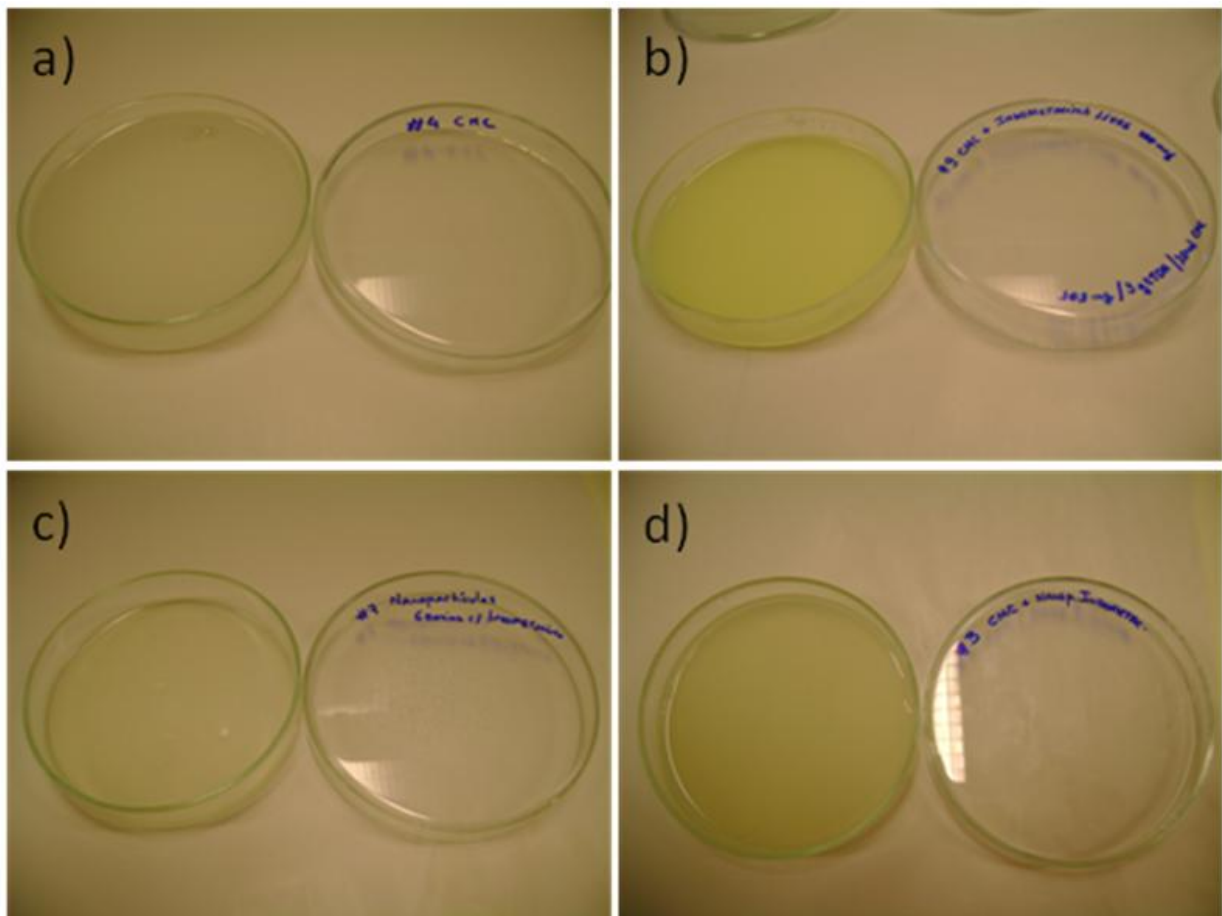


Figure. a) CMC-based system; b) CMC with free indomethacin;c) Indomethacin-loaded nanoparticles and d) Indomethacin-loaded nanoparticles in CMC-based system.

An antibacterial coating based on silver loaded in a polymer/sol-gel hybrid matrix

Pedro J. Rivero, A. Urrutia, P. Aldaz, J. Goicoechea, I.R. Matías, F.J. Arregui
Public University of Navarra (UPNA), Campus Arrosadia S/N, Pamplona, Spain
pedrojose.rivero@unavarra.es

In this work it is proposed a novel antibacterial surface composed of an organic-inorganic hybrid matrix of tetraethoxysilane (TEOS) and a weak polyelectrolyte like *Poly(acrylic acid sodium salt)* (PAA) which are deposited on glass slides by sol-gel method using the dip-coating technique [1]. This work is focused in the *in situ* synthesis of Ag nanoparticles (NPs) which are responsible of the antibacterial activity.

The weak polyelectrolyte PAA is used to create ion-binding sites in the starting solution by pH manipulation. This polyelectrolyte has been used earlier to bind Ag^+ via ion exchange (using AgNO_3 10mM) [2, 3]. The silver cations (Ag^+) formed electrostatic pairs with the carboxylate groups from PAA. The carboxylate-bounded Ag^+ ions were reduced *in situ* to produce zero-valent silver (Ag^0) with dimethylaminoborane (DMAB 10mM) which acted as reduction agent. The UV-VIS absorbance spectrum confirms the existence of silver nanoparticles inside the coating due to the existence of an absorption peak near 410 nm (see Figure 1a). Such narrow absorption bands are typical of silver nanoparticles and they are originated by the Surface Plasmon Resonance (SPR) phenomenon [4, 5].

In this work the impact of the organic-inorganic ratio and the number of dip/reduction cycles on the total amount of synthesized silver nanoparticles has been studied. Figure 1a shows a direct relation between the number of dip/reduction cycles and the total amount of Ag nanoparticles. Moreover if the organic/inorganic molar ratio is increased, this also results into a rise of the number of nanoparticles, as it is shown in Figure 1b. The morphology of such surfaces was studied by Atomic Force Microscopy (AFM). The resultant coating was uniform and homogeneous, showing a smooth surface with a roughness of 7,5 nm (RMS). The topography and phase AFM images of the coating reveal is shown in Figure 2, and reveals the presence of a slight phase separation at the microscale, with the appearance of slightly different phase domains, which suggest different mechanical properties of each region.

The coated surfaces were tested in bacterial cultures of genus *Lactobacillus plantarum* to observe their antibacterial activities. Thus, *L. plantarum* were inoculated in a "MRS Broth" aqueous medium and incubated at 37° C for 24hours. The antibacterial activity was carefully measured by optical method. Figure 3 shows the results in two substrates placed on agar slabs after 24 h. The first one, Figure 3a, shows one reference substrate (uncoated) where it is obvious to observe a high number of *Lactobacillus plantarum* colonies that grow up randomly in the whole agar slab. The second one, Figure 3b, shows the coated substrate where it is easy to differentiate between the coated area (where there is no growth of colonies) and the uncoated area and the rest of the slab (where the growth of colonies is high as it was expected). These results confirm the high antibacterial property of the coatings based on silver loaded in a polymer/sol-gel hybrid matrix.

References:

- [1] M. Marini, S. De Niederhausern, R. Iseppi, M. Bondi, C. Sabia, M. Toselli and F. Pilati, *Biomacromolecules*, **vol. 8** (2007) 1246-1254.
 [2] Z. Li, D. Lee, X. Sheng, R. E. Cohen and M. F. Rubner, *Langmuir*, **vol. 22** (2006) 9820-9823.
 [3] X. Zan and Z. Su, *Thin Solid Films*, (2010), *article in press*.
 [4] T. C. Wang, R. E. Cohen and M. F. Rubner, *Adv Mater*, **vol. 14** (2002) 1534-1537.
 [5] A. J. Nolte, M. F. Rubner and R. E. Cohen, *Langmuir*, **vol. 20** (2004) 3304-3310.

Figures:

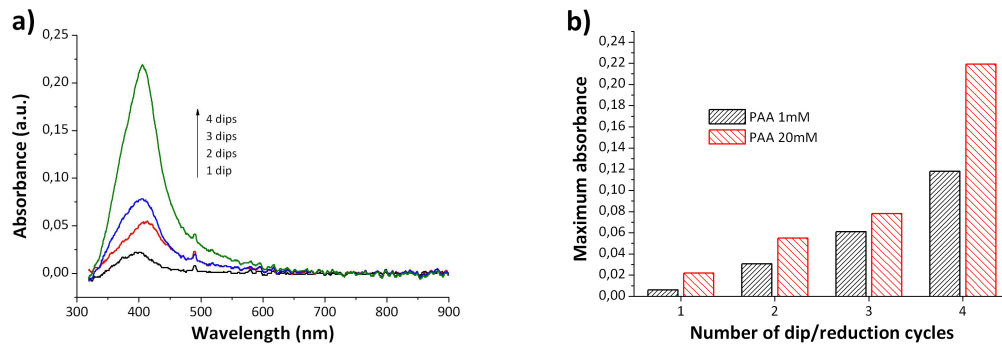


Figure 1: UV-VIS absorption spectra of the coating film (a) with different number of dip/reduction cycles (PAA 20mM), (b) with different ratio molar of organic/inorganic

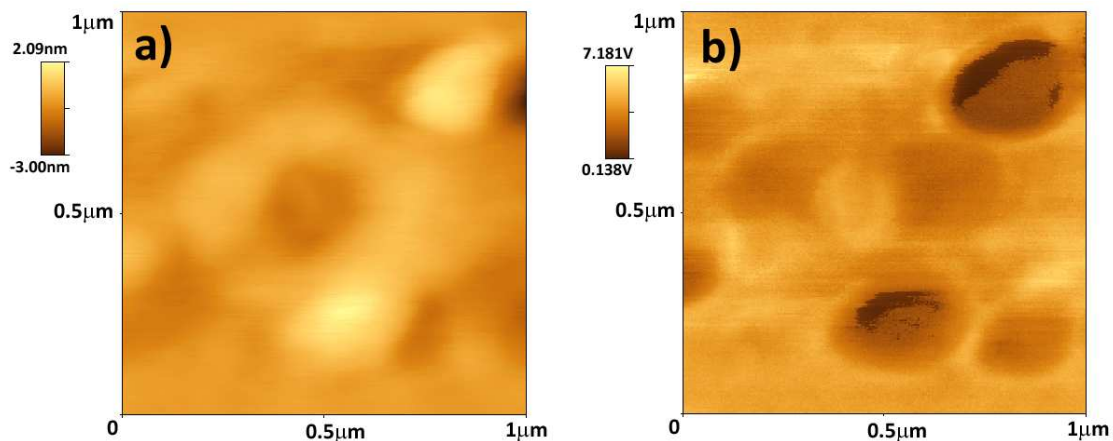


Figure 2: AFM images of the coating substrate: (a) height; (b) phase

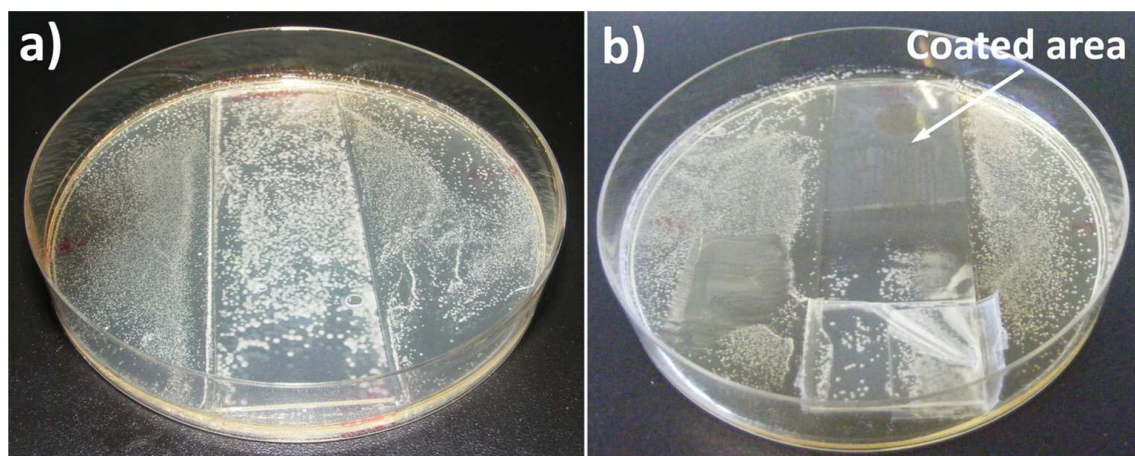


Figure 3: Bacteria growth on culture plates after 24 hours: (a) uncoated substrate; (b) coated substrate

Fabrication of silica hollow microcoils with mesoporous walls

Carlos Rodríguez-Abreu^{1,2}, Neus Vilanova², Conxita Solans², Masaki Ujihara³,
Toyoko Imae³, and Seiji Motojima⁴

1. International Iberian Nanotechnology Laboratory (INL), Avda. Central nº100, Edificio dos Congregados, 4710-229, Braga, Portugal
2. Instituto de Química Avanzada de Cataluña. Consejo Superior de Investigaciones Científicas (IQAC-CSIC) Jordi Girona 18-26, 08034 Barcelona, Spain
3. Graduate Institute of Engineering, National Taiwan University of Science and Technology, 43 Keelung Road, Section 4, Taipei, Taiwan
4. Toyota Physical & Chemical Research Institute, Nagakute, Aichi 480-1192, Japan
crodriguez@inl.int

Hollow silica microcoils have been prepared by using functionalized carbon microcoils (CMCs) as hard templates [1,2] and surfactant aggregates as soft templates. The obtained materials have been characterized by electron and optical microscopy, small angle X-ray scattering, thermogravimetry and porosimetry (gas sorption analysis). The obtained hollow microcoils resemble the original hard templates in shape and size. Moreover, they have mesoporous walls (pore size ≈ 3 nm) with some domains where pores are ordered in a hexagonal array, originated from surfactant micelles. As a result the surface area of the silica microcoils is much higher than that of the original CMCs used as templates. The obtained silica microcoils also show preferential adsorption of cationic fluorescent dyes. A mechanism for the formation of silica microcoils is proposed.

References

- [1] Motojima, S.; Chen, X., Bull. Chem. Soc. Jpn. **80** (2007) 449.
[2] Adhikari, P.D.; Tai, Y.; Ujihara, M.; Chu, C-C. ; Imae, T.; Motojima, S., J. Nanosci. Nanotechnol. **10** (2010) 833.

Figures

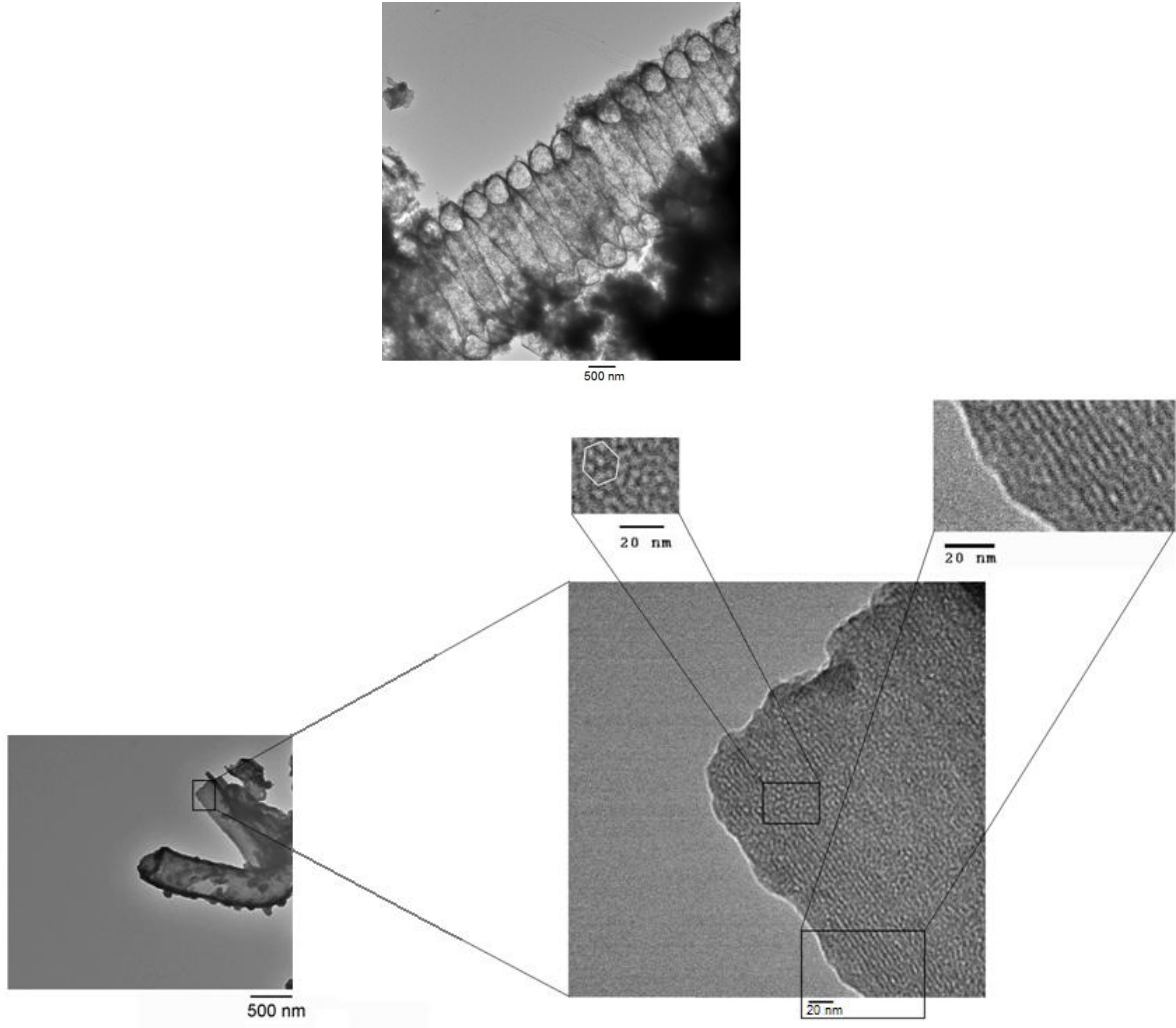


Figure 1: TEM images of sections of silica hollow microcoils.

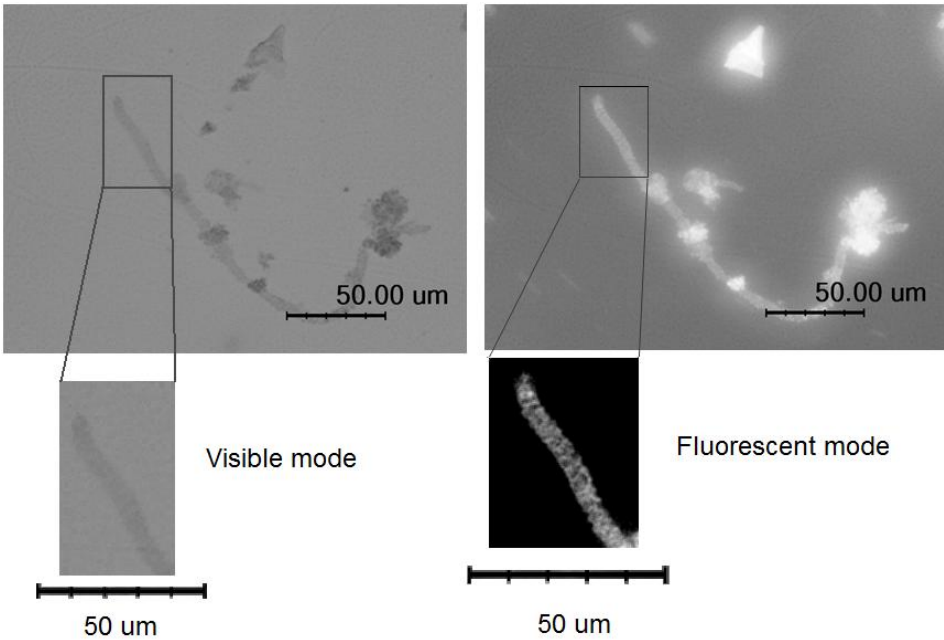


Figure 2: Visible and fluorescent microscopic images of hollow silica microcoils after soaking them in aqueous solutions of rhodamine B

Lossy-mode resonance based optical fiber pH sensors

C. R. Zamarreño*, M. Hernaez, I. Del Villar, P. J. Rivero, I. R. Matias, F. J. Arregui
Public University of Navarra, Campus Arrosadia, Pamplona, SPAIN
carlos.ruiz@unavarra.es

Different type of resonances can be supported by thin-film coated substrates [1]. Among them, lossy-mode resonances (LMRs) have been recently explored for the fabrication of indium tin oxide and titanium oxide based optical fiber refractometers [2-3]. These devices take advantage of optical fiber properties, such as portability, light-weight and easy multiplexation in wavelength among others [4], as well as the benefits associated to the LMRs, such as the non-dependence with the polarization of light or the generation of multiple resonances without modifying the optical fiber geometry [2-3]. LMR-based devices also permit the utilization of additional layers onto the sensitive coating in order to detect diverse substances or chemical compounds [5]. However, LMRs can be also generated by the utilization of many other materials different than metal oxides or semiconductors.

Here, it is described the fabrication of LMR-based optical fiber pH sensors by means of the deposition of thin polymeric structures onto the exposed core of 200/225 μm core/cladding diameter optical fibers (FT200EMT, Thorlabs Inc.). The materials used for the coating fabrication are the polycation *poly(allylamine hydrochloride)* (PAH), the polyanion *poly(acrylic acid)* (PAA) and the colorimetric pH indicator known as neutral red (NR). The coatings have been fabricated by using the well-known Layer-by-Layer (LbL) electrostatic self-assembly technique as it has been already described in previous works of our group [5-6]. Moreover, PAH/PAA structure has shown thickness dependence with the pH of the surrounding medium, known as swelling/deswelling [7], which has been exploited before in the fabrication of pH sensors [8].

A white light source (AQ4303-B, ANDO Inc.) was connected at the input of the fiber in a typical optical transmission setup in order to introduce light through the sensitive region, as it is represented in Fig. 1. The output of the fiber was connected to the single end of a bifurcated optical fiber, which was attached at the other end to two spectrometers (HR4000 and NIR512 from Oceanoptics Inc.) in order to obtain the spectral information in the range between 500 nm and 1700 nm.

Absorbance spectra were collected as the coating thickness was increased up to 100 bilayers. Three different resonances were originated during the coating fabrication process as it is observed in Fig. 2. Two of these resonances (2nd and 3rd) remained visible within the studied range at the end of the fabrication process. Then, [PAH+NR/PAA]₁₀₀ coated optical fiber was immersed into different pH solutions in order to observe the shifts of the second and third resonances as a function of the coating thickness variations. As it is represented in Fig. 3, both, second and third resonances, shift forward and backward as the pH of the surrounding medium is varied between 5.0 and 4.0 for different intervals. Hence, wavelength at maximum absorbance or resonance wavelength can be used in order to determine the pH of the surrounding medium. Wavelength based detection technique permits the fabrication of robust and power fluctuation immune optical fiber sensors. Furthermore, the presence of two different resonances permits the realization of dual reference measurements and the associated improvement in the signal to noise ratio. Wavelength shifts of both, second and third resonances, have been obtained by monitoring the maximum absorbance wavelength during the pH variation sequence as it is represented in Fig. 4. Here, it is observed that the second resonance wavelength shift is larger (~30 nm), approximately double, than that of the third resonance (~15 nm), which indicates that the second resonance is more sensitive to pH variations.

To sum up, polymer coated optical fiber has been fabricated and characterized as LMR-based optical fiber pH sensors for the first time. Moreover, these devices take advantage of wavelength detection and the utilization of two references. Finally, the fabrication of LMR-based devices by means of the deposition of polymeric coatings presents a first step towards the application of many other coatings with different properties and applications in chemistry, biology among others.

References:

- [1] F. Yang, J. R. Sambles, *J. Mod. Opt.*, **44**(6), (1997) 1155-1163.
- [2] I. Del Villar, C. R. Zamarreño, M. Hernaez, F. J. Arregui, I. R. Matias, *J. Lightwave Tech.*, **28**(1) (2010) 111-117.
- [3] M. Hernaez, I. Del Villar, C. R. Zamarreño, F. J. Arregui, I. R. Matias, *Appl. Opt.*, **44**, (2010) 3980-85
- [4] B. Lee, S. Roh, J. Park, *Sens. Actuators B*, **15** (2009) 209-221.
- [5] C. R. Zamarreño, M. Hernaez, I. Del Villar, I. R. Matias, F. J. Arregui, *Sens. Actuators B*, (2010)
- [6] J. Goicoechea, C. R. Zamarreño, I. R. Matias, F. J. Arregui, *Sens. Actuators B*, **132**, (2008) 305-311.
- [7] K. Itano, J. Choi, M. F. Rubner, *Macromolecules*, **38**(8), (2005) 3450-3460.
- [8] J. Goicoechea, C. R. Zamarreño, I. R. Matias, F. J. Arregui, *Sens. Actuators B*, **138**, (2009) 613-618

Figures

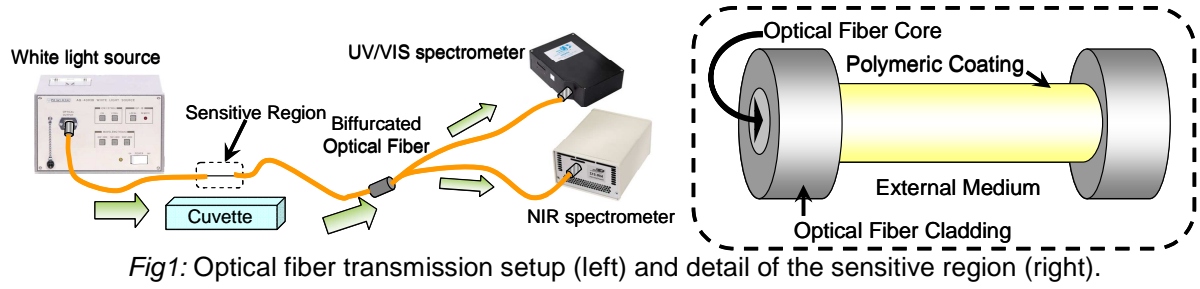


Fig1: Optical fiber transmission setup (left) and detail of the sensitive region (right).

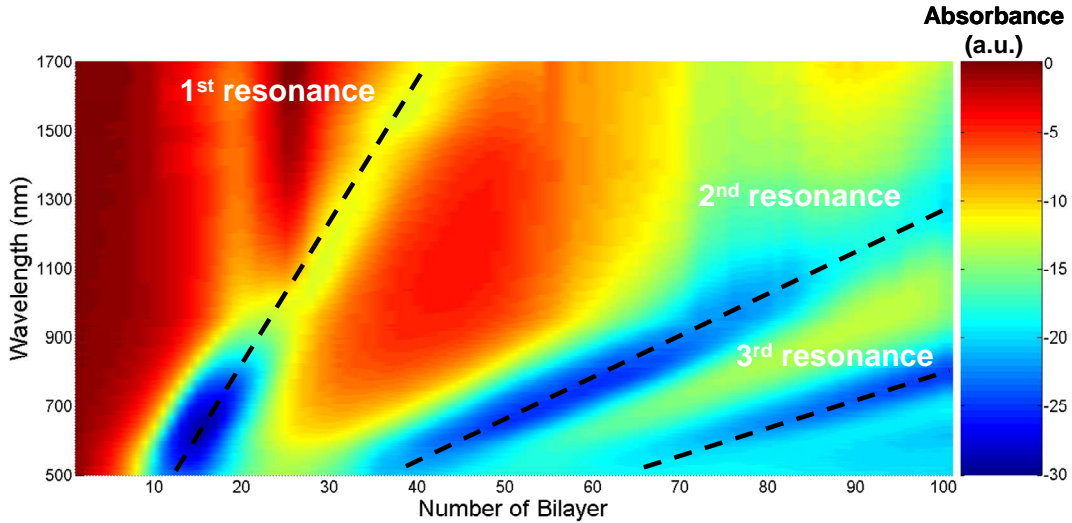


Fig2: Spectral response as a function of the number of bilayers added.

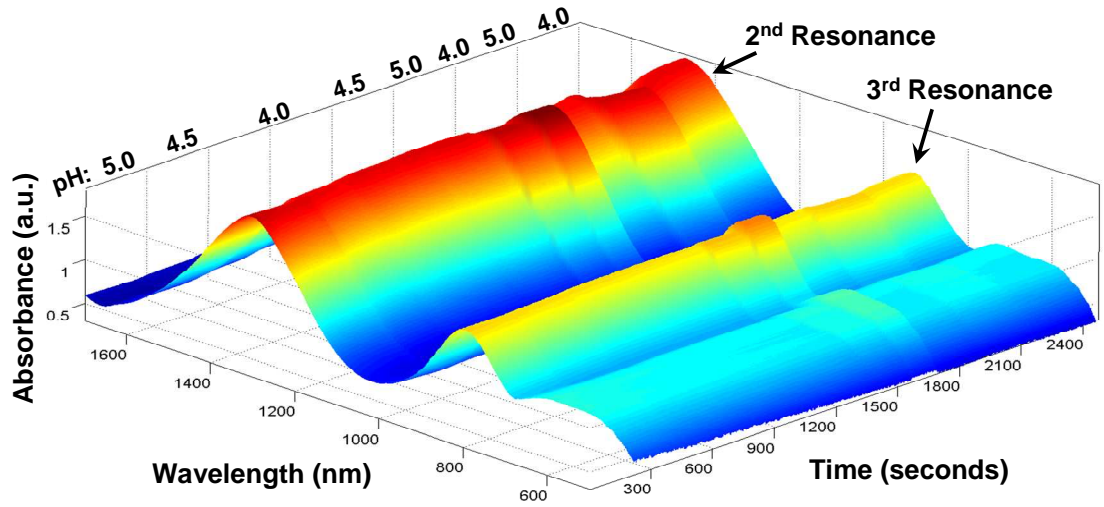


Fig3: Spectral response as a function of the pH of the external medium for a [PAH+NR/PAA]₁₀₀ device.

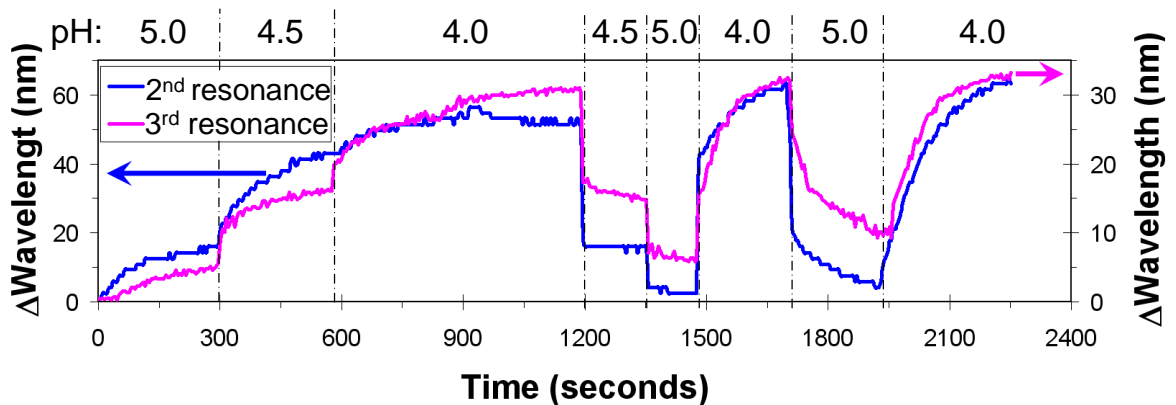


Fig4: Wavelength absorbance maxima shift for the 2nd and 3rd resonances as a function of the pH.

Adhesion and Energy Dissipation on the Formation of One-Atom Contact on Au and Pb

G. Sáenz-Arce¹, A. Castellanos-Gomez², G. Rubio-Bolinger², C. Untiedt¹

¹LT-NanoLab, Departamento de Física Aplicada, Universidad de Alicante, Campus de San Vicente del Raspeig, E-03690 Alicante, Spain

²Departamento de Física de la Materia Condensada (C-III).
Universidad Autónoma de Madrid, Campus de Cantoblanco, 28049 Madrid, Spain.

giovanni.saenz@ua.es

Quartz Tuning Fork (TF) has been recently successfully implemented in force detection schemes for scanning probe microscopy applications[1, 2, 3, 4]. Here we report its use as a nanotribometer for studying energy dissipation and the forces in the formation of a single atom contact. The idea behind such a noncontact mono-atomic energy dissipation detector, is to take advantage of the mechanical resonance of a TF which has a large Q-factor and elastic constant which in our set-up is a function of the tip-sample dissipative forces. Finally, we report measurements of the shift in the resonance frequency and the Q-factor degradation of the oscillating TF, either as a function of the tip-sample voltage or distance. These experiments have been done on Au and Pb close to the superconducting transition temperature in high vacuum.

References

- [1] S. Morita, et. al. Noncontact Atomic Force Microscopy, Nanoscience and Technology (Springer-Verlag, Berlin (2002)
- [2] F. Giessibl APL. 73 (1998) 3956
- [3] A. Castellanos-Gomez, et al. Nanotechnology 20 (2009) 215502
- [4] G. Rubio-Bollinger, et. al. PRL (2004) 116803-1

Figures

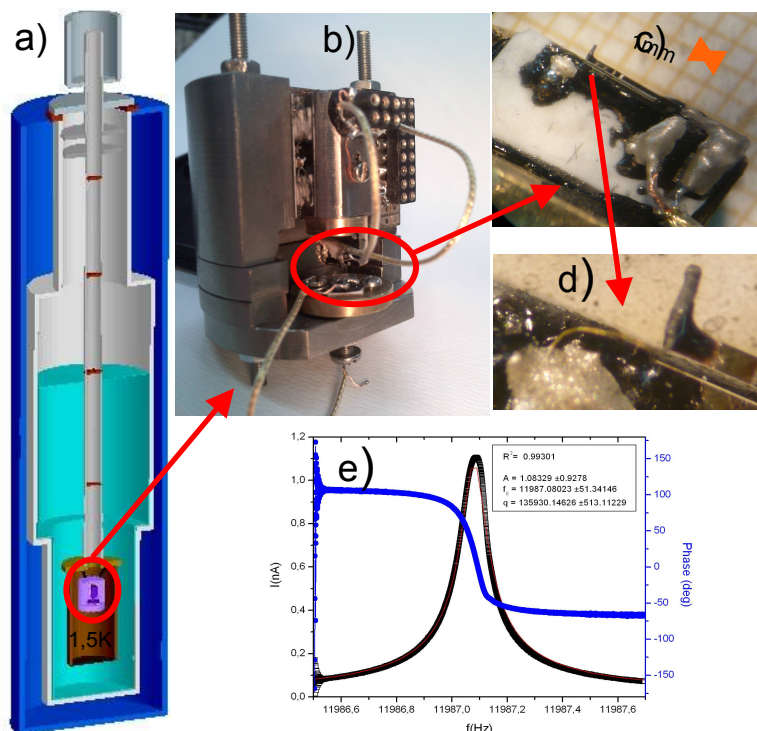


Figure1: Experimental Set up. a,b) The low temperature set-up is shown. The STM/AFM is hanged by springs from the top of a cup situated at the bottom part of a dipstick. We use the qPlus sensor with the tip isolated from the TF-electrode. We welded Pb (0.125mm diameter) wire with Au (0,025mm), which is attached to the front side of the free TF prong with non conductive epoxy. We cut the tip before making high vacuum and low temperature to reduce the quantities of lead oxide.

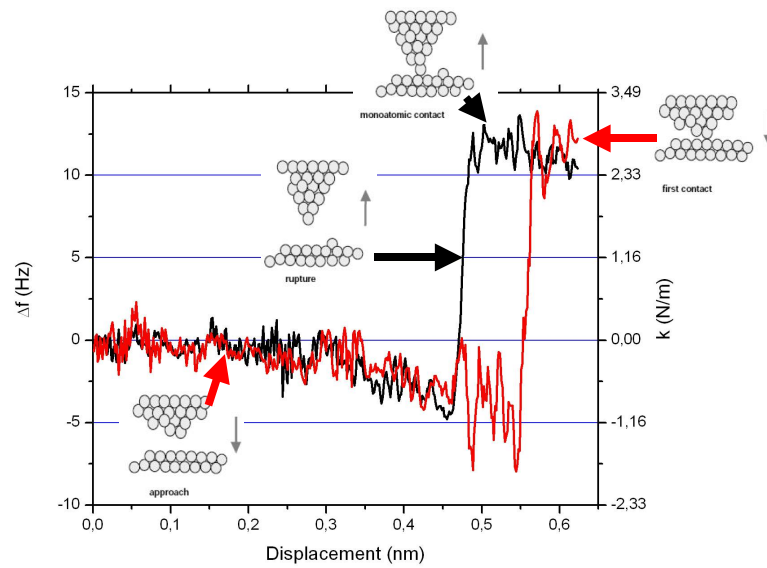


Figure2: Changes of the TF's frequency in the process of formation of a Pb one-atom contact at 4.2K.

Synthesis of Few Layer Graphene by Electrochemical Intercalation and Exfoliation Induced by a Polymeric Surfactant

Horacio J. Salavagione², Gustavo M. Morales¹, Pablo Schifani¹, Gerardo Martínez², Gary J. Ellis², Carmen Ballesteros³, César A. Barbero¹,

¹ Universidad Nacional de Río Cuarto. Departamento de Química. Ruta Nacional 36 Km 601, X5804ZAB, RíoCuarto, Córdoba, Argentina,

² Instituto de Ciencia y Tecnología de Polímeros, CSIC, Juan de la Cierva 3, 28006 Madrid, España

³ Universidad Carlos III de Madrid, Departamento de Física., Avenida Universidad 30, 28911 Leganés, España

horacio@ictp.csic.es

Graphene, one-atom-thick planar sheet of sp^2 -bonded carbon atoms, is a quasi-2-dimensional (2D) material. The fascinating properties of graphene and few layer graphene (FLG) have made it one of the most promising materials.

However, graphene suffers from a problem that is common to many novel materials, the lack of a method for producing it in large quantities. So, fully exploiting the properties of graphene requires yet the development of a method for their mass production. The exfoliation of expandable graphite via graphite intercalation compounds (GICs) can be one of the most attractive methods for this proposes because this process, which has been studied considerably in the past is cheap and scalable.² The electrochemical intercalation and subsequent exfoliation of graphite is a well known phenomenon in the field of lithium-ion batteries using carbonaceous material.

Here we report a simple method to produce graphene that combines the anodic and cathodic electrochemical intercalation/expansion of graphite in aqueous perchloric acid and posterior expansion by microwave radiation and exfoliation with ultrasound radiation (Figure 1).

The morphological characterization of the EG shows the typical worm-like shape of the EG since our method rely in the intercalation/expansion principle.

Raman results suggest that the material integrity is retained, and the pre-treatment has no negative influence on the material integrity. The level of exfoliation and the structure of the material dispersed have been analyzed by TEM and Raman, confirming that few-layer graphene have been successfully produced (Figure 2).

Graphene is usually dispersed in organic solvents such as NMP and o-DCB. Here we reported the dispersion of few layer graphene in water with the aid of a polymeric surfactant. The polymer is a PVA modified with perylene groups. The aromatic planar molecules ensure interaction with graphene while the polar polymer confers to the system solubility in water.³

The absorption spectrum of PVAPery/Grf dispersions confirms the presence of graphene laminates. In addition, upon exposure to a laser beam, the Tyndal scattering effect is observed for the PVAPery/Grf dispersions (Figure 3).

The presence of dispersed graphene laminates was further confirmed by Raman and NIR spectroscopy as well as with fluorescence measurements.

Acknowledgments. Financial support from the Spanish Ministry of Science and Innovation (MICINN) (MAT2009-09335) is grateful acknowledged.

References

[1] A. K. Geim, K. S. Novoselov, *Nature Mater.* 6 (2007) 183

[2] D.D.L Chung, *Journal of Materials Science*, 37 (2002) 1475.

[3] J. M. Englert, J. Röhl, C. D. Schmidt, R. Graupner, M. Hundhausen, F. Hauke, A. Hirsch, *Adv. Mater.* 21 (2009) 4265

Figures

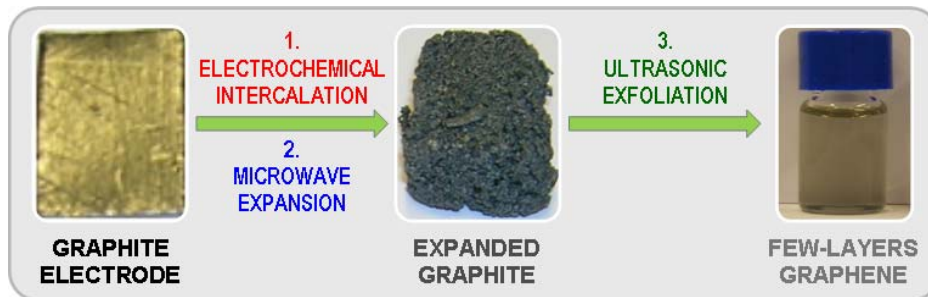


Figure 1. Schematic representation of the process to produce few layer graphene from a graphite electrode

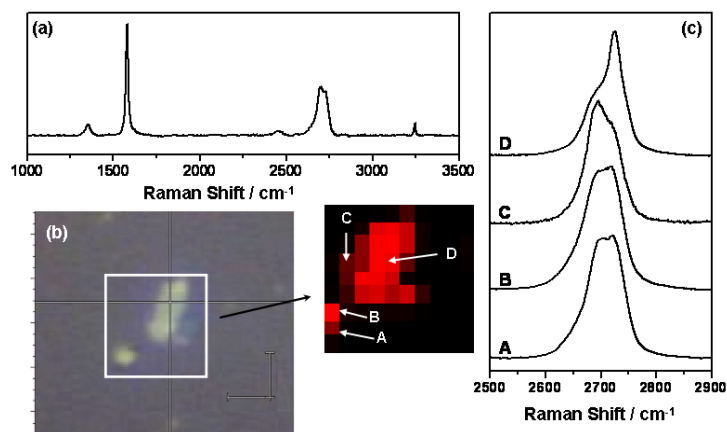


Figure 2. (a) Raman spectrum observed from exfoliated -1V FLG sample deposited on a quartz slide, (b) optical image of a typical deposit on the quartz slide and false-color map of the zone indicated, and (c) representative spectra from the points indicated of the 2D region of FLG.



Figure 3. The Tyndal scattering in a solution of PVA-Perylene containing dispersed few layer graphene

Cohesive strength of ZnO:Ga thin films deposited at room temperature

A.P. Samantilleke^{1#}, L. Rebouta^{1*}, L. Rubio-Peña², S. Lanceros-Mendez¹, P. Alpuim¹, S. Carvalho¹

1 Centro de Física, Universidade do Minho, Azurém, 4800-058 Guimarães, Portugal

2 University of Cadiz, Engineering School, C/ Chile, 1. 11002 Cádiz, Spain

Presenting author (anura@fisica.uminho.pt)

* Corresponding author (rebouta@fisica.uminho.pt)

Abstract

The main purpose of this work is the deposition of transparent conducting oxide (TCO) films on polymers with electromechanical and electro-optical properties, in order to develop applications such as flexible touch screens and keyboards. Transparent conducting ZnO:Ga (GZO) films have been deposited by dc magnetron sputtering, on glass, Polyethylene naphthalate (PEN) and poly (vinylidene fluoride) – (PVDF) substrates. Samples were prepared at room temperature while varying the working pressure. The deposition rate was approximately 30 nm/min and the thicknesses of films were between 100 and 700 nm. Electrical resistivity of $8.8 \times 10^{-4} \Omega \cdot \text{cm}$ has been obtained for films deposited on glass, while a resistivity of $2.2 \times 10^{-3} \Omega \cdot \text{cm}$ has been attained in similar coatings on polymers.

Tensile tests were performed in order to investigate the crack onset strain, the coating cohesive strength as well as the influence of mechanical strain on the electrical properties. The crack onset strain is similar for different GZO coatings and occurs for nominal strains around 1 %. The cohesive strength of coatings, which was evaluated from the initial part of the crack density evolution was found to be between 1.3 and 1.4 GPa. For these calculations, a Young's modulus of 112 GPa, which was evaluated by nanoindentation using thick GZO films deposited on glass, was used.

Nanostructured hybrid ZnO thin films for energy conversion

A. P.Samantilleke^{1#}, M. Moya², M. Mollar², B. Mari^{2*},

¹Centro de Física, Universidade do Minho, Braga 4710-057, Portugal.

² Department de Física Aplicada-IDF, Universitat Politècnica de València, Camí de Vera s/n, 46022, València, Spain

Presenting author: anura@fisica.uminho.pt

* Corresponding author: bmari@fis.upv.es

A new class of hybrid material consisting of a mixture of inorganic and organic components is currently leading the way in the search for new multifunctional materials. Such materials are well suited for use in low cost devices for photovoltaic conversion of sunlight. In this context, ZnO is an abundant and cheap material that can be easily synthesized and tailored for hosting several types of organic dyes.

In this work we report on hybrid films based on ZnO/organic dyes prepared by electrodeposition using Tetrasulphonated Copper Phthalocyanines (TS-CuPc) and Eosin-Y (EOY). Both the morphology and porosity of hybrid ZnO films are highly dependent on the type of dyes used in the synthesis. Different morphologies were obtained using TS-CuPc and Eosin-Y in aqueous media. These morphologies, as well as the porosities of the hybrid films, were characterized using SEM, TEM and AFM techniques. Photoelectrochemical methods were used to assess the photosensitivity of the ZnO/dye hybrid films, revealing a high photosensitivity for ZnO/Eosin-Y films and a very weak photoresponse for ZnO/TS-CuPc films.

This study asserts that even if the absorption coefficient of TS-CuPc is much higher than that of Eosin-Y, the energy levels of TS-CuPc do not correlate well with that of ZnO and thus photoelectrons cannot reach the conduction band of ZnO. On the contrary however, in ZnO/Eosin-Y hybrid films, the excited photoelectrons between the Eosin-Y levels can be extracted through ZnO, with the porosity of ZnO/Eosin-Y also easily controlled.

CdSe Quantum dot sensitized solar cells with a CdS capping layer

A.P.Samantilleke^{a*}, L.F.F.F. Gonçalves^b, M.F.Cerqueira^a, M.J.M. Gomes^a, C.J.R Silva^b,

^a Centro de Física, Universidade do Minho, Braga 4710-057, Portugal. ^b Centro de Quimica, Universidade do Minho, Braga 4710-057, Portugal.

(* author for correspondence: anura@fisica.uminho.pt)

In photoelectrochemical cells (PEC), the photon-to-electron conversion efficiency is limited as the majority of the solar spectrum is not absorbed due to the wide bandgap of the TiO₂ (E_g = 3.2 eV) electrode. Dye sensitized solar cells (DSSC) often use TiO₂ as the photoanode (for its stability and its inherent corrosion resistance in aqueous electrolytes), along with dye as a sensitizer in order to extend the absorption into the visible. However, in solar cells, the use of semiconductor nanocrystalline (nc) or quantum dots (QD) as a sensitizer has several advantages over dyes. The absorption spectrum of the solar cell can be tuned to match the spectral distribution of the solar spectrum by controlling the size of nanocrystals, in order to tune the band gap of QDs. Also, nanocrystals possess a large extinction coefficient due to their quantum confinements and intrinsic dipole moments, leading to rapid charge separation. QDSC using nanocrystalline semiconductors such as CdSe, have been used as the light energy harvesting assemblies with some success in TiO₂-based electrodes [1]. Solid state solar cells containing nanocrystalline CdSe have also proven attractive [2]. Therefore, in this work, nc-CdSe was used to fabricate QDSC. Nanoparticle TiO₂ films (~5 nm thick) were prepared using a paste made from Degussa P25 onto the conducting glass substrates. Colloidal CdSe QDs were synthesized by a reverse micelle method and linked through a surface assembly onto a titania (TiO₂) nanoparticle surface. A thin film of CdS was chemically deposited on a QD sensitized TiO₂ photoanode using the established chemical bath deposition and spin coating methods. Room temperature Raman scattering was performed on the samples in order to characterize the microstructure and also to determine the average crystal size of the nanoparticles to complement the optical study. Correlation between the obtained microstructure and properties are made.

The optical absorbance of the pristine CdSe colloidal particles shows a blue shift in the absorption edge with decreasing particle size suggesting a quantum size effect, as the energy bandgap shifts from 1.74 eV (710 nm, bulk) to the observed 2.45 eV (520 nm). The CdSe particle size (diameter), determined by Brus model [3] is about 4.8 nm. The photon-to-electron conversion efficiency (IPCE) of the composite electrode, while employed as the photoanode in a photoelectrochemical cell containing a redox electrolyte and a Pt electrode, was measured. The composite electrode showed higher stability for photocurrent generation than the TiO₂ electrode alone, according to photocurrent transient responses. Furthermore, the effect on the photocurrent of the composite solar cell of the CdS thin coating over QDs and CdSe particle size is discussed in the paper.

Reference

- [1].Eugenia Marti'nez-Ferrero, Ivan Mora Sero', Josep Albero, Sixto Gime'nez, Juan Bisquert and Emilio Palomares, Physical Chemistry Chemical Physics, 12 (12)(2010) 2819.
- [2].HyoJoong Lee,Mingkui Wang, Peter Chen, Daniel R. Gamelin, Shaik M. Zakeeruddin, Michael Grätzel and Md. K. Nazeeruddin, Nano Letters, 9(12)(2009)4221.
- [3].I.Brus, J.Chem. Phys., 80(1984)4403.

EFFECTS OF DRAW RATIO ON THE STRUCTURE AND PROPERTIES OF POLYCARBONATE FILMS REINFORCED BY AN AMORPHOUS POLYAMIDE NANOCOMPOSITE

P. Santamaría, J. I. Eguiazabal, J. Nazabal

Departamento de Ciencia y Tecnología de Polímeros and Instituto de Materiales Poliméricos
"POLYMAT", P^o Manuel de Lardizabal 3, 20018 San Sebastián (SPAIN)
pablo.santamaria@ehu.es

INTRODUCTION

There has been in the recent years an increasing scientific and technological interest in the use of layered clays to improve certain properties of polymeric materials (mainly mechanical, barrier and thermal properties), and it has been established as a very effective route to produce polymer nanocomposites (Nc's) with wide commercial applications.¹ The key to these property improvements is to achieve high levels of dispersion or eventual exfoliation of the clay, so that it is present in the polymeric matrix in the form of platelets with nanometer scale thickness and consequently with high aspect ratios.¹ Recently, the research has been also focused in the use of highly exfoliated Nc's as dispersed phases in different polymer blends to develop ternary systems.²

Packaging is one of the application fields for which Nc's are highly attractive, because the property improvements mentioned before could allow such materials to be employed as innovative solutions to satisfy the demanding requirements. The combination of this technology with that of polymer blends could spread out the applications of the base polymers and lead to the development of new materials with enhanced performance.

Polycarbonate (PC) and amorphous polyamides (aPA) are polymers with wide applications in packaging technology. Besides, aPA based Nc's (nano-aPA) have shown wide exfoliation levels due to the good compatibility of aPA with layered silicates.³ Blends of PC/nano-aPA have been less studied and too little attention has been paid to film extrusion of these blends. The aim of this work is to study the structure and properties of extruded films based on PC/nano-aPA blends and, taking into account the ability of aPA to fibrillate during processing, to establish the effect of the draw ratio (DR) on the fibrillation and the final properties of the films.

EXPERIMENTAL

In a first step, the Nc based on aPA with 4 wt% of organically modified montmorillonite (Nanomer I30) was obtained in the melt state using a co-rotating twin-screw extruder. The resulting Nc was melt mixed with PC to obtain a 75/25 PC/nano-aPA blend. The reference PC/aPA blend without montmorillonite was also processed at the same conditions. The films were obtained by reextruding the blend pellets in a single extruder equipped with a flat die. A water cooled 3-Roller Calender was used to collect the films, and the take-up velocity was varied from 1.5 to 10.5 m/min. The DR was calculated as the ratio of die gap to the final film thickness. Mechanical properties were measured by means of tensile tests in both machine (MD) and transverse (TD) directions. Thermal properties were determined by means of calorimetric analyses. The orientation was evaluated by means of birefringence and the morphology was observed by scanning electron microscopy (SEM).

RESULTS AND DISCUSSION

The obtained films exhibited good surface properties. Films prepared from the PC/aPA blend were colourless and transparent, whereas those of the PC/nano-aPA blend had a yellowish colour with less clarity than the pure blend. The phase behavior of the blends, studied by DSC, showed two clear Tg's at the positions of the pure components, indicating the presence of two pure amorphous phases.

Figure 1 shows SEM photomicrographs of the cryogenically fractured surfaces of PC/aPA (Figure 1a) and PC/nano-aPA (Figure 1b) films at low DR. As can be seen, the dispersed phase size was in both cases very small. As can also be seen comparing Figure 1a and Figure 1b, the presence of clay in the dispersed phase did not appear to modify the compatibility between the PC and aPA.

With respect to the mechanical performance, Figure 2 shows the tensile modulus of PC/aPA and PC/nano-aPA films as a function of DR in both the MD and the TD. As can be seen, the modulus in the

MD was around 1.5 GPa higher than in the TD. As the DR increased, the modulus in the MD slightly increased whereas that in the TD remained invariable. This behaviour is consequence of the uniaxial orientation of the polymer chains during stretching. Figure 2 also shows higher modulus in the PC/nano-aPA films in both the MD and the TD, indicating the reinforcing effect of the clay presence in the dispersed phase of the blend. The yield stress was also higher in the PC/nano-aPA blend, due to the contribution of the clay, and increased with the DR.

Acknowledgements: The financial support of the Spanish "Ministerio de Ciencia e Innovación" (project n. MAT2007-60153) is gratefully acknowledged. P. Santamaría also acknowledges the grant awarded by the Basque Government.

References

- [1] D. R. Paul, L. M Robeson, *Polymer*, **49 (15)** (2008) 3187.
 [2] I. Goitisoló, J. I. Eguiazabal, J. Nazabal, *Composites Science and Technology*, **70 (5)** (2010) 873.
 [3] Y. Yoo, D. R. Paul, *Polymer* **49 (17)** (2008) 3795.

Figures

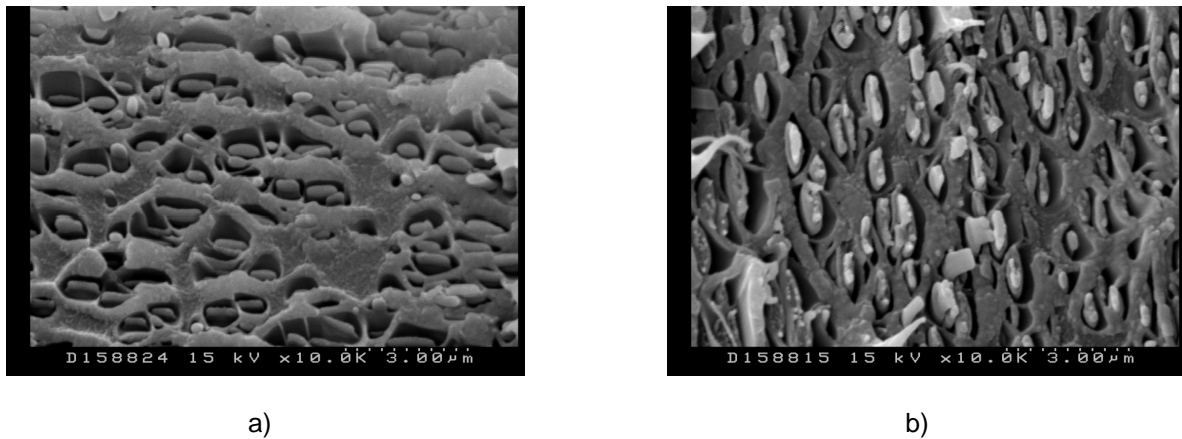


Figure 1. SEM photomicrographs of cryogenically fractured surfaces of PC/aPA (Figure 1a) and PC/nano-aPA (Figure 1b) films at low DR.

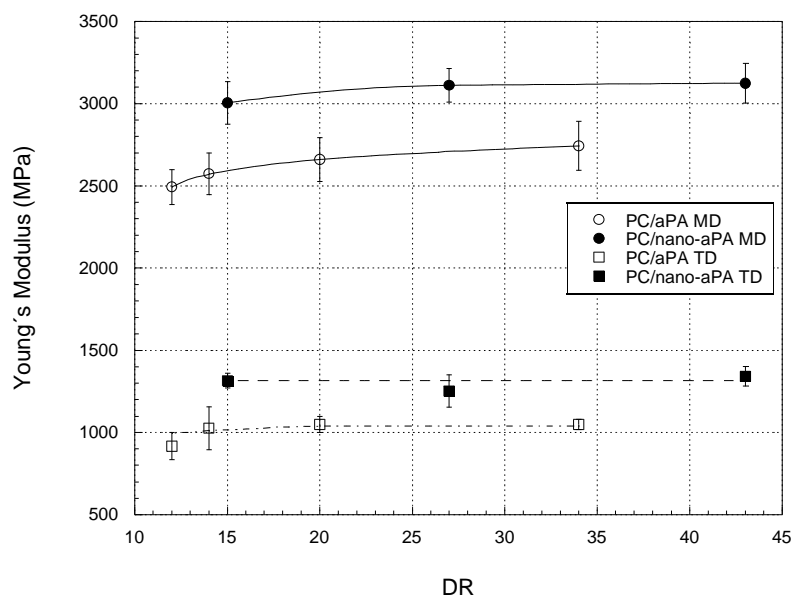


Figure 2. Tensile modulus of the PC/aPA and PC/nano-aPA blends as a function of the DR in both the MD and the TD.

Long term oxidization and phase transition of InN epitaxial nanotextures

E. Sarantopoulou^(a), Z. Kollia^(a), G. Dražič^(b), S. Kobe^(b),

^(a) National Hellenic Research Foundation, 48 Vassileos Constantinou Avenue, Athens 11635
Greece.

^(b) Josef Stefan Institute, Department of Nanostructured Materials

Jamova 39, 1000 Ljubljana Slovenia

esarant@eie.gr

The long term oxidization (aging) of hcp-InN (wurtzite, InN-w) epitaxial nanotextures synthesized on Si substrates is analyzed. The densely packed layers of InN-w nanotexture (5-100 nm), were eventually oxidized by atmospheric oxygen through the formation of an intermediate amorphous In-O_x-N_y (indium oxynitride) phase, directly identified with high resolution transmission electron microscopy.

The hcp-InN single-phase nanotexture was continuously transforming to a bi-phase alloy hcp-InN /bcc-In₂O₃ texture. The oxidization process is associated to the large accumulation of charges on the periphery of nanotextures, which increases the reactivity of oxygen locally.

Using energy-dispersive X-ray spectroscopy and selected area electron diffraction, it was found that the concentration of bcc-In₂O₃ phase in the alloy, was higher at the texture areas of small size (~5nm) in comparison to the larger texture dimensions (>30nm).

Visibility enhancement of Graphene on multiple substrates

Peter Schellenberg¹, Michael Belsley¹, Hugo Gonçalves¹, Cacilda Moura¹, Tobias Stauber²

¹Center of Physics, University of Minho, Campus de Gualtar, 4710-057 Braga, Portugal

²Department of Condensed Matter Physics, University Autónoma of Madrid,
Campus of Cantoblanco, E-28049Madrid, Spain

peter.schellenberg@fisica.uminho.pt

In order to take advantage of the enormous potential of graphene for future electronic micro-circuits, nanophotonic assemblies, coatings and other microstructured graphene based devices, it is essential to develop graphene visualization techniques, which reliably and rapidly deliver images of graphene and graphene based structures.

A multitude of optical techniques have been put forward to this end, for example based on the exploitation of refractive index differences. Several imaging methods are based on Raman and Rayleigh scattering, or on fluorescence quenching of dyes by graphene layers. Generally these methods require relatively complex equipment or an optimized substrate coating. Here, we report on two novel and easy to use techniques for the identification of potential graphene flakes.

One technique aims to increase the contrast of the graphene and multilayer graphene structures by reducing background intensity by using immersion microscopy. The second technique exploits hydrophobicity differences between substrate and graphene structures to enhance their visibility. This second method can be employed to quickly and easily visualize graphene and few-layer graphite on a wide variety of substrates without the need for any specific surface modification or preparation. To our knowledge, there is no other currently available method that is capable of readily visualizing graphene flakes on plastic surfaces, untreated dielectrics and uncoated metals.

Optical probe of quantum shot noise reduction at a single atom contact

Natalia L. Schneider¹, Guillaume Schull², and Richard Berndt¹

¹ Institut für Experimentelle und Angewandte Physik,
Christian-Albrechts-Universität zu Kiel,
D-24098 Kiel, Germany
nschneider@physik.uni-kiel.de

² Institut de Physique et Chimie des Matériaux de Strasbourg,
UMR 7504 (CNRS - Université de Strasbourg),
67034 Strasbourg, France

Visible and infra-red light emitted at a Ag-Ag(111) junction has been investigated from tunneling to single atom contact conditions with a scanning tunneling microscope. The light intensity varies in a highly nonlinear fashion with the conductance of the junction and exhibits a minimum at conductances close to the conductance quantum. The data is interpreted in terms of current-noise at optical frequencies, which is characteristic of partially open transport channels.

Molecular simulation of Dendritic Core-Multi-Shell (CMS) Nano transporter

Amir Sedighi^{a,b}, Marcus Weber^a, Peter Deuffhard^a, Monika Schäfer-Korting^b

^aKonard-Zuse -Zentrum für informationstechnik Berlin, Computational Molecule Design
Group, Berlin, Germany

^bInstitute of Pharmacy, Pharmacology and Toxicology, Freie Universität Berlin, Germany

Email: sedighi@zib.de

Our research focused on molecular simulation of Core Multi-Shell (CMS) Nano transporter. CMS is a novel nano transporter with lots of compatibilities that makes this nano carrier distinct from the others.

Limited matrix compatibility is one of the basic problems of such a carrier systems. They can either transport non-polar molecules into an aqueous environment or, if the system relies on inverted micellar architecture, transfer polar molecules into a hydrophobic environment such as an organic medium. Therefore, the generation of nano compartments that are compatible with various environments such CMS should solve many solubility and stability problems of active agents.

New multi shell design and properties are based on a hyperbranched polymeric core surrounded by double layered shells. This type of system can encapsulate and transport a wide variety of compounds ranging from non-polar to ionic molecules in a broad matrix spectrum including non-polar and polar organic as well as aqueous environments. This CMS consist of three different part, Poly Glycerol (PG) Core which is hydrophilic, surrounded by hydrophobic parts of alkyl chain and monomethyl poly ethylene glycol (mPEG). Single size of this structure is about 8-10 nm and when it gets aggregated as a carrier in a different size between 20-50 nm.

To simulation of this novel nano carrier, Molecular Dynamic in Gromacs and methods of Conformational dynamic has been used. All the simulations are in (NVT) ensemble. Single parts of the structures and Surface simulated with the solvent (water) and intended drug(Morphine) is also located into the simulations. For the preliminary results and progressing the coarse-grained model, the morphine location on the CMS Nano carrier has been detected by calculating Free energies and entropies of morphine in different places of the structure.

References:

1. M. Klimm, A. Bujotzek, M. Weber: Direct Reweighting Strategies in Conformation Dynamics, MATCH Comm. Math. Comp. Chem., accepted for publication, 2010
2. S. Kuchler, M. Radowski, T. Blaschke, M. Dathe, J. Plendl, R. Haag, M. SchäferKorting, K. Kramer: Nanoparticles for skin penetration enhancement – A comparison of a dendritic coremultishell nanotransporter and solid lipid nanoparticles, Eur. J. Pharm. Biopharm., 2009, 71(2):243250
3. E. Burakowska, R. Haag, Dendritic polyglycerol coredoubleshell architectures: Synthesis and transport properties, Macromolecules, 2009, 42, 55455550,
4. A. Bujotzek, M. Weber: Efficient Simulation of ligandreceptor bindingprocesses using the conformation dynamics approach, J. Bioinf. Comp.Biol. (accepted), April 2009.

Figures:

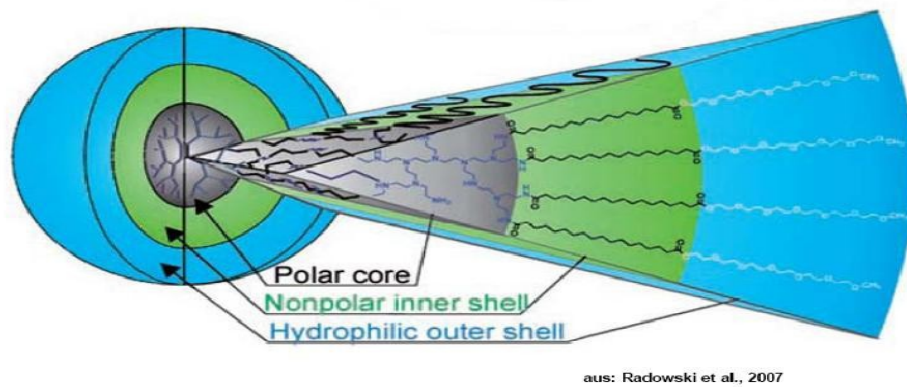


Figure-1: Single structure of CMS which content of three different parts; Two Polar and a Non polar in the middle of the structure.

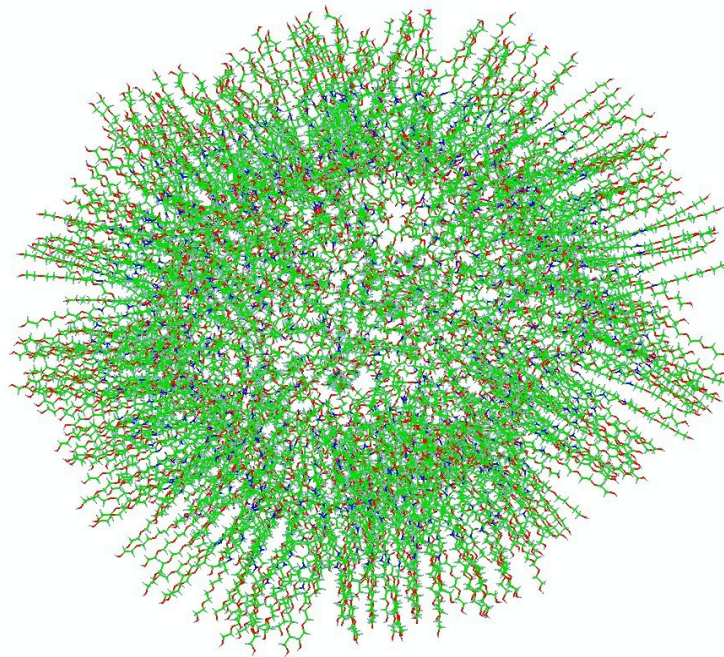


Figure-2: CMS coarse-grained model

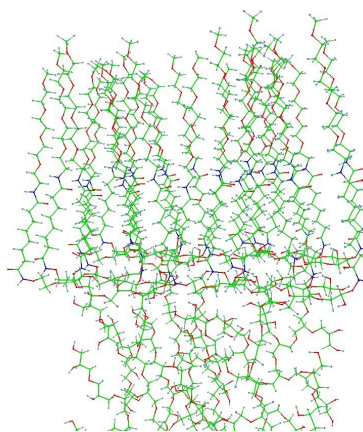


Figure-3: Surface model of CMS

4e transport of a supercurrent in two-contact SQUID with anharmonic by current - phase dependence

Sergeyev D.M.

*Aktobe State Pedagogical Institute, avenue Moldagulova 34 A, Aktobe, Kazakhstan
serdau@rambler.ru*

New materials nanoelectronics – Josephson junction (JJ) with anharmonic by current - phase dependence (ACPD) recently are intensively investigated [1]. JJ with ACPD have a number of features in comparison with "traditional": occurrence half-integral of steps Shapiro on current-voltage characteristic (CVC) at influence of a microwave of a signal, increase of size of plasma frequency, supervision of a minimum quantum interference at fractional meanings of the normalized magnetic flow [2,3] etc. However these phenomena of the strict proof have not found.

In the given work is considered two-contact SQUID with ACPD. In anharmonic SQUID each junctions JJ_1 , JJ_2 is possible to consider as set two JJ $JJ_1' + JJ_1''$, $JJ_2' + JJ_2''$, describing by functions (fig. 1):

$$j_{s1}(\varphi) = j_{c1} \sin \varphi + j_{c2} \sin 2\varphi, \quad j_{s2}(\varphi) = j_{c3} \sin \varphi + j_{c4} \sin 2\varphi, \quad (1)$$

$$j_{c2} = k \cdot j_{c1}, \quad j_{c4} = k \cdot j_{c3}, \quad (2)$$

where j_{s1} , j_{s2} – supercurrents JJ_1 , JJ_2 , k – coefficient (factor) anharmonicity ($k < 1$).

In work [4] was theoretically predicted, that in a chain of four JJ, placed in a cross magnetic field, the pairing superconducting (Cooper) pairs and their transport (4e-transport) through weak links takes place.

Let's consider, anharmonic two-contact SQUID representing as four JJ (fig. 1) and for the description we use the theory 4e of transport of a supercurrent. In our opinion, in anharmonic JJ besides 2e of transport, takes place 4e transport of a supercurrent. Anharmonic part of a supercurrent creates condition for pairing Cooper pairs (for 4e transport of a supercurrent), then expression (1) is possible to present as:

$$j_s(\varphi) = j_{2e} \sin \varphi + j_{4e} \sin 2\varphi. \quad (3)$$

For calculation of effective potential SQUID with anharmonic by current - phase dependence have taken advantage of expression for four JJ, closed a kind of a rhombus, the kind of effective potential is submitted in a fig. 2 a [4]. As it is visible, in 2e a mode the tunneling occurs on short ways (red lines), and in a mode 4e on long (green lines). However existence 4e of transport of a current does not forbid to existence 2e to a mode. At reduction of factor anharmonicity $k \rightarrow 0$, is suppressed 4e transport of a current, i.e. coupled Cooper of pair is split on 2 pairs.

The existence 4e of transport of a supercurrent, well describes experimental results.

In a mode 2e of transport of a supercurrent of a step Shapiro arise on CVC as a result of the appendix to them of external microwaves of signals with frequency f at voltage:

$$V_{2e} = \frac{\hbar}{2e} \frac{d\varphi}{dt} = \frac{\hbar}{2e} \cdot 2\pi f = \Phi_0 f. \quad (4)$$

There is a capture Josephson of frequency by external frequency.

In a mode 4e of transport of a current at presence anharmonicity by current - phase dependence means replacement $2e \rightarrow 4e$, i.e. the steps Shapiro owe to be shown twice more often at voltage:

$$V_{4e} = \frac{\hbar}{4e} \frac{d\varphi}{dt} = \frac{\hbar}{4e} \cdot 2\pi f = \frac{\Phi_0}{2} f = \frac{V_{2e}}{2}. \quad (5)$$

Feature SQUID with ACPD is at influence of a magnetic flow (quantum interference) occurrence of minima in half-integral (fractional) meanings $\Phi = \frac{\Phi_0}{2} = \frac{\hbar}{4e}$, which is caused $4e$ by transport of a current (fig. 2, b).

Thus, is established, that in SQUID with anharmonic by current - phase dependence the pairing Cooper of pairs and $4e$ transport of a supercurrent takes place. $4e$ transport of a current essentially influences properties SQUID. Response on influence of a magnetic field in another way, gives an opportunity to create new magnetic nanofacility on SQUID with anharmonic by current - phase dependence.

References:

- [1] I. N. Askerzade, Technical Physics Letters, **17** (2007) 10-15.
- [2] D. M. Sergeyev, and K. Sh. Shunkeyev, in: Proceeding 3rd International Conference Fundamental Problems of HTSC, Moscow – Zvenigorod, Russia, (2008) 344–345.
- [3] D. M. Sergeyev, Izvestija vuzov. Physics **9/2** (2008) 208–210.
- [4] L. B. Ioffe, and M. V. Feigel'man, Phys. Rev. B, **22** (2002) 224503.
- [5] B. Doucot, and J. Vidal, Phys. Rev. Lett. **22** (2002) 227005.

Figures:

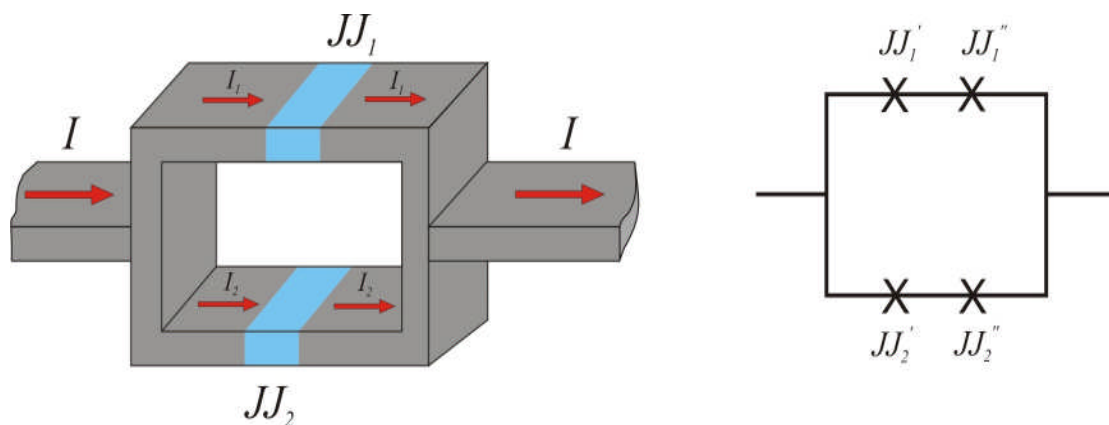


Figure 1 - Two-contact SQUID with anharmonic by current - phase dependence

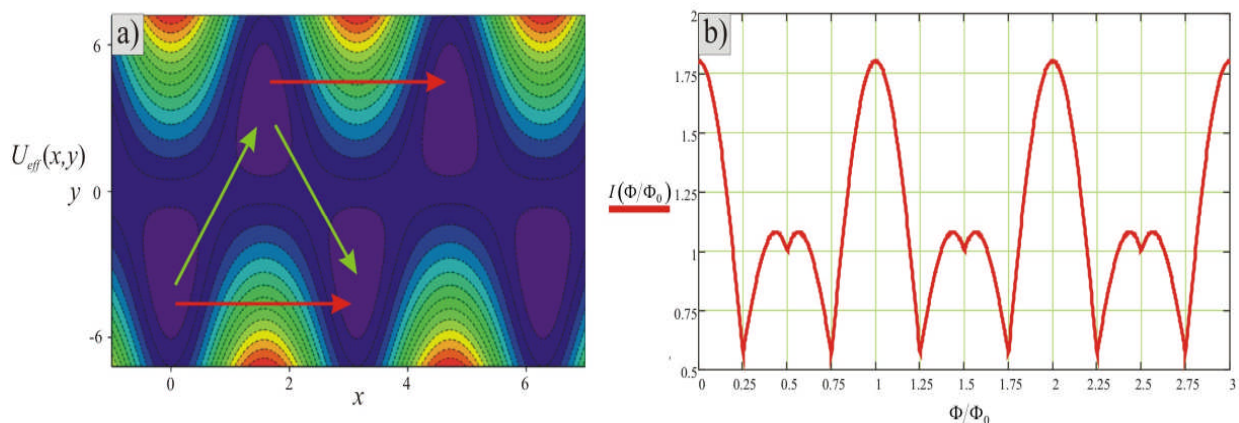


Figure 2 - a) Effective potential JJ with anharmonic by current - phase dependence, b) Dependence a supercurrent-magnetic flow in anharmonic SQUID

Formation and properties of iron nanoparticles for nucleating CNTs in floating-catalyst chemical vapor deposition process

Jing Shen, Jinbo BAI

Laboratory of Mechanics of Soils, Structures and Materials,
CNRS UMR 8579, Ecole Central Paris, 92295 Chatenay-Malabry, France
Email: reearth2008@gmail.com

1. Introduction

For the ultimate goal of being capable of growing CNTs with specific chirality by wisely manipulating the growth conditions, a thorough understanding of CNT growth mechanisms, especially the role of metal catalyst is required. Despite the wealth of information on catalyst's morphology, chemical composition, and aggregate state obtained from in-situ experiments and theoretical calculations, there is still a lack of studies on the initial stage of CNT nucleation with the presence of metal particles. In this work, the formation and properties of iron nanoparticles (NPs) for nucleating CNTs in floating-catalyst chemical vapor deposition (CVD) process is studied by first-principle Density-Functional Theory (DFT) calculations. A schematic of this process is depicted in Fig 1. For comparison, we first calculated the properties and formation process of small iron NPs with atom numbers up to 20. Then in the next step we calculated the interactions between iron atoms and carbon atoms or small molecules like C_6H_6 . As a result, we are able to predict the formation process of iron NPs in the gas phase far from supersaturation, and we could also predict the possible nuclei for CNT growth.

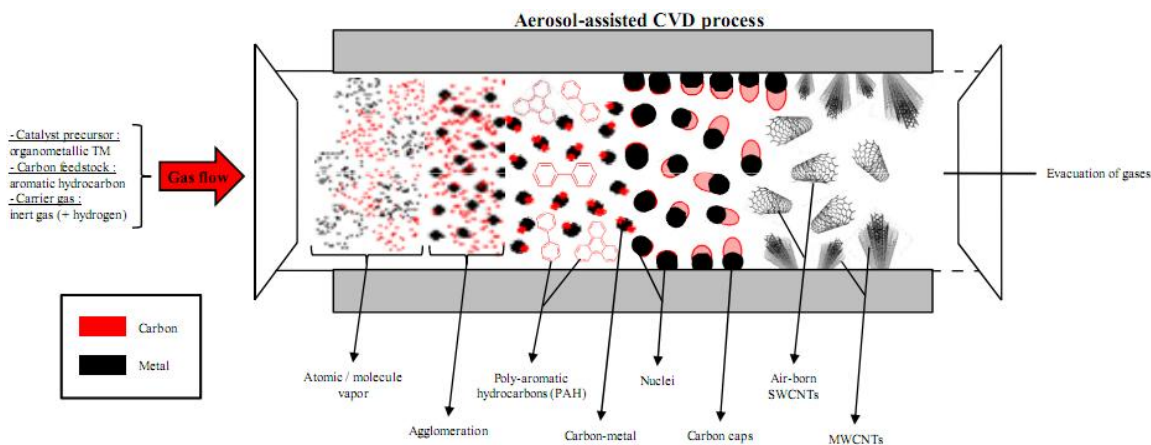


Fig 1. Schematic of floating-catalyst CVD process for growing CNTs.

2. Computational details

The DFT computational scheme implemented in the SIESTA code uses numerical atomic orbitals as basis sets to solve the single-particle Kohn-Sham equations. In these calculations, we used a double-zeta basis with single-zeta polarization functions, with orbital confinement energy of 0.001 Ry in order to achieve linear scaling. The core electrons were represented by nonlocal, norm-conserving Troullier-Martins pseudopotentials factorized in the Kleinman-Bylander form. Fe pseudopotential is generated by relativistic atomic calculations with nonlinear core corrections to account for the large overlap of the core charge with the $3d$ orbitals of Fe. Here we use the valence configuration $3d^74s^1$ to generate atomic Fe pseudopotential. For carbon, non-relativistic atomic calculations without core corrections are implemented to the ground-state configuration of carbon. Both pseudopotentials have been thoroughly tested for transferability in various configurations. Our calculations were performed within Generalized Gradient Approximation (GGA) for the exchange-correlation potential as parameterized by Becke gradient exchange functional and Lee, Yang, Parr correlation functional. We used a supercell geometry with a $30\text{\AA} \times 30\text{\AA} \times 30\text{\AA}$ unit cell, and a 200 Ry cutoff to define the finite real space grid for numerical integration.

3. Results and discussion

3.1. Results for pure iron clusters with atom numbers up to 20

Studies on the formation of metal clusters from supersaturated metal vapor have shown that the size

distribution of small metal clusters (with atom number $n \leq 20$) is determined not only by the growth statistic, but also depends on the stability of the clusters. However, in a typical floating-catalyst CVD process for CNT synthesis, as a rough estimate, the number density of Fe atoms in the gas phase is at least 100 times lower than in supersaturated metal vapor. Therefore, studying the structures and properties of small Fe particles is of great importance for understanding their formation and catalytic effects in CNT growth process. For comparison, small and pure Fe particles have been studied by first principle DFT calculations. Their lowest-energy structures were obtained by choosing various initial configurations and relaxing them using a conjugated gradient method. Fig 2 shows the most stable structure of a Fe_{19} particle.

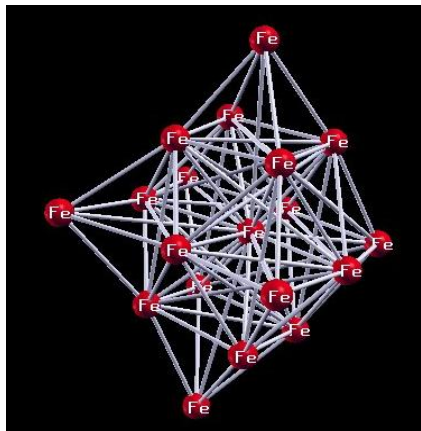


Fig 2. Most stable structure of Fe_{19} .

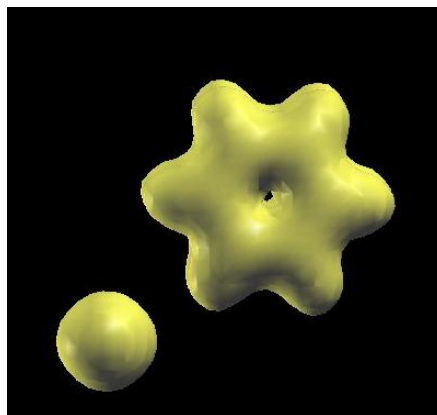


Fig 3. Relaxed configuration of Fe atom-benzene molecule system.

3.2 The interaction between Fe atoms and C atoms/molecules

Theoretical and experimental studies have shown that, in CNT growth condition, catalyst precursors like ferrocene quickly break down to release Fe atoms and other small carbon molecules like C_2 , C_3 , etc. Moreover, carbon molecules like C_2H_2 thermally break down to give C_6H_6 and C_4H_4 molecules. As the result of complex chemical and physical reaction in the gas phase, Fe particles gradually form and catalyze CNT nucleation. Therefore by unraveling these gas-phase reactions using DFT calculations, the mechanisms of Fe particle formation and catalysis in nucleating CNT can be explicitly explained. Fig 3 shows the interaction between a Fe atom and a benzene molecule.

4. Conclusion

In floating catalyst CVD of CNTs, iron NP formation is more complex than in condensation of supersaturated iron vapor. The chemical and physical reactions between Fe atoms and C atoms/molecules determine the nucleation of Fe particles and their ability to nucleate CNTs.

Development of photocatalytic nanomaterials for pollution control, using thin film deposition techniques (*sol-gel*, PVD)

L.F. Oliveira, P.J.G. Coutinho, C.J. Tavares

Centre of Physics, University of Minho, Braga, Portugal

filipasoliveira@gmail.com

The aim of this study regards the development of photocatalytic titanium dioxide (TiO₂) based nanomaterials for pollution control. Particularly, by synthesizing nanostructured coatings using physical vapor deposition (PVD) and Langmuir-Blodgett (LB) deposition techniques.

These materials have a good hydrophilicity and an optimum photocatalytic efficiency, when comparing to a commercial standard. Therefore, this self-cleaning capability foresees potential applications in the building materials, particularly for ceramic panels (tiles, bricks) and glass panes [1].

The PVD thin films were produced in reactive sputtering mode, using a pure titanium target in a atmosphere of Ar/O₂:N₂, whereas the LB thin film deposition consisted in using a water floating monolayer of TiO₂ nanoparticles in a matrix of DTAB or CTAB surfactant.

The photocatalytic efficiency was evaluated by monitoring the degradation of an organic dye (Methylene Blue 0.1 μM) following an irradiation with UV-A light in the presence of the photocatalyst.

For the PVD films, it was possible to correlate the relationship between the working gas flow (argon) used during the deposition and the first-order rate constant (*k*) for the degradation of the dye [2].

It was found that for the PVD films produced with an argon flow of 275 sccm a better photocatalytic performance was attained, with a first-order rate constant equal $2.6 \times 10^{-3} \text{ min}^{-1}$. (figure 1). This evidence can be ascribed that for a higher deposition pressure a subsequent enhancement of porosity in the films is achieved, resulting in a larger surface area for the dye (pollutant) adsorption. Furthermore, the thickness of the films increases up to a threshold of 275 sccm, decreasing afterwards due to the decrease in mean free path of the impinging flux on the substrates during deposition and inherent inhibition of adatom mobility. The optical band-gap was determined from Tauc plots and was calculated to be 3.18 eV for the best coatings. The crystallinity of these films was characterized by X-ray diffraction (XRD) and the results show that anatase is the polymorph phase which is more stable and provides better photocatalytic efficiency (figure 2) [3].

The TiO₂ nanoparticles obtained by sol-gel method were characterized by dynamic light scattering (DLS) and scanning electron microscopy in transmission mode (STEM). These results yield evidence that the nanoparticles are spherical and have size distributions centered between 100 and 400 nm, as seen in figure 3.

References

[1] T. Tölke, A. Kriltz, A. Rechtenbach, *Thin Solid Films*, 518, **2010**, 4242–4246.

[2] C. J. Tavares, S. M. Marques, T. Viseu, V. Teixeira, J. O. Carneiro, E. Alves, N. P. Barradas, F. Munnik, T. Girardeau, J.-P. Rivière, *Journal of Applied Physics*, 106, **2009**, 113535;

[3] N. R. Mathews, E. R. Morales, M.A. Cortés-Jacome, J.A. Toledo Antonio, *Solar Energy*, 83, **2009**, 1499–1508.

Figures

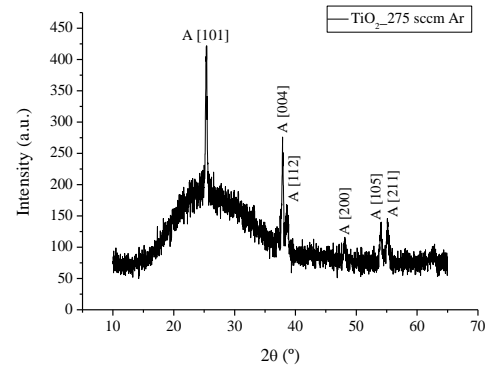
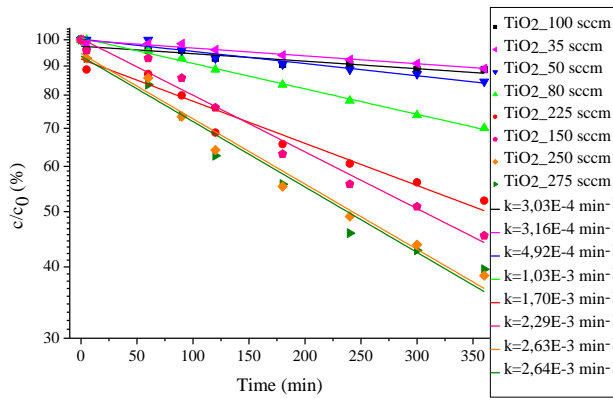


Figure 1 - Relative decrease in Methylene Blue concentration as a function of UV-A irradiation time for titania thin films deposited by sputtering with varying argon (working gas) flow rate.

Figure 2 - XRD pattern for titania thin film deposited with a 275 sccm flow of argon.

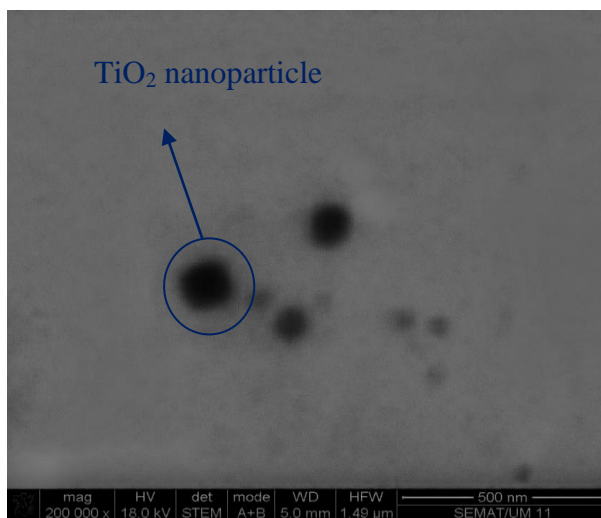


Figure 3 - Scanning electron microscopy image acquired in transmission mode (STEM) for the TiO₂ nanoparticles produced by sol-gel method.

Acknowledgements

The authors kindly acknowledge the financial support from the Portuguese FCT scientific program NANO/NTec-CA/0046/2007.

Sputter-Deposition of Copper Nanoparticles onto Granular Polymeric Spacers for Enhancing Cell Wall Structure of Sintered Highly Porous Aluminum Materials

Tsutomu Sonoda, Kiyotaka Katou

National Institute of Advanced Industrial Science and Technology (AIST), 2266-98 Anagahora, Shimoshidami, Moriyama-ku, Nagoya 463-8560, Japan
tsutomu.sonodat@aist.go.jp

Powder metallurgy processing has become more important in recent years, because not only higher performance in quality, reliability or durability, of metallic materials but also smaller amount of resource and energy necessary for fabricating the materials have been more earnestly demanded from the standpoint of environmental protection. In the conventional powder metallurgy processing, however, some inhomogeneous distribution of additive metallic elements over the alloy matrix is inevitable, because its approach is based on mixing additive metal powder with basic metal one. Hence it can be noted that the coated powder approach significantly decreases the inhomogeneous distribution of additive metallic elements over the alloy matrix [1], where the basic metal powder is coated with the additive metal film instead of mixing the additive metal powder with the basic metal one. Moreover, making use of this coated powder approach, it is also expected that the powder coated with the additive metal film can be sintered at lower temperature than the powder non-coated with the metal film, in case that the melting point of the film metal is lower than that of the powder metal.

On the other hand, cellular metallic materials can be also fabricated in the powder metallurgy processing by combining with a space-holder method. And it is noted that the mechanical properties or the compressive properties in particular of the cellular metallic materials are influenced by their cell wall structures. Hence it is expected that the compressive properties of cellular metallic materials fabricated in the powder metallurgy processing could be improved by enhancing the cell wall structures of the sintered porous compacts. In the present work, therefore, the deposition of copper onto acrylic resin powder in its self-convective motion [2-7] by magnetron DC sputtering was examined in order to prepare granular polymeric spacers coated with the metal, aiming at enhancing the cell wall structure of sintered highly porous aluminum materials. Furthermore the effects of the sputter-deposition of copper onto the spherical polymeric spacers on cell wall structures of the sintered porous compacts were investigated. The schematics for the enhancement of the cell wall structures in sintered porous compacts are shown in Fig.1, compared with an ordinary non-enhanced cell wall structure.

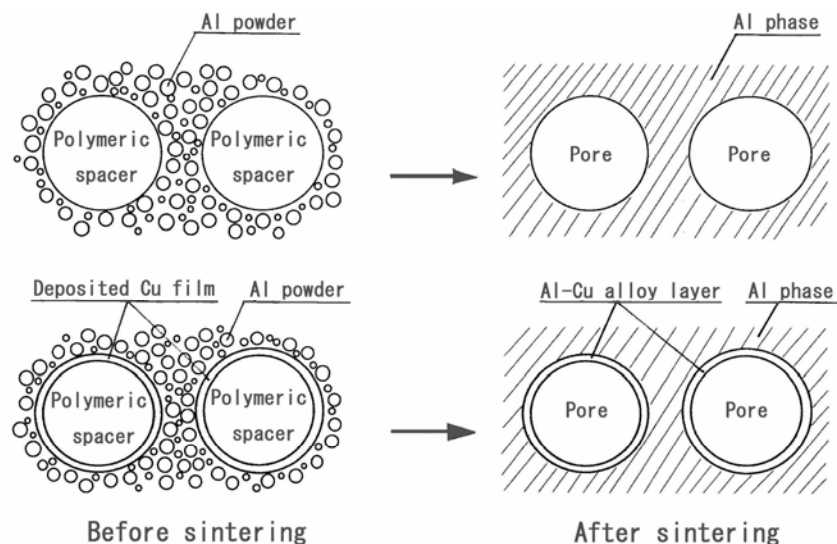


Figure 1. Schematics for the enhancement of the cell wall structures in sintered porous compacts shown in the downside, compared with that for an ordinary non-enhanced cell wall structure shown in the upside.

A vibrating-source for applying perpendicular vibration to the acrylic resin powder developed in order to perform so-called “powder-coating” in this study. A planar magnetron DC sputtering system (ANELVA Corp. type SPF210H) with a 200-mm diameter and 130-mm height stainless steel chamber was used.

The vibrating-source was installed onto a substrate holder of the sputtering system. A planar magnetron sputtering system (ANELVA Corp. type SPF210H) with a 200-mm diameter and 130-mm height stainless steel chamber was used. A planar target used for this study was a 100-mm diameter pure copper (Cu) disk. Acrylic granules (particle size: around 300 μ m in diameter, 3.03 g) was put onto the stainless petri-dish, which is mounted on the substrate holder and can be vibrated with the amplitude of 1mm at the frequency of 10Hz in the vacuum chamber. The self-convection phenomenon of the titanium powder occurred in the vacuum chamber evacuated to 5 \times 10 Pa when a perpendicular vibration was applied to the powder. Argon gas was introduced at a desired flow rate into the vacuum chamber evacuated to 1 \times 10⁻² Pa or less.

The sputter-deposition of the copper film onto the titanium particles was carried out during the self-convection of the acrylic powder. The sputtering conditions examined in this study were as follows. Discharge voltage and current were fixed at 420V and at 0.1A, respectively. The argon flow rate was fixed at 15.0 ml/min, where the gas pressure in the chamber was regulated at 22 Pa by adjusting the exhaust through the main gas valve. The deposition time for sputtering was fixed for 30 min.

Then the fabrication of porous aluminum materials was carried out in an ordinary powder metallurgy processing combined with a space-holder method using the prepared Cu coated acrylic powder in ordinary powder metallurgy processing. The tablets with 20mm in diameter were made of the pure aluminum powder mixed with a desired amount of the Cu coated acrylic powder as a space-holder, by being pressed in a cylinder with a piston. Both tablets consisting of the coated acrylic powder were pre-sintered at 400 degree centigrade for 2 hours in an argon atmosphere for the sublimation of the resinous spacer material and then sintered at 650 degree centigrade for 2 hours in a vacuum.

The effects of the sputter-deposition of copper onto the granular polymeric spacers on cell wall structure of the sintered porous aluminum materials were investigated. The porous structure of the obtained sintered compacts was observed by SEM. On the other hand, the distribution of copper atoms in the cellular aluminum materials was measured by qualitative analysis using an EPMA.

Under visual observation, the color tone of the acrylic powder obtained after the sputter-deposition looked red brown or coppery, i.e., the color tone of sputtered pure copper deposits, while that before the sputter-deposition had looked white or semi-transparent, i.e., the color tone of the acrylic powder. Thus it was assumed that the acrylic powder was coated with the copper deposits. Figure 2 shows typical optical micrographs of the acrylic resin granules before the sputter-deposition and those obtained after the sputter-deposition. The surface of the obtained granules appeared to be covered with deposited copper thin film without any peelings. Thus it was confirmed that the sputtered copper could be adherently deposited onto the surface of the acrylic resin granules.

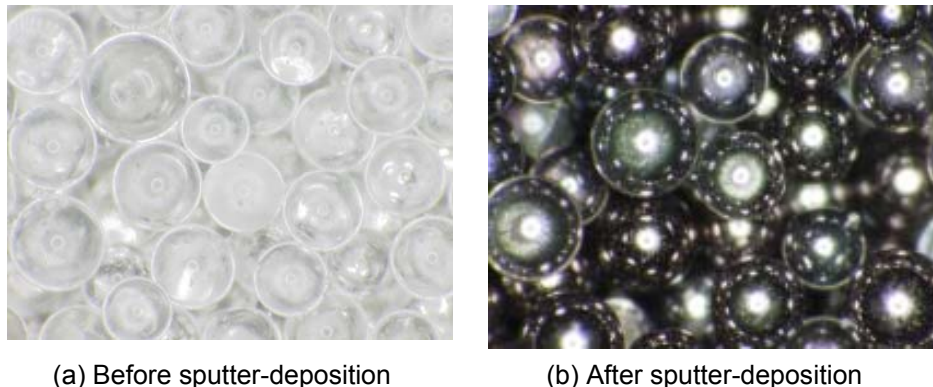


Figure 2. Optical micro-graphs of the acrylic resin granules before the sputter-deposition (a) and those obtained after the sputter-deposition (b).

The sintered compact obtained from the aluminum powder mixed with the copper sputter-deposited acrylic resin powder was solid and uniform, and its porosity was around 70%. Under the SEM image, it was found that the porous structure of the sintered aluminum compacts consisted of a cell structure with spherical pores of several hundred micro-meters in diameter. According to EPMA analysis, K α X-ray peaks for Cu atoms as well as those for Al atoms were definitely detected on at the vicinity of the cell walls, while those only for Al atoms was detected on the matrix area. Thus it was found that Cu atoms were distributed at the vicinity of its cell walls, concluding that cell wall structures could be enhanced by this processing.

Alteration in Structure of Nanometer Films of Polymethine Dyes

Anton Starovoytov, Elena Kaliteevskaya, Valentina Krutyakova, Tatyana Razumova

St. Petersburg State University of Information Technologies, Mechanics and Optics
49 Kronverkskiy pr., St. Petersburg, Russia
Anton.Starovoytov@gmail.com

The regularities responsible for the component composition and spectral parameters of thin films of polyatomic organic molecules on glass are described. Changes in the component composition of the film and in the spatial orientation of its components induced by laser radiation or heating are explored.

A priority direction in science and engineering related to nanophotonics requires the development, research, and application of new optical materials. Organic nanostructures (molecules and aggregates), along with traditional nanoparticles (semiconducting, carbohydrate, and metallic), are also of interest for this purpose. Stable thin solid films of organic dyes are interesting practical objects. Organic films are widely used in photoelectric solar energy converters, as photorefractive and electroluminescent media, and for information recording. A photo-induced irreversible change in the structure and spatial orientation of the nanocomponents with respect to the substrate gives a principal possibility to record and read out long-term information (Write-Once-Read-Many optical memory disk) by non-destructive optical methods.

Objects of study are symmetric polymethine dye belonging to the homologous series. It was found that the equilibrium composition of the polymethine films is determined by the degree of asymmetry induced in the intramolecular electron density distribution by the interaction between cationic molecules and surface negative charges of the substrate. The presence of components (all-trans-isomers, cis-isomers of different type, dimers, and J-aggregates) depends on the surface concentration of polymethine molecules (fig. 1) and electron-donating ability of end heterocyclic groups (Φ), as well on the length of a polymethine chain.

In thin films, two types of the component orientation differing in the orientation angles θ_i of polymethine chain with respect to the normal to the layer surface are present (fig. 2). The molecules with the first type of orientation can change neither the orientation angle nor the component composition. The molecules of the second orientation type, when heated to 120⁰C or exposed to resonance photoexcitation, irreversibly vary both orientation angles and component concentrations (N_i) and finally convert to the layer of the first type (fig. 3). The dissociation of dimers, decrease in the relative concentration of cis-isomers and the increased number of J aggregates and all-trans-isomers are responsible for the above changes. Heating to < 100⁰C causes composition of the layer vary only reversibly and does not affect the orientation angles of its components.

The above results may be explained by the effect exerted by asymmetry of the electron density distribution, which is induced in the course of the interaction between the cationic molecule and the negatively charged substrate, on the equilibrium component composition of the layer. The irreversible reorientation of the molecule with respect to the substrate affects the interaction with the surrounding molecules and the substrate. As consequence, the intramolecular electron density distribution and the equilibrium component composition of the layer corresponding to it change. When orientation is not affected by light or heat, then stereoisomerization and variations of component composition of the layer will be only reversible.

We used the obtained experimental results to suggest the energy model for all-trans isomer reorientation in a symmetric dicarbocyanine dye layers. In the terms of this model, the isomerization of a molecular fragment around the third bond of the chain is the initial stage of the rearrangement.

The photoexcitation mechanism differs from the mechanism of thermal excitation only in the first stage, involving either excited- or ground- state molecule. After completing this stage, both thermally and photoexcited molecule is in the same intermediate ground-state configuration, with all subsequent stages for thermally and photo- induced rearrangement the same.

The above mechanisms differ by the height of the isomerization barrier and by the temperature of layer, which determine the probability and yield of the isomerization and the relative yields from the intermediate to the initial configuration (layer of type 2) or from the intermediate to the rearranged configuration (layer of type 1).

Figures

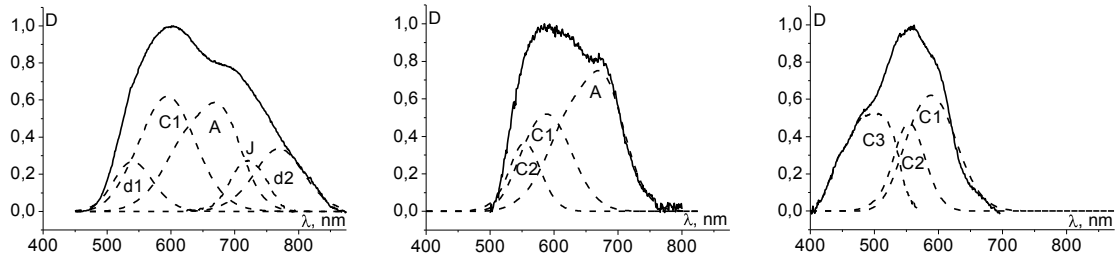


Figure 1: The normalized absorption spectra of symmetric dicarbocyanine dye layers ($\Phi = 57^\circ$) and the spectra of molecular components of the layers spin-coated on glass. Maximum optical absorption density D_{\max} : 0.0405 (left), 0.0052 (center), and 0.0027 (right).

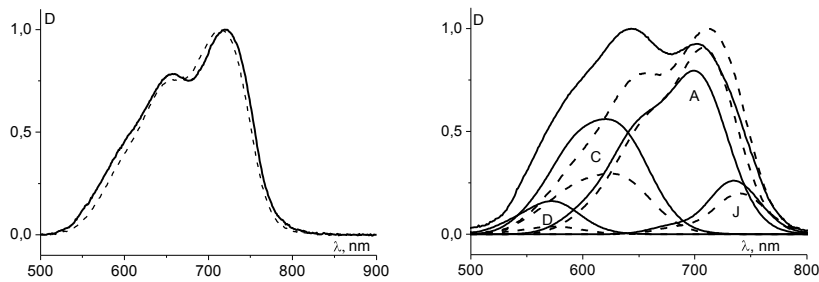


Figure 2: Absorption spectra of symmetric dicarbocyanine dye layers ($\Phi = 45^\circ$) of types one (left) and two (right) with the average electron-donating ability before (solid line) and after (dashed line) the exposure to the single-pulse radiation from a ruby laser.

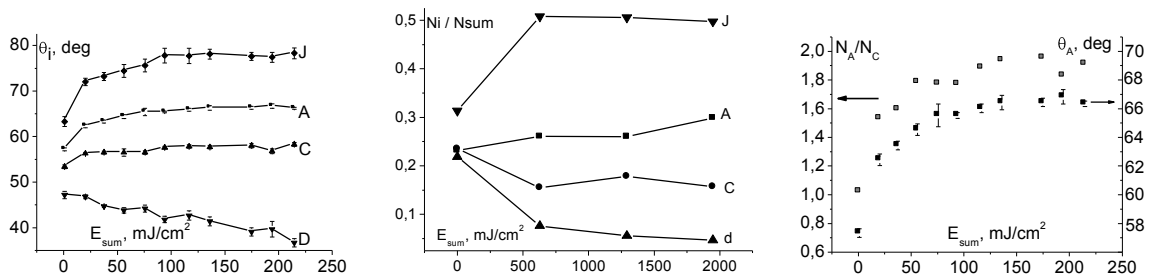


Figure 3: The orientation angles (left, right) and the relative concentration of layer components (center, right) vs. the total energy of excitation by a single-pulse ruby laser radiation. Symmetric dicarbocyanine dye layer ($\Phi = 45^\circ$).

Surface studies to improve graphene growth on 4H-SiC for nanoelectronics

Andrew J Strudwick, Graham L Creeth, Christopher H Marrows

School of Physics and Astronomy, University of Leeds, Leeds, LS2 9JT, United Kingdom
phy4ajs@leeds.ac.uk

Since being successfully isolated in 2004, there has been a great rush to produce large areas of high quality graphene. This has been caused by the unusual physical and electronic properties of graphene. The high electron mobilities and high electron velocity coupled with its structural stability make graphene an ideal candidate for post-CMOS development. To allow graphene to be used in this capacity commercially wafer-scale areas of good quality graphene material need to be produced. A technique which shows promise in this development is the thermal decomposition of silicon carbide substrates [1, 2]. In this work studies of this growth technique have been carried out for varying annealing times and temperatures in both UHV ($<10^{-10}$ mbar) and at a higher partial pressure by the use of an alumina cap situated at a small separation above the 4H-SiC chip.

Low energy electron diffraction (LEED), Raman microscopy and Atomic Force Microscopy (AFM) have been used to characterize these samples. LEED carried out is used to indicate the onset of graphene growth on the C-terminated face of silicon carbide by the presence of a ring pattern, which is associated with the turbostratic nature of the graphene growth on the C-terminated face.

Raman data shows the annealed samples to be carbon rich, as identified by the presence of the D, G and 2D bands, which can be seen when a background silicon carbide spectrum is subtracted from the data. It has been seen through Raman measurements that the position of the 2D peaks shifts with annealing time. Annealing times of 45 minutes give a positive shift of 60cm^{-1} away from 2645cm^{-1} whereas annealing times of 15 minutes give short positive shifts of around $1\text{-}2\text{cm}^{-1}$. Positive shifts in 2D peak have been linked to compressive strains within the graphene layer [3] so it appears that the amount of strain within our graphene is varying with anneal time.

AFM data shows the lateral grain size present within a sample, this increases notably between samples annealed in an open geometry (10s nm) and samples annealed with an alumina cap (100s nm). This can be attributed to the increase in partial pressure of silicon above the SiC chip during capped annealing leading to a decrease in the sublimation rate of silicon out of the SiC. Step edges observed by AFM show the graphene films present to be 5-10 layers thick.

This work was supported by the EPSRC and Intel.

References

- [1] Berger, C; et al, J.Phys. Chem. B. 2004, **108**, 19912.
- [2] Seyller, T; et al, Phys. Stat. Sol. (b). 2008, **245**, 1436–1446.
- [3] Mohiuddin, T.M.G; et al, Phys. Rev. B. 2009, **79**, 205433

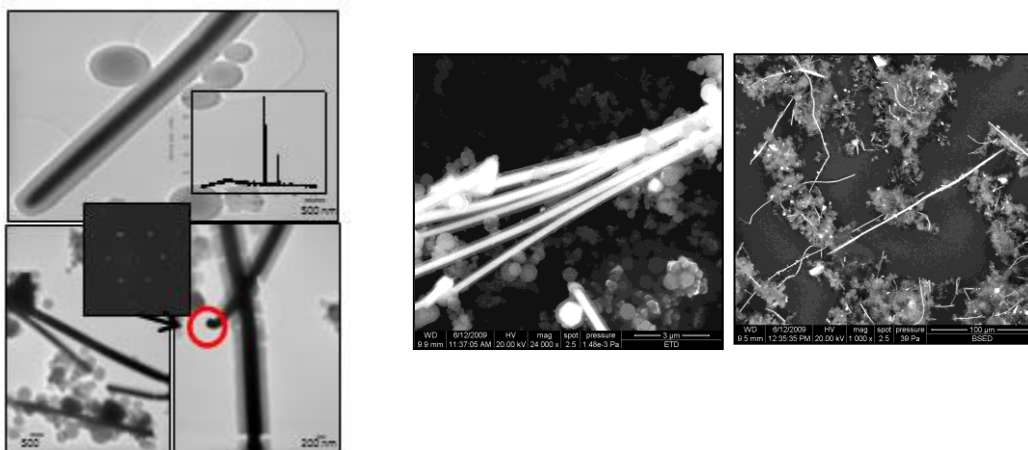
Hydrothermal Synthesis of Metal-Polymer Hybrid Nanostructures. Polypyrrole-coated Copper Nanocables

Jullieith Suárez-Guevara, Omar Ayyad, David Muñoz-Rojas and Pedro Gómez-Romero*

Centro de Investigación en Nanociencia y Nanotecnología, CIN2 (CSIC-ICN)
Campus UAB, 08193 Bellaterra (Barcelona), Spain
e-mail: pedro.gomez@cin2.es

Nanoparticles, nanotubes and nanowires are some of the most studied objects being developed by nanotechnologists. Noble metals have been widely used for these purposes given their ease of formation and stability. However, the fabrication of multicomponent or core-shell nanoparticles or nanowires is a more complex task.

In our group we have developed a line of work on the synthesis of hybrid nanostructures formed by metals (with Ag as a prototypical material) and conducting polymers [1-3] or biopolymers.[4] Hydrothermal techniques have played an important role in the fabrication of these structures. We present here several of the wide variety of hybrid materials prepared along this line, including Ag@PPy nanoparticles, Ag@PPy nanosnakes and AgCN@PPy nanotubes. Among these materials we will make special emphasis on the newest member of the family, namely Cu@PPy nanocables.[5] Thus we will present the first synthesis of polypyrrole-coated copper nanowires (Cu@PPy). These nanostructures are formed by rods of metallic copper coated with polypyrrole forming wires of a few hundred nanometers in diameter and lengths up to a few hundred microns, as seen on TEM (left) and SEM (center and right) photographs below.



These samples contain a large number of nanowire structures together with abundant globular formations of PPy. It should be remarked that the metallic copper core is single-crystalline in nature as showed by the SAED pattern.

Reference

- [1] Muñoz-Rojas, D., Oro-Sole, J., Ayyad, O., Gomez-Romero, P. *Small*. **4** (2008). 1301–1306.
- [2] Muñoz-Rojas, D., Oro-Sole, J., Gomez-Romero, P. *Journal of Physical Chemistry C*. **51**(2008). 20312-20318
- [3] Muñoz-Rojas, D., Oro-Sole, J., Gomez-Romero, P. *Chemical Communications*. **39**(2009). 5913-5915.
- [4] Ayyad, O., Munoz-Rojas, Oro-Sole, J., Gomez-Romero, P. *Journal of Nanoparticle Research*. **1**(2010). 337-345.
- [5] Submitted for publication.

Photodynamic effect on cytomechanical and morphological properties of HeLa cell lines

Katerina Tomankova¹, Hana Kolarova¹, Petr Kolar¹, Milan Vujtek², Klara Safarova²

¹*Department of Medical Biophysics, Faculty of Medicine and Dentistry, Institute of Molecular and Translational Medicine, Palacky University in Olomouc, Hnevotinska 3, 775 15 Olomouc, Czech Republic*

²*Centre for Nanomaterial Research, Faculty of Science, Palacky University in Olomouc, Slechtitelu 11, 783 71 Olomouc, Czech Republic
katerina.tomankova@upol.cz*

High resolution imaging of biological structures and their changes induced by different agents such as drugs and toxins is commonly performed by fluorescence and electron microscopy (EM). Recently, AFM has been shown to be a suitable tool for imaging biological structures and their modifications [1]. In addition to accurate morphological and cytomechanical information atomic force microscopy (AFM) provides a unique opportunity to study of living individual cells at the nanometer scale. Although high-resolution imaging is possible with EM, the requirements for fixation and staining of samples for image contrast severely limits the study of living organisms. AFM would be an attractive technique for studying these organisms because they could be maintained and imaged in biocompatible conditions. Moreover, AFM is capable of simultaneous nanometer spatial resolution and piconewton force detection allowing for detailed studies of cell surface morphology and monitoring of cell-tip interaction [2]. We present a method that images and mechanically characterized whole cells are studied by atomic force microscopy. We used a HeLa cell line (cervix carcinoma cell), which is sensitive to photodynamic therapy (PDT), DMEM growth media as a scanning surrounding, atomic force microscopy NT-MDT Aura for cytomechanical measurement, and scanning electron microscopy Hitachi Su 6600 for control images of the cells. In summary, elastic properties of intact cell can indicate mechanical characteristics of cells. On the other hand, cell elasticity changes can offer the degree or value of cells damage for example after PDT.

Acknowledgement

This work has been supported by the Projects of the Ministry of Education of the Czech Republic MSM6198959216, MSM6198959218, 1M6198959201, Czech Science Foundation GACR 202/09/1151 and CZ.1.05/2.1.00/01.0030.

Reference

[1] Sullivan CJ, Venkataraman S, Retter ST, Allison DP, Doktycz MJ. 2007. Comparison of the indentation and elasticity of *E. coli* and its spheroplasts by AFM. *Ultramicroscopy* 107, 934-942.

[2] Riethmuller C, Schaffer TE, Kienberger F, Stracke W, Oberleithner H. Vacuolar structures can be identified by AFM elasticity mapping. *Ultramicroscopy* 107, 895-901.

Optimal ^{99m}Tc radiolabeling of fullereneol $\text{C}_{60}(\text{OH})_{22-24}$ - potential tracer for scintigraphic investigation of kidneys and urinary bladder.

^{1*}Dj. Trpkov, ¹O. Neskovic, ¹J. Cveticanin, ¹T. Maksin and ²A. Djordjevic
¹Vinca Institute of Nuclear Sciences, P.O. Box 522, 11000 Belgrade, Serbia.

²Department of Chemistry, Faculty of Science, University of Novi Sad,
Trg Dositeja, Obradovića 3, 21000 Novi Sad, Serbia

*djordjet@vinca.rs

Influences of structural properties on the stability of fullereneol and ^{99m}Tc complexes, $[\text{}^{99m}\text{Tc}(\text{CO}_3)_3(\text{H}_2\text{O})_3]\text{C}_{60}(\text{OH})_{22-24}$, were studied using experimental mass spectrometric techniques, MALDI TOF, magnetic mass spectrometer and HPLC. We performed the dynamic and static scintigraphy of dog, using new synthesized radiopharmaceutical $[\text{}^{99m}\text{Tc}(\text{CO}_3)_3(\text{H}_2\text{O})_3]\text{C}_{60}(\text{OH})_{22-24}$.

After 24 hours, we detected the activity in kidneys and urinary bladder. Pharmacokinetic investigations performed in this study are of key interest for the further complexes of fullereneol in human in vivo research.

fullereneol, MALDI TOF, radiopharmaceutical, in vivo

Using chemical coprecipitation method to prepare magnetite magnetic fluids and explore its applications in hyperthermia

Hong-Yi Chen ^(a), Chang-Shu Tsai ^(a*), Tsz-Rou Chen ^(b), Kwo-Ping Chang ^(a),
Yuan-Ron Ma ^(c)

^(a) Institute of Radiological Sciences, Tzu Chi College of Technology, 97005, Hualien, Taiwan, R.O.C.

^(b) Department of Counseling and Clinical Psychology, National Dong Hwa University, 97003, Hualien, Taiwan, R.O.C. ^(c) Department of Physics, National Dong Hwa University, 97401, Hualien, Taiwan, R.O.C.

Correspondence Author : Chang-Shu Tsai ^(a*)

E-mail : fred@tccn.edu.tw ; FAX : 886-3-857-8941 ; TEL : 886-3-857-2158

Address : 880, Sec.2, Chien-Kuo Road, Hualien, Taiwan, 97005 R.O.C

In recent years, researches of hyperthermia have been widely conducted. One of the focuses is magnetic fluid hyperthermia (MFH), which is to place the magnetic fluid in alternating magnetic field and to increase the temperature of local tumor to 41-46°C for eliminating tumor cells[1]. In this study, the chemical coprecipitation method was employed for magnetic nanoparticles and then the formula of SAR was to evaluate its capability in converting the energy into heat per time and mass[3]. As a result, magnetic nanoparticles have been an important factor in determining the efficiency of hyperthermia.

Eleven different kinds of parameters, including the preparation time (0.5hr, 1hr, 1.5hr, 2hr, 2.5hr, 3hr etc.), temperature (30°C, 60°C, 70°C, 80°C, 90°C, 100°C etc.), pH(4, 10, 12 etc.), different ratios of iron salts ($Fe^{2+} : Fe^{3+} = 1:1, 1:1.5, 1:2, 1:2.5, 1:3, 1:3.5, 1:4$ etc.), different alkaline media (NH_4OH and $NaOH$), different concentration (1g/ml, 7 g/ml, 14 g/ml, 28 g/ml, 50 g/ml etc.), different drying time (12hr and 24hr) and in comparison with $Fe^{2+}:Fe^{3+}=1:1\sim 1:4$; different shaking time (0.5min, 1 min, 5 min, 10 min, 15 min etc.) and in comparison with $Fe^{2+}:Fe^{3+}=1:1$ and 1:2. The samples which are well-prepared in the magnetic fluid (75kHz) adjusted the power of electric current (125A, 200A, 300A, 400A, 500A, 600A etc.). After the repetitively heating the same sample, and XRD spectra, the magnetite of the sample was identified by its reaction. Finally, all of the best parameters from samples were in comparison to the commercial magnetic nanoparticles (< 50nm, Sigma Aldrich).

The SAR of pH=10 and 12 both were higher than that of pH=4, and there is no distinct difference between pH=10 and 12 ($p=0.4229$). In the preparation time, when the temperature reached 90°C and 100°C, the SAR was higher than other samples under different temperatures, and showed no distinct difference ($p=0.4163$). Moreover, we also concluded from the study that the SAR in different ratios of magnet. 1:1, 1:1.5, 1:2, are higher than that in others, and there is no distinct difference among the three of them [1:1 and 1:1.5($p=0.3683$), 1:1 and 1:2($p=0.4742$), 1:1.5 and 1:2($p=0.4269$)].

Furthermore, the SAR from the sample of NH_4OH was higher than other sample of $NaOH$, and both of them showed distinct differences ($p=0.001407$). The SAR from the samples under 3 hours of preparation time was higher than others, and showed distinct differences from all the other samples. Even though the SAR from the sample of 1g/ml concentration was higher than others, it took more time for it to reach the temperature for hyperthermia. Therefore, we chose to use the sample of 50g/ml concentration, which can reach the temperature for hyperthermia faster, comparatively. In the process of

preparation, using the ferric salts from different brands, Mallinckrodt, Nihon Shiyaku, Sigma Aldrich showed no distinct difference (Mallinckrodt: Nihon Shiyaku, $p=0.1430$; Mallinckrodt: Nihon Shiyaku, $p=0.1620$; Nihon Shiyaku: Sigma Aldrich, $p=0.4029$).

Setting the shaking time to 0.5 min, both the SAR from the samples of 1:1.5 and 1:2 ratios were lower, comparing with other samples which showed no distinct difference. In the drying time, except that $Fe^{2+}:Fe^{3+}$ was in the ratios of 1:2:5 and 1:3:5 and had its SAR increased after 24hr of drying, other samples no distinct difference. In adjusting the electric current of magnetic fluid, the SAR of the sample increased with the amplification of electric current. In the repeatedly heated samples, except that the SAR of $Fe^{2+}:Fe^{3+}$ resulted in 1:3~1:3.5 and showed no distinct difference, the SAR of other samples declined drastically. As a result, the best parameter for preparation time is 3hr and $pH=10$, the best preparation temperature is $90\text{ }^{\circ}C$, the best brand is the $Fe^{2+}:Fe^{3+} = 1:1, 1:1.5, \text{ and } 1:2$ from Sigma Aldrich, the best proportion of concentration is 50g/ml, and the best shaking time was 1min every time before heating. In the end, comparing our samples ($Fe^{2+}:Fe^{3+}$ is 1:1~1:2) with the commercial magnetic nanoparticles, they all showed distinct differences as the following, Commercial:1:1 ($p=0.0021$); Commercial:1:1.5 ($p=0.0001$); Commercial:1:2 ($p=0.0006$). There is no distinct difference in the sample of $Fe^{2+}:Fe^{3+}$ as 1:1~1:2 (1:1 compares with 1:1.5, $p = 0.1061$; 1:1 compares with 1:2, $p = 0.1147$, 1:1.5 compares with 1:2, $p = 0.2659$). In the long run, the sample with dextran, and study their changes after heating will be under continuous observation.

Reference

- [1] A.Jordan, R.Scholz, P.Wust, H.Fahling, R.Felix, J.Magn.Magn.Mater.201, (1999) 413-419.
- [2] B.R.Jarrett, M.Frendo, J.Vogan and A.Y.Louie, Nanotec.18 (2007) 035603.
- [3] I.Hilger, K.Fruhauf, W.Andra, R.Hiergeist, R.Hergt, W.A.Kaiser, Acad Radiol.9 (2002)198-202.
- [4] R.Massart,IEEE.Trans.Magn,17, (1981) 1247.

Atomic force microscopy characterization of nanoparticles on rough surfaces

Petr Klapetek¹, **Miroslav Valtr**¹, David Nečas², Ota Salyk³

¹*Department of Nanometrology, Czech Metrology Institute, Okružní 31, 638 00 Brno, Czech Republic*

²*Department of Physical Electronics, Faculty of Science, Masaryk University, Kotlářská 2,
611 37 Brno, Czech Republic*

³*Institute of Physical and Applied Chemistry, Faculty of Chemistry, Brno University of Technology,
Antonínská 548/1, 601 90 Brno, Czech Republic*

pklapetek@cmi.cz

Nanoparticle analysis is an important challenge in present nanoscale metrology. Nanoparticles are used in many fields of research and technology and their proper characterization is therefore very important. Besides the fact that there are several general approaches to nanoparticle analysis (optical methods, microscopy), results of them differ mutually very often due to different effects of non-ideal measurement conditions.

Nanoparticle analysis can be performed using scanning probe microscopy methods (namely atomic force microscopy - AFM). If the isolated nanoparticles are deposited on an ideally flat substrate and they are spherical, the size of a nanoparticle can be determined easily from the AFM image by measuring the nanoparticle image height. However, for non-ideal particles and curved substrates many questions arise from the point of particle analysis in AFM image processing software. In this contribution algorithms for non-ideal nanoparticle analysis on rough and curved substrates will be presented. Particle aspect-ratio measurement, agglomerated particles analysis, particle orientation analysis and similar topics will be addressed. Moreover, an analysis of uncertainties due to tip-sample convolution effects on results of statistical particle analysis will be presented.

Examples will be given for nanoparticles prepared using different methods and using different materials (gold, palladium, polystyrene). For all the algorithms presented, an open source application Gwyddion (<http://gwyddion.net>) will be used.

Textile fibres with metal nanoparticles: new technologies for industry

Inês V. Osório^a, Ricardo Ramos^b, Leonor Soares^c, Eulália Pereira^c, Rui Igreja^b, Ricardo Franco^a, João Cortez^a

^a REQUIMTE, Departamento de Química, Faculdade de Ciência e Tecnologia da Universidade Nova de Lisboa, Campus de Caparica, 2829-516 Caparica, Portugal

^b CENIMAT, I3N, Faculdade de Ciências e Tecnologia, Universidade Nova de Lisboa, 2829-516 Caparica, Portugal

^c REQUIMTE, Departamento de Química, Faculdade de Ciências da Universidade do Porto, R. Campo Alegre, 687, 4169-007 Porto, Portugal

ines.osorio@dq.fct.unl.pt

The development of novel technologies to improve existing materials and develop novel ones is extremely important for the technical textile market. EM radiation fields generated at near-field by mobile phones or far-field by e.g. radiofrequency towers generate considerable concern to human health[1,2].

We propose the concept of deposition or immobilisation of a nanometric layer of metal nanoparticles (NPs) on the surface of textile fibres, resulting in high levels of conductivity that lead to EM field dissipation by the textiles through a Faraday Cage effect[3].

Our approach, in departure from previous methodologies, will be the targeted use of specific ligands to ensure the immobilisation of metal nanoparticle (NPs). This rational design will permit low temperature immobilisation of metal NPs onto different fibre compositions in a targeted manner by controlling the NP amount immobilised onto the fibres, thus providing a tuneable EM shielding (EMS) for a wide range of EM frequencies; allow the production of EMS clothing with high standards of comfort and resistance to washing and wear, at a low cost.

Our approach involves the synthesis of silver nanoparticles (AgNPs) in solution and then the application binding onto textile fibres. The AgNPs were synthesised following the borohydrate method[4]. This method uses water as solvent and the AgNPs obtained have a average size of 8-10 nm (Fig. 1). A stability study of these particles showed they aggregated at NaCl concentrations greater than 40 mM and at pH lower than 4. These nanoparticles were functionalized with ligands that allow an increase in conductivity and shielding of wool and cotton. The conductivity measurements show that the treated fabrics have a shielding effect that blocks the EM radiation.

Another property of great interest to the textile industry is the production of the new self-cleaning textiles. We propose the use of nanoparticles followed by a polymer application to achieve this goal. These textiles are being developed with ZnO NP's by a seeding growth method[5]. SEM images (Fig. 2a) indicate that these nanoparticle seeds grow directly on cotton fibres, and in a second reaction they grow to form nanorods. So far, the contact angle obtained with the use of silanes as hydrophobic polymer layer were up to 138° (Fig 2b). The use of silanes and other polymers are currently under investigation to find out what will be the best hydrophobic polymer (that does not involved fluorocarbon compounds) as capping and allow an increase in contact angle to above 150°.

This work is part of the project QREN-ADI-5518-METALFUN, funded by the ERDF via QREN (Quadro de Referência Estratégico Nacional), a Portuguese funding body, in collaboration with Devan-Micropolis, Moreira da Maia, Portugal. The authors also wish to acknowledge the collaboration of Eng. Raquel Vieira (Micropolis) in this work.

References:

1. <http://www.who.int/mediacentre/factsheets/fs322/en/index.html>, WHO study, June 2007.
 2. Kundi M., Mild K., Hardell L., Mattsson M. 2004. *J. Toxicol. Environmental Health, Part B*, 7:351–384.
 3. Gindrup W., Vinson, R. 1998, United States Patent 5786785.
 4. Hynning D. and Zukoski, C. (1998) *Langmuir*, 14, 7034-7046.
 5. Bi Xu and Zaisheng Cai, *Appl. Surf. Scien.*, 254, 2008, 5899-5904
- Figure 1. TEM photograph of AgNPs synthesized.

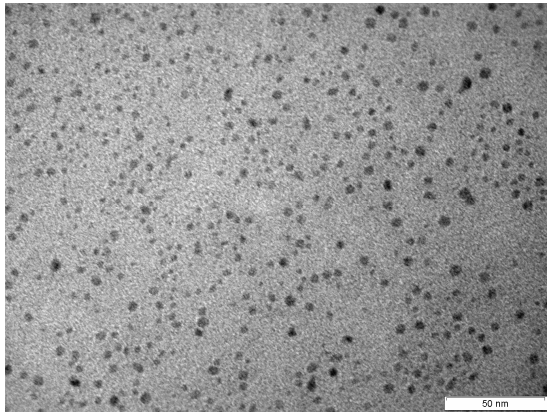
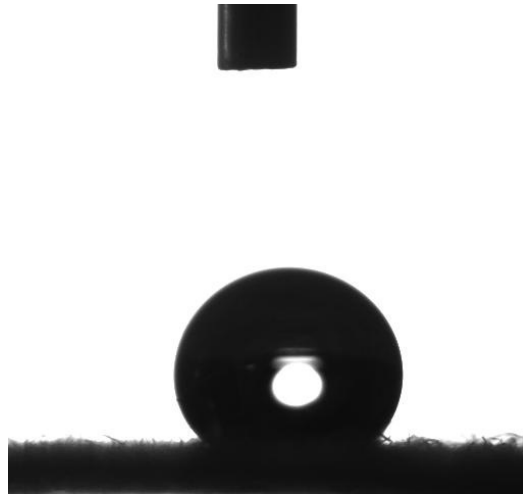
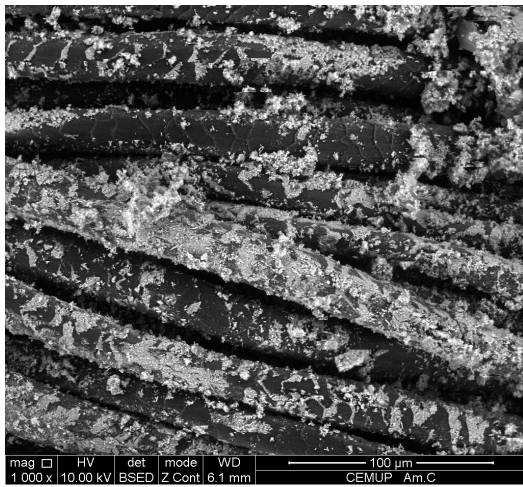


Fig 2 – a) SEM images of ZnO seeds in cotton and b) a water droplet with 5 μ L and a contact angle of 140 $^\circ$.



Stability, electronic structure and conductivity of monoatomic Mo wires inside carbon nanotubes

A. Vega,¹ A. García-Fuente,¹ V. M. García-Suárez,² J. Ferrer²

¹Departamento de Física Teórica, Atómica y Óptica. Universidad de Valladolid, Spain

²Departamento de Física. Universidad de Oviedo, Spain
vega@phenix.fam.cie.uva.es

We study the electronic, structural and transport properties of monoatomic Mo wires encapsulated inside single-walled carbon nanotubes. We used the SIESTA code [1] for the structural relaxation, while the transport properties were calculated with the non-equilibrium Green's functions formalism SMEAGOL [2]. We have simulated Mo wires inside single-walled carbon nanotubes with zigzag and armchair chiralities of different radii. We have found that the ground state of these systems is always formed by non-magnetic Mo dimers (Fig. 1) with interatomic distances similar to those of the periodic monoatomic Mo wire in the free-environment [3]. The minimum radius for a nanotube to be able to encapsulate a monoatomic Mo wire was found to be around 2.8 Å. Equidistant Mo wires, which are magnetic with both an antiferromagnetic and a ferromagnetic spin isomers, are also possible when the Mo concentration is decreased, although they are much higher in energy. We have calculated the band structure, densities of states and transmission channels for different thicknesses and chiralities, and we have then compared with those of the Mo wire in the free-environment and of the empty carbon nanotube (Fig. 2). For certain nanotubes, when we encapsulate a long Mo wire inside it (which is an insulator), the resulting system has a metallic behavior, independently of the insulating or metallic character of the nanotube.

[1] J. M. Soler et al, J. Phys.: Condens. Matter **14**, 2745 (2002)

[2] A. R. Rocha et al., Nature Materials **4**, 335 (2005)

[3] A. García-Fuente et al., Nanotechnology **21**, 095205 (2010)

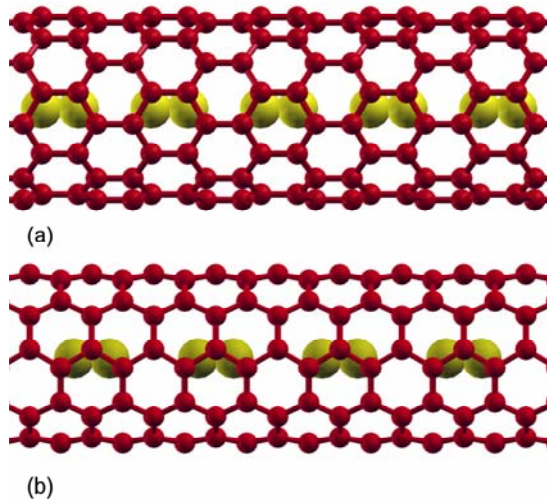


Fig.1: Ground state of a Mo wire inside (a) a (9,0) zigzag nanotube and (b) a (5,5) armchair nanotube.

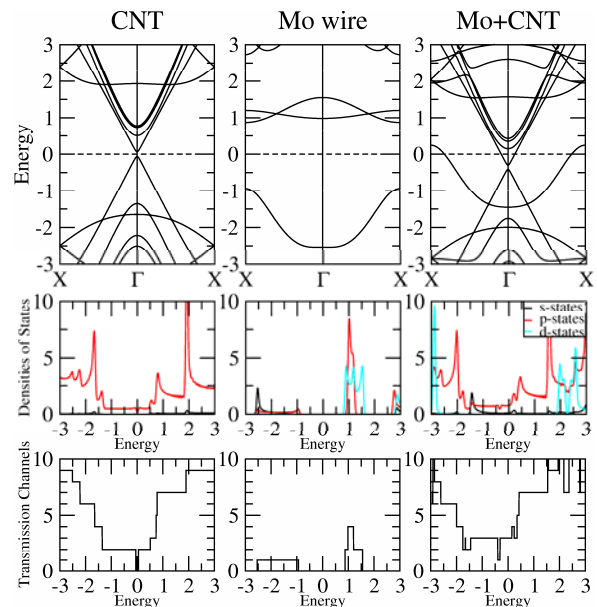


Fig 2: Band structure, projected densities of states and transmission channels of the system formed by a Mo dimerized wire encapsulated inside a (9,0) carbon nanotube compared with those of its components separately. All energies are in eV and referred to the Fermi level.

A PCR-Au-nanoprobes combined approach for detection of mutations associated with antibiotic resistance in *Mycobacterium tuberculosis*

Bruno Veigas¹; Diana Machado^{2,3}; João Perdigão⁴; Isabel Portugal⁴;
Isabel Couto^{2,5}; Miguel Viveiros^{2,6}; Pedro Baptista¹

¹ CIGMH/DCV, Faculdade de Ciências e Tecnologia, Universidade Nova de Lisboa, Caparica, Portugal;

² Unidade de Micobactérias, Instituto de Higiene e Medicina Tropical, Universidade Nova de Lisboa (IHMT/UNL);

³ UPMM (IHMT/UNL);

⁴ Centro de Patogénese Molecular/URIA, Faculdade de Farmácia, Universidade de Lisboa, Lisboa, Portugal;

⁵ Centro de Recursos Microbiológicos (CREM), Universidade Nova de Lisboa

⁶ COST ACTION BM0701 (ATENS)

Contact: bmrveigas@gmail.com

Tuberculosis (TB) is one of the leading causes of infection in humans, causing high mobility and mortality all over the world. The rate of new cases of multi and extensively drug resistant tuberculosis (MDR/XDR-TB) continues to increase [1], representing a serious health problem with serious implications in the containment of the disease [2]. In most cases, anti-TB drug resistance has been related to mutations in several loci within the pathogen's genome. The development of fast, cheap and simple screening methodologies would be of paramount relevance for the early detection of these mutations, and essential for the timely and effective diagnosis and management of MDR/XDR-TB patients.

The use of gold nanoparticles derivatized with thiol-modified oligonucleotides (Au-nanoprobes) has led to new approaches in molecular diagnostics - nanodiagnosics. Based on the differential non-cross-linking aggregation of Au-nanoprobes we were able to develop a colorimetric method for the detection of specific sequences with a single base resolution at room temperature [3,4] – Figure 1.

Here, we present a simplified approach for the rapid detection of *M. tuberculosis* complex (MTBC) strains and for the simultaneous detection of mutations associated with rifampicin resistance. This low-complexity assay enabled for detection of mutations D516V and S531L from MTBC clinical specimens with remarkable sensitivity in a few hours. This approach is being extended to further relevant mutations at other loci. This type of assay may prove to be useful in the initial management of suspected TB cases, especially from areas known to harbor high rates of MDRTB.

References:

[1] World Health Organization. Anti tuberculosis drug resistance in the world: report No. 4. Geneva, Switzerland: WHO; (2008).

[2] Martins M, Viveiros M, Couto I and Amaral L. Int J Tuberc. Lung. Dis. (2009) 13:569-73.

[3] Baptista PV, Montewka MK, Oles JP, Doria G and Franco R. Clin. Chem. 52, No. 7, (2006).

[4] Doria G, Franco R and Baptista PV. IET Nanobiotechnology, 1(4) (2007) 53-57.

Acknowledgments:

We acknowledge Fundação para a Ciência e a Tecnologia, Portugal for funding (CIGMH). This work was partially supported by Project PTDC/BIA-MIC/71280/2006 and PTDC/SAU-BEB/66511/2006; and PTDC/FIS/74274/2006 (BV). D. Machado was supported by grant SFRH/BD/65060/2009.

Figures:

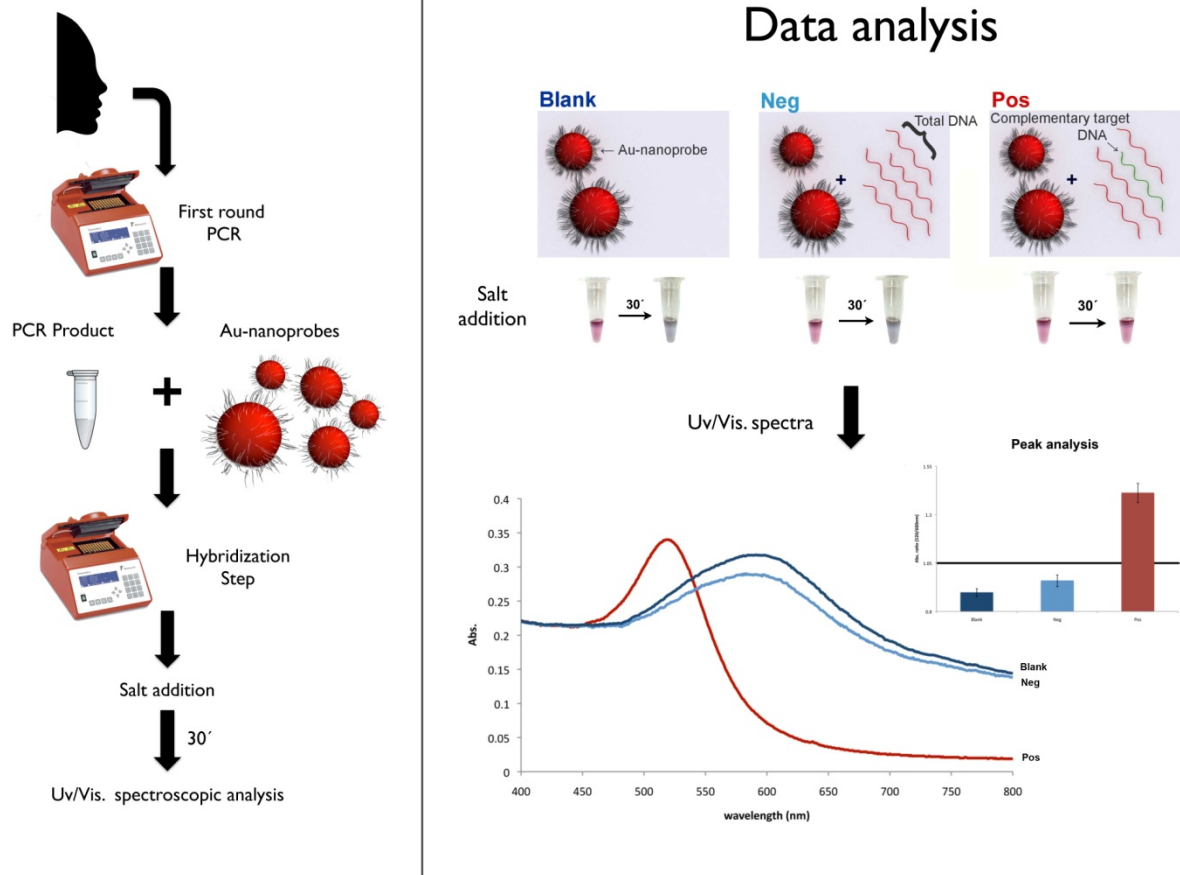


Figure 1- Au-nanoprobe strategy for detection of MTBC members and mutations associated with rifampicin resistance. Schematic representation of the detection with gold nanoprobes. The assay consists on visual comparison of test solutions before and after salt induced Au-nanoprobe aggregation: Au-nanoprobe alone – Blank; in the presence of a complementary DNA sequence – “POS”; and in the presence of a non-complementary DNA sequence – “NEG”.

Interactions of heparine with polymethinium salts capped gold nanoparticles in aqueous environment.

Lenka Veverková, Kamil Záruba, Vladimír Král

Institute of Chemical Technology, Department of Analytical Chemistry,
Technická 5, 166 28 Prague 6, Czech Republic,
Lenka.Veverkova@vscht.cz

Anions and anionic biopolymers play a fundamental role in a wide range of chemical and biological processes. Development of receptors which are designed for these analytes is an important branch of modern chemistry [1,2]. One of the major challenges in supramolecular chemistry is the design of receptors for selective anion recognition. Nature has developed selective protein receptors even for structurally very similar biologically important anions, e.g., including phosphate and sulfate binding proteins [3]. The design of synthetic receptors for selective sulfate over phosphate recognition in aqueous media has been a significant challenge. In the case of polysulfates, such as heparin, two types of optically-responsive synthetic receptors have been studied. One of these is using cationic boronic sensors [4].

Nowadays, gold nanoparticles are often prepared by chemical reduction of Au(III) [5]. Sodium citrate belongs to the most usable reducing agents [6] to prepare citrate stabilized gold nanoparticles. Mercapto-derivatives have been commonly used as modifiers of gold nanoparticles in recent years. 3-Mercaptopropionic acid (3-MPA) represents such a compound. At basic pH nanoparticles modified by 3-MPA have negative charge on the surface due to carboxylate groups. This allowed immobilization of polymethinium salts (**1**, **2**) which have positive charge due to quaternary nitrogen atoms by ionic bond. It is also possible to immobilized polymethinium salts by direct immobilization to non-modified gold nanoparticles because of their negative surface charge.

The method based on the reduction of $K[AuCl_4]$ by citrate was used to prepare 15 nm average size gold nanoparticles (ref. 5). The immobilization of porphyrin conjugates was carried out by two different ways of ionic interaction. First, direct immobilization of polymethinium salts on nanoparticles, second, immobilization of polymethinium salts on 3-MPA premodified gold nanoparticles. Such prepared nanoparticles were purified by centrifugation and characterized. Interactions of heparine with polymethinium salts in water were studied by UV-Vis spectroscopy.

Immobilization of **1** and **2** on gold nanoparticles (GNP) prevents the polymethinium salts from aggregation in water. Comparative experiments with free **1** and **2** versus GNP-MPA-1, GNP-MPA-2 in water revealed a strong influence of the immobilization of the polymethinium salts on their interactions with heparine. The selectivity of polymethinium salts towards heparine remains the same with comparison to free polymethinium salts in the solution.

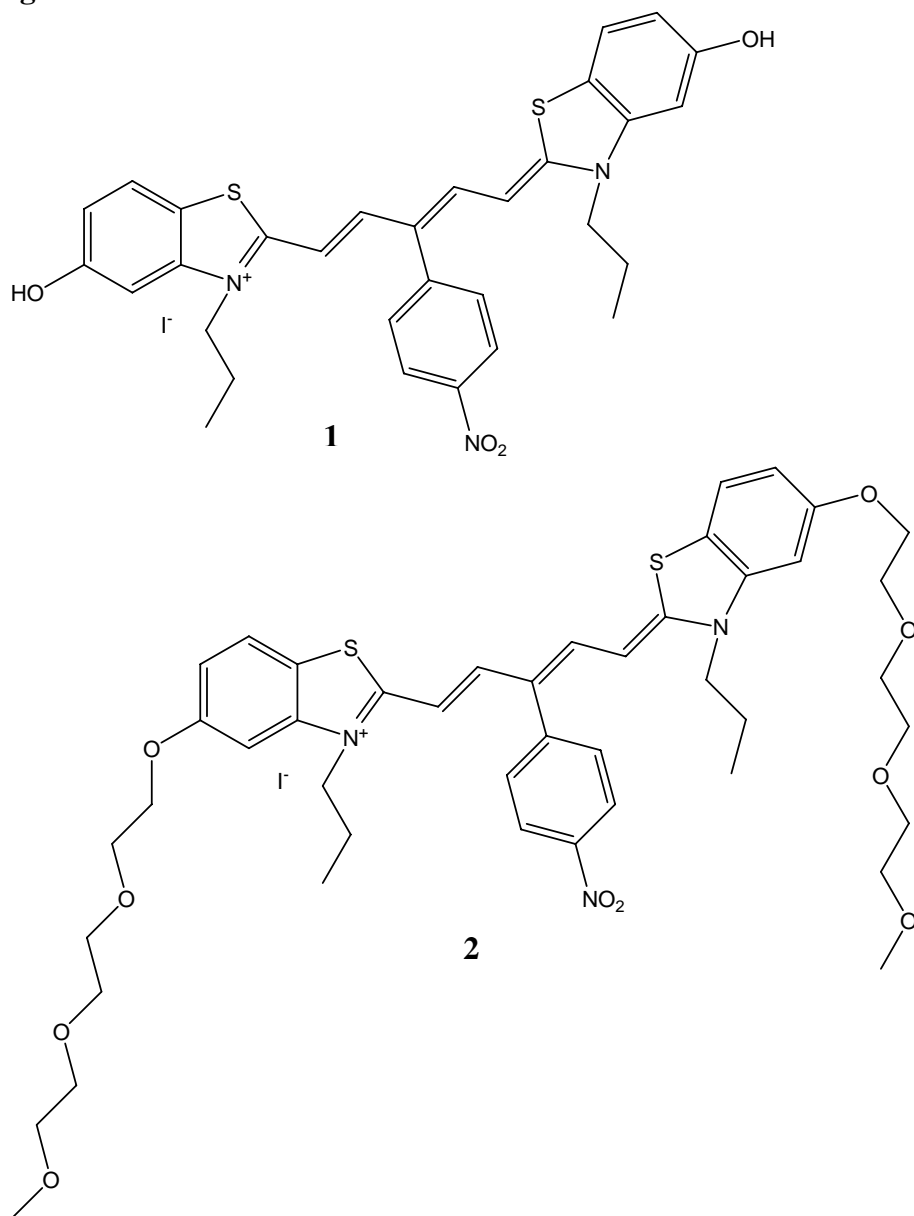
The financial support from the MSMT6046137307, LC512, KAN200100801 and KAN200200651 is gratefully acknowledged.

References:

- [1] Piatek P., Lynch and, V. M., Sessler J. L., J. Am. Chem. Soc., **126** (2004), 16073.
- [2] Singh N. J., Jun E. J., Chellappan K., Thangadurai D., Chandran R. P., Hwang I. C., Yoon J. and Kim K. S., Org. Lett., **9** (2007), 485.

- [3] Shrestha S., Salin L. E., Ensor C. M. and Daanert S., *Biotechnol. Bioeng.*, **78** (2002), 517.
[4] Zhong Z. and Anslyn E. V., *J. Am. Chem. Soc.*, **124** (2002), 9014.
[5] Shipway N. A., Katz E., Willner I., *Chem. Phys. Chem.*, **1** (2000) 1655.
[6] Turkevitch J., Stevenson P. C., Hillier J., *Discuss. Faraday Soc.*, **11** (1951) 55.

Figures:



Structural and electrical characterization of Si_{1-x}Ge_x nanocrystals embedded in Al₂O₃ matrix

E. M. F. Vieira¹, S.R.C. Pinto¹, A.G. Rolo¹, A. Chahboun^{1,2}, S. Levichev¹, M. Buljan³, S. Bernstorff⁴, O. Conde⁵ and M. J. M. Gomes¹

¹ Physics Department and Centre of Physics, University of Minho, 4710 – 057 Braga, Portugal,

² LPS, Physics Department, Faculty of Sciences, BP 1796, Fès, Morocco

³ Rudjer Boskovic Institute, Bijenicka cesta 54, 10000 Zagreb, Croatia

⁴ Sincrotrone Trieste, 34012 Basovizza, Italy

⁵ Physics Department, University of Lisbon and ICEMS, 1749-016 Lisboa, Portugal

Contact@-E-mail: eliana_vieira@fisica.uminho.pt

SiGe-based heterostructures are receiving a lot of interest not only from the point of view of device applications but also from the scientific point of view [1]. This is because SiGe heterostructures have a high potential to improve the state of Si devices particularly for very large scale integrated circuits (VLSIs) and add such new functions as optics and also provide a new scientific field of materials growth and characterization relating to the lattice mismatch between Si and Ge.

In order to fabricate high performance devices with Si_{1-x}Ge_x nanocrystals, it is necessary to know and control their structural and electrical properties [2] which depend on several factors including particle size, shape and atomic composition.

In this work, Si_{1-x}Ge_x nanostructures embedded in Al₂O₃ dielectrics were produced by RF-sputtering. Raman spectroscopy, Grazing Incidence X-ray diffraction (GIXRD) and Grazing Incidence Small Angles X-ray scattering (GISAXS) techniques were used for the structural characterization of the produced systems. The analyses showed the formation of Si_{1-x}Ge_x nanocrystals after a subsequent annealing (Figs. 1 and 2), and the nanocrystal size distribution and arrangement properties were determined. The electrical properties and carrier's retention effect in the formed nanostructures were studied by current-voltage characterization (Fig. 3).

References

[1] Y. Shiraki, and A. Sakai, Surf. Sci. Rep., vol. **59**, (2005) pp. 153-207

[2] L.J. Lauhon et al, Nature (London), vol. **57** (2002) pp.420

Figures

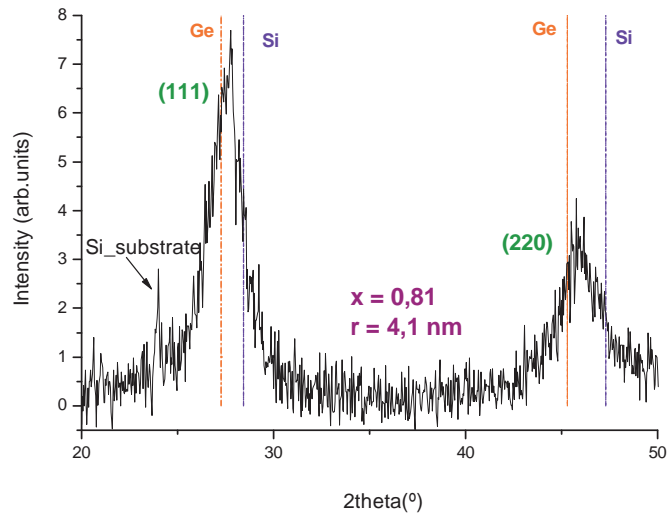


Fig.1. GIXRD pattern of $\text{Si}_{1-x}\text{Ge}_x$ NCs in alumina matrix. The two peaks are associated with the crystallographic planes of the $\text{Si}_{1-x}\text{Ge}_x$ alloy, respectively. The composition x and the NCs size are indicated on the figure.

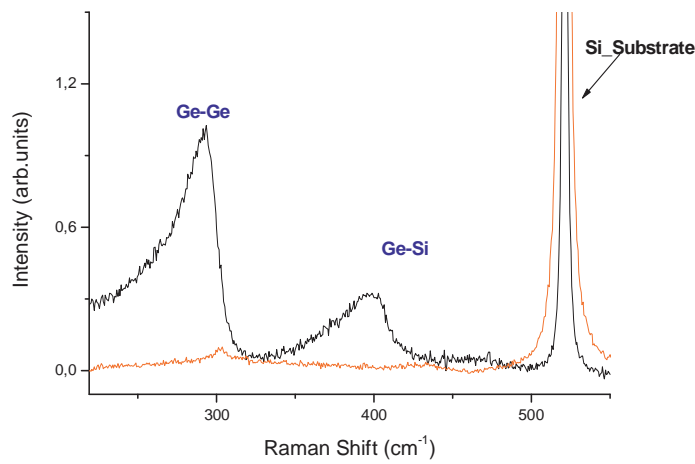


Fig.2. Raman spectra of the sample (black) and Si substrate (red). The two peaks near 300 and 400cm^{-1} correspond to the Ge-Ge and Ge-Si optical phonon modes, respectively.

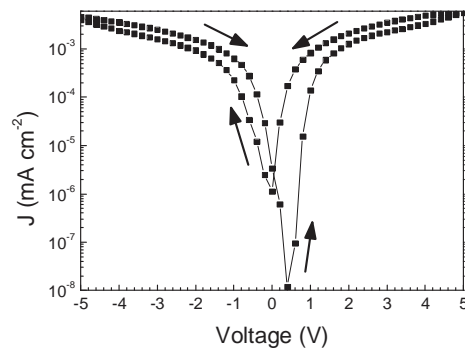


Fig.3. Semi-log plot of current – voltage characteristic of an $\text{Al}/\text{Al}_2\text{O}_3/\text{SiGe NCs} + \text{Al}_2\text{O}_3/\text{Al}_2\text{O}_3/\text{Al}$ device. The arrows indicate the sweep directions.

Gold Nanoparticles Stability studies in physiological mediums

Laura Vivero¹, Hanna Parkkola¹, Judith Sendra¹, Joaquín Querol¹, Pablo G. Cambero², Marc Ramis¹

1- Endor Nanotechnologies
2- Instituto de Salud Carlos III

E-mail: laura.vivero@endornanotech.com, marc.ramis@endornanotech.com

The use of nanomaterials in biomedical application has attracted enormous attention due to their distinct physical and biochemical properties at the nano-scale [1]. The stability of the nanomaterial is one of the key factors for each specific application. Recently, gold nanoparticles (GNPs) have been used in the medical field because of their biocompatibility, versatile coating chemistry and also unique optical properties. Therefore, the study of GNPs stability in physiological mediums is of current importance.

Several GNPs stability studies have been already reported in water solution [2, 3]. However, most biological studies require a physiological medium with high salt concentration. The presence of salts in the medium can cause GNPs instability. The aim of this study is to investigate the stability of GNPs in saline media. We have compared non-coated GNPs and Hyaluronan coated GNPs (HA-GNPs) in different saline solutions.

GNPs stability study was performed in embryo, daphnia, fish and worm physiological mediums. Each specific medium has a different saline concentration. All GNPs samples were analyzed at different times by UV-VIS, Dynamic Light Scattering (DLS) and TEM in order to examine the stability of the GNPs.

In summary, results demonstrated that HA-GNPs were stable in all saline medium while GNPs were not. The UV-VIS showed a maximum peak at 520nm when GNPs were stable and this peak diminished when GNPs aggregated. DLS technique showed the different size of GNPs. When GNPs aggregated, particle size was bigger than with non aggregated, stable GNPs. HA-GNPs expressed the same size at different times of analysis. GNPs were visualized by TEM which showed that GNPs had an irregular shape but HA-GNPs presented a spherical shape.

In conclusion, non-coated GNPs aggregate in saline mediums tested in this work. However, HA-GNPs are stable. GNPs instability could be due to the interactions between highly concentrated electrolytes in the medium and the GNPs non-coated surface.

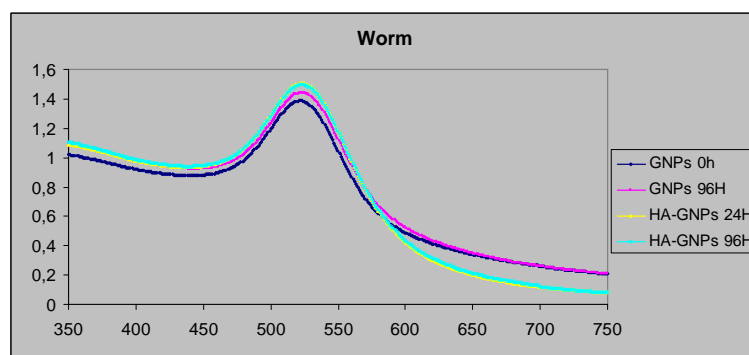
References

- [1] Elodie Boisselier and Didier Astruc, Chem Soc Rev, 38 (2009) 1759-1782.
- [2] Isaac Ojea-Jimenez and Victor Puentes, J.A.M.CHEM.SOC, 131 (2009) 13320-13327.
- [3] Wenting Zhao, Li Lin and I-Ming-Hsing, Langmuir, 26(2010) 7405-7409

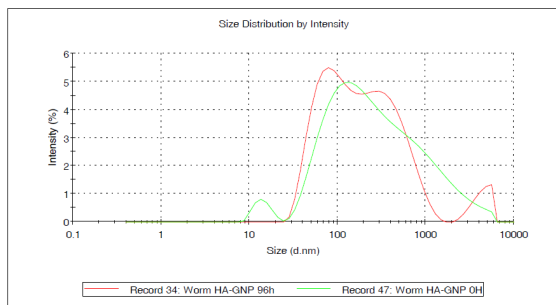
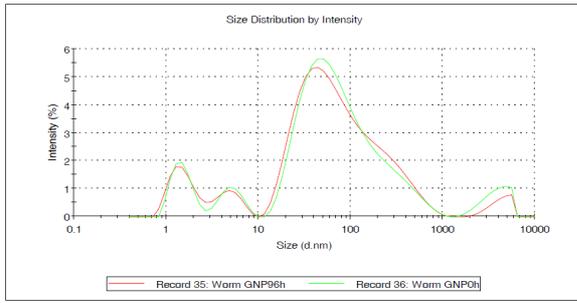
Figures: representative results

Worm

- UV-Vis

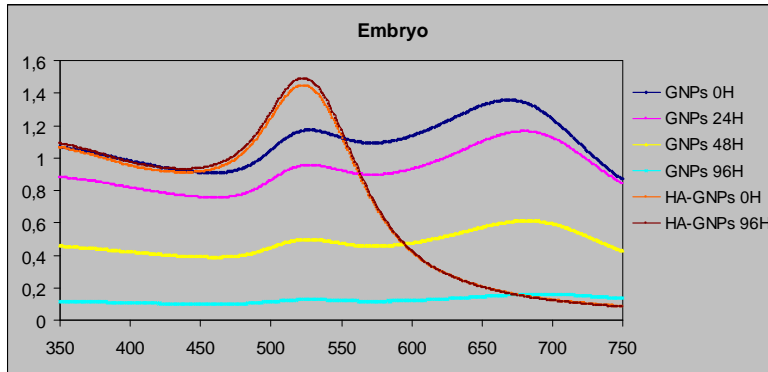


- DLS

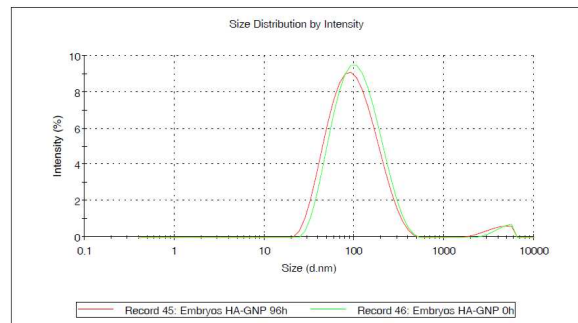
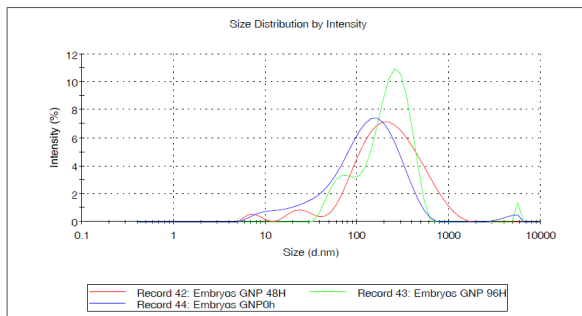


Embryos

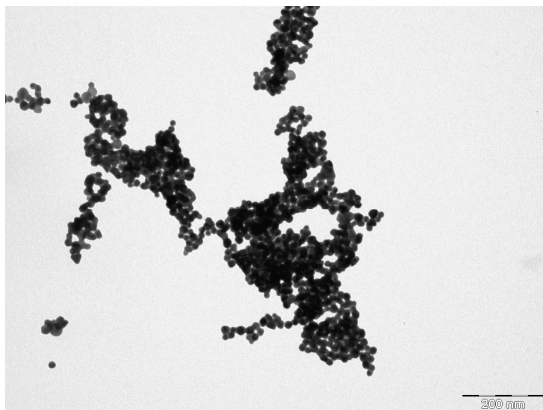
- UV-Vis



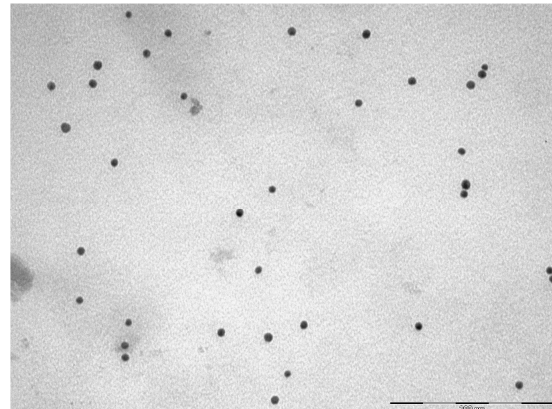
- DLS



- TEM



GNP aggregated



HA-GNPs

Mechanics of lipid nanotube networks and containers

Voinova M.V., Adams K., Karlsson R., Cans A.-S., Engelbrektsson J., Zhang B., Eves D.J., Heien M.L., Ewing G.

Chalmers University of Technology, S-412 96Gothenburg, Sweden

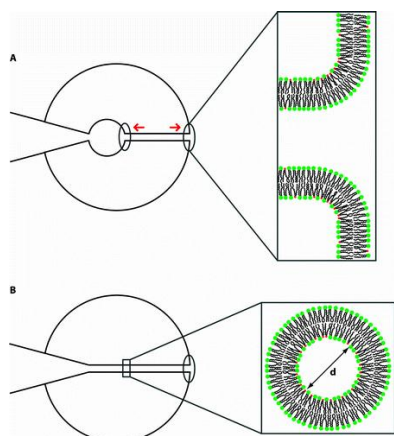
marina.voinova@chalmers.se

Lipid vesicle is an attractive mechanical model of cell plasmatic membrane since demonstrates similar elastic properties and global and local geometrical transformation yet contains no specific proteins responsible for the local curvature in living cells. It was found [1-3] that the application of the localized mechanical force produces lipid tethers (lipid nanotubes), water-filled cylindrical structures of radius $\sim 0.5 \mu\text{m}$. The peculiarities of the mechanical properties of lipid nanotubes (LNTs) originates from the fluidity of the tube wall and their mesoscopic size which makes shape fluctuations an important contribution to the membrane tension. The shape of a structure is a result of the interplay between the curvature elasticity effects maintaining the original geometry and the membrane tension which tends to reduce the nanotube radius and therefore diminish the free energy of the system. Recently, a spectacular work on formation of a microscopic network of lipid nanotubes connected with containers-vesicles has been reported in [2,3]. It was proved that lipid nanotubes can mediate an intravesicular transport of fluid and microparticles. This transportation could be induced by a mechanical perturbation of a given vesicle by causing a shape deformation [2] and a concomitant directed flow of membrane lipids. These interesting findings open perspectives towards controlled transportation of substances between lipid microcontainers-vesicles via bioorganic LNTs channels.

In this study we present a physical analysis of mechanics and transport phenomena in the system of surface-immobilized lipid bilayer vesicles (microcontainers) conjugated with a common lipid nanotube (LNT) pulled from its wall in different geometry. This work has been motivated by recent experimental precision measurements of lipid nanotube diameter utilising an artificial cell model [1] and correlations between the membrane deformation and enhanced transport of encapsulated substances between two interconnected containers-vesicles by creation of a lipid flow [2].

References

- [1] Adams K.L., Engelbrektsson J., Voinova M.V., Zhang B., Eves D.J., Karlsson R., Heien M. L., Cans A.-S., Ewing G. *Analytical Chemistry*, **82** (2010) 1020.
- [2] Karlsson, M., Davidson M., Karlsson R., Karlsson A., Bergenholtz J., Konkoli A., Jesorka, A., Lobovkina T., Hurtig, J., Voinova M. V., Orwar O. *Ann. Rev. Phys. Chem.*, **55** (2004) 613.
- [3] Karlsson R., Karlsson R., Karlsson M., Cans A.-S., Strömberg A., Ryttsen F., and Orwar O. *Nature*, 409 (2001) 150.



Strong carbon nanotube doping by *m*-tweezer molecules

A. Wurl, T. Reumann¹, E. M. Peréz², N. Martín² and Ch. Klinke¹

¹Institute of Physical Chemistry, University of Hamburg, Grindelallee 117, 20146 Hamburg, Germany;

²Departamento de Química Orgánica, Facultad de Química, Universidad Complutense, E-28040 Madrid, Spain

wurl@chemie.uni-hamburg.de

Carbon nanotube field effect transistors (CNTFETs) have attracted more and more attention in recent years due to their intrinsic advantages compared to transistors made from bulk material: First, the atomic scale and therefore quantum confinement of the channel leads to extreme sensitivity to the environment. Second, tuning of the characteristics of CNTFETs is possible through chemical processing of pristine nanotubes, opening up a broad spectrum of applications. We chose a supramolecular approach to realize electrostatic doping of CNTFET devices. By exploiting non-covalent forces, namely van-der-Waals, π - π , and concave-convex interactions [1], a host-guest complex is formed between single-walled carbon nanotubes (SWCNT) of CNTFET devices and electroactive ligand molecules. This supramolecular association results in charge transfer to the transistor channel and gating at the same time, since net charge is generated in the ligands.

We chose ligand structures with an extended π -electron system and a bivalent, tweezers-like design [2] which ensures efficient complexation and geometrically matches the CNT in its two-fold symmetry. The two recognizing units are connected covalently by a *meta*-substituted aromatic spacer, giving rise to the term "*m*-tweezer".

Electrostatic doping effects of the ligands are studied by measuring transfer characteristics of CNTFET devices as well as by confocal Raman spectroscopy of SWCNTs in solution. SWCNT-ligand interactions are modelled by DFT calculations.

Apart from being able to tune the transfer characteristic of CNTFET devices, this method provides a concept for a chemical sensor in the way that the non-covalent association of an organic ligand to a SWCNT can be monitored by the current flow in a CNTFET.

References

[1] T. Kawase *et al.* Angew. Chem., Int. Ed., **42** (2003) 1621.

[2] E. M. Peréz *et al.* J. Am. Chem. Soc., **128** (2008) 7172.

[3] E. M. Peréz *et al.*, Chem. Commun. (2008) 4567-69.

Figures

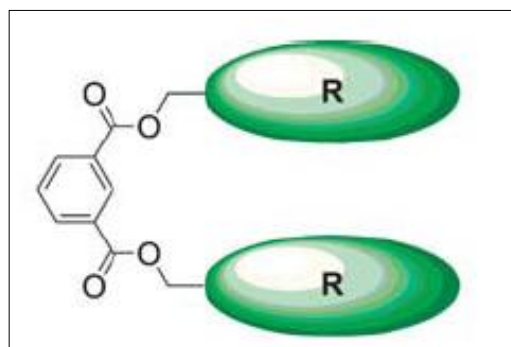


Figure 1: Structural concept of *m*-tweezer [3].

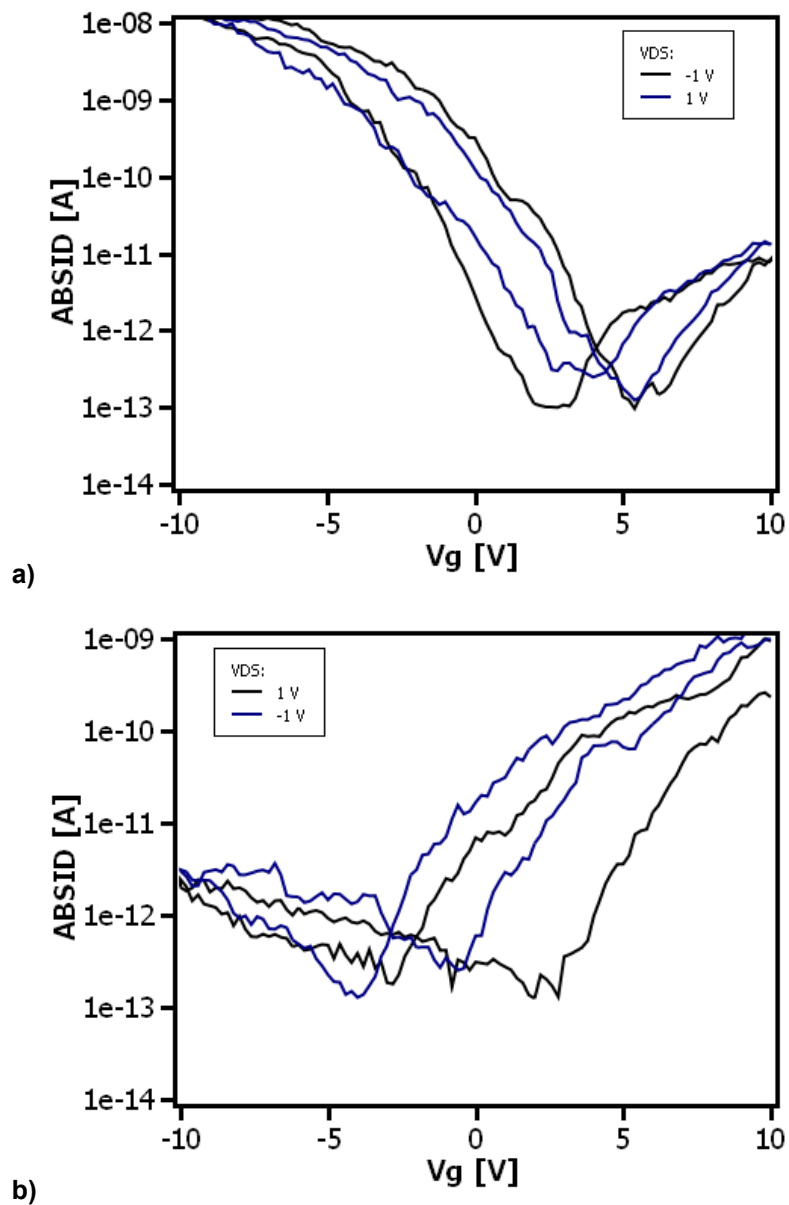


Figure 2: Typical CNTFET transfer characteristics. **a)** Pristine device showing p-type polarity (hole transport). **b)** After electrostatic doping with a π -donor *m*-tweezer ligand, the transistor polarity has changed to n-type (electron transport).

Study on oxidation layer of single core Nickel nanobeads

E. Xuriguera¹, M. Benelmekki², M. Segarra¹, Ll. Martínez³

¹Diopma, IN2UB, Departament de Ciència dels Materials i Enginyeria Metal·lúrgica, Universitat de Barcelona, Martí i Franquès 1, E-08028 Barcelona, Spain

²Centro de Física, Universidade do Minho, Braga, Portugal

³Sepmag Tecnologies, Parc Tecnològic del Vallès, Barcelona, Spain

xuriguera@ub.edu

Magnetic separation is one of the technological applications of magnetic nanoparticles (MNP). Magnetic separation of organic compounds, proteins, nucleic acids and other biomolecules and cells from complex reaction mixtures is becoming the most suitable solution for large production in bioindustrial purification and extraction processes. Optimal magnetic properties can be achieved by the use of metals like nickel, instead of commercial magnetic nanobeads with unclear magnetic behaviour and high cost. However, they are extremely sensitive to oxidation and degradation under atmospheric conditions.

Ni nanoparticles (NPs) were synthesised by conventional solution reduction process. The obtained NPs were surfactated in citric acid and then coated with silica to form single core Ni nanobeads. In this work, the research is focused on the study of surfactated nickel NPs, since they have suffered oxidation before silica coating.

The surfactated nickel nanoparticles were characterized by Atomic Force Microscopy (AFM). Later, citric acid was removed to observe shape and size of nickel oxidated NPs with High Resolution Transmission Electron Microscopy (HRTEM) and determine morphology and structure of oxidation layer by means of Electron Energy Loss Spectroscopy (EELS) [1]

The nickel nanoparticles were polycrystalline with an average size of 50nm. The presence of nickel oxide superficial layer was confirmed by the elemental ratio between Ni and O observed in the EEL spectra [2] and by the FFTs of HRTEM images. EEL spectra along one particle showed that the layer of nickel oxide was not continuous and the thickness was not homogenous. To confirm this, a map of NiO and Ni distribution in a whole particle was obtained through multiple linear least-squares (MLLS) method fitting of a spectrum in cross section geometry.

The authors would like to thank Sonia Estradé, Serveis Científicotècnics de la Universitat de Barcelona, for help with the HRTEM and EELS analyses.

References

- [1] S. Barth, S. Estrade, F. Hernandez-Ramirez, F. Peiro, J. Arbiol, A. Romano-Rodriguez, J. R. Morante and S. Mathur, *Crystal Growth and Design*, **9 (2)** (2009) 1077-1081.
- [2] L. Cave, T. Al, D. Loomer, S. Cogswell and L. Weaver, *Micron.*, **37** (2006) 301.

CHARACTERIZATION AND PROPERTIES OF POLYAMIDE 12 NANOCOMPOSITES MODIFIED BY A GRAFTED ELASTOMER

A. Zabaleta, I. González, J. I. Eguiazábal and J. Nazabal

Dpto. de Ciencia y Tecnología de Polímeros and Instituto de Materiales Poliméricos POLYMAT.
Facultad de Ciencias Químicas UPV/EHU, Paseo Manuel Lardizábal 3, 20018, San Sebastián, Spain.
asier.zabaleta@ehu.es

Introduction

There is an increasing interest in the possibility of linking polymer nanocomposite production by clay addition, to blending with a second tough component. This will offer the possibility to overcome the tendency to notch sensitivity and low-notched fracture toughness of nanocomposites by means of rubber modification. In this way, the technique of rubber toughening brittle polymers (that deform by crazing), later extended to ductile polymers (mostly deformed by shear), could also be used for nanocomposites. This would mean that the only major mechanical property that is not enhanced upon organoclay addition, i.e. toughness, could increase with respect to that of the matrix, and that the decrease in stiffness observed upon rubber addition in toughened blends could be counteracted by the presence of the organoclay (OMMT)^{1,2}.

Polyamide 12 (PA12) is a semi-crystalline polyamide that offers a good combination of thermal and mechanical properties, which make it suitable for a number of industrial applications. This PA12 is able to form exfoliated PNs with commercially available organically modified clays, but to the best of our knowledge, no work has been published concerning its toughening. This gives us the opportunity to study (i) whether toughening is possible in PA12 PNs (ii) the morphological position of the brittle/tough (B/T) transition by means of the interparticle distance, and (iii) the parameters that influence the position of the B/T transition.

Experimental

The PNs were obtained in two extrusion steps. The PA12/OMMT matrix with 3% OMMT was obtained in a twin screw extruder. Subsequently, a maleinized styrene/ethylene-butylene/styrene copolymer (mSEBS) was added up to 30% in a second extrusion step, before injection molding. The PA12/mSEBS blends were prepared as a reference in one step. The characterization of the nanostructure was carried out by X-ray diffraction (XRD) and transmission electron microscopy (TEM), the surfaces of cryogenically fractured specimens were observed by scanning electron microscopy (SEM) and the phase structure was analyzed by dynamic mechanical analysis (DMA). The mechanical properties were determined by Izod impact and tensile tests.

Results y discussion

The nanostructure analysis revealed that the clay layers stayed in the PA12 matrix and that the additional processing, required to incorporate the rubber, did not lead to any compaction of the widely exfoliated layers. The morphology of the rubber particles in the PNs was homogeneous, with particle sizes slightly larger than those of the corresponding blends, due to limitations imposed by the OMMT on the compatibilizing effect of the mSEBS. The presence of the exfoliated OMMT and the modification with rubber (25%) led to a polymer nanocomposite in which high toughness (the notched impact strength was 25 times that of the PA12 matrix) (Figure 1) and ductility (the elongation at break was 210%) were produced simultaneously. This indicates that these materials were tough throughout an unusually wide range of strain rates and mode of fracture conditions. The brittle/tough transition of PNs occurred at a τ_c smaller than that of the blends. Taking into account that the extrinsic parameters (testing conditions) that influence τ_c were constant, and that the difference in interfacial adhesion between the PNs and the blends should increase τ_c , the observed behaviour of τ_c must be attributed to the higher modulus of the PNs.

Acknowledgements: The financial support of the Spanish “Ministerio de Ciencia e Innovación” (Project Number MAT2007-60153) is gratefully acknowledged. A. Zabaleta also acknowledges the grant awarded by the Ministerio de Ciencia e Innovación.

References

- [1] Y. Yoo, L. Cui, P. J. Yoon, D. R. Paul. *Macromolecules* **43** (2010) 615.
[2] I. González, J. I. Eguiazábal, J. Nazábal. *Composites Science and Technology* **66** (2006) 1833.

Figures

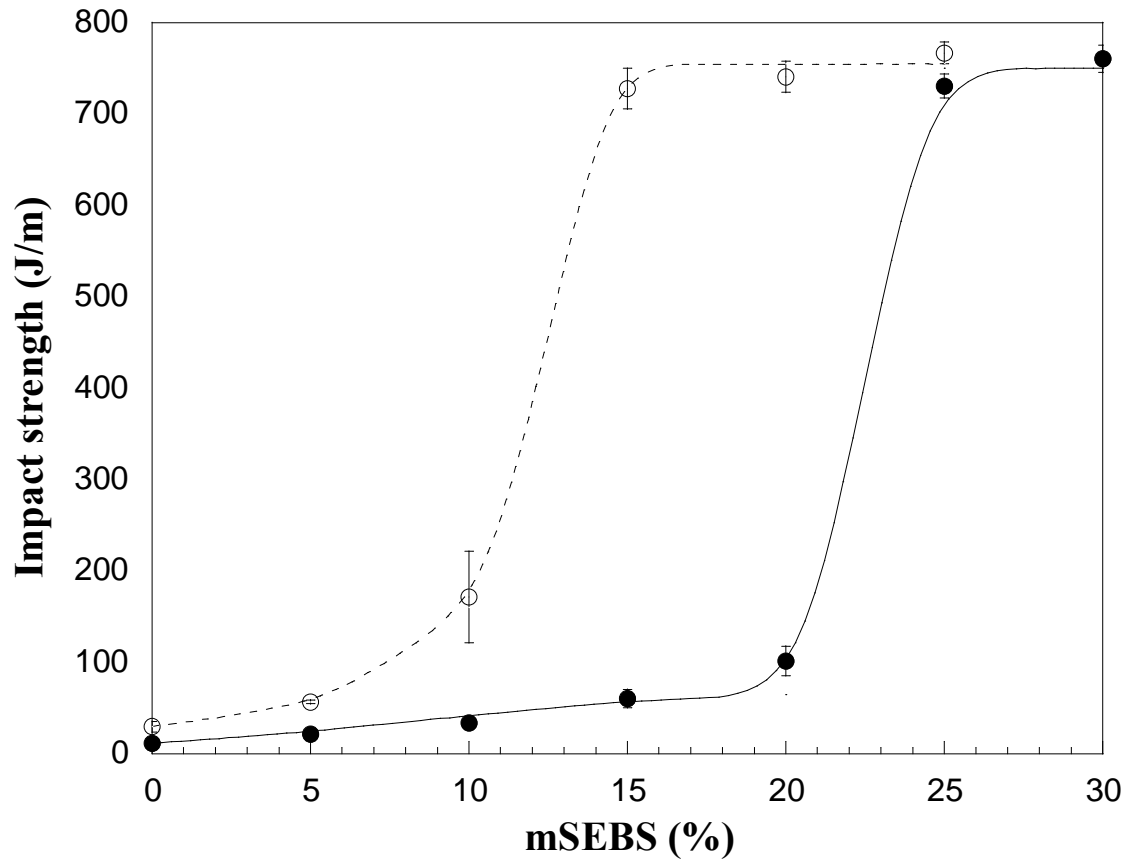


Figure 1. Notched Izod impact strength of the PNs (solid symbols) and reference blends (open symbols) versus mSEBS content.

Zinc Sulphide has been known as a luminescence material and doping it with transition metals has been done in order to reach photoluminescence with max intensity in various regions of electromagnetism spectrum.

Mehdi Zohrabi

Tarbiat Moalem University, Iran

zh_als@yahoo.com

Sources of coherent, monochromatic short-wavelength infrared (1-2 μm) light are essential in telecommunications, biomedical diagnosis and optical sensing. Today, semiconductor lasers are made by epitaxial growth on a lattice-matched single-crystal substrate. This strategy is incompatible with direct growth on silicon. Colloidal quantum dots synthesized in solution can, in contrast, be coated onto any surface. Here we show a 1.53 μm laser fabricated using a remarkably simple process: dipping a glass capillary into a colloidal suspension of semiconductor quantum dots.

We developed the procedures to produce a smooth low-scattering-loss film inside the capillary, resulting in a whispering gallery mode laser with a well-defined threshold. While there exist three prior reports of optical gain in infrared-emitting colloidal quantum dots [1,2,3], this work represents the first report of an infrared laser made using solution processing.